**Australian Government**

Geoscience Australia

*pmd*\*CRC

Final Report

# 3D Geological models of the eastern Yilgarn Craton Project Y2

September 2001–December 2004

*R.S. Blewett and A.P. Hitchman (editors)*

**Record**

**2006/05**
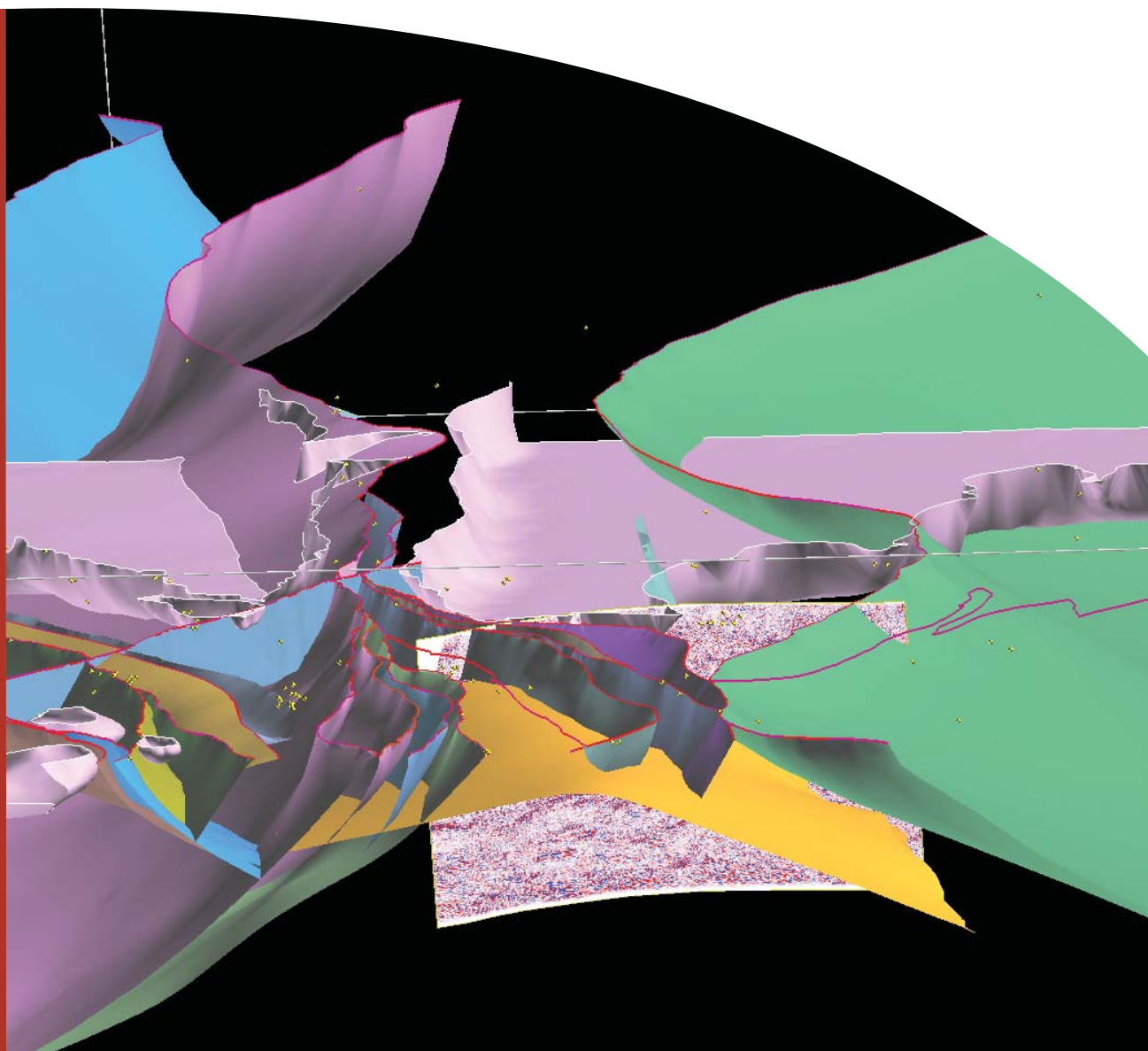
Final Report

# 3D Geological models of the Eastern Yilgarn Craton Project Y2

September 2001 – December 2004

by

R.S. Blewett and A.P. Hitchman (editors)

**Australian Government**
**Geoscience Australia**

*pmd**CRC

# Forward

This Geoscience Australia Record 2006/05 is the public release of a confidential final report to the sponsors of the Predictive Mineral Discovery Cooperative Research Centre (*pmd*\*CRC) Y2 project. This record is available in digital format only, but was released as a printed document to the sponsors.

# Y2 project (*pmd*\*CRC): 3D geological models of the eastern Yilgarn Craton

# Executive Summary

## Introduction

*R.S. Blewett*

Ore deposits are focal points of large-scale energy and mass flux systems (Hronsky, 2004) and it is important to recognise the system even though the precise genetic links with mineralisation may be unclear. Spatial prediction depends on the architecture and dynamics of ore systems, and it is paramount to have a good knowledge of the complex processes at a variety of scales. Understanding of these processes at the province and sub-province scale will help first-order evaluation and ranking of one terrane over another.

The eastern Yilgarn Craton (EYC) is one of the most intensely mineralised areas of continental crust containing numerous world-class gold and nickel deposits. Within the Yilgarn, however, there are clearly province to sub-province scale geodynamic processes that were important in localising gold-rich mineral systems. Understanding the 4D evolution of the province and sub-provinces provides the starting point in which to constrain the P–T and geodynamic histories of the various terranes as well as the architecture of the gold systems.

## Project goals and deliverables

The Y2 project is a predictive mineral discovery Cooperative Research Centre (*pmd*\*CRC) collaborative project between Geoscience Australia (GA), the Geological Survey of Western Australia (GSWA) and the University of Western Australia (UWA). It also involved significant collaboration with the Australian National University's Research School of Earth Sciences (RSES), AngloGold Ashanti, Goldfields St Ives, WMC Resources, and Placer Dome Asia Pacific.

The principal goal of the Y2 project was to determine the 3D architecture and its evolution through time. The Y2 project title is "to build accepted 3D geological models of the EYC to enable prediction of where within the terrane the location of major gold deposits is likely to occur". It is envisaged that the new tools and new understanding developed by the Y2 project not only benefit the sponsors in their endeavours in the Yilgarn, but in a generic sense in other terranes of interest.

In order to achieve the project goal, six key deliverables were designed:

1. An integrated geological and geophysical 3D map (model) for three specific regions within the EYC. These regions were the Kalgoorlie-Ora Banda region, the Leonora-Laverton region, and the Norseman-Wiluna region, the first two being nested within the later model;
2. Interpreted seismic sections for the 2001 seismic recorded in the Leonora-Laverton region;
3. Tomographic model of the Kalgoorlie-Ora Banda region which links the region's velocity structure from the surface, through the base of the crust to the base of lithosphere with the integrated geological and geophysical 3D geological models;
4. Map of chalcophile elements across selected portions of the EYC;

5. Assessment of the utility of the new 3D data versus the 2D data at a regional scale, and;
6. Prospectivity analysis of the derived 3D models.

All deliverables (except the abandoned deliverable 6[1]) were completed on time and within budget. Deliverable 3 considered the greater Yilgarn Craton.

## *Project achievements*

The *pmd*\*CRC Y2 project operated for a little over three years, and in this time has more than met its goal and deliverables. This final report brings together a vast wealth of new knowledge, information and data, with all the source and derivative data, various presentations, papers, animations and posters etc.

At the start of the project the Y2 team was inexperienced in building 3D maps, and the early attempts were relatively crude and clumsy. Now, after more than three years of learning and testing, the project team has achieved an excellent result and methodology for building rigorous 3D maps.

The main achievement of the Y2 project has been the building of comprehensive 3D maps of Kalgoorlie-Kambalda and the Norseman-Wiluna region. The maps were built on a foundation of 2D solid geology maps from government agencies, universities and industry. These data were integrated with various geophysical data sets (seismic reflection, refraction, broadband recording, receiver function, gravity and magnetic data, plus various derivatives such as "worms"), geochemical data sets (e.g., from P624), and geochronological data sets (from AMIRA P624 and earlier projects as well as published data).

The result of this integration is a more-holistic understanding of the EYC from a five questions approach. This understanding is outlined both in the maps and associated data sets, as well as this final report. The Y2 project has had its principal impact on answering the architecture question (Q2). The project has contributed to the geodynamics (Q1), drivers and pathways (Q3), fluids and their sources/reservoirs (Q4), and metal transport and deposition (Q5) questions.

The report is structured around the six key deliverables. Chapter 1 sets the geological scene and defines the tectono-stratigraphic nomenclature used throughout. Chapter 2 describes the work flow process devised to build the 3D maps. Chapter 3 discusses the seismic reflection and wide-angle reflection data and interpretations. Chapter 4 incorporates the mapping of the lithosphere and its velocity structure by using broadband seismic recording (tomography) and receiver function data (velocity profiles). Chapter 5 concerns the mapping of the chalcophile elements. Chapter 6 assesses the utility of 3D as opposed to 2D methodology, and discusses the structural history. Chapter 7 is a brief outline of the prospectivity analysis conducted by the *pmd*\*CRC A1 project using Y2 project data. Chapter 8 is a synthesis chapter arranged by the five questions. Many of the new ideas and understanding built on the data and observations of the earlier chapters are developed. Chapter 9 has the project conclusions. Chapter 10 presents the scope of the next phase of the CRC as recommendations for future work. Extensive appendices follow each chapter, including all pertinent publications and deliverables. Acknowledgements as well as an outline of all data sources and intellectual property, and references complete the report.

---

[1] Deliverable six was abandoned following sponsors agreement at the December 2003 review.

## *Regional framework*

New subdivisions of the EYC have been proposed. In the main, these build on the ideas of AMIRA project P624. The Gindalbi Terrane has now been included as a domain within the Kurnalpi Terrane. The Kalgoorlie and Burtville Terranes lie west and east respectively. The terranes and domains are fault and/or unconformity bound, the bounding faults have been defined, and disparate names have been rationalised into fault systems. A summary of the stratigraphic evolution is included, along with a time-space chart of each domain/terrane from the publicly available data. These data provide the temporal framework for the 3D map.

The following subheadings describe the new findings in each of the five questions. Further details may be found throughout the report, appendices, and the 3D map.

## *Question 1: Geodynamics*

The broadband data provide a unique view of the crust and mantle lithosphere. The main conclusion concerns the interpretation of the fast S-wave velocity layer at 100-120 km in the lithosphere. The layer is likely to represent the residue from High-Ca granite magmatism which ceased around 2660 Ma that was delaminated from the base of the crust. The result of delamination was a thermal spike at the base of the thinned crust, resulting in crustal melting and the generation of the Low-Ca granite suite. These later granites are temporally associated with the late orogenic gold (Cassidy et al., 2002a). The passage of mantle plumes and the presence of subduction zone slabs appear to not be imaged.

The main contractional event across the EYC involved ~east-west shortening during $D_2$. An orogenic surge model has been proposed to account for the diachroneity of the $D_2$ deformation, Late Basins and the emplacement of the Mafic granites and termination of the High-Ca granites. Much of the architecture and large-scale faults were developed and active during this event. The orogenic surge model also accounts for the relationship where the Late Basins and granites cut earlier stages of $D_2$, are deposited/emplaced in an extensional regime during $D_2$, and yet are overprinted by $D_2$ contraction. The diachroneity of $D_2$ deformation and associated granites and basins may explain some of the age differences found across the EYC. The driving force of the upper-crustal surge was the imbrication of the mid crust from behind and below. This mid-crustal deformation likely drove fluids via newly developing pathways into a pre-prepared architecture. These metamorphic fluids and alteration would have reduced the strength of the active part of orogen, and maintained a high-strain focus at the toe of the foreland wedge. In this way, the generation and driving processes of fluids are linked in one geodynamic model. Early versions of the model were tested numerically and the results implied that the model is mechanically viable. Numerous analogues of have been discussed in support of the model. Alternative models of remnant ocean basins and strike-slip basins were found to be inapplicable to the EYC geodynamic setting.

## *Question 2: Architecture*

There are clear differences in the endowment of the various terranes of the EYC. A conclusion from the analysis of the receiver function data is that there are architectural differences in terms of the velocity structure (i.e., lithology) between the terranes. The Kalgoorlie Terrane is on average faster than the Australian average (to which the other terranes are similar), but has a significant velocity drop at around 10 km depth. The velocity anomaly under the Kalgoorlie Terrane has been interpreted as a function of greater volumes of Low-Ca granites, which are temporally associated with a major thermal change in granite type across the Yilgarn Craton at the same time as gold was deposited.

The Kurrawang Basin and Zuleika Fault region is known for significant gold deposits. New findings suggest that the basin is not a simple syncline, rather it comprises two synclines separated by a largely faulted anticline. The fault that divides the basin is a moderately west-dipping splay from the steep listric west-dipping Zuleika Fault. This interpretation differs from previous interpretations.

The Ida Fault, although largely unmineralised, is a fundamental boundary of the Yilgarn Craton. The tracing of this boundary beneath a younger thrust (Waroonga Fault System) suggests significant late-stage contraction following the relatively late-stage extensional movement on the Ida Fault. This observation has implications for geodynamics through the structural history and any late-stage gold mineral systems.

The Kalgoorlie Terrane's architecture is built on a 'Golden Corridor'. The unifying theme to this corridor is the relationship between the major faults and regional anticlinoria, with periodic undulations or perturbations resulting in elongate domes. The Golden Corridor stretches from Kambalda possibly to Plutonic, with locations under thin cover providing new opportunities for exploration (i.e, north of Wiluna).

The question of whether there are deep penetrating faults was considered from a modelling perspective (was it mechanically possible) and an interpretation of the data. The observation that world-class deposits occur near deep faults was being tested. Breaking the entire crust with a single fault plane under contraction is mechanically difficult to achieve, but is easier under extension. The process is facilitated by the presence of water/fluid. The seismic data suggest that the terrane bounding faults, and therefore the amalgamation of the terranes, was relatively thin-skinned and its subsequent deformation (post-'$D_2$') involved a thick-skinned component. It is likely that these through-going crustal penetrating faults developed late in the orogenic process (post-'$D_2$') and represent late-stage extensional collapse, probably assisted by (mineralising?) fluids.

## Question 4: Drivers and pathways

The question regarding fluid flow drivers and pathways was not answered specifically. The orogenic surge model was proposed to explain a number of tectono-thermal and temporal features of the orogen. The model predicts some degree of topography (which was numerically modelled) which may have driven fluids. The model also involves localised stress switching (through fault reactivation and inversion), which is an effective method for driving differing fluids or tapping different reservoirs. The model also accounts for the Mafic-type granites and Late Basins, both may have provided different fluids to the general orogenic/metamorphic fluid. The model implied that the whole crust was involved and that deformation in the mid crust (imbrication) may have driven fluids into a structurally pre-prepared architecture.

## Question 4: Fluids, their sources and reservoirs

The question of fluid sources and reservoirs was explored by considering the nature of the strong areas of reflectivity in the seismic data, and whether these regions represented alteration from fluid flow. Numerical modelling determined that there are regions of stagnant fluid in the viscous lower crust. The stagnant fluids were modelled between a downward flowing and upward flowing system. Implied mineral alteration (reflectivity) will be asymmetric in the sense that it will be different on the upper and lower surfaces of the layers. Future seismic imaging may be able to distinguish between the symmetric alteration patterns (bright spots in the upper crust) as opposed to asymmetric alteration (as bright spots in the lower crust).

Examination of the temporal and geometrical relationships of the strong reflectors (detachments) suggested that the low-angle shears (LASHs), which are developed high in the crust, were the (palaeo)brittle-ductile transition at their time of formation. This conclusion has important implications for fluid flow and a source or reservoir for mineralising fluids. The ability to track the history of the development of this surface in the crust through time has implications for the geodynamic evolution of the region. The cycles of deformation, uplift and erosion appear to be broadly tracked in the seismic data.

The 3D map of Kalgoorlie-Kambalda incorporated a published 2D isograd map, and built 3D surfaces from this. Despite a number of assumptions in the process, the following observations were made. Anomalous low metamorphic grade areas have been identified as regions of possible fluid down-flow zones, associated with the interaction between meteoric fluids and gold-rich fluids. Anomalous areas of higher metamorphic grade may correspond to zones rich in mafic granites/porphyries and the indicators of favourable regions for gold. The metamorphism overprints the $D_2$ architecture.

## Question 5: Metal deposition

One of the most compelling discoveries of the project was the relationship between domes and the location of large mineral deposits. There is an empirical relationship, both globally and in the EYC, between domes and mineralisation. The domes occur at three levels in the crust and are stacked and linked by breaching faults, resulting in an ever increasingly focussed fluid being channelled upwards.

The domes are best mapped by seismic reflection data, however 3D gravity inversions have also successfully mapped them regionally, allowing a rapid and inexpensive method for detecting them. Granites appear to be intimately involved in the domes. This has been long understood from simple 2D map patterns. The emplacement of granites and vein systems into dilational sites depends on their position with respect to the neutral surface of the regional folds. The underlying 'core' of the domes appears to comprise granite laccoliths (Mafic-type?). They have a flat base, probably co-developed with the sole thrust, and convex or domal upper surface. The upper surface is folded in harmony with the regional anticlinoria.

These domes are superimposed on the Golden Corridor, providing a highly efficient pathway and trap. Fluids are focussed upwards into the apices of the domes, which may act as a reservoir that is tapped on breaching by late faults. The pathways of the domes are shear zones and upper granite contacts, both being domed by a process of emplacement, cross folding, and/or thrust culmination development. The underlying granite core provides suitable heat and/or fluid, and the overlying Late Basins add a seal to the system (and fluids?).

## Future directions

The Y2 project team was instrumental in driving the next phase of the *pmd*\*CRC research in the Yilgarn. Future work is outlined in Chapter 10, which is the Y-New project plan.

A clear gap in the work of the Y2 and Y3 projects is one of scale. The Y2 project has been constructing 3D maps analogous to 1:250 000 scale and smaller (Norseman-Wiluna), and 1:100 000 scale (Kalgoorlie-Kambalda). No one would site a drill hole on the basis of a 1:100 000 scale geological map. Larger scale mapping would be conducted.

In contrast, the Y3 project has been spatially limited in their work, restricted to small areas of a few deposits. Taking these data and concepts up to the next scale (camp and district) is the next challenge.

The intermediate (between Y2 and Y3 scales) district scale understanding of both the architecture and fluid systems is needed for a more scale-independent integration of the targeting ability of the more detailed work and the conceptual framework of the regional work. The Y-New project will endeavour to achieve this and apply the learnings of Y2 outlined in this report.


## *Appendix i*

Presentation made at the Perth December 2004 project development team meeting outlining the Y2 project objectives (**Appendix i pdt 2004 Blewett deliverables.pdf**)

# Chapter 1: Geological Evolution of the eastern Yilgarn Craton (EYC), and terrane, domain and fault system nomenclature

*K.F. Cassidy*

Much of the information in the Geological Evolution section has been presented previously in the form of AMIRA reports and Geoscience Australia publications and presentations. This overview provides the framework for the various studies of the Y2 project.

## Introduction

Models for the crustal evolution of the Yilgarn Craton have changed in the last 25 years from generally autochthonous greenstone development on sialic crust (Gee et al., 1981, Groves and Batt, 1984) to allochthonous models that highlight the importance of accretionary tectonics (Myers, 1995), and for each model there are fundamental implications for the type of mineral system that will be developed. Recent models highlight the importance of mantle plumes and long-lived convergent margins for both gold and nickel (Barley et al. 1998, Cassidy and Champion, 2004).

Over the past ten years, extensive studies of the Yilgarn Craton through the AMIRA P437A (Barley et al., 2002), P482/M281 (Cassidy et al., 2002b) and P624 (Barley et al., 2003) projects, in conjunction with current projects within the *pmd*\*CRC, have resulted in a much better understanding of the tectonic evolution of the Yilgarn Craton, particularly the highly mineralised eastern Yilgarn. A number of regional studies have concentrated on the felsic rocks that make up the bulk of the Yilgarn Craton in order to provide key constraints on the evolution of the craton. The felsic rocks from across the Yilgarn represent 'crustal probes' that constrain the age and extent of basement terranes (imaged by the various seismic processes and outlined in Chapters 3 and 4). A collage of crustal fragments is revealed that implicates both autochthonous and allochthonous crustal development (Cassidy and Champion, 2004). The resulting crustal evolution of the Yilgarn places significant constraints on the development of various metallogenic associations that may provide some important implications for terrane selection.

## Evolutionary history of the Yilgarn Craton

The preserved Yilgarn Craton consists of meta-volcanic and -sedimentary rocks and granites that formed principally between ca. 3.05 and 2.6 Ga (Figure 1-1), with a minor older component (to >3.7 Ga). Voluminous granite intrusion between 2.76 and 2.62 Ga was coincident with Neoarchean orogeny resulting in amalgamation and assembly of several cratonic elements to form the present Yilgarn Craton. High-Ca and Mafic granites have a range of ages that overlaps closely with the age of supracrustal rocks, and commonly contain significant zircon inheritance with a range of ages generally <3.1 Ga. In the central and western part of the craton, High-Ca/Mafic granites have ages between 2.72 and 2.68 Ga, in contrast to a 2.675 and 2.655 Ga peak in the east. 2.655 Ga marks a distinct switch from High-Ca/Mafic to Low-Ca magmatism. Low-Ca granites, with ages between 2.655 and 2.63 Ga, occur across the craton. Syenitic granites have a restricted age range from 2.665 to 2.64 Ga, and are spatially restricted to the eastern Yilgarn.
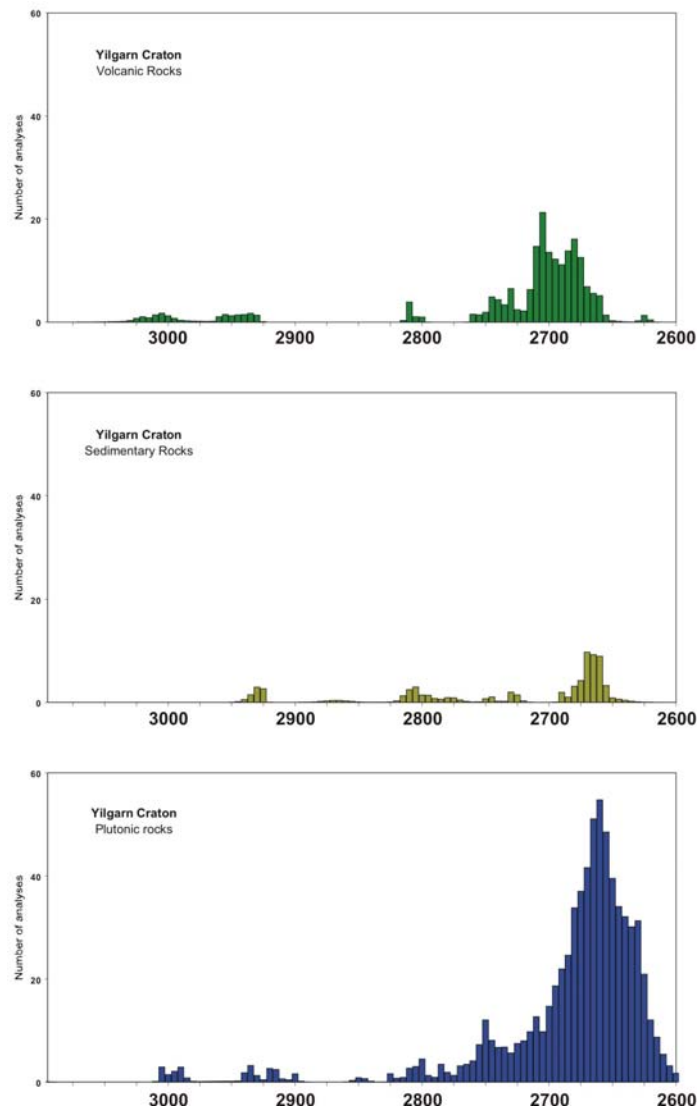
**Figure 1-1: Histogram of U-Pb zircon ages for volcanic, plutonic and sedimentary rocks of the Yilgarn Craton. Minor ages up to 3.7 Ga are excluded from this figure.**

## Crustal evolution model for the Yilgarn Craton

Previous subdivisions of the Yilgarn Craton have been on the basis of greenstone morphology (Gee et al., 1981) or fault-bounded tectono-stratigraphy (Myers, 1995; 1997; Barley et al., 2002; 2003). Incorporation of data from felsic magmatic rocks that form over 70 % of the craton provides additional key constraints on the evolution of the Yilgarn from the earliest forming events at >3.7 Ga to major plutonism between ~2.76 and 2.63 Ga (Cassidy et al., 2002b; Cassidy and Champion, 2004).

In conjunction with studies of supracrustal sequences (Swager, 1997; Krapež et al., 2000; Pidgeon and Hallberg, 2000; Barley et al., 2002; 2003), these data indicate that the main components of the craton are (Figure 1-2, Table 1-1):

- Narryer Terrane in the NW part of the craton, that comprises ~3.73-2.6 Ga high-grade gneiss, and supracrustal and granitic rocks; and host to metasedimentary rocks famous for their >4.4 Ga detrital zircons (Wilde et al., 2001).
- South West Terrane in the SW part of the craton that comprises >3.2-2.6 Ga high-grade gneiss, and supracrustal and granitic rocks.
- Youanmi Terrane comprising ~3.01-2.63 Ga greenstones and granitic rocks. It incorporates the Southern Cross and Murchison provinces of Gee et al. (1981), and

includes the Cue Domain that may constitute a separate terrane. It is named the 'Youanmi Terrane' after the Youanmi Fault, invoked by Myers (1995) as the bounding fault between his west Yilgarn superterrane and east Yilgarn superterrane.

- Kalgoorlie Terrane: series of >2.76-2.63 Ga granite-greenstone domains. This forms part of the Eastern Goldfields Province of Gee et al. (1981), and approximates the Kalgoorlie Terrane of Myers (1997). See also 'Terrane, Domain and Fault Nomenclature' section in this chapter.
- Kurnalpi Terrane: a complex series of ~2.95-2.63 Ga granite-greenstone domains. Forms part of the Eastern Goldfields Province of Gee et al. (1981), and incorporates the Gindalbie, Kurnalpi and Laverton Terranes of Myers (1995, 1997). See also 'Terrane, Domain and Fault Nomenclature' section in this chapter.
- Burtville Terrane: poorly defined ~2.95-2.63 Ga granite-greenstone domains. Forms part of the Eastern Goldfields Province of Gee et al. (1981), and incorporates the Duketon Terrane of Barley et al. (2002, 2003). See also 'Terrane, Domain and Fault Nomenclature' section in this chapter.

| Terrane | Crust Age | Greenstones | Komatiites | Granites/gneisses | Gold | Nickel | VHMS |
|---|---|---|---|---|---|---|---|
| | (Ga) | (Ga) | | (Ga) | (orogenic) | (komatiite) | |
| Narryer | 3.4–3.8 | ?3.73 | no | 3.73-3.6, ~3.48, 3.3 | no | no | no |
| | | (anorthosites) | | 3.0, ~2.75, 2.68–2.62 | | | |
| South West | 3.0–3.5 | ?3.2–3.0, | ? | ?3.2, ~2.8, | minor | no | no |
| | | ?2.8, 2.7 | | 2.68–2.62 | | | |
| Youanmi | 3.0–3.4 yes | 3.01–2.92, 2.81, | Al-depleted and | | 3.01–2.92, ~2.81, | | minor |
| | | 2.76–2.74 | Al-undepleted | 2.76–2.68, 2.66–2.62 | | | |
| *Cue Domain* | 2.9–3.0 | 3.01–2.92, 2.81, | Al-depleted | 3.01–2.92, ~2.81, | yes | no | yes |
| | | 2.76–2.74 | | 2.76–2.68, 2.66–2.62 | | | |
| Kalgoorlie | 2.8–3.05 | ?2.94, ?2.81, | Al-undepleted | ~2.81, ~2.76, | yes | yes | no |
| **(all Domains)** | | 2.74–2.66 | > Al-depleted | 2.69–2.68, 2.67–2.63 | | | |
| Kurnalpi | | | | | | | |
| *'young' Domains* | 2.8–2.9 | 2.71–2.68 | ? (Bulong) | ~2.7, 2.68–2.66, | minor | no | minor |
| **(Gindalbie, Murrin, Menangina)** | | | | 2.65–2.63 | | | |
| *'old' Domains* | 2.9–3.1 | >2.8, 2.72–2.68 | yes | ~2.95, ~2.71, | yes | yes | no |
| **(Laverton, Edjudina, Linden)** | | | | 2.68–2.66, 2.65–2.63 | | | |
| Burtville | 2.8–>3.0 | 2.81, 2.77–2.66 | yes | ~2.95, ~2.8, ~2.77 | minor | ? | no |
| **(Duketon, Merolia, Yamarna)** | | | | 2.69–2.63 | | | |

**Table 1-1. Summary characteristics of crust, greenstones, granites and mineralisation for the various terranes of the Yilgarn Craton (modified from Cassidy and Champion, 2004).**

The terranes and domains of the EYC are illustrated in Figure 1-3; see "Terrane, Domain and Fault Nomenclature" section in this chapter for further discussion on terrane and domain delineation and bounding fault systems. A space-time framework for the terranes and domains of the EYC is presented in Figure 1-4 (appended in Appendix 1-1). The framework clearly delineates variations in ages of volcanism and plutonism for the various terranes across the eastern Yilgarn with some domains containing significantly older greenstone assemblages and/or granite-gneiss.
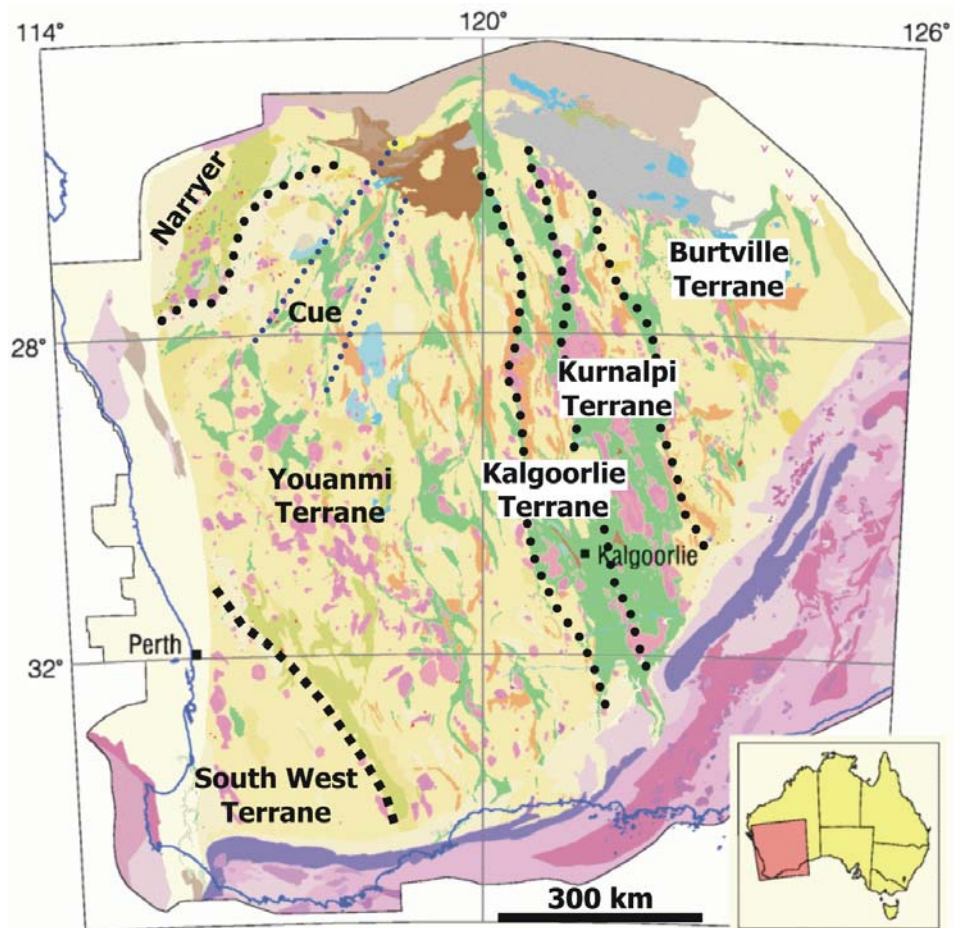


**Figure 1-2: Subdivision of the Yilgarn Craton based on Nd isotope and zircon crystallisation and inheritance data from felsic magmatic rocks, in conjunction with studies of the supracrustal sequences. (Modified from Cassidy and Champion, 2004).**

4
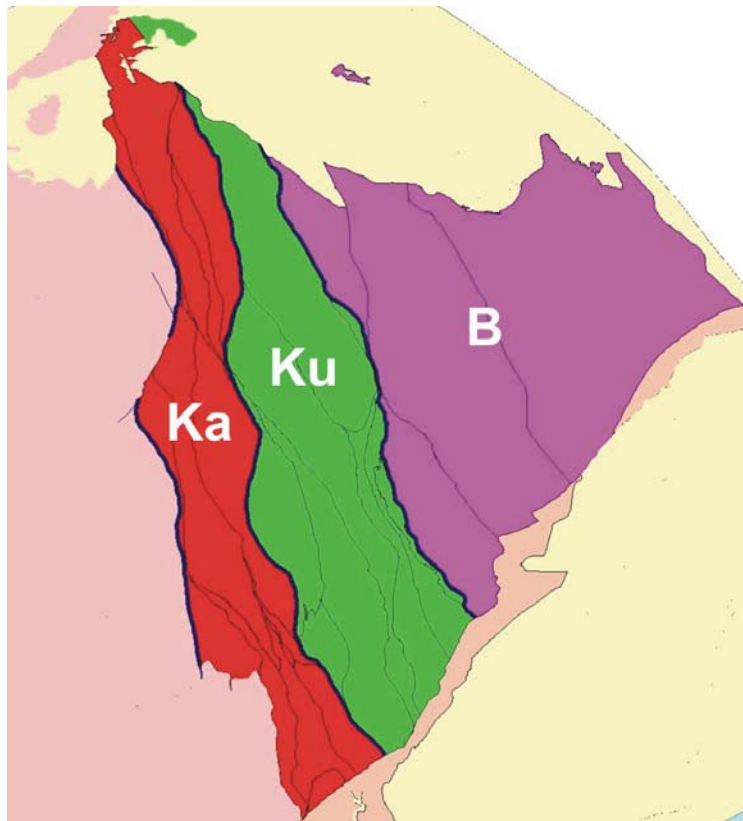
**Figure 1-3: Terranes of the EYC. Each terrane is divided into a number of domains outlined in black. Ka = Kalgoorlie, Ku = Kurnalpi, B = Burtville.**

## Nd isotope data and zircon inheritance patterns

On the basis that most of the granites have had interaction with older continental crust, Nd model ages and the age(s) of zircon inheritance can provide strong constraints on the make-up and evolution of the Yilgarn Craton. A map of the Nd isotopes (Figure 1-5) shows model ages for granites from across the Yilgarn Craton. In virtually all cases the Nd model age is significantly older than crystallisation age of the host granite and/or felsic volcanic rock, generally 200-300 My and sometimes over 500 My older.

There are a number of obvious divisions, with the central/western Yilgarn comprising relatively consistent block (?protocraton) of 3.3-3.1 Ga old crust, except for a belt of younger 3.0-2.95 Ga model ages in the north-west part of the terrane (Cassidy and Champion, 2004). The Nd 'map' also clearly highlights the distinct isotopic character of the northwestern Yilgarn with model ages generally older than 3.3 Ga; this approximates the Narryer Terrane.

A distinct 'break' that approximates the Ida Fault marks the possible eastern margin of the Youanmi Terrane. East of this is an isotopically complex region that can be divided into several poorly defined zones (the EYC and the region covered by the 3D crustal model of this project). Virtually all granites east of the Ida Fault have Nd model ages <3.1, and generally <2.95 Ga. The boundaries to these isotopic domains trend with the tectonic grain of the region, suggesting that differences are east to west. This has implications for the polarity and nature of the early extension (D$_E$) and the subdivision of the eastern Yilgarn (see Chapter 5).
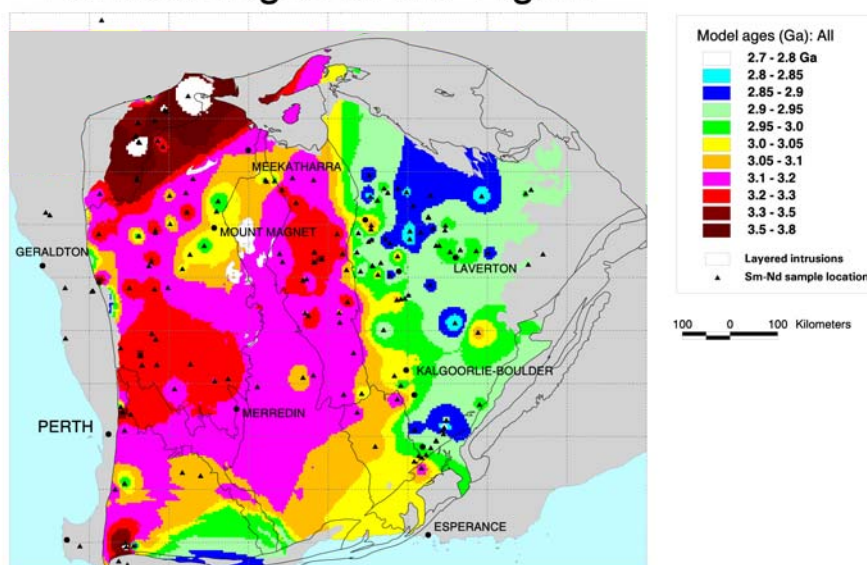
**Figure 1-5: Map of Nd model ages for plutonic rocks of the Yilgarn Craton.**

The zircon inheritance patterns for the EYC clearly show a strong similarity between the Youanmi and Kalgoorlie Terranes, with the Kurnalpi and Burtville Terranes in the EYC displaying a consistently different pattern (Figure 1-6). Of note, is a dominant 2.81 Ga population in the Youanmi and Kalgoorlie Terranes, with 2.81 Ga inheritance only found within 'old' domains in the Kurnalpi and Burtville Terranes. The other important populations are the 2.74-2.73 Ga zircons in granites and felsic volcanic rocks in the Kalgoorlie Terrane, a characteristic feature not present in the other eastern Yilgarn terranes (Cassidy and Champion, 2004).

The zircon inheritance data in combination with changes in felsic volcanism, and a subtle change in the age of High-Ca, Mafic and Low-Ca granites, are all consistent with the Kalgoorlie-Kurnalpi Terrane boundary marking a fundamental crustal 'break'. TTG-type dacite to rhyolite submarine volcanic and sedimentary rocks of the Kalgoorlie Sequence (incorporating the Black Flag Group) (Brown et al., 2001; Barley et al., 2002) represent a series of mainly submarine (back-) arc or intra-arc basins. In contrast, in terranes of the eastern Yilgarn, the main felsic volcanic associations are arc-rift-related bimodal basalt-rhyolite sequences and calc-alkaline arc-type sequences. The volcanism and deposition of the Kalgoorlie Sequence overlaps with emplacement of the High-Ca and Mafic granites in the Kalgoorlie Terrane, whereas in the terranes of the eastern Yilgarn, a major influx of High-Ca and Mafic granites postdate greenstone deposition.
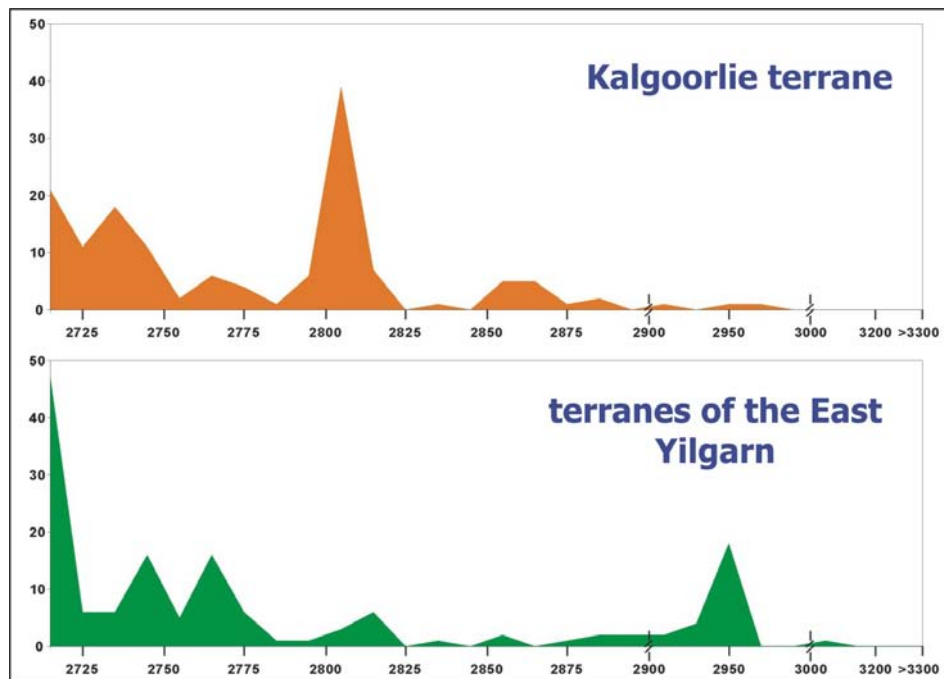
**Figure 1-6: Histogram of zircon inheritance ages for plutonic rocks of the EYC (modified from Cassidy and Champion, 2004).**

It is also interesting to note that the type of Proterozoic alkaline ultrabasic rock changes from dominantly kimberlites in the Kalgoorlie Terrane to lamprophyres and carbonatites in the Kurnalpi and Burtville Terranes. This change is consistent with a fundamental 'break' on the eastern side of the Kalgoorlie Terrane, which is mapped as the Ockerburry Fault.

The data indicate a complex history of crustal recycling throughout the Mesoarchaean and Neoarchaean. Autochthonous development for much of the granite-greenstone terranes in a continental environment is implicated. Voluminous granite intrusion, between 2.76 and 2.63 Ga, was coincident with Neoarchaean orogeny that resulted in the amalgamation and assembly of several cratonic elements to form the present Yilgarn Craton.

In the EYC, and perhaps for the whole craton, the preferred tectonic environment is a subduction setting, possibly a long-lived accretionary margin. The importance of interaction with pre-existing continental crust for the majority of granites in the Yilgarn Craton cannot be over emphasised. In fact, quartzofeldspathic gneisses contain rare xenocrystic zircons up to ~3.8 Ga, though typically younger than 3.1 Ga, consistent with involvement of old crust.

## Tectono-stratigraphic components of the eastern Yilgarn terranes

Incorporation of key results from the AMIRA P624 project (Barley et al., 2003) with new information resulting from the Y2 project has provided a much better understanding of the tectono-stratigraphy and evolution of the EYC. Important outcomes include:

1. The greenstone belts in the EYC contain at least three tectono-stratigraphic terranes, defined on the basis of distinctive volcanic facies and geochemistry, and age of volcanism that ranges from >2.81 to 2.66 Ga, and were tectonically juxtaposed after ~2.66 Ga (Barley et al., 2003). From southwest to northeast, these are the Kalgoorlie, Kurnalpi and Burtville Terranes (Figures 1-3 and 1-4). Each terrane contains a number of domains defined largely as fault-bounded geologically-contiguous blocks within terranes.

- Tholeiitic, komatiitic and calc-alkaline volcanic and sedimentary rocks that developed dominantly between ~2.72 and 2.66 Ga, form the bulk of the successions in the eastern Yilgarn, and generally young towards the west, such that the greenstone succession in the Kalgoorlie Terrane contains the youngest volcaniclastic units (Barley et al., 2002, 2003).
- The intensely mineralised Kalgoorlie Terrane is an amalgamation of young (<2.71 Ga) and old (>2.74 Ga) tectonostratigraphic associations. Enclaves or domains of older (>2.74 Ga) greenstone successions (Kambalda and Wiluna Domains, Leonora district in the Boorara Domain) are present in the Kalgoorlie Terrane (Barley et al., 2002). Further research is required on those older enclaves as to whether they represent autochthonous basement to the younger rock units.
- The <2.71 Ga greenstone successions in the southern Kalgoorlie Terrane are divided into the 2.71–2.69 Ga tholeiitic and komatiitic mafic-ultramafic (Kambalda Sequence) and 2.69–2.66 Ga felsic volcaniclastic (Kalgoorlie Sequence) sequences (Barley et al., 2002, 2003). The Kalgoorlie Terrane includes similar greenstone successions in the Boorara and Yandal Domains.
- The Kalgoorlie Sequence (incorporating the Black Flag Group) is a TTG volcaniclastic association restricted to the Kalgoorlie Terrane and was deposited in an extensional, deep-marine, strike-slip intra-arc basin, between 2.69 and 2.66 Ga. Several depositional and magmatic sequences in the Kalgoorlie Sequence can be grouped into unconformity-bounded tectonic stages that record uplift-subsidence cycles related to transtensional strike-slip tectonics (Barley et al., 2003).
- The Kurnalpi Terrane includes 2.715–2.705 Ga mafic volcanic rocks, intermediate calc-alkaline complexes, feldspathic sedimentary rocks, and mafic intrusive rocks and 2.695–2.675 Ga bimodal HFSE-enriched rhyolite-basalt and intermediate-felsic calc-alkaline complexes that extend along a linear belt (principally in the Gindalbie Domain) at the eastern edge of the Kalgoorlie Terrane. The 2.71– 2.715 Ga andesite-derived volcaniclastic rocks, and fine-grained sandstone-shale units ("BIF") in the eastern part of Kurnalpi are separated out as the Edjudina Domain (Barley et al., 2002). The Bulong Domain at the southern part of the Kurnalpi Terrane comprises lithologies from the Kurnalpi and Kalgoorlie Terranes that are inferred to have been tectonically interleaved along a complex terrane boundary.
- Geochemistry indicates distinct petrogenesis in 2.715-2.66 Ga felsic rocks in the Kalgoorlie and Kurnalpi Terranes, which now form adjacent parallel terranes. Rocks of the ~2.72–2.68 Ga Edjudina, Murrin and Menangina Domains are interpreted as representing an arc basin, whereas geochemical similarity between intermediate rocks in these domains and the Gindalbie Domain, combined with the trends in age, εNdT and the distinct volcanic facies suggest that rocks of the Gindalbie Domain represents a rifting phase of the Kurnalpi Terrane (or similar) arc. In combination, distinct arc-related terranes formed over a ~60 My period, and are possibly related to the same convergent margin, but were probably not adjacent during volcanism (Barley et al., 2002; 2003).
- The ~2.81 Ga Laverton Domain includes <2808 Ma mafic and ultramafic volcanic rocks, BIF, fine-grained tuffaceous sediments, and possibly <2.87 Ga mafic and ultramafic volcanic rocks and BIF of the Dingo Range greenstone belt (Barley et al., 2003). With the Edjudina and Linden Domains may actually form three sub-domains, with the Laverton Domain assemblages possibly unconformity-bound not fault-bound and representing autochthonous basement to the younger rock units.
- The Duketon Domain in the Burtville Terrane includes ~2805 Ma intermediate and felsic volcanic rocks and associated mafic (± ultramafic) rocks in the central and eastern part of the Duketon greenstone belt as well as greenstone assemblages dominated by mafic and ultramafic volcanic and fine-grained sedimentary rocks east

of Laverton. The Merolia and Yamarna Domains contain poorly understood variably deformed and metamorphosed mafic and felsic volcanic and sedimentary sequences.

- SHRIMP U-Pb zircon data show three main peaks in age of the volcano-sedimentary sequences: 2.65-2.72, 2.81, and 2.95-3.05 Ga. Nd data suggest marginal arcs rather than purely oceanic arc systems, and recycling of crust (2.8 - >3.0 Ga) along a complex convergent margin, with the youngest crust represented by rocks of the Gindalbie Domain and some intermediate volcanic rocks from the Menangina and Murrin Domains of the Kurnalpi Terrane. Hf data suggest there were periods of addition of newly generated crust/lithosphere (+ve εHf) and that these episodes also reworked crust that originally formed at ~3.05 Ga or earlier (Barley et al., 2003). Overall, there is a dominance of continental margin signatures as well as evidence of magmatic recycling of older arc-related crust. The terranes were possibly part of same arc/back-arc system dismembered and then re-assembled by accretionary tectonics.

2. The history of granite magmatism, with the exception of the High-HFSE granites, is broadly similar across the EYC (Champion and Sheraton, 1997; Cassidy et al., 2002b; Champion and Cassidy, 2002). High-Ca, Mafic and High-HFSE granites correspond to specific volcanic associations in the greenstone belts in terms of timing as well as chemistry. Low-Ca and Syenitic granites have no extrusive equivalents preserved in the EYC.

- Most granite groups occur across the EYC, with High-HFSE and Syenitic granites the most localised, being largely, but not exclusively, concentrated within a NNW zone characterised by young Nd model ages that approximately corresponds to domains (Gindalbie, Menangina, Murrin) in the western part of the Kurnalpi Terranes. There is no obvious geographic localisation of geochemical subgroups within any of the granite groups (Champion and Cassidy, 2002).
- Most magmatism occurred between ~2.72 Ga and 2.63 Ga, with remnants of older (>2.74 Ga) granites and older inherited zircons most prevalent within the Kalgoorlie Terrane, and Laverton, Linden and Duketon Domains, consistent with the Sm-Nd isotopic data which clearly indicates extensive older crust must have been present (Cassidy and Champion, 2004).
- Although each granite/volcanic group was long-lived, there are distinct periods where particular groups are most common: 2.72 to 2.68 Ga was variably dominated by High-HFSE, high-Al TTG-type High-Ca and Mafic magmatism; 2.675 to 2.655 Ga was dominated by transitional TTG-type High-Ca, with lesser Mafic (sanukitoids) and Syenitic magmatism; post ~2.655 Ga was dominated by Low-Ca with lesser Syenitic and minor Mafic magmatism (Champion and Sheraton, 1997; Champion and Cassidy, 2002).
- High-HFSE (and associated Mafic) granites exhibit a broad decrease in ages from east to west (Cassidy et al., 2002a). A similar decrease is evident in the geochronological data for felsic and intermediate volcanism in the Kurnalpi Terrane.
- The period ~2.675–2.66 Ga is characterised by High-Ca and lesser Mafic and Syenitic magmatism across all the terranes within the EYC. High-Al TTG-type High-Ca and Mafic granites that are geochemically similar to TTG-related volcaniclastic rocks that are confined to the Kalgoorlie Sequence in the Kalgoorlie Terrane are present throughout the EYC, including intrusive dykes and plutons into older intermediate volcanic-dominated sequences in the Kurnalpi Terrane.
- The switch in granite style from High-Ca and Mafic granites to Low-Ca dominated magmatism at ~2.655 (-2.65 Ga) was preceded, and partly accompanied, by 'late' (2.66 to 2.65 Ga) High-Ca and Mafic magmatism (Champion and Cassidy, 2002; Blewett et al., 2004b). This appears to be confined to (certainly concentrated within), the Kalgoorlie Terrane, suggesting that this region was the main locus of magmatism

at this time. Many of these 'late' granites are transitional-TTG-type High-Ca and 'sanukitoid'-like Mafic granites, suggesting the switch in granite type from High-Ca/Mafic to Low-Ca granites subsequent to ~2.655 Ga accompanied availability of a metasomatised mantle source for the High-Ca/Mafic granites, at least in the Kalgoorlie Terrane, as well as a tectonic trigger to promote derivation of Low-Ca granites through melting of older granitoid material within the crust (see Chapter 8).

- High-Ca and Mafic granite groups are similar in all provinces indicating that similar overall processes were involved in the genesis of these granites. These granites, however, have distinct age profiles in each of the terranes, suggesting that these processes have recurred but at different times.

- The High-Ca, Low-Ca, and High-HFSE granites have a clear crustal component involved partly or solely within their genesis (Champion and Sheraton, 1997; Champion and Cassidy, 2002). Compilation of Nd model age data for these granites shows that the crust within the EYC becomes older both east and west of a NNW zone approximating the western part of the Kurnalpi Terrane and its northern extension. Also, there is a clear isotopic break between the Kalgoorlie Terrane and the Youanmi Terrane that must represent a major crustal break, i.e. the eastern Yilgarn crust represents younger crustal growth onto the pre-existing Youanmi 'proto-craton' (Cassidy and Champion, 2004).

- Favoured tectonic models indicate a variety of arc environments pre ~2.655 Ga that maintain a pre-existing continental crust component with or without various rifting regimes (Champion and Cassidy, 2002). Earlier (pre-2.655 Ga) changes in type of felsic magmatism are interpreted to represent variations within an overall subduction-related environment. It is speculated that the change at ~2.68 Ga, from high-Al TTG-type Mafic and bimodal/High-HFSE, to transitional TTG-type High-Ca-dominated, may relate to some form of terrane accretion at this time, particularly given that widespread magmatism within the Youanmi Terrane effectively ceased at this time (Cassidy et al., 2002b).

- The change at ~2.655 Ga to widespread, continued and voluminous Low-Ca dominated-magmatism indicates a distinct change in the thermal regime of the crust and a similar process occurring craton-wide for the first time. Low-Ca magmatism continued from 2.65 to ~2.63 Ga across the entire craton (see Chapter 8).

3. Late-Stage Sequences are younger coarse siliciclastic sequences (Late Basins) that unconformably overlie, or are in fault contact with, the volcano-sedimentary successions, transgress terrane boundaries and on the basis of SHRIMP dating of detrital zircons are interpreted to have been deposited <2.655 Ga (Krapež et al., 2000; Barley et al., 2003).
  - Two facies types are recorded in the Late-Stage Sequences: (i) turbidites, and (ii) fluvial deposits. SHRIMP detrital zircon studies suggest that the fluvial facies are older than turbidite facies (Krapež et al., 2000; Barley et al., 2002).

  - The Late-Stage Sequences are preserved in structural basins adjacent to major terrane and domain-boundary faults, and their preservation may reflect orogenic uplift. The basins indicate that regional orogeny pre- and post-dated their deposition at ~2.655 Ga (Blewett et al., 2004c). The sequences overlap the terranes, post-date D1 and $D_{2a}$ and were increasing in depth and length up to their abrupt deformation during ENE-WSW shortening [$D_{2b}$], and were followed by the emplacement of Low-Ca granites, syenites, lamprophyres and porphyries between ~2.65 and 2.63 Ga.

  - SHRIMP dating of detrital zircons indicate multiple older sources with ages of ~2.73, ~2.81, ~2.85, ~3.00 and less commonly >3.40 Ga, corresponding to ages of greenstones and granites, but some (~2.95–3.00, >3.40 Ga) have no recognised source in the EYC (Barley et al., 2002; 2003). Whole rock Nd and detrital zircon Hf data are consistent with a complicated history involving both mantle-derived magmatism and

recycling of older crust since ~3.1 Ga (Barley et al., 2003). With the exception of some zircons from the Kurrawang and Jones Creek conglomerates, the age and isotopic characteristics of these sources reflect major magmatic and crust-forming episodes in the eastern Yilgarn, accompanied by significant recycling of crust generated in the previous magmatic episodes.

4. The integrated geological and metallogenic framework developed for the granite-greenstone terranes provides the basis for a geodynamic model for the EYC and implications for the relationship between this evolution and the generation of gold mineral systems. A four-dimensional geodynamic reconstruction of the EYC indicates that continental "growth" occurred through combined magmatic-arc processes and Cordilleran-style terrane accretion (Barley et al., 2003). It is likely that exposed supracrustal belts of the eastern Yilgarn are the eroded remnants of (para-autochthonous) terranes that were accreted onto the eastern margin of a pre-existing continent.
- Volcanosedimentary sequences in the Kalgoorlie and Kurnalpi Terranes are structurally bound fragments of arc-related and marginal-basin crust that possibly lay along the same convergent margin, but not in their present relative positions. The terranes were tectonostratigraphically different, particularly with respect to volcanic petrogenesis. The terranes were severed from their parent geotectonic settings and amalgamated to produce an Eastern Goldfields superterrane, possibly during $D_1$ (Barley et al., 2003). Sequences in the Bulong Domain represent a tectonic melange caught up in the suture between the Kalgoorlie and Kurnalpi Terranes.
- The tectonostratigraphic terranes have a common post-D1 record of overlapping synorogenic basin formation linked to a tectonic environment that culminated in peak ENE-WSW shortening. Late-Stage Sequences are preserved in structural basins close to terrane- and domain-bounding faults (Barley et al., 2003). They are coeval with the early stages of compressive orogenic deformation and the emplacement of Low-Ca granites, syenites, lamprophyres and porphyries between ~2.655 and 2.63 Ga.
- Late-stage sequences in all terranes are deformed by continuing ENE-WSW-directed orogeny ($D_{2b}$) (Blewett et al., 2004b; 2004c), which is interpreted to result from thin-skinned thrusting (accretion) of the terranes onto the Yilgarn Craton, most likely along the Ida Fault System.
- Continued province-scale transpressive deformation fragmented the terranes into structural domains. A late-stage of differential uplift may relate to regional-scale extension, but not necessarily as a continuation of collisional and transpressive tectonics.
- Gold mineralisation is related to orogeny of the EYC and is not a single event with a single cause. Gold mineralisation occurred during D2-D4, coincident with crustal thickening, but also peak metamorphism, emplacement of lamprophyres, porphyries, syenites, and Low-Ca granites (thermal pulse). Understanding the uplift and thermal history between ~2.655 and 2.625 Ga are critical to predicting the location of gold mineralisation.

## *Space–Time evolution of the Yilgarn Craton*

A series of time slices to illustrate the space–time evolution of the Yilgarn Craton is presented to provide constraints for answering Q1 and Q2 of the 'Five Questions':
- What are the P-T and geodynamic histories (Q1)
- What is the architecture of the system (Q2)

### Pre-3.0 Ga time slice
The oldest supracrustal sequences in the Yilgarn Craton are poorly constrained with

evidence for pre-3.0 Ga sequences in the Narryer, South West and Youanmi Terranes based on Nd depleted-mantle model ages (TDM) and limited U-Pb geochronology providing maximum depositional ages of metasedimentary successions. Meta-sedimentary rocks and quartzites from these terranes have a complex provenance with a spectrum of ages up to 4.4 Ga (Wilde et al., 2001; Wyche et al., 2004). Quartzites at the base of the exposed successions in the Illaara and Maynard Hills greenstone belts (Youanmi Terrane) have maximum depositional ages of ca. 3130 Ma, with detrital zircons ranging up to 4.35 Ga. Quartzofeldspathic gneisses in the Youanmi, Kalgoorlie and Duketon Terranes contain xenocrystic zircons generally <3.1 Ga consistent with involvement of old crust. A similar situation emerges from detrital/xenocrystic zircons in the greenstone sequences, with the exception of the Kurnalpi and possibly Duketon Terranes that contain only rare pre-2.95 Ga zircons.

In the Narryer Terrane, granitic gneisses and mafic layered intrusions have crystallisation ages up to 3.73 Ga and Nd $T_{DM}$ ages up to 3.9 Ga (Nutman et al. 1993). There are no constraints on the tectonic setting, although the presence of the 3.73 Ga Manfred Complex, a layered complex of anorthosite, gabbro and ultramafic rocks, may imply the presence of an even older pre-existing (?cratonic) mass.

The emerging picture suggests that the 3.3-3.1 Ga Youanmi Terrane represents the main crustal nucleus of the Yilgarn Craton (Figure 1-7). Evidence for a pre-3.05 Ga origin for most of this region is based on Nd and Hf isotopic data and >3.05 Ga xenocrystic zircons indicating interaction with a significant 3.4-3.1 Ga felsic (?crustal) component (see also Griffin et al., 2004).
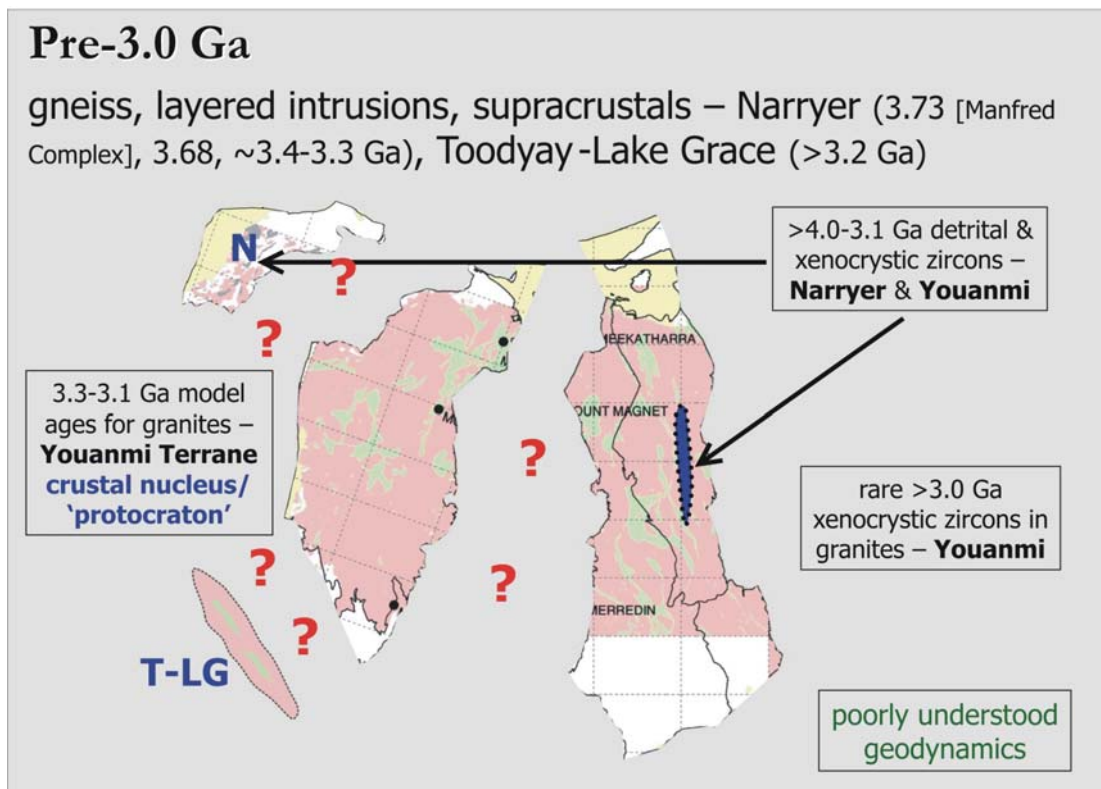


**Figure 1-7: Schematic outlining the key tectonic features of the pre ~3.0 Ga time slice for the Yilgarn Craton. (Modified from Cassidy and Champion, 2004).**

## 3.0 to 2.9 Ga time slice

The Youanmi Terrane contains abundant 3.01 - 2.93 Ga mafic-ultramafic volcanism and minor quartzites, felsic volcanism and sedimentary rocks (Figure 1-8). The Youanmi

Terrane may represent an amalgam of fragments that were assembled possibly during a ~3.0-2.95 Ga orogeny, and certainly prior to 2.81 Ga, although the tectonic environment pre-2.8 Ga is little understood.

It includes an isotopically distinct domain in the Mount Magnet-Meekatharra region. The 'Cue' Domain is characterised by ultramafic/mafic and felsic volcanic rocks and some granites that have Nd TDM ages that are essentially the same as their U-Pb zircon crystallisation ages. This is the only domain in the Yilgarn Craton with this characteristic and is best explained as representing juvenile crustal growth. Of note is that this region contains significant VHMS mineralisation, such as that at Golden Grove. It is not known whether the ~3.0-2.95 Ga 'Cue Domain represents a separate terrane, or the margin of older crustal blocks.

New U-Pb geochronology and Nd and Hf isotope data for supracrustal and granitic rocks in the Dingo Range and Duketon areas indicate a previously unrecognised 'older crustal' fragment in the EYC. On the basis of Nd isotope data, the 'old' domain forms an elongate belt subparallel to the younger belts, overlaps with the Laverton and Linden Domains in the Kurnalpi Terrane and the western part of the Duketon Domain (Burtville Terrane), and potentially allochthonous with respect to the surrounding eastern Yilgarn terranes. Further work is needed to determine the extent of the old belt and to further constrain its evolution.
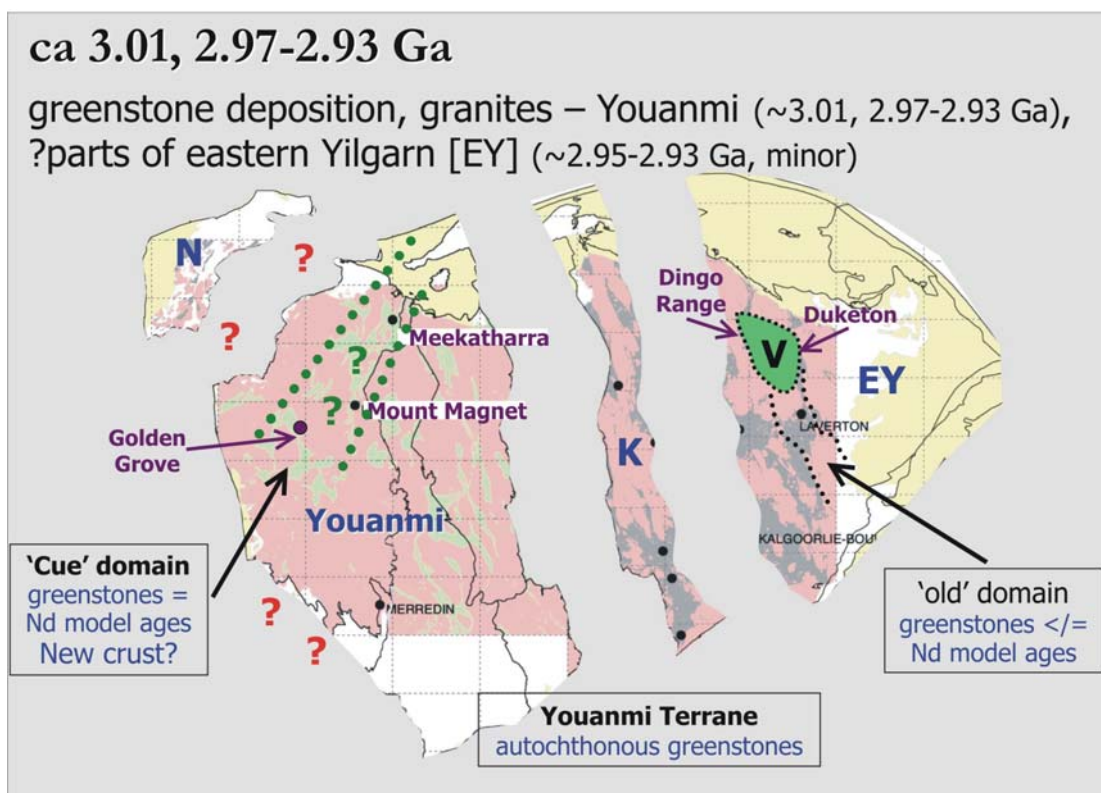


**Figure 1-8: Schematic outlining the key features of the ~3.01-2.93 Ga time slice for the Yilgarn Craton, including greenstone deposition and felsic magmatism in the western Youanmi Terrane and minor 'old' greenstones in the northeastern parts of the eastern Yilgarn [EY]. (Modified from Cassidy and Champion, 2004).**

## 2.81 Ga time slice

Along the eastern margin of the 'Cue' Domain are a series of layered mafic intrusions, including the large ~2.81 Ga Windimurra and Narndee intrusions (Figure 1-9). The Youanmi Terrane also contains minor ~2.81 Ga felsic volcanic rocks and granites principally in the region surrounding the mafic intrusions. The mafic intrusions and felsic

13

volcanism are consistent with some form of rift environment at ~2.81 Ga that is possibly plume-related, although the relationship of the ~2.81 Ga granites to this event is unknown. Modern drainages in the northern part of this region contain abundant ~2.81 Ga detrital zircons (Griffin et al., 2004) that were likely sourced from the felsic magmatism.

Minor 2.81 Ga granites also characterise the Kalgoorlie Terrane. Younger granites, felsic volcanic and metasedimentary rocks in both terranes also contain abundant zircon inheritance of this age. These data indicate that the Kalgoorlie Terrane has strong affinities with the Youanmi Terrane, at least at ~2.81 Ga, suggesting that it represents an exotic terrane, or perhaps a crustal block rifted off the Youanmi Terrane and re-accreted.
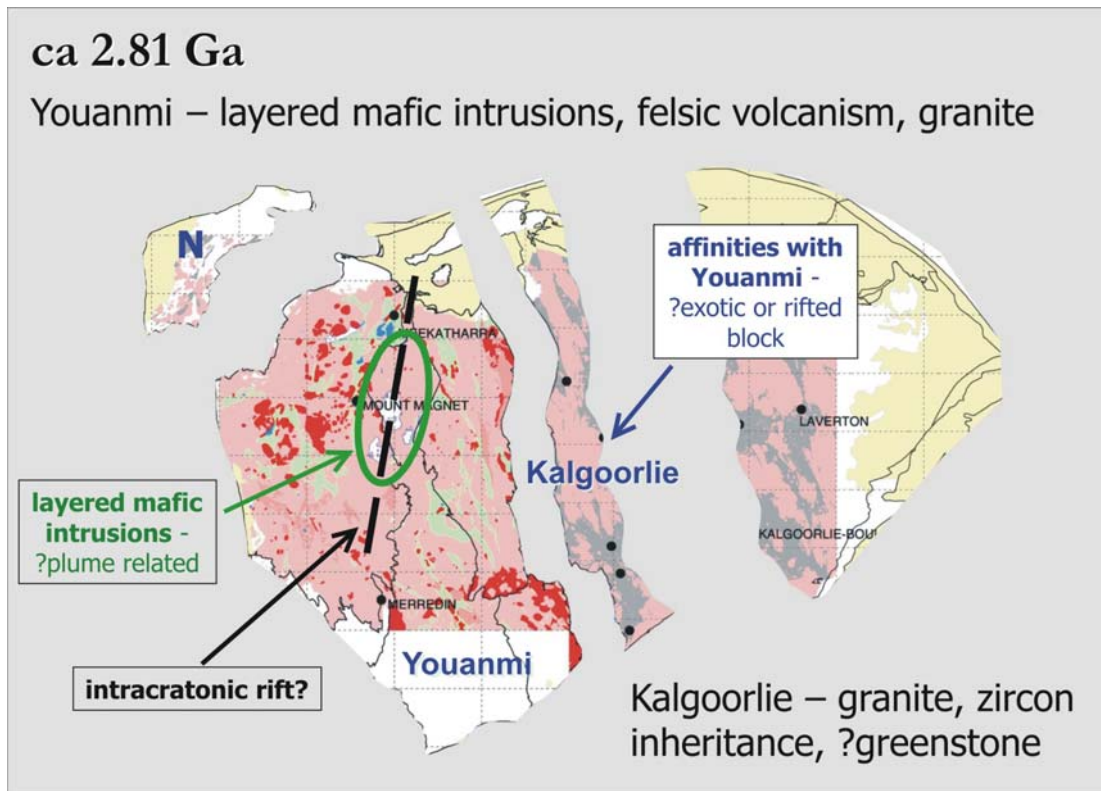


**Figure 1-9: Schematic outlining the key features of the ~2.81 Ga time slice for the Yilgarn Craton specifically possibly plume-related activity associated with layered mafic complexes and incipient rifting (modified from Cassidy and Champion, 2004).**

## 2.76 to 2.73 Ga time slice

There is significant felsic volcanism, (transitional- and) high-Al TTG-type granites and minor siliciclastic sedimentary rocks across the Youanmi Terrane that range from ~2.76 Ga in the northwest to 2.73 Ga in the southeast (Figure 1-10). 2.76-2.75 Ga sanukitoid granitoids are also present in the 'Cue' Domain. The sanukitoid granites indicate derivation from a metasomatised mantle source, perhaps previously metasomatised during juvenile (?arc) magmatism responsible for the ~2.95 Ga ultramafic, mafic and felsic volcanism in the 'Cue' Domain.

Post 2.8 Ga, the craton appears to be dominated by convergent tectonics. The Narryer and South West Terranes are thought to have accreted to the Youanmi Terrane post 2.8 Ga. Nutman et al. (1993) suggest that the 3.73-3.3 Ga Narryer Gneiss Complex forms part of an allochthonous terrane emplaced over the Youanmi Terrane at ~2.75 Ga. The 2.76-2.73 Ga felsic volcanism and high-Al TTG-type granites in the Youanmi Terrane and 'late' ~2.75 Ga granites in the Narryer Terrane may be related to such a collision.

There is also evidence for minor 2.74-2.73 Ga felsic volcanism, Hich-Ca and High-HFSE granites in the Kalgoorlie Terrane. High-HFSE granites, generally interpreted to be subvolcanic intrusions related to felsic volcanism, are present in the northern part of the Kalgoorlie Terrane. Other studies suggest a felsic volcanic succession underlying the dominant Kambalda-type mafic-ultramafic sequence, which is consistent with this concept. In addition, younger granites, felsic volcanic and metasedimentary rocks from the Kalgoorlie Terrane contain abundant 2.74-2.73 Ga inherited zircon, an inheritance age that is not represented in rocks from either the Kurnalpi or Burtville Terranes. This is consistent with the premise that the Kalgoorlie Terrane either represents an exotic terrane or perhaps a crustal block rifted off the Youanmi Terrane and re-accreted.
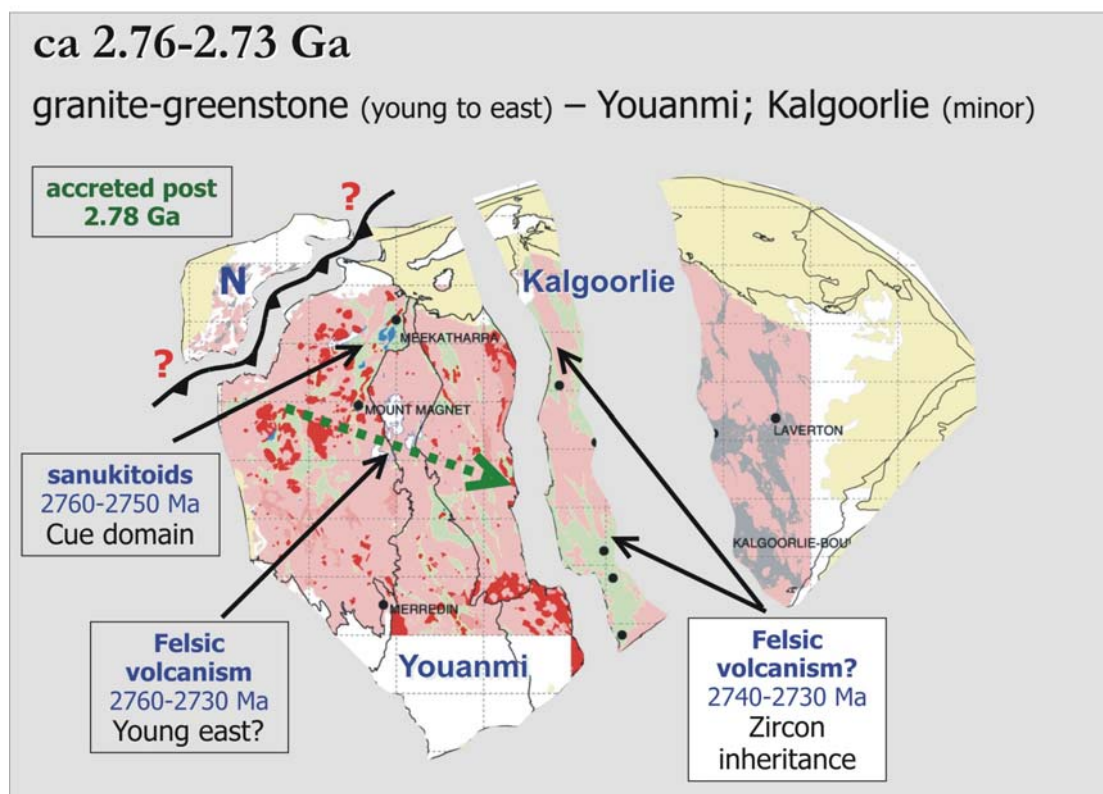


**Figure 1-10: Schematic outlining the key features of the ~2.76-2.73 Ga time slice for the Yilgarn Craton including east-younging felsic volcanism across the Youanmi Terrane and coeval sanukatoid magmatism in the Cue Domain. (Modified from Cassidy and Champion, 2004).**

## 2.72 – 2.68 Ga time slice

Abundant High-Ca (mainly high-Al- and transitional-TTG) and minor Mafic granites were emplaced from 2.72 to 2.68 Ga in the Youanmi Terrane (Figure 1-11). The origin of the abundant plutonism at this time is poorly understood.

This contrasts with the Kalgoorlie, Kurnalpi and Burtville Terranes where this time interval is characterised by abundant mafic-ultramafic, intermediate and felsic volcanism, and subordinate granites. The principal greenstone-forming event in the Kalgoorlie Terrane was the deposition of a 2.71-2.69 Ga submarine, plume-related mafic-ultramafic volcanic succession (Kambalda Sequence) as well as the initial stages of arc-related felsic volcanic rocks of the Kalgoorlie Sequence (the 2.69-2.68 Ga Spargoville assemblages: Krapež et al. 2000). Minor high-Al TTG-type High-Ca and rare Mafic granites intruded at this time, in contrast to the Youanmi Terrane. The abundant plutonism of the latter may reflect geodynamic processes outboard of the terrane.

In contrast, the Kurnalpi (and possibly Burtville Terrane) Terrane is characterised by calc-

alkaline intermediate volcanic sequences (2.72-2.695 Ga), overlain by mafic-ultramafic sequences (~2.7 Ga). Minor high-Al TTG-type High-Ca and Mafic granites were emplaced at 2.7-2.69 Ga. A series of rifted-arc sequences are also present terminating with abundant 2.69-2.68 Ga bimodal basalt-rhyolite sequences in the Gindalbie Domain on the western margin of the Kurnalpi Terrane. Subvolcanic High-HFSE intrusions mimic the ages of the bimodal sequences and provide good geochronological constraints on these sequences. Tectonic models for these sequences are poorly constrained, although the age of the rift-arc sequences progressively changes from ca. 2.72 Ga in the east to ca. 2.68 Ga at the western boundary, implying possibly eastward-dipping subduction at the margin of an older continental fragment (see discussion in Chapter 3).

The relationship between the Kalgoorlie and Kurnalpi Terranes is poorly understood, although contrasting volcanic associations, zircon inheritance patterns in granites and felsic volcanic rocks, and Nd TDM ages, suggests there may not have been a direct geotectonic link between them prior to ~2.68 Ga.
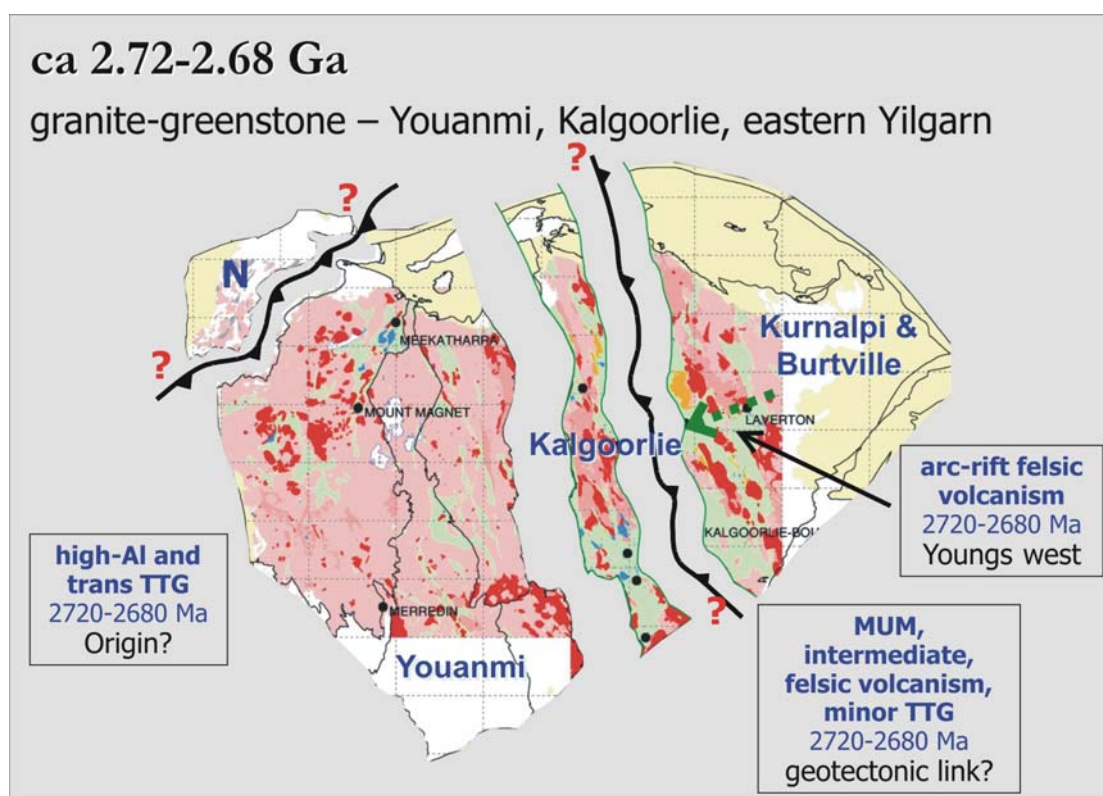


**Figure 1-11: Schematic outlining the key features of the ~2.72-2.68 Ga time slice for the Yilgarn Craton including west-younging arc/arc-rift felsic volcanism in the Kurnalpi Terrane, coeval mafic-ultramafic volcanism in Kalgoorlie Terrane, and high-Al- and transitional-TTG- type felsic magmatism in the Youanmi Terrane (modified from Cassidy and Champion, 2004).**

## 2.68 – 2.66 Ga time slice

The time period 2.68-2.66 Ga represents the dominant period for emplacement of abundant High-Ca (mainly transitional TTG-type) and a variety of Mafic granites, including sanukitoid-like plutons, in the Kalgoorlie, Kurnalpi and Burtville Terranes (Figure 1-12). Volcanism appears to have ceased in the Kurnalpi and Burtville Terranes, whereas the TTG-related felsic volcanic and sedimentary rocks of the Kalgoorlie Sequence were mainly deposited in submarine, possibly back-arc, basins in the Kalgoorlie Terrane (Barley et al., 2002). The geochemistry of these sequences is similar to that of the voluminous High-Ca and Mafic granites that intruded during the same time interval. It is interpreted that the Kalgoorlie, Kurnalpi and Burtville Terranes were in close proximity by this time,

although amalgamation may not have taken place until 2.66 Ga or later (Barley et al., 1998; 2003).

Felsic magmatism had virtually ceased elsewhere in the Yilgarn, with the exception of rare High-Ca (transitional TTG-type) granites in the Youanmi, Narryer and South West Terranes.
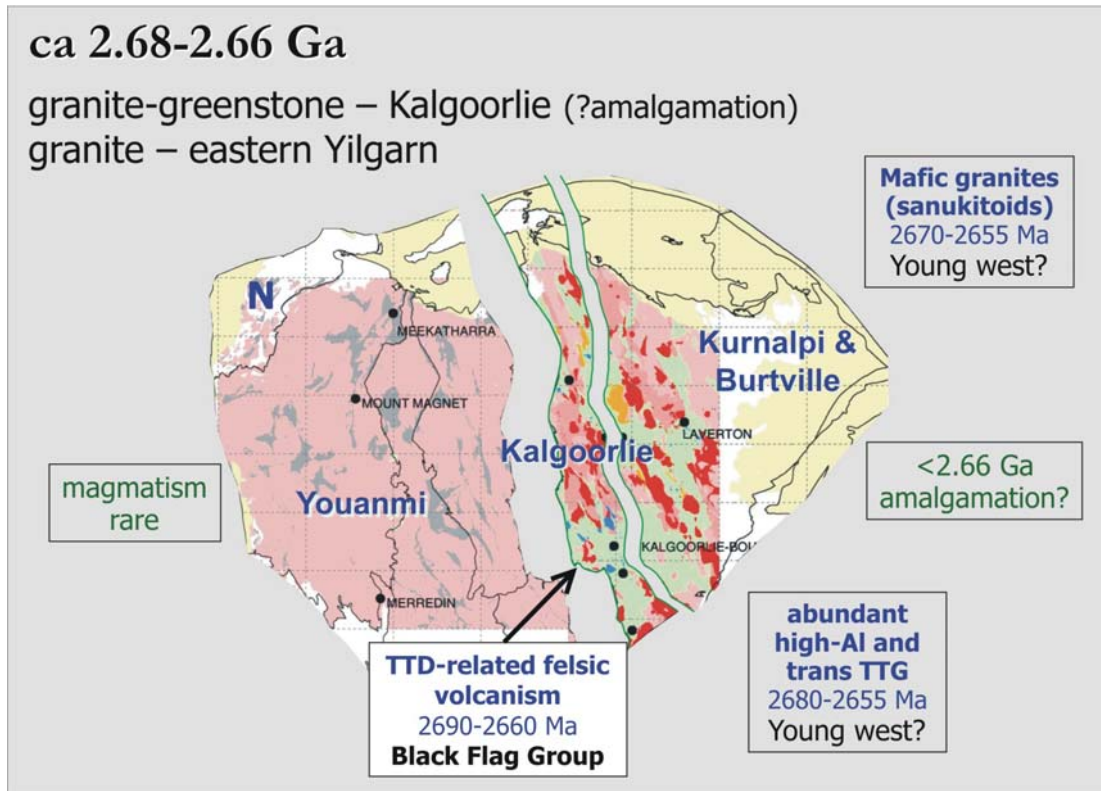


**Figure 1-12: Schematic outlining the key features of the ~2.68-2.66 Ga time slice for the Yilgarn Craton including abundant high-Al and transitional-TTG high-Ca granites (in red) across the eastern Yilgarn and TTG-related felsic volcanism in the Kalgoorlie Terrane. (Modified from Cassidy and Champion, 2004).**

## 2655 Ma time slice

The ~2655 Ma time slice marks a significant change in the evolution of the Yilgarn Craton, as it represents the switch from High-Ca and Mafic to Low-Ca magmatism. A number of High-Ca (transitional TTG-type) and Mafic (sanukitoid-like) granites were emplaced in the Kalgoorlie Terrane at this time (Figure 1-13) and mark the upper age constraint on orogeny in this terrane (Blewett et al., 2004c). At the same time, minor Low-Ca and Syenitic granites were emplaced in the Kurnalpi and Burtville Terranes. Many of these post-date at least one stage of regional folding indicating that orogeny had started prior to this time. The Kurnalpi and Burtville Terranes have a distinctive geohistory but must have been part of the Yilgarn Craton prior to the switch from High-Ca/Mafic to Low-Ca magmatism at ~2655 Ma.

From this time, abundant Low-Ca granites were emplaced across the craton, and are considered to mark the main interval of orogeny. Some researchers (Qiu and Groves, 1999) invoke a collisional orogeny and accompanying granulite-facies metamorphism in the southwest part of the Craton at this time.
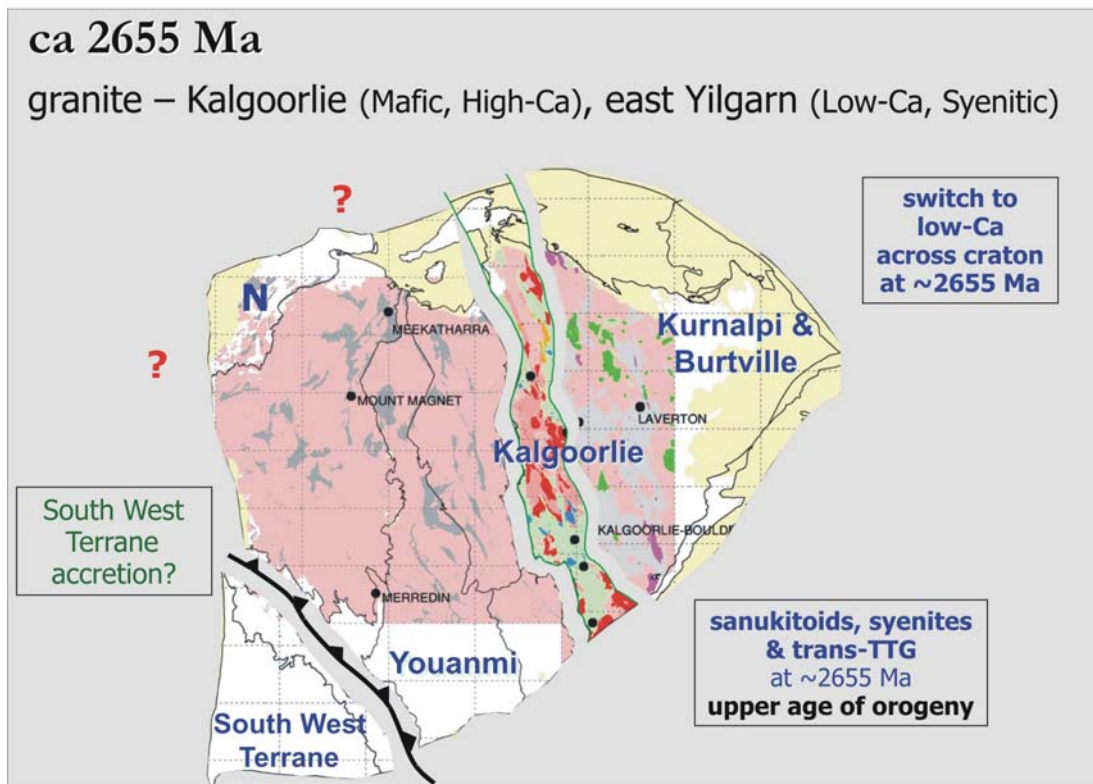
**Figure 1-13: Schematic outlining the key features of the ~2655 Ma time slice for the Yilgarn Craton that marks the switch from lower crustal- to upper mantle-derived High-Ca and Mafic granites (in red) to crustally-derived Low-Ca granites (in green) across the entire Yilgarn Craton. Note that High-Ca granites intruded only in the Kalgoorlie Terrane at this time. (Modified from Cassidy and Champion, 2004).**

## 2.65 – 2.63 time slice

From 2.65 to 2.63 Ga in the eastern Yilgarn and possibly as young as 2.6 Ga in the western Yilgarn, Low-Ca granites were emplaced across the Yilgarn Craton, including the Narryer and South West Terranes (Figure 1-14). This clearly indicates a shift in the thermal regime of the crust, with Low-Ca granites representing high-temperature, intracrustal melting of variably older felsic to intermediate crust. Minor Syenitic granites continued to be emplaced throughout the Kurnalpi Terrane during this time period.

As in the Superior Province, and other Archaean provinces world-wide, the development of a 'late-granite bloom' is the last magmatic event prior to 'cratonisation'. A craton-scale tectonic event is required to explain the Low-Ca magmatism. The Low-Ca magmatism may reflect a fundamental change in tectonics to extensional tectonics (?orogenic collapse), although some researchers suggest that lithospheric delamination best explains the observed geological and geophysical features (see discussion in Chapter 4 and Chapter 8).
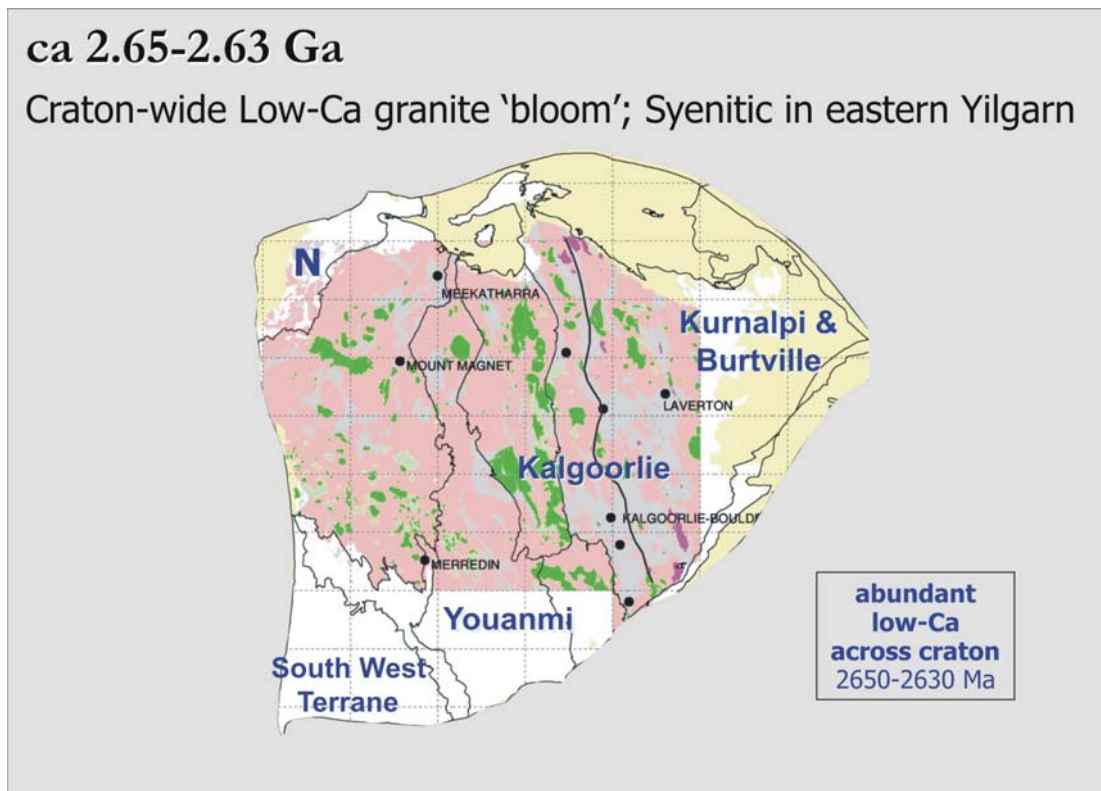
**Figure 1-14: Schematic outlining the key features of the ~2.65-2.63 Ga time slice for the Yilgarn Craton notably the intrusion of abundant crustal melt-derived Low-Ca granites (in green) across the entire Yilgarn Craton, and syenitic granites (in purple) restricted to the Kurnalpi and Burtville Terranes. (Modified from Cassidy and Champion, 2004).**

## *Terrane, domain and fault system nomenclature*

*D.C. Champion*

The terrane and domain nomenclature was first used for the eastern Yilgarn Craton (EYC) by the Geological Survey of Western Australia (GSWA). The GSWA defined terranes as being fault-bounded regions grouping rock packages with similar geological assemblages and histories, contrasting with other terranes with their own distinctive geology. Domains were defined largely as fault-bounded geologically-contiguous blocks within terranes.

Swager and Griffin (1990), Swager et al. (1992) and Swager (1994) subdivided the southern EYC into a number of terranes (e.g., Kalgoorlie, Gindalbie, Kurnalpi), and the terranes (especially Kalgoorlie) into domains. This subdivision was extended by the GSWA (e.g., Myers, 1995) to cover the whole of the EYC.

Subsequent work on terranes and domains was undertaken by the P437A and P624 AMIRA projects. This work resulted in largely minor modifications to the original GSWA terrane and domain definitions in the western half of the EYC, and more extensive refinement, and introduction of additional terranes and domains, for the eastern half.

Further refinement of the EYC terranes and domains, was undertaken by the Y2 project of the *pmd*\*CRC, as part of the geological-synthesis required to build the 3D map of the EYC. This refinement included recognition of new domains and terranes in the very easternmost part of the EYC, and rationalisation, including amalgamation, of some terranes in the western half.

The final process involved a meeting on the 5th of December, 2004 of key personnel from GSWA, and participants of the AMIRA P437A, AMIRA P624, and *pmd*\*CRC Y2 projects (essentially from Geoscience Australia (GA) and University of Western Australia (UWA)), to rationalise and agree on a standardised terrane and domain nomenclature for the EYC. The first half of this paper presents the new nomenclature adopted at this meeting.

A key facet of the 3D map construction was the establishment and building of the interconnected systems of faults required to separate each terrane and domain. The resultant 'fault systems' were each given their own nomenclature, e.g., Hootanui Fault System (the fault system forming the eastern boundary of the Kurnalpi Terrane). This procedure was undertaken to simplify the nomenclature for the region and to simplify discussion and reporting of features and results of the 3D map. The second section of this report details the individual fault systems, both graphical (2D and 3D) and textual. In particular, the component faults/shears of each system are given, using GSWA-standardised fault/shear nomenclature as shown on GSWA and GA-GSWA solid geology maps.

## Terranes and domains in the EYC
### Kalgoorlie Terrane

| Terrane | West margin | East margin | Comments |
|---|---|---|---|
| **Kalgoorlie** (Figure 1-15) | Ida FS Wahroonga FS (Figure 1-16) | Ockerburry FS (Figure 1-16) | Originally defined by Swager et al. (1992) and Swager and Griffin (1990), for southern part of EYC. Terrane boundary extended by Myers (1995) to cover the whole of EYC. Myers (1995) confined Kalgoorlie Terrane, in the north to being west of Perseverance Fault (Figure 1-16). Northern boundaries subsequently modified (moved to east) by P437A and P624 AMIRA projects. A number of domains were proposed for the southern Kalgoorlie Terrane by Swager et al. (1992), most of which are still current and largely follow the original boundaries as defined (though often extending further north). Exceptions include the abandonment of the Bullabulling Domain and the introduction of the Depot Domain (P437A, P624, *pmd*\*CRC Y2). Extension of the Kalgoorlie Terrane to the east of the Perseverance FS resulted in the addition of 3 domains (Wiluna, Moilers and Jundee). |
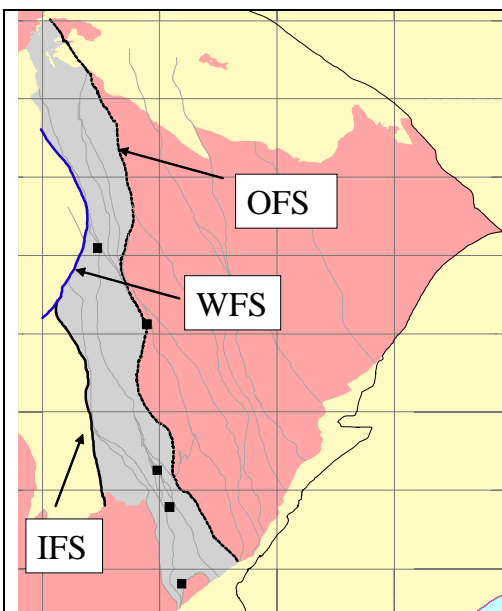


**Figure 1-15: Kalgoorlie Terrane with bounding fault systems. OFS = Ockerburry FS; WFS = Waroonga FS; IFS = Ida FS.**



Kalgoorlie Terrane Fault Systems

Faults from east to west:
Ockerburry FS
Mt McClure FS
Bardoc FS
Kunanalling FS
Ida FS
WaroongaFS

3X vertical exaggeration
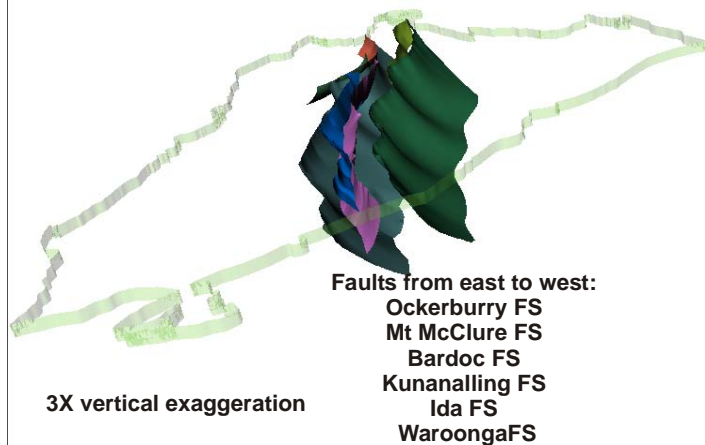
**Figure 1-16: 3D interpretation of the Fault Systems of the Kalgoorlie Terrane. View looking to the northwest.**

### Domains of the Kalgoorlie Terrane

| Domain | West margin | East margin | *Comments* |
|---|---|---|---|
| **Coolgardie** (Figure 1-17A) | Ida FS, Waroonga FS | Kunanalling FS | Largely as defined by Swager et al. (1992), although extended to the north, and newly defined Depot Domain excised. |
| **Depot** (Figure 1-17A) | Kunanalling FS | Zuleika Sh. | As defined by Y2, separated from the Coolgardie based on inferred significance of the Kunanalling FS. |
| **Ora Banda** (Figure 1-17A) | Waroonga FS, Zuleika Sh., Kunanalling FS | Bardoc FS | Largely as defined by Swager et al. (1992), although extended further to the north. |
| **Kambalda** (Figure 1-17B) | Bardoc FS | Lefroy FS | Largely as defined by Swager et al. (1992). |
| **Parker** (Figure 1-17B) | Lefroy FS, Boorara FS | Ockerburry FS | Largely as defined by Swager et al. (1992). |
| **Boorara** (Figure 1-17B) | Waroonga FS, Bardoc FS, Lefroy F | Perseverance FS, Ockerburry FS | Largely as defined by Swager et al. (1992), although extended further to the north. |
| **Wiluna** (Figure 1-17B) | Perseverance F | Koonoonooka FS | New domain, resulting from extension of Kalgoorlie Terrane, to the east of the Perseverance FS (P437A, P624). |
| **Moilers** (Figure 1-17B) | Koonoonooka FS | Mt McClure FS | New domain, resulting from extension of Kalgoorlie Terrane, to the east of the Perseverance FS (P437A, P624). |
| **Jundee** (Figure 1-17B) | Mt McClure FS | Ockerburry FS | New domain, resulting from extension of Kalgoorlie Terrane, to the east of the Perseverance FS (P437A, P624). |
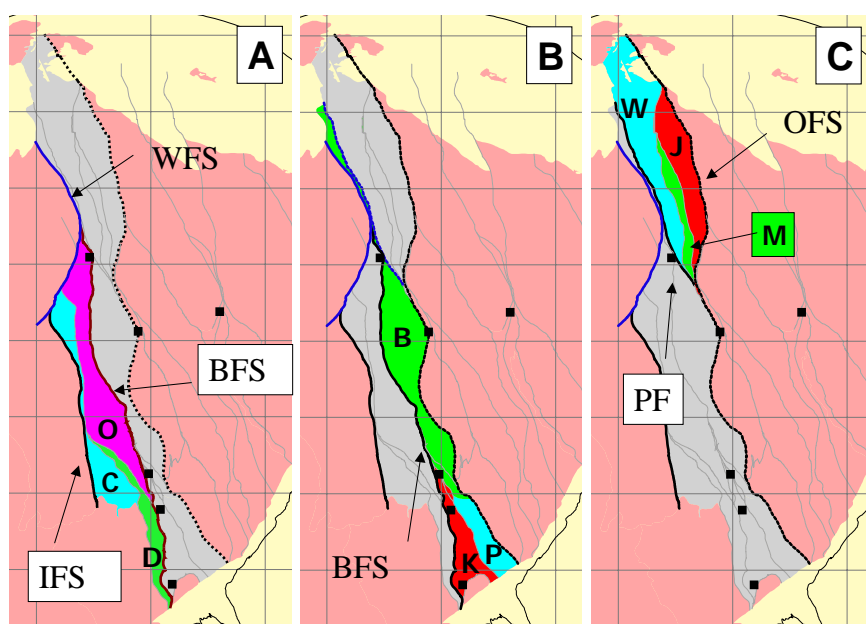


**Figure 1-17: Domains of the western (A), central (B) and eastern (C) parts of the Kalgoorlie Terrane, as follows: O = Ora Banda, D = Depot, C = Coolgardie, B = Boorara, P = Parker, K = Kambalda, W = Wiluna, J = Jundee, M = Moilers. Fault systems: IFS = Ida, BFS = Bardoc, WFS = Waroonga, PF = Perseverance, OFS = Ockerburry.**

**Kurnalpi Terrane**

| Terrane | West margin | East margin | *Comments* |
|---|---|---|---|
| **Kurnalpi** (Figure 1-18) | Ockerburry FS (Figure 1-19) | Hootanui FS (Figure 1-19) | Originally defined by Swager et al. (1992), Swager and Griffin (1990) and Swager (1994), for southern part of EYC. Terrane boundary extended by Myers (1995) to cover whole of EYC. Myers (1995) confined Kalgoorlie Terrane, in the north to being west of Perseverance Fault (Figure 1-2). Northern boundaries subsequently modified (moved to the east) by P437A and P624 AMIRA projects. <br><br> As originally defined, and as also defined by P437A and P624, the Kurnalpi Terrane was separate from the Gindalbie and Laverton Terranes. Following the nomenclature meeting between GSWA, UWA and GA, held at GSWA (Dec, 2004), the Kurnalpi Terrane has been expanded to include both the Gindalbie and Laverton Terranes (the latter having been downgraded to domain status). |
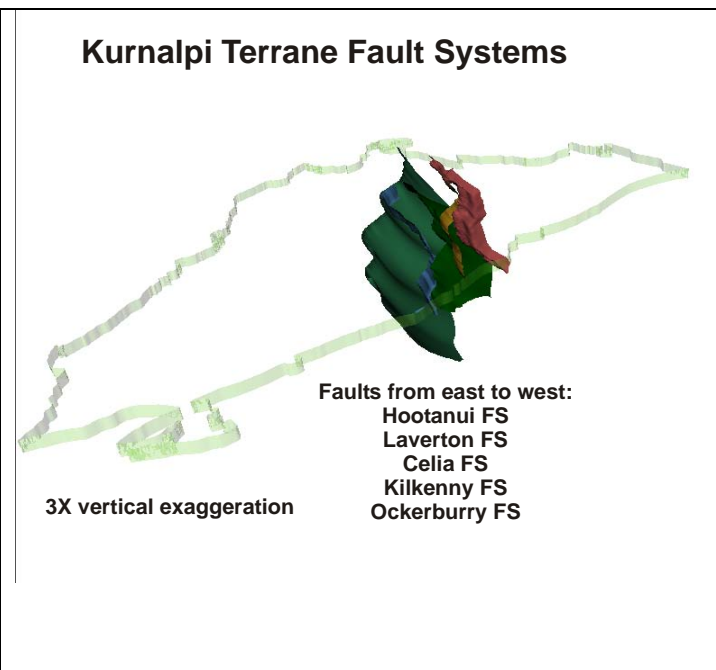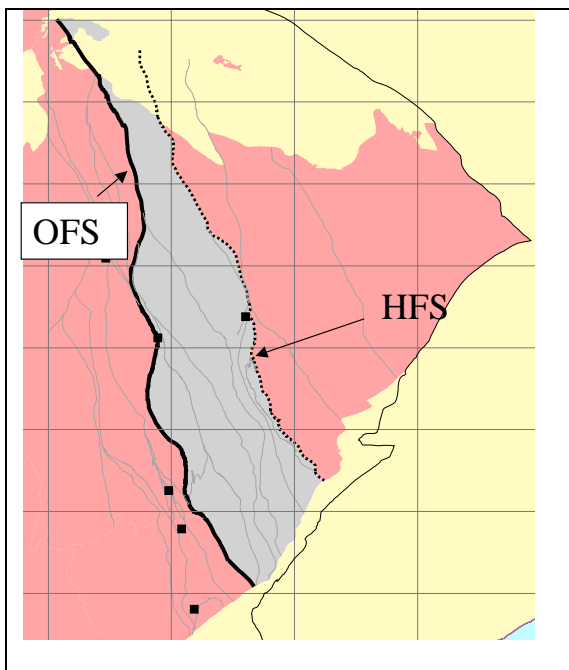


**Figure 1-18: Kurnalpi Terrane with bounding fault systems; OFS = Ockerburry FS, HFS = Hootanui FS.**



**Figure 1-19: 3D interpretation of the Fault Systems of the Kurnalpi Terrane. View looking to the northwest.**

## Domains of the Kurnalpi Terrane

| Domain | West margin | East margin | *Comments* |
|---|---|---|---|
| **Bulong** (Figure 1-20A) | Ockerburry FS | Emu FS | Originally part of Gindalbie Terrane, e.g., Swager (1994); but excised by the Y2 project because of its complex geology which appears to comprise parts of both the Kalgoorlie and Kurnalpi Terranes. The Bulong Domain has a complex faulted boundary with the Gindalbie Domain to the north. |
| **Gindalbie** (Figure 1-20A) | Ockerburry FS | Emu FS, Kilkenny FS | Largely as defined by GSWA, e.g., Swager, 1994, although now downgraded to domain status and minus the southern portion (now the Bulong Domain). |
| **Menangina** (Figure 1-20A) | Emu FS | Kilkenny FS | New domain subdivision of the Kurnalpi Terrane, introduced by the Y2 project. |
| **Murrin** (Figure 1-20A) | Kilkenny FS | Celia FS | New domain subdivision of the Kurnalpi Terrane, introduced by the Y2 project. |
| **Laverton** (Figure 1-20B) | Ockerburry FS Celia FS | Hootanui FS Laverton FS | Largely as defined by GSWA, e.g., Myers (1997), although eastern margin reduced by AMIRA P437A/P624 projects. Edjudina and Linden domains may actually form 3 sub-domains, possibly unconformity-bounded rather than fault-bounded. |
| **Edjudina** (Figure 1-20B) | Celia FS | Laverton FS | Largely as defined by early GSWA work, e.g., Swager (1994, 1997), although defined at terrane status. Later work, e.g., Myers (1997), expanded the Edjudina Terrane to include all the region to the east. This work follows the AMIRA P437A/P624 projects in restricting Edjudina to be a thin north-south domain within the Kurnalpi Terrane. |
| **Linden** (Figure 1-20B) | Laverton FS | Hootanui FS | Largely as defined by early GSWA work, e.g., Swager (1994, 1997), although following modifications of the AMIRA P437A, P624 projects. |
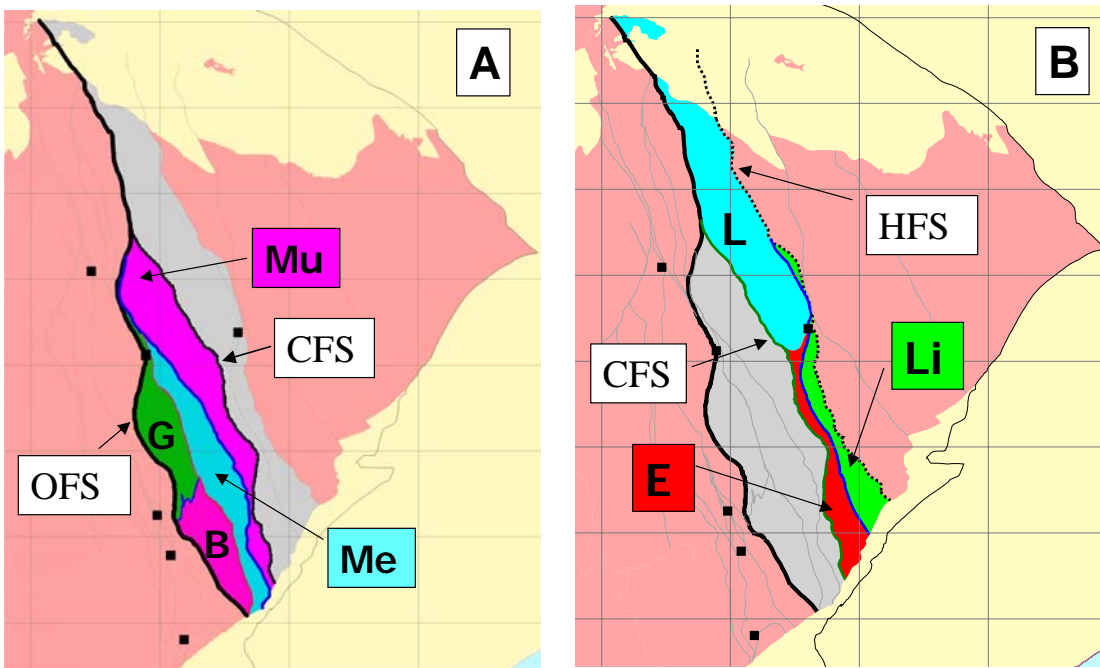
**Figure 1-20: Domains of the western (A), and eastern (B) parts of the Kurnalpi Terrane, as follows: G = Gindalbie, B = Bulong, Me = Menangina, Mu = Murrin, L = Laverton, Li = Linden, E = Edjudina. Fault systems: HFS = Hootanui, CFS = Celia, OFS = Ockerburry.**

## The Burtville Terrane

| Terrane | West margin | East margin | *Comments* |
|---------|-------------|-------------|------------|
| **Burtville** (Figures 1-21, 1-22) | Hootanui FS (Figure 1-22) | Edge of craton? (Figure 1-22) | Poorly understood region, in which, with the exception of the very westernmost part of the terrane, no terranes or domains have been described or defined. Based largely on seismic data, the Y2 project defined 3 terranes (Duketon, Merolia, Yamarna). As a result of the nomenclature meeting between GSWA, UWA and GA, held at GSWA (Dec, 2004), these have now been downgraded to domain status, and united to form the Burtville Terrane. |

**Burtville Terrane Fault Systems**

Faults from east to west:
Yamarna FS
Turnback FS
Hootanui FS

3X vertical exaggeration
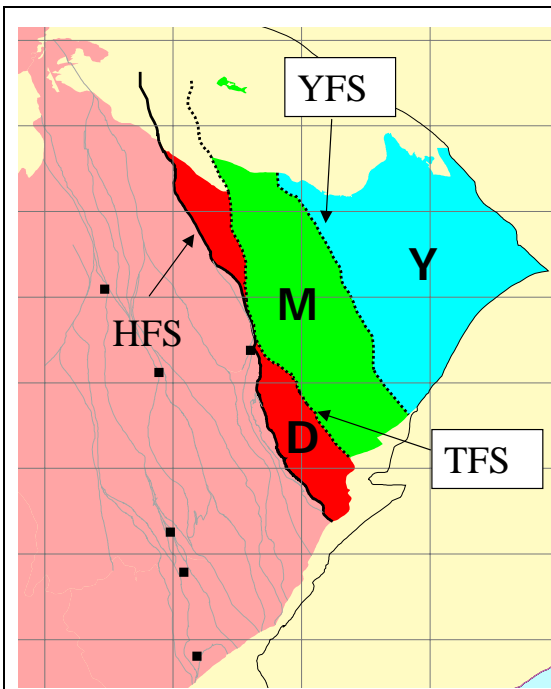
| **Figure 1-21:** Burtville Terrane with domains and bounding fault systems, as follows: D = Duketon, M = Merolia, Y = Yamarna. Faults Systems: HFS = Hootanui FS, TFS = Turnback FS, YFS = Yamarna FS. | **Figure 1-22:** 3D interpretation of the Fault Systems of the Burtville Terrane. View looking to the northwest. |
|---|---|
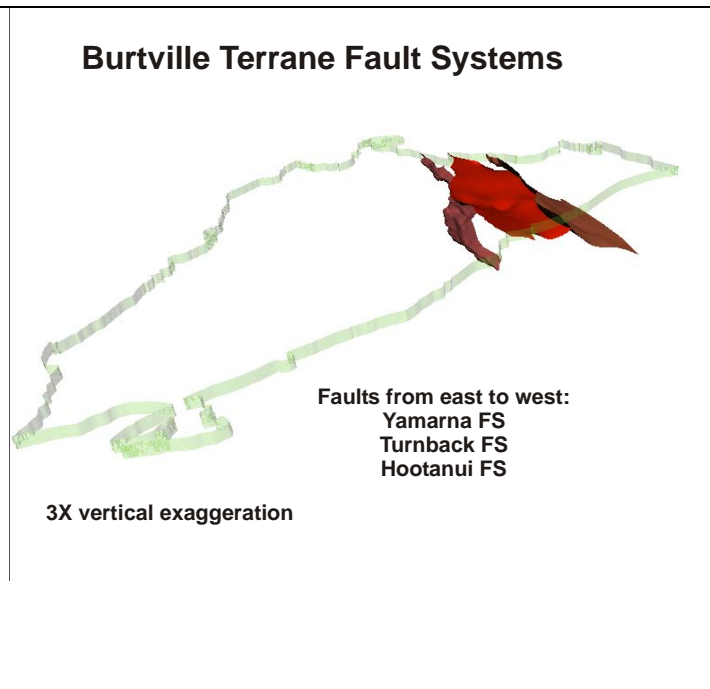
## Domains of the Burtville Terrane

| Domain | West margin | East margin | *Comments* |
|---|---|---|---|
| **Duketon** (Figure 1-21) | Hootanui FS (Figure 1-22) | Turnback FS (Figure 1-22) | Poorly understood, with little available geological information. Defined by the AMIRA P437A and P624 projects. |
| **Merolia** (Figure 1-21) | Turnback FS (Figure 1-22) | Yamarna FS (Figure 1-22) | Poorly understood, with little available geological information. Defined by the Y2 project. |
| **Yamarna** (Figure 1-21) | Yamarna FS (Figure 1-22) | Edge of craton? | Poorly understood, with little available geological information. Defined by the Y2 project. |

## Terrane fault systems and domain-bounding faults

**Yamarna Fault System**

**Eastern boundary of**: Merolia Domain, Burtville Terrane

**Western boundary of**: Yamarna Domain, Burtville Terrane

**Component faults** (north to south): Yamarna Fault (new name, Y2 project)

**Principal interpretation**: aeromagnetic data, seismic data

**Dip direction**: East

**3D interpretation of fault:** Figure 1-24.

**Plan view of faul**t: Figure 1-23.
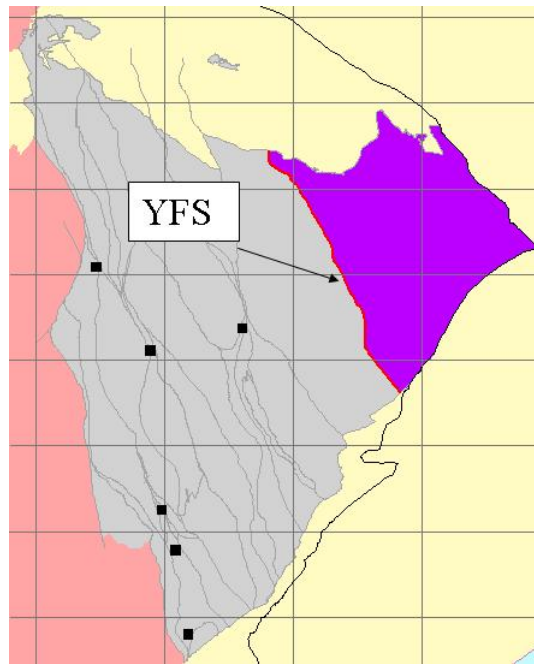


**Figure 1-23: Plan view of Yamarna Fault System (YFS), and Yamarna Domain (purple).**

# Burtville Terrane Fault Systems



Hootanui FS    Turnback FS    Yamarna FS
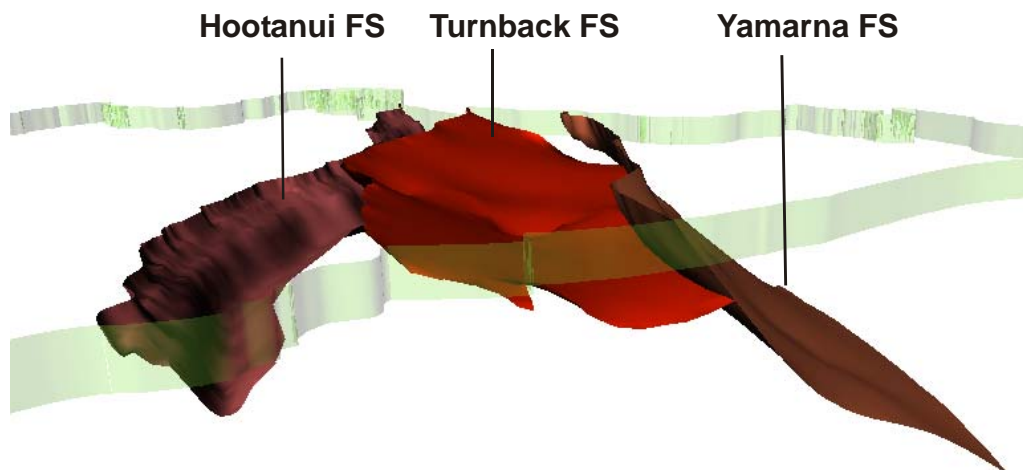
**3X vertical exaggeration**

**Figure 1-24: 3D interpretation of the terrane and domain bounding fault systems of the Burtville Terrane.**

## Turnback FS

**Eastern boundary of**: Merolia Domain, Burtville Terrane.

**Western boundary of**: Duketon Domain, Burtville Terrane.

**Component faults** (north to south):
Unnamed fault (Liu et al., 2001)
Hootanui Fault (Liu et al., 2001)
New fault (Y2 project).

**Principal interpretation**: aeromagnetic data, seismic data

**Dip direction**: East

**3D interpretation of fault:** Figure 1-24.

**Plan view of faul**t: Figure 1-25.
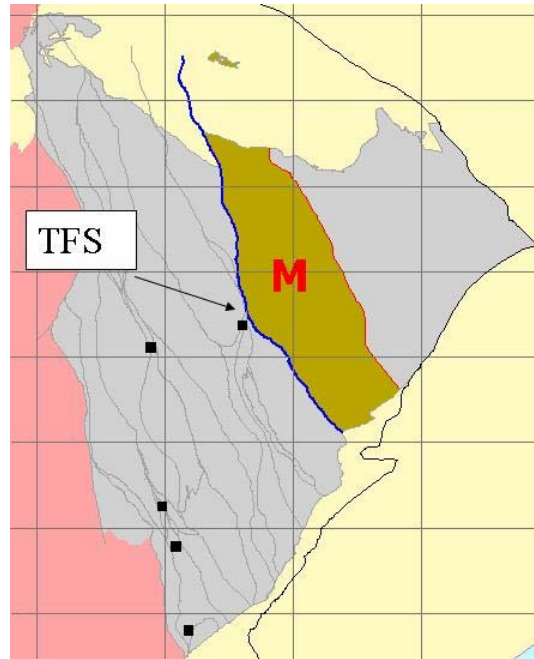


**Figure 1-25: Plan view of the Turnback Fault System (TFS), and Merolia Domain (M).**

## Hootanui FS

**Eastern boundary of**: Kurnalpi Terrane, and Laverton Domain, Kurnalpi Terrane

**Western boundary of**: Burtville Terrane, and Duketon Domain, Burtville Terrane

**Component faults** (north to south):
unnamed (Liu et al., 2001)
new (Y2 project)
central part of Hootanui Fault (Liu et al., 2001)
Laverton Fault (Liu et al., 2001)
Brumby Fault (Liu et al., 2001)

**Principal interpretation**: aeromagnetic data, seismic data

**Dip direction**: East

**Plan view of faul**t: Figure 1-26.

**3D interpretation of fault:** Figure 1-24 and Figure 1-27.
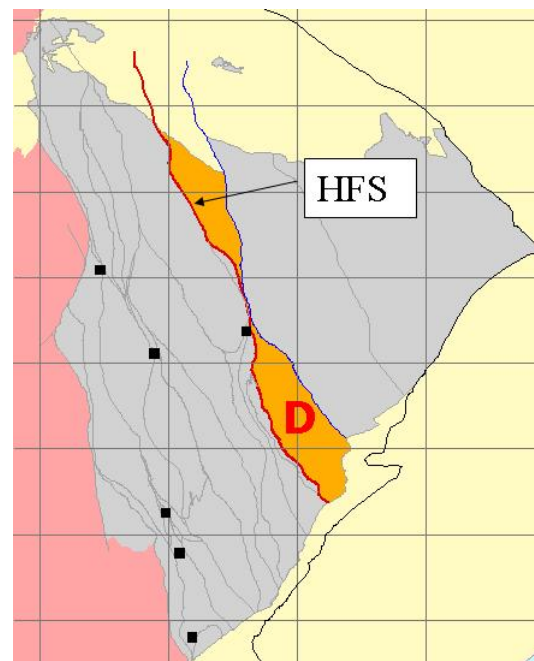


**Figure 1-26: Plan view of Hootanui Fault System (HFS), and Duketon Domain (D).**

**Kurnalpi Terrane Fault Systems**

Ockerburry FS    Emu FS    Kilkenny FS    Celia FS    Laverton FS    Hootanui FS

3X vertical exaggeration
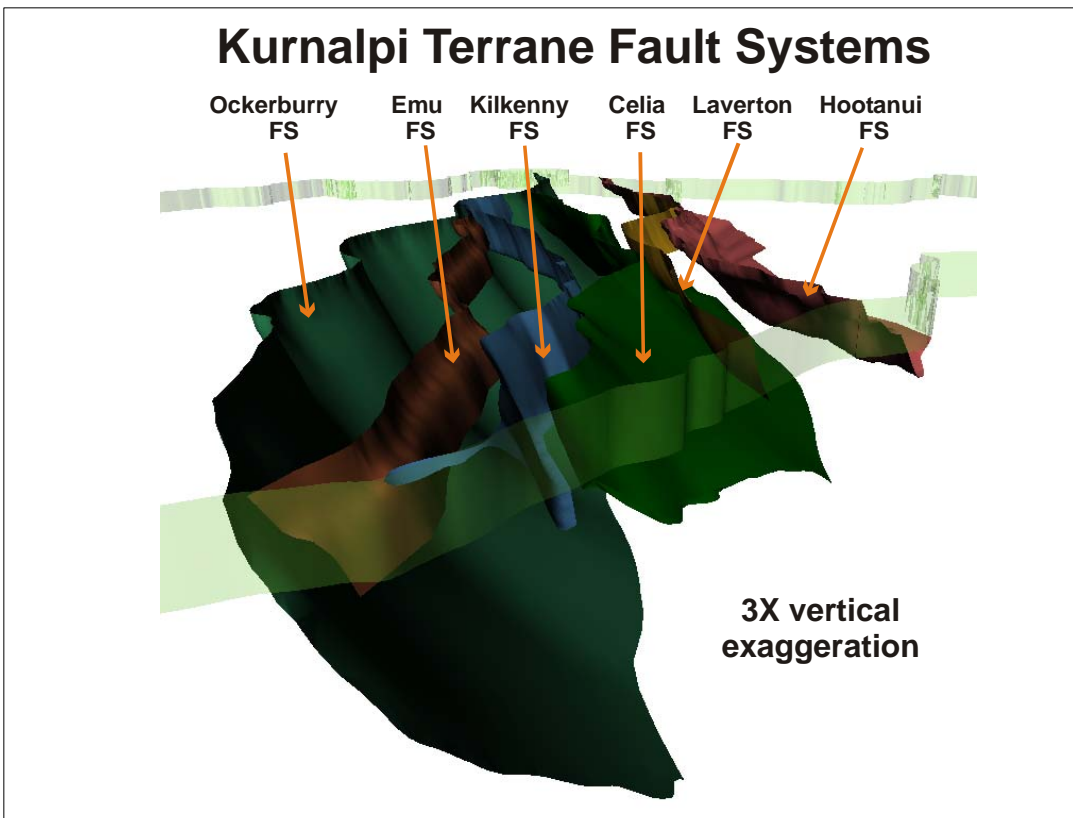
**Figure 1-27: 3D interpretation of the terrane- and domain-bounding fault systems of the Kurnalpi Terrane.**

## Celia Fault System

**Eastern boundary of**: Murrin Domain, Kurnalpi Terrane

**Western boundary of**: Laverton Domain, Kurnalpi Terrane

**Component faults** (north to south):
Ninnis Fault (Liu et al., 2001)
Claypan Fault (Swager, 1994)
Unnamed fault (Swager, 1994)
New fault (Y2 project)

**Principal interpretation**: aeromagnetic data, seismic data, previous geology

**Dip direction**: East

**3D interpretation of fault:** Figure 1-27.

**Plan view of fault**: Figure 1-28.



CFS

M
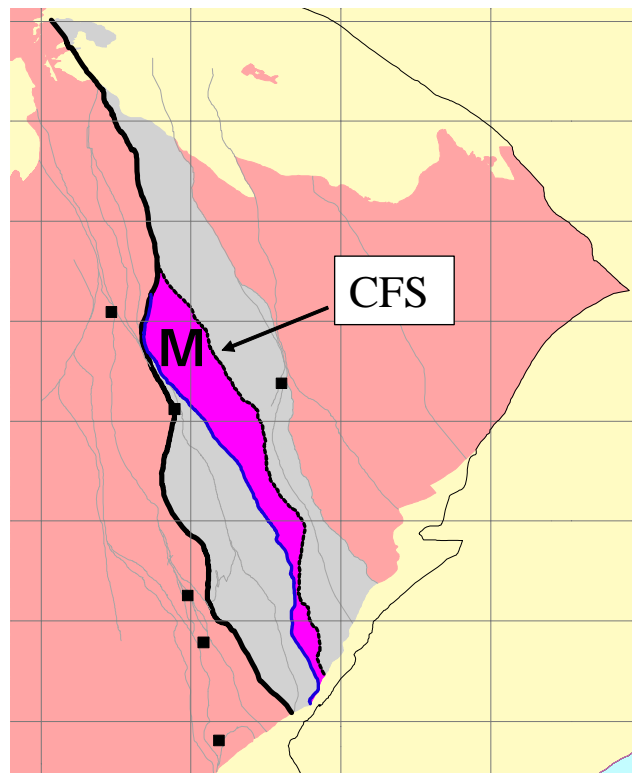
**Figure 1-28: Plan view of the Celia Fault System (CFS). Murrin Domain (M) in pink; Kurnalpi Terrane in grey.**

## Kilkenny Fault System

**Eastern boundary of**: Laverton Domain, Kurnalpi Terrane

**Western boundary of**: Murrin Domain, Kurnalpi Terrane

**Component faults** (north to south):
Kilkenny Fault (Liu et al., 2001)
Yilgangi Fault (Liu et al., 2001; Swager, 1994)
Unnamed fault (Swager, 1994)
New fault (Y2 project)

**Principal interpretation**: aeromagnetic data, seismic data, previous geology

**Dip direction**: East

**3D interpretation of fault:** Figure 1-27

**Plan view of fault**: Figure 1-29.
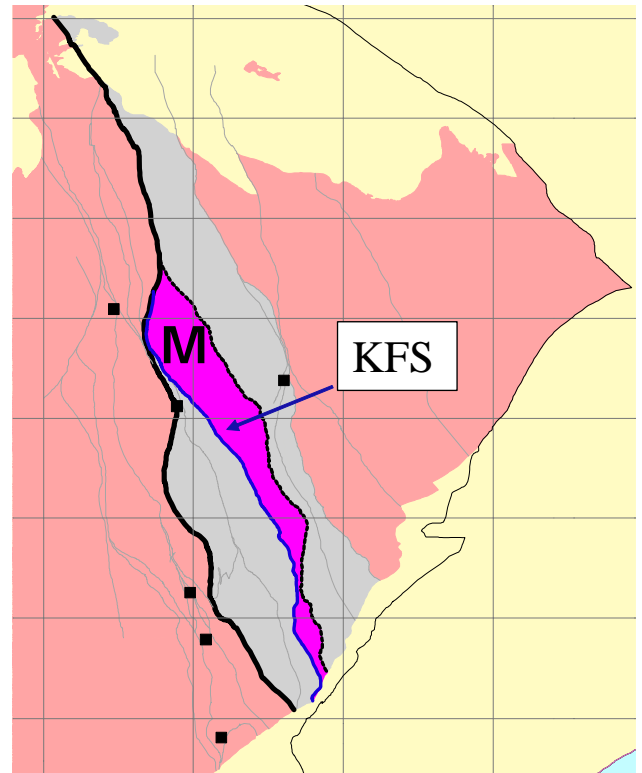


**Figure 1-29: Plan view of the Kilkenny Fault system (KFS). Murrin Domain (M) in pink; Kurnalpi Terrane in grey.**

## Emu Fault System

**Eastern boundary of**: Menangina Domain, Kurnalpi Terrane

**Western boundary of**: Gindalbie and Bulong Domains, Kurnalpi Terrane

**Component faults** (north to south):
Melita-Emu Fault (Liu et al., 2001)
Emu Fault (Swager, 1994)
Avoca Fault (Swager, 1994)
Cowarna Fault (Swager, 1994)
Unnamed Fault (Swager, 1994)
New fault (Y2 project)

**Principal interpretation**: aeromagnetic data, previous geology

**Dip direction**: West

**3D interpretation of fault:** Figure 1-27.

**Plan view of fault**: Figure 1-30
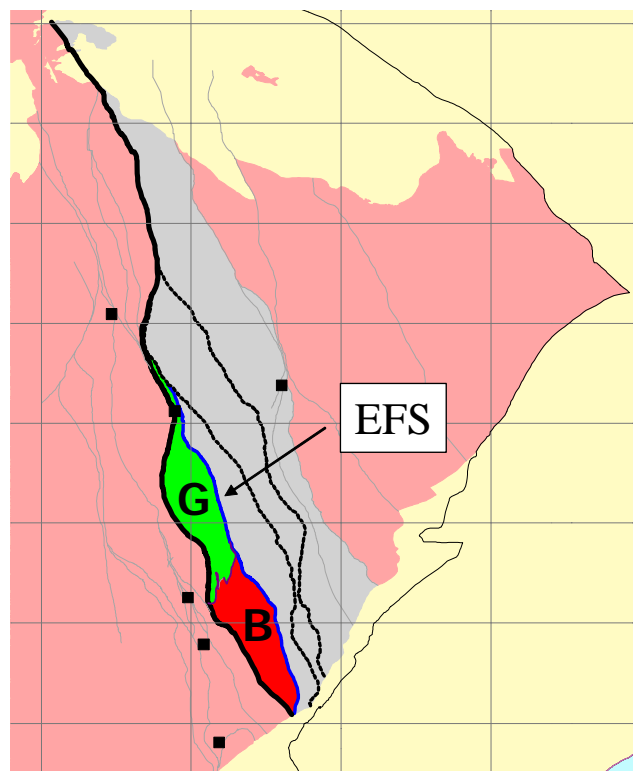


**Figure 1-30: Plan view of the Emu Fault System (EFS). Gindalbie Domain (G) in pink; Bulong Domain (B) in red; Kurnalpi Terrane in grey.**

## Ockerburry Fault System

**Eastern boundary of**: Kalgoorlie Terrane; Jundee Domain, Kalgoorlie Terrane; Boorara Domain, Kalgoorlie Terrane; Parker Domain, Kalgoorlie Terrane

**Western boundary of**: Kurnalpi Terrane; Bulong Domain, Kurnalpi Terrane; Gindalbie Domain, Kurnalpi Terrane; Murrin Domain, Kurnalpi Terrane; Laverton Domain, Kurnalpi Terrane

**Component faults** (north to south):
Ninnis (Liu et al., 2001)
Mount Grey Fault (Liu et al., 2001)
Ockerburry Fault Zone (Liu et al., 2001)
Mt George Shear Zone (Liu et al., 2001)
New fault (Y2 project)
Mt Monger Fault (Swager and Griffin, 1990; Swager, 1994)

**Principal interpretation**: aeromagnetic data, seismic data, previous geology

**Dip direction**: East

**3D interpretation of fault:** Figures 1-27, 1-32, 1-33, 1-36.

**Plan view of faul**t: Figure 1-31.
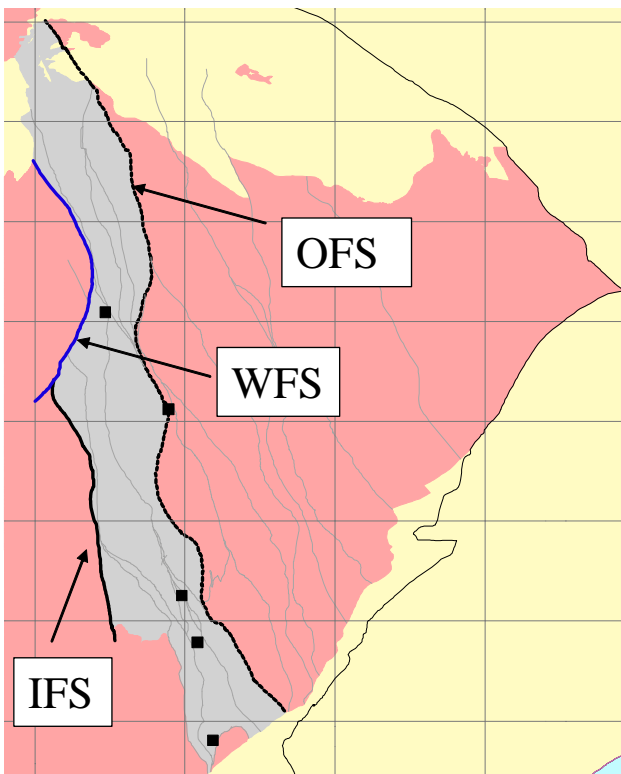


Figure 1-31: Fault systems defining the Kalgoorlie Terrane. OFS = Ockerburry FS; WFS = Waroonga FS; IFS = Ida FS. Kalgoorlie Terrane shown in grey.

# NE Kalgoorlie Terrane Fault Systems

Waroonga FS  Ida FS  Bardoc FS  Perseverance FS  Mt McClure FS  Ockerburry FS

Looking North-West

3X vertical exaggeration
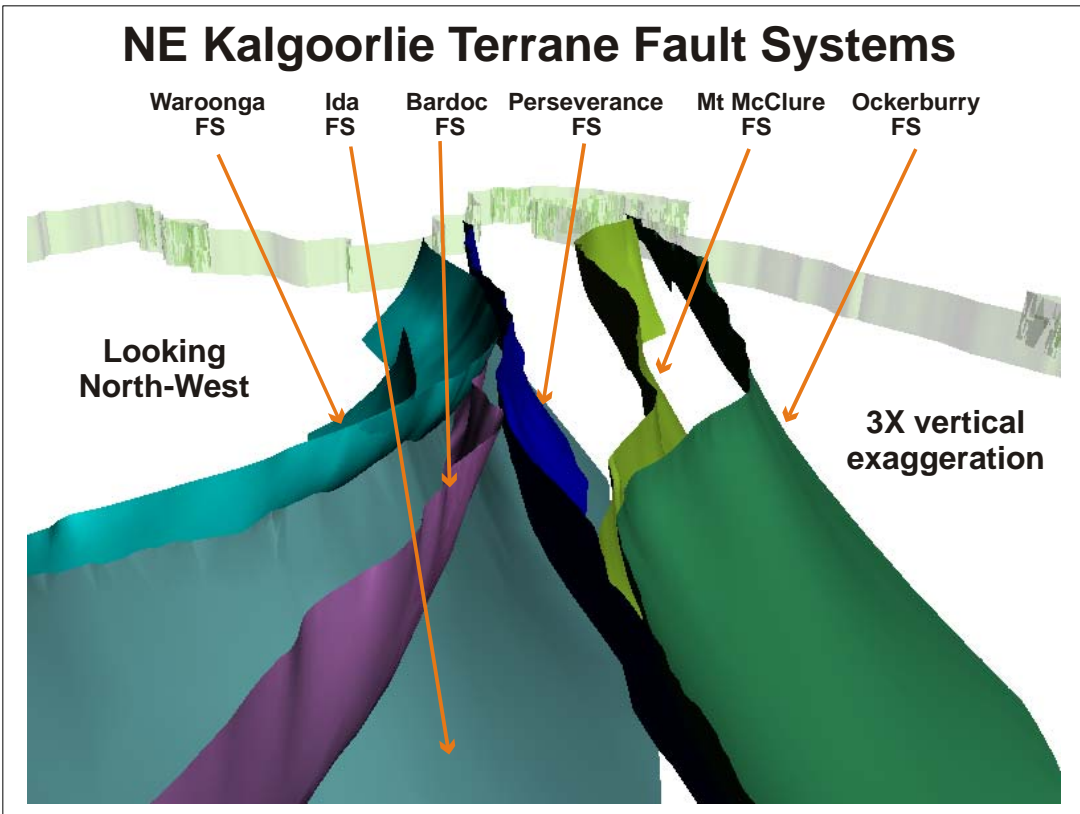
**Figure 1-32: 3D interpretation of the terrane- and domain-bounding fault systems of the northeastern part of the Kalgoorlie Terrane.**

# Central Kalgoorlie Terrane Fault Systems

Ida FS  Bardoc FS  Lefroy FS  Perseverance FS  Ockerburry FS

Looking North-West

3X vertical exaggeration
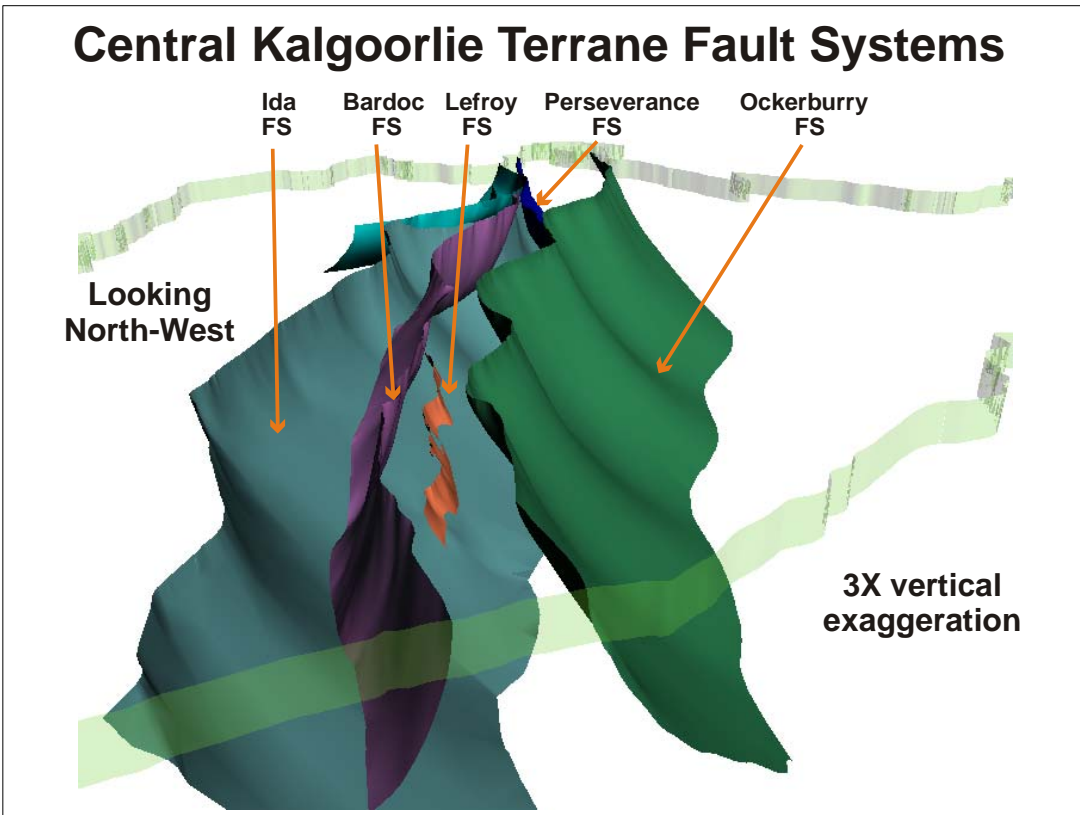
**Figure 1-33: 3D interpretation of the terrane- and domain-bounding fault systems of the central part of the Kalgoorlie Terrane.**

## Mt McClure Fault System

**Eastern boundary of**: Jundee Domain, Kalgoorlie Terrane

**Western boundary of**: Moilers Domain, Kalgoorlie Terrane

**Component faults** (north to south):
Unnamed fault (Liu et al., 2001)
Moilers Shear Zone (Liu et al., 2001)
Mt McLure Fault (Liu et al., 2001)

**Principal interpretation**: aeromagnetic data, previous geology

**Dip direction**: East

**3D interpretation of fault:** Figure 1-32.

**Plan view of faul**t: Figure 1-34.

## Koonoonooka Fault System

**Eastern boundary of**: Wiluna Domain, Kalgoorlie Terrane

**Western boundary of**: Jundee Domain, Kalgoorlie Terrane;
Moilers Domain, Kalgoorlie Terrane

**Component faults** (north to south):
west part of Moilers Shear Zone (Liu et al., 2001)
New fault (Y2 project)
Unnamed fault (Liu et al., 2001)

**Principal interpretation**: aeromagnetic data, previous geology

**Dip direction**: West

**3D interpretation of fault:** Not shown.

**Plan view of faul**t: Figure 1-34.
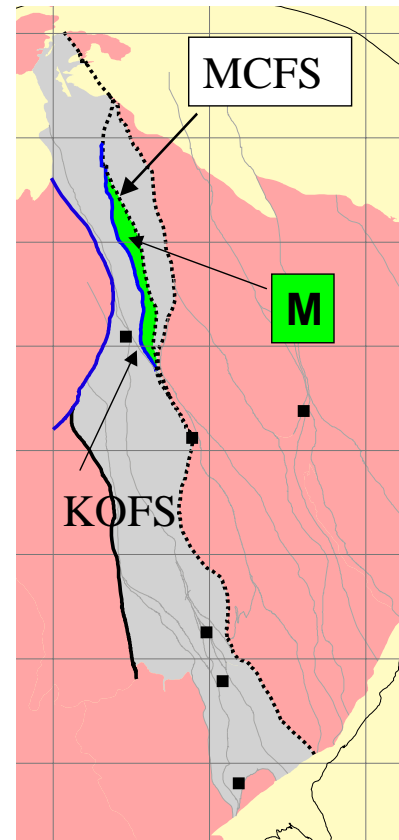


**Figure 1-34: Plan view of the Mt McClure Fault System (MCFS) and the Koonoonooka Fault system (KOFS). Moilers Domain (M) in green; Kalgoorlie Terrane in grey.**

## Perseverance Fault

**Western boundary of**: Wiluna Domain, Kalgoorlie Terrane; Moilers Domain, Kalgoorlie Terrane

**Eastern boundary of**: Boorara Domain, Kalgoorlie Terrane

**Component faults** (north to south):
New fault (Y2 project)
Perseverance Fault (Liu et al., 2001)

**Principal interpretation**: aeromagnetic data, previous geology

**Dip direction**: East

**3D interpretation of fault:** Figures 1-32, 1-33, 1-36.

**Plan view of faul**t: Figure 1-35



**Figure 1-35 (right): Plan view of the Perseverance Fault (PF). Moilers Domain (M) in green; Jundee Domain (J) in red; Wiluna Domain (W) in blue. Kalgoorlie Terrane in grey.**
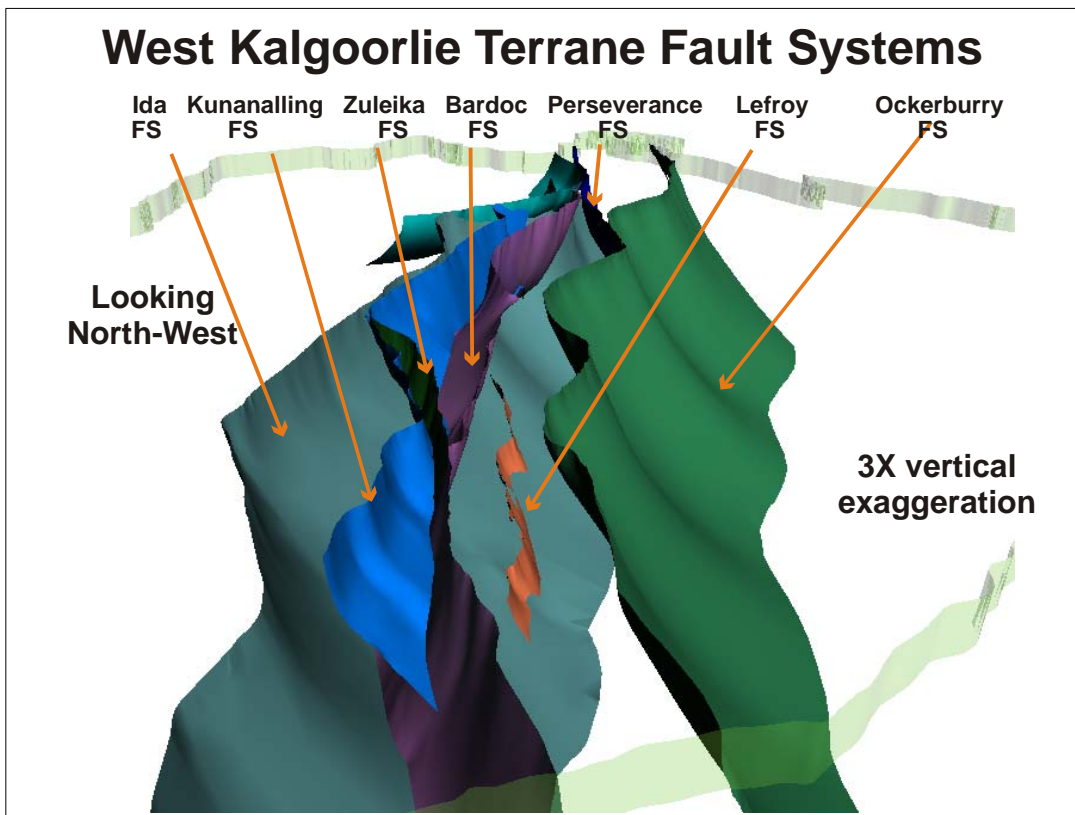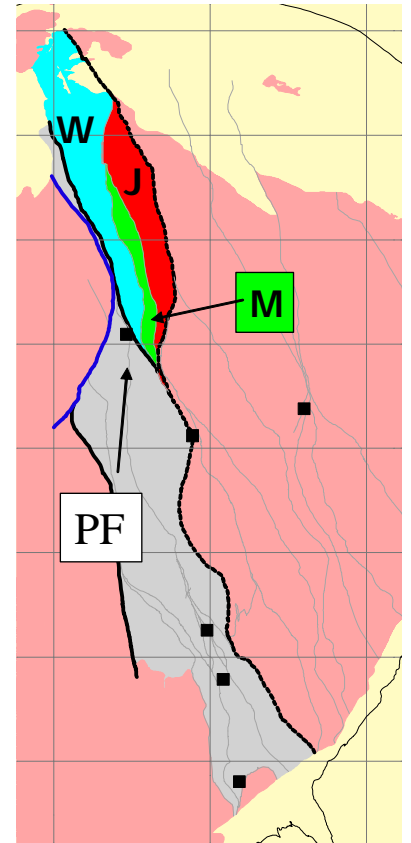


**Figure 1-36: 3D interpretation of the terrane- and domain-bounding fault systems of the western part of the Kalgoorlie Terrane.**

## Bardoc Fault System

**Eastern boundary of**: Boorara Domain, Kalgoorlie Terrane; Kambalda Domain, Kalgoorlie Terrane

**Western boundary of**: Ora Banda Domain, Kalgoorlie Terrane; Depot Domain, Kalgoorlie Terrane

**Component faults** (north to south):
unnamed fault (Liu et al., 2001)
Menzies Shear (Swager and Griffin, 1990)
Bardoc Deformation Zone (Swager and Griffin, 1990)
Abattoir Shear (Swager and Griffin, 1990)
part of Zuleika Shear (Swager and Griffin, 1990)
unnamed fault (Swager and Griffin, 1990)
new fault (Y2 project)

**Principal interpretation**: aeromagnetic data, previous geological interpretation, detailed Placer Dome and Goldfields Ltd geology, seismic data

**Dip direction**: West

**3D interpretation of fault:** Figures 1-32, 1-33, 1-36.

**Plan view of faul**t: Figure 1-37.
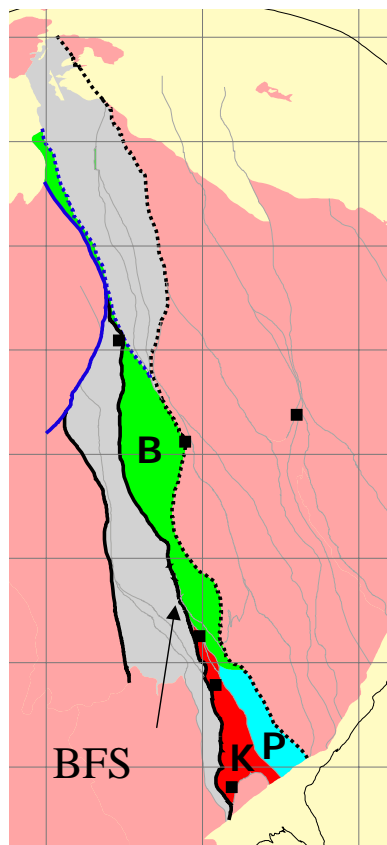


Figure 1-37: (above). Plan view of the Bardoc Fault System (BFS). Parker Domain (P) in blue; Kambalda Domain (K) in red; Bardoc Domain (B) in green. Kalgoorlie Terrane in grey.

## Lefroy Fault System

**Eastern boundary of**: Kambalda Domain, Kalgoorlie Terrane

**Western boundary of**: Boorara Domain, Kalgoorlie Terrane; Parker Domain, Kalgoorlie Terrane

**Component faults** (north to south):
Lefroy Fault (Swager and Griffin, 1990)
Woolibar Fault (Swager and Griffin, 1990)
Unnamed faults (Swager and Griffin, 1990)
New fault (Y2 project)

**Principal interpretation**: aeromagnetic data, seismic data, Goldfields Ltd detailed geology and unpublished data.

**Dip direction**: East

**3D interpretation of fault:** Figures 1-33, 1-36.

**Plan view of faul**t: Figure 1-38
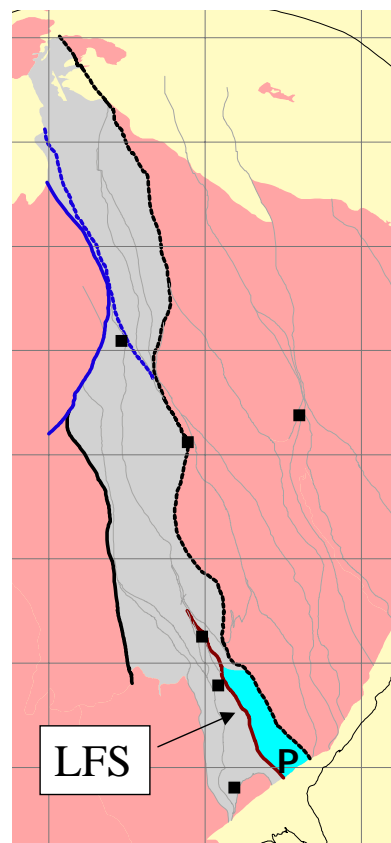


Figure 1-38 (right): Plan view of the Lefroy Fault System (LFS). Parker Domain (P) in blue. Kalgoorlie Terrane in grey.

## Ida Fault System

**Eastern boundary of**: Kalgoorlie Terrane;
Coolgardie Domain, Kalgoorlie Terrane

**Western boundary of**: Youanmi Terrane; Southern Cross Province

**Component faults** (north to south):
Ida Fault (Swager and Griffin, 1990)

**Principal interpretation**: aeromagnetic data, seismic data

**Dip direction**: East

**3D interpretation of fault:** Figures 1-32, 1-33, 1-36.

**Plan view of faul**t: Figure 1-39.
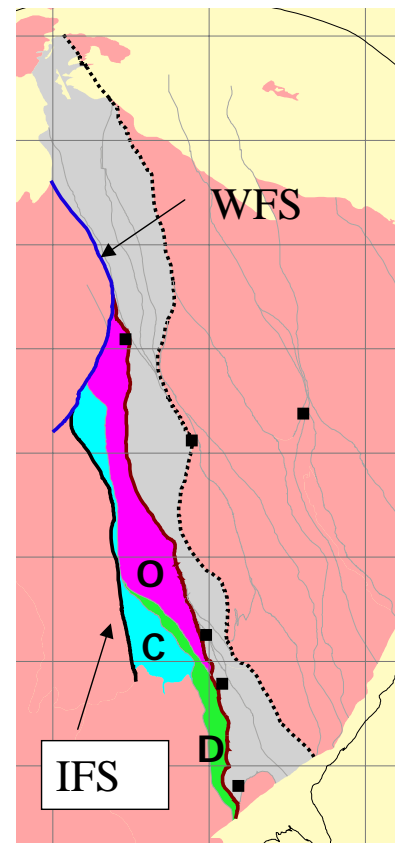


Figure 1-39: Plan view of the Ida Fault System (IFS), and the Waroonga Fault System (WFS). Ora Banda Domain (O) in pink; Depot Domain (D) in green; Coolgardie Domain (C) in blue. Kalgoorlie Terrane in grey.

## Waroonga Fault System

**Eastern boundary of**: Kalgoorlie Terrane;
Coolgardie Domain, Kalgoorlie Terrane;
Boorara Domain, Kalgoorlie Terrane;
Ora Banda Domain, Kalgoorlie Terrane.

**Western boundary of**: Youanmi Terrane; Southern Cross Province

**Component faults** (north to south):
Erawalla Fault (Liu et al., 2002)
Miranda Fault (Liu et al., 2002)
Waroonga shear zone (Liu et al., 2001)

**Principal interpretation**: aeromagnetic data, previous geology

**Dip direction**: west

**3D interpretation of fault:** Figure 1-32; also on Figure 1-36 but unlabelled.

**Plan view of faul**t: Figure 1-39.

## Zuleika Fault System

**Eastern boundary of**: Depot Domain, Kalgoorlie Terrane

**Western boundary of**: Ora Banda Domain, Kalgoorlie Terrane

**Component faults** (north to south):
Zuleika Shear (Swager and Griffin, 1990)

**Principal interpretation**: aeromagnetic data, Swager and Griffin (1990), detailed Placer Dome geology, seismic data.

**Dip direction**: West

**3D interpretation of fault:** Figure 1-36.

**Plan view of faul**t: Figure 1-40.



**Figure 1-40 (right): Plan view of the Zuleika Fault System (ZFS). Ora Banda Domain (O) in pink. Kalgoorlie Terrane in grey.**
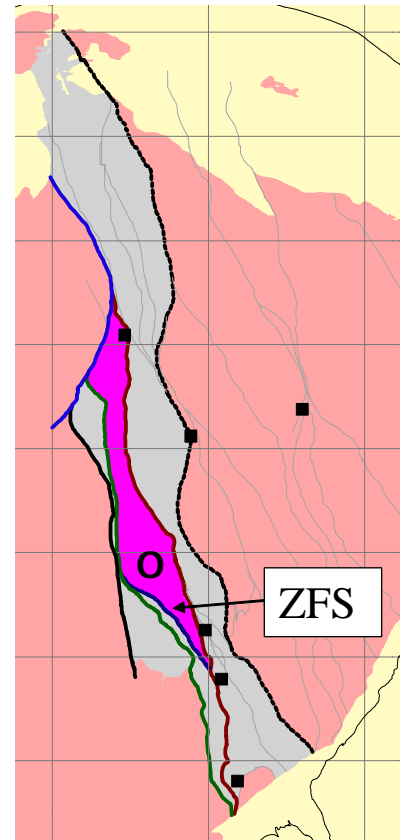
## Kunanalling Fault System

**Eastern boundary of**: Coolgardie Domain, Kalgoorlie Terrane

**Western boundary of**: Depot Domain, Kalgoorlie Terrane,
Ora Banda Domain, Kalgoorlie Terrane

**Component faults** (north to south):
northern Zuleika Shear (Swager and Griffin, 1990)
Kunanalling Fault (Swager and Griffin, 1990)
new fault (Y2 project)

**Principal interpretation**: aeromagnetic data, Swager and Griffin (1990); detailed Placer Dome geology, seismic data

**Dip direction**: East

**3D interpretation of fault:** Figure 1-36.

**Plan view of faul**t: Figure 1-41.



**Figure 1-41 (right): Plan view of the Kunanalling Fault System (KFS). Coolgardie Domain (C) in blue. Kalgoorlie Terrane in grey.**
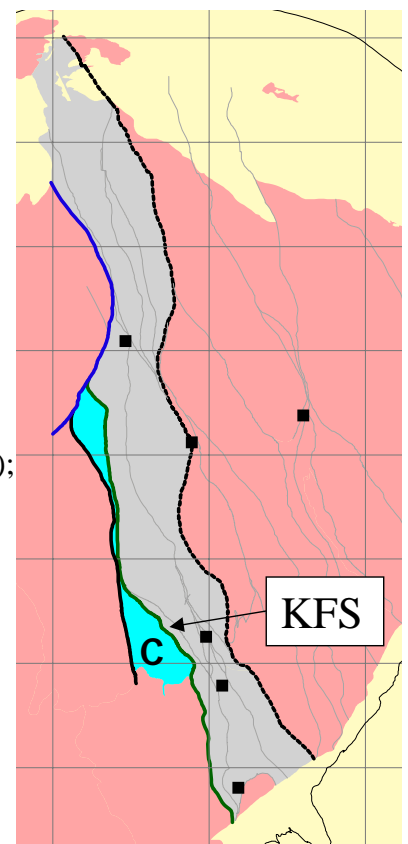
## *Appendix 1:*

1-1: An A2 scale time-space chart of published geochronology jpeg file complements the 3D map **Appendix 1_1 time space plot (Fig 1_4).pdf**

1-2: **Appendix 1_2 pdt 2004 Cassidy time_space.pdf** was presented at the December 2004 PDT meeting in Perth.

1-3: **Appendix 1_3 pdt 2004 Champion regional_setting.pdf** was presented at the December 2004 PDT meeting in Perth.

1-4: **Appendix 1_4 Champion regional geology Dec 04 update.pdf** is an update of the Champion presentation at eth December 2004 PDT meeting in Perth.

1-5: **Appendix 1_5 Cassidy&Champion SEG 2004 Abstract.pdf** is the abstract of the paper presented at the SEG meeting in September 2004 in Perth.

# Chapter 2: An integrated geological and geophysical 3D map for the EYC

*P.A. Henson*

## Introduction

One of the chief outputs of the *pmd*\*CRC Y2 project is a new 3D map depicting the structural and lithological architecture of the eastern Yilgarn Craton (EYC). This map is the result of the integration and validation of geological and geophysical data sets using software specifically designed to manipulate and visualise spatial data in 3D. The 3D maps with their respective metadata may be found in Appendix 2 at the end of this chapter.

A seamless solid geology map of the region has been constructed by integrating industry, state and federal government data sets. This solid geology map formed the starting point for all other interpretations within the region. Understanding the third dimension is not a trivial task and there has been much historical debate about such seemingly minor issues as the dip of faults. These issues have arisen because we have few geological techniques that can unambiguously image the subsurface architecture in polydeformed terrains like the EYC.

3D maps are becoming common place in academic research and company exploration and resource definition processes. They provide a suitable medium in which multidisciplinary data can be stored, displayed and interpreted. This 3D medium allows all spatially referenced data to be viewed in absolute x, y and z coordinates, and significantly improves our understanding over that obtained using a traditional 2D GIS package.

Mineral systems are clearly three dimensional and, in order to understand them, it is logical to import relevant data into virtual 3D space. This approach allows us to track the processes and symptoms of a mineral system as we see it today, enhances our understanding of the third dimension, and improves targeting techniques through increased insight into the manifestation of mineral system signatures in x, y and z coordinates.

## *Building a 3D map*

### Essential elements

The initial planning is critical in the construction of a 3D map, and should be given careful thought. The first step is to define the spatial region that the map is to cover; the second step is to decide what questions the map must address. Careful consideration of both these issues will help define the parameters of the project and, in turn, determine the data needed to complete the task.

When the x and y boundaries of the region have been decided, an approximate depth should be chosen for the model in order to build surfaces compatible with the map scale. In this respect the 3D map can be likened to a 2D equivalent, where maps are constructed at different scales and the density of data depends on the regions they cover (eg. 1:250 000 compared to 1:1 000 000 scales). This issue of scale is even more important in a 3D environment due to the practical constraints imposed by hardware and software. If not properly managed, these issues can cause significant problems in constructing and displaying the 3D map.

A variety of elements go into making a 3D map, many of which are essential to get right at the outset. The description below is a guide to the construction process although it is not an exact set of procedures. The process can be highly variable and specific details will depend on the direction and scope of an individual project.

**Hardware**
Although it sounds intuitive, hardware can be a limiting factor when performing the computationally intensive tasks common in constructing a 3D map. The manipulation, construction and display processes exceed the capabilities of most general-purpose office computers. 3D space requires additional computational power to operate efficiently without downtime for the operator.

It is difficult to identify exact hardware specifications, due to the variable requirements of different 3D software packages. Additionally, it would not be appropriate to state what is suitable today due to the rapid advancement in computing capabilities. Instead, it should be noted that to operate efficiently a high-end computer is needed, with processor and RAM specifications at the top of the desktop range. In addition, this platform will also require a high-end video card (e.g., NVIDIA Quadro FX 3000) to facilitate smooth display and manipulation of the data.

**Software**
A multitude of 3D software packages already exist (eg. Gocad 2.0.8, Vulcan, FracSys and Rino), and many new ones are in development. Several factors must be decided before a suitable package is selected, including price, longevity, functionality, compatibility and display capabilities. All of these issues are significant in the initial selection process.

Importing and manipulating 2D data is often best done using a 2D GIS package; it is therefore important that suitable export and import functionality exists between the 2D and 3D packages used in a project. There also needs to be an interface between geophysical programs and the 3D software, although most packages now produce output that can be readily imported into a variety of other software. In this way, data from forward and inverse potential-field modelling and seismic lines can be imported and displayed in 3D space.

**Solid geology**
The foundation for all interpretations in the third dimension is the accurate identification of spatially referenced lithological units and faults at surface; the 'solid geology'. Solid geology is an essential component of the process and without an accurate data set the determination of geometries in the third dimension is problematic.

Surface geological boundaries have topographic relief. Consequently, all lithological and fault boundaries are draped on a digital elevation model (DEM) of the project area. By following this initial procedure an accurate spatially referenced framework in xyz space may be constructed, onto which all other interpretations in the third dimension can be based.

**Data**

Constructing 3D maps of the EYC has followed a process of 2D, 2.5D and 3D data integration to constrain subsurface geometries. A broad range of data sets acquired from federal government, state government, industry and academic sources have been used in this study. This strong emphasis on integration is essential in the 3D environment because data become part of the overall data set and have associated spatial context and real geological implications.

Early acquisition of all available data needed for the project is preferable. Addition of significant data after the process is under way may necessitate reassessment of the specifications of the 3D map and could significantly delay the map building process. Since data are paramount in the validation of interpretations in the third dimension, particular emphasis should be placed on combining structural and lithological data with geophysical techniques to verify the architecture of geometries in the subsurface.

## Workflow and processes: eastern Yilgarn and Kalgoorlie region

The power of using 3D as a geological interpretive tool is derived from data integration and display. Using this medium we can no longer make interpretations in isolation or simply from 2D data alone, and we can't ignore relationships with other pertinent data simply because they don't fit our model. It is a powerful way of validating our hypotheses and cross checking geological relationships derived from multidisciplinary data sources and techniques (Figure 2-1). Geological data combined with geophysical methods have proved well suited to 3D space, which allows a combination of techniques to operate within the same spatial context, ensuring internal consistency of the data.
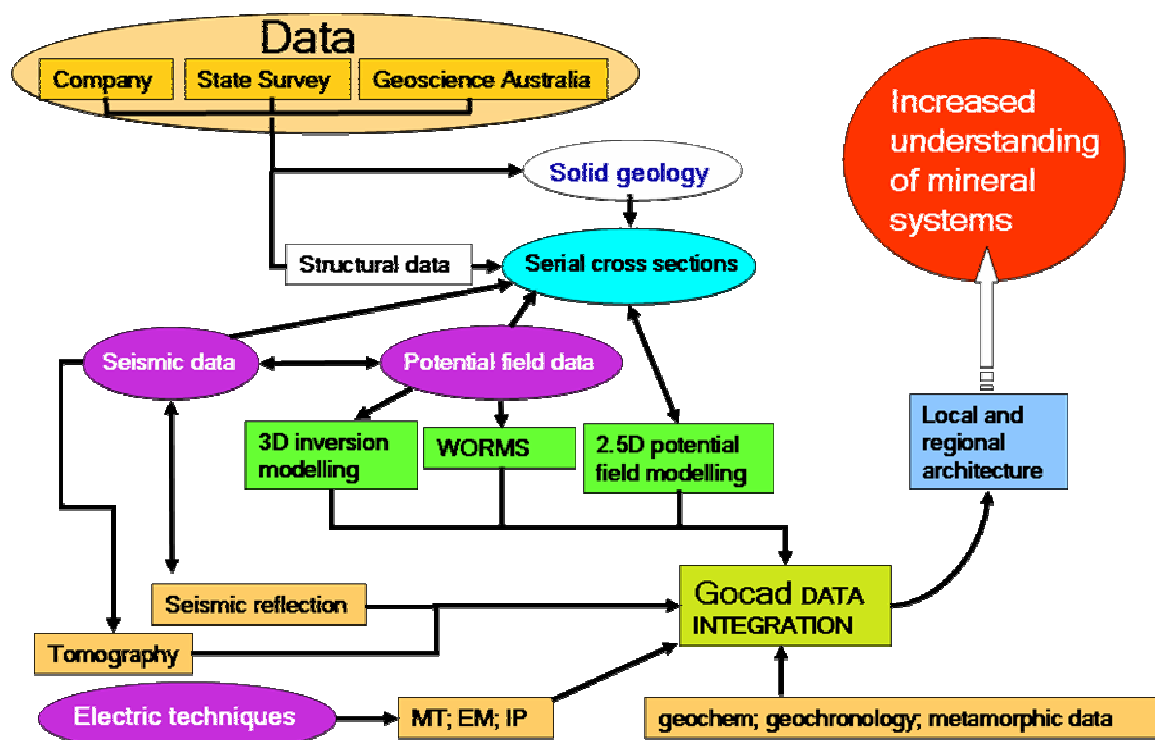
**Figure 2-1: Workflow diagram for the construction of a 3D map.**

The decision was made to base the 3D map on the detailed 1:100 000 geology due to its spatial accuracy. This accuracy enabled mine-scale 3D maps to be imported into the final regional 3D map without the significant misfit problems that may have been encountered if a more generalised data set had been used.

Stratigraphic units have been grouped (generalised) to enable regional integration of spatially referenced data and to limit the size of the final project. These units were imported into Gocad as dxf files and represent the surface expression of the simplified solid geology as line work (poly lines). The fault coverage has also been generalised to limit the total size of the project. The combined solid-geology and fault-coverage line work has been draped on a DEM to produce a seamless coverage of the field area.

A summary of the process of interpreting the subsurface geometries of lithological units and faults follows:

- determine the stratigraphy and rock relationships;
- incorporate structural readings derived from map patterns, field studies and publications, to interpret the dip of stratigraphic units and of major faults;
- construct a series of regional 2D cross sections to represent geometries in the third dimension (both ~north-south and ~east-west oriented lines);
- validate cross sections using potential-field forward modelling (we used Encom's ModelVision software); modelling a series of individual cross sections in unison helps validate the geometries on a regional basis; this extensive process sometimes requires several iterations to match both the surface expression of the geology (structural readings) and the observed field;
- translate the modelled sections into Gocad objects using an 'AWK' script;

- import the cross sections into Gocad, locating them 3D space, and;
- use cross sections as a basis for constraining 3D surfaces.

## Geological and geophysical constraints

Potential-field and seismic-reflection data have been crucial in providing constraints for the map. These data have delineated subsurface geometries and lithological relationships not evident from surface observations. The workflow process applied to these data sets is discussed later in this chapter.

The construction of serial cross sections across the EYC has proven to be a significant part of building the 3D map. They provide an important link between structural/lithological observations and geophysical constraints. Linking these two disciplines provides greater understanding from the available data and, upon completion, results in a data set against which all other interpretations can be compared.

### Rock relationships
The relationship of all stratigraphic units must be determined prior to the construction of cross sections; these relationships will constrain geologically feasible geometries and relationships between units (Figure 2-2).
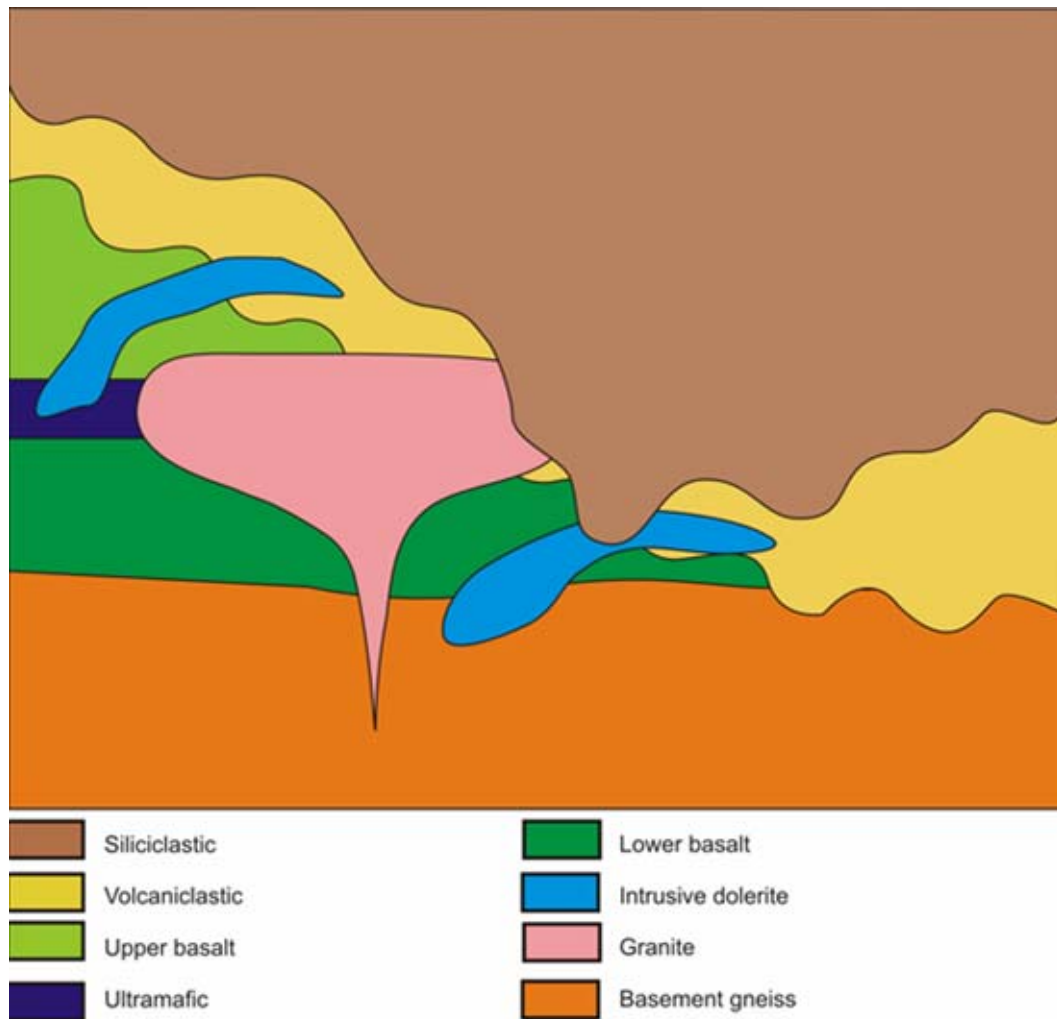
**Figure 2-2: Rock relationship diagram for the Kalgoorlie-Kambalda region.**

The first stage of cross section construction involved drawing a series of geological sections on tracing paper overlying A0 printouts of the solid geology. This step ensured geometrical consistency between parallel cross sections and enabled all structural readings to be incorporated in the initial interpretations (Figure 2-3). Cross sections for potential-field modelling were generally constructed to a depth of five to ten kilometres; the geometry of deeper structures was determined using seismic reflection data.

An integral part of the process was the interpretation of the dip of all fault and stratigraphic unit boundaries. This was a substantial task requiring literature searches, map analysis, potential-field techniques and seismic interpretation to determine the most-valid geometry for each feature. The interpretation of composite magnetic and gravity images of the area and the use of gravity 'worms' to determine dip in critical locations were important components of this stage of the process. These methods allowed an approximate thickness of mafic units to be determined and also enabled dip azimuth to be interpreted where a dramatic contrast in gravity or magnetic signals occurred.

44
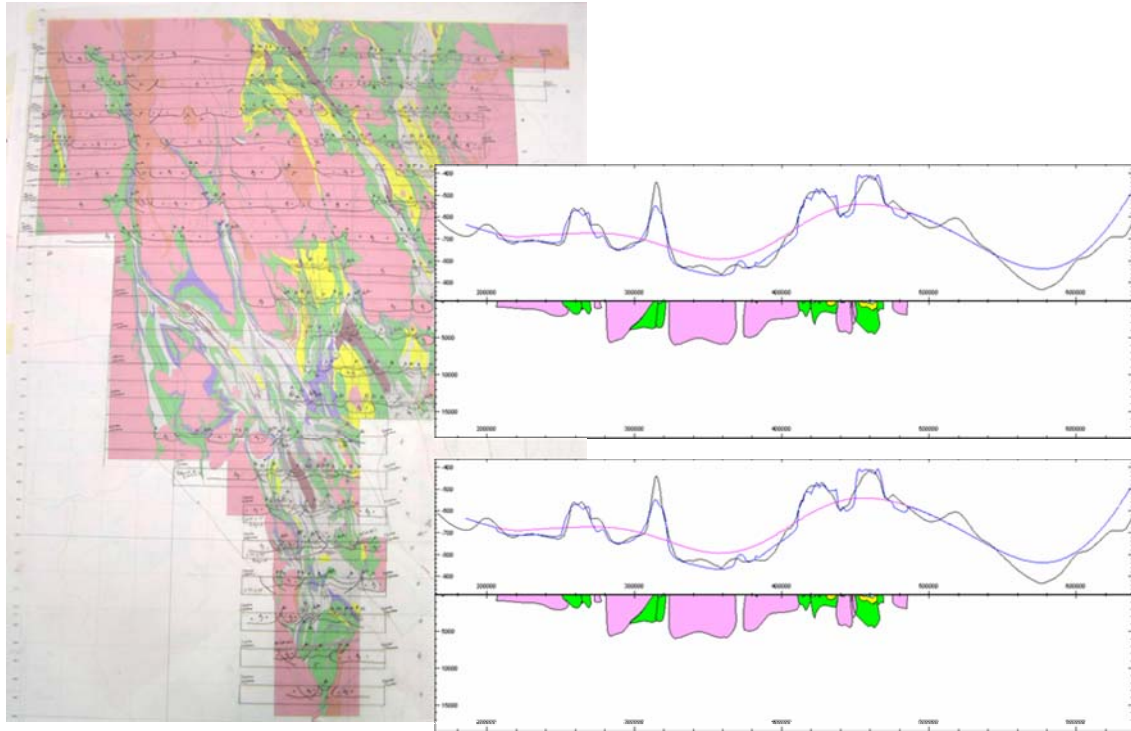
**Figure 2-3: Image of the construction phase of serial cross sections and two potential-field modelled sections validating the thickness and geometries of the initial interpretations.**

## 2.5D potential-field forward modelling

Following the initial stage of incorporating structural and lithological surface readings into serial cross sections, potential-field forward modelling was used to constrain the lithological thicknesses and the dip of faults. Using this methodology, testable geometries were developed.

Potential-field modelling produces non-unique solutions, however, the incorporation of structural readings and architecture when constructing the initial geological models significantly narrowed the range of acceptable solutions. Additionally, where available, seismic data were directly compared (in 3D space), enabling the final cross sections to be evaluated using an independent technique. During this process, all of the original geometries where honoured, where possible, to maintain the structural and lithological constraints at surface. On completion, the digitised cross sections were exported from ModelVision into Gocad using an 'AWK' script written by Malcolm Nicoll (GA) to translate them from 2D to 3D format.

Figure 2-3 shows a subset of the hand-drawn cross sections overlain on a map of the solid geology, with two examples of modelled sections. A detailed description of the forward-modelled data sets used to constrain the 3D map is given in **Potential-field data sets for building 3D maps** later in this chapter.

## 3D inverse modelling

In addition to 2.5D forward modelling, 3D analysis has been undertaken using the University of British Columbia – Geophysical Inversion Facility (UBC-GIF) inversion software to produce a 3D interpretation of the gross geology (see **Potential-field data sets for building 3D maps** later in this chapter for more details).

45

Gravity inversion attempts to predict subsurface geometries by modelling the observed field (gravity or magnetics) using 'real' geological constraints (observations and interpretations of the geology). This is a complex process in which the final output is only as good as the geological constraints that are initially fed into the model; a somewhat circular argument! However, in order to truly understand the subsurface a critical level of geological understanding is essential prior to attempting the inversion process.

There is a close correlation between the base of greenstone derived from 2.5D forward modelling and the 3D inversion modelling result. This means that the regional surface defining the base of greenstone can be confidently interpolated between the cross sections on both the regional and Kalgoorlie-Kambalda models. We believe that this is a novel application of the various techniques, aiming to achieve the greatest rigour in the final 3D map.

**Seismic reflection data**

Seismic data have played a complementary role in constraining subsurface geometries (see Chapter 3 for details). These data provided a unique tool for imaging structures in regions where no density or magnetic contrast was observed using potential-field techniques. Seismic data are particularly useful at depths below 5 km to constrain structures below the base of greenstone. A series of low-angle domical structures within the basement felsic gneiss, not identified by other techniques, were interpreted using seismic data (Figure 2-4).
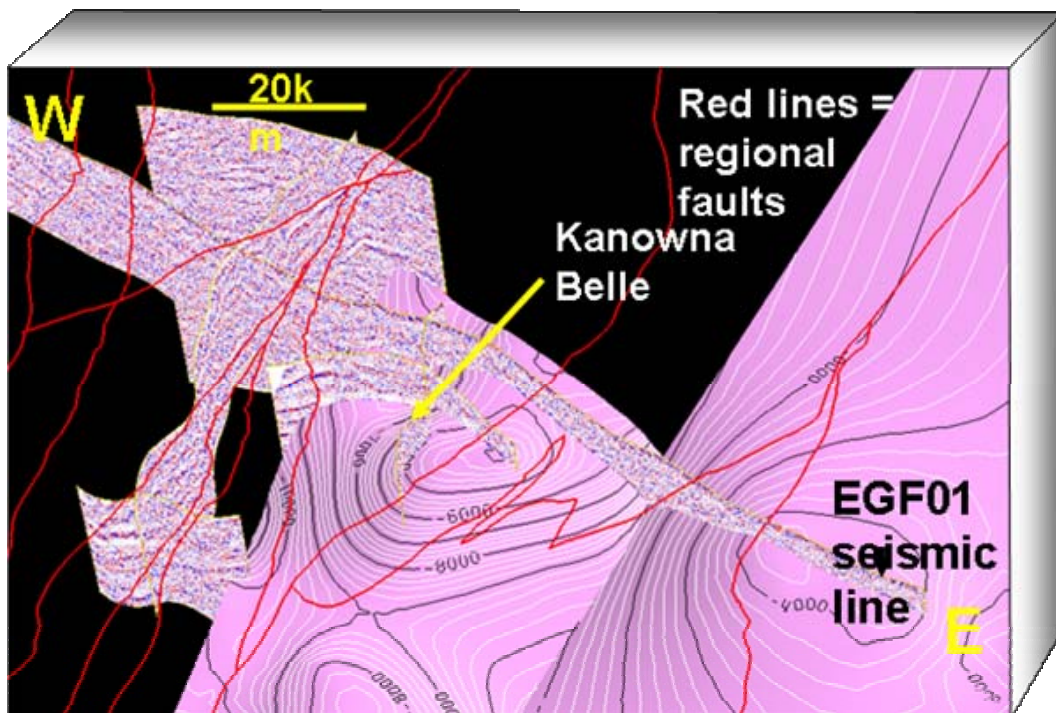


Figure 2-4: Seismic lines in 3D space delineating a domical structure beneath Kanowna Belle.

Seismic reflection data has proved an integral part of interpreting the third dimension and provide one of the few avenues for interpreting deep structures (to the Moho). Historically, these data were interpreted using paper printouts of individual lines on which major stratigraphic boundaries and faults were identified. This method allows

limited correlation with cross lines or other lines that may identify structures along strike. Additionally, seismic lines commonly follow existing roads and are often curved, adding to the complexity of reflector geometries if viewed only in 2D.

The EYC is a complexly deformed terrain comprising several orthogonal deformations which have produced a variety of geometric shapes. An assortment of curved and dipping reflectors result, having relationships difficult to unravel on a 2D plane. The introduction of 3D technologies has allowed us to import seismic reflection lines into 3D space, in effect, displaying the absolute location of each reflection and taking into account non-linearity in the seismic line (Figure 2-5). The advantages of this method include:

- interconnection between two intersecting seismic lines allows direct correlation of similar reflectors;
- correlations can be drawn between two or more unconnected seismic lines that have similar structures or lithologies, by sighting between them in 3D space;
- bends in seismic lines allow for increased understanding; when a dipping fault intersects a bend in a line at ~90º, an apparent dip of the fault can be determined, and;
- in 3D space, direct seismic interpretation can be performed providing connectivity between all the seismic lines within a given region.
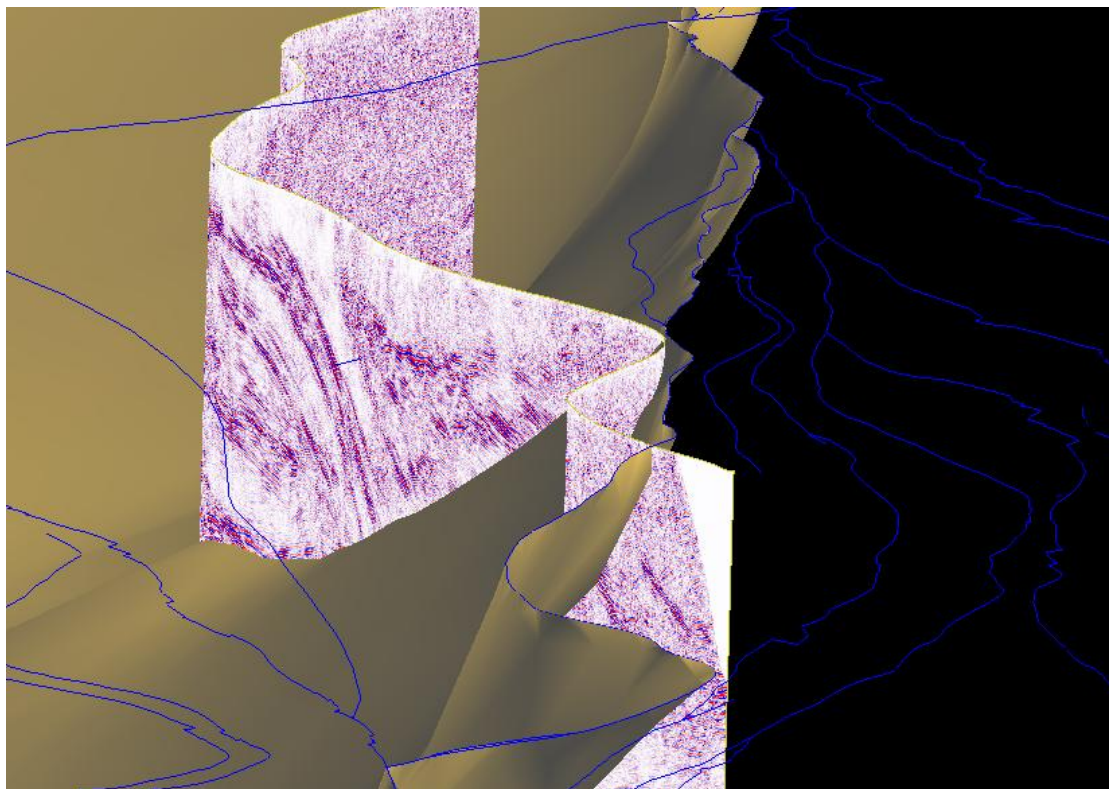


**Figure 2-5: Example of the Bardoc Fault (gold) intersecting the curved mig99Y4 seismic line (speckled maroon and white surface) in 3D space. Surface fault traces are shown in blue.**

The visualisation and interpretation of seismic reflection lines in 3D space has proven to be a major improvement compared to conventional paper copy techniques. Through

visualisation all pertinent relationships can be addressed leading to a greater understanding of the geometries in the subsurface.

All interpretations of the seismic data were "validated" by 2.5D forward modelling of gravity and magnetic data. The validation of the interpretations and the repeatability of reflectors at the same place on intersecting lines supports the veracity of these data and their interpretation.


## Linework and Surfaces

### Linework
The 3D map is in effect a 3D GIS; it allows a variety of spatially referenced data to be imported and it operates in a very similar way to 2D GISs. The linework in 3D is similar to a 2D GIS in that it is made up of a series of nodes and links (Figure 2-6).

However, a major difference between 2D and 3D GIS is related to digitising. In 2D, the reference is always a 2D plane and any digitised line is constrained to lie on that plane. In 3D space, digitised lines are tied to a 3D reference surface, otherwise they may snap to a point anywhere in front of, or behind, an image. This misalignment can also occur if anything is visible in the foreground. Hence, it is preferable to have few objects visible during the digitising process.
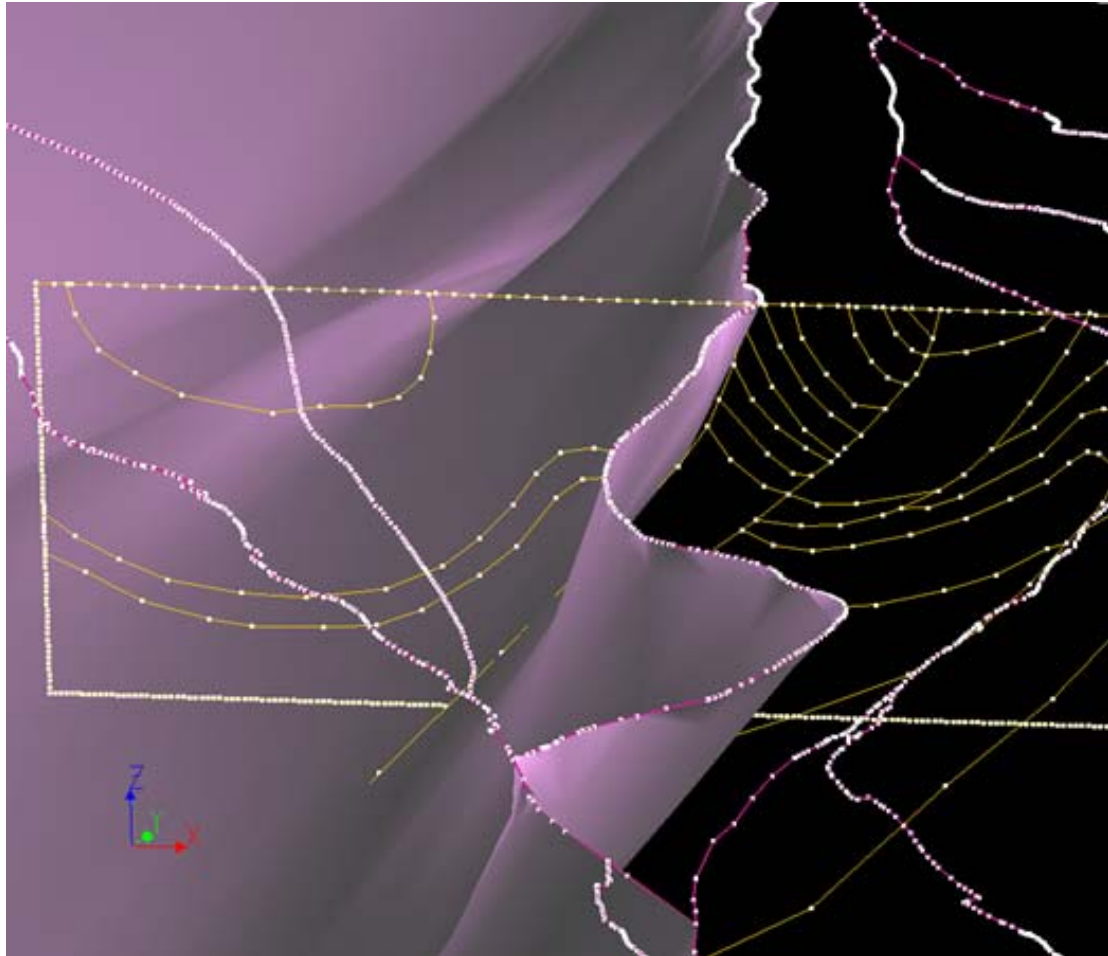
**Figure 2-6: Image of a fault (purple surface) constrained by a potential-field modelled cross section (orange linework) in 3D space.**

### Surface construction

Surfaces can be constructed using a variety of techniques. As a general rule, the number of triangular facets in a surface should be minimised to aid in reducing the final size of the completed project. Unfortunately, this often means a trade-off against the accuracy that may be needed if further manipulation of the surface is required at a later date.

There are basically three different ways to create a surface using Gocad 2.0.8. A surface can be created using a closed curve, two curved parts or several curved parts. When creating a surface using a closed curve, the complete border is pre-defined and a surface is created within this boundary (Figure 2-7).

49
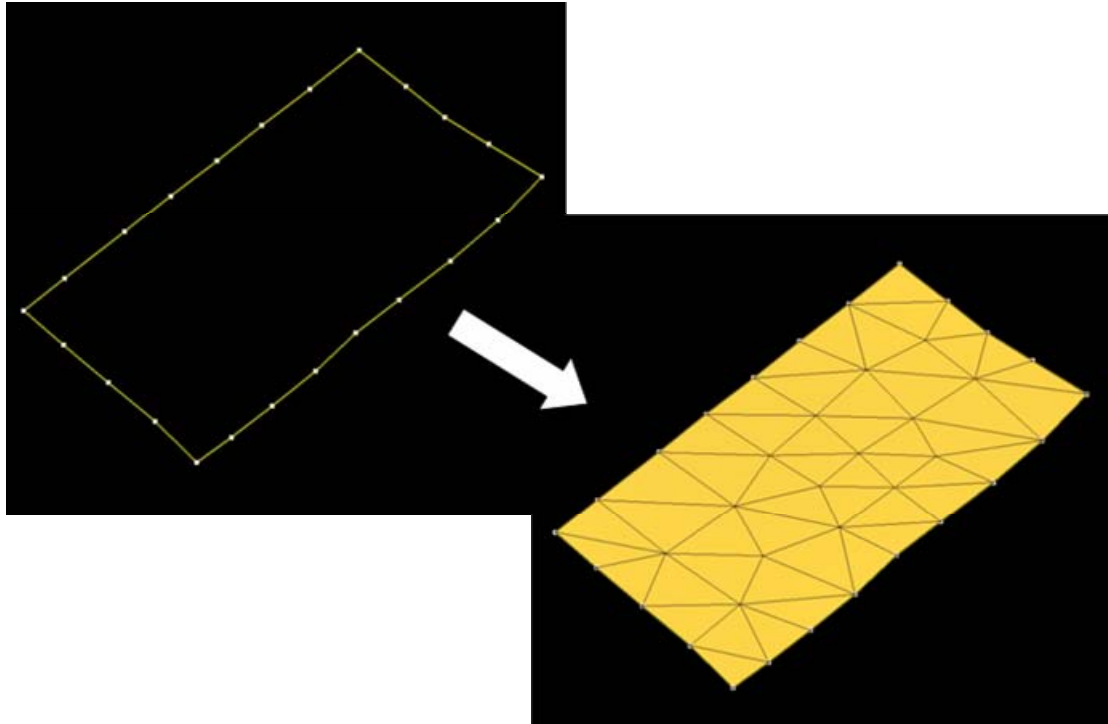
**Figure 2-7: Surface construction using a closed curve function in Gocad.**

An additional method of surface construction is to use two or more lines (Figure 2-8A). One of the advantages of this method is that there is no need to define the whole perimeter of the surface, instead the interpolation process links the lines and builds a surface from them. It produces a surface that is a series of rows of triangles sub-parallel to the original lines (Figure 2-8B). An additional interpolation process (the Gocad method beautify triangles for equilaterality) can convert the triangular facets into homogenous triangles, which are more suitable for manipulation (Figure 2-8C).
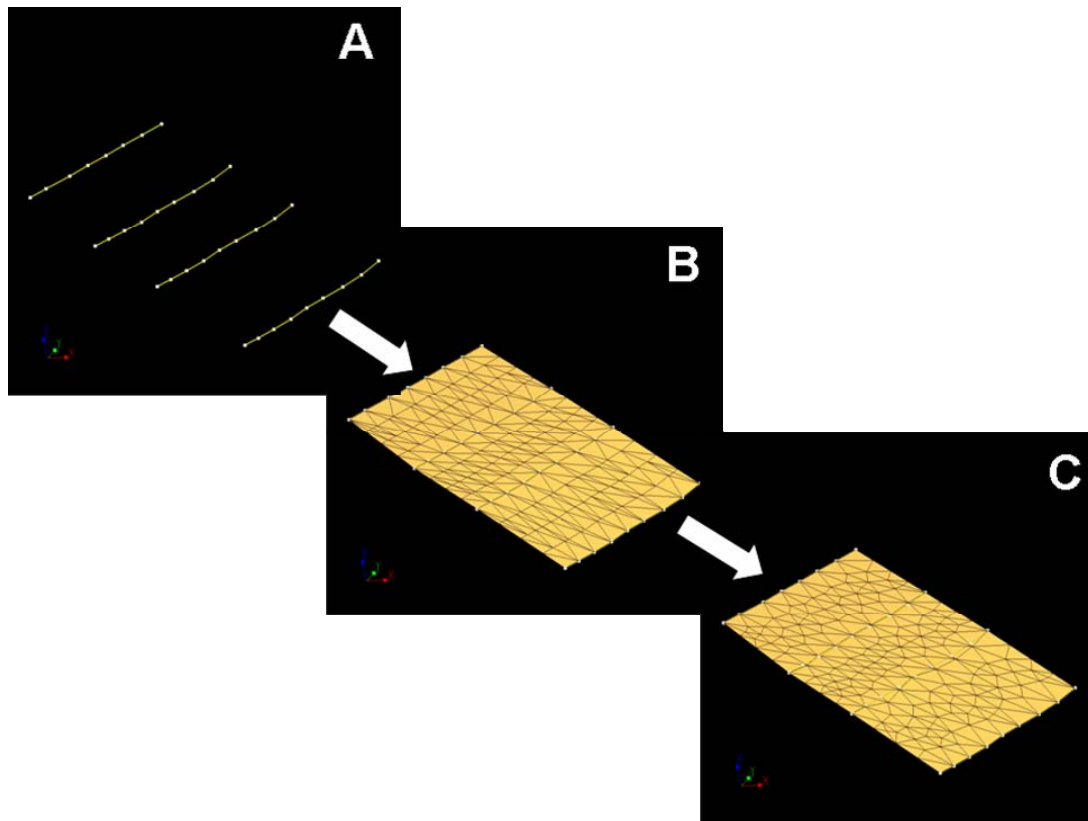
**Figure 2-8: Surface construction from several parts.**

## Constraining a surface

A surface can be 'rubber sheeted' into any geometry using constraints. Once the surface is constructed, a line, surface or point can be used to 'rubber sheet' the surface into any required shape. Figure 2-9 shows how a surface can be constrained using a line to 'rubber sheet' it into position. It must be noted that the surface is a series of flat triangular facets which will only conform to a complex constraint if there are enough triangular facets to bend into position. If there are insufficient triangular facets in a surface it will not exactly fit the constraint; hence, a more-detailed surface may be needed.
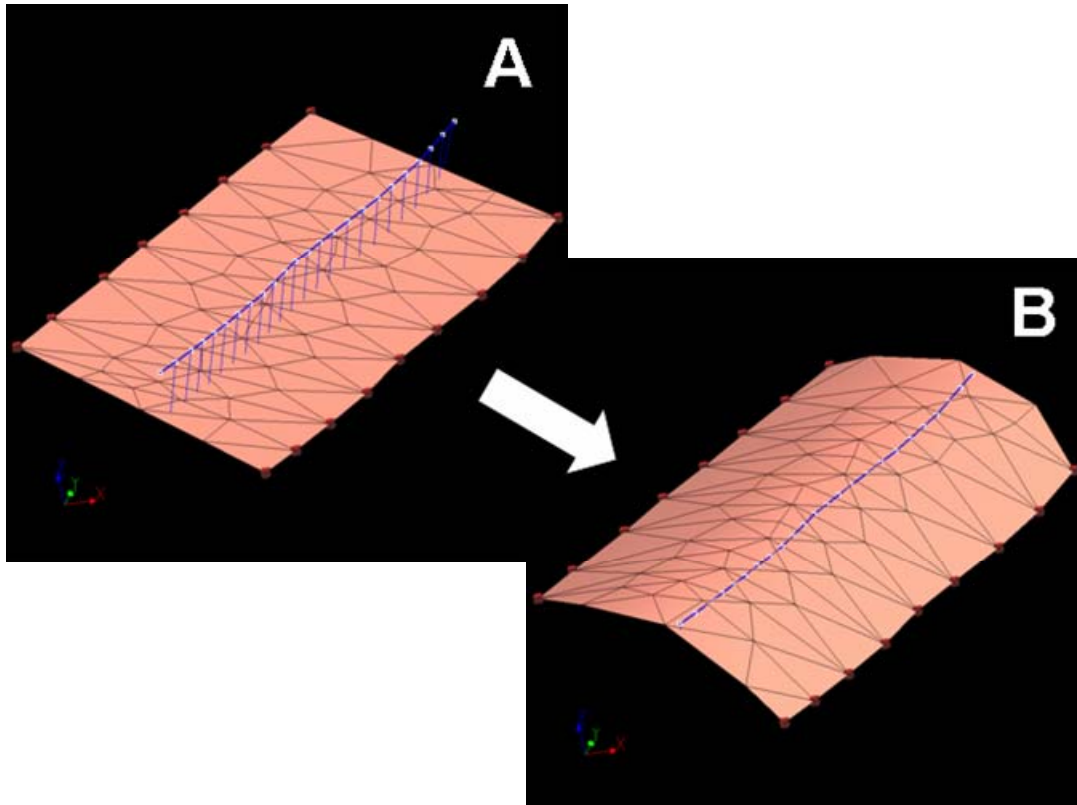
**Figure 2-9: Constraining a surface using a line ('rubber sheeting').**

### Construction of multiple surfaces

The construction of multiple surfaces can follow a variety of paths although it is always preferable to build major fault surfaces first. Faults always cross-cut and displace lithological units and, therefore, provide a starting point for the model. The construction of granites should follow fault construction, and then the construction of all other lithological boundaries. When constructing surfaces that define lithological boundaries it is preferable to extend them through the pre-defined fault surfaces and cut them to produce seamless joins between surfaces. By following this process a coherent 3D map can be produced and, by creating surfaces that are seamless, further volume calculations can be performed on them at a later date (Figure 2-10).
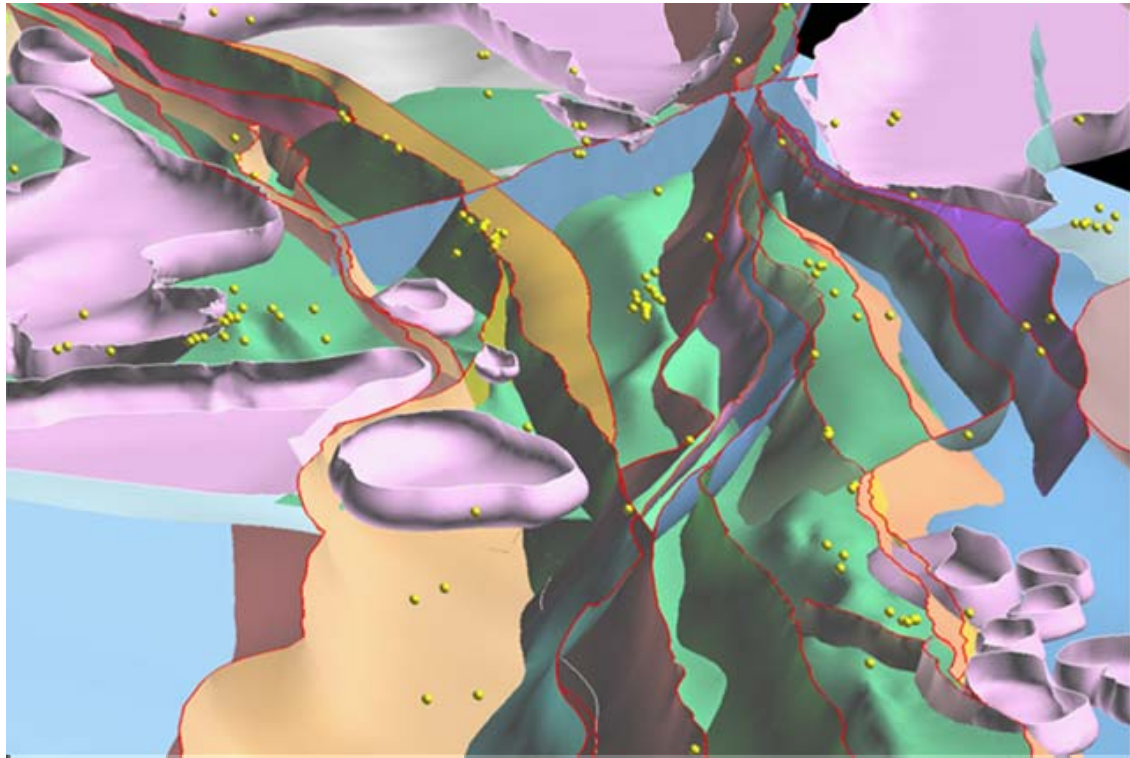
**Figure 2-10: Image of the Kalgoorlie-Kambalda 3D map, showing Au deposits (yellow spheres) and surface fault traces (red lines).**

## *Potential-field data sets for building 3D maps*

*A.P. Hitchman*

The application of potential-field data has been a critical component of the 3D map building process. How these data were used is described in the preceding sections. The following sections are a more-detailed documentation of the potential field data sets used in building the 3D maps.

## Methods and constraints

A range of potential-field data sets have been modelled to advance the 3D understanding of the depth of greenstone sequences, and their relationship to granitic intrusions, in the EYC. Forward and inverse modelling of gravity and magnetic data, and multiscale edges (worms), have contributed to the development of new structural insights for the region. Table 2-1 lists the data sets used and Figure 2-11 shows where they are located in the EYC.

**Forward modelling**

Forward modelling allows the gravity and magnetic responses of virtual geological models to be assessed (Grant and West, 1965). By constructing a geological model and assigning suitable densities and magnetic susceptibilities to each lithological unit the expected gravity and magnetic anomalies associated with the model may be determined. Comparison of the modelled anomalies with observed data allows the suitability of the model to be gauged and suggests where possible modifications may be made. Iterative refinement to accommodate these modifications, while maintaining

53

the integrity of the model, leads to an improved understanding of the subsurface geology.

A number of important limitations apply to forward modelling methods. Their primary shortcoming is the non-uniqueness of their solution; the same gravity anomaly may be produced by bodies of increasing density and depth, and the same magnetic anomaly by bodies of increasing susceptibility and depth. Consequently, an almost infinite number of geological structures can be invoked to explain an observed gravity or magnetic anomaly.

A practical limitation on potential-field modelling is the paucity or inaccessibility of density and magnetic-susceptibility rock-property data. Although geological samples are routinely collected they are seldom subjected to physical property analysis. Consequently, for potential-field modelling purposes the physical properties of the modelled geological units commonly need to be inferred from data collected in similar geological settings elsewhere.

A further complication is that, where they do exist, measured physical parameters from individual samples don't necessarily represent bulk values for geological units well. This issue of scalability results primarily from the significant property variability that is common within lithological units. Such variability is due to a range of factors including compositional variability, chemical and thermal history, age and depth of burial, and degree of weathering. Emerson (1990) and Trench et al. (1993), for example, indicate that Yilgarn greenstones may vary in density by up to 0.5 g/cm$^3$. Nevertheless, in the modelling conducted for the Y2 project, petrophysical properties of the individual crustal units have been assumed to be homogenous. Importantly, Bourne et al. (1993) suggest that modelled depth estimates may be in error by kilometres due to inappropriate selection of greenstone/granite density contrasts.

Furthermore, the forward modelling techniques used in this project are restricted to two dimensions. Obtaining an understanding of geology in the third dimension requires subsequent interpolation between individual 2D models. Where strike-continuity is poor, the correlation of geological units between sections can be problematic.

Despite these limitations, 2.5D potential-field modelling is currently one of the few ways of interpreting subsurface geometries. It is a tool that can test geometries in the third dimension and provides a framework for evaluation against other methods such as seismic reflection data.

Consequently, potential-field forward modelling is most effectively used in combination with additional information from a range of sources, including geological observations, and drillhole and seismic data. A successful match of modelled and observed potential-field data does not imply the uniqueness of the solution but, at best, indicates that the model is consistent with the observed data.

| No. | Name | Field | Method | Description |
|-----|------|-------|--------|-------------|
| *Regional data sets* | | | | |
| 1 | Norseman–Wiluna | gravity | worms | generated using GA method |
| 2 | Norseman–Wiluna | magnetics | worms | generated using GA method |
| 3 | Norseman–Wiluna | gravity | forward | 36 E-W sections, 20 km separation |

| 4 | Norseman–Wiluna | gravity | inverse | 302×552×15 km model, 2×2×1 km cells |
|---|---|---|---|---|
| *Local data sets* | | | | |
| 5 | Leonora–Laverton | gravity | forward | 9 E-W sections, 20 km separation |
| 6 | Rason | gravity | forward | 6 E-W sections, 20 km separation |
| 7 | Kalgoorlie-Kambalda | gravity | forward | 15 E-W sections, 10 km separation |
| 8 | NY1 seismic line | gravity | forward | |
| 9 | Minerie | gravity | inverse | 76×86×10 km model, 1×1×0.5 km cells |
| 10 | Kalgoorlie | magnetics | worms | generated using GA method |

**Table 2-1: Potential-field modelling methods used in the development of the EYC 3D structural map.**
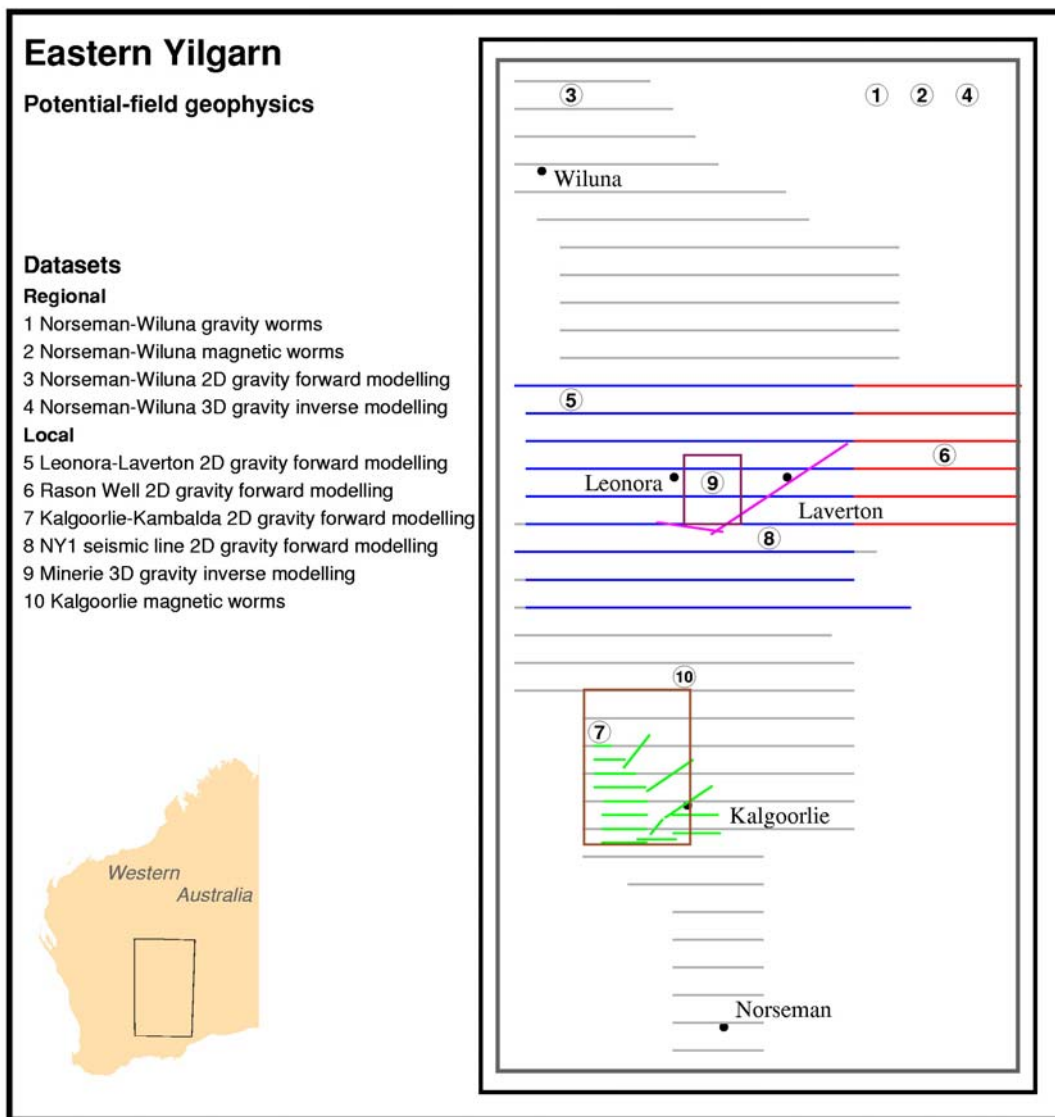


**Figure 2-11: Potential-field methods applied to understanding the 3D architecture of the EYC.**

## Inverse modelling

Inverse modelling, or "inversion", is an automated process for determining a density or magnetic-susceptibility distribution that reproduces the observed gravity or magnetic anomaly subject to a set of parameters and constraints. In this process a starting distribution of physical properties is iteratively adjusted and, with each

iteration, the response of the model is computed. The misfit between the observed and modelled data is used to guide the adjustment of the model. Once a specified number of iterations is completed, or the fit between observed and modelled data is sufficiently good, the modelling process is concluded and the "best fit" property distribution is then used to interpret lithology.

Improved models are obtained by including *a priori* geological information in the initial reference model. The inversion process then attempts to produce a final model that matches both the observed potential-field data and the existing understanding of geological relationships and structural geometries. Constraints implemented in the inversion may be derived from the known surface geology, drillhole data and additional geophysical data such as reflection seismic interpretations. Even if the actual subsurface geology is poorly known it is possible to add some geometrical constraints to inversion models where there is a broad-scale understanding of crustal geometry. For instance, in the Yilgarn it is known that greenstone belts represent only a thin layer of the total crust; hence the inversion carried out in this study has been constrained to produce a model that represents this shallow layer rather than allowing thick or transcrustal units.

Inverse modelling is routinely applied in both two and three dimensions for a range of geophysical data. This study used the commercially available UBC-GIF inversion package GRAV3D (Li and Oldenburg, 1996; Li and Oldenburg, 1998). The inversion method implemented in GRAV3D permits a single density value for each cell and allows the smoothness with which modelled densities vary from cell to cell to be specified by a user-defined smoothness parameter. It also includes a customisable depth-weighting function that governs the depth and vertical extent of bodies. The software does not provide an estimate of the uncertainty in the model; however statistical analysis may be used to determine a level of confidence in the final model. The complexity of the inverse problem means that resultant models are highly simplified and cannot be expected to represent finely nuanced geological detail.

Since a "forward" computation of the modelled response is made with each iteration, inversion models are subject to the same limitations as forward models. Additionally, as inversion is a form of minimisation it is possible that an acceptable solution may simply represent a local minimum in the misfit function, and that a better fit may be obtained with a different model that may represent the global minimum. Due to the computational intensity of the inversion process there is also an inevitable trade-off between available computing power and desired model size and detail. Finally, and perhaps most significantly, the final result is strongly dependent on the parameters chosen and constraints applied when setting up the inversion process. For this reason, the plausibility of the final model is closely linked to the properties and specifications delineated in the starting model.

**Multiscale edges**
Multiscale edges, or "worms", have recently been developed to derive from potential-field data additional information on the 3D orientation (dip) of geological contacts and other planar features (Hornby et al., 1999; Boschetti et al., 2000). The dip of a structure is investigated by computing the loci of the maximum horizontal gradient on a series of upward continued data layers.

The approach is based on two key assumptions. Firstly, that the maximum horizontal gradient in potential-field anomalies indicates a boundary between underlying units of differing physical properties; and, secondly, that upward continued levels of data tend to be influenced by geological structure at increasing depth. This relationship between upward-continuation level and depth is not a direct one, however, so care must be taken when using worms to interpret depth information. Bearing in mind this cautionary note, worms can provide guidance on the location and approximate orientation of geological contacts as a starting point for forward and inverse modelling.

## Specific data sets

### Norseman-Wiluna gravity worms

Grided Bouguer-anomaly gravity data for the EYC were obtained from Geoscience Australia's online Geophysical Archive Data Delivery System (http://www.geoscience.gov.au/gadds). This grid used a standard 800 m cell size and was derived from a number of publicly available data sets in the region, in which original data-point separations ranged from hundreds of metres to 10 km.

Using these data, worms were computed for a series of upward continued layers to a height of 65 km. Examples of these worms are shown in Figure 2-12 overlain on the greyscale Bouguer gravity anomaly. They give initial information on the regional orientation of boundaries between structural units possessing different densities. In conjunction with gravity and magnetic anomaly images, these regional worms have provided initial indications of the orientation of contacts in preliminary interpretations. They are represented by the Gocad object worms_nws_new_ah_group.gp in the 3D map.
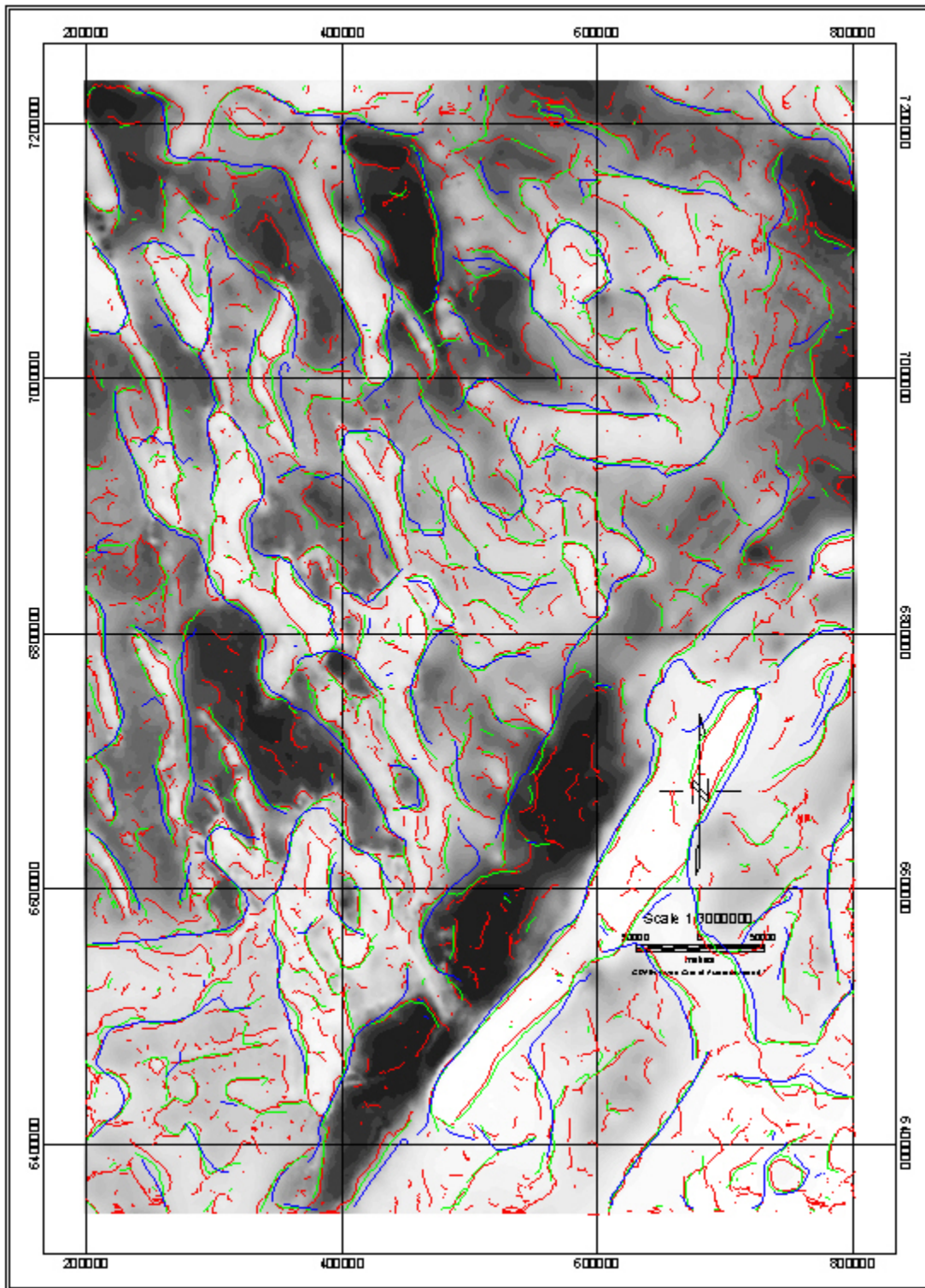
**Figure 2-12: Regional gravity worms obtained from upward continued layers at 5264 (red), 11541 (green) and 21627 m (blue).**

### Norseman-Wiluna magnetic worms

A set of worms has also been obtained using magnetic-field data spanning the EYC. These worms were derived from a 250 m-cell total-intensity grid upward continued to 10884 m. They provide initial information on the regional orientation of boundaries between structural units possessing different magnetic properties. Figure 2-13

displays these worms and exemplifies their capacity to delineate broad magnetic structure.
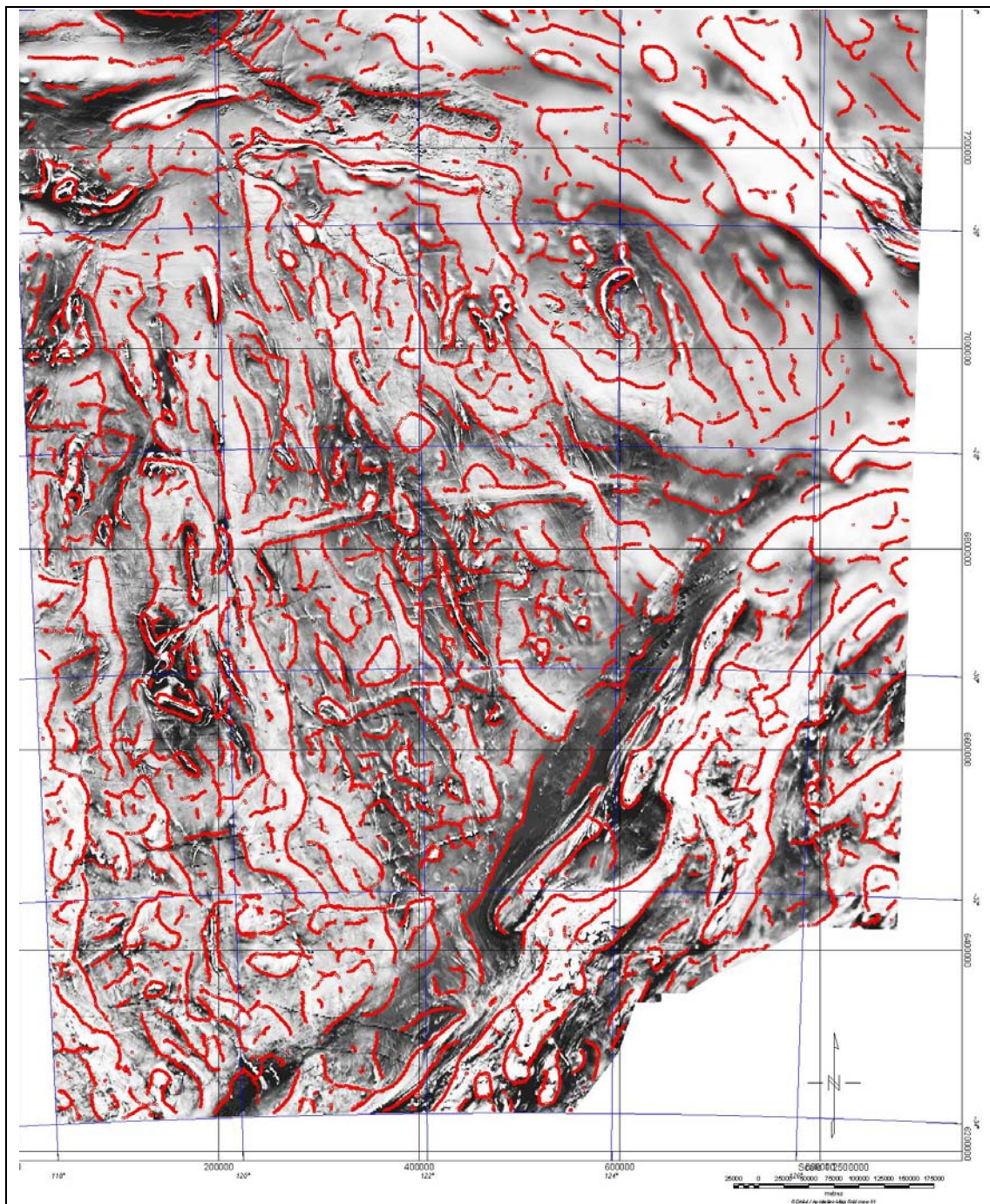


**Figure 2-13: Regional magnetic worms for an upward continued layer of 10884 m, overlain on original TMI data.**

## Norseman-Wiluna 2.5D gravity forward modelling

Thirty-six geological cross sections describing the inferred regional relationships between the greenstone, granitic, felsic volcanic, sedimentary and gneissic units that comprise the eastern Yilgarn were used as a starting point for regional forward modelling. These E-W cross sections were prepared at a 20 km spacing and

represented the anticipated geology to a depth of 10 km (for example, see Figure 2-14).
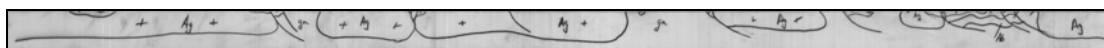


**Figure 2-14: Initial geological cross section used in forward modelling: width 300 km, depth 10 km. NB The vertical exaggeration in this figure is a factor of 10.**

For each section, the boundaries of lithological units were digitised and subsequently represented as polygons in the forward-modelling software (ModelVision). Each polygon was then assigned a density characteristic of its represented lithology, shown in Table 2-2. These density data were based on a geophysical study of greenstones in the Kambalda-Widgiemooltha area of the province (House et al., 1999) and have also formed the basis for modelling described in other studies (Bell, 2002).

| Lithology | Density $g/cm^3$ |
|---|---|
| Granitoid | 2.65 |
| Gneiss | 2.65 |
| Sedimentary | 2.70 |
| Felsic volcanic | 2.74 |
| Mafic/ultramafic | 2.90 |
| Background | 2.71 |

**Table 2-2: EYC lithological densities (House et al., 1999).**

The particular goal of this exercise was to model the greenstone sequences, especially their depth and relationship with granitic intrusions. Prior to modelling, a regional field estimated to represent the response of geological features not pertinent to this goal was subtracted from the data. Since greenstone sequences tend to possess a horizontal spatial wavelength of less than 100 km this regional field was derived by applying a low-pass filter with a cut-off wavelength of 140 km to the observed anomaly.

The 800 m grided Bouguer anomaly gravity data for the EYC was used for this modelling. The non-uniform spacing of the original data points (ranging from hundreds of metres to 10 km) means that lithological features of limited horizontal extent may not be represented in the grided gravity data in areas with relatively sparse data coverage.

Using the digitised geological sections as a starting point the dimensions of polygons, and their contacts with adjacent polygons, were adjusted to improve the agreement between the modelled and observed gravity data. No adjustment of assigned physical properties was made to the polygons. Figure 2-15 shows an example of a modelled cross section, and the complete set of thirty-six sections is shown in Figure 2-16. These cross sections are represented by the Gocad object regional_xsection_01_to_36_group.gp in the 3D map. Appendix 2-7 contains the full set of ModelVision files used to constrain the cross sections.
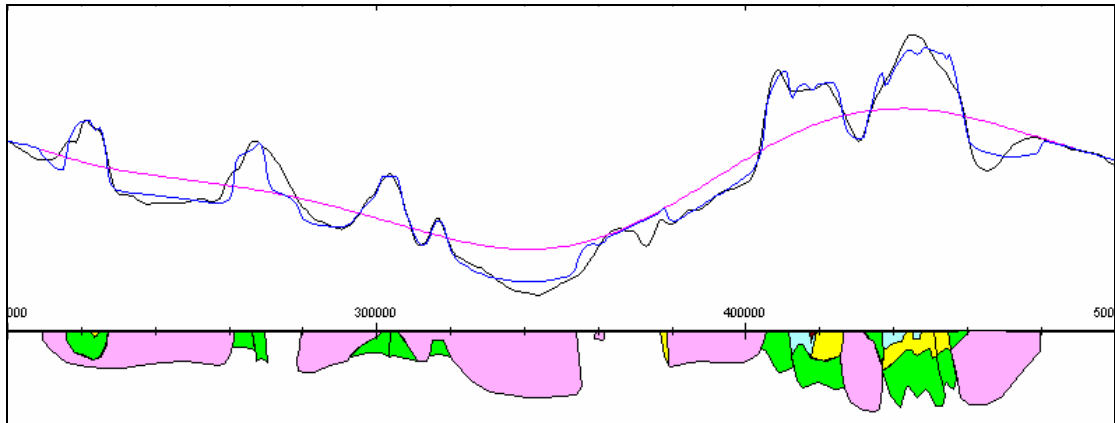
**Figure 2-15: The digitised geological cross section and associated modelled (blue), observed (black) and regional (pink) gravtiy anomalies.**



Azimuth:333 Inclination:22
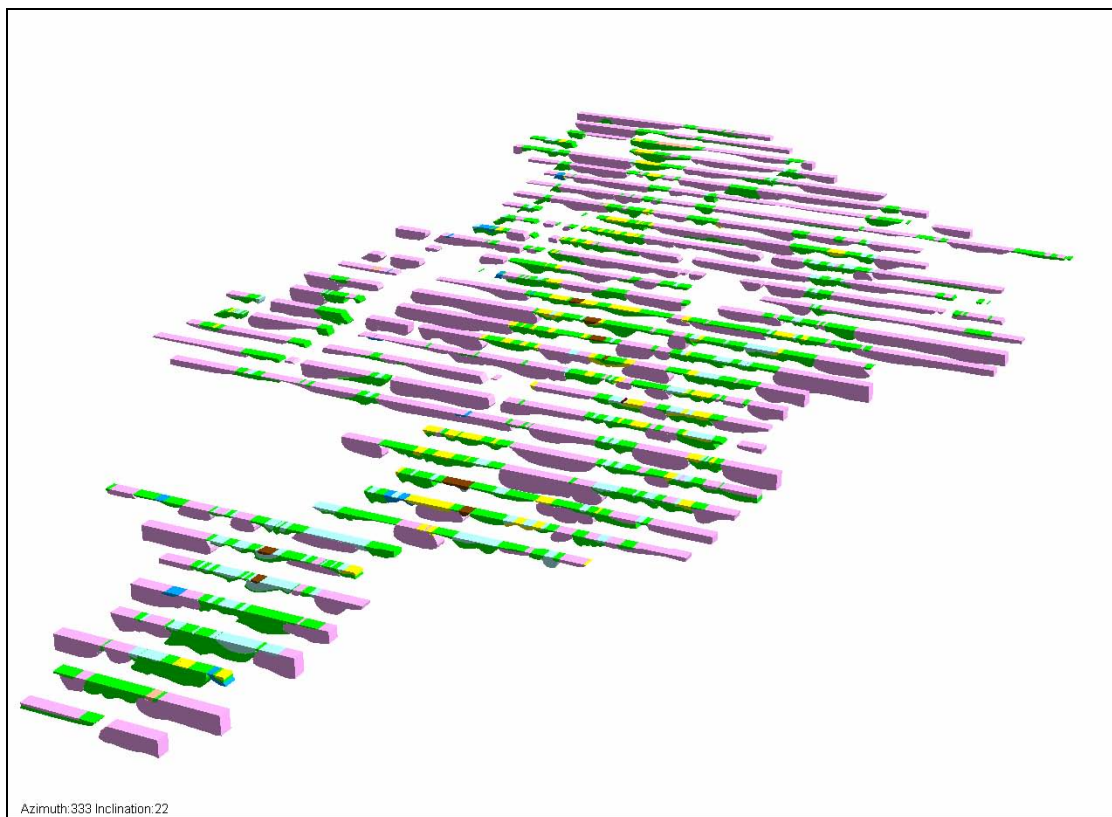
**Figure 2-16: 3D perspective view of the thirty-six modelled E-W cross sections, each spaced 20 km in a N-S direction (see Appendix 2-7).**

### Norseman-Wiluna 3D gravity inverse modelling

Inversion modelling was used to characterise the 3D geometries of major lithologies and structures in the EYC (Barlow, 2004a; see Appendix 2, **Barlow2004a_3D_NW_inversion.pdf**). The model was represented by a 550×300×15 km mesh comprising 625140 cells of 2×2×1 km. In this method, lithological units are represented by a collection of cells possessing the same physical property.

The initial application of this technique involved an unconstrained inversion of the observed Bouguer gravity anomaly and resulted in geometries that did not honour the surface geology or resemble realistic geology at depth. Consequently, an improved starting model with realistic geological and geometrical constraints was developed; it included key lithological elements, expected physical properties and unit thicknesses and orientations, derived from known surface geology, seismic data and potential-field forward modelling.

Two significant constraints were applied. The first was that the density distribution of surface cells was governed by the known outcrop geology. As shown in Figure 2-17 the locations of outcropping greenstone and granite were extracted from the geology coverage of the 2D GIS and used to assign densities to the uppermost cells of the initial model. The densities of cells below the surface layer were not prescribed. By adding surface constraints to the starting model a simple distinction could be made between outcropping granite and greenstone units.

After several iterations using only surface constraints it became apparent that the gross geometry of these units needed to be modified by applying a depth constraint which forced the inversion to spread laterally rather than vertically, to resemble a laterally extensive flood basalt sheet. Hence, the second constraint, based on seismic reflection data and potential-field forward modelling, was that the thickness of the high-density greenstones was limited to around 4 km. This constraint was imposed by setting the depth-weighting function to produce bodies that spread laterally rather than vertically.

The current inversion model has been constrained using the surface distribution of two lithologies, granite and greenstone. This is a preliminary model of subsurface geometries due to the gross simplification of the units, and was developed as a first pass to constrain the geometries laterally. Through this work a greater understanding of the inversion process has been gained. Based on this experience, it should be emphasised that a totally unconstrained inversion model of either magnetic or gravity data will bear little resemblance to the true geology and should be treated with caution.
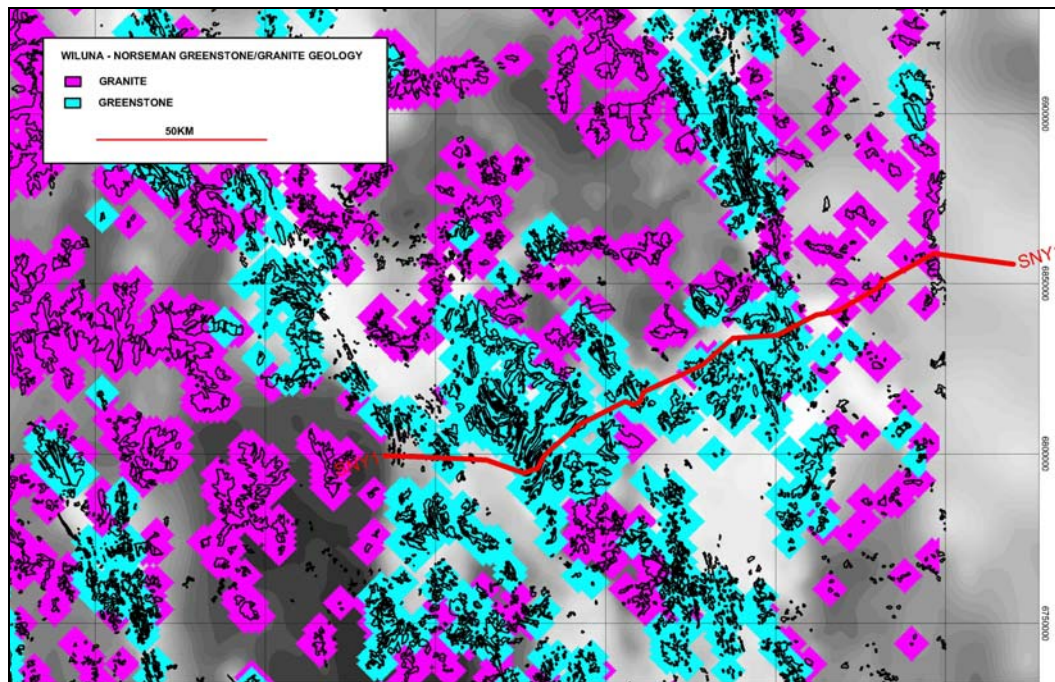
**Figure 2-17: The digitised locations of high-density greenstone (green) and low-density granite (purple), overlain on the greyscale Bouger gravity anomaly.**

Figure 2-18 shows the initial model, in which cells representing the high-density greenstone are shown in red and the low-density granites in dark blue. The final model produced by the inversion process is shown in Figure 2-19. Its surface density distribution is well defined, as anticipated, and it possesses laterally extensive high-density features representing greenstone sequences. Some of the suggested higher densities evident below the greenstone units result from the model constraint that density values vary smoothly from cell to cell. Hence the transition from the high-density surface units to the modelled low-density structures at depth may be more abrupt than suggested in Figure 2-19.

The data from this modelling exercise are represented in the 3D map by the Gocad objects invers_grav_02.ts to invers_grav_05.ts.

63
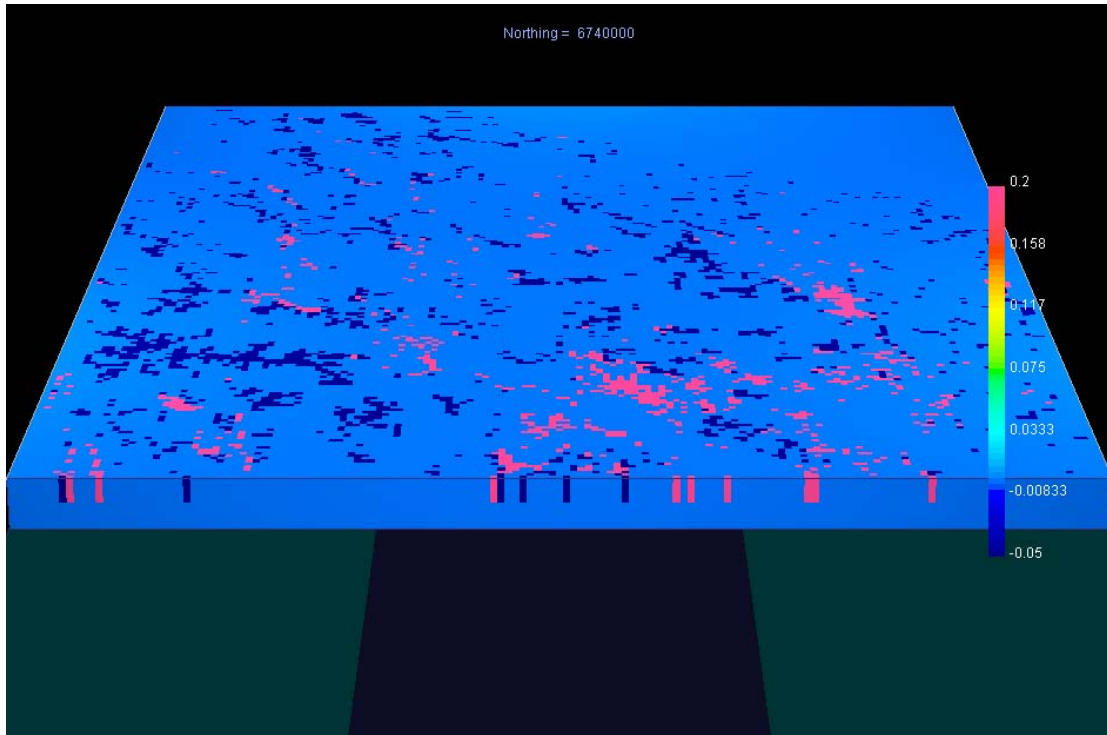
**Figure 2-18: The initial model used for the inversion process. The coloured scale bar describes the contrast from a background density value of 2.6 g/cm$^3$ (see Barlow 2004a).**
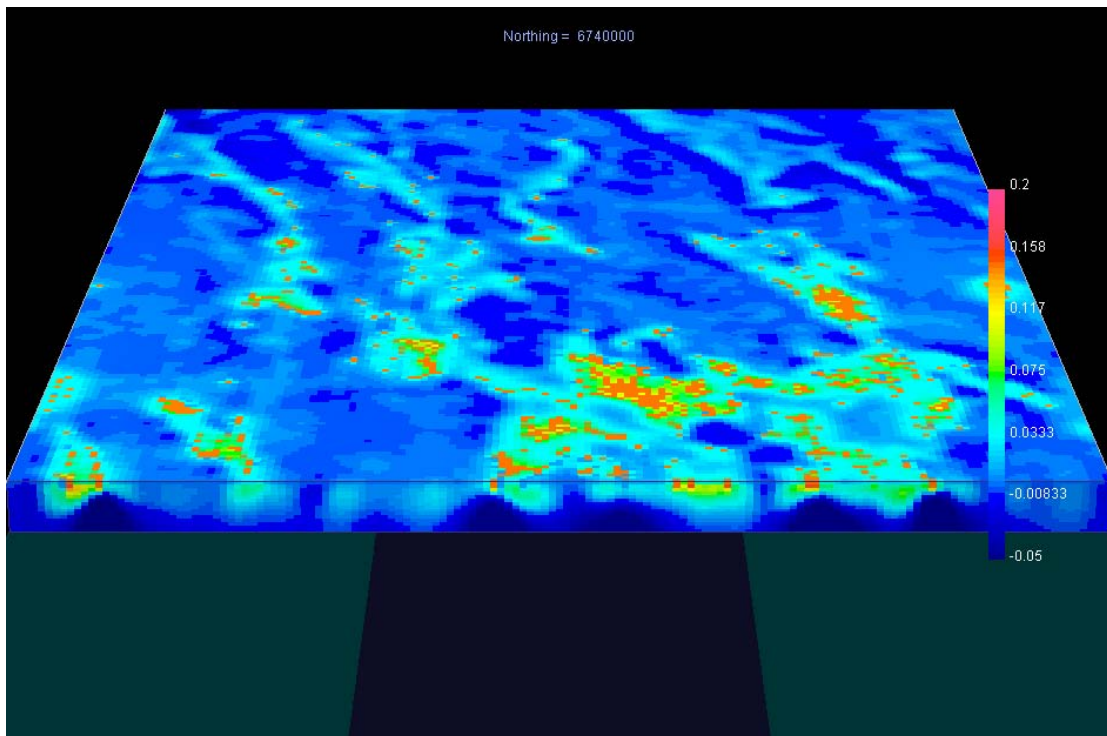


**Figure 2-19: The final inversion model representing the relationships between greenstones (+0.2 g/cm$^3$) and granites (-0.1 g/cm$^3$), sliced E-W at 6740000mN (see Barlow, 2004a).**

### Leonora–Laverton 2.5D gravity forward modelling

Forward modelling of gravity data in the Leonora-Laverton area employed nine east-west cross sections spaced 20 km apart and representing anticipated structure to a

depth of 15 km (Bell, 2002). The initial representation of these sections was based on interpretation of magnetic, gravity, seismic, and surface geology data previously collected in the area. Figure 2-20 shows an example of one of the nine modelled sections, and indicates the increased level of detail over and above that contained in the regional modelling shown in Figure 2-15.
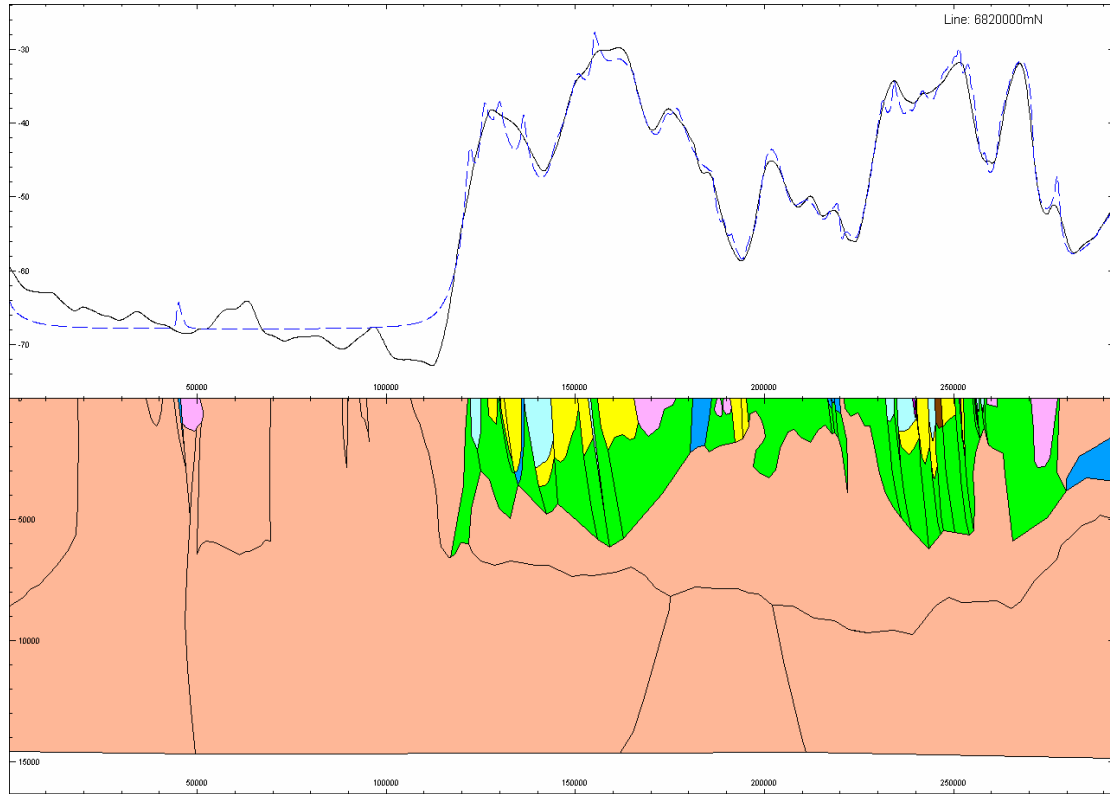


**Figure 2-20: Leonora-Laverton gravity forward modelling cross section. The observed anomaly is shown in black and the modelled anomaly in blue.**

### Rason 2.5D gravity forward modelling

In the Rason area, gravity forward modelling was performed using six 10 km-deep east-west cross sections spaced 20 km apart. As with previous forward-modelling exercises the initial sections were developed using an understanding of the geology inferred from available magnetic, seismic, and surface geology data. Figure 2-21 shows an example of one of the modelled cross sections.
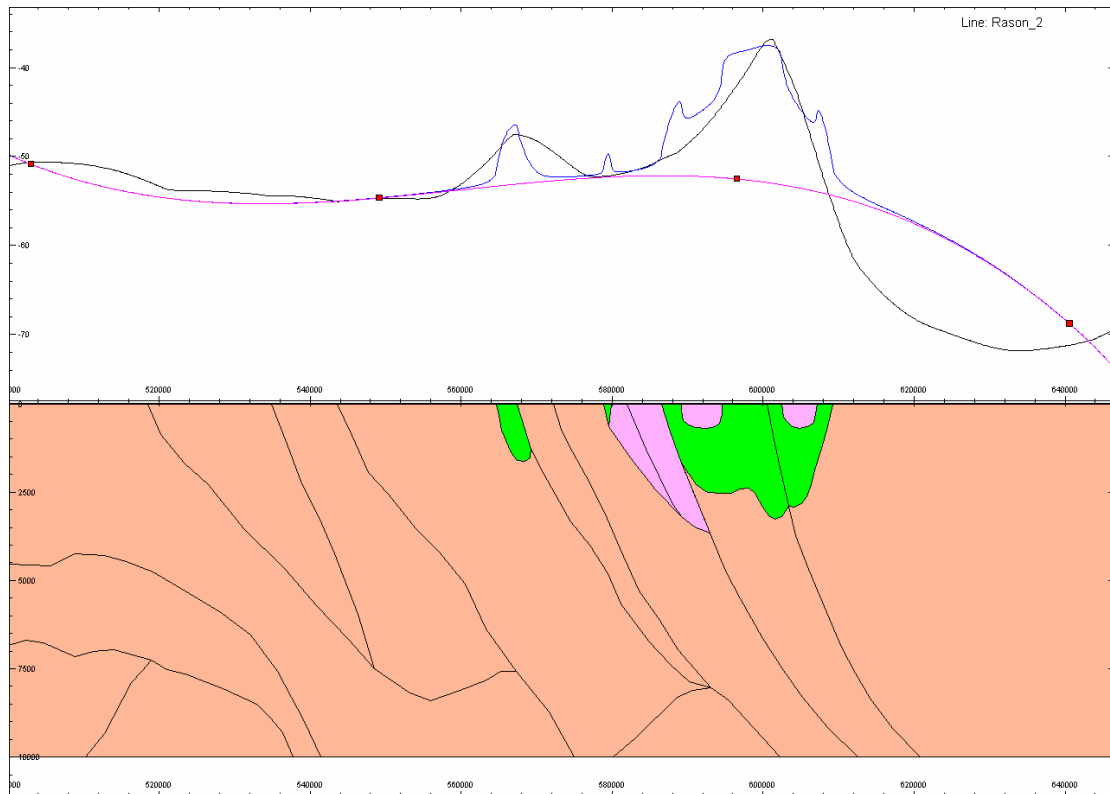
**Figure 2-21: Rason gravity forward modelling cross section. The observed anomaly is shown in black, the modelled anomaly in blue, and the regional field in pink.**

## Kalgoorlie-Kambalda 2.5D gravity forward modelling

In the Kalgoorlie-Kambalda area fifteen closely spaced and variably oriented cross sections were modelled to a depth of 5 km. These sections were oriented to cross cut the major lithological features in the area and to provide a densely packed 2.5D picture which lent itself to 3D interpretation. Figure 2-22 shows an example of one of the fifteen cross sections modelled in the Kalgoorlie-Kambalda area. These cross sections are represented in the 3D map by the Gocad object kal_sections_01_15_group.gp.
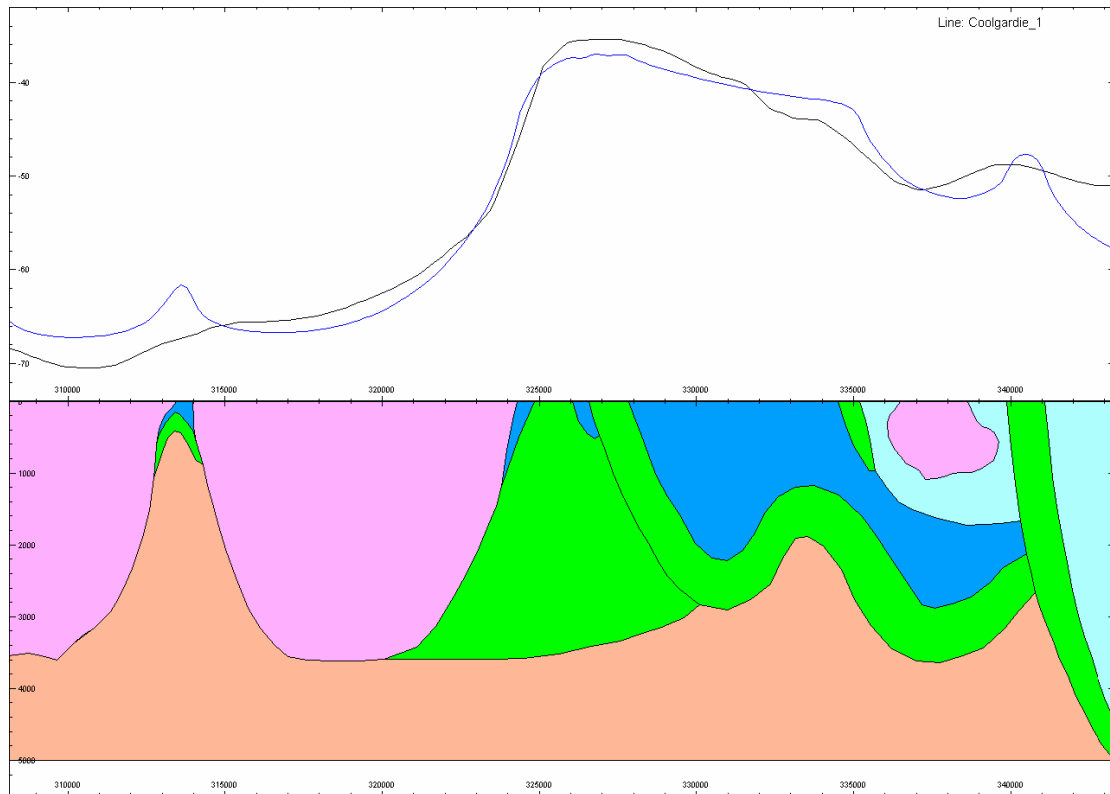
**Figure 2-22: Kalgoorlie-Kambalda gravity forward modelling cross section. The observed anomaly is shown in black and the modelled anomaly in blue.**

### NY1 seismic line 2.5D gravity forward modelling

The 01AGSNY1 line was a deep-reflection seismic traverse acquired in the north Yilgarn in 2001 (Jones et al., 2002). The line commenced at Leonora, passed Laverton and terminated at Lake Yeo, and comprised a total of 384 km of data. Figure 2-17 indicates the location of 01AGSNY1. Chapter 3 contains the full interpretation of this and other seismic lines acquired in 2001.

2.5D forward modelling of two subsections of the line, using both magnetic and gravity data, was carried out to support geological interpretation of the seismic data. Figure 2-23 shows the modelling of 100 km of the western section of the line. The interpretation of this line is represented in Gocad as the object seismic_leon_interp_ny1_11_03_group.gp.

67
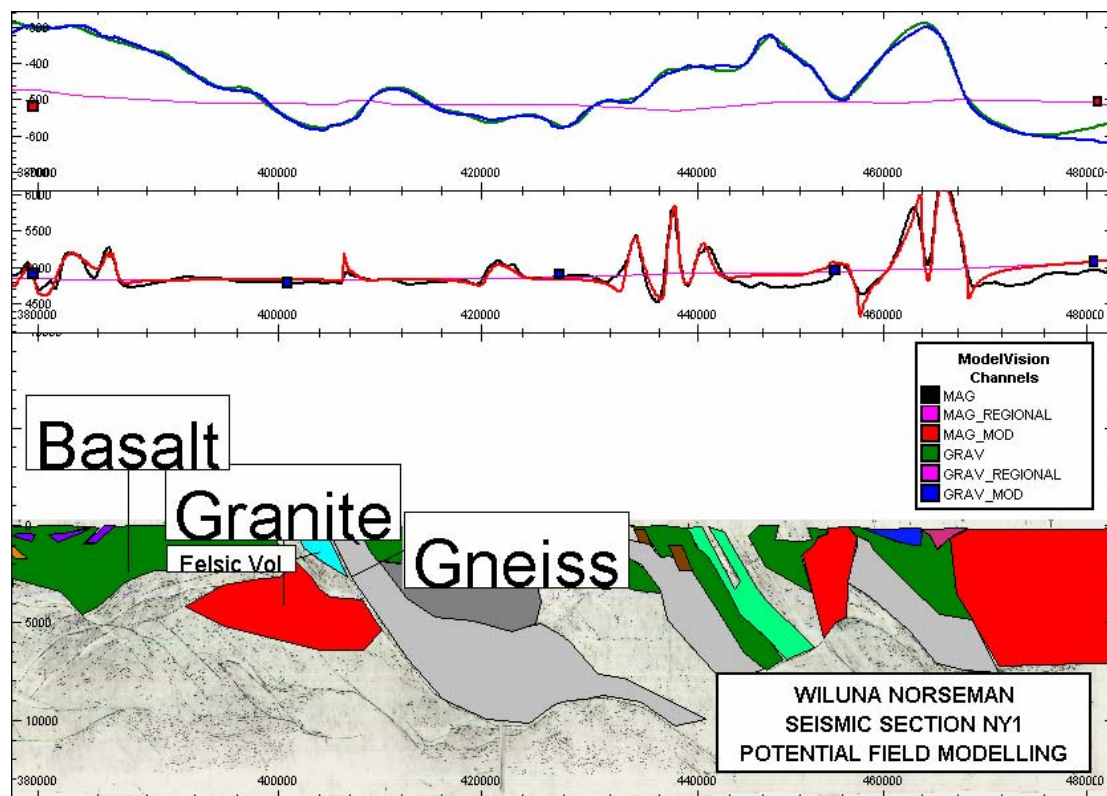
**Figure 2-23: Eastern portion of 01AGSNY1 seismic line, gravity and magnetics forward modelling cross section.**

### Minerie 3D gravity inverse modelling

A petrophysical study of the Minerie 1:100 000 map sheet area, conducted by Dr Bruce Groenewald of the Geological Survey of Western Australia, formed the basis of this modelling exercise. The systematic sampling of over 300 sites produced extensive information on the spatial variability of petrophysical parameters and provided invaluable data for constraining a detailed gravity inversion model.

Figure 2-24 shows the final model produced by this process, and Figure 2-25 compares a slice through the model with the forward modelled NY1 seismic line. The inversion result was a close match to the seismic interpretation completed before the inversion process was run. This independent test, yet again, supports the essential architecture defined by the seismic reflection data

Barlow (2004b) concluded that in order to harness the full benefit of the detailed petrophysical data set higher-resolution gravity data than the available 2-km station spacing were needed. Consequently, this modelling exercise did not add substantially to the information already provided by regional inverse modelling. Nevertheless, by using the high-resolution 01AGSNY1 seismic transect and its associated potential-field model (Figure 2-23) new insights have been developed into the value of detailed petrophysics for the purposes of inversion.

In addition to the density measurements used in this gravity modelling, the Minerie petrophysical data set also provides comprehensive susceptibility values over typical rocks encountered in the EYC. The Minerie petrophysical study and associated

inversion modelling are described in detail in Barlow (2004b), see Appendix 2 (**Barlow2004b_3D_Minerie_inversion.pdf**).
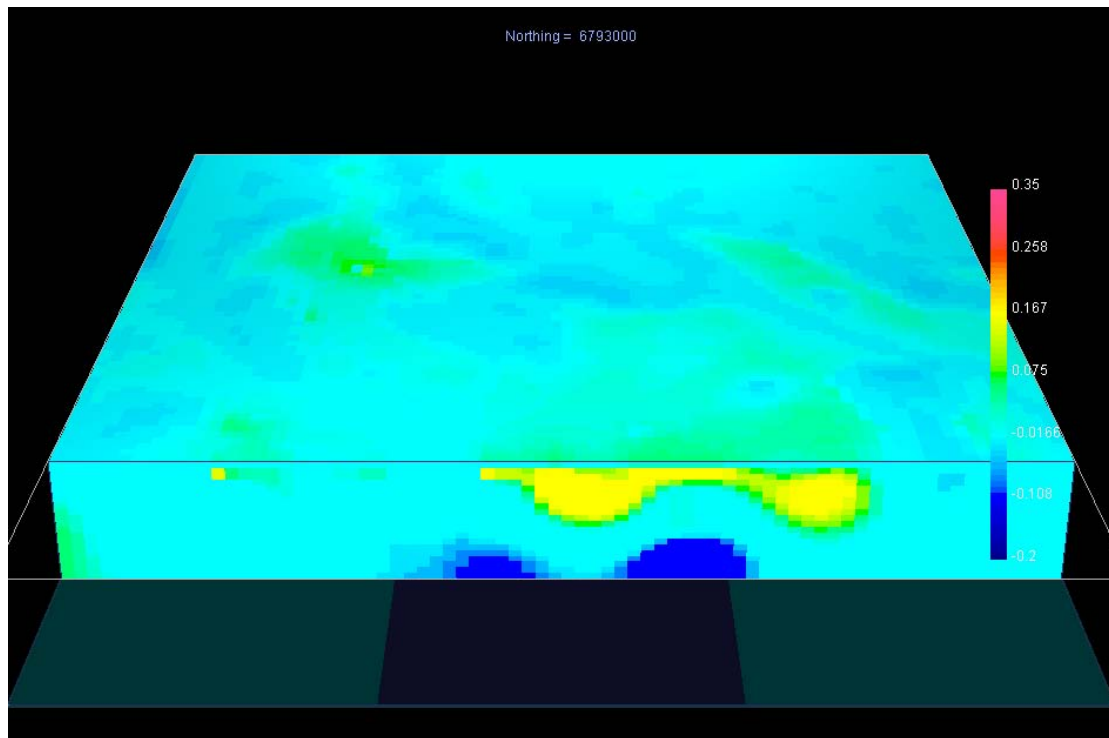


**Figure 2-24: Minerie detailed gravity inversion final model.**
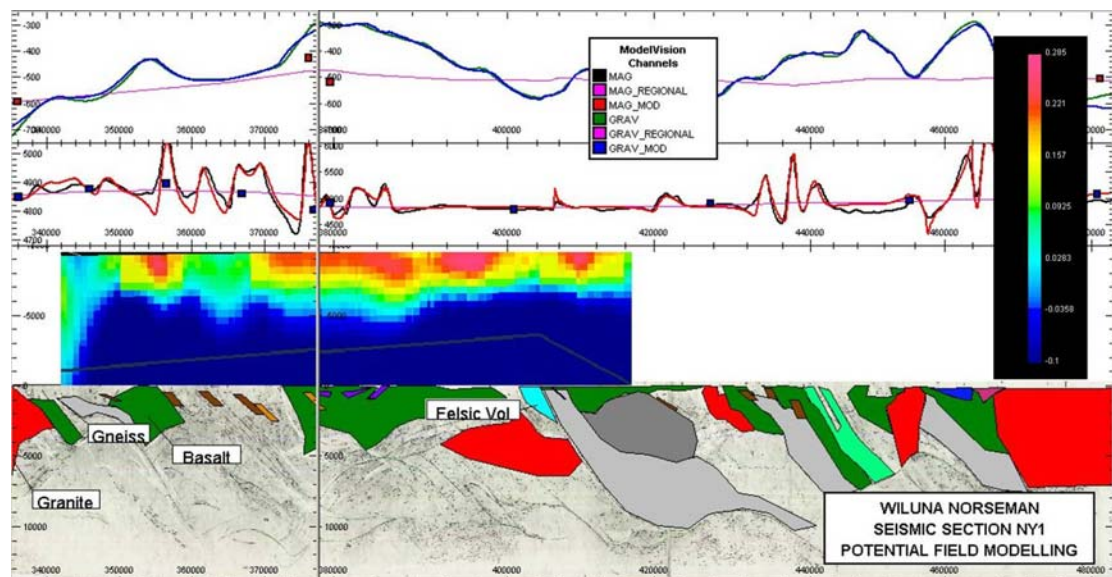


**Figure 2-25: Comparison of the results of forward and inverse modelling of the NY1 seismic line.**

## Kalgoorlie magnetic worms

A set of worms has been obtained using magnetic-field data for the Kalgoorlie area. These worms were derived from a 250 m-cell total-intensity grid upward continued to levels between 250 m and 5411 m. They provide initial information on the orientation of boundaries between structural units possessing different magnetic properties, and were used in initial interpretations of the magnetic structure of the Kalgoorlie area.

69

Figure 2-26 displays the Kalgoorlie magnetic worms for a range of upward continued levels.

A report on the *Distortion Effects of Faults on Gravity "Worm" Strings* was prepared by Robin O'Leary, a Geoscience Australia graduate employee, as part of his training. The work is not part of the *pmd*\*CRC but has relevance to Y2's work and has been included in Appendix 2 (**OLeary_2003_Worm_Evaluation.pdf**).

The task was to determine whether upward continued gravity-anomaly worms can be used as a tool to determine the dip direction of structures known to cross-cut lithologies (i.e. intersect the bedding at an angle) and consequently offset stratigraphy. The question was asked because ambiguous worm dips were noted along the trace of the Zuleika fault zone. The conclusion was that stratigraphy, and especially the dip of the ultramafic layers and their juxtaposition with low-density granites, had a greater impact on the worm orientation than did the fault dip. The Zuleika dips west.
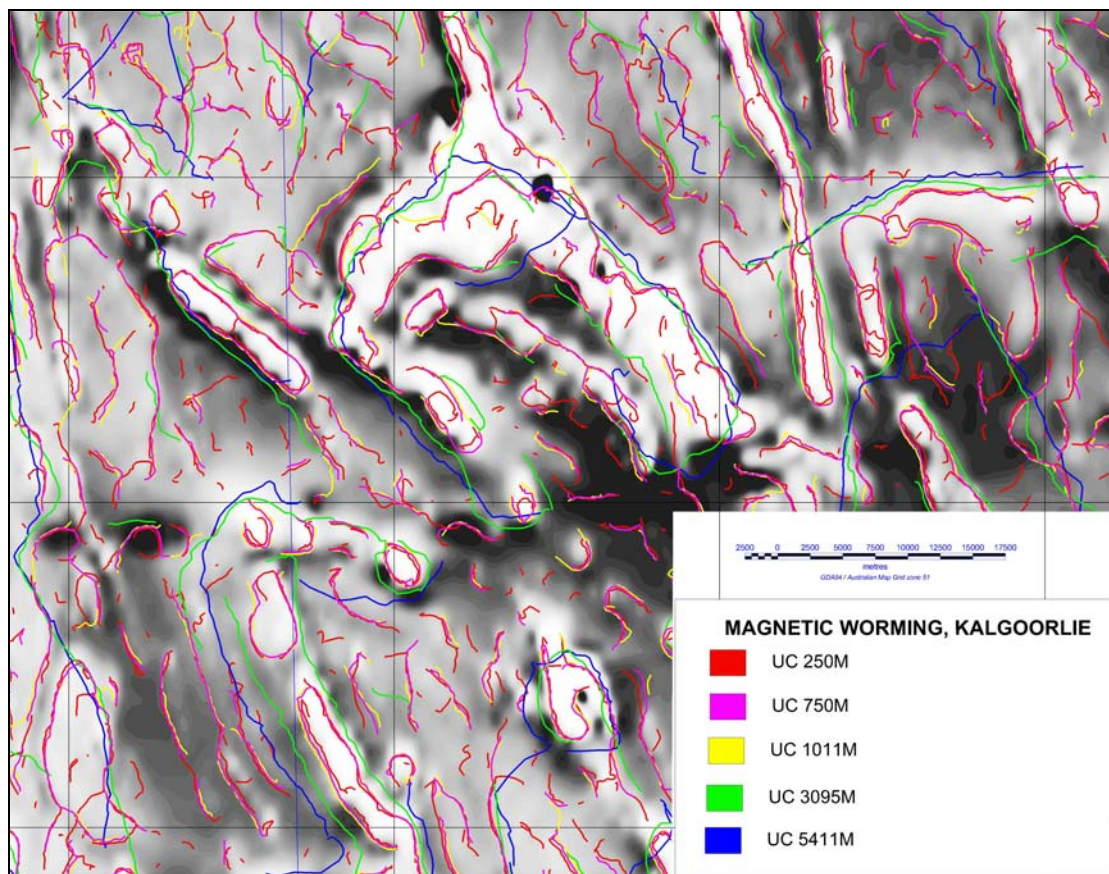


**Figure 2-26: Kalgoorlie worms derived from magnetic data upward continued to 250, 750, 1011, 3095 and 5411 m.**

## 3D joint inversion

As part of Geoscience Australia's assessment of the capabilities of the GeoModeller software package (formerly know as 3D WEG), a joint inversion of gravity and magnetic-field data was carried out for the Kambalda area of the EYC. This inversion was conducted during the closing stages of the Y2 project and, consequently, its very preliminary results have not been incorporated into the 3D map.

However, GeoModeller appears to offer exciting new opportunities for the potential-field modelling of geological structure. Following further development and testing it will be integrated into GA's analysis regime where it is expected to facilitate new insights into the 3D character of the EYC and other Australian provinces. Figure 2-27 is an example of the 3D volumes, representing lithological units, which are produced by GeoModeller.
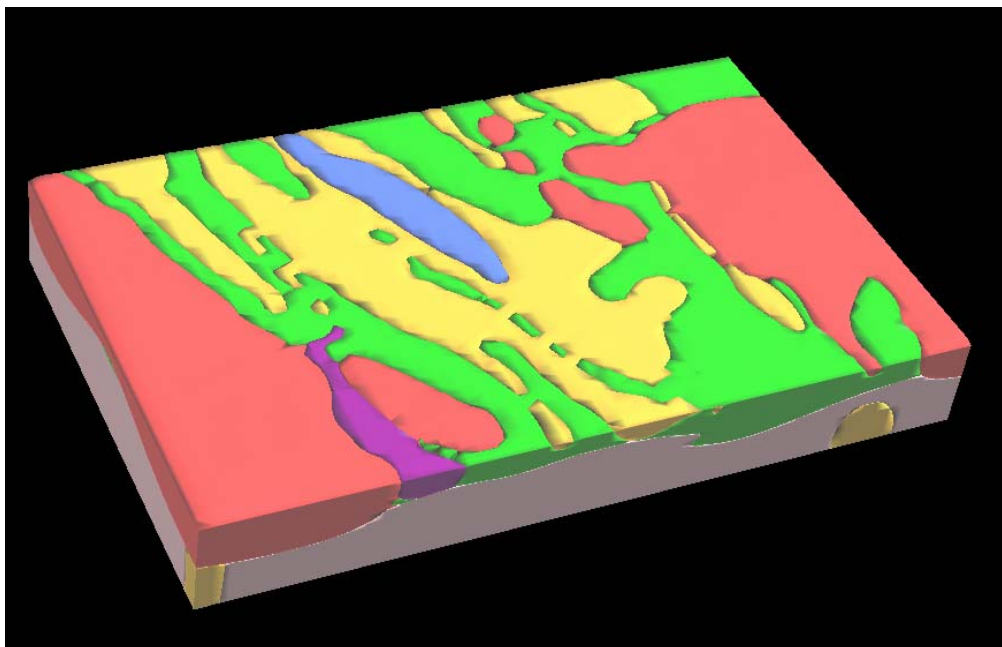


**Figure 2-27: Inversion model of the Kambalda area of the EYC, produced by Geomodeller using a joint inversion of gravity and magnetic-field data.**

## Outcomes from potential-field modelling

Potential-field modelling has improved the understanding of the complex relationship between greenstones and intrusive granitic units in the EYC. This modelling has helped shaped the development of the 3D map described in the previous sections. Specific outcomes of this modelling are described below.

Regional forward modelling has delineated the northwest-trending greenstone sequences prevalent in the eastern Yilgarn and has helped elucidate their structural relationship with felsic volcanic and sedimentary rocks also present in the region (Whitaker et al., 2002). Modelling has helped constrain the depth of the contact between greenstones and underlying granite/gneiss, and supports earlier estimates of greenstone thickness generally in the range <1 to 4 km but up to 6 km in the south of the province (Blewett et al., 2002b). The present modelling suggests a variety of orientations of this contact in addition to the predominantly east-dipping orientation described in Blewett et al. (2002b).

High-level granitic plutons are also evident in the gravity modelling though their thickness is difficult to constrain due to the similarity of their of their density and that of the pervasive underlying gneissic elements in the terrane (Whitaker et al., 2002). Granite thicknesses shown in Figure 2-16 are therefore speculative. Examples of

granites internal to greenstones are also present in the model. The data appear to constrain these features to thin sheets, as described in Blewett et al. (2002b).

The cross sections in Figure 2-16 suggest substantial greenstone thickness variability over short distances. East-west variability is readily observed in the east-west oriented sections, however the 20 km separation between sections means that north-south thickness variability is inadequately mapped over short distances by this forward modelling exercise.

Evidence of the north-south continuity is provided by the 3D inversion model, however, which gives a broad representation of the greenstone/granite geometry and relationships to a depth of 15 km. By correlating the inverted structure with greenstone units modelled in the 2.5D cross sections, the north-south continuity of the sequences can be inferred.

This regional perspective is supplemented by local studies that provide detail on a scale not possible in broader studies.

2.5D forward modelling in the Leonora-Laverton district (Bell, 2002) has provided additional structural information including

- indications of greenstone thickness of approximately 6 km east of the Celia Fault,
- suggestion that the greenstone package west of the Kilkenny shear zone thickens from about 3 km in the south to perhaps 8 km in the north,
- the Raeside Batholith – greenstone contact dips approximately 40° E,
- in the southern Leonora-Laverton area the Celia Fault dips approximately 35° E, and,
- evidence that some discrete granitoids in the Malcolm and Murrin domains are underlain by greenstones.

Detailed modelling also suggested greenstone thickness of 1 to 4 km in the vicinity of Kalgoorlie-Kambalda; and suggests possible interleaved greenstone/ultramafic sequences up to 4 to 5 km thick. Similarly, modelling in the Rason area suggests a predominantly gneissic geology with evidence of limited emplacements of greenstone and granite between 2 and 3 km thick.

The Minerie detailed inversion exercise adequately modelled the greenstone structure but was impeded in adding significant detail to the regional inversion model due to the relative sparseness of gravity data (2 km station separation). The availability of the detailed petrophysical study in the Minerie area did improve the correlation between the surface physical properties calculated by the inversion, and those attributed to the mapped geology.

## *Implications for predictive mineral discovery*

The integration of geological and geophysical data to construct a 3D map of EYC geology has highlighted the following issues which are pertinent to predictive mineral discovery:

- a good pre-existing understanding of the geology before model-building begins is essential;
- high-quality, high-resolution geophysical data sets are critical;
- developing geological interpretations that are consistent with all available geophysical and geological data is essential;
- when using inverse modelling, a well-constrained starting model is preferable;
- the ability to visualise, integrate and analyse a variety of data in a virtual 3D working environment is invaluable;
- 2D and 3D software packages which have compatible data formats are helpful;
- working in 3D allows the processes and symptoms of a mineral system as it is today to be tracked, and;
- targeting techniques are significantly enhanced through increased insight into the manifestation of mineral system signatures in three dimensions.

## *Appendix 2*

2-1: Metadata for Norseman-Wiluna 3D Map (**includes data**)
2-2: Metadata for Kalgoorlie-Kambalda 3D Map (**includes data**)
2-3: Source of Solid Geology datasets for Norseman-Wiluna (**includes data**)
2-4: Metadata for Seismic Gocad depth (***includes data***)
2-5: Metadata for Seismic Gocad objects (***includes data***)
2-6: Metadata for Model Vision files (***includes data***)
2-7: Directory of 3D map screen snapshots (**jpeg files**)
2-8: GIS data (*not available in this product*)
2-9: Henson, P.A., 2004. *How to build a 3D map: Y2 learnings and development of a workflow process*, PDT meeting, Perth, November 2004 (**Appendix 2_9 Henson 3Dmap methodology.pdf**).
2-10: Barlow, M., 2004a. *Yilgarn constrained gravity inversion. pmd*CRC internal report (**Appendix 2_10 Barlow 2004a 3D Inversion process.pdf**).
2-11: Barlow, M., 2004b. *Density and susceptibility characterisation of the Minerie 100,000 geology sheet: implications for detailed gravity inversion. pmd*CRC internal report (**Appendix 2_11 Barlow 2004b Minerie Inversion Report.pdf**).
2-12: O'Leary, R., 2004. *Distortion Effects of Faults on Gravity "Worm" Strings*. Geoscience Australia internal report
(**Appendix 2_12 O'Leary 2003 worm_evaluation.pdf**).
2-13: Hitchman, A.P., 2004. *Eastern Yilgarn Cratonic architecture: Tests and applications of potential-field forward and inverse modelling*, PDT meeting, Perth, November 2004 (**Appendix 2_13 Hitchman potential field constraints.pdf**)
2-14: Eleven screen snap shots of examples of the Geomodeller joint inversion outputs from Kalgoorlie (**jpeg and tif files**)
2-15: Images from Barlow 2004b report (**bmp and tif files**)
2-16: Database of rock property determinations from Minerie 1:100 000 sheet (**Excel files**)
2-17: A presentation on the early established work flow process may be found in **Appendix 2_17 3D model work flow.ppt.**

## *Appendix 2-1: Metadata for Norseman-Wiluna 3D Map*

*T. Brennan*

     Notes:
- Created with Gocad version 2.0.8
- UTM projection;   MGA Zone 51;   datum GDA94
- ahd - Australian height datum
- kal – data for the Kalgoorlie/Kambalda area
- nws – data for the Norseman-Wiluna area
- datasets with ahd in the name have been projected up to the DEM surface (where 'ahd zero' is used the height of the data is zero)
- The Gocad 'group' objects can be ungrouped into their individual lines, points or surfaces.
- Some common datasets appear in both models.

**nws_chalcophyles**

GA whole rock analyses for nws area. The Gocad properties function can be used to display the different elements.
chalcophyles_pts.vs  -  pointset
chalcophyles_surfaces.ts  -  surface
geochemxyz.xls  -  spreadsheet data

**nws_cross_sections**

cross-section group files - used  to constrain the model surfaces
kal_xsections_01_to_15_group.gp
kal_xsections_10k_revised_group.gp
kam_xsections_01_to_06_revised_group.gp

regional xsection files:  (01_to_36) for nws area
xline files:   these contain the cross-section position lines

**nws_data_source_outlines**    (all in MGA Zone 51)

craton_boundary_zero_ahd.pl - Craton Boundary
province_boundary_zero_ahd.pl - Province boundaries
Proterozoic_boundary_edge_surface.ts - Edge of NWS project area
source_of_data_outlines_zero_ahd.pl – see source of solid geology data.doc
source_of_data_sufaces_group.gp – see source of solid geology data.doc

**nws_dem_surfaces**

dem_nws_2000_surf.ts  -  DEM digital elevation model
    2000m cell size - 131560 points, 262916 triangles
    clipped from GA's 9 second DEM of Australia - version 2
    simplified in Gocad to 8280 points and 16256 triangles.

dem_nws_4000c_surf.ts  -  DEM with 4000m cell size

**nws_deposits**

minloc_nws_deposits_ahd.vs - all deposits from the Minloc database
ozmin_nws_all_deposits_ahd.vs - all deposits from the Ozmin database
ozmin_nws_au_deposits_ahd.vs - gold deposits only from the Ozmin database

**nws_faults_lines**

fltsys_nws_ahd.pl – all lines coded as a major fault system (from solgeol dataset)

**nws_faults_surfaces**

a_Proterozoic_boundary_edge_surface.ts – boundary surface of regional dataset
fault_surfaces_nws_group.gp - major fault surfaces and boundary surface (grouped)

individual fault surfaces:-
flt_Bardoc_nws.ts
flt_Celia_nws.ts
flt_Emu_nws.ts
flt_Erawalla_nws.ts
flt_Hootanui_nws.ts
flt_Ida_nws.ts
flt_Ida_nws_original.ts
flt_Kilkenny_nws.ts
flt_Kunanalling_nws.ts
flt_Laverton_nws.ts
flt_MtMcClure_nws.ts
flt_Ockerburry_nws.ts
flt_Perseverance_nws.ts
flt_Turnback_nws.ts
flt_Waroonga_nws.ts
flt_Yamana_nws.ts

**nws_geochem**

carbonatites_yilgarn.vs - point locations from GA Ozrox database
kimberlites_yilgarn.vs - point locations from GA Ozrox database
lamprophyres_yilgarn.vs - point locations from GA Ozrox database

sm_nd_points_yilgarn.vs - point locations from GA Ochem database

yilgarn_sm_nd_surface_1.ts – Yilgarn surface of sm-nd model age
yilgarn_sm_nd_surface_2.ts – Yilgarn surface of sm-nd model age

P482 data displayed as voxets:-
yilgarn_granite_hfse_image.vo
yilgarn_granite_hfse_image_granite_hfse@@  - data
yilgarn_granite_high_ca_image.vo
yilgarn_granite_high_ca_image_granite_high_ca@@  - data
yilgarn_granite_low_ca_image.vo
yilgarn_granite_low_ca_image_granite_low_ca@@  - data

yilgarn_granite_mafic_image.vo
yilgarn_granite_mafic_image_granite_mafic_0@@  - data
yilgarn_granite_syenite_image.vo
yilgarn_granite_syenite_image_granite_syenite@@  - data

**nws_gravity_inversion**

invers_grav_05_1000.ts – final isosurface of gravity inversion

summary of gravity inversion process.doc

**nws_greenstone_base**

greenstone_base_nws.ts   –   regional base of greenstone
   created from serial cross-sections and constrained by the regional gravity inversion
   surface and seismic reflection data
greenstone_base_kal_part_of_regional_surf.ts   -   Kalgoorlie part of base
greenstone_base_xsect_lines_nws.pl   –   cross-section lines used to construct the surface
outlines_of_granites_nws.pl   –   outlines used to constrain base of greenstone surface

**nws_low_angle_shear_surfaces**

Low angle shear zones (detachment), interpreted surfaces from seismic reflection data:-
faults_lash_surfaces_group.gp -  all lash surfaces grouped together
Lower_lash_surface_1.ts
Lower_lash_surface_2.ts
Lower_lash_surface_3.ts
Lower_lash_surface_4.ts
Lower_lash_surface_5.ts
Upper_lash_surface.ts

**nws_map_sheet_index**

map_sheet_index_100k.pl – for nws project area
map_sheet_index_250k.pl – for nws project area

**nws_seismic_interp**

seismic lines – K1,K2,K3,K4 Y1,Y2,Y3,Y4,Y5
 seismic_kal_interp_by_line_group.gp
 seismic_kal_interp_by_type_group.gp

seismic line EGF01
 seismic_kal_interp_egf01_group.gp

seismic line NY1
  seismic_leon_interp_ny1_11_03_group.gp

**nws_solid_geology_lines**

 granite_high_ca.pl – polyline of High-Ca granite (from P482)
 granite_low_ca.pl – polyline of Low-Ca granite (from P482)
 granite_mafic.pl – polyline of Mafic granite (from P482)
 granite_syenite.pl – polyline of Syenitic granite (from P482)

 solg_kal_kam_all_ahd.pl  - solid geology,  full version (Kalgoorlie area)
 solg_kal_kam_simp_ahd.pl  -  solid geology,  simplified version (Kalgoorlie area)

 solg_nws_all_lines_zero.pl  -  solid geology,  full version (nws area)
 solg_nws_simp_lines_zero.pl  -  solid geology,  simplified version (nws area)

**nws_tomography**

 nws_moho_surf.ts - Base of crust (Moho) surface for Norseman-Wiluna
 receiver_functions.vs -
 refraction_moho_pics.vs – Estimate of Base of crust (Moho) from seismic refraction
 data

**nws_topo**

 roads_nws.pl - main connecting roads
 towns_nws_pointset_group.gp - main towns

**nws_worms**

 worms_nws_new_ah_group.gp  -  gravity vector worms
   maximum upward continued level: 65km
   source: GA's Bouger gravity anomaly 800m grid, worms processed by GA

**yilgarn_granite_surfaces**

 data from AMIRA granites project  -  (all data in UTM, MGA Zone 51)
 granite_hfse_image.vs – 2 bit tiff image of 'hfse' granite distribution as coloured
 polygons
 granite_high_ca_image.vs - 2 bit tiff image of 'high_ca' granite distribution as
 coloured
   polygons
 granite_low_ca_image.vs - 2 bit tiff image of 'low_ca' granite distribution as
 coloured
   polygons
 granite_mafic_image.vs - 2 bit tiff image of 'mafic' granite distribution as coloured
   polygons
 granite_syenite_image.vs - 2 bit tiff image of 'syenite' granite distribution as
 coloured
   polygons

## Appendix 2-2: Metadata for Kalgoorlie-Kambalda 3D Map

*T. Brennan*

Notes:
- Created with Gocad version 2.0.8
- UTM projection;   MGA Zone 51;   datum GDA94
- ahd - Australian height datum
- kal – data for the Kalgoorlie/Kambalda area
- nws – data for the Norseman-Wiluna area
- datasets with ahd in the name have been projected up to the DEM surface (where 'ahd zero' is used the height of the data is zero)
- The Gocad 'group' objects can be ungrouped into their individual lines, points or surfaces.
- Some common datasets appear in both models.

**kal_alteration_data**

polygons created from pmd*CRC Y3 project data around Kanowna Belle (2003)
alkali_fspar_domains.ts
wavelengths_high_ALOH_surf.ts – Aluminium hydroxide
wavelengths_low_ALOH_surf.ts – Aluminium hydroxide

**kal_cross_sections**

cross-section group files - used  to constrain the model surfaces
kal_xsections_01_to_15_group.gp
kal_xsections_10k_revised_group.gp
kam_xsections_01_to_06_group.gp
kam_xsections_01_to_06_revised_group.gp

regional xsection files:  (01_to_36) for nws area

xline files:   these contain the cross-section position lines

**kal_data_source_outlines**

model_full_edge_surface.ts
outline_granite_interp_zero.pl
outline_leon_neal_zero.pl
outline_model_area_ahd.pl
outline_nws_solgeol_zero.pl
outline_reliability_diagram_ahd.pl
outline_reliability_diagram_zero.pl
outline_swager_data_zero.pl

source_of_data_surfaces_group.gp  -  see source of solid geology data.doc
source_of_data_outlines_zero_ahd.pl  -  see source of solid geology data.doc

**kal_dem_surface**

dem_final_surface.ts

DEM - digital elevation model; clipped from GA's 9 second grid - DEM of Australia version 2; simplified in Gocad to 8280 points and 16256 triangles

**kal_deposits**

minloc_deposits_kal_ahd.vs – all deposits from the Minloc database
ozmin_kal_au_deposits_ahd.vs – gold deposits from the Ozmin database

**kal_fault_lines**

Named fault lines at DEM surface:-
flt_abattoir_east_top_line.pl
flt_bardoc_top_line.pl
flt_black_flag_top_line.pl
flt_boorara_dc1_top_line.pl
flt_boorara_dc2_top_line.pl
flt_boorara_top_line.pl
flt_boulder_lefroy_top_line.pl
flt_boulder_top_line.pl
flt_dc3_top_line.pl
flt_emu_top_line.pl
flt_ida_top_line.pl
flt_kanowna_dc3_top_line.pl
flt_kanowna_top_line.pl
flt_kunanalling_01_top_line.pl
flt_kunanalling_02_top_line.pl
flt_kunanalling_03_top_line.pl
flt_kunanalling_top_line.pl
flt_lefroy_east_top_line.pl
flt_lefroy_top_line.pl
flt_mthunt_north_top_line.pl
flt_mthunt_south_top_line.pl
flt_ockerburry_top_line.pl
flt_ph1_top_line.pl
flt_ph2_top_line.pl
flt_speedway_top_line.pl
flt_zuleika_01_top_line.pl
flt_zuleika_top_line.pl

faults_all_top_lines.gp – all named faults surface lines (see above), as one group

fltall_ahd.pl – all lines coded as faults (from solgeol dataset)
fltnam_ahd.pl – minor named faults (from solgeol dataset)
fltsys_ahd.pl – all lines coded as a major fault system (from solgeol dataset)

**kal_fault_surfaces**

(Note1: if the file has 'up' in the title it is the upward continued surface above the DEM)
(Note2: all surfaces [where appropriate] intersect the DEM surface)

faults_lower_surfaces_group.gp – all fault surfaces (below DEM) grouped together
faults_upper_surfaces_group.gp – all fault surfaces (above DEM) grouped together

flt_abattoir_east_surf.ts
flt_bardoc_surf.ts
flt_bardoc_up_surf.ts
flt_black_flag_surf.ts
flt_black_flag_surf_deep_old.ts
flt_boorara_dc1_surf.ts
flt_boorara_dc2_surf.ts
flt_boorara_surf.ts
flt_boorara_up_surf.ts
flt_boulder_surf.ts
flt_boulder_up_surf.ts
flt_boulder_up_surf_a.ts
flt_boulder_up_surf_b.ts
flt_bulla_01_surf_yamarny.ts
flt_bulla_02_surf.ts
flt_bulla_03_surf.ts
flt_bulla_04_surf.ts
flt_bulla_surf.ts
flt_dc3_surf.ts
flt_ida_01a_surf.ts
flt_ida_01b_surf.ts
flt_ida_01c_surf.ts
flt_ida_01d_surf.ts
flt_ida_surf.ts
flt_ida_up_surf.ts
flt_kanowna_surf.ts
flt_kunanalling_01_surf.ts
flt_kunanalling_02_surf.ts
flt_kunanalling_03_surf.ts
flt_kunanalling_surf.ts
flt_kunanalling_up_surf.ts
flt_lefroy_east_surf.ts
flt_lefroy_surf.ts
flt_lefroy_up_surf.ts
flt_mthunt_north_surf.ts
flt_mthunt_north_up_surf.ts
flt_mthunt_south_surf.ts
flt_mthunt_south_up_surf.ts
flt_near_ag56.ts
flt_ockerbury_surf.ts
flt_ockerbury_up_surf.ts
flt_ph1_surf.ts
flt_ph2_surf.ts
flt_speedway_surf.ts
flt_speedway_up_surf.ts
flt_zuleika_01_surf.ts
flt_zuleika_surf.ts

flt_zuleika_up_surf.ts

**kal_granite_surfaces**

individual granite surfaces:-
  'ahd' – at DEM surface
  'up' – upward continued
  'base' – below DEM

grouped granite surfaces:-
granite_flat_ahd_surfaces_group.gp – at DEM
granite_lower_surfaces_group.gp – below DEM
granite_upper_surfaces_group.gp – above DEM

**kal_gravity_inversion**

invers_grav_05_1000.ts – final isosurface of gravity inversion

summary of gravity inversion process.doc

**kal_greenstone_surfaces**

Individual base of greenstone surfaces (1 to 14) that have been constrained by
Kalgoorlie-Kambalda cross sections

greenstone_base_kal_part_of_nws.ts – Kalgoorlie part of the nws regional dataset
  constrained by regional cross sections and gravity inversion surfaces

greenstone_base_kal_surfaces_group.gp – all Kalgoorlie base of greenstone
surfaces (1-14)
  constrained by Kalgoorlie-Kambalda cross sections, grouped together

**kal_komatiite**

2 surfaces of one komatiite unit:
auk02_lower_surf.ts
auk02_upper_surf.ts

**kal_late_basin**

latebasin_1_to_10_surf_group.gp
individual late basin surfaces (1 to 10)

**kal_lithology_surfaces**

lith_kurrawang_east_surf.ts
lith_merougil_surf.ts

**kal_low_angle_shear_surfaces**

faults_lash_surfaces_group.gp - 6 low angle shear surfaces grouped together

6 individual low angle shear surfaces (plus a larger regional surface)

**kal_map_sheet_index**

map_sheet_index_100k.pl – for nws project area
map_sheet_index_250k.pl – for nws project area

**kal_metamorphic**

meta_facie_all_classes.vs – metamorphic point data, Mickuki and Roberts (2003)
meta_facie_c0_undefined.vs
meta_facie_c1_unmetamorphosed.vs
meta_facie_c2_lower_greenschist.vs
meta_facie_c3_greenschist.vs
meta_facie_c4_greenschist_amphibolite.vs
meta_facie_c5_lower_amphibolite.vs
meta_facie_c6_mid_amphibolite.vs
meta_facie_c7_upper_amphibolite.vs
meta_facie_c8_granulite.vs
metamorphic_bg_amph_iso.ts – isosurface of blue-green amphibole isograd,
        Mickuki and Roberts (2003)
metamorphic_biotite_iso.ts – isosurface of biotite isograd
        Mickuki and Roberts (2003)
metpet_iso_biotite_lines.pl
metpet_iso_mafic_lines.pl
metpet_key_pelite.vs
metpet_project_area.pl

metamorhpic_binns76_yilgarn_lines.pl

**kal_moho**

moho_kal_surface.ts
receiver_functions.vs
refraction_moho_pics.vs

**kal_seismic_interp**

seismic lines – K1,K2,K3,K4 Y1,Y2,Y3,Y4,Y5
seismic_kal_interp_by_line_group.gp
seismic_kal_interp_by_type_group.gp

seismic line EGF01
    seismic_kal_interp_egf01_group.gp

seismic line NY1
    seismic_leon_interp_ny1_11_03_group.gp

**kal_solid_geology_lines**

selected polygon lines from main solgeol (granite-interp) linework:

granite_high_ca_yilgarn.pl
granite_low_ca_yilgarn.pl
granite_mafic_yilgarn.pl
granite_syenite_yilgarn.pl

main solid geology linework:
solg_kal_kam_all_ahd.pl – detailed version
solg_kal_kam_simp_ahd.pl  – simplified version

**kal_solid_geology_surfaces**

solgeol_a_all_surfaces_group.gp  – all solid geology units (at DEM surface level)
solgeol_ab_surfaces_group.gp  - greenstone
solgeol_af_surfaces_group.gp  – felsic igneous
solgeol_ag_surfaces_group.gp  - granite
solgeol_agn_surfaces_group.gp  – granitoid gneiss
solgeol_ao_surfaces_group.gp  – metagabbro, metadolerite
solgeol_as_surfaces_group.gp  – sedimentary rocks
solgeol_asc_surfaces_group.gp  – polymict conglomerate
solgeol_aslb_surfaces_group.gp  – late basins
solgeol_au_surfaces_group.gp  - ultramafic
solgeol_lp_surfaces_group.gp  - lamprophyre
solgeol_prot_surfaces_group.gp  – proterozoic

**kal_topo**

roads_kal.pl  – main connecting roads
towns_kal_pointset_group.gp  – main towns

roads_nws.pl – main connecting roads (nws area)
towns_nws_pointset_group.gp  – main towns (nws area)

**kal_worms**

grav_worms_kal_new_ah_group.gp
    gravity vector worms - maximum upward continued level: 13km
    source: GA's Bouger gravity anomaly 800m grid; worms processed by GA

## Appendix 2-3: Source of Solid Geology datasets for Norseman-Wiluna

*T.Brennan*
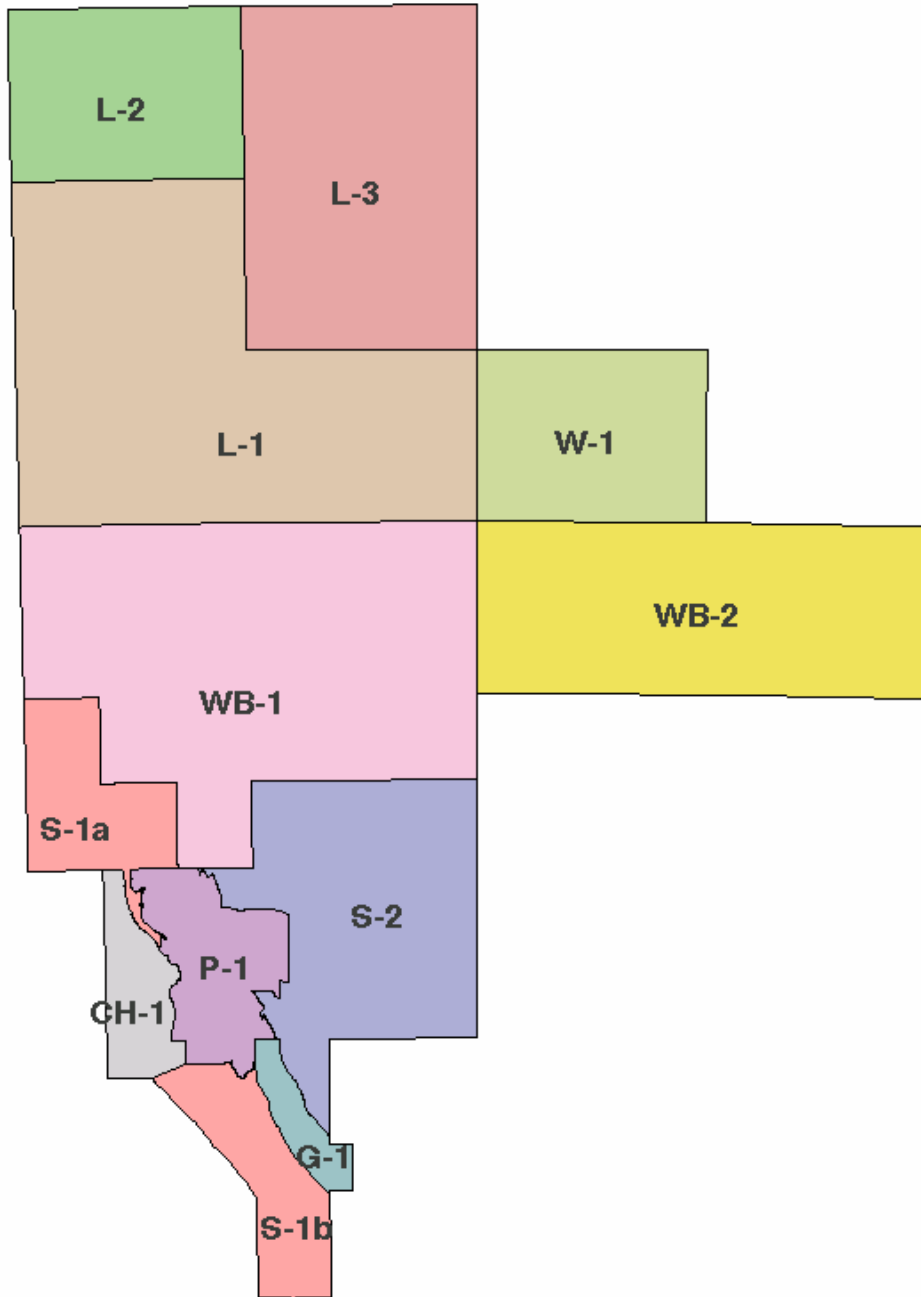


**Map of data sources for the solid geology**

***********************************************************************************

Whitaker, A.J. and Blewett, R.S., 2002. Leonora-Neale transect 1:500 000 solid geology map. Geoscience Australia, Canberra.


**WB-1** - Solid geology interpretation at 1:100 000 scale based on published 1:100 000 and 1:250 000 scale geological maps (first & second editions), GA's 400m line spacing aeromagnetic data, Fugro's 200m line spacing aeromagnetic data, and GA's regional gravity data.

**WB-2** Aeromagnetic interpretation at 1:250 000 scale, greenstone not subdivided, based on published first-edition 1:250 000 scale geological maps, GA's 3000m, 400m, & 200m line spacing aeromagnetic data, and GA's regional gravity data.

***********************************************************************************

Liu, S.F., Stewart, A.J., Farrell, T.R., Whitaker, A.J., and Chen, S.F., 2000. Solid geology of the north-eastern goldfields, Western Australia (1:500 000 scale map). Geoscience Australia, Canberra. With some minor modification by the Y2 project.

**L-1** Detailed interpretation based on published 1:100 000 and 1:2500 000 scale geological maps (first and second editions), GA's 400m line spacing aeromagnetic data, and detailed company 100m line-spacing aeromagnetic data for some areas.

**L-2** Interpretation based on published first-edition 1:250 000 scale geological maps and GA's 400m line spacing aeromagnetic data, mainly to highlight the Yilgarn Craton's margin, the distribution of Proterozoic rocks and the Earaheedy Basin.

**L-3** Very limited interpretation of aeromagnetic data. Also data from Whitaker, A.J. and Bastrakova, I.V. 2002. Yilgarn Craton Aeromagnetic Interpretation 1:1 500 000 scale map. Geoscience Australia

***********************************************************************************

**CH-1** Champion, D.C. and Henson, P.A., unpublished data. Solid geology interpretation at 1:100 000 scale based on published 1:100 000 and 1:250 000 scale geological maps (first and second editions), Fugro 200m line spacing aeromagnetic data (used with permission), and GA's regional gravity data.

**S-1a** , **S-1b**. Swager, C.P, and Griffin, T., 1990 (compilers). Geology of the Archaean Kalgoorlie Terrane, northern and southern sheets. Geological Survey of Western Australia. Interpretation locally modified by current project largely to edge match with more detailed solid geology interpretations.

**P-1**. Placer Dome solid geology interpretation - detailed interpretation based on published 1:100 000 geological maps and detailed company maps at various scales, drill hole information, and detailed company aeromagnetic and gravity data. Interpretation simplified for current project.

**W-1**. Whitaker, A.J. and Bastrakova, I.V. 2002. Yilgarn Craton Aeromagnetic Interpretation 1:1 500 000 scale map. Geoscience Australia.

**S-2**. Swager, C.P., 1994. Geology of the greenstone terranes in the Kurnalpi-Edjudina region, Geol. Survey of Western Australia, Report 47 & accompanying map.

**G-1**. Goldfields Ltd solid geology interpretation - detailed interpretation based on published 1:100 000 geological maps and detailed company maps at various scales, drill hole information, seismic interpretation, and detailed company aeromagnetic and gravity data. Solid geology interpretation simplified for current project.

## *Appendix 2-4: Metadata for Seismic Gocad depth*

*T.Brennan*

    Note:

        all objects created using GOCAD 2.0.8

        unless stated all objects are UTM MGA Zone 51, GDA94

        unless stated all objects are for the entire Yilgarn Craton

        all objects in the zone 50 have been projected as if in zone 51.

**seismic_refraction_data**

        35 objects (data from Geoscience Australia)

        data restricted to the Norseman-Wiluna region

        mig01NY1_18s2_depth.xs – object of seismic section as named

        mig01NY1_pt1_4s2.xs – object of seismic section as named

        mig01NY1_pt2_4s2.xs – object of seismic section as named

        mig01NY2_16s2_depth.xs – object of seismic section as named

        mig01NY2_6s2_depth.xs – object of seismic section as named

        mig01NY3_16s2_depth.xs – object of seismic section as named

        mig01NY3_6s2_depth.xs – object of seismic section as named

        mig01NY4_16s2_depth.xs – object of seismic section as named

        mig01NY4_6s2_depth.xs – object of seismic section as named

        mig91EGF1_20s2_depth.xs – object of seismic section as named

        mig91EGF1pt_6s2_depth.xs – object of seismic section as named

        mig91EGF2_20s2_depth.xs – object of seismic section as named

        mig91EGF2_6s2_depth.xs – object of seismic section as named

        mig91EGF3_20s2_depth.xs – object of seismic section as named

        mig91EGF3_6s2_depth.xs – object of seismic section as named

        mig97K1_5s2_depth.xs – object of seismic section as named

        mig97K2_5s2_depth.xs – object of seismic section as named

        mig97K3_20s2_depth.xs – object of seismic section as named

        mig97K3_6s2_depth.xs – object of seismic section as named

        mig97K4_20s2_depth.xs – object of seismic section as named

        mig97K4_6s2_depth.xs – object of seismic section as named

        mig99Y1_16s2_depth.xs – object of seismic section as named

        mig99Y1_6s2_depth.xs – object of seismic section as named

        mig99Y2_16s2_depth.xs – object of seismic section as named

        mig99Y2_6s2_depth.xs – object of seismic section as named

        mig99Y3_16s2_depth.xs – object of seismic section as named

        mig99Y3_6s2_depth.xs – object of seismic section as named

        mig99Y4_16s2_depth.xs – object of seismic section as named

        mig99Y4_6s2_depth.xs – object of seismic section as named

        mig99Y5_16s2_depth.xs – object of seismic section as named

        mig99Y5_6s2_depth.xs – object of seismic section as named

   **data from Goldfields, St Ives**

        data restricted to the St Ives region

        REV02stives_3s2_depth.xs – object of seismic section as named

        REV02stives_VEL_3s2_depth.xs – object of seismic section as named

        VIC02stives_3s2_depth.xs – object of seismic section as named

        VIC02stives_VEL_3s2_depth.xs – object of seismic section as named

## *Appendix 2-5: Metadata for Seismic Gocad objects*

*T. Brennan*

Note:

all objects created using GOCAD 2.0.8

unless stated all objects are UTM MGA Zone 51, GDA94

unless stated all objects are for the entire Yilgarn Craton

all objects in the zone 50 have been projected as if in zone 51.

**receiver_functions**

13 objects

data from three sources

1) Anya.gp from Reading, Kennett and Dentith, 'Seismic structure of the Yilgarn Craton, Western Australia'
2) Geoff.gp from Clithero thesis and Brian Kennett (RSES, ANU)
3) *pmd*\*CRC and Reading (WP sites) in Reading, Kennett and Goleby, 'The deep seismic structure of Precambrian terranes within the West Australian Craton and implications for crustal formation and evolution', in prep, Precambrian Research.

site locations from both pmd\*CRC work and Brian Kennett (RSES, ANU)

rec_fn_Anya.gp – object containing receiver functions published by Anya Reading

rec_fn_Geoff.gp – object containing receiver functions published by Geoff Clithero

rec_fn_Wpsites.gp – object containing receiver functions from *pmd*\*CRC WP sites

rec_fn_WPsites_VpVs.gp - object containing Vp/Vs ratios from *pmd*\*CRC WP sites

recfn_basestations.vs – object showing location of base station recording sites for receiver function studies

recfn_skippy.vs – object showing location of skippy recording sites for receiver function studies

recfn_wp.vs – object showing location of *pmd*\*CRC WP recording sites for receiver function studies

recfn_wr.vs – object showing location of WR recording sites for receiver function studies

recfn_ws.vs – object showing location of WS recording sites for receiver function studies

recfn_wt.vs – object showing location of WT recording sites for receiver function studies

recfn_wv.vs – object showing location of WV recording sites for receiver function studies

recfn_ww.vs – object showing location of WW recording sites for receiver function studies

recfn_wx.vs – object showing location of WX recording sites for receiver function studies

**seis_surfaces**

1 object

data from receiver function, refraction profiles and seismic reflection sections

moho_surf_yilgarn.ts – depth to Moho surface

**seismic_reflection**

10 objects

data from Geoscience Australia

data restricted to the Norseman-Wiluna region

seismic_locations_Yilgarn.pl – object showing the location of seismic
   reflection traverses within the eastern Yilgarn Craton

seis_egf1_interp_20s.gp – object containing interpretation of central portion of
   1991 seismic traverse EGF01

seis_kcgm_interp_20s.gp – object containing interpretation of the 4 1997
   KCGM seismic traverses

seis_interp_y1_20s.gp – object containing interpretation of the 1999 seismic
   traverses Y1

seis_interp_y2_20s.gp – object containing interpretation of the 1999 seismic
   traverses Y2

seis_interp_y3_20s.gp – object containing interpretation of the 1999 seismic
   traverses Y3

seis_interp_y4_20s.gp – object containing interpretation of the 1999 seismic
   traverses Y4

seis_interp_y5_20s.gp – object containing interpretation of the 1999 seismic
   traverses Y5

seis_ny1_interp_20s.gp – object containing interpretation of the 2001 seismic
   traverses NY1

historical_sites.vs - -object showing location of pre-1980 seismic traverses

**seismic_refraction**

3 objects

data from Clive Collins, Geoscience Australia

refraction_moho_picks.vs – object showing depth to Moho from refraction
   picks.

refraction_stations.vs – object of refraction recording station locations

refraction_shots.vs - object of refraction shot locations

**teleseismic_swave_skippy**

2 objects

data from Brian Kennett (RSES, ANU)

swave_volume.vo – s-wave velocity volume of the Yilgarn Craton, to a depth
   of 350km

swave_isosurf_48.ts – object of region with high s-wave velocities > 4.8 km/s

**wide_angle_Fomin**

3 objects

data from Geoscience Australia

data restricted to the Laverton-Leonora region

wide_angle_stationloc.vs – object showing location of wide-angle stations

wide_angle_depth.gp – object with wide-angle results, displayed in depth (m).
   This is the display most commonly used.

wide_angle_twt.gp – object with wide-angle results, displayed in two-way-
travel time (ms)


## *Appendix 2-6: Metadata for Model Vision files*

*T.Brennan*

The files within this folder relates to the ModelVision modelling undertaken for the pmd*CRC's Y2 project.

**\*.lin** are the potential field import files for ModelVision. That were obtained from Geoscience Australia's gravity and magnetic grid of Western Australia.

**\*.tkm** are the exported ModelVision model files that were subsequently imported into Gocad

**\*_modified\*** are the modified models created through endeavouring to match the interpreted geological sections to the gravity data. Files without this naming convention are the orginal geological sections drawn by the project's geologists.

# Chapter 3: Seismic reflection studies of the northeastern Yilgarn Craton

*B.R. Goleby and R.S. Blewett*
Much of the seismic data have been presented previously. All presentations and reports, data, interpretations and images are provided in one of the Appendices in this chapter or as Gocad objects within the 3D map (Appendix 2-4 and 2-5). A summary is provided here for clarity.

## *Introduction*

The understanding of a region's 3D architecture is an essential tool in the interpretation, understanding, and prediction of that region's mineral deposits. Indeed, architecture is a key ingredient in the five questions. Seismic data (especially reflection data) have proved invaluable for constraining the geometry of the eastern Yilgarn Craton (EYC) below the base of the greenstones. This is because there is insufficient variation in density and magnetisation rock properties for potential-field methods (see Chapter 2) to be used effectively. Furthermore, the resolution of potential-field techniques decreases dramatically with depth and there is little property contrast between the largely felsic crust or basement and the greenstone sequences.

The process of construction and calibration of a 3D map usually results in a quantum increase in the understanding of the three dimensional structural relationships within the region. Several of the questions that are important in this process are:

- understanding and assessing the deep crustal architecture including the lithosphere;
- understanding structural controls on the late-stage evolution, processes and deformation history, and;
- understanding deformation processes and timing within known deposits so that exploration strategies based on structural targets at all scales can be formulated.

Two seismic reflection techniques were employed in the Y2 project: deep seismic reflection profiling using Vibroseis sources (Goleby et al., 2003), and wide-angle reflection profiling using the same source (Fomin et al., 2003). Results are outlined below and copies of papers, posters and PowerPoint presentations are attached in Appendix 3.

Seismic reflection techniques can assist in answering the fundamental questions outlined above. The *pmd*\*CRC Y2 project made use of the existing deep seismic reflection data that was recently acquired as well as earlier deep seismic traverses acquired in the EYC. Figure 3-1 shows the location of the northeastern Yilgarn deep seismic reflection traverses. Figure 3-2 shows the locations of the 1991, 1997 and 1999 Yilgarn Seismic Traverses in the southern Kalgoorlie Terrane.

## *Deep seismic reflection results*

## Scientific objectives

The broad scientific objectives of the 2001 Northeastern Yilgarn Seismic Survey were to:

- investigate the thickness of the crust within the Leonora-Laverton region and compare it with the thickness of the crust in the Kalgoorlie region and with regions to the east and to the west;
- investigate variations in the seismic characteristics of the crust between different regions within the EYC;
- determine the presence and geometry of any major boundaries within the Leonora-Laverton region;
- determine if a detachment surface exists within the Leonora-Laverton region and, if present, determine the lateral extent and depth variation of this surface;
- determine the thickness and internal geometry of the granite-greenstone in the Leonora-Laverton region and the geometry of any major internal structural features within the region. This was achieved by:
  - imaging the internal geometry of the granite-greenstone succession,
  - identifying deformation surfaces within and/or bounding the greenstone package,
  - determining the relationship of the bounding surfaces of a greenstone package to mapped/identified faults systems,
  - imaging the granite-greenstone contacts,
  - determining regional variations of the structure of the granite-greenstone succession,
  - identifying the sequence of deformational history within the greenstone terrane using kinematic indicators identified within the seismic data, and,
  - investigating the cumulative effects of the successive deformations ($D_1$ - $D_4$) on the greenstone belt;
- determine the predominant structural style within the Leonora-Laverton region, both within the deeper crust and in the upper succession, and attempt to provide constraints on the relative timing and importance of contractional, extensional, and strike-slip tectonics during the evolution of the EYC;
- map the form of granite intrusions within the Leonora-Laverton region and compare these with the Kalgoorlie region; and,
- image possible fluid flow pathways through the granite-greenstone succession.
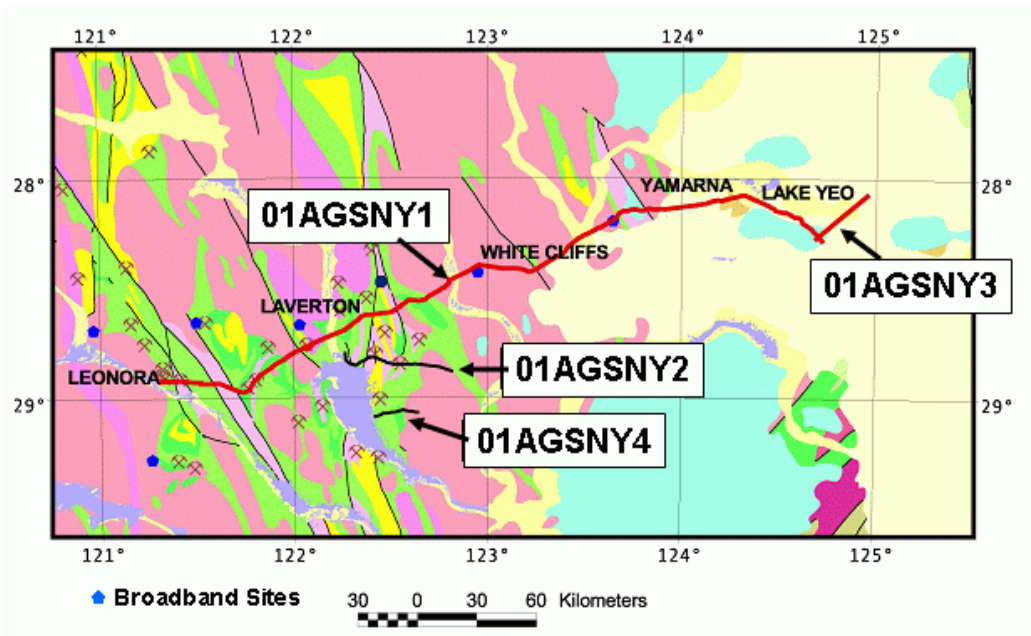
**Figure 3-1: Location of the 2001 Northeastern Yilgarn Deep seismic traverses.**
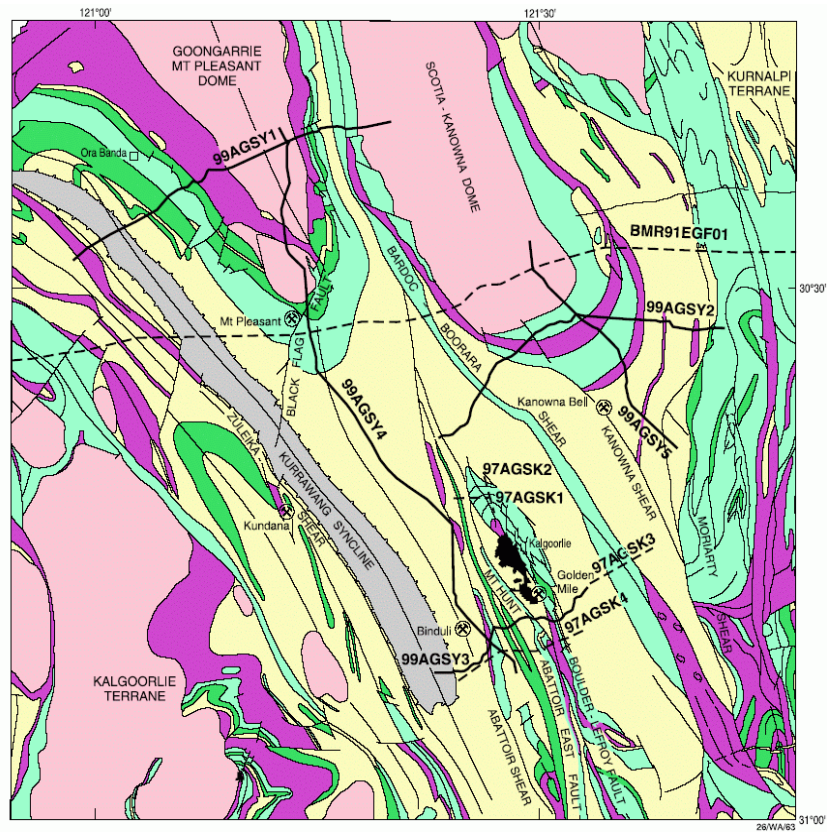


**Figure 3-2: Location of the 1999 Yilgarn Deep seismic traverses. The central portion of the 1991 Eastern Goldfields traverse 91EGF01 is shown as the east-west oriented dotted line. These seismic lines were the initial data sets for the detailed Kalgoorlie-Kambalda 3D map.**

92

## Scientific results

The 2001 Northeastern Yilgarn Seismic Survey achieved the above objectives, in particular providing detailed information on crustal architecture of the region at depth. In addition to the seismic reflection data, two additional seismic related experiments were acquired to improve our knowledge of the regions velocity structure. These experiments were a wide-angle reflection profile experiment (discussed below) and a passive-listening broadband experiment (discussed in Chapter 4).

*Milestones and outputs achieved*
- The 1999 deep seismic lines were re-interpreted and included in the Kalgoorlie-Kambalda 3D map. These interpretations were included as figures in the scientific journal, Australian Journal of Earth Sciences, published in December 2002 (see **Appendix3-1_Goleby_etal_AJES_49#6_pdf**).
- Interpretation of the 2001 seismic data was completed. These data were prepared for release and are available on a set of CDs and as downloadable PDFs from http://www.ga.gov.au/rural/projects/20011019_19.jsp.
- The data are reproduced here:
  **Appendix3-22_Seismic_section_01AGSNY1.pdf**;
  **Appendix3-23_Seismic_section_01AGSNY3.pdf**;
  **Appendix3-20_Seismic_section_processing.pdf**; **and**
  **Appendix3-21_Seismic_section_releasenotes.pdf**).
- The interpretation of the 2001 seismic was presented in August 2002. The results were published as a set of workshop notes.
- The workshop notes from the above 2001 GSWA-*pmd*\*CRC-GA seismic workshop were updated after the workshop and published as a GA Record (see **Appendix3-4_GARecord_2003_28.pdf**).
- Several papers and a poster were prepared on seismic results and presented at the 10th deep seismic meeting in New Zealand (see **Appendix3-3_Goleby_etal_tectonophysics_2004.pdf**). Considerable interest in the results was expressed.
- A paper prepared on integrating the seismic results was presented at the SEG 2004 Conference (see **Appendix3-12_Goleby_seg2004.pdf**).
- Several papers and a poster on seismic results were presented at 11th deep seismic meeting in Canada (see **Appendix3-11_Yilgarn_3D_seismix2004.pdf**).

## Methodology and output delivery

The methodology and output promised by the *pmd*\*CRC included:
- Undertake processing and interpretation of the 2001 regional deep seismic reflection data collected as part of the Leonora-Laverton deep seismic reflection transect. Geoscience Australia provided the seismic data as an in-kind contribution to the *pmd*\*CRC, and the GSWA component was a cash contribution. The processing and interpretation of the 2001 seismic reflection and wide-angle reflection data were completed within Geoscience Australia for the *pmd*\*CRC.
- Document and distribute the results from the Leonora-Laverton deep seismic reflection transect (see **Appendix3-4_GARecord_2003_28.pdf**).

These outputs were achieved.

## Seismic Interpretations

The published interpretations of the new seismic data acquired for the Y2 project are summarised in the Figures 3-3 through 3-6. It should be pointed out that several of these interpretations have been further modified during the construction of the 3D map. These updated interpretations have not jet been published; they are however included in the 3D map.
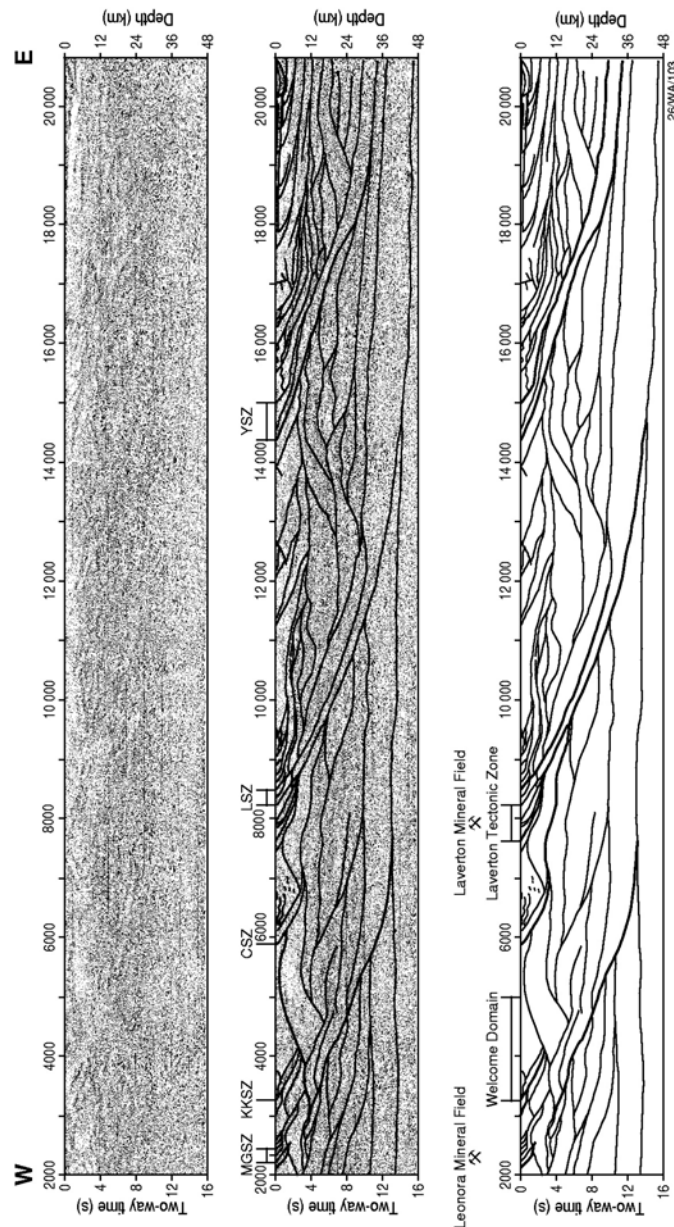


**Figure 3-3: 2003 interpretation of the 2001 Northeastern Yilgarn Traverse – 01AGSNY1. This interpretation has been further refined during the construction of the 3D map.**

94
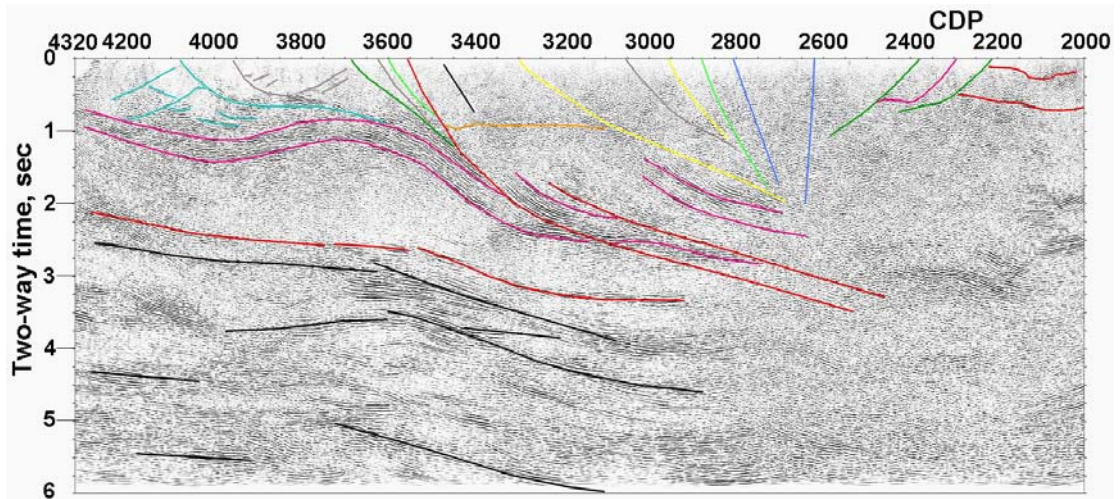
**Figure 3-4: 2003 interpretation of the 2001 Northeastern Yilgarn Traverse – 01AGSNY2. This interpretation has been further refined during the construction of the 3D map.**
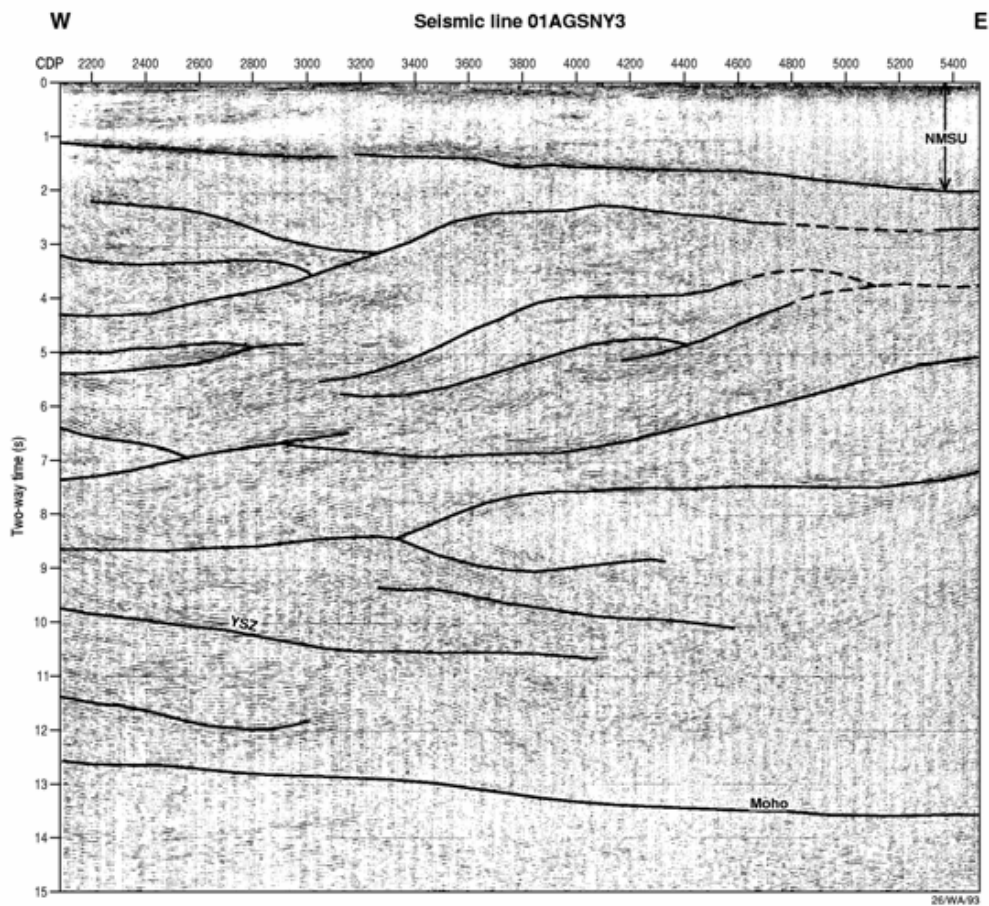


**Figure 3-5: 2003 interpretation of the 2001 Northeastern Yilgarn Traverse – 01AGSNY3. This interpretation has been further refined during the construction of the 3D map.**

95
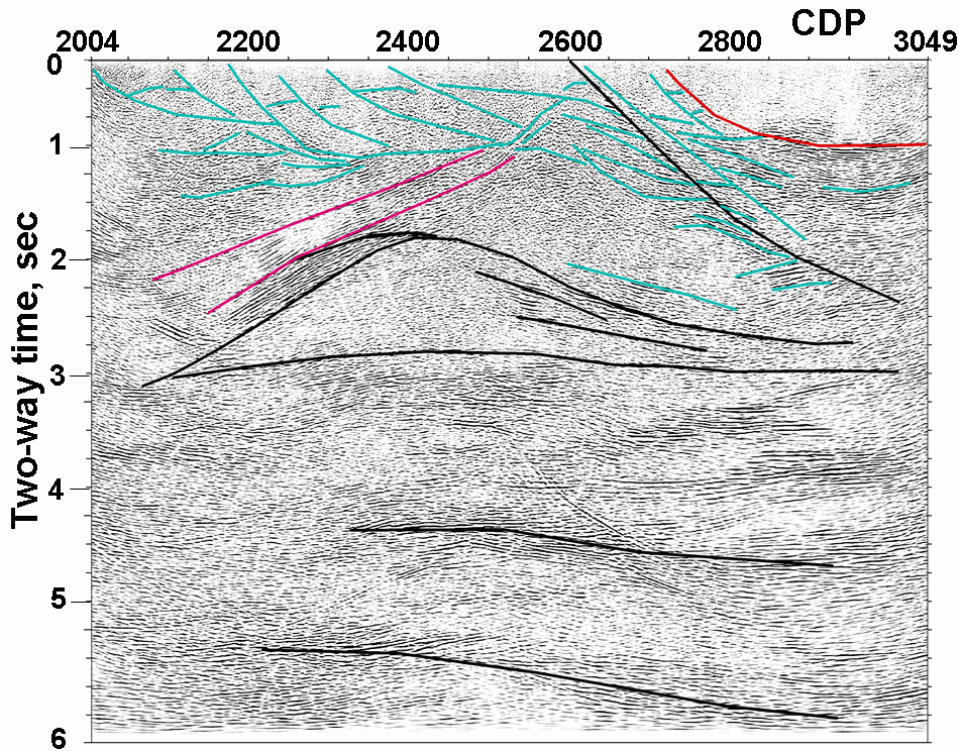
**Figure 3-6: 2003 interpretation of the 2001 Northeastern Yilgarn Traverse – 01AGSNY4. This interpretation has been further refined during the construction of the 3D map.**

## Main seismic features of the Northeastern Yilgarn seismic transect

This section has been reproduced from Goleby et al. (2003), which is available in Appendix 3-4 and 3-22. The north-eastern Yilgarn deep seismic reflection transect is characterised by several prominent features (Figure 3-3), which are related to the seismic characteristics of the crust. These features include:

1. a change in the thickness of the crust across the north-eastern Yilgarn Craton;
2. a subdivision of the crust into three broad layers;
3. a series of strongly aligned reflectors that many faults sole onto (a detachment);
4. a prominent east dip to the majority of the reflections, and;
5. three east-dipping crustal-penetrating shear zones.

## Crustal thickness

The crust is approximately 40 km thick in the Leonora-Laverton region, and thickens eastwards towards the Albany-Fraser Province; a feature also noted on the previous EYC seismic data (Goleby et al., 2000). There is a prominent sub-horizontal thin band of reflections that are interpreted as the Moho. The reflectors define the seismic base of the crust. There is no refraction data in the region to confirm that this boundary is the Moho, however, refraction to the southwest indicates that the Moho is at a similar depth. The Moho's seismic character and its position is similar, although a bit deeper, to that interpreted by Goleby et al. (2000) on the regional EYC traverse 91EGF01.

96

The Moho is interpreted to be at about 13.5 s (40 km) beneath the town of Leonora, deepening to about 15.5 s (46 km) at the eastern end of the traverse. This deepening of the Moho is achieved by a series of ramps and flats, with the Moho generally sub-horizontal for long sections, and then ramping down over a short distance. These features are similar to those seen in the regional Eastern Goldfields Traverse 91EGF01.

## The EYC as a three-layered crust

Based on the overall seismic characteristics seen in the section, the crust is subdivided into three sub horizontal layers. The lowest layer is considered to be a ductile lower crustal unit. There are only two instances where dipping reflections are seen in this layer and they both relate to interpreted deep-penetrating shears zones (see below).

The upper surface of this sub-horizontal layer is defined by a sudden change in reflection character to a zone where large packages of dipping reflectivity are the norm. The seismic reflectivity in this middle level is characterised by numerous prominent east-dipping reflections that can be subdivided into large units that have similar seismic character, producing large-scale, lozenge-like, mid-crustal bodies. Drummond et al. (2000) described duplex structures in the mid crust of the 91EGF01 seismic line related to 'D$_2$' thrusting and imbrication. Similar features are evident in segments of the 01AGSNY1 line.

The boundary between the middle and upper layers is diffuse and irregular in geometry. The upper layer is far more complex and variable in its seismic character.

## One or more detachments?

The concept of a regional detachment was formulated from work on the regional 91EGF01 seismic line (Goleby et al., 1993). More detailed work on newer (higher quality) lines (see Figure 3-2) and 01AGSNY1 has shown that there is unlikely to be a single 'detachment' plane.

A feature noted in the 01AGSNY1 line around Leonora was that the strong reflectors were more complex (folded and faulted) at the highest levels compared to deeper levels (~2 s TWT). The interpretation here was that the strong reflectors were developed by shearing, possibly facilitated by fluids, around the brittle-ductile transition. With further deformation (exhumation) the old brittle-ductile transition would be deformed and uplifted while the neo-detachment would remain at a relatively stable crustal level (all things being equal). The analogy was drawn from modern earthquake hypocentres concentrating at these levels (depths) and the strong reflectivity imaged at these levels (see Chapter 8 for further discussion).

## The east dip of most of the EYC reflectors

There is a very pronounced dip to the east for the majority of the reflectivity seen along the seismic traverse, both in the middle and upper levels of the crust. West-dipping features are also imaged, but these are restricted to a few locations. The east-dipping reflections generally have a shallow dip, typically around 30°.

## Deep penetrating shear zones

Within this east-dipping architecture, there are three prominent east-dipping zones of reflectivity that cut deep into the crust. These three deep-penetrating shear zones divide the north-eastern Yilgarn Craton into four distinct domains, and are interpreted to represent the Mount George Shear Zone, the Laverton Shear Zone and the Yamarna Shear Zone. The Yamarna Shear Zone dips at about 30° and is wider at the surface than at depth. The shears can be traced from the surface to the lower crust and, in two cases, to the Moho. The Laverton and the Yamarna Shear Zones are the more clearly defined, whereas the Mount George Shear Zone appears to have been intruded by later granite emplacement or subsequent deformation. All three deep penetrating shear zones have a complex geometry, suggesting that these zones have seen several episodes of deformation.

There has been debate within the project team as to whether this reflectivity is a single plane (as shown in the 3D map). Detailed examination of the reflectors, especially near the detachment, show that it is difficult to interpret a single plane cutting through the crust. This is especially true of the Ockerberry Fault which is imaged on both the 01AGSNY1 line and 91EGF01 line. The Ockerberry Fault is a terrane boundary and yet it appears thin skinned. Faults such as the Celia and Laverton may cut the detachment, yet they are relatively minor faults within terranes. The inference from these observations is that terrane accretion may have been thin-skinned thrusting and the subsequent deformation (especially late extension) occurred along different boundaries within the terranes. See Chapter 1 for a discussion of the fault and terrane nomenclature.

## Implications for predictive mineral discovery

Seismic reflection data have proved to be an invaluable tool for defining a regional architecture. Furthermore, the technique is being increasingly applied at mine and camp scales for target generation purposes (Ned Stolz *pers. comm.*, 2004).

The Y2 project made much use of the seismic reflection data in the construction and validation of the 3D map (see Chapter 2). This map has the most detail, rigour and understanding in areas where the density of seismic data is greatest.

The seismic reflection survey imaged a series of prominent east-dipping crustal-penetrating shear zones, which correlate at the surface with mapped terrane boundaries (Swager, 1997).

Within the EYC, the major gold deposits are all spatially associated with these major structures. The Laverton Tectonic Zone, within the EYC, is a highly mineralized corridor, controlled by one of these shear zones. It contains several world-class gold deposits plus many smaller deposits. Other faults unrelated to main crustal-penetrating structures do not appear to be as economically well endowed. In the upper crust, low angle shear zones splay off the major crustal-penetrating structures. In the mantle there is an indication that the southeast-dipping body is not just a single dipping body but rather a series of southeast-dipping segments; the breaks correlating

with the general location of the major crustal-penetrating structures. Overall, the resultant mantle and crustal geometry assisted in focusing upward moving fluids and then distributing them into the overlying complexly deformed greenstones.

## *Wide-angle refraction studies*

*T. Fomin*

## Introduction

During the acquisition of seismic data in the Leonora-Laverton region in 2001, a wide-angle refraction survey was carried out to supplement the deep seismic reflection studies. The following extract is taken from Fomin et al. (2003) (see **Appendix3-2_as_eg34p147_150.pdf**), which summarises the overall project.

'The major objectives were to obtain velocity information for the upper crust from high-density refraction information for offsets of up to 60 km, and to carry out a comparative study of near-vertical and wide-angle seismic images of the crust in the study area. The survey deployed 120 short period recorders at a spacing of 500 m. Acquisition parameters used for the wide-angle reflection experiment were selected so that it would fit into the schedule and technology of the reflection survey. The signals were recorded by refraction and reflection equipment simultaneously. The major challenge in processing the wide-angle data was to manage the huge set of data collected during the survey. The processing sequence included sorting into receiver and source gathers, cross-correlation with reference sweeps and stacking original seismic traces to form single source point traces, producing seismograms from individual traces, and finally creating seismic record sections from separate seismograms. High amplitude seismic signals from Vibroseis sources were recorded to at least 50 km offsets in the first arrivals, and later arrivals were observed down to 12 s near the sources. A preliminary upper crustal model developed from the wide-angle data shows that the thickness of a high-velocity layer, corresponding to greenstone rocks, is 4.0-4.5 km. The boundary separating this layer from a low-velocity layer below it is possibly a compositional boundary between greenstones and underlying felsic gneisses. There is no evidence for high-velocity material below this boundary. Assuming the Moho is associated with the deepest reflections modelled, total crustal thickness in the region can be speculatively estimated to be in the range of 32-37 km. This model will be refined when more processed data become available for modelling.'

## Methodology

The following extract is taken from Fomin et al. (2003) (see **Appendix3-2_as_eg34p147_150.pdf**), which describes the methodology for collecting the wide-angle data.

'The 64-km long recording array was centred in the Leonora-Laverton Tectonic zone with vibration points extending beyond it by 75 km to the west and 35 km to the east, up to the White Cliffs area (Figure 3-7).
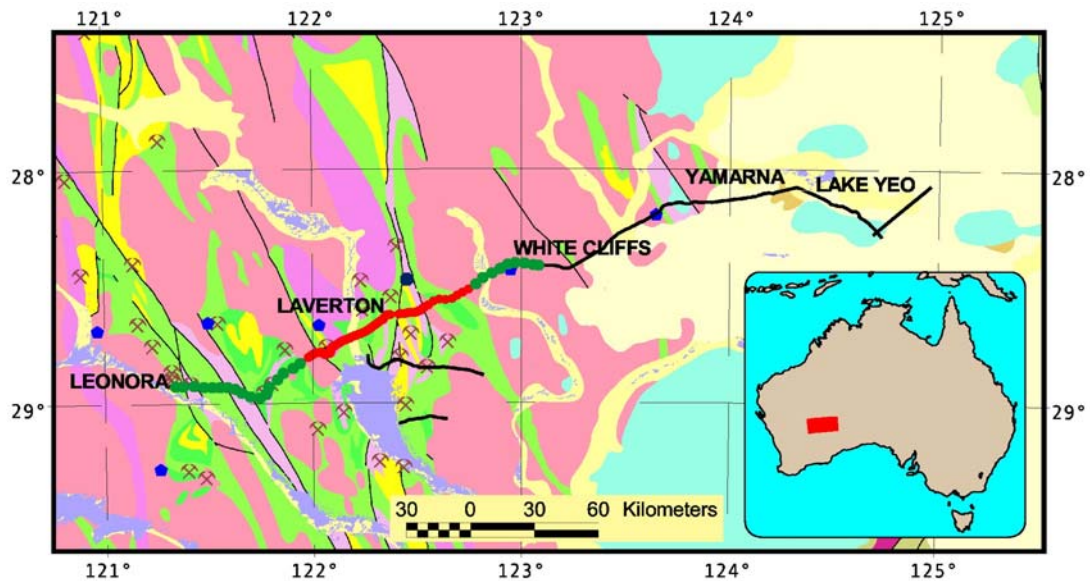
**Figure 3-7: Location map of the 2001 North-eastern Yilgarn deep seismic survey over the simplified geology. Wide-angle survey shown as a dotted line coincident with the regional reflection transect. Wide-angle recording array – red dots, extended beyond recording array by additional 75 km of vibration points in the west and additional 35 km in the east - green dots.**

Three IVI 60 000 lb vibrators were used as the energy source. Short period portable recorders, designed and built by the Research School of Earth Sciences at Australian National University, recorded the seismic signal on solid-state memory cards.

The wide-angle survey was completed in two weeks in August 2001 and included four stages: deployment of instruments, recording, replacement of full memory cards, and retrieval of the equipment. These stages overlapped because of the complex work schedule designed to enable most efficient utilisation of recording time and equipment. The 120 short period portable instruments were deployed at a spacing of 500 m as a fixed recording array. The recorders ran continuously during the whole survey, and memory cards were replaced every fourth day for every station. Vertical component geophones were used for almost all of the recording stations because of difficulties of servicing three-component geophones and memory volume considerations. The extension of the effective length of the line by positioning vibration points beyond the recording array on both ends resulted in achieving maximum offsets of more than 150 km. The recording array was extended by 23 km in the east to enable recording, at increased offsets, of an 8 tonne underground blast at the Sons of Gwalia mine.

The major challenge of the experiment was to collect wide-angle data utilising the acquisition parameters of a typical reflection survey. These parameters were selected from experience of previous Vibroseis reflection surveys in the Yilgarn region. The only modification made to the conventional reflection parameters was an increase of the sweep length from 8 s to 12 s. The seismic source and recording parameters are shown in Table 3-1. The offsets and number of recorded sweeps varied for different

100

recording stations, depending on the day of deployment and collection of instruments.'

**Recording parameters**

| Type of recorders | ANU, short period portable |
|---|---|
| Number of recorders | 120 |
| Spacing interval | ~500 m |
| Sample rate | 10 ms |
| Type of seismometer | 1 Hz , one-component vertical |
| Listening time | continuous |
| **Energy source parameters** | |
| Vibrator type | IVI Hemi 60 |
| Number of vibrators | 3 |
| Number of vibrator points | 2137 |
| Vibrator points interval | 80 m |
| Number of sweeps at each source point | 3 |
| Source move-up | 15 m |
| Sweep length | 12 s |
| Sweep frequency | 7–56, 12–80, 8–72 Hz |

**Table 3-1: Recording parameters for the wide-angle seismic reflection survey.**

## Scientific results

The wide-angle Vibroseis experiment with a passive recording array in the northern Yilgarn Craton proved the effectiveness of using reflection source acquisition parameters for collecting high-quality wide-angle seismic data to offsets of at least 70 km.

An upper crustal model developed from the wide-angle data shows that the thickness of a high-velocity layer (6.2–6.6 km/s), corresponding to greenstone rocks, is 4.0–4.5 km (Figure 3-8). The velocities are lower below this layer and may correspond to felsic gneisses. This exercise demonstrates that velocity information interpreted from wide-angle data recorded from a Vibroseis source can be used to constrain the geological interpretation of coincident near-vertical reflection data.
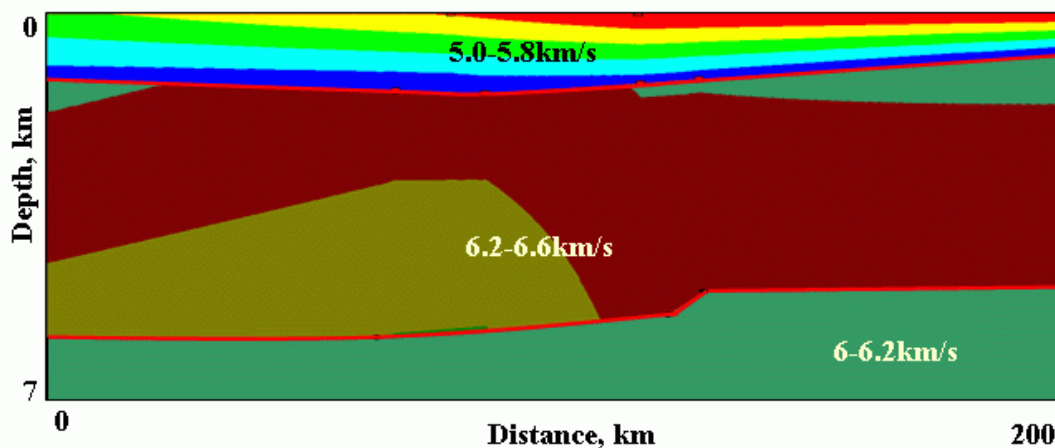


**Figure 3-8: 2D velocity model for the upper crust, Leonora-Laverton Tectonic Zone, Western Australia.**

This upper crustal model has been further refined and the results are shown in Figure 3-9. See **Appendix3-15_tfomin_talk_seismix2004.pdf** for more information.
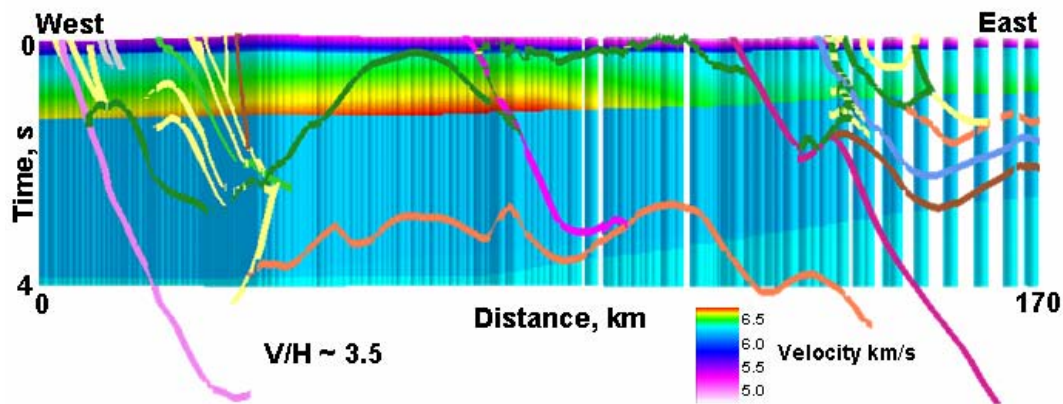


**Figure 3-9: The wide-angle data, plotted with the deep seismic reflection interpretation to show similarities and differences between the two methods.**

## Recommendations for survey parameters interpreted from findings

Fomin et al. (2004) (see **Appendix3-19_tfomin_poster_Seismix04.pdf**) recommends the following survey parameters:

1. Shot and recorder intervals:
   - 240 m vibration point interval
   - 5-10 km recorder interval – for building a velocity model
   - 1-1.5 km recorder interval – for stacking wide-angle data.
2. Use a longer sweep (~30 s ?) – to build lower crustal velocity model.
3. Use a recording station sample rate of at least 4-6 ms – for better resolution of stacked sections.

## Conclusions

The following conclusions may be drawn from this wide-angle refraction study:

- Wide-angle surveys supplement reflection data by providing velocity information for the upper crust.
- These supplementary surveys provide an opportunity to compare the velocity model derived from wide-angle data with a structural image obtained from the deep seismic reflection data.
- The experiment has proved the effectiveness of using a Vibroseis source for collecting wide-angle data simultaneously with reflection survey.
- The velocity model for the upper crust demonstrates the possibility of differentiating high velocity mafic rocks from low velocity rocks.

- Wide-angle reflections from the lower crust are not sufficient to build an accurate velocity model, lower crustal refractions in the first arrivals are required to constrain this model better but unfortunately the signal was too weak to achieve this.
- Reflection horizons and changes in reflectivity patterns mapped by the reflection technique will not necessarily coincide with velocity boundaries imaged by wide-angle reflection technology due to different wavelengths and different interference styles.
- The stacked wide-angle seismic section has both similarities and differences with the conventional reflection section. More work is needed to identify additional uses of the wide-angle section.
- A more accurate geological interpretation is possible using a combination of wide-angle and reflection seismic techniques.

## Investigation of advanced seismic processing techniques; improving the resolution of near surface seismic data derived from deep crustal reflection seismic surveys.

*C. Heath*

Most of the seismic data collected by the Australian National Seismic Imaging Resource (ANSIR) is designed to image the deep crust and therefore requires long recording times. The purpose of this study was to investigate the possibility of reprocessing the first few seconds of these data, to improve the imaging of near surface geological features. The full report is attached as a PDF document in Appendix 3-5 (**Appendix3-5_Heath_reflection_report.pdf**).

Seismic line 99AGSY4 was chosen for this purpose. This line intersects a deformed Archaean sedimentary succession. It was anticipated that reprocessing might improve the resolution of the succession.

Initial reprocessing, involving standard processing techniques, improved the resolution within the top 500 ms (1.5 km) of the line. This improvement was achieved by re-picking the first break energy mutes. Advanced processing techniques, involving dip move-out processing and frequency-wave-number filtering were investigated, but were found not to enhance the data resolution.

Pre-stack migration was found to result in the greatest improvement of data quality, and in changing the nature and characteristic of many of the reflectors. However, this was only a preliminary study and it is not yet clear if some of the changes are artefacts of the processing technique, or reflect geological reality.

Further work in pre-stack migration and pre-stack depth migration is suggested as a means of clarifying these issues and further improving the data. Until such processing is completed it is suggested that care be taken in interpreting the nature of the sedimentary units within the sedimentary succession.

## *Implications for predictive mineral discovery*

Seismic reflection data provide an excellent image of the crustal architecture of a region. However, what is often missing is good lithological information at depth. Some lithological information is obtained through the projection of known surface geology to depth, while other information is suggested through the use of potential-field modelling where modelled density and susceptibility values provide some indication on the broadest lithological possibilities.

Combining the wide-angle refraction and reflection techniques provides a further parameter to narrow down likely lithological variations. This is then important in understanding the distribution of particularly favourable rock units or regions at depth.

Improvements could be made to the upper two seconds of the seismic reflection data. Pre-stack migration is a very labour-intensive process but, as the seismic reflection data were instrumental in building the 3D map, improved and specialised processing of the upper parts of the data should be carefully considered.

## *Appendix 3*

### *Papers*

3-1: **Appendix3-1_Goleby_etal_AJES_49#6.pdf** is a PDF of the paper: B.R. Goleby, R.J. Korsch, T. Fomin, B. Bell, M.G. Nicoll, B.J. Drummond and A.J. Owen, 2002. Preliminary 3-D geological model of the Kalgoorlie region, Yilgarn Craton, Western Australia, based on deep seismic-reflection and potential-field data. *Australian Journal of Earth Sciences*, 49, 917–933.
```
Published with the permission of the Geological Society of
Australia.
```
3-2: **Appendix3-2_as_eg34p147_150.pdf** is a PDF of the paper: Fomin, T., Crawford, A. and Johnstone, D., 2003. A wide-angle reflection experiment with Vibroseis sources as part of a multidisciplinary seismic study of the Leonora-Laverton Tectonic Zone, Northeastern Yilgarn Craton. *Exploration Geophysics*, 34, 147–150.

3-3: **Appendix3-3_Goleby_etal_tectonophysics_2004.pdf** is a PDF of the paper: B.R. Goleby, R.S. Blewett, R.J. Korsch, D.C. Champion, K.F. Cassidy, L.E.A. Jones, P.B. Groenewald, P. Henson, 2004. Deep seismic reflection profiling in the Archaean northeastern Yilgarn Craton, Western Australia: implications for crustal architecture and mineral potential. *Tectonophysics*, 388, 119–133.
```
"Reprinted from Tectonophysics, 388, Goleby et al., Deep seismic
reflection profiling in the Archaean northeastern Yilgarn Craton,
Western Australia: implications for crustal architecture and
mineral potential, Copyright (2004), with permission from
Elsevier".
```

### *Reports*

3-4: **Appendix3-4_GARecord_2003_28.pdf** is a PDF of the Geoscience Australia Record: Goleby, B.R., Blewett, R.S., Groenewald, P.B., Cassidy, K.F., Champion, D.C., Jones, L.E.A., Korsch, R.J., Shevchenko, S. and

Apak, S.N., 2003. The 2001 Northeastern Yilgarn Deep Seismic Reflection Survey. *Geoscience Australia*, *Record* 2003/28. 143pp.

3-5: **Appendix3-5_Heath_reflection_report.pdf** is a PDF of the report: Heath, C.J., Goleby, B.R., Fomin, T., 2004. Investigation of advanced seismic processing techniques; improving the resolution of near surface seismic data derived from deep crustal reflection seismic surveys. Unpublished *pmd*\*CRC report, 39p.

## *Abstracts*

3-6: **Appendix3-6_abstract_DeepSeismicMeeting_NZ.pdf** is a PDF of the abstract: Fomin, T., Crawford, A.R. and Johnstone D.W., 2002. Conventional vibroseis technique expanded to yield high quality wide-angle data in northeastern Yilgarn, Western Australia, *in* Goleby, B., Drummond, B., Bannister, S. and Henrys, S. (comp) 2002. *The 10th International Symposium on Deep Seismic profiling of the Continents and their Margins, Programme and Abstracts*, Huka Village Conference Centre, Taupo, New Zealand, 6-10 January 2002. Institute of Geological and Nuclear Sciences, Information Series, 52, Lower Hutt, New Zealand: Institute of Geological and Nuclear Sciences Limited. p62.

3-7: **Appendix3-7_Blewett_SGTSG_2003_Abstract.pdf** is a PDF of the abstract: 'On the deep crustal structure of the late Archaean eastern Yilgarn Craton: a comparison to Palaeozoic and modern analogues' by Richard Blewett, Paul Henson, Bruce Goleby, David Champion, Kevin Cassidy, and Bruce Groenewald presented at the 2003 SGTSG Conference.

3-8: **Appendix3-8_aseg_abstract_2003.pdf** is a PDF of the abstract: Fomin, T., and Arcidiaco, A., 2003. Wide-angle reflection seismic experiment with vibroseis source as part of multidisciplinary seismic study through the Leonora-Laverton tectonic zone, northern Yilgarn. 16th ASEG Geophysical Conference and Exhibition, Adelaide, South Australia.

3-9: **Appendix3-9_tf_abstract_barossa.pdf** is a PDF of the extended abstract: Fomin, T., 2004. Models of the upper crust from wide-angle and reflection studies, Northeastern Yilgarn: Why we need both. *in* A.C. Barnicoat and R.J. Korsch (Editors) *Predictive Mineral Discovery Cooperative Research Centre - Extended Abstracts from the June 2004 Barossa Conference.* Geoscience Australia, Record 2004/09.

3-10: **Appendix3-10_tfomin_abstract_seismix2004.pdf** is a PDF of the abstract: Fomin, T., Goleby, B.R. and Nicoll, M., 2004. Some lessons from combined interpretations of wide-angle and conventional reflection data in the northern Yilgarn, Western Australia. Seismix 2004, the 11th International Symposium on Deep Seismic profiling of the Continents and their Margins, Programme and Abstracts, 26 September-1 October 2004, Centre des congrès, Mount-Tremblant, Quebec, Canada.

3-11: **Appendix3-11_Yilgarn_3D_seismix2004.pdf** is a PDF of the abstract: 'Using of seismic data to build three-dimensional models of the crust and upper mantle: An example from the Yilgarn Craton, Australia' by B.R. Goleby, B.L.N. Kennett, T. Fomin, A.M. Reading, B.J. Drummond, R. Blewett, P. Henson, S. Fyshwick, D.C. Champion, M. Nicoll and T. Brennan. Seismix 2004, the 11th International Symposium on Deep Seismic profiling of the Continents and their Margins, Programme and Abstracts, 26

September-1 October 2004, Centre des congrès, Mount-Tremblant, Quebec, Canada.

3-12: **Appendix3-12_Goleby_seg2004.pdf** is a PDF of the abstract: 'Seismic: A key tool in understanding crustal architecture and mineral systems' by B.R. Goleby, R.S. Blewett, B.L.N. Kennett, L.E.A. Jones, R.J. Korsch, B.J. Drummond, T. Fomin, A.M. Reading, K.F. Cassidy, D.C. Champion, P. Henson, P.B. Groenewald, M. Nicoll and T. Brennan. Submitted to the Society of Economic Geologists Conference, Perth, September, 2004.

*Talks*

3-13: **Appendix3-13_nz_talk_onscreen.pdf** is a PDF of the PowerPoint presentation: Fomin, T., Crawford A., and Johnstone, D., 2003. Conventional vibroseis technique expanded to yield high quality wide-angle data in the Northeastern Yilgarn, Western Australia. *The 10th International Symposium on Deep Seismic profiling of the Continents and their Margins*, 6-10 January 2002, Taupo, New Zealand - Talk

3-14: **Appendix3-14_Blewett_SGTSG_2003.pdf** is a PDF of the PowerPoint presentation: 'On the deep crustal structure of the late Archaean Yilgarn Craton: A comparison with Palaeozoic and Modern Analogues' by R.S. Blewett, P. Henson, B.R. Goleby, D.C. Champion, K.F. Cassidy and P.B. Groenewald presented at the 2003 SGTSG meeting.

3-15: **Appendix3-15_tfomin_talk_seismix2004.pdf** is a PDF of the PowerPoint presentation: Fomin, T., Goleby B.R., and Nicoll, M., 2004. Lessons from combined interpretations of wide-angle and conventional reflection data in the northern Yilgarn, Western Australia. *11th International Symposium on Deep Seismic profiling of the Continents and their Margins*, 26 September-1 October 2004, Mount-Tremblant, Canada – Talk.

3-16: **Appendix3-16_pdt2004_Goleby_seismic.pdf** is a PDF of the PowerPoint presentation: 'Application of seismic Application of seismic techniques for imaging of lithospheric techniques for imaging of lithospheric' presented at the final Y2 meeting in Perth, December 2004.

*Posters*

3-17: **Appendix3-17_ANSIR_poster__openday_2002.pdf** is a PDF of the poster: Fomin, T., Crawford, A., Arcidiaco, A., and Percival, T., 2002. Refraction/wide-angle seismic studies with vibro source to reveal velocity structure of the Leonora-Laverton tectonic zone, northern Yilgarn. *ANSIR Open Day 2002* - Poster.

3-18: **Appendix3-18_Wideangle_poster_Barossa.pdf** is a PDF of the Poster: Fomin, T., 2004. Models of the upper crust from wide-angle and reflection studies, Northeast Yilgarn: *Why we need both. Predictive Mineral Discovery Cooperative Research Centre, Barossa Conference* – Poster.

3-19: **Appendix3-19_tfomin_poster_seismix2004.pdf** is a PDF of the Poster presentation: Fomin, T., Goleby B.R., and Nicoll, M., 2004. Lessons from combined interpretations of wide-angle and conventional reflection data in the northern Yilgarn, Western Australia. *11th International Symposium on Deep Seismic profiling of the Continents and their Margins*, 26 September-1 October 2004, Mount-Tremblant, Canada – Poster.

### Processing documentation and release notes

3-20: **Appendix3-20_Seismic_section_processing.pdf** is a PDF of the article: 'Seismic data acquisition and processing – 2001 Northern Yilgarn seismic reflection survey (L154)' by L.E.A. Jones, B.R. Goleby, D.W. Johnstone and T.J. Barton *in* Geology, geochronology and geophysics of the north eastern Yilgarn Craton, with an emphasis on the Leonora-Laverton transect area: Proceedings of papers presented at an industry workshop held in Perth, 20 June, 2002, K.F. Cassidy (ed). Geoscience Australia, Record 2002/18, 111-118.

3-21: **Appendix3-21_Seismic_section_releasenotes.pdf** is a PDF of the article 'Release of the GA-GSWA-*pmd*\*CRC seismic reflection data, 2001 Northern Yilgarn seismic survey' by T.J. Griffin and C. Pigram *in* Geology, geochronology and geophysics of the north eastern Yilgarn Craton, with an emphasis on the Leonora-Laverton transect area: Proceedings of papers presented at an industry workshop held in Perth, 20 June, 2002, K.F. Cassidy (ed). Geoscience Australia, Record 2002/18, 101-103.

### Seismic Images

3-22: **Appendix3-22_Seismic_section_01AGSNY1.pdf** is an image of seismic section 01GA_NY1.

3-23: **Appendix3-23_Seismic_section_01AGSNY3.pdf** is an image of seismic section 01GA_NY3.

3-24: Directory **Appendix3-24seismic_skeleton_images** is a directory containing seismic skeletonisation images of 01AGSNY1 and NY3, and 91EGF1 seismic lines have been generated by Arie van der Velden (University of Calgary, Alberta, Canada). They are included as *tif* files for completeness.

# Chapter 4: Tomographic studies of the Yilgarn lithosphere

*B.R. Goleby, R.S. Blewett and A.M. Reading*

## Introduction

As part of the process of understanding a region's distribution of mineral deposits, it is essential to understand its 3D crustal architecture. Mineral deposits are the product of the focussing of enormous mass and energy fluxes at a range of scales from global to deposit. A key task is to attempt to map the signatures of this passage of mass and energy through the lithosphere. At the crustal scale, these signatures can be mapped by seismic reflection methods and, to a lesser extent, seismic refraction methods. However, at the lithospheric scale, seismic tomography methods must be used.

The eastern Yilgarn Craton (EYC) is well covered by these seismic data sets and hence allows the construction of a well-constrained 3D geological map. There is of course never enough coverage of seismic to get 3D detailed images. Existing seismic reflection data provide excellent 2D crustal architecture along key transects. This 2D architecture must be in-filled, at crustal or lithospheric scale, through the use of seismic tomography data sets at a range of scales.

The *pmd*\*CRC recognised this requirement and, as part of the Y2 project, facilitated the collection of tomographic data at the province scale to assist in the construction of a crustal-scale 3D geological map of the EYC. This tomography data is used to produce a velocity model of the central portions of the EYC, concentrating on the Kalgoorlie-Kambalda and Leonora–Laverton-Menzies regions, to show the provinces' velocity structure from the surface, through the base of the crust, the base of lithosphere and well into the mantle.

## Tomography background

Seismic tomography uses energy received from distant earthquake sources at a range of azimuths to build a velocity image of the volume of the earth through which the seismic waves have travelled. An earthquake releases different forms of seismic energy which travel through the earth. These forms of energy include P-waves (compression), S-waves (shear) and surface waves, with the latter occurring in several forms. These waves may travel directly to the receiver or may follow a path that has included reflection from one or more sub-surface structural features. Each of these ray paths is given a code to identify its path through the sub-surface. For example, Pn is an up-going P-wave that is reflected back from a feature between the Moho and the base of the asthenosphere (i.e. in the upper mantle); Sn is an S-wave that has travelled through the same path.

When a seismic event is recorded the record is a combination of P-waves, S-waves and

surface waves. Figure 4-1 shows the three components (vertical, and two horizontal) of a distant earthquake recorded in Australia. These different components are used to construct images of P-wave velocity, Vp, S-wave velocity, Vs, and Vp/Vs distributions within the sub-surface.
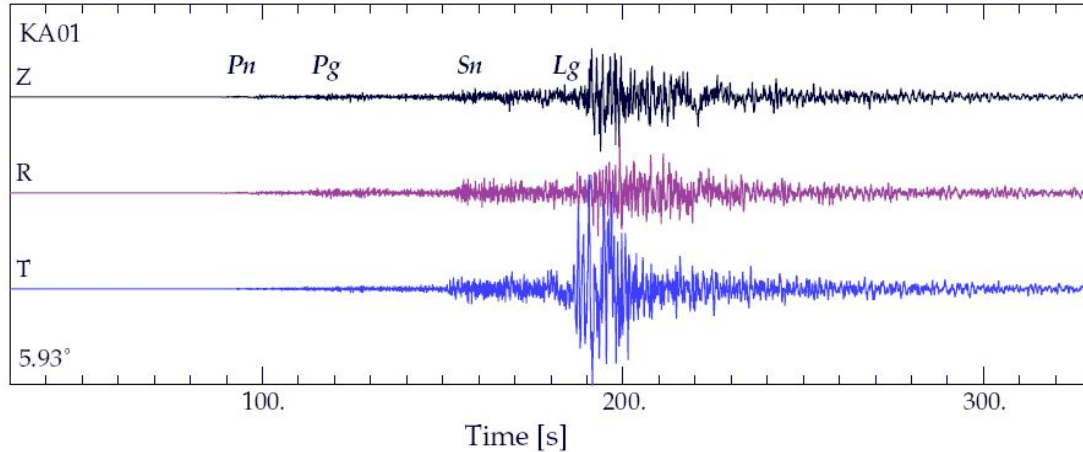


**Figure 4-1: The three components of a seismic wave recorded on a 3-component seismometer showing P-waves, S-waves and surface waves (in this case Lg). This image has been provided by Brian Kennett, RSES, ANU.**

Seismic tomography data are recorded on instruments deployed along line profiles or as array surveys. Energy from a distant earthquake travels to the recording site through rocks with differing properties. These differences can be divided into variations in rock properties in the vicinity of the earthquake source, variations within the mantle and variations within the crust beneath the recording site. An assumption in the method is that, particularly for deep earthquakes, the source and mantle rock properties variations are very small and the main variations are at the recording site. This means changes in seismic energy from different earthquakes at different azimuths can be used to compute velocity (and hence density) estimates within the crust beneath the recording site.

## Project linkages and collaboration

In early 2001 the *pmd*\*CRC developed a proposal to undertake a multi-phase tomographic study using instruments administered by the Australian National Seismic Imaging Resource (ANSIR). The initial ANSIR proposal is attached as Appendix 4-1 and the proposed deployment sites are shown in Figure 4-2. The initial phase of the subproject involved a *pmd*\*CRC and Research School of Earth Sciences (RSES, ANU) collaborative deployment of 12 broadband recorders, followed by a *pmd*\*CRC deployment of 4 broadband recorders.

Planning of the survey was supervised by *pmd*\*CRC staff. Through RSES, ANSIR provided trained staff to assist in the deployment and maintenance of the broadband recorders. The Geological Survey of Western Australia provided vehicles for all instrument deployments and an accompanying staff member for several of the deployments (Appendix 4-2). This contribution reduced the costs of the survey greatly

and allowed more flexibility in planning. RSES provided the necessary expertise to process and interpret the tomographic data in exchange for full access to the data for use in future projects.
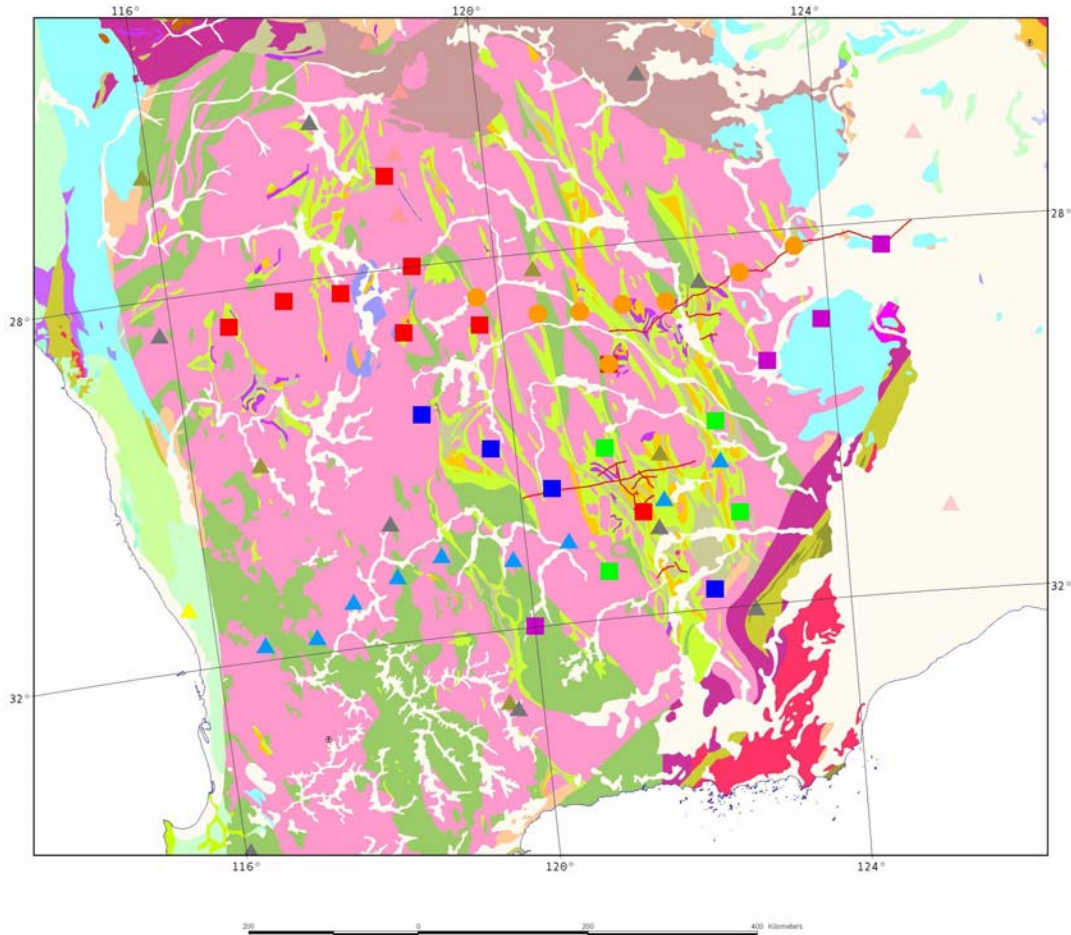


**Figure 4-2: Proposed locations of broadband recorders for the seismic tomography study, on a geological map of the Yilgarn Craton. Deployment of recorders was staggered: phase 1 (orange dots), coincident with deep seismic reflection transect; phase 2 (red squares) extend transect to west and link to old north-south traverse (pink triangles); phase 3 (blue squares) northwest – southeast traverse across mineralised – non-mineralised belts; phase 4 (green squares) concentration within mineralised region; phase 5 (purple squares) northeast – southwest traverse across mineralised – non-mineralised belts.**

## *Goal and objectives of the tomography subproject*

The Y2 project had four objectives, and the overriding objective relevant to the tomography subproject was:

'The project will also collect some additional data to improve our understanding of the velocity structure of the Kalgoorlie-Ora Banda region. These data will be in the form of a tomographic survey which will link the region's velocity structure from the surface,

through the base of the crust to the base of lithosphere with the integrated geological and geophysical 3D geological maps.'

In order to achieve this goal, the four specific scientific objectives of the tomography subproject were, initially:

1.  to investigate the velocity structure of the granite-greenstone succession within the Kalgoorlie region of the EYC,
2.  to investigate the crustal–upper mantle velocity structure (receiver function analysis) in geologically different crustal blocks within the Kalgoorlie region of the EYC,
3.  to investigate the upper mantle and crustal Vp and Vs velocity structure from interpretation of refracted wave arrivals from mine blasts, and,
4.  to augment the 'Skippy' data set with additional data recorded in the Yilgarn using distant earthquakes.

The subproject focused predominantly on objectives 1 and 2 above, particularly using S-wave seismic modes, since these data sets were expected to contribute most significantly to achieving the overriding goal.

Following initial theoretical modelling of mine blast and instrument planned offset distances, it became clear that the sampling capability of the recording instruments would not allow the upper crustal (granite-greenstone succession) Vp and Vs velocity structure to be adequately resolved. Consequently, objective 3 was deferred until such time as higher sample rate instruments are available. However, mine blast data were still recorded and are available for inclusion in future larger scale seismic studies.

All of the seismic data collected (Vp, Vs and surface waves) have been made available to RSES for inclusion in studies of the Yilgarn that use distant earthquakes (e.g., Skippy-like data sets for infill of the seismic velocity structure of the Yilgarn Craton). Some of these data sets are already being analysed by RSES PhD students.

The major milestones of the subproject were the completion of the collection of tomography data in December 2002, and the integration of these data into the 3D map in June 2003.

## *Key deliverable*

The key deliverable of the tomography subproject was:

*'A tomographic model of the Kalgoorlie-Ora Banda region which links the region's velocity structure from the surface, through the base of the crust to the base of lithosphere with the integrated geological and geophysical 3D geological maps.'*

The model derived by this subproject meets this deliverable. The development of this model is described below.

## Tomography experiment

The *pmd*\*CRC tomography survey was designed to investigate whether anomalous crustal and/or upper mantle velocities exist beneath the highly-mineralised regions of the EYC compared to 'normal' velocities beneath barren regions within and away from the EYC. The premise being tested was that the gold mineralising process, and its related geodynamic process, had altered or deformed the lower crust and/or upper mantle and, in doing so, changed the velocity structure.

Therefore the experiment focussed on the world-class 'Golden Mile' area of the Kalgoorlie region, and used additional sites outside this mineralised zone to get an indication of background velocity structure. The experiment needed to map velocity variations from the surface, through the base of crust, to the base of lithosphere. The resulting tomographic model would then provide additional constraints on the region's 3D structure.

The design of the tomographic data acquisition was similar to that used during ANU's 'Skippy' project (e.g., van der Hilst et al., 1994), which operated between 1983 and 1996. For the *pmd*\*CRC tomography subproject, broadband data were acquired using a series of staggered deployments over the EYC, with a concentration of instruments in the Eastern Goldfields between Kalgoorlie, Leonora and Laverton. The experiment ran for nearly 2 years and was extended well into the adjacent provinces to image craton-scale crustal variations. Table 4-1 gives broadband equipment information.

The first deployments were designed to determine whether any measurable large-scale velocity differences exist in the crust and upper mantle beneath provinces within the Yilgarn Craton, in particular if there is any significant velocity variation between the mineralised EYC and the less-mineralised to barren regions on either side (e.g., Southern Cross Province). Depending on the results of this initial work, further deployments were planned to determine the areal extent of any velocity difference relative to the mineralised region.

The first two deployments were along an east-west transect (see Figure 4-3; purple stars and large red stars westward continuation including WP01, WP02, WP03 and WP06), and aimed to determine the 1D crustal velocity functions from each of the identified provinces within the Yilgarn Craton. Additional recording sites (WP04 and WP11, Figure 4-3) were positioned to add 1D velocity functions to an earlier north-south transect (gold dots, Figure 4-3).

The next two deployments were orientated to collect data along two orthogonal profiles running from the barren terranes adjacent to the Kalgoorlie region into and through the highly-mineralised 'Golden Mile' region of the Eastern Goldfields. The centre of this array is coincident with the region of the 1999 reflection survey, and focuses on crustal velocities in this section of the Eastern Yilgarn. Four broadband instruments were use per field operation for these and subsequent surveys. Recording site spacing is somewhere between 20 km and 50 km, following the rule of thumb that the shallower the depth of investigation, the closer the seismometer spacing.

| Initial deployments | |
|---|---|
| Recorders | 4× Reftek 72A-02 16 bit, 6 channel, 600 Mbyte disc recorders; 6× Nanometrics Orion recorders |
| Seismometers | Broadband seismometers for Refteks; Guralp CMG40T seismometers for Orions |
| Ancillary | Power supply and timing equipment |
| Subsequent deployments | |
| Recorders | 4× Reftek 72A-02 recorders |
| Seismometers | Broadband seismometers |
| Ancillary | Power supply and timing equipment |

**Table 4-1: Summary of broadband equipment used during tomographic survey deployments.**

The initial broadband recorder sites proposed are shown in Figure 4-2, and the final successful recorded sites are shown in Figure 4-3. Figure 4-2 indicates the four pronged approach to the *pmd*\*CRC's tomography subproject:

1. The orange coloured sites were collected coincident with the north-eastern deep seismic traverse 01AGSNY1 to provide some deeper velocity information along this transect.
2. The red coloured sites extend the orange line across the Yilgarn Craton to give a 2D lithospheric velocity image of the craton. An additional two sites were located in a north-south orientation to link with stations that crossed the Capricorn Orogen. These sites, and those to the south, provide a 2D north-south lithospheric velocity image of the craton.
3. The blue sites add to a northwest–southeast diagonal crossing of the Southern Cross – EYC, to investigate if there are any finer velocity variations associated with mineralised – non-mineralised terranes.
4. The purple sites add to a northeast – southwest diagonal crossing of the Southern Cross – EYC, to investigate is there are any finer velocity variations associated with mineralised – non-mineralised terranes and, in conjunction with the blue sites, provide information on 3D variations.
5. The green sites are more-closely spaced sites that provide finer velocity detail in the mineralised Kalgoorlie Terrane.

Each deployment of the broadband recorders lasted approximately 3 months. From past experience, this length of deployment was judged to be enough time for a sufficient data to be recorded. Prior to the instruments being redeployed, the world earthquake catalogue was consulted to confirm that sufficient large-magnitude earthquakes, at suitable distances and range of azimuths, had occurred in the preceding 3 months to provide enough data to determine a velocity at that site. Instruments were then moved to the next defined site to build up a 3D velocity coverage of the region. Although not all the initial sites could be occupied, the original fundamental philosophy was followed, and the final recording sites provided excellent coverage to meet the goal and objectives of the

tomography subproject.

All sites (labelled WP) were located within granites. This site selection assisted in removing any additional near-surface velocity variation caused by large variations in upper crustal rock types (greenstones). The results from these sites are given in Appendix 4-3.
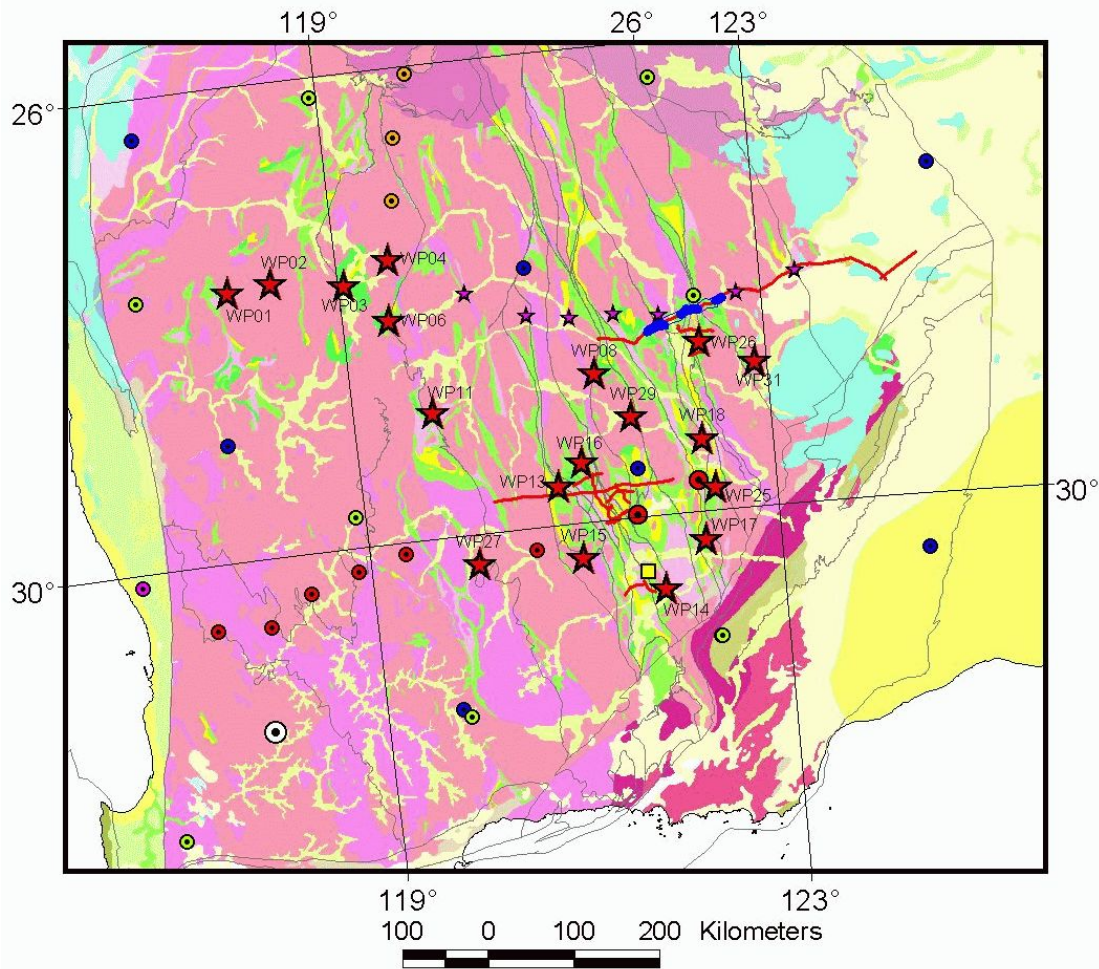


**Figure 4-3: Geological map of the Yilgarn Craton showing final locations of broadband recorders (red stars). The large red stars are successful deployment sites; the small purple stars show the initial east-west deployment. Coloured dots are earlier sites used in conjunction with the purple stars to assess craton-scale velocity variation. The yellow square is the Kambalda seismological station. The blue dotted line is the position of the passive-listening experiment aimed at collecting wide-angle reflection data (see later).**

## Broadband results

Broadband studies tend to focus on investigations of the mantle lithosphere.

The lithosphere is defined as the Earth's rigid outer layer. The only difference between it

114

and the underlying asthenosphere is its different rheological properties. Over time the lithosphere acts as a rigid shell whereas the asthenosphere behaves as a viscous fluid. The base of the lithosphere is defined as the 1300º C isotherm as this is where mantle rocks change from being rigid to more ductile. The boundary between the lithosphere and the asthenosphere is the seismically imaged low velocity zone (LVZ), where S-waves, which are sensitive to changes in shear modulus, are slowed down. The lithosphere is between 250 km and 300 km thick beneath shield areas, however, it is better defined beneath the oceans.

Broadband refers to the frequency range of the recorded seismic signal. Broadband recording implies a sampling pass-band from at least 0.5 to 100 s, in contrast to short-period instruments designed to record the higher frequency end of this band. The broadband technique records seismic waves whose wavelength is of the order of 10 to 50 km, a range that is of greatest interest both for the study of earthquake foci and for structural investigations.

The data collected during the deployment of the WP tomography sites have been provided to RSES, ANU, for inclusion in their Australia-wide Vp, Vs and surface wave studies of the continent. In return, RSES will provide updated Vp, Vs and surface wave images of the Australian continent. One such image, a 75 km depth slice beneath Australia, is shown in Figure 4-4. Blue colours indicate S-wave velocities faster than the world average. With time, further refinements of this model of the lithospheric velocity structure will be undertaken; as will Vp and surface wave images of the Australian lithosphere.

Initial indications support the earlier observations (eg Reading et al., 2003, Appendix 4-4); Reading and Kennett, 2003, Appendix 4-5) that the Yilgarn Craton has a low velocity crust that is underlain by mantle with a shear wave velocity faster than the world average (see Figures 4-5, 4-6, 4-7, 4-8 and 4-9). The teleseismic S-wave speed volume shows a higher-velocity, southeast dipping body approximately 70 km beneath the Murchison Province, increasing to approximately 100 km beneath the Ida Fault, then to approximately 120 km (see Figure 4-10). There are currently two suggestions as to what this higher-velocity body represents. These are a fossil southeast-dipping subduction zone, or a delaminated lower crustal restite layer. This topic is further discussed in Chapter 8.

Although the spacing of the sample points, and hence the griding of the teleseismic S-wave volume is coarse, there is an indication that this body is not just a single southeast dipping body but rather it is broken into a series of segments. We also note that there is a first order spatial correlation of these breaks with the main province boundaries mapped within the Yilgarn Craton.

The broadband teleseismic data indicate that the lithosphere beneath the Yilgarn Craton is of the order of 220 km deep (B.L.N. Kennett, *pers. comm.*). We also know that we can categorise the mantle beneath the Yilgarn and Pilbara Cratons as being **fast, depleted, refractory, cold, less dense, dry, strong, buoyant**; whereas the mantle beneath the

eastern part of Australia is **slow, undepleted, fertile, warm, dense, wet, weak, less buoyant**.

We can therefore infer that the mantle beneath the Yilgarn consists of harzburgite (i.e. peridotite or clinopyroxene-poor lherzolite), with the 100-120 km deep, high S-wave speed body indicating a compositional change from harzburgite to garnet lherzolite, or the change from garnet lherzolite to eclogite. We do not see a pronounced low velocity zone (LVZ) beneath the Yilgarn Craton. Current theories (Revenaugh and Jordan, 1991) suggest the LVZ is caused by preferential orientation of highly anisotropic olivine crystals during deformation at the boundary between the highly anisotropic lithosphere and the underlying isotropic asthenosphere (i.e. mechanical decoupling occurring where there is a change from dislocation to diffusion creep deformation (Karato, 1992)). This occurs at a depth of approximately 220 km beneath the cooler and/or drier continents but is shallower beneath wet and/or hot regions.
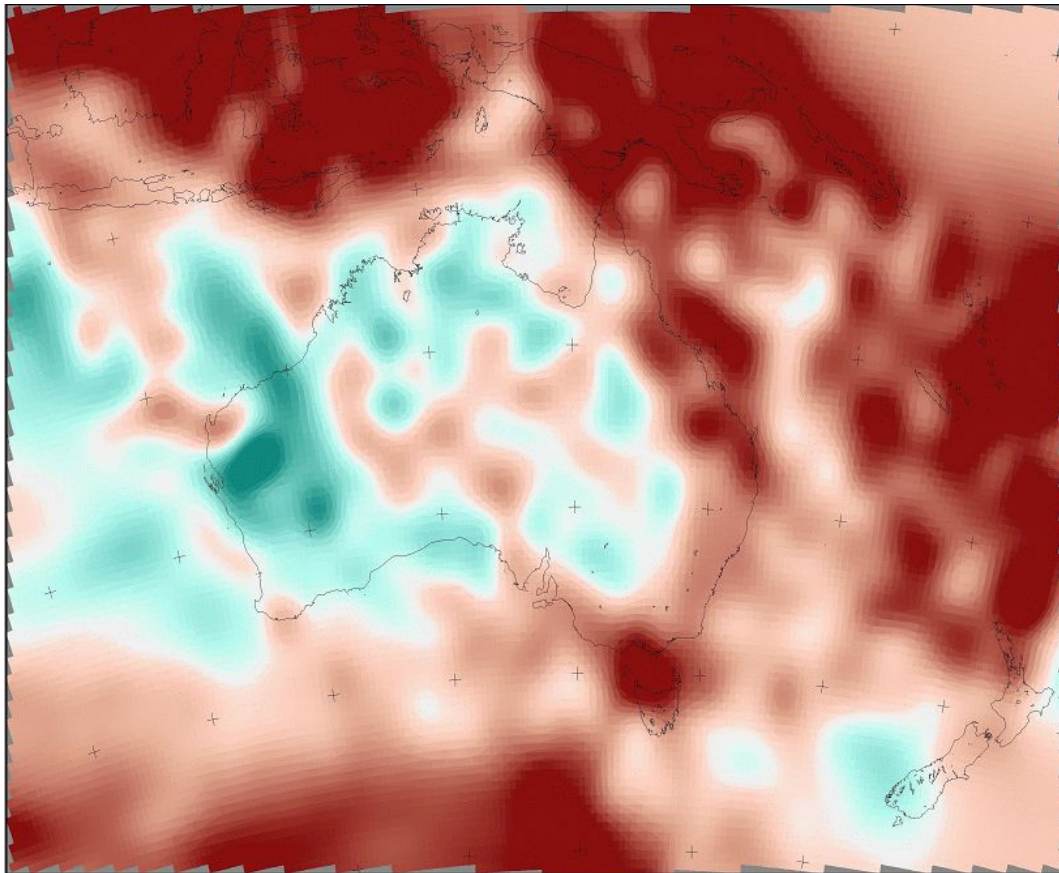


**Figure 4-4: Image of the 3D shear wave speed structure of the lithosphere beneath Australia at a depth of 75 km. Red/brown colours indicate S-wave velocities slower than the world average, blue colours indicate S-wave velocities faster than the world average. Image courtesy of B.L.N. Kennett, RSES, ANU.**

Kimberlite xenocryst data (Graham et al., 2004) indicate that the lithosphere beneath the Eastern Goldfields was either melt metasomatised prior to emplacement of the kimberlites or the lithosphere is relatively less refractory (i.e. melt depleted). Graham et

al. (2004) further suggests that the lithosphere beneath the EYC played a significant role in determining the petrophysical characteristics of the magmas that were emplaced into the EYC crust. This suggests that the lithospheric structure seen today is probably similar to that of the Archaean, as there has been very little deformation since the last magmas were emplaced.
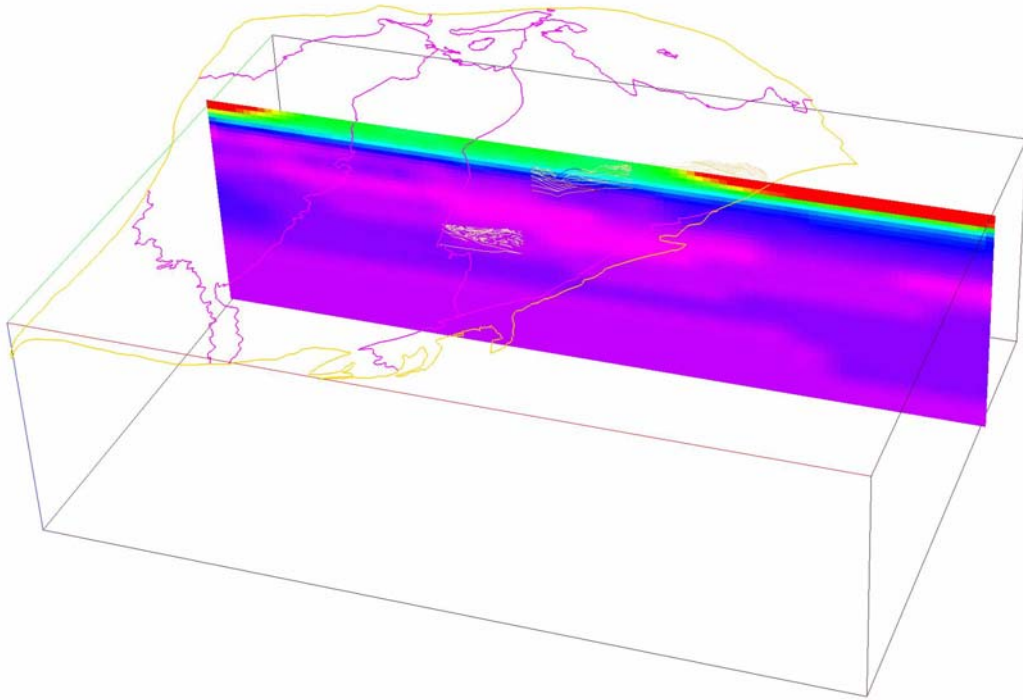


**Figure 4-5: Image of the 3D shear wave speed structure of the lithosphere beneath the Yilgarn Craton on an east-west vertical slice through the latitude of the north-eastern Yilgarn deep seismic reflection traverse 02GA_NY1. Pinker colours indicate S-wave velocities faster than the world average; blue colours indicate S-wave velocities slower than the world average. The yellow line is the surface outline of the Yilgarn Craton; purple lines are the main province subdivisions.**
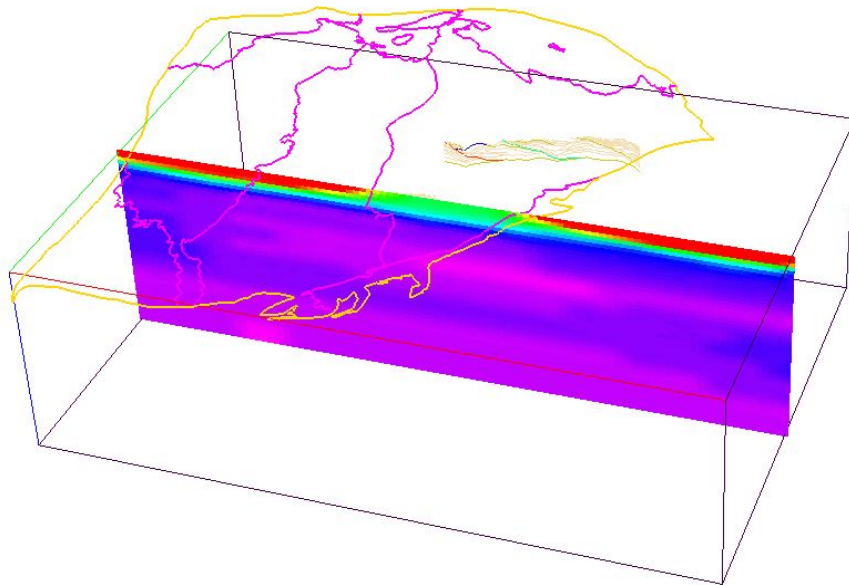
**Figure 4-6: Image of the 3D shear wave speed structure of the lithosphere beneath the Yilgarn Craton on an east-west vertical slice through the latitude of the 1991 deep seismic reflection traverse 91BMREGF01. Pinker colours indicate S-wave velocities faster than the world average; blue colours indicate S-wave velocities slower than the world average. The yellow line is the surface outline of the Yilgarn Craton; purple lines are the main province subdivisions.**
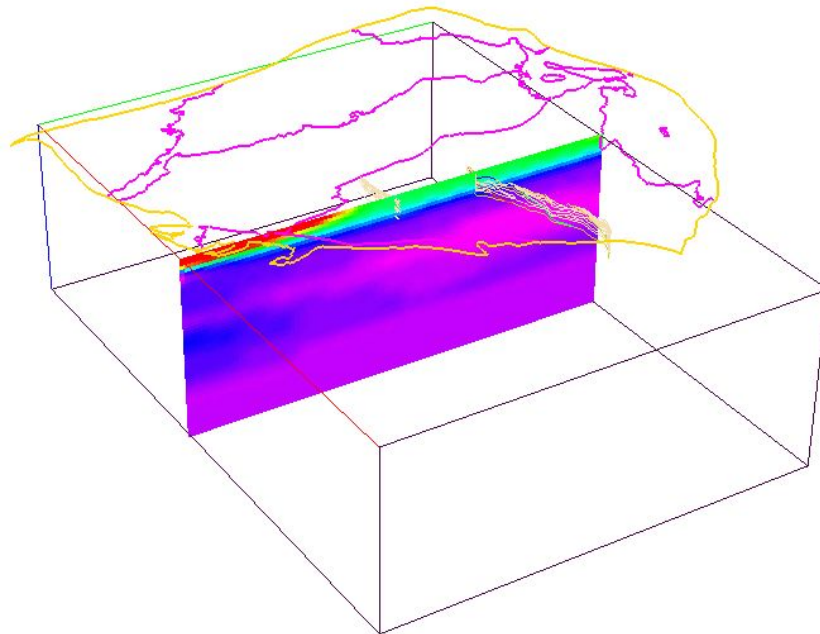


**Figure 4-7: Image of the 3D shear wave speed structure of the lithosphere beneath the Yilgarn Craton on a north-south vertical slice along the approximate longitude of the Kalgoorlie Terrane. Pinker colours indicate S-wave velocities faster than the world average; blue colours indicate S-wave velocities slower than the world average. The yellow line is the surface outline of the Yilgarn Craton; purple lines are the main province subdivisions.**

118
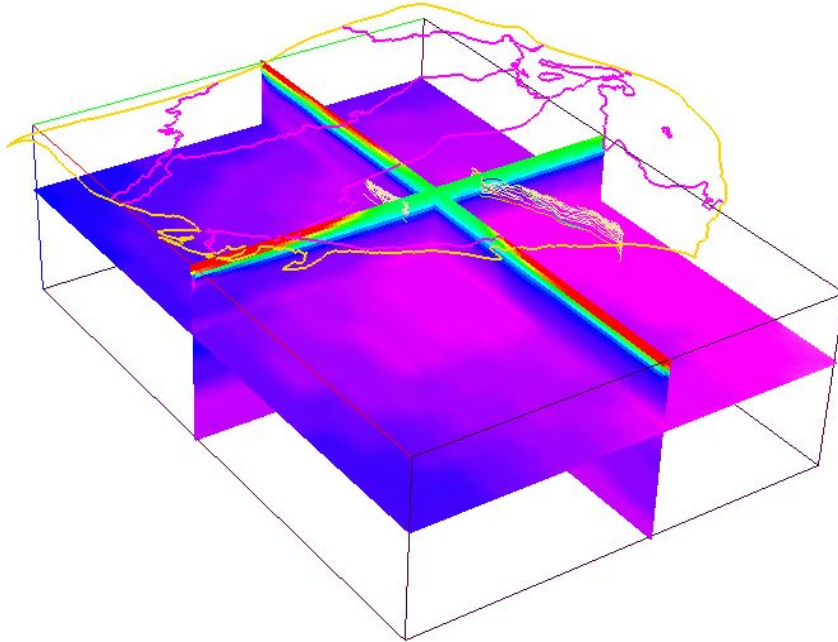
**Figure 4-8: Image of the 3D shear wave speed structure of the lithosphere beneath the Yilgarn Craton on 3 slices through the shear wave speed velocity volume. Pinker colours indicate S-wave velocities faster than the world average; blue colours indicate S-wave velocities slower than the world average. The yellow line is the surface outline of the Yilgarn Craton; purple lines are the main province subdivisions.**
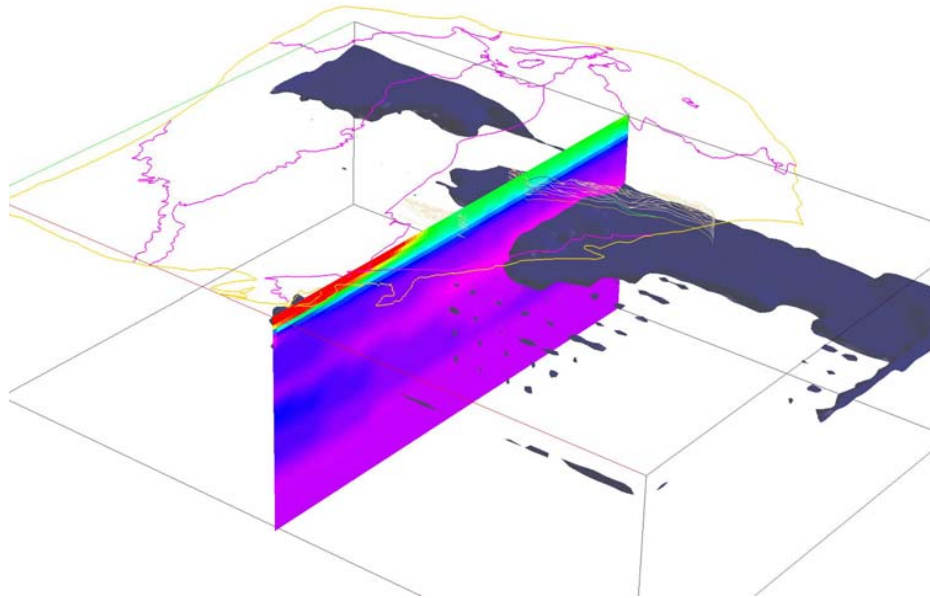


**Figure 4-9: Image of the 3D shear wave speed structure of the lithosphere beneath the Yilgarn Craton on a north-south vertical slice along the approximate longitude of the Kalgoorlie Terrane. Dark grey/black volume encloses the region of the mantle with shear wave speeds greater than 4.8 km/s. Pinker colours indicate S-wave velocities faster than the world average, blue colours indicate S-wave velocities slower than the world average. The yellow line is the surface outline of the Yilgarn Craton; purple lines are the main province subdivisions.**

119
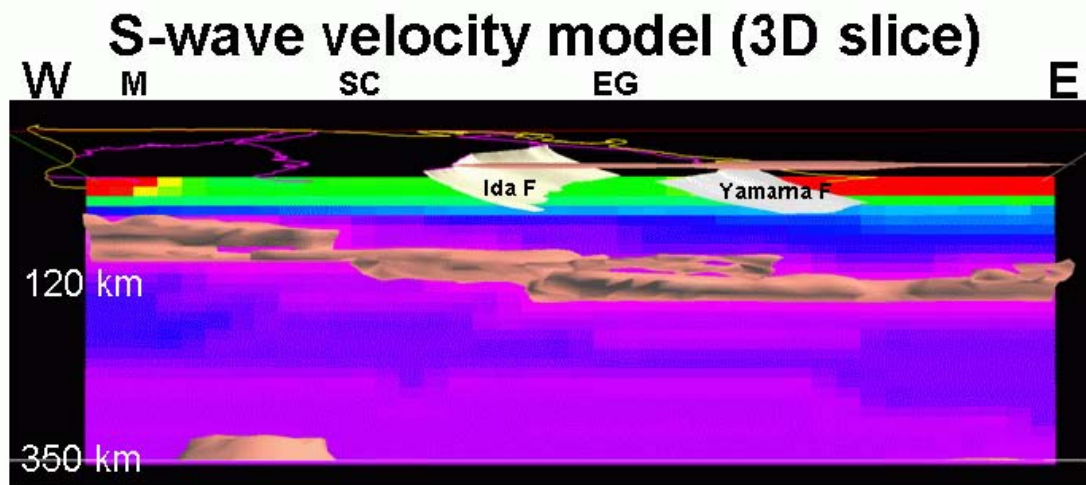
**Figure 4-10: 3D Image of the lithosphere beneath the Yilgarn Craton, looking northwards from a depth of approx 100 km. The velocity spectra changes colour from green to blue at the Moho. Two of the regional crustal penetrating shear zones, the Ida Fault and the Yamarna Fault, are shown as east dipping white-coloured surfaces. Pinker colours indicate S-wave velocities faster than the world average; blue colours indicate S-wave velocities slower than the world average. The yellow line is the surface outline of the Yilgarn Craton; purple lines are the main province subdivisions.**

## Receiver function results

A description of the receiver function method is best given in the following extract from Reading et al., in prep (Appendix 4-6). References cited in the extract below are given in Appendix 4-6.

*'The principles of the receiver function approach and the methods used to calculate the waveforms used in the modelling of structure were described by Reading et al.,(2003a). A more general description is given by Stein and Wysession, 2003. In summary, the signal due to the structure beneath the receiving station is extracted from the 3-components of the digital broadband record by deconvolving the vertical component with the horizontal component in the radial (source-to-receiver) direction (Ammon, 1991). Receiver functions were calculated in this way according to the method of Shibutani et al. (1999). The calculated receiver functions are stacked for each station, further reducing noise and enhancing the signal due to the receiver structure. Inherent in this approach is the assumption that the structure beneath the station may be approximated by a 1-D layered structure such that energy from all azimuths produces the same receiver waveform. Small departures from this assumption in the form of gently dipping layers do not strongly affect the analysis (Langston, 1977). The frequency of the incoming signal corresponds to a footprint on the Moho of several km across. The structure obtained are thus unaffected by small intrusive bodies or other structure that are less than a km in extent. The best-fitting structure is obtained from the stacked receiver function waveforms by searching the solution space using an algorithm that is well-suited to the non-linear relationship between the receiver waveform and Earth structure. As in previous work*

120

*(Reading et al., 2003a) we use the Neighbourhood Algorithm (Sambridge, 1999) that uses adaptive techniques to search the solution space in an efficient manner and also provides a means of visualising the best-fit structure against other structures that also fit the observed waveform almost as well.'*

## *Deployment summaries*

Table 4-2 provides position information for all broadband recorder deployments. Of the 23 sites occupied, 18 sites were successful in recording usable data, while 5 sites had instrument malfunctions and no recoverable data existed. This was a 78% data recovery rate.

| Station | Location | Latitude (dec degrees) | Longitude (dec degrees) | Height (mASL) |
|---------|----------|------------------------|-------------------------|---------------|
| WP01 | Wagga | -28.32100 | 116.93550 | 300 |
| WP02 | Munbina | -28.24150 | 117.44183 | 304 |
| WP03 | Challa | -28.29450 | 118.30233 | 427 |
| WP04 | Anketel | -28.03517 | 118.83667 | 479 |
| ~~WP05~~ | ~~Yarrabubba~~ | -27.12333 | 118.81567 | 491 |
| WP06 | Youangarra | -28.68050 | 118.82500 | 427 |
| ~~WP07~~ | ~~Bulga Downs~~ | -28.50867 | 119.76133 | 444 |
| WP08 | Jeedamya | -29.28233 | 121.25717 | 454 |
| WP11 | Diemels | -29.66167 | 119.31233 | 448 |
| ~~WP12~~ | ~~Riverina~~ | -29.75917 | 120.56983 | 445 |
| WP13 | Credo | -30.46283 | 120.81100 | 417 |
| WP14 | Binneringie | -31.53683 | 122.09800 | 275 |
| WP15 | Nepean | -31.21350 | 121.09317 | 424 |
| WP16 | Mt Vetters | -30.21133 | 121.08483 | 387 |
| WP17 | Cowarna | -31.02283 | 122.59850 | 327 |
| WP18 | Edjudinia | -29.96917 | 122.54633 | 386 |
| WP25 | Kanowna | -30.47550 | 122.70783 | 371 |
| WP26 | Mt Weld | -28.95000 | 122.51667 | 452 |
| WP27 | Mt Clara | -31.25683 | 119.82317 | 452 |
| ~~WP28~~ | ~~Riverina~~ | -29.75833 | 120.57000 | 437 |
| WP29 | Mendleyarri | -29.76383 | 121.72433 | 372 |
| ~~WP30~~ | ~~Cat Camp~~ | -31.68000 | 120.28700 | 475 |
| WP31 | Coglia | -28.87100 | 122.77950 | 512 |

**Table 4-2: Summary of seismometer information for instruments used during deployments.**

Table 4-3 provides seismometer and recorder information for all broadband recorder deployments. The 'Riverina' recording site was occupied twice in an attempt to obtain

data in this area. Although different recorders and seismometers were used on each occupation, both times were unsuccessful.

| Station | Location | Seismometer | Serial | Recorder | Disc1 |
|---------|----------|-------------|--------|----------|-------|
| WP01 | Wagga | 3ESP | T3137 | 7017 | AO4 |
| WP02 | Munbina | 3ESP | T3238 | 7023 | 51122 |
| WP03 | Challa | 3ESP | T3139 | 7018 | 51120 |
| WP04 | Anketel | 3ESP | T3136 | 7019 | 51124 |
| ~~WP05~~ | ~~Yarrabubba~~ | 3ESP | T368 | 7020 | 5168 |
| WP06 | Youangarra | 40T | T4666 | 7024 | 5169 |
| ~~WP07~~ | ~~Bulga Downs~~ | 3ESP | T3207 | 7169 | 51123 |
| WP08 | Jeedamya | 3ESP | T367 | 7022 | 5167 |
| WP11 | Diemels | 40T | T4664 | 461 | 51116 |
| ~~WP12~~ | ~~Riverina~~ | 40T | T4674 | 7170 | 51121 |
| WP13 | Credo | 40T | T4661 | 467 | 51117 |
| WP14 | Binneringie | 40T | T4657 | 465 | 51114 |
| WP15 | Nepean | 40T | T4666 | 7023 | 51123 |
| WP16 | Mt Vetters | 40T | T4674 | 7024 | 51120 |
| WP17 | Cowarna | 40T | T4664 | 7017 | 5169 |
| WP18 | Edjudinia | 40T | T7018 | 7018 | 5348 |
| WP25 | Kanowna | 40T | T3666 | 7024 | 51123 |
| WP26 | Mt Weld | 40T | T7018 | 7018 | 5169 |
| WP27 | Mt Clara | 40T | T4666 | 7017 | 51116 |
| ~~WP28~~ | ~~Riverina~~ | 40T | T4664 | 7017 | 5348 |
| WP29 | Mendleyarri | 40T | T4664 | 7024 | A04 |
| ~~WP30~~ | ~~Cat Camp~~ | 40T | T4674 | 7023 | 51120 |
| WP31 | Coglia | 40T | T4661 | 7018 | 51123 |

**Table 4-3: Summary of number of earthquake events used during deployments.**

For each site, a number of teleseismic earthquakes have been recorded. The number of earthquake events usable is given in Table 4-4.

| Station | Location | No Events |
|---------|----------|-----------|
| WP01 | Wagga | 3 |
| WP02 | Munbina | 8 |
| WP03 | Challa | 8 |
| WP04 | Anketel | 7 |
| WP06 | Youangarra | 5 |
| WP08 | Jeedamya | 2 |
| WP11 | Diemels | 8 |

| | | |
|---|---|---|
| WP13 | Credo | 8 |
| WP14 | Binneringie | 7 |
| WP15 | Nepean | 16 |
| WP16 | Mt Vetters | 9 |
| WP17 | Cowarna | 18 |
| WP18 | Edjudinia | 16 |
| WP25 | Kanowna | 6 |
| WP26 | Mt Weld | 5 |
| WP27 | Mt Clara | 25 |
| WP29 | Mendleyarri | 2 |
| WP31 | Coglia | 12 |

**Table 4-4: Summary of number of earthquake events used during deployments.**

The results from each of the successful broadband recording sites are given in Appendix 4-3. Figure 4-11, from Reading et al. (in prep), shows the results from three sites, one in the Southern Cross Province (WP13) and two in the EYC (WR07 and WP18).

Rather than repeating all the results, the reader is referred to Reading et al. (in prep) in Appendix 4-6 for further discussions on the data analysis. A summary of the results of the receiver function is best given in the following extract from Reading et al. (in prep; Appendix 4-6).

*'The Precambrian terranes of the West Australian Craton show seismic structures that are characteristic of each of the large terrane groups; Pilbara, Murchison, Southwest, Southern Cross, Eastern Goldfields and Capricorn Orogen. There is notable consistency in structure through the Pilbara, Murchison and Southern Cross Terranes. A proposed mechanism for the formation of an especially sharp Moho is the extensive reworking of crustal rocks such that the lower crust becomes more felsic and lower in seismic velocity, leading to a sharper discontinuity across the seismic Moho. Structure is more variable across the Southwest and Eastern Goldfields terranes. It is likely that the seismic structure was 'frozen in' to each terrane prior to the assembly of the craton. The receiver function method is now established as a tool for mapping crustal units in regions of limited exposure and is a practical and economic alternative to seismic refraction experiments.'*

These observations are illustrated in Figure 4-12.
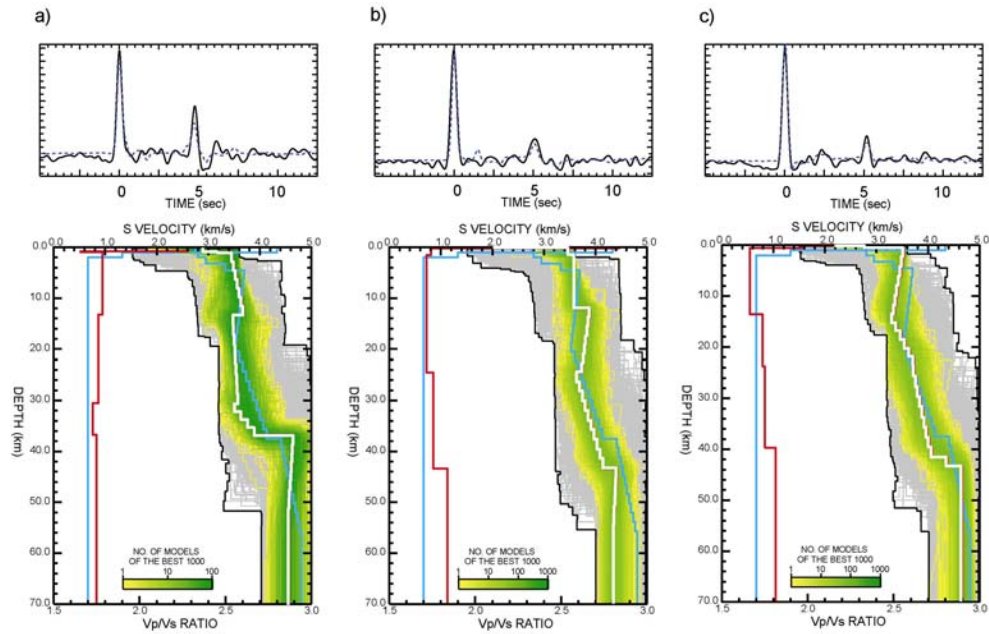
**Figure 4-11: Diagram from Reading et al. (in prep). Observed and best-fit synthetic receiver functions and seismic velocity plots for stations in the a) Southern Cross (WP13) and b) & c) Eastern Goldfields (WR07 and WP18) Terranes. The seismic velocity plots show the best-fit structure (broad white line) corresponding to the best-fit synthetic receiver function. The aqua line is a Yilgarn reference model. The green density plots behind the white lines all correspond to the same number of iterations and hence give a comparative indication of the regions of solution space which might also contain a well-fitting structure. The Vp/Vs velocity ratios for the site (red) and the Yilgarn reference (aqua) are shown to the left of each plot.**

Although there is a marked variation in velocity profile between the various terranes, it has not been possible to distinguish between mineralised and non-mineralised areas within the same domain.

**Murchison**

S VELOCITY (km/s)

Moho depth 34 km (e.g. WR05)
Sharp
Simple upper crust
Velocity gradient in lower crust
Structure very consistent across terrane

**Southwest**

S VELOCITY (km/s)

Moho depth 36 km (e.g. WT04)
Sharp away from terrane edges
Discontinuity in upper crust
High velocity gradient zone above Moho
HVGZ thickens towards the west

**Southern Cross**

S VELOCITY (km/s)

Moho depth 38 km (e.g. WT08)
Very sharp
Simple upper crust
Constant velocity lower crust
Structure consistent across terrane

**Eastern Goldfields**

S VELOCITY (km/s)

Moho depth 42 km (e.g. WV05)
Sharp
Discontinuity in upper crust
Lower crust velocity gradients variable
Structure generally very variable
Moho much shallower towards the south

**Pilbara**

S VELOCITY (km/s)

Moho depth 32 km (e.g. MBWA)
Very sharp
Discontinuity in upper crust
Velocity gradient in lower crust
Moho deeper in the south of the craton

**Capricorn Orogen**

S VELOCITY (km/s)

Moho depth 44km (e.g.WR04)
Broad
Discontinuity in upper crust
Velocity gradient throughout lower crust
Structure variable
Moho sometimes hard to define

**Figure 4-12: Diagram from Reading et al. (appendix 4-4) summarising average velocity functions for each province. The grey area behind the white velocity function plot is an indication of the regions of solution space which might also contain a well-fitting structure.**

## *Implications for predictive mineral discovery*

These teleseismic and receiver function data sets support the conclusion that the lithosphere below the Yilgarn Craton is far more complex than originally suggested. The broadband data indicate the lithosphere beneath the Yilgarn is of the order of 220 km deep and that there is evidence of a higher velocity mantle body that dips to the east-southeast. This mantle body varies in depth from approximately 70 km beneath the Murchison Province to approximately 120 km at the eastern margin of the craton. The receiver function results show an eastward thickening of the Yilgarn Craton crust.

## *Appendix 4:*

4-1: **Appendix4-1_ANSIR_application_Y2_tomography.pdf** is a PDF of the submitted ANSIR proposal 'The Velocity Structure of the Yilgarn Crust and Upper Mantle: Receiver Function and Teleseismic Analysis' for the *pmd*\*CRC's tomography work.

4-2: **Appendix4-2_Field_Photos.pdf** is a PDF of photographs taken during acquisition of the tomography survey.

4-3: **Appendix4-3_RecFn_Results.pdf** is a PDF of the receiver function results produced as part of the *pmd*\*CRC'S Y2 tomography investigations of the Yilgarn Craton.

4-4: **Appendix4-4_Reading_etal_ajes_50_3.pdf** is a PDF of the paper '*Seismic structure of the Yilgarn Craton, Western Australia*' by Reading, A.M., Kennett, B.L.N. and Dentith, M.C.

4-5: **Appendix4-5_Reading&Kennett_ajes_50_3.pdf** is a PDF of the paper 'Lithospheric structure of the Pilbara Craton, Capricorn Orogen and northern Yilgarn Craton, Western Australia, from teleseismic receiver functions' by Reading, A.M. and Kennett, B.L.N. Published with the permission of the Geological Society of Australia.

4-6: **Appendix4-6_Reading_etal_PRECAMBRIANRESEARCH_draft.pdf** is a PDF of draft paper '*The deep seismic structure of Precambrian terranes within the West Australian Craton and implications for crustal formation and evolution*' by Reading, A.M., Kennett, B.L.N. and Goleby, B.R. This paper outlines initial results of the received function analysis.

4-7: **Appendix4-7_VRML_images.pdf** is a description and screen snapshots of VRML of tomography data.

4-8: **Appendix4-8_Goleby_etal_seismix04.pdf** is a PDF of the paper reprinted from Tectonophysics, 388, Goleby, B.R., Blewett, R.S., Korsch, R.J., Champion, D.C., Cassidy, K.F., Jones, L.E.A., Groenewald, P.B., and Henson, P.A., Deep seismic reflection profiling in the Archaean northeastern Yilgarn Craton, Western Australia: implications for crustal architecture and mineral potential, 119-131, Copyright (2004) with permission from Elsevier.

4-9: **Appendix4-9_Tomography_depth slices.pdf** is a PDF of depth slices from teleseismic data set.

4-10: **Appendix4-10_Tomography_talk.pdf** is a PDF of Mineral Division talk with emphasis on teleseismic data sets.

4-11: **Appendix4-11_SEG04_Goleby.pdf** is a PDF of a PowerPoint presentation presented at the 2004 Society of Economic Geologists meeting, Perth, September, 2004.

4-12: **Appendix4-12_pdt2004_Goleby_tomography.pdf** is a PDF of a talk on 'Application of seismic Application of seismic techniques for imaging of lithospheric techniques for imaging of lithospheric architecture' presented at the final Y2 wrap-up meeting, Perth, December, 2004.

4-13: **Appendix4-13_pdt2004_Blewett_lithosphere.pdf** is a PDF of a talk on 'Lithospheric Geodynamics: a seismic view of the Yilgarn Craton' presented at the final Y2 wrap-up meeting, Perth, December, 2004.

4-14: **Appendix4-14_Depth_Slices_Images** is a folder of 30 tif images of successive depth slices through the tomography volume. Each slice is 12.5 km apart.

4-15: **Appendix4-15_RecFn_Result_Images** is a folder of 18 jpeg images of receiver function data.

4-16: **Appendix4-16_Tomo_Vrml** is a vrml model of the tomography volume. The browser plugin Blaxxun is required, and can be downloaded for free on: http://www.blaxxun.com/en/products/contact/index.html

# Chapter 5: Chalcophile and key element distribution in the EYC

*A.A. Kalinowski*

## Introduction

The initial goal of this subproject was to produce a map of chalcophile elements within the basement rocks across selected portions of the east Yilgarn Craton (EYC). The purpose of this study was discussed at length at the Y2 PDT meeting in Perth in February 2003, however, and its role and relevance in the overall Y2 project re-evaluated.

The feeling of the industry sponsors present at the meeting was that there was a large amount of restricted data within companies and that they were conducting this type of research already. Consequently, at the meeting it was decided to stop further work on this objective. The results from the work already completed were to be written up and displayed on the project page of the *pmd*\*CRC website for comment. Sponsors suggested that the report include information on what had been achieved in analysis of regional bedrock geochemistry data and on correlating various chalcophile-element distributions and bedrock and faults locations. This report was completed before the end of that quarter and delivered to sponsors, and put on TWIKI by March 2003.

## Objectives and aims of the chalcophile subproject

The aim of the geochemical analysis was to seek to identify regional chalcophile corridors within the bedrock (partly as a complement to CRCLEME's regolith studies) which could be used as an aid in locating gold prospects. Two aspects of the regional geochemistry were considered:

1. the distribution of chalcophile elements from bottom-hole whole-rock geochemistry along the seismic line EGF01, and
2. the regional distribution of chalcophile and trace elements by creating geochemical contour maps from available data.

The geochemical analysis data (mainly bottom-hole geochemistry) was obtained from Geoscience Australia, the Geological Survey of Western Australia and a little from companies. BHP Billiton had already compiled most of these data, however it became impractical to gain access to this data set.

The relevant elements were compiled into a database and then plotted. These plots are shown in the attached PDFs. A few selected images are included herein.

The main milestones of this subproject were the preparation of an initial report by March 2003 and the compilation of available chalcophile elements and maps of various

chalcophile elements by June 2003.

**Work progress:**
Geochemical data were obtained from Geoscience Australia and the Geological Survey of Western Australia, analysed for duplication and plotted. These data images were presented at the 2003 Y2 Project Development Team meeting in Perth between 10/2/03 and 12/2/03.

Outputs prepared as part of this subproject include PowerPoint presentations showing:

1. chalcophile and other trace element distributions along the 1991 deep seismic reflection traverse 99-EGF01 (see **egf01_geochemistry.pdf**), and,
2. chalcophile and other trace element distributions throughout the EYC (see **yilgarn01_geochemistry.pdf**).

Maps of the chalcophile elements are included as layers in the 3D map (see Appendix 2.1 **nws_chalcophyles**).

## *Methodology*

Once the data were collated two aspects of the regional geochemistry were worked up. These were the distribution of chalcophile elements from bottom-hole whole-rock geochemistry along the seismic line EGF01, and the regional distribution of chalcophile and trace elements by creating geochemical contour maps from available data.

### Distribution of chalcophile elements along the seismic line EGF01

Bottom-hole geochemistry values were plotted as profiles, along with the location of known faults and lithology in an attempt to identify possible geochemical leakage along crustal-scale faults.

The location of the seismic traverse EGF01 is shown in Figure 5-1. An example of the output produced for this component of the work is shown in Figure 5-2. The complete results are contained in **egf01_geochemistry.pdf**.

### Regional distribution of chalcophile and trace elements

Data were read into both Arcview and Petrosys for griding and plotting. To assist in the identification of geochemical leakage along crustal scale faults, the major fault systems were imported into Petrosys and were used as a constraint in the griding process.
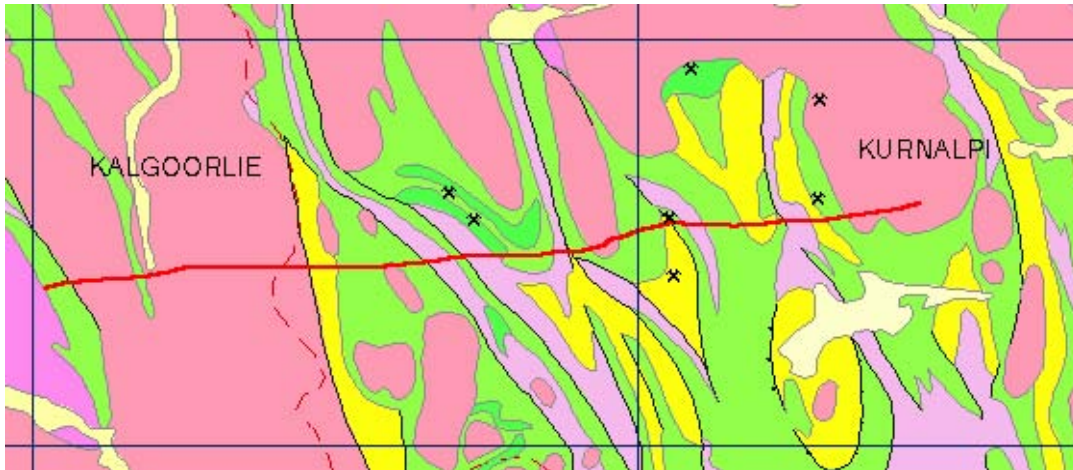
**Figure 5-1: The Kalgoorlie Seismic Transect EGF01 (thick red line) on the Kalgoorlie and Kurnalpi 1:250 000 sheets. The dotted line is a magnetic boundary. Derived from the GA database.**

In summary, the key points of this aspect of the work were:

- Petrosys, a program usually applied to petroleum geology, was used to produce geochemical grids and contour maps.
- Data from Geoscience Australia's geochemical database (Ozchem) were used to produce geochemical grids and contour maps for the EYC.
- Grids were generated using the Distance Weighted Averages (DWA) interpolation method with, unless otherwise stated, a 200 m × 200 m cell size.
- The area covered by the grids is the entire EYC region from 119º45'E to 123ºE and 33ºS to 25ºS.
- Minimum values were generally set at an estimated background level to eliminate background "noise". Input values were adjusted to produce the best grids. These values are stated next to the images.
- Major faults were included in the final stages of the griding process. These faults were current in January 2003.
- A combination of the best grids and contours were produced, together with a small reference geological map.

The location of the sample points used in the regional work and an example of the output produced for this component of work is shown in Figure 5-3. The complete results are shown in **yilgarn_geochemistry.pdf.**
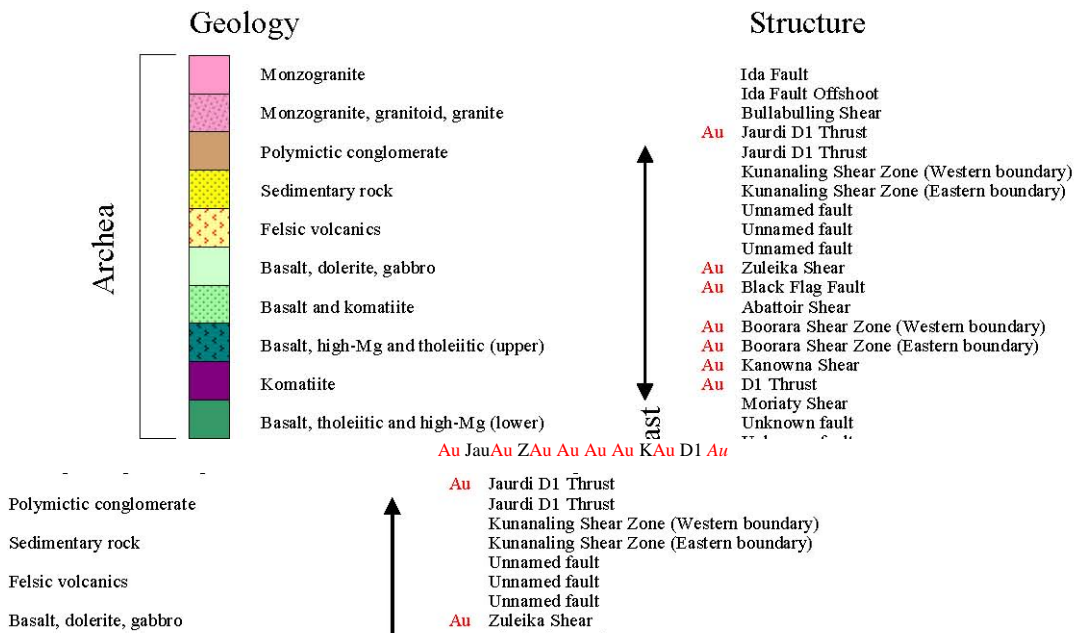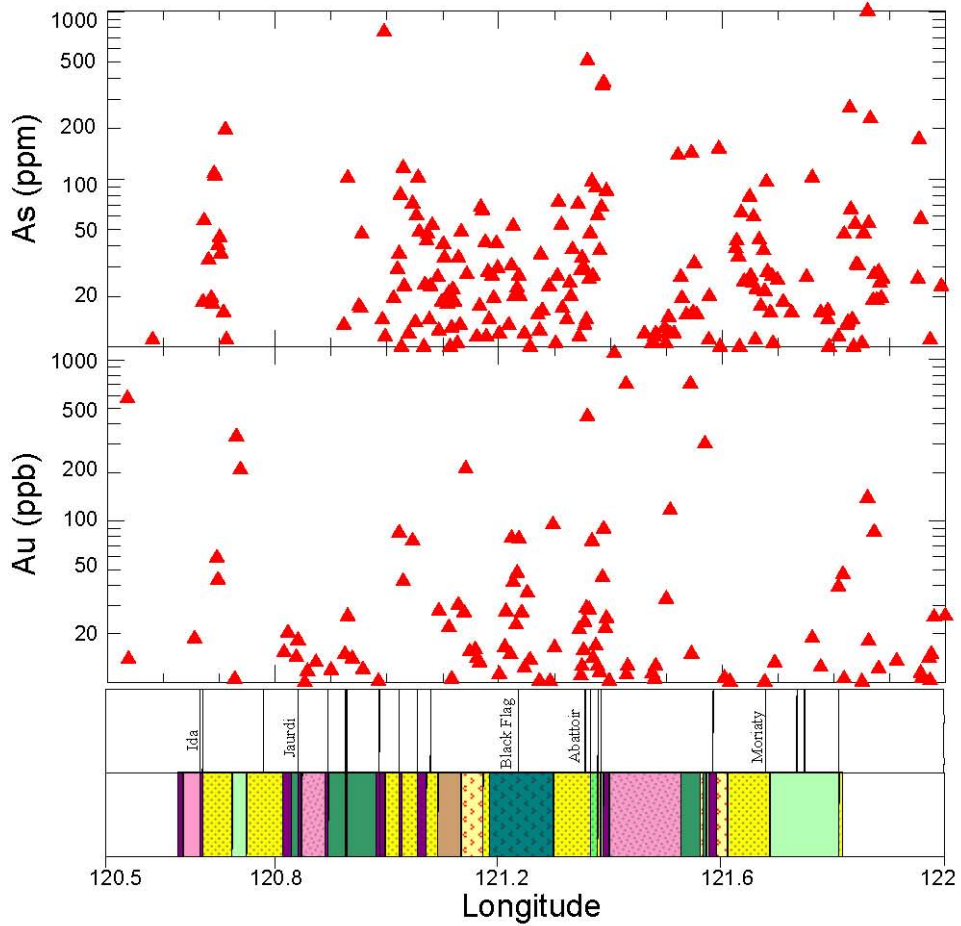
**Figure 5-2: Au and As variations along part of the Kalgoorlie Seismic Transect EGF01. Main faults plotted over general lithology. Data derived from the GA database.**
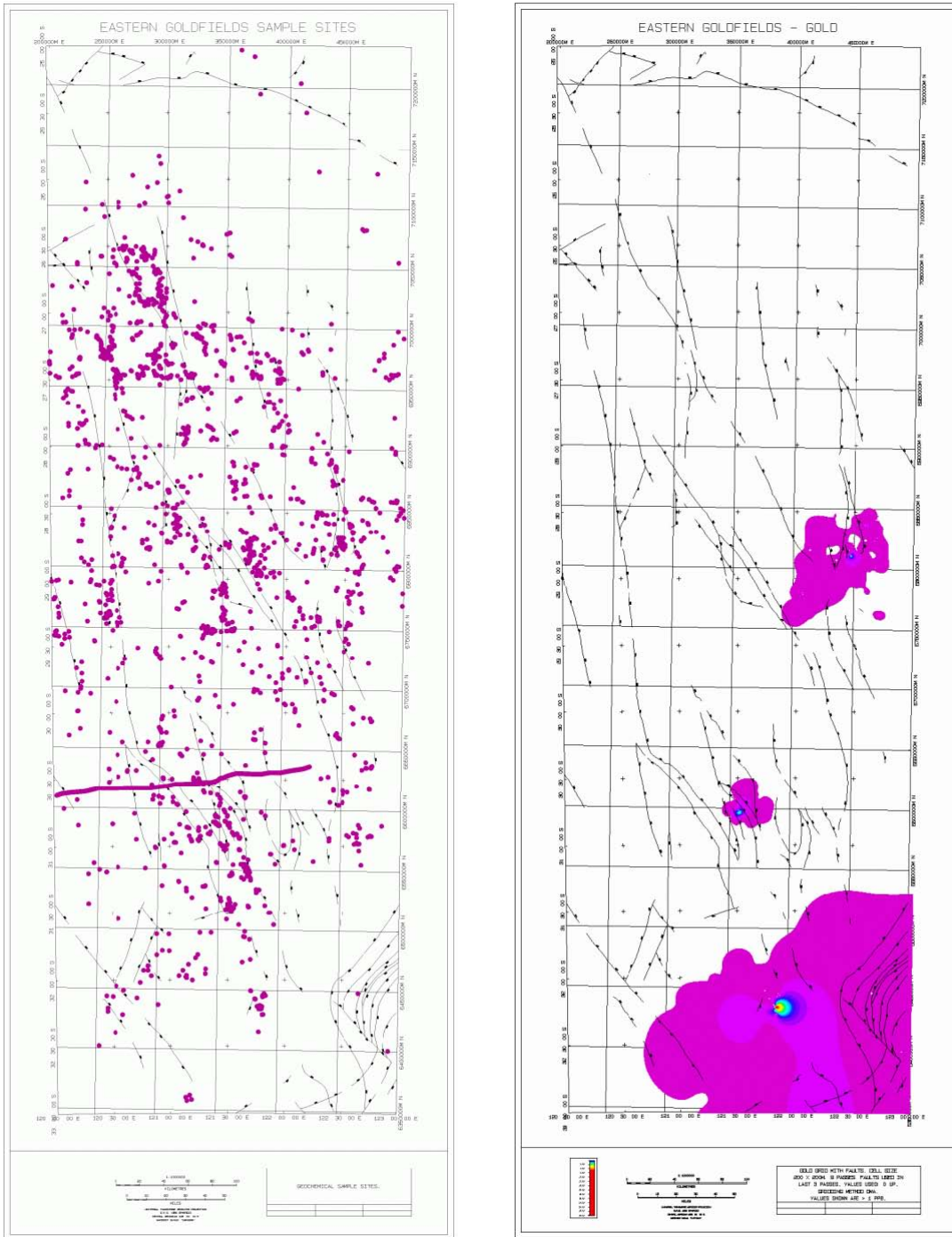
**Figure 5-3: Sample locations used for analysis of the regional distribution of chalcophile and trace elements within the EYC, and an example of the output for one element. Main province scale faults plotted over general lithology. Data derived from the GA database.**

**Some questions addressed during the work:**

- What is the distribution of elements in the Kalgoorlie area?

- Are any elements associated with gold?
- Do any elements increase/decrease systematically with gold?
- Are there any broad halos?
- Which elements correspond to the underlying lithology and which are lithology independent?
- Which elements correspond directly to faults/fluid conduits?
- Which elements correspond to faults linked with mineralisation?
- What do S, O and C isotopes in the veins and around the deposits show?
- Is the fluid source magmatic? Connate? Metamorphic?
- Is there an association between gold and granites?

## Implications for predictive mineral discovery

This work supported the following:

- The geochemical approach to exploration for gold has been used successfully in the past in the EYC.
- Gold and arsenic have been identified as the best indicators of mineralisation.
- Most exploration has therefore been constrained both spatially (to company leases), and chemically (to gold and arsenic).
- It is therefore important to assess the geochemistry, chalcophile, and key element distribution in the bedrock on a regional scale through contouring and geochemical profiling.
- Although the geochemical data used here are not as dense (spatially) as company data, they have the advantage of being well distributed on a regional scale, as well as encompassing a suite of elements.

This work indicated that:

- As expected from studies on a local scale, areas of high gold and arsenic generally coincide on a regional scale, and these areas also tend to coincide with faults or fault junctions.
- Arsenic appeared to be a good indicator of mineralisation from a regional perspective.
- Arsenic 'halos', however, are spatially almost as restricted as gold anomalies (from a regional perspective).
- The distribution of Au and As seems to be more closely related to faults and fault junctions than lithology.
- The distribution of Ag is similar to that of Au, and so could be an indicator of mineralisation but not a vector to it.
- The distributions of Ni, Cr, Zn, Cu are controlled much more by lithology than structure.
- Several of the elements investigated are particularly useful as vectors to gold mineralisation.
- These elements are much more useful as local indicators of mineralisation.

## Points of interest

- Gold seems to be the best tracer of gold-deposit-associated fluid pathways.
- Arsenic seems to be associated with gold to some extent. In some cases, anomalously high As values are recorded in conjunction with anomalously high Au values, however, in other cases, high Au values are accompanied by very low As values. Although this does limit the usefulness of As in estimating fluid pathways or pinpointing Au deposits, it does support the theory that these chemical signatures are primary and not due to leaching of deposits. The variability of arsenic abundance could well be due to the extraction of As from the fluid as it moves through sulphur-rich rocks.
- There is both a temporal and spatial association between gold and granites/granitoids, however, there is not necessarily a genetic link between the two. Metamorphism to granulite grade of the lower crust would have dehydrated the lower and middle crust of a great deal of water. The fluid travelling through crustal-scale structures carrying gold would have caused mineralisation in structures in the middle crust. The same metamorphic event and consequent de-watering would have caused crustal melting and therefore granite emplacement pre- and post-mineralisation. Both the fluid and the magma would have used the same crustal-scale structures to travel through. Thus, they are both spatially and temporally associated, with some gold deposits in granitoids, although the granites are not necessarily the source of either gold or fluid.
- Elements thought to have some association with gold include:
  - silver, although it doesn't seem to be very abundant,
  - bismuth, which has very low abundances is sometimes associated with gold and at other times completely separated,
  - molybdenum, although again abundances are very low, and,
  - tungsten, which unfortunately either wasn't analysed or was present below detection levels.
- Lithology is likely to have a strong influence on the following elements:
  - nickel, which has an almost exclusive association with komatiite flows,
  - copper and zinc are likely to be associated with mafic rocks – basalts and komatiites, and,
  - lead and rubidium are likely to be associated with granites or sediments.

## Gold and trace elements

There are a number of elements which could potentially be associated with gold deposits through being carried in the same fluid. Some elements are associated with the ore, some are associated with wall rock alteration, and others are depleted in the ore zone or wall rock.

- Ore metal (local) associated elements include Au, Ag, W, As, Te, Sb, Cu, Pb, Bi, Sn.
- Wall rock alteration includes $CO_2$ (carbonate), K, S (pyrite) ±B, V, Ba, Rb, Li, Sr enrichment.

- Depletion or remobilisation of the following elements/minerals from the ore zone can occur: Na, Ca, $Fe_2O_3$.
- In addition there are element ratios which could be useful in tracing fluid pathways and gold occurrences. Some examples include K/Rb, K/Na, K/Ba, Te/Au, Ag/Au, Au/Ag, Sb/Au, Te/Se, Cu/Pb.
- Geochemical dispersion halos of the following elements are useful on a regional scale: Au, As, enriched pisolites, enriched/anomalous soils, BIFs.

## Other element trends and associations

Rubidium and lead are both incompatible elements and as such will be found in primary melts such as granites and granitoids. Figure 5-4 is a graph showing the essentially 1:1 relationship between these two elements, excluding a few outlying values.
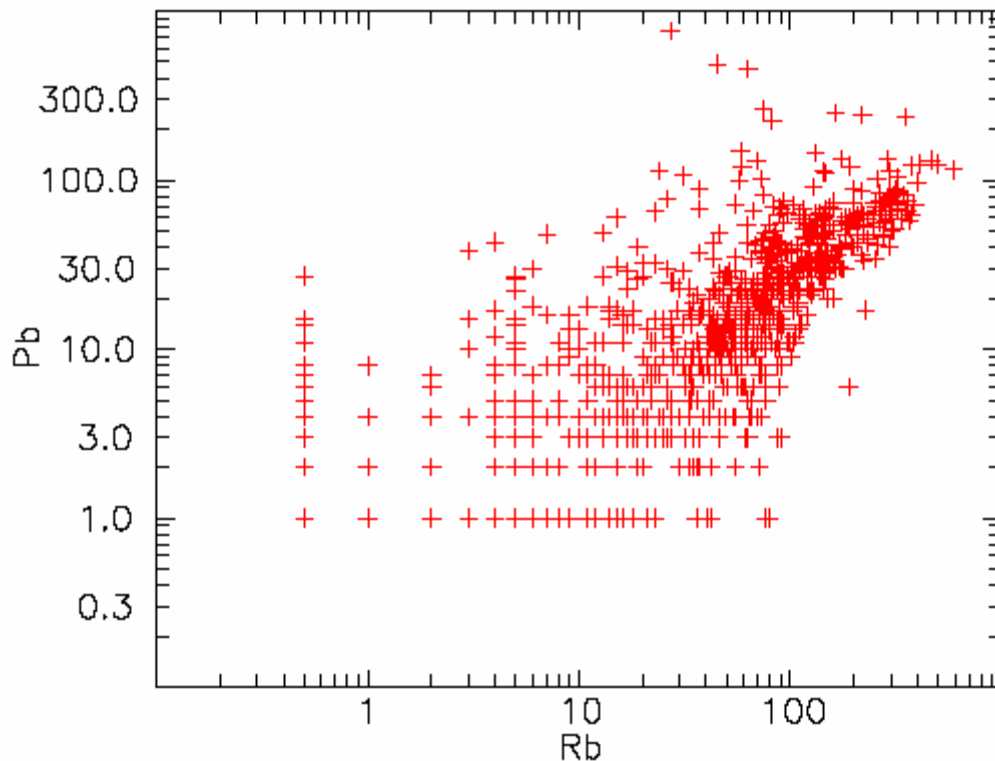


**Figure 5-4: Plot of Pb vs Rb along the seismic line. Data derived from the GA database.**

## Geochemistry along seismic line EGF-01

The seismic transect EGF01 was completed in 1991. It is 213 km in length, oriented approximately east-west, and is some 30 km north of Kalgoorlie (Figure 5-1). Major features of the EYC granite-greenstone terrane (including rock types and structures) were encountered along its length including its boundary with the Southern Cross Terrane.

Sample material was collected from the bottom (nominally 40 m depth) of each shot hole (giving a total of 883 samples) and analysed for 30 trace elements (Goleby et al., 1993). An effort was made to collect and analyse only bedrock samples. Inevitably, however, regolith samples were incorporated into the collection due the depth of regolith cover in the Yilgarn craton, and so the results should be regarded with caution.

Samples were analysed by X-ray fluorescence using the method of Norrish and Chappell (1977). Concentrations were obtained for the following elements: Ag, As, Ba, Be, Bi, Ce, Cr, Cu, Ga, Ge, Hf, Li, Mn, Mo, Nb, Nd, Ni, Pb, Rb, Sc, Se, Sn, Ta, Th, U, V, Y, Zn and Zr. In addition, the same samples were analysed at the Geological Survey of Western Australia for Au, Pt and Pd.

## Chemistry compared to structures and geology

The abundance of each element was plotted against the geology and structure encountered by the seismic line (according to maps current in November 2002). One of the outcomes of the analysis of the seismic line was to reinforce the idea that the best geochemical indicator of gold mineralisation is gold itself.

Anomalies in the distribution of gold along the seismic line reflect the positions of faults rather than changes in lithology (Figure 5-5). The limited mobility of gold ensures tight, discrete peaks which, where they exist, correspond directly to individual structures. From this evidence and the current consensus on the orogenic, structure-hosted nature of the gold deposits in the Yilgarn Craton it can be concluded that where positive gold anomalies exist in conjunction with faults, the faults are most likely associated with mineralisation which may exist within the fault or, more often, within splays.

This consistent relationship between gold and faults or shear zones leads to two further hypotheses.

Firstly, a structure not associated with a positive gold anomaly was either not a mineralising fluid conduit (not connected to the mineralising network of faults) by being a later or inactive structure at the time of mineralisation; or the fault/shear was the 'backbone' of the plumbing system and so was completely flushed of its gold residue by syn- and post-mineralisation fluids. It is probable that very little gold would have precipitated in this type of fluid conduit. A possible example is the Ida fault.

Secondly, positive gold anomalies not obviously associated with recognised structures are either inconsistent anomalies (not fault related) possibly associated with, for example, porous basin sequences; or, more likely, are indicative of faults which have not been identified. In support of the latter hypothesis, at least two positive anomalies were recognised that were used to identify two previously unknown faults between the Ida Fault to the west and the Bullabulling Shear to the east (Figure 5-2).

After assessing the abundance of gold along the seismic traverse, a background value of 10 ppb for gold was selected. Of all the analyses, the element found to be most closely

associated with gold mineralisation was arsenic (background value 10 ppm). The distribution of gold and arsenic is shown compared to structures and geology (current in November 2002) for the EYC section of the seismic line, from 120º30'E to 122º00'E in Figure 5-2.
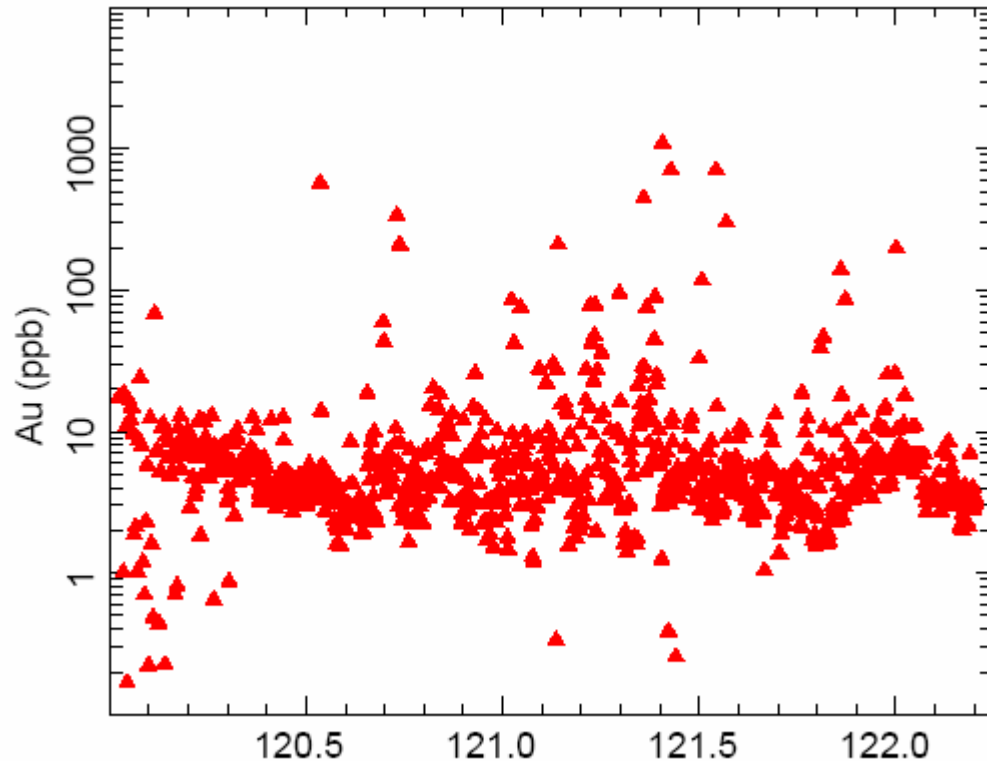


**Figure 5-5: Log graph of abundance of Au along the seismic traverse (longitude on x-axis).**

## *Summary*

Questions raised but not resolved include:

- What elements show a correlation with Au?
- For elements that don't show a correlation, is there a dependence on rock type (i.e. felsic > 50% $SiO_2$, mafic, < 50% $SiO_2$)?
- Correlation of seismic line samples with faults and lithology.
- As expected from studies on a local scale, in general areas of high gold, gold and arsenic coincide. Is this relationship applicable on a regional scale?
  - if so, arsenic should be a good indicator of mineralisation from a regional perspective,
  - however, arsenic 'halos' are spatially almost as restricted as gold anomalies (from a regional perspective).
- Are there much more useful local indicators of mineralisation?
- The distribution of Au and As seems to be more closely related to faults and fault

junctions than lithology. Is this actually indicating fluid movement up crustal penetrating faults as suggested?

In summary, this study of the chalcophile distribution and geochemistry in the EYC indicates that:

- the geochemical approach to exploration for gold has been successfully applied in the past in the EYC,
- gold in particular, and arsenic, have been identified as the best indicators of mineralisation,
- most exploration has therefore been constrained both spatially (to company leases) and chemically (to gold and arsenic), and,
- there has been a change in emphasis from geochemistry to attempting to understand the evolution of the EYC and the tectonic setting of gold deposits.

## *Appendix 5:*

5-1    A PowerPoint presentation showing chalcophile and other trace element distributions along the 1991 deep seismic reflection traverse 99-EGF01 (see **Appendix 5_1 egf01_geochemistry.pdf**).

5-2    A PowerPoint presentation showing chalcophile and other trace element distributions throughout the EYC (**Appendix 5_2 yilgarn01_geochemistry.pdf**).

5-3    Original figures for chalcophile variations along seismic traverse EGF01 and for regional variation (see **Appendix 5_3 chalcophile maps.pdf**).

5-4    A PDF of a summary of CRCLEME report P241A describing geochemical variation in the regolith (see **Appendix 5_4 Summary_P241A.pdf**).

# Chapter 6: An assessment of the utility of the new 3D data versus the 2D data at a regional scale: geodynamic insights

*R.S. Blewett*

## Introduction

The uptake and now routine process of building regional and semi-regional 3D maps by sponsors of this project is a clear measure of the added utility of developing a 3D understanding (with time) versus traditional 2D approaches.

The process of building a 3D map necessitates a far greater degree of rigour than that needed for traditional 2D maps and GIS data sets, because it requires each adjacent relationship to be considered in 3D. From this approach a temporal understanding of all unit and event relationships is developed.

Development of a structural framework and its likely geodynamics were not an explicit task or deliverable for the Y2 project. However, the model building process has meant that aspects of the structural paradigm for the eastern Yilgarn Craton (EYC) were questioned. The following section is a summary of the structural history as ascertained by carefully examining map patterns, drawing validated serial cross section, and constructing 3D surfaces and volumes.

## Structural history

### $D_E$

Extension has been recognised as a major event in the development of the EYC architecture (Hammond and Nisbet, 1992; Williams and Whitaker, 1993, Oversby, 1994; Swager, 1997; Brown et al., 1999; SRK Consulting, 2000). Hammond and Nisbet (1992) suggested that extension may have occurred episodically over a 200 Ma timeframe. The timing, polarity, and number of extensional events remain enigmatic. However, all workers have extension ($D_E$) as older than the onset of the regional contractional events.

The principal tectono-stratigraphic changes in the lower mafic-ultramafic sequences of the Kalgoorlie Terrane occur east to west across an essentially north-south tectonic grain (Figure 6-1). Brown et al. (1999) mapped the shape of the Ni ore troughs around Kambalda and concluded that they were structurally controlled by east-west extension during volcanism. They suggested that faults such as the Boulder Fault may have initiated as extensional structures. Across the entire EYC, isotopic changes and differences in zircon inheritance in the supra- and super-crustal rocks are also greatest across the north-south architecture (Cassidy et al., 2002a; Chapter 1). These observations suggest that the main extensional polarity was probably east-west in the EYC.
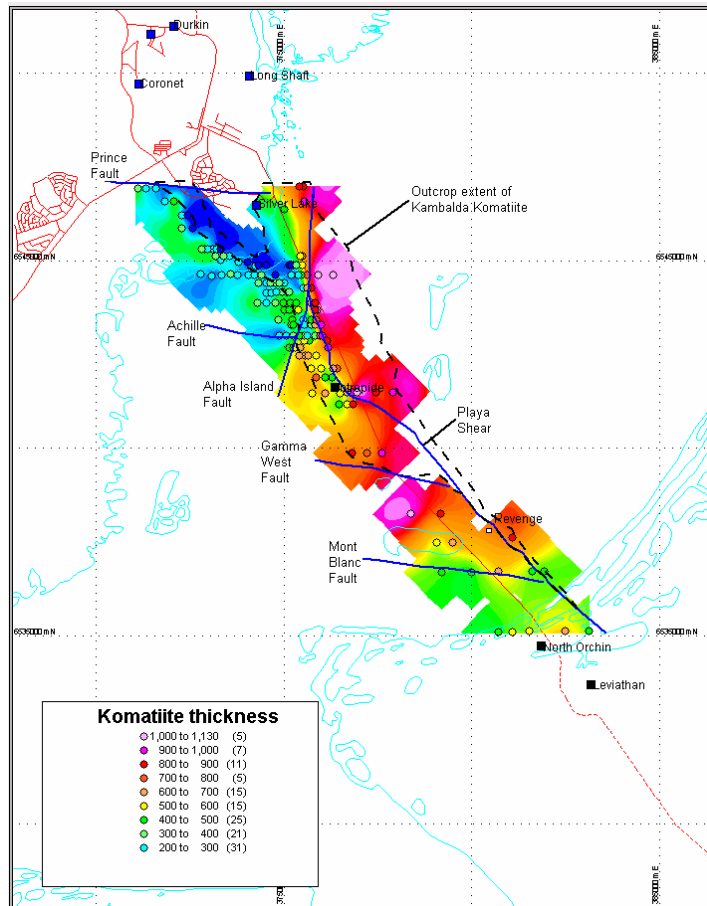
**Figure 6-1: Map of komatiite thickness from the Kambalda dome area showing the possible relationship between north-south fault control and ultramafic volcanism (from Karen Connors, St Ives Goldfields).**

Some workers ascribe a ~north-south polarity to the extension, with greenstone top to the SSE (Hammond and Nisbet, 1992; Williams and Whitaker, 1993; SRK Consulting, 2000), with the high-grade sheared contacts and telescoped metamorphic gradients around many of the north- or south-closing gneiss domes interpreted as metamorphic core-complexes. The north-south or NNW-SSE trending faults that bound domains in the Kalgoorlie Terrane (Swager et al., 1992), and the other terrane boundaries (Myers, 1997), would have acted as transfer structures during SSE-directed extension. Passchier (1994) suggested that the $D_1$ recumbent folds were related to the extension and that this was poly-directional. This ~north-south extension around Lancefield and Leonora overprint the mafic-ultramafic stratigraphy (e.g., at the Tarmoola mine north of Leonora; Fairclough and Brown, 1998).

Map patterns in the Kalgoorlie Terrane (Swager and Griffin, 1990) show major changes in the basal contact relationships of the Black Flag Group with the underlying mafic-ultramafic (lower) sequence (Figure 6-2; Appendix 6-1). If these map patterns are correct, they imply significant unroofing and erosion prior to and during Black Flag Group deposition/volcanism. Alternatively, the basal contact is partly structural and there are extensional detachments excising stratigraphy with the Black Flag Group in the upper plate (hangingwall). Recent work in the Boorara Domain (see Figure 1-3B) has revealed that the upper sequence does occur and is conformably

140

overlain by felsic volcanic and volcaniclastic rocks of the Black Flag Group
(Trofimovs et al., 2004).
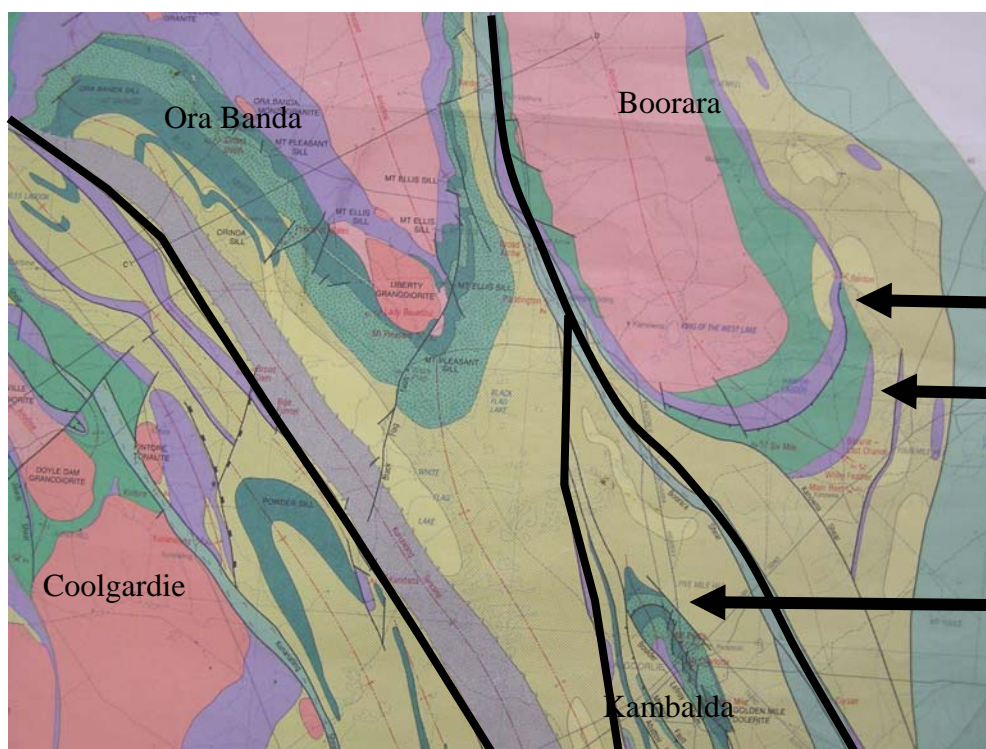


**Figure 6-2: Changes in the relationship between the Black Flag Group (yellow) and lower mafic-ultramafic sequences. Map patterns (from Swager and Griffin, 1990) show the Black Flag Group 'down cutting' through the komatiite into the lower basalt in the Boorara Domain. Compare with more 'complete' stratigraphy in the Kambalda Domain.**

In contrast to Trofimovs et al., (2004), Krapež et al. (2000) described a basal unconformity to the Black Flag Group of the Kalgoorlie Terrane, together with a number of unconformities within the Group (Figure 6-3). The unconformity between the Spargoville Formation and the Black Flag Formation lies between 2686 Ma and <2669 Ma. A significant metamorphic event occurred at around 2675 Ma across all terranes of the eastern Yilgarn, with melting, leucosome and gneiss development at this time (Cassidy et al., 2002b). Significant unroofing (extension) is implied at 2675 Ma because high-grade gneisses are cross cut by relatively undeformed and unmetamorphosed granites that are within error of the gneiss age (Cassidy et al., 2002b). Extension was also suggested as the likely driver for this metamorphic event in the external granites of the EYC (Blewett et al., 2004a).

The preferred model for the early extensional development of the EYC was for at least two main extensional episodes. The first recognisable event was ~east-west directed extension with the development of the mafic-ultramafic sequences in the Kalgoorlie Terrane at around 2.7 Ga. This extension may have been associated with the rifting of the eastern terranes (Kurnalpi and Duketon) from an ancestral Younami craton whose margin was located at (or near) the Ida Fault. The next major extensional event occurred between 2695 Ma and 2670 Ma, with a significant event at ~2675 Ma. A core complex model (Figure 6-4) is proposed for the 2675 Ma period, with lower-plate high-grade gneiss domes being extruded north and south coeval with upper-plate sedimentation/volcanism of the Black Flag Group.
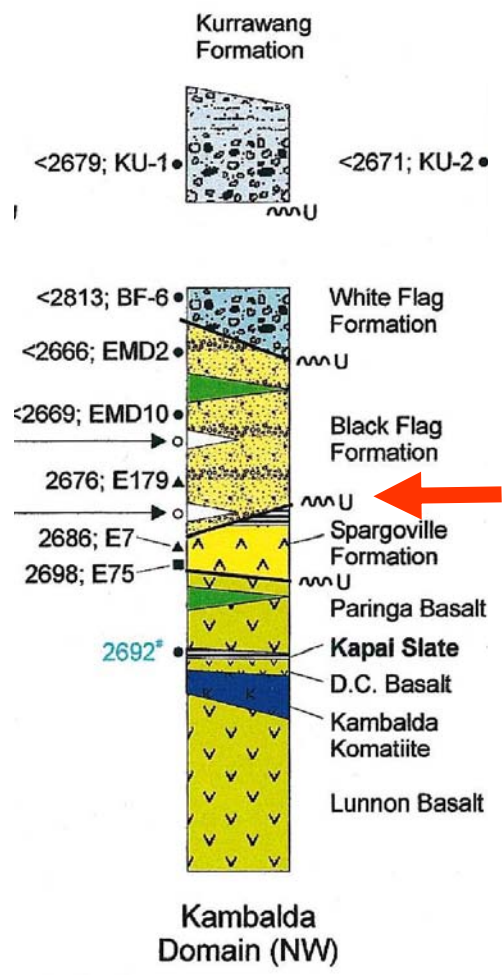
**Figure 6-3: Stratigraphic column for the Kambalda Domain of the Kalgoorlie Terrane (after Krapež et al., 2000). Note the series of unconformities through the sequence and the major change between the Spargoville and the Black Flag Formations at ca. 2675 Ma. Note the uniformity (red arrow) at the base of the Black Flag Formation at around 2675 Ma.**
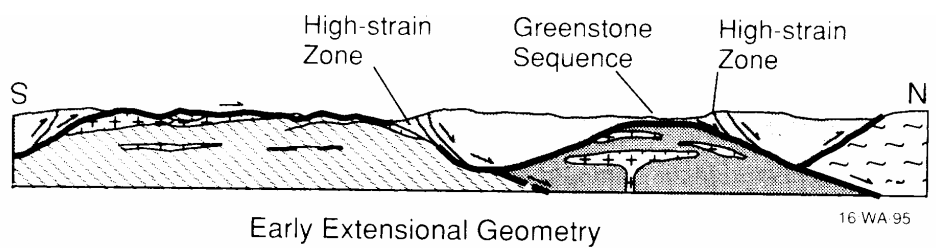


**Figure 6-4: Model of core-complex extension for exhumation of granite gneisses in the lower plate and greenstones (eg Black Flag Group) in the upper plate above a low-angle detachment (from Williams and Whitaker, 1993). The timing is interpreted to be 2675 Ma (see text for discussion).**

# $D_1$ – what is it?

The D$_1$ event has been described by a number of workers (Archibald, 1979; Martyn, 1987; Swager and Griffin, 1990; Hammond and Nisbet, 1992; Swager et al., 1992; Williams and Whitaker, 1993; Passchier, 1994; Swager, 1997; Stewart, 1998; Chen et al., 2001; Davis, 2002). Most interpret the event to involve north-south contraction, with south over north thrusting and recumbent folding, with some stratigraphic duplication. The stratigraphic duplication is largely based upon the assumption that there is one komatiitic marker unit (Swager et al., 1992; Rattenbury, 1993), and that this is extrusive.

Recent work in the Canadian Abitibi has shown that there is a sequence of discrete temporally separated komatiite events or flows (Ayer et al., 2002b). The geochronology of the komatiites in the Yilgarn is not (in general) as precise as in Canada. However, the komatiites in the Murrin Murrin area of the Gindalbi Domain were younger than those at Kambalda (Mark Doyle pers. comm. 2003), raising questions about the assumed age of 2705 Ma (Claoue-Long, et al., 1988) for this 'marker' unit.

Recent work around Agnew has suggested that the komatiites are both intrusive and extrusive (e.g., Trofimovs et al., 2004). This means that repetitions of komatiite may be stratigraphic and not structural duplication.

Examination of map patterns around the southern part of Kambalda (Figure 6-5) show that the so-called D$_1$ Republican and Fosterville thrusts cut 'F$_2$' folds (blue arrows), and are not folded by the 'F$_2$' folds. On superposition arguments alone, this relationship suggests that a post-'D$_2$' stage of ~north-south contraction overprinted an entire stage of 'D$_2$' east-west contraction (see also Blewett et al., 2004a).
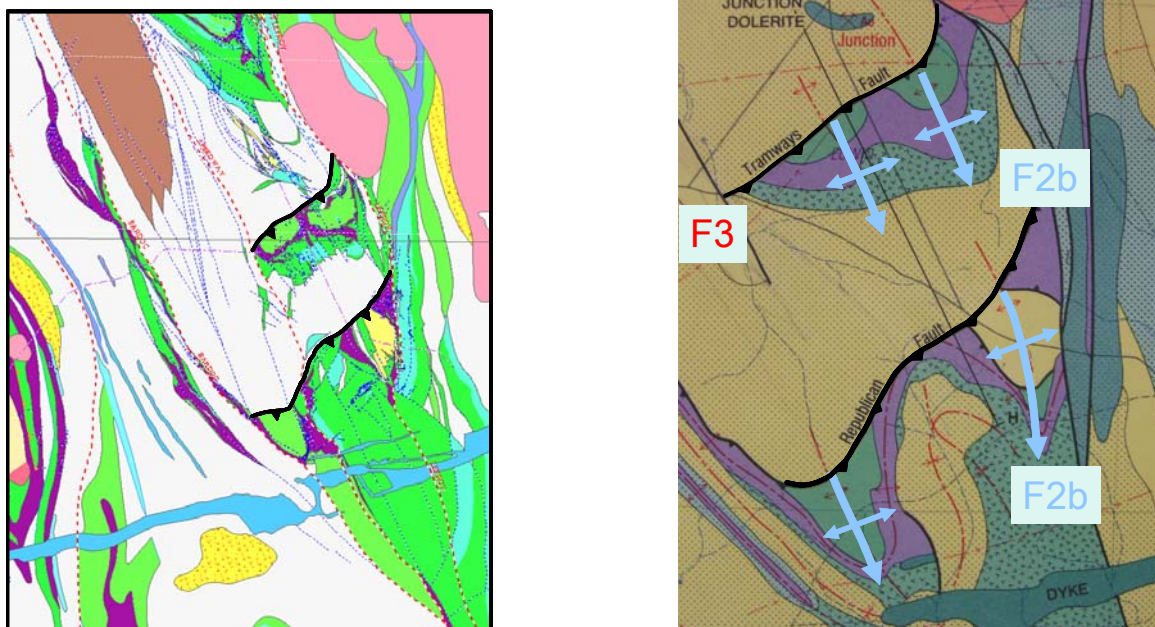


**Figure 6-5: Map patterns around southern Kambalda showing a post-'D$_2$' stage of ~north-south contraction. NNW-directed D$_3$ thrusts (Tramways, Replication) overprint NNW-trending 'F$_2$' folds. If they were D$_1$, then they would be folded by 'F$_2$'.**

The $D_1$ event is noted in many of the gneissic outcrops of the so-called external granites (Blewett et al., 2004a). Isoclinal recumbent folding (Figure 6-6) of the gneissic layering (dated at ~2675 Ma) records north- and south-directed movements (similar to that described by Swager et al., 1992 for the greenstones). What is unclear is whether these folds developed during contraction, or are simply a response to ongoing extension (cf. Harris et al., 2004). Passchier (1994) also suggested that $F_1$ folds were related to extensional events around Leonora.
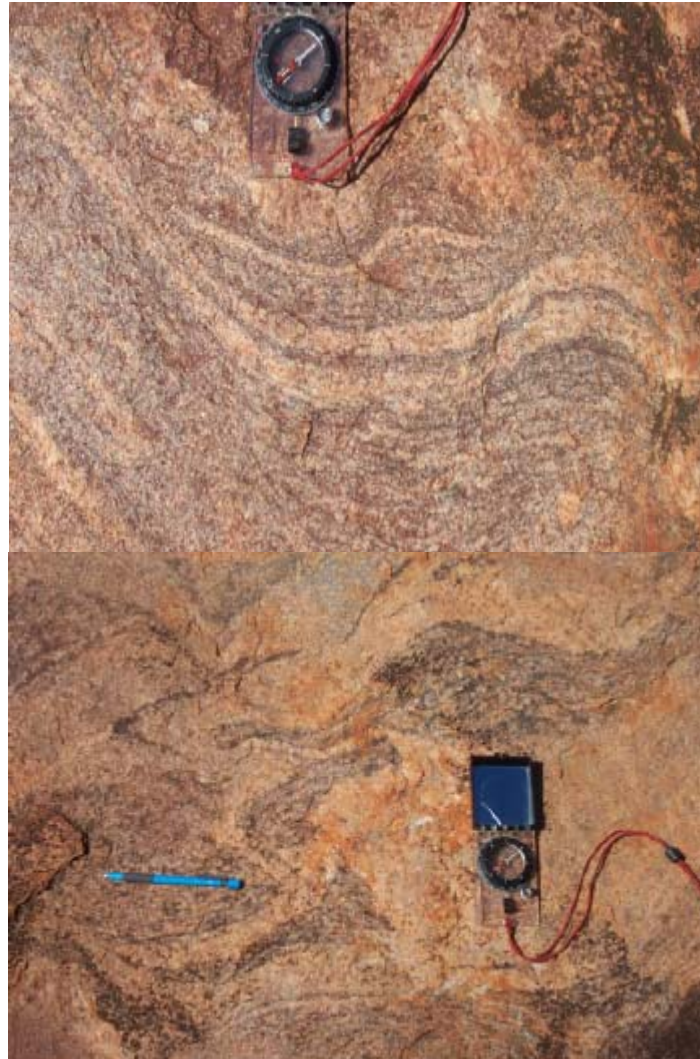


**Figure 6-6: Gneissic fabric (developed during $D_E$) isoclinally folded by $F_1$ and refolded by upright '$F_2$' folds (Blewett et al., 2004a). From Moon Rocks SE of Laverton.**

Stewart (1998) identified an early fabric that was folded by the main '$F_2$' folds around the Welcome Well and Murrin Murrin area of the Gindalbi Domain. In the greenstones further east, there is limited evidence for $D_1$ structures (except for the granites east of Laverton; Blewett et al., 2004a).

Refolded fold patterns (Type II) with NNW folds overprinting recumbent isoclinal originally east-west trending folds ($F_1$) occur in parts of the Kalgoorlie Terrane (Figure 6-7). They were also mapped on magnetic data at Lawlers and north of Leonora (Blewett and Whitaker, 2002).

144

The presence of $D_1$ structure is not universal across the EYC. In many places it may be a fabric that is parallel to bedding/layering. Evidence for contraction and duplication is limited and it is possible that much of what has been described as $D_1$ contraction was extensional in origin.
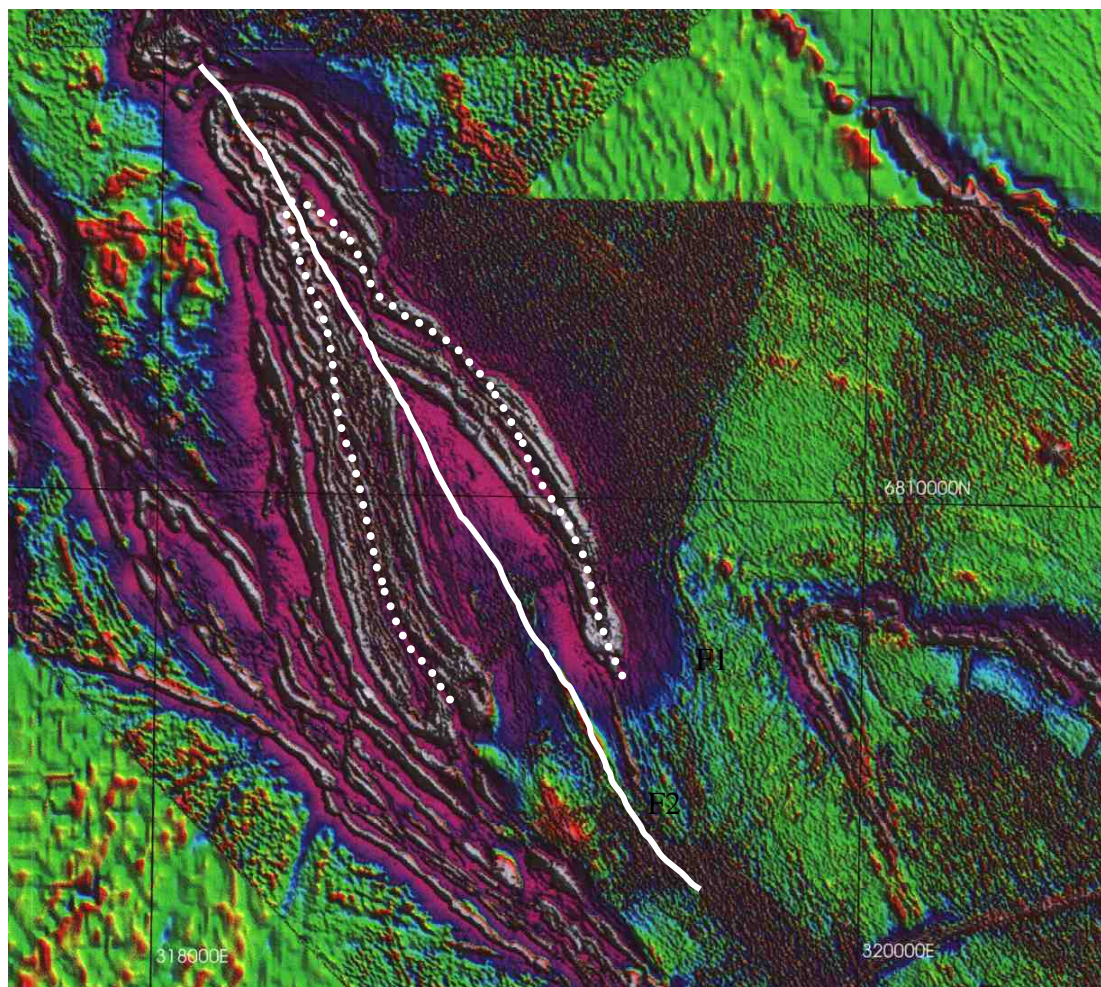


**Figure 6-7: Regional Type II fold interference map pattern developed in mafic-ultramafic rocks east of Kintore. The $F_1$ axis is the dotted line and the NNW-trending solid white line is the '$F_2$' axial trace.**

## '$D_2$' – it's a bit more complex than we thought

A re-examination of the deformation events has shown that '$D_2$' (Kalgoorlie Orogen of Weinberg et al., 2003) was not a single progressive event. Rather, it involved several stages of switching of the tectonic mode (contraction-extension switching) between ~2665 Ma and ~2655 Ma (Blewett et al., 2004c; Appendix 6-2). Not only was the '$D_2$' event associated with deformation, but also the emplacement of significant granite batholiths (Figure 6-8; Table 6-1), and the deposition and inversion of the Late Basins (Blewett et al., 2004c). Based on available geochronology, it is also likely that this sequence of '$D_2$' events was diachronous, younging from east to west (Blewett et al., 2004d).

**Table 6-1: Age constraints on 'D$_2$' events**

| Area/domain | Event | Upper limit Ma | Lower limit Ma | Comments | References |
|---|---|---|---|---|---|
| Kurnalpi Terrane (Welcome Well area) | D$_{2a}$ | ca. 2705 | 2662±5 | D$_{2a}$ overprints D$_1$, and also has a maximum age of the youngest sequence | Cassidy et al., 2002 |
| | D$_{2e}$ | | 2662±5 | Cross-cutting monzodiorite dyke at Yilgangi | Black et al., 2002; |
| | | | 2660±5 | Bulla Rocks Monzogranite cuts faults that cut the Pig Well-Yilgangi basin | |
| | D$_{2b}$ | ≤2660±5 | | The Bulla Rocks Monzogranite is located in the hinge zone of a macroscale F$_{2b}$ anticline | Black et al., 2002 |
| | | | 2662±5 | Cross-cutting monzodiorite dyke at Yilgangi | Nelson, 1996 |
| | D$_3$ | <2635 | | Youngest Low-Ca granites | Nelson, 1997; Cassidy et al., 2002 |
| Ora Banda Domain | D$_{2a}$ | | 2666±5 | | |
| | D$_{2e}$ | ≤2657±4 | | Maximum depositional age of the Kurrawang basin | Fletcher et al., 2001 |
| | D$_{2b}$ | 2666±5 | | | |
| | | 2648 ± 6 | | post-D$_2$ Liberty Granodiorite | |
| | D$_3$ | | 2640 ±8 | The Clark Well Granite, a stitching pluton across post D$_3$ extensional movement on the Ida Fault | Nelson, 1996 |
| | | | | | Bateman, et al., 2002 |
| Kambalda Domain | [1]D$_1$ | ~2673 | ~2660 | Golden Mile Fault with W-directed thrusting cuts porphyry dykes at Kalgoorlie | Bateman et al., 2001 |
| | D$_2$ | 2658 ± 3 | | pre-D$_2$ porphyry dykes at Mt Shea | Krapež et al., 2000 Kent, 1994 |
| Boorara Domain | D$_{2a}$ | 2655 ± 6 | | pre-D$_2$ porphyry dykes at Kanowna Belle | Davis, 2002; Ross et al., 2003 |
| | D$_{2b}$ | | | | |
| | D$_{2c}$ | | 2640 ±6 | By correlation with regional framework (Swager, 1997) | Davis, 2002 |

---

[1] D$_1$ is a local name and is correlated with 'early' D$_2$ by Bateman et al., 2001.

Unravelling these separate and complex stages of the 'D₂' event is important for:

- establishing regional deformation correlations and the timing of events;
- establishing fold geometries through time and their impact on the rotation and/or translation of early structures and any mineral deposits from their original position/orientation (Bateman et al., 2002);
- establishing the kinematics and timing of fault and shear zone activity;
- understanding fluid flow and the changing axes of mean-stress to identify dilational and constrictional areas,
- understanding the significance of granite emplacement and the formation of Late Basins, and;
- an improved understanding of Archaean tectonic processes in relation to younger and generally better understood orogens.
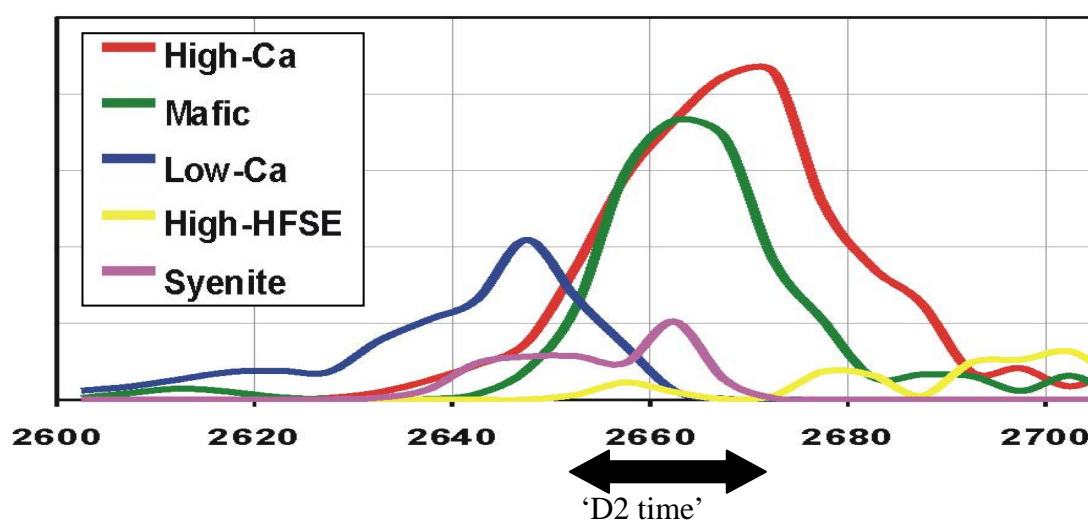


**Figure 6-8: Emplacement age histogram of the five granite groups (Champion and Sheraton, 1997) for the EYC. Note the age peaks of the mafic and the syenitic types and the waning age of the High-Ca type corresponding to the time of 'D₂' orogenesis.**

The following section characterises the 'D₂' event in terms of the relationship between deformation, magmatism, and basin development.

## 'D₂' deformation

The published ages of the 'D₂' event range from >2665 Ma (Swager, 1997) to <2655 Ma (Krapež et al., 2000; Weinberg et al., 2004). Figure 6-9 shows estimates of the ages of deformation, granite magmatism and Late Basin formation in the east, central (Kurnalpi) and the west (Kalgoorlie). Like the granite temporal patterns, the deformation ages young from east to west, with ages around 2665 Ma in the east to about 2657 Ma in the west. 'D₂' did not involve a single contractional event, but multiple stages with both contraction and extension (see Blewett et al., 2004c).

The sequence of 'D₂' deformation events involved an early stage of ~east-west shortening (D₂ₐ), followed by extension with basin formation, granite emplacement

(mafic and syenite) and normal fault movement ($D_{2E}$), and finally a second stage of ~east-west (ENE-WSW) contraction ($D_{2b}$). These features are well illustrated by the geometry and geological relationships that occur in the Kurnalpi Terrane (Welcome Well area) and the Kalgoorlie Terrane (Ora Banda, Kambalda, and the Boorara Domains) of the central and southern EYC.

The first east-west contractional event initiated a series of north-trending upright macroscale $F_{2a}$ folds with wavelengths of 3-10 km and was associated with west-directed thrusts or reverse faults (Figure 6-10). The seismic reflection data from across the area reveal a pronounced moderate east dip to most structures (Goleby et al., 2002a). The Kilkenny shear zone is a wide zone of parallel reflectors (Figure 6-11) developed during west-directed thrusting during $D_{2a}$ contraction (Blewett et al., 2002; 2004c).
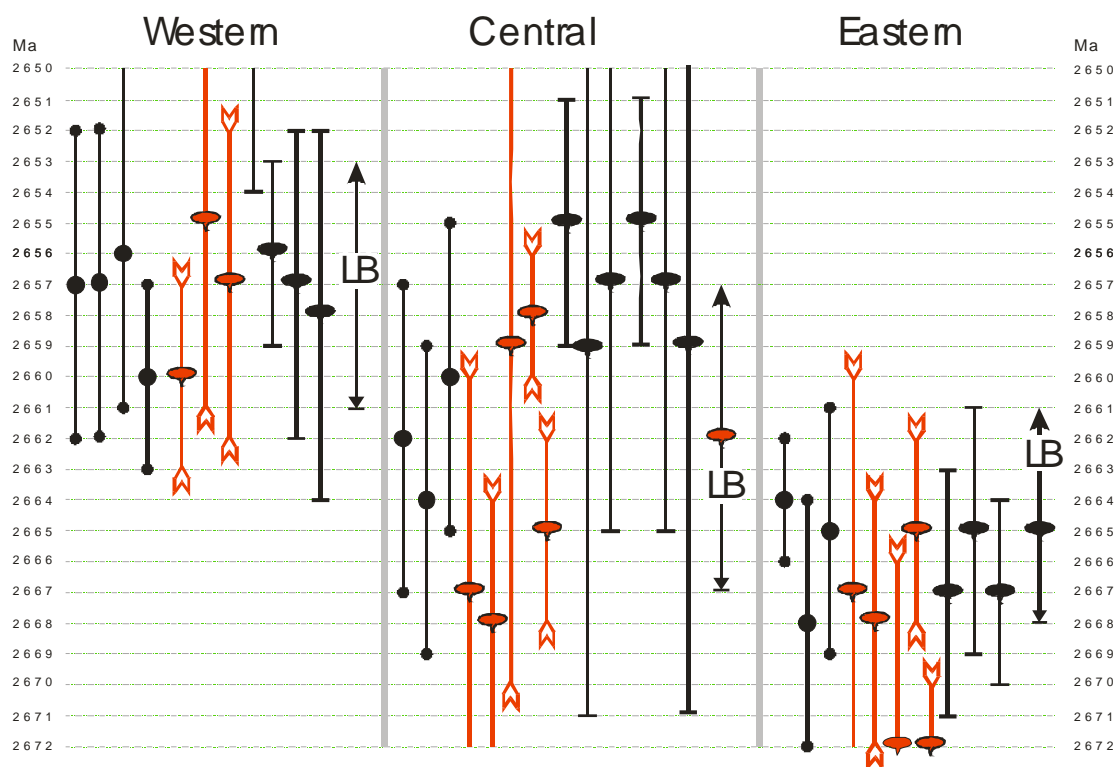


**Figure 6-9: Compilation of deformation, High-Ca and Mafic granite type, and Late Basin age ranges for Laverton (east) compared with Gindalbi/Kurnalpi (central) and Kalgoorlie (west). Black dots – '$D_2$' ages; red balloons – youngest High-Ca granites; black balloons – Mafic granites; LB – Late Basins.**

The Pig Well (Late) Basin comprises polymictic conglomerate deposited by northerly-sourced alluvial fans into a down-faulted $D_{2E}$ extensional graben (Hallberg, 1985). The basin trends NNW, and cuts the $D_{2a}$ macroscale fold hinges and their associated thrusts/reverse faults, with a partly faulted unconformity on the east (Figures 6-10, 6-11). The Pig Well Basin, like most Late Basins, fines upwards, with deeper water turbidites preserved in the youngest parts of the thickest basins (Krapež et al., 2000). These fining-up basins are atypical of foreland basins (which generally coarsen upwards due to hinterland propagation into the foreland), and they do not display the complex interplay between evolving structure and sedimentology typical of strike-slip basins (Crowell, 1979). Sedimentologically they are more like

intercontinental or back-arc extensional basins (Brooks et al., 1984). The east-dipping Kilkenny shear zone defines the western margin of the hangingwall basin (Figure 6-10), which is 2–8 km wide (Hallberg, 1985), 1.5 km deep and cutting moderately east-dipping $D_{2a}$ shears or faults (Goleby et al., 2002a). Aeromagnetic and gravity data clearly show the truncation of north-trending $D_{2a}$ and refolded $D_1$ structures by the basin. Key evidence for coaxial extension ($D_{2E}$) superimposed on an earlier east-west shortening event ($D_{2a}$) is provided by the NNW-trending basin and its marginal faults overprinting north-trending structures in its basement.
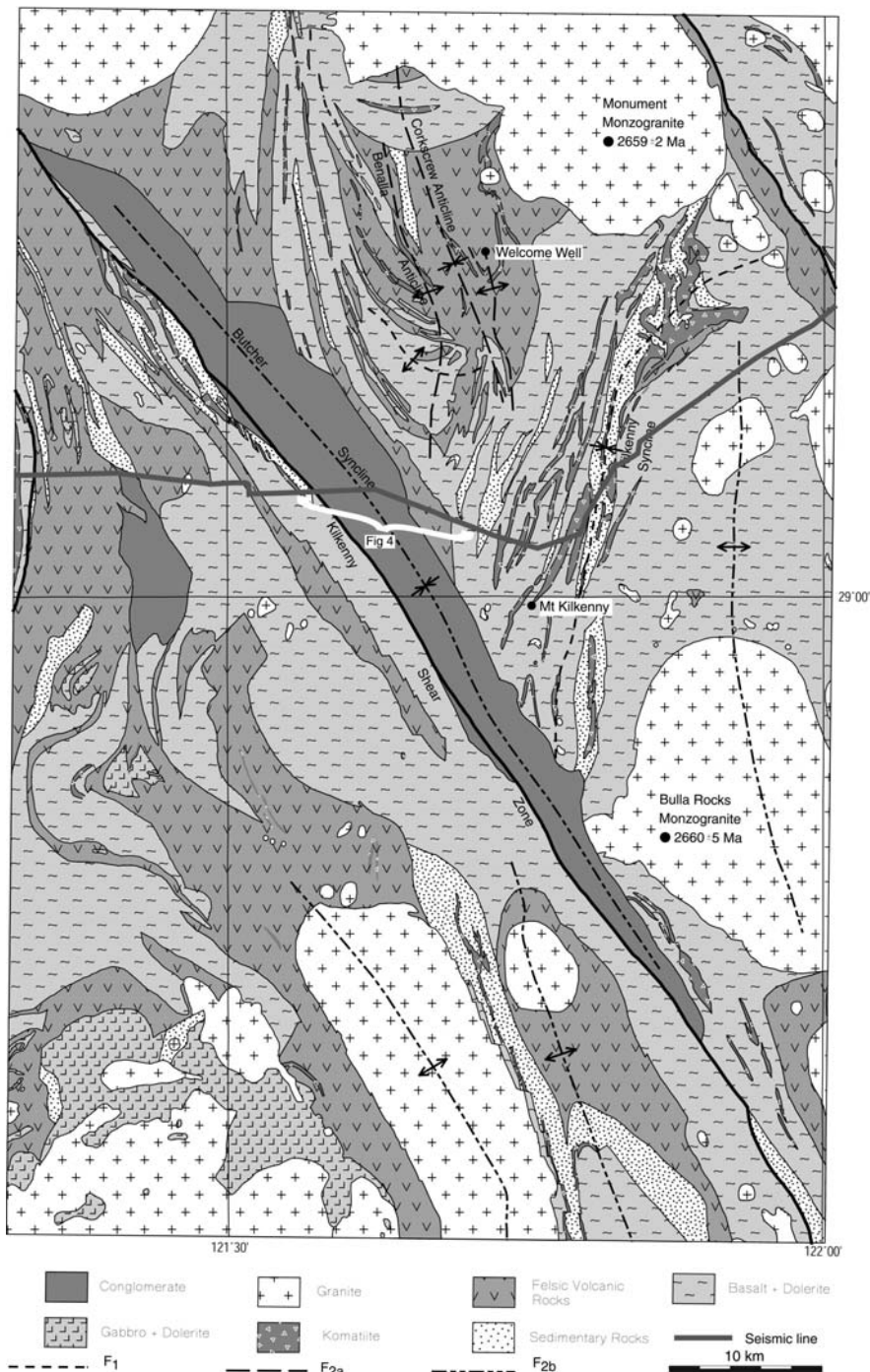


**Figure 6-10: Geological map of the Welcome Well Mt Kilkenny area showing $D_{2a}$ folds being overprinted by the Pig Well Late Basin and associated $D_{2b}$ synform.**
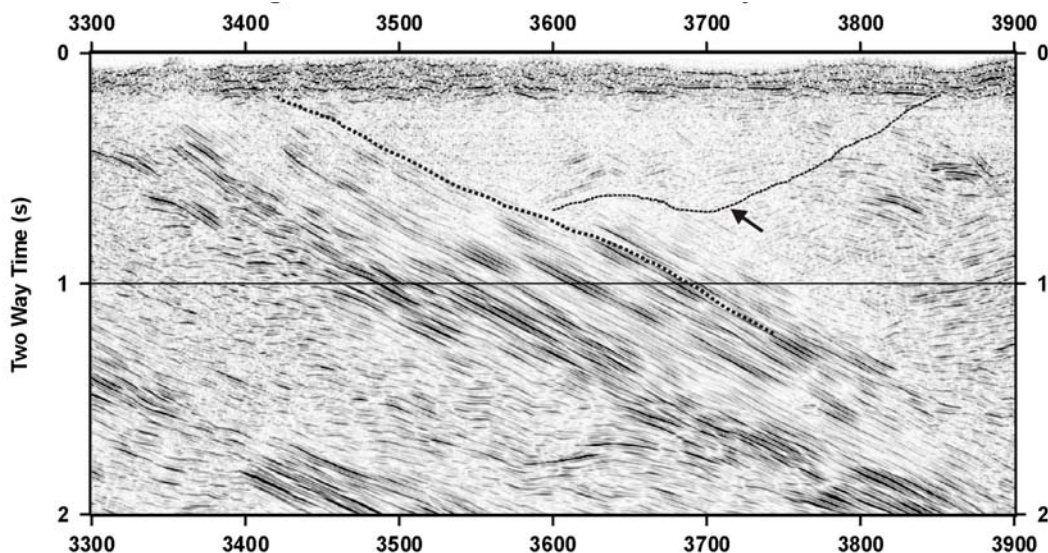
**Figure 6-11: Segment of seismic reflection profile from the 01AGSNY1 line (Goleby et al., 2003) through the Pig Well Late Basin. Note the unconformity (arrow) of the basin developed on prefolded ($D_{2a}$) basement. Open folding ($D_{2b}$) in the basin is also visible.**

Following (or during?) sedimentation in the Pig Well Basin, the $D_{2E}$ extensional basin-bounding faults were inverted, and the sequence deformed during renewed east-west contraction (Figure 6-11). Previously, this shortening event was interpreted as regional '$D_2$', so that the $D_{2a}$ structures described above, and those described below, were considered a single finite deformation event (Hammond and Nisbet, 1992; Swager, 1997; Krapež et al., 2000; Weinberg et al., 2003). The Butcher Syncline is an upright macroscale $F_{2b}$ fold that trends NNW and plunges sub-horizontally in the centre of the Pig Well Basin (Figure 6-10). An open synformal structure is clear on seismic data (Figure 6-11), consistent with the mostly shallow dips (Hallberg, 1985). Regional $D_{2b}$ contraction flattened cobble clasts and developed a penetrative NNW-trending $S_{2b}$ fabric, and also significant mylonites (Hallberg, 1985). The $D_{2b}$ shortening event was ~east-west (ENE-WSW) oriented, largely co-axial with $D_{2a}$ (and the strike of the Pig Well Basin), further tightened the $D_{2a}$ folds (Type 0 fold interference), steepened fold limbs, and reactivated earlier $D_{2a}$ thrusts (e.g., the Kilkenny shear zone as a west-directed thrust [Figure 6-11]). The same relationships have been described by Smith (2004) for the Granny Smith Late Basin near Laverton to the east, and are outlined in Figure 6-12.

Evidence for a complex (polyphase) regional '$D_2$' event has been reported across the EYC. Detailed structural studies around Kalgoorlie (Bateman et al., 2001; 2002), Laverton (Davis, 2001), and Mulgarrie (Davis, 2002), and Scotia-Kanowna Dome areas (Davis, 2002) show that there are multiple coaxial contractional events that developed the intense NNW-trending structural grain and associated fabrics. Coaxial '$D_2$' extension has now also being recognised. For example in the Laverton area, Davis and Maidens (2003) and Newton et al. (2002) have described a late '$D_2$' orogenic collapse event that occurred in tandem with the last stages of ENE-WSW directed regional '$D_2$' shortening.

150
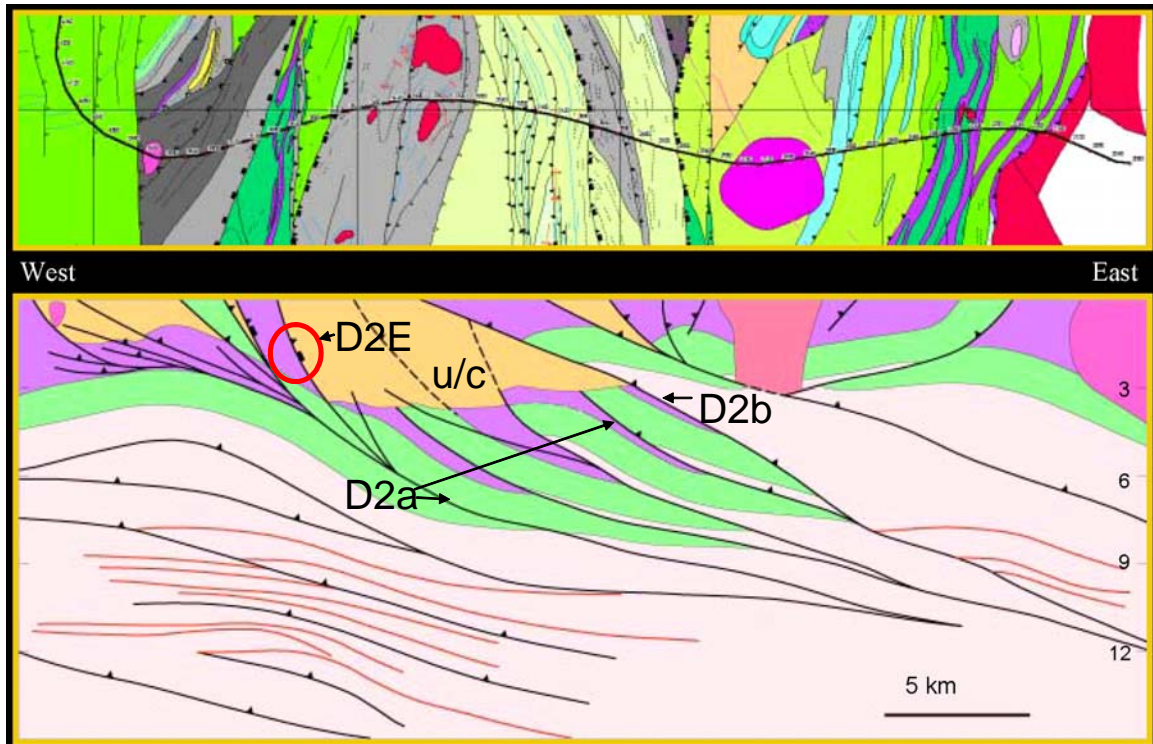
**Figure 6-12: Interpretation of seismic line 01AGSNY2 by Smith (2004). The Granny Smith Late Basin (Laverton district) sits with an unconformity on previously thrusted (D$_{2a}$) basement. Basin bounding fault on the west has both contractional and extension movements (D$_{2E}$). The Late Basin is overthrust and deformed by an out-of sequence thrust in the east (D$_{2b}$).**

## 'D$_2$' and granites

Champion and Sheraton (1997) classified the granites of the Yilgarn into five geochemical groups or types. The syenitic and mafic types intrude greenstones and are known to be important in the formation of a number of deposits (e.g., Wallaby, Granny Smith, Kanowna Belle, Bindula, St Ives, Tarmoola).

The syenitic and mafic types are syn-D$_2$ in age (Figure 6-9). The High-Ca granite type was largely terminated with or by the onset of the D$_{2a}$ contractional events. In detail, there is a diachronous range of emplacement ages from east to west of the mafic granites and the youngest age of the High-Ca granites. For example, in the Laverton area the mafic granites are around 2665 Ma, and corresponding mafic granites in the Kalgoorlie area are around 2657 Ma (Figure 6-9). Similarly, the youngest eastern High-Ca granites are around 2665 Ma, while the youngest western High-Ca granites are around 2655 Ma. Both the end of High-Ca magmatism and the onset of mafic type granite magmatism occur during the 'D$_2$' event. As the ages of mafic granite magmatism and youngest High-Ca granite magmatism in the central regions overlap those to the east and the west (Figure 6-9), there is a suggestion of a diachronous progression of 'D$_2$' from east to west.

## Timing of 'D$_2$'

The 'D$_2$' event was associated with deformation, granite emplacement, and Late Basin sedimentation and inversion (Blewett et al., 2004c). The ages of the granites and Late Basins provide time limits on various stages of the 'D$_2$' event.

151

In the east, the Granny Smith Basin places lower and upper limits on the timing of $D_{2a}$ and $D_{2b}$, respectively in the Laverton Terrane (eastern region). The basin lies with an unconformity on prefolded basement (Gower, 1976; Hronsky, 1993; Smith, 2004) and is intruded by the mafic-type Granny Smith Granodiorite (2665 ±4 Ma; Hill et al., 1992). Hence $D_{2a}$ is constrained to be older than this age and $D_{2b}$ as younger than this age.

In the centre, the Pig Well-Yilgangi Basin places lower and upper limits on the timing of $D_{2a}$ and $D_{2b}$, respectively in the Kurnalpi Terrane (central and west region). The intrusion of the 2662 ±5 Ma Yilgangi porphyry (Nelson, 1996) into the basin constrains $D_{2a}$ as older and $D_{2b}$ as younger than this age. Additional age constraints come from cross-cutting granitoids (Figure 6-10), including: the Bulla Rocks Monzogranite (2660 ±5 Ma; Black et al., 2005), and the Monument Monzogranite (2659 ±2 Ma; Dunphy et al., 2003). These plutons intrude the Pig Well-Yilgangi Basin, providing a minimum age of ~2661 Ma for $D_{2a}$ and $D_{2E}$ (Table 6-1). These intrusions are deformed by $D_{2b}$, providing a maximum age for this event in the terrane (Figure 6-10).

In the west, the Kurrawang Basin also provides age limits on '$D_2$' deformation in the Ora Banda Domain of the Kalgoorlie Terrane (Figure 6-13). Based on the youngest detrital zircon populations, this Late Basin was deposited after 2657 ±4 Ma (Fletcher et al., 2001), which (although within error) has a younger median age than its correlative to the east, the Pig Well-Yilgangi Basin. The age determinations of cross cutting granites in the Ora Banda Domain are within error of those in the Kurnalpi Terrane (Figure 6-10). However the median ages are 3-5 My younger in the west compared to the east. The youngest phase of the Kanowna Belle porphyry to be overprinted by $D_{2a}$ has an age of 2655 ±6 Ma (Ross et al., 2001; 2004). More precise ages of pre-$D_{2b}$ granites include Golden Cities (2656 ±3 Ma; GA unpublished data), Split Rocks (2657 ±5 Ma; Nelson, 1996), and the Mt Shea Porphyry (2658 ±3 Ma; Krapež et al., 2000). A minimum age for $D_{2b}$ is provided by the 2648 ±6 Ma Liberty Granodiorite (Figure 6-13; Kent, 1994). These maximum ages for $D_{2a}$ and $D_{2b}$ at Ora Banda, Kambalda, and Boorara Domains of the Kalgoorlie Terrane, as well as the Late Basin age, are on average ~5 My younger than their respective events in the Kurnalpi Terrane to the east.

## The correlation of regional deformation events

The chronological paradigm for the regional deformation of the EYC to date has been largely pinned to '$D_2$' structural elements (see Swager, 1997, and references therein). These '$D_2$' structural elements strike mostly NNW-SSE, and include a pervasive metamorphic foliation, upright folds with gentle NNW- or SSE-plunging hinges, and reverse faults. Structural elements deformed by '$D_2$' structures are interpreted as '$D_1$', and structural elements that deform '$D_2$' are interpreted variously as '$D_3$' and '$D_4$'. If, as we contend, the '$D_2$' event was polyphase, then care is needed in correlating local features with the regional framework.

**Figure 6-13: Map of the Ora Banda Domain of the Kalgoorlie Terrane showing the Kurrawang Late Basin cutting across an F$_{2a}$ fold and itself folded into an F$_{2b}$ synform.**

The multiple stages of coaxial deformation across the EYC resulted in significant foliation reactivation and crenulation (e.g., Bateman et al., 2001; Davis, 2001), so

errors are likely if one simply uses the dominant 'S$_2$' fabric as a temporal marker for correlation. Inferences about tectonic mode (contraction-extension) based on folds and shear zones also need to be viewed with caution. This is because the extensional stage of the orogeny (D$_{2E}$) would have developed folds on listric-bounding shears (roll-overs), similar to those mesoscale folds generated during the shortening stages (cf. Harris et al., 2002). For example, Davis (2001) described late 'D$_2$' orogenic collapse along flat-lying ductile fabrics that might be mistaken for contractional (thrust) structures. These ductile fabrics were interpreted to be associated with the emplacement and remobilisation of gold mineralisation at the world-class Wallaby and Sunrise deposits of the Laverton area. This extension was thought to have occurred in tandem (lateral extrusion) with the last stages of ENE-WSW directed regional 'D$_2$' shortening (Davis and Maidens, 2003).

Constraining or correlating a single 'D$_2$' structural element at a specific outcrop or mineral deposit to a regional framework is therefore difficult, because 'D$_2$' was clearly different things in different places at different times!

Further west in the Youanmi Terrane (Southern Cross Province), Chen et al. (2004) correlated local 'D$_3$', which developed during ~east-west contraction and was associated with sinistral strike-slip shearing, with 'D$_2$' in the EYC. Based on the age of 2656 ±3 Ma granites cross-cut local 'D$_3$' shears (age from Qiu et al., 1999), Chen et al. (2004) suggested a maximum age of ~2655 Ma for 'D$_3$' in the Youanmi Terrane. This age is within the range of 'D$_2$' ages for the Kalgoorlie Terrane, suggesting that the Wangkathaa Orogeny may represent the docking of the EYC with the Youanmi Terrane (see also Chen et al., 2004).

Deep seismic reflection profiling has revealed that west-verging regional 'D$_2$' thrusts in the mid crust to top of the lower crust are continuous between the EYC and the Youanmi Terrane (Drummond et al., 2000). These data suggest that the the 'D$_2$' event was broad in its lateral extent (area) and likely affected the entire depth of the crust.

## The regional tectonic architecture

The present architecture of the EYC is a function of multiple small strain events. Unravelling the various stages of infinitesimal strain is an important process in restoring the present architecture (Bateman et al., 2002). Restoration becomes difficult in the EYC where at least two stages of coaxial ~east-west shortening occurred. This is because structures developed during D$_{2a}$ would have been further deformed during D$_{2b}$. For example, F$_{2a}$ folds will further tighten during D$_{2b}$ contraction (Type 0 fold interference), making identification of two stages of shortening difficult. An additional complication is the tightening of F$_{2a}$ folds during D$_{2E}$ extension (see Swager, 1997), especially as roll over structures in the hangingwall of listric normal faults (of inverted D$_{2a}$ thrusts). These two stages of shortening and consequent rotation need to be factored into any restoration of pre-D$_{2b}$ (or Late Basin) geometries and architecture (see also Bateman et al., 2002).

The seismic reflection data (Goleby et al., 2003) show a remarkably consistent 30º dip through the crust, and across nearly 400 km of the strike of the EYC, despite at least two stages of ~east-west shortening. One might expect in a foreland-propagating fold-thrust belt that hinterland (eastern) thrust horses become progressively back rotated

and steepened as piggy backs above successive footwall collapse as new frontal thrusts initiate (Butler, 1983). The consistent geometry of the major structures suggests that any back rotation of thrusts in the east (hinterland) during $D_{2a}$ was restored by an approximately equivalent (or greater) extensional inversion ($D_{2E}$) before the subsequent $D_{2b}$ shortening. Alternatively, the mode of thrusting was out-of-sequence (Butler, 1983) and thrusting stepped back successively into the hinterland (east), so that earlier thrusts in the west were largely unaffected by later thrusts in the east. The indication of an age progression for the Wangkathaa Orogeny (younger in the west not the east) likely invalids this alternative hypothesis.

## Low-pressure high-temperature metamorphism

Peak metamorphism across the EYC was late in the deformation history (post $D_{2b}$), and was of the low-pressure high-temperature type (Binns et al., 1976; Archibald, et al., 1978; Hallberg, 1985; Mikucki and Robert, 2003; Chapter 8). The fact that high-pressure metamorphic assemblages were not developed, despite two stages of ~east-west shortening, suggests that the coaxial $D_{2E}$ extension (collapse) restored much of (or more than) any crustal thickening due to earlier $D_{2a}$ contraction. Subsequent $D_{2b}$ shortening therefore began from a partly 'restored' base level and as a result did not thicken the crust to an extent where high pressures were developed at the present level of erosion. The late-stage (2655-2630 Ma) Low-Ca granite suite develops low-pressure aureoles (see Mikuki and Robert, 2003) that overprint the earlier regional metamorphism described above. These granites were emplaced into relatively high levels, suggesting that exhumation and uplift occurred in later stages of the Wangkathaa Orogeny.

An analogy might be the low-pressure metamorphism accompanying convergence during the Variscan Orogeny of NW Iberia (Arenas and Catalan, 2003). Here, syn-convergent extensional shear zones allowed re-equilibration of the orogenic wedge by tectonic denudation of an allochthonous unit during its emplacement (in the hangingwall), and by thinning and extension in the footwall of the advancing thrust sheet.

## Archaean tectonic processes

One of the paradoxes of orogenic belts is the common observation of extension occurring simultaneously with contraction (or soon after) and episodic switches between these tectonic modes (Lister et al., 2001 and references therein).

Several hypotheses have been proposed for generating tectonic mode switching. These hypotheses need to explain why an orogen (e.g., EYC) undergoes extension following prolonged contraction, while convergence continues across the orogen (and with the same movement vector). Four hypotheses are outlined:

1. Extension or orogenic collapse is thought to follow delamination of a thickened lithospheric root because the gravitational potential of the overlying lithosphere is raised, significant heat is advected into the remaining lithosphere, thereby reducing its strength (Houseman et al., 1981; Platt et al., 2003). The model predicts a time lag of 20-30 My between initial collision and collapse, which is inappropriate for the rapid switching in the EYC.
2. Slab drop-off or slab-tear would allow hot asthenosphere to replace the mantle wedge, providing a heat source that would significantly reduce the strength of the

lithosphere and allow it to extend. This mechanism would permit rapid switching in tectonic mode. A subducting slab would hinder delamination of a thickened root. If Archaean subduction was flat or at a low angle, then it would likely further restrict delamination.

3. Hinge migration of a subducting slab (see Hamilton, 1998) results in extension of the overriding plate during retreat (e.g., NW Pacific), or contraction during slab advancement (e.g., northern Andes). The rate of change of migration will determine the stress state in the upper plate, and thus control switching in tectonic mode (Platt, 1986; Lister et al., 2001). Extension will occur if the rate of roll back increases, even if the rate of overall convergence remains (Dewey, 1980). Roll-back is likely to produce diachronous patterns of extension (Platt et al., 2003).

4. Crustal thickening, due to folding and thrusting of an orogen under contraction, will build a gravitational instability that is relieved by extensional collapse (or rapid erosion). Orogenic surge (Lister et al., 2001) is a mechanism where the front of the orogen surges over its foreland along a low-angle basal thrust at a rate that is greater than the overall rate of shortening across the orogen. As a result, the orogen undergoes overall extension; much of it accommodated on inverted thrusts that were active during the crustal thickening phase in the overlying (and hinterland) slices. This is an effective mechanism to cause a switch in tectonic mode in the overlying (hangingwall) slices, despite the orogen still being under contraction.

All of these processes above (1-4) imply a plate-tectonic influence and that these processes in the late Archaean may not have been too dissimilar to those found in younger orogens. Hypothesis 3 and/or hypothesis 4 are considered the most likely causes of the switching in tectonic mode for the EYC. Hypothesis 4 is favoured and further developed in Chapter 8.

## World-class orogenic gold mineral systems

There is common consensus that **most** of the gold in the EYC was deposited relatively late in the deformation history (i.e., $D_3$ and $D_4$), was post peak metamorphism, and was associated with second- and third-order structures related to major shear zones (Clark et al., 1989; Swager, 1989; McNaughton et al., 1990; Groves et al., 2000). The observation that many Late Basins are mineralised (e.g., Pig Well, Scotty Creek, Kurrawang, etc) demonstrates the partial uplift/exhumation and erosion of greenstones in the waning stages of orogenesis (Groves et al., 1984). Vearncombe et al. (1989) also showed that reactivated shear zones were important for localising gold. The Wangkathaa Orogeny involved reactivation of faults with thrust, normal, and strike-slip movements, that developed and subsequently deformed basins derived from uplifted areas (i.e., granite detritus).

In terms of fluid flow, the Wangkathaa Orogeny was an important component of the orogenic gold mineral system. It generated:

- $D_{2a}$ contraction which developed the necessary structural (fault) architecture;
- $D_{2E}$ extension which partly exhumed the orogen, inverted earlier faults resulting in basin formation, and facilitated fluid infiltration, and;
- $D_{2b}$ (and $D_3/D_4$?) coaxial contractional regimes which provided a mechanism to drive fluid flow and produce dilational traps.

Similar relationships between faults and late basin sequences occur within the Archaean Abitibi Province of eastern Canada. Here the mineralised 2680-2674 Ma (approximately 20 My older than the EYC) Timiskaming Assemblage (Ayer et al., 2002a), occurs as narrow corridors of clastic sedimentary and volcanic rocks, displaying many similarities to the Late Basins of the EYC. Additionally, the basins in both regions occupy areas proximal and parallel to regional scale (first- and second-order) faults (Swager et al., 1992; Ayer et al., 2002b), suggesting that Late Basins indicate repeated fault activity (inversion) and are potentially pointers to fluid flow.

## D2x or D3

A post '$D_2$' stage of north-south contraction was described in the discussion about regional $D_1$. McMath (1953) described the regional cross folding around Coolgardie as having a NNW-trending first phase and a later ENE-trending cross phase. He noted that cross folding was first described by Gustafson and Miller (1937) with east-west trends overprinting NNW trends in Kalgoorlie. McMath (1953) with his examination of mines and general structural trends at the time suggested that:

- the greatest deposits (leases) occur on the eastern margin of Coolgardie dome (the dome is anticlinorial in character);
- the major gold centres are grouped about the "cross–fold" axes of various orders of magnitude, and;
- the major producers are associated with anticlinal "cross–fold" axes, fewer and smaller deposits are associated with synclinal "cross–fold" axes.

Ellis (1939) and Matheson (1939) also described the regional cross folding by east-west folds on the main NNW trending folds in the Southern Cross region (Figure 6-14). They suggested that refolding was not only important for the location of the gold deposits, but also the metamorphic grade.

North-south or NNW-SSE contraction post-'$D_2$' events have been widely noted in both the internal and external granites of the central EYC (Blewett et al., 2004a; Figure 6-15). The change from predominantly east-west contraction to NW-SE contraction occurred just before the switch to Low-Ca magmatism (<2655 Ma).

Mineral deposits such as Tarmoola, Sunrise Dam, Wallaby, and the St Ives region are considered to have developed during late NW-SE contraction (Duuring et al., 2001; Tornotora, 2002; John Miller pers. comm., 2004). The periclinal nature (double plunge) of the main '$F_{2b}$' syncline-anticline pairs in the southern Kalgoorlie Terrane may also reflect a north-south contractional overprint during $D_3$ (Figure 6-5).

The detachment, base of greenstone, and many other prominent seismic reflectors are folded in both east-west and north-south lines (Figure 6-16). Swager (1997) interpreted the domical nature and periclinal plunges as a function of '$D_2$' thrust culminations. Little evidence is preserved in the seismic data for significant development of thrust horses, raising the possibility that the development of the domes was a late feature and involved a component of refolding. The significance of the domes is discussed further in Chapter 8.
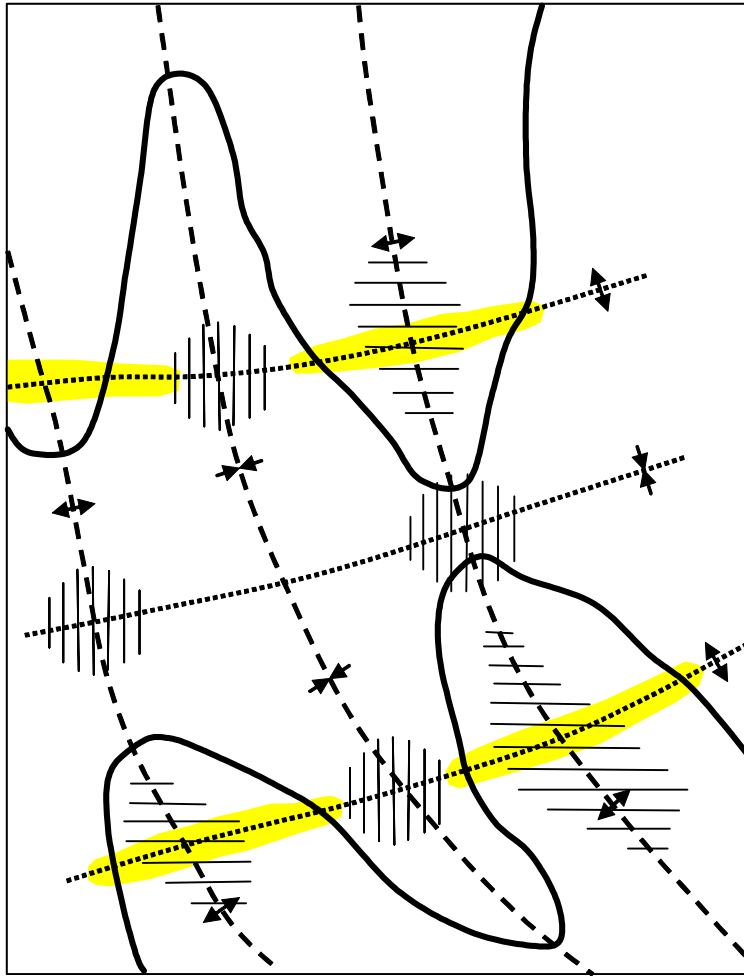
**Figure 6-14: Most Au deposition in the Southern Cross is located at cross folding (domes) (Ellis, 1939).**

| Regional | Southern Cross | Kalgoorlie | Greenstones | Kurnalpi Gindalbie Laverton | Merolia |
|---|---|---|---|---|---|
| 14 →← | | →← | | →← | ⇒⇐ |
| 13 | | | | | ⇩ ⇧ ? |
| 12 →← | | →← | D4 →← | ⇒⇐ | →← |
| 11 | | | | | |
| 10 | | 2647±4 | D3 | | ~2638 |
| 9 | | | ? | | |
| 8 | | | D3 | 2664±5 | |
| 7 →← | ⇒⇐ | →← | | →← | →← |
| 6 | | 2652±5 | D2b | 2662±5 | |
| 5 | | | D2E | 2667±4 | 2664±2 |
| 4 →← | | →← | D2a →← | ⇒⇐ | →← |
| 3 | | | D1 | | 2663±7 |
| 2 ↔ | | ↔ ~2675 | De ↔ | ⇐⇒ | ↔ ~2675 |
| 1 →← | | →← ~2800 | | ~2710 | ~2770 |

Major change to D$_3$ NW-SE contraction

**Figure 6-15: Main NW-SE D$_3$ contractional change occurs just before Low-Ca magmatism in granites (Blewett et al., 2004a).**

## Implications for predictive mineral discovery

The major implication for predictive mineral discovery is an improved understanding of the structural and event history of the EYC. There are gaps in knowledge regarding the early (pre-accretion) history, especially the nature and role of extension in developing the region's architecture.

Significant findings for predictive mineral discovery are:
- diachronous deformation and its link with magmatism and Late Basin development;
- periodic stress switches and mode changes between contraction and extension, and;
- development of a domal geometry.
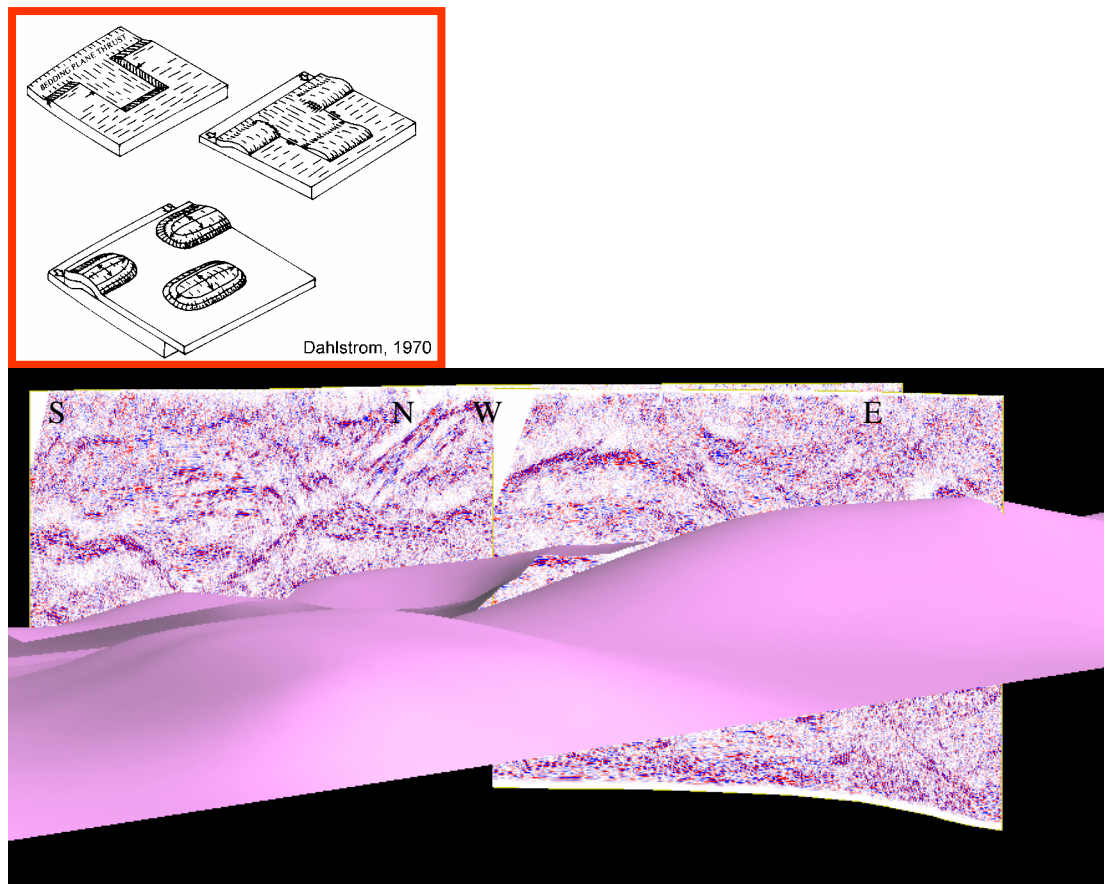
**Figure 6-16: An alternative model for the domal geometry and double plunging D$_2$ structures in the Kalgoorlie Terrane (see Swager, 1997). Lateral ramps and thrust culminations may develop domes (Dahlstrom, 1970). Domical reflectors from the Kalgoorlie 3D map do not show evidence for thrust horses stacking up to develop culminations.**

The diachronous development of deformation means that it is difficult to correlate one event with another simply on absolute time. The linkage of the main tectono-thermal events (deformation, magmatism, metamorphism and sedimentation) permit more realistic geodynamic models to be inferred (see Chapter 8).

The role of stress switching both in direction and mode has a major impact on fluid flow (Sibson, 1990). Linking these switches with the tectono-thermal events permits the construction of a more predictive framework.

Domes are favourable trap and fluid focus regions. The mapping in 3D of this architecture has certain predictive power. Linking the development of the dome architecture with an understanding of the geodynamics described above is important for the age of gold mineralisation and the role of magmatic and/or basinal fluids. If domes focussed fluids and they developed by cross-folding, then gold deposition would be post-'D$_2$' and D$_3$ in age. These hypotheses are in contrast to the one regarding active fluid mixing (Neumayr, 2004). A conclusion of this is that there was more than one mineralising event.

## *Appendix 6*

6-1:  **Appendix 6_1 Henson et al Barossa poster.pdf** is the structural history poster presented at the pmd*CRC Barossa conference June 2004.

6-2:  **Appendix 6_2 Blewett et al (Wangathaa).pdf** is a copy of the 2004 paper describing the $D_2$ orogenic event and its relationship with the Late Basins.

```
"Reprinted from Precambrian Research 130, Blewett, R.S., Cassidy,
K.F., Champion, D.C., Henson, P.A., Goleby, B.R., Jones, L., and
Groenewald, P.B., 2004, The Wangkathaa Orogeny: an example of
episodic regional 'D2' in the late Archaean Eastern Goldfields
Province, Western Australia., 139-159, Copyright (2004), with
permission from Elsevier".
```

# Chapter 7: Prospectivity analysis

*R.S. Blewett*

The prospectivity analysis output was terminated on the decision of sponsors at the December 2003 PDT meeting in Perth. The reason being that more-sophisticated prospectivity analysis tools were being developed external to the *pmd*\*CRC. The trade-off was for the project to concentrate on the 3D map.

Having said this, the *pmd*\*CRC A1 project has been considering why some faults are mineralised and others are not. The A1 project presented a paper at the December 2004 PDT meeting in Perth, a copy is found in Appendix 7-1 (**Appendix 7_1 BierleinMoreyA1_YilB5.pdf**). Relatively simple 2D GIS prospectivity analysis was conducted on the GIS built by the Y2 team.

The following extract is from the A1 project update, and pertains to the concept of breaching of domes as being prospective. The results from the A1 project confirm this hypothesis/observation.

The A1 project asked:
*Is mineralisation associated with major faults that intersect structural domes?*

The parameters in the GIS considered were:

1.  faults with a strike length >100 km,
2.  position of regional anticline and syncline axes, and,
3.  mineral occurrences.

The resulting analysis showed that domes are better mineralised than the average crust or keels (Figure 7-1), and that the intersection of domes with long faults is significantly more endowed (Figure 7-2).
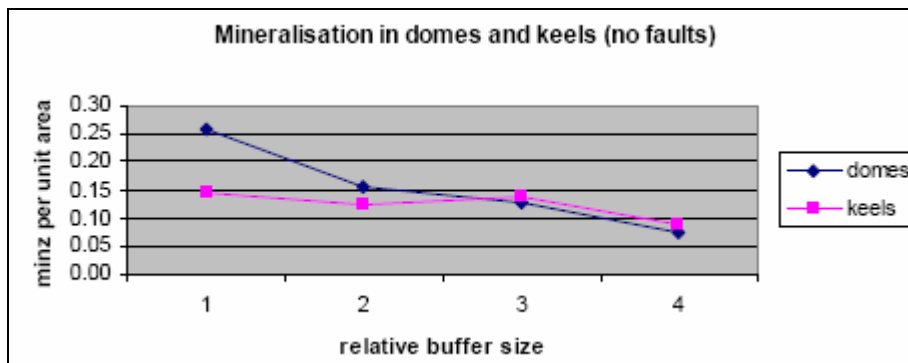


**Figure 7-1: Domes are more endowed than keels (synclines), and there is a significant difference up to 10 km from a dome axis (Buffers 5, 10, 20, 40 km from dome axis).**
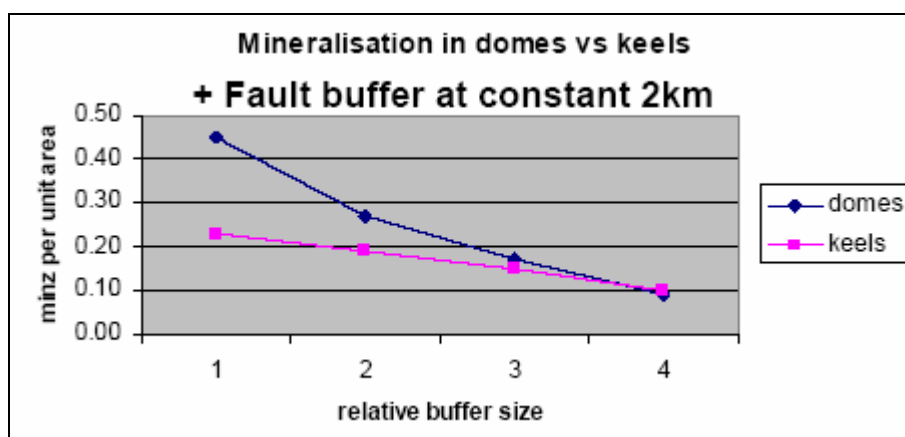
**Figure 7-2: Domes with adjacent faults are even more endowed than keels (synclines), and there is a significant difference up to 20-km from a dome axis (Buffers 5, 10, 20, 40 km from dome axis).**

Another question was:

*Does gold occur preferentially within the hanging wall of major faults?*
The A1 project tested the HW and FW side of faults against mineralisation hypothesis. They used a 2 km buffer on five of the major east-dipping faults. The result was that there is no significant difference in mineralisation on either side of the fault.

A summary of the A1 project prospectivity work (Table 7-1) shows that domes or anticlines and an adjacent fault are the most endowed parts of the Kalgoorlie Terrane. These concepts are further discussed in Chapter 8.

| Factor Mineralisation Intensity | Mineral rank | Mineral prod'n |
|---|---|---|
| average Yilgarn | 0.01 | 5 |
| long gravity worms | 0.05 | 34 |
| bends; all faults | 0.10 | 173 |
| jogs; all faults | 0.14 | 340 |
| fault major >100km | 0.04 | 18 |
| synclines | 0.14 | 44 |
| anticlines | 0.26 | 67 |
| **intersection anticline, major fault** | **0.45** | **430** |
| intersection syncline, major fault | 0.23 | 120 |
| small faults near major faults | 0.09 | 130 |
| small faults away from major faults | 0.08 | 30 |
| intersection fault, bend | 0.08 | 30 |
| intersection of fault, dome and bend | 0.13 | 40 |

**Table 7-1: Comparisons between the tests shows that a major fault intersecting an anticline obtains the highest score in these tests.**

## *Appendix 7*

7-1: **Appendix 7_1 BierleinMoreyA1_YilB5.pdf** is a copy of the A1 project paper presented at the December 2004 PDT meeting in Perth.

# Chapter 8: A 5Qs synthesis and predictive mineral discovery

*R.S. Blewett*

The following chapter is a "Five Questions" (5Qs) synthesis of the eastern Yilgarn Craton (EYC) based on the results of the Y2 project. Most of the project was focussed on answering the architecture question. The five questions are:

1.  What is the geodynamic setting and PT history?
2.  What is the architecture?
3.  What are the fluids, their source and/or reservoirs?
4.  What are the fluid flow drivers and pathways?
5.  What are the metal transport and deposition processes?

The 5Qs is a mineral systems approach to understanding a mineral deposit holistically. The ideas originated from the work of the Australian Geodynamics CRC (AGCRC). However, a mineral systems approach is not new (and not simply adapted from the petroleum system). Ellis (1939) first described the mineral system where "*the occurrence of gold in certain localities and its non-occurrence in others is dependent mainly on three factors, all of which must be present together before gold deposition can take place*". These factors are:

1.  a source of supply;
2.  a suitable pre-existing rock-structure, such as fracture zones or other lines of weakness in which the gold and its associated gangue minerals can be deposited, and;
3.  there must be suitable rock types in which essential precipitants (e.g., Fe) freely occur, favourably situated with respect to the source of supply and the geological structure.

Ellis (1939) asks the question, why is gold localised in zones along a favourable horizon or line of deposits? Using the 3 essential factors, it is structure (factor 2) that is especially important because granite (factor 1) and greenstone (factor 3) are widely distributed (in Ellis's interpretation).

## Question 1—Geodynamics and PT history

Geodynamics is the science dealing with dynamic processes or forces within the earth. The geodynamic processes and forces that have been described or quantified with the tools available to this project include:

*   the character of the mantle lithosphere and its relationship to possible slabs, mantle plumes, or delamination;
*   the deformation history and orogenic processes, and;
*   analogues for Yilgarn geodynamic models.

The following section is a synthesis of the Y2 project's results in terms of geodynamics.

## The velocity anomaly at 100-120 km in the upper-mantle lithosphere

Chapter 4 described the velocity structure of the crust and mantle lithosphere. A feature of note was the relatively fast velocity anomaly (4.8 km/s S-wave) that dipped gently to the southeast at around 100-120 km depth (Figure 8-1). The precise thickness of the layer is difficult to ascertain, but it is interpreted to be around 20-25 km thick. Details of the velocity layering in the lithosphere are presented as a series of depth slices in the Appendix of Chapter 4.
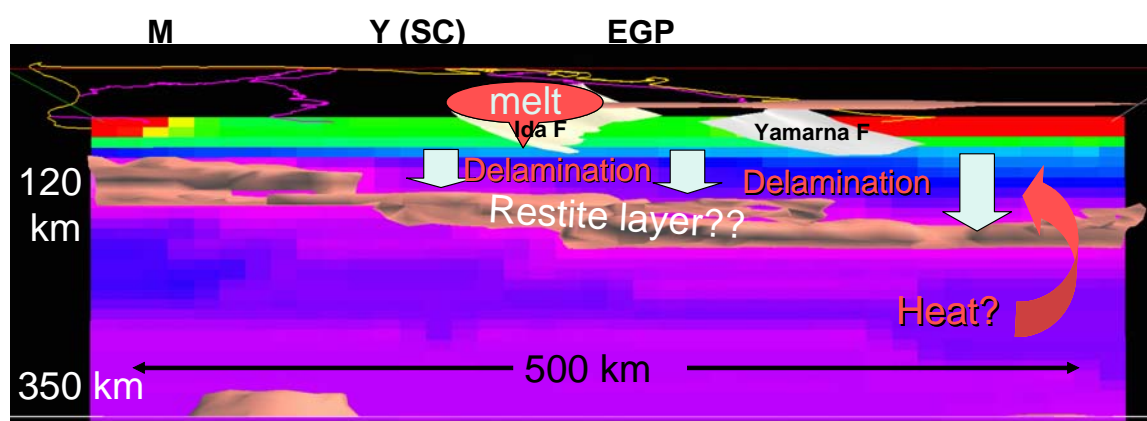


**Figure 8-1: The 4.8 km/s S-wave high-velocity layer in pink in the upper mantle lithosphere may be the eclogitic remains (restite) of lower crustal melts (High-Ca granites). This dense layer (fast velocity) then delaminated at the onset of the $D_{2a}$ contraction (termination of High-Ca magmatism), allowing heat from the mantle (with high ambient temperatures from earlier 2.7 Ga plume influence) to partially melt the crust and generate the Low-Ca granite type. Model after Smithies and Champion (1999). Alternatively, the high-velocity layer may be a fossil subduction zone or slab.**

Certain inferences can be made about the nature and impact of this high-velocity layer and the role of any mantle plumes in the creation or disruption of this layer. The layer could be interpreted as:

1. a fossil slab from southeast-directed subduction between the Narryer and western Youanmi Terranes at ca. 2.75 Ga (see Cassidy et al., 2002a)?, or
2. a delaminated restite layer from High-Ca magmatism.

## Velocity layer as a fossil slab?

Based on largely geochemical evidence, subduction has been proposed at various times, places and with various polarities across the Yilgarn Craton. For example, at 2760-2730 Ma, collision of the Narryer Terrane with the Youanmi Terrane was interpreted as the result of SE-directed subduction (Cassidy and Champion, 2004). Also, west-directed subduction has been proposed under the Kalgoorlie Terrane at ~2700 Ma (Morris and Witt, 1997). What impact or signature would a subduction zone leave on the lithosphere of the Yilgarn?

To answer this question, one should consider modern systems. Subduction zone slabs in modern systems are characterised by **fast** S-wave velocities. Figure 8-2A shows the fast velocity structure associated with the subduction of the Pacific plate beneath the Japanese arc (Fukao et al., 2001). Tomographic images of this subduction shows the oceanic plate or slab as relatively fast (0.5% higher than average P-wave velocity) for the entire mantle volume below Japan and eastern China (Fukao et al., 2001). This velocity anomaly has been presented as an isosurface (http://www.geo.uu.nl/~bijwaard/), and an animation (Appendix 8.1). A number of important observations are revealed in this animation:

1. most of the plate material in the upper mantle flattens on the upper-to-lower mantle transition;
2. there is a narrow conduit connecting the upper mantle plate material with a large volume in the lowermost mantle (the so-called "graveyard"), and;
3. the 'slab' has a complex 3D shape with holes and tears in it.
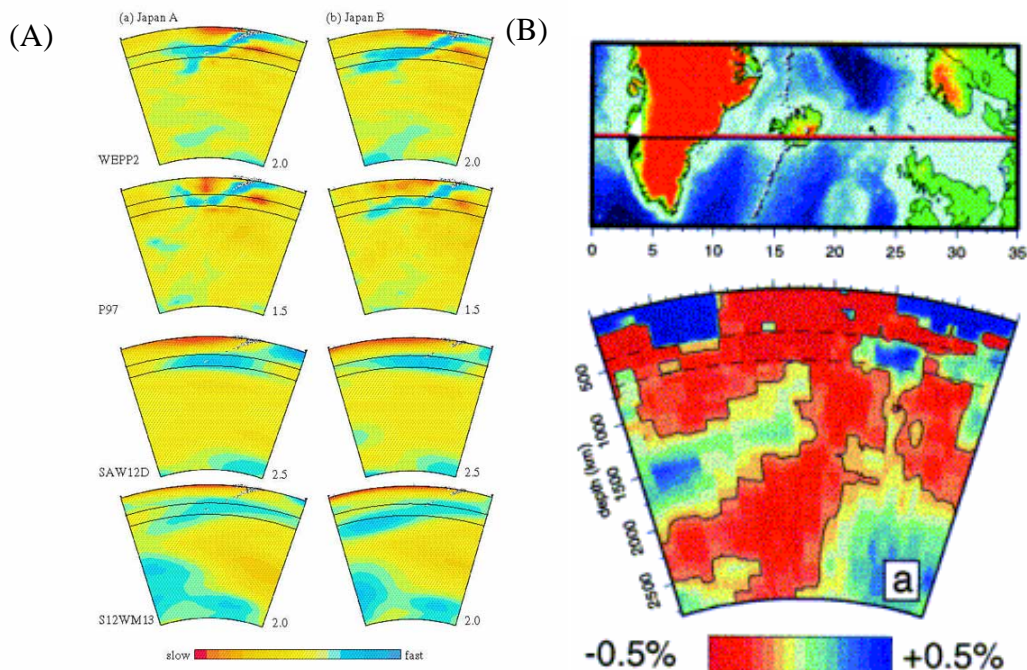


**Figure 8-2: (A) The fast velocity structure associated with the subduction of the Pacific plate beneath the Japanese arc (Fukao et al., 2001); (B) Cross section through the model of Bijwaard et al. (2004) showing a large plume-shaped anomaly (with respect to reference model ak135 [Kennett et al., 1995]) in the mantle below Iceland. A 0.15% velocity contour is indicated in black for clarity. The separate layers are well-resolved in the lower mantle, but less well-resolved in the upper mantle. Dashed lines indicate the 410 and 660 km discontinuities.**

In contrast to the modern Japanese example, the high-velocity layer is at relatively shallow mantle levels under the Yilgarn, and is geometrically relatively simple. However, this simplicity may be a function of the coarse sampling resolution of the broadband data. The high-velocity layer cannot be both the signature of a slab from opposing southeast- and west-directed subduction events. It is unlikely that the high-velocity layer represents a slab (see also discussion of mantle plumes below).

## Velocity layer as delaminated restite?

Delamination is the removal of the lower part of the lithosphere, commonly resulting in melting under continents. By removing the lower lithosphere, the mantle can rise to higher levels, depressurise, and partially melt. There are two conditions that must be met before delamination can occur:

1. The lower parts of the lithosphere have to be gravitationally unstable by being more dense than the underlying material. The lower lithosphere can be more dense because of an intrinsic compositional difference, such as having buoyant mantle residuum beneath it, or it can become more dense through cooling, or by consisting of denser minerals.
2. The viscosity must be lowered. For lithosphere to detach and begin to flow downward under the influence of gravity, its viscosity must be low enough to allow flow (Rayleigh-Taylor instability). The flowing material is still completely solid, but it behaves according to the rules of fluid dynamics on a geological time scale.

Champion and Sheraton (1997) defined the principal granite types across the Yilgarn Craton (see Chapter 1). The High-Ca and Low-Ca types dominate the granite types by area (60% and 20% respectively). High-Ca granite types have a long-lived age range up to ~2660 Ma, and have been interpreted as lower-crustal to upper-mantle melts developed during subduction (Champion, 1997). Low-Ca granite types are high-temperature (A type), and were emplaced after 2655 Ma (most ~2640 Ma) across the entire Yilgarn. They have been interpreted as mid-crustal melts caused by a significant thermal addition near the base of the crust some 5-40 My after the peak High-Ca magmatism (Champion, 1997). Champion and Sheraton (1997) and Smithies and Champion (1999) suggested that the delamination or convective thinning of a dense, garnet-rich, lower crust (restite from extraction of earlier voluminous High-Ca granite magma) advected heat into the base of the crust. This heat then allowed widespread crustal anatexis, and emplacement during late-orogenic extensional collapse. Many of the latest features, for example fault movements, inferred from the seismic reflection data support late extension (Swager, 1997). The presence of the relatively flat Yilgarn Moho (Drummond et al., 2000a; Goleby et al., 2004) indicates some form of lower crustal thermal erosion or modification by delamination (Nelson, 1992).

What evidence exists for a dense delaminated layer from early High-Ca lower-crustal melting? The velocity structure of the Yilgarn crust today shows it is essentially felsic (Drummond et al., 1993; Fomin, 2003) with no evidence of dense garnet-rich restite (eclogite or garnet amphibolite) down to 40-45 km depth. Rudnick (1995) has suggested that delaminated lower crustal layers return to the mantle (below the depth visible in the seismic reflection data). Evidence supporting the Smithies and Champion (1999) delamination model for the generation of the Low-Ca granites includes:

1. a flat Moho with a gentle east dip;
2. a crust that is thin (~40 km) relative to the depths inferred from geochemistry and petrophysics;
3. a fast S-wave velocity layer at 100-120 km that dips gently to the southeast, and;

4.  a relatively simple layering of the lithosphere (suggesting the features are relatively late – see discussion on mantle plumes below).

Adding the 20-25 km thickness of the high-velocity layer to the base of the crust, and taking account of up to 10 km of post Archaean erosion, a 2.65 Ga crustal thickness of around 70-75 km can be inferred. This restored estimate of crustal thickness and rheology is consistent with the inference based on geochemical models (Smithies and Champion, 1999).

The concept of crustal delamination and upper-mantle metasomatism is reflected in the alkali chemistry and diamond pathfinder indicators (Mark Mitchell, De Beers, *pers. comm.*, 2004). The degree of metasomatism increases to the east, consistent with the greater distance between the present crustal base in the east than the west (Figure 8-1). For example, the garnets present in kimberlites (2.5-2.3 Ga) are less Ca-saturated from east to west, suggesting a more refractory mantle in the east (Graham et al., 2004). The syenite magmatism (synchronous with Low-Ca granite magmatism) is limited to the terranes east of Kalgoorlie (Champion and Sherton, 1997). Based on Sr-Nd isotope variations, these syenites were derived from a re-fertilised subcontinental lithospheric mantle (Graham et al., 2004). The high-velocity layer is deepest to the east (Figure 8-1), consistent with a greater amount of delamination and therefore enrichment or re-fertilisation of the upper mantle.

The preferred model is for delamination of a dense (high-velocity) High-Ca restite at the onset of $D_{2a}$ contraction. The delamination provided heat into the base of the now thinned (delaminated) crust and re-fertilisation of the subcontinental lithospheric mantle. Mafic granites and early syenites were emplaced during localised extensional events associated with '$D_2$' orogenesis. Later syenites (direct from the mantle) and the Low-Ca granite crustal melts, reflect the time delay in heating the new crustal base and ongoing extension at the end of the $D_{2/3}$ contractional events.

## Mantle plumes or not?

Some workers have suggested that the ~2.7 Ga mafic-ultramafic sequences in the Kalgoorlie Terrane were the product of a large-scale mantle plume melting event. Others have suggested that all of the felsic magmatism across the entire Yilgarn was the result of plume tectonics (e.g., Campbell and Hill, 1988; 1992). Mantle plumes are thermal pulses generated in the deep Earth. Assuming the lithospheric stratification is old, the passage of a plume through the mantle would have a visible impact on any stratification. Modern mantle plumes are characterised by low velocities in both P- and S-waves.

Bijwaard et al. (2004) imaged a large-scale low-velocity anomaly beneath the Iceland hotspot in the central North Atlantic Ocean (Figure 8-2B). Similar low velocities are present below Yellowstone, the Society Islands, the Canary Islands, and central Africa. The mantle below Iceland proves to be one of the places to demonstrate good resolution for the entire mantle plume. Care is needed in comparison because much of the Iceland imagery is deeper than the available tomography for the Yilgarn (which continues to a depth of 350 km; see Chapter 4).

The stratification of the mantle lithosphere in the Yilgarn shows no evidence of the passage of a mantle plume (low-velocity holes). This suggests that the mantle plume rose to an elevation below the base of the lithosphere (below 350 km), or that its passage to higher elevations has been obliterated by younger processes. The latter interpretation is preferred, and is consistent with the high-velocity layer being a relatively young feature (<2.7 Ga) and related to younger magmatism and delamination as discussed above.

## Implications for predictive mineral discovery

The broadband seismic data provide a unique view of the crust and mantle lithosphere. The main conclusion concerns the interpretation of the fast S-wave velocity layer at 100-120 km in the lithosphere. The layer is likely to represent the residue from High-Ca granite magmatism which ceased around 2660 Ma, that was delaminated from the base of the crust. The result of delamination was a thermal spike at the base of a thinned crust which resulted in melting and generation of the Low-Ca granite suite. These later granites are temporally associated with the late orogenic gold (Cassidy et al., 2002a). The passage of mantle plumes and the presence of subduction zone slabs appear not to have been imaged.

There is controversy over whether all the gold mineralisation occurred in a crustal continuum late in the orogenic cycle, or throughout the orogenic cycle (cf. Groves, 1993; Yeats et al., 2001). Geochronological and structural evidence does indicate that a number of gold events have occurred. However, a significant period of gold mineralisation occurred across the Yilgarn late in the orogenic cycle (2640-2630 Ma) and was temporally linked with a palaeostress switch (Blewett et al., 2004a) and Low-Ca granitoid magmatism (Champion and Sheraton, 1997).

Delamination of a thickened crustal root and the generation of late (low-pressure) crustal melt granitoids have been temporally linked (Smithies and Champion, 1999; Qiu and Groves, 1999). Qiu and Groves (1999) proposed that the delamination was of sufficient scale to drive the gold-bearing giant upper-crustal fluid system with lateral and vertical flow at the scale of hundreds and tens of kilometres respectively. Delamination is a large-scale geodynamic process which is conceptually value to predictive mineral discovery in that it explains the temporal link between the late Low-Ca granites and syenites across the craton and the late craton-wide gold event.

## A new tectonic model for the Eastern Yilgarn Craton: orogenic surge

Details of the deformation history are outlined in Chapter 6. The following section is a discussion of the orogenic surge model (Blewett et al., 2004b; 2004d) for the development of 'D$_2$' in the EYC. The process of switching tectonic mode (compression-extension) while under the same general contractional orogen can occur in a number of ways (Figure 8-3).

**Vertical block 'escape' or channel flow**
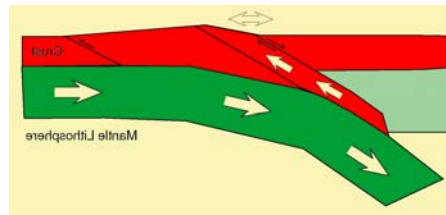


**Underplating and wedge extension**
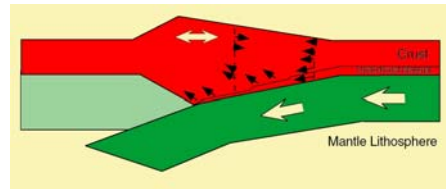


**Slab roll back**



**Post-orogenic collapse**



**Slab detachment/break off**
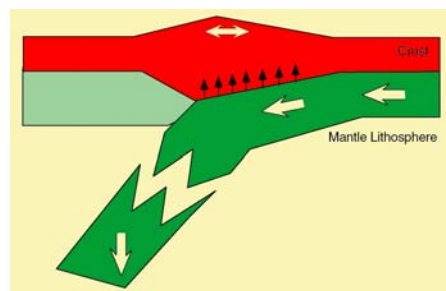


**Figure 8-3: Five alternative models for switching between contraction and extension. Models include channel flow, underplating with wedge extension, slab roll back, post-orogenic collapse, and slab break off. Difficulties with these alternative models include: the likely flat subduction in the Archaean, the wide orogen, the whole crust is involved, the rapid and diachronous switches, and the few high-pressure rocks exposed.**

The EYC is divided into a number of domains or terranes (Swager, 1997) separated by moderately east-dipping faults with a west-directed vergence (Goleby et al., 2002). Within each domain, there was a similar cycle of at least two stages of east-west shortening ($D_{2a}$ and $D_{2b}$), separated by extension and basin formation ($D_{2E}$). Between the domains, however, the timing of this cycle was "out of phase" by ~3-5 Ma (younger in the foreland to the west). Figure 8-4 illustrates that during the first stage of compression $D_{2a}$ (~2661 Ma) in the west or southwest (Kalgoorlie), further east (Kilkenny district) was experiencing $D_{2E}$ extension and the deposition of the Pig Well

Basin adjacent to inverted earlier (~2665 Ma) $D_{2a}$ thrusts. Similarly, when the Kurrawang Basin was being deposited (~2657 Ma) during $D_{2E}$ in the west, the Pig Well Basin to the east was being inverted by a phase of $D_{2b}$ compression (Figure 8-4). Further east, it is likely that an earlier couplet existed between the Kilkenny district and the Laverton district. Here, the >2665 ±4 Ma Granny Smith Late Basin (Hill et al., 1992) unconformably ($D_{2E}$) overlies a previously folded basement sequence ($D_{2a}$), and it was itself deformed during later $D_{2b}$ regional folding. This is ~3-5 My older than similar events in the Kilkenny district (Figure 8-4).
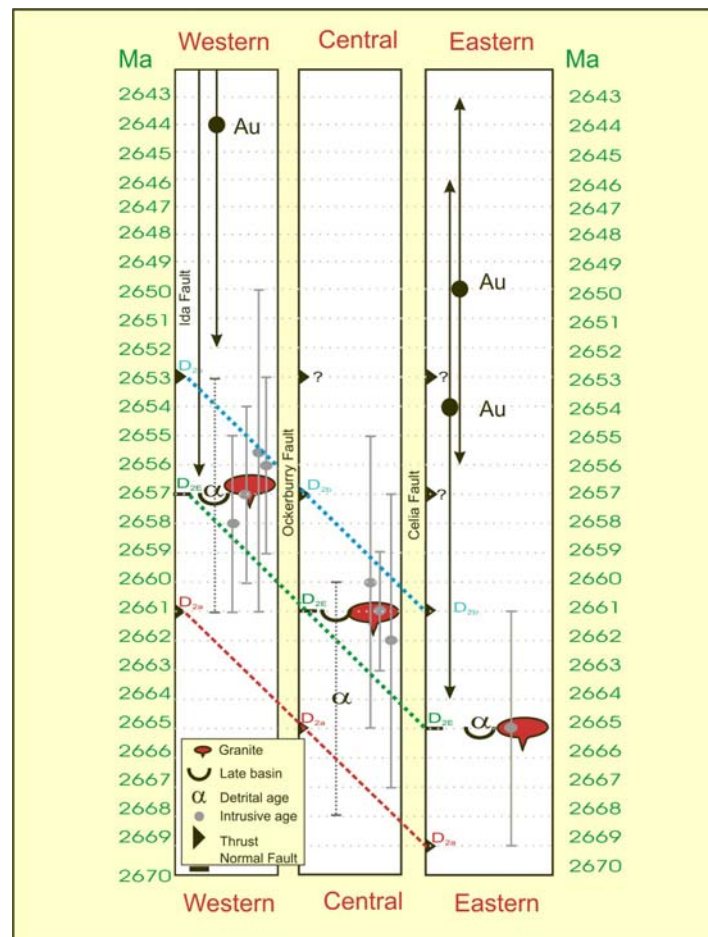


**Figure 8-4: '$D_2$' orogenesis time lines across the EYC. Published ages for direct gold from Brown et al. (2002), Veilricher et al. (2003) and Salier et al. (2004). '$D_2$' ages young diachronously to the west (SW). Syn-gold ages overlap the last stages of '$D_{2b}$' contraction.**

A tectonic model needs to account for extension following prolonged contraction, while convergence continues across the orogen (with a similar movement vector). A number of alternative models are presented (Figure 8-3), however they do not readily account for the:

- great width of the orogen;
- rapidity of the switches;
- diachroneity;
- lack of high-pressure rocks, and;
- hypothesis that a slab was likely to be flat in the Archaean.

172

Blewett et al. (2004b; 2004d) proposed an alternative model – orogenic surge, to account for the unique features of the development of the 'D$_2$' orogeny in the EYC. This orogeny was diachronous, rapid, involved granite magmatism and emplacement, and basin development and inversion. Crustal thickening builds a gravitational instability that is commonly relieved by extensional collapse (or rapid erosion). Orogenic surge (Lister et al., 2001, and references therein) is a mechanism in which footwall collapse along a newly initiated low-angle frontal thrust allows the orogen to surge over its foreland at a rate that is greater than the overall rate of shortening across the orogen (Figure 8-5). As a result, the orogen undergoes overall extension; much of it accommodated on inverted thrusts that were active during earlier crustal thickening in the overlying (and hinterland) slices. This is an effective mechanism to cause an episodic switch in tectonic mode in the overlying (hangingwall) slices, despite the orogen still being under contraction.

# Orogenic surge – summary of the process
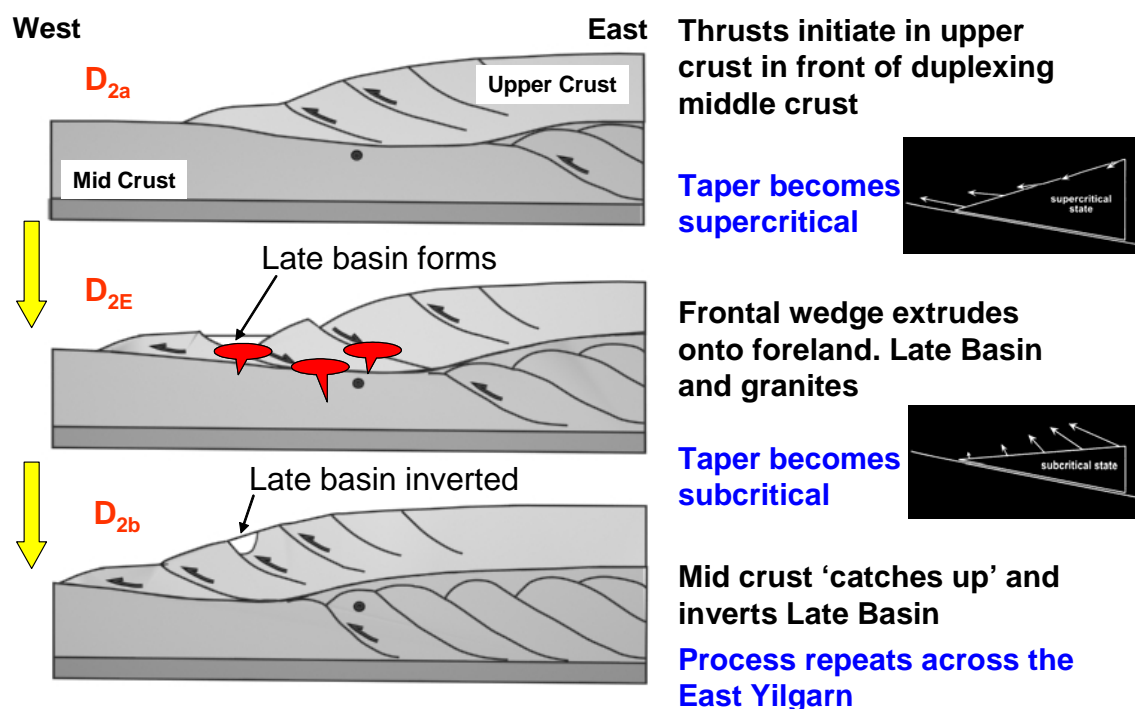


Figure 8-5: A schematic diagram illustrating the surging of the foreland above a duplexing mid-crust. During the surge, localised extension occurs on previous thrusts and permits mafic-type granite intrusion and space for Late Basins to be deposited. The mid crust "catches up" with the upper crust and inverts the basins and reactivates faults as thrusts. The process repeats across the EYC. Deep fluids are driven from below and behind the upper crust which is out of phase with the mid crust. This means that orogenic gold will occur late in the cycle in a pre-prepared upper-crustal architecture.

The orogenic surge model (Figures 8-5; 8-6) is an elegant explanation for the geometry, kinematics and timing of the tectono-thermal phases associated with the diachronous passage of a compression-extension couplet across the EYC. We envisage a process whereby a 'D$_2$' deformation wave passes diachronously between domains at a rate of ~3-5 My from east to west from ~2670 Ma to ~2650 Ma, and that

this wave was driven by the duplexing and thickening of the mid crust (see Chapter 3).

For each successive domain, the following process (Figure 8-5) is proposed:

1. Far-field stress from the plate margin to the east initially thickened the crust during $D_{2a}$. Thickening was accomplished by west-directed thrusting, on major crustal penetrating structures, on thin-skinned thrusts, and driven by duplexing in the mid-crust, together with upright folding during $D_{2a}$. Foreland basins likely developed in advance of the frontal thrusts. A gravitational instability (critical taper) was developed.
2. The gravitational instability was released by a rapid west-directed surge of the frontal wedge out over the foreland, accommodated on a low-angle frontal thrust. Contraction occurred at the front and extension in the adjacent hinterland. This extension at upper-crustal levels resulted in flooding and rapid deepening of Late Basins, which mostly developed as half-grabens in the east-dipping hangingwall of the $D_{2E}$ inverted (normal) faults. Differential movement of glacier ice is an analogy, with thrusting at the toe and crevasse development "upstream".
3. Ongoing plate convergence and duplexing in the mid crust inverted the $D_{2E}$ extensional faults as $D_{2b}$ thrusts. Locally, the $D_{2b}$ inversion more than restored the earlier $D_{2E}$ extension so that most of the basins were elevated and stripped. The basins were folded and metamorphosed as out-of-sequence thrusts brought basement over the basins (e.g., at Laverton).
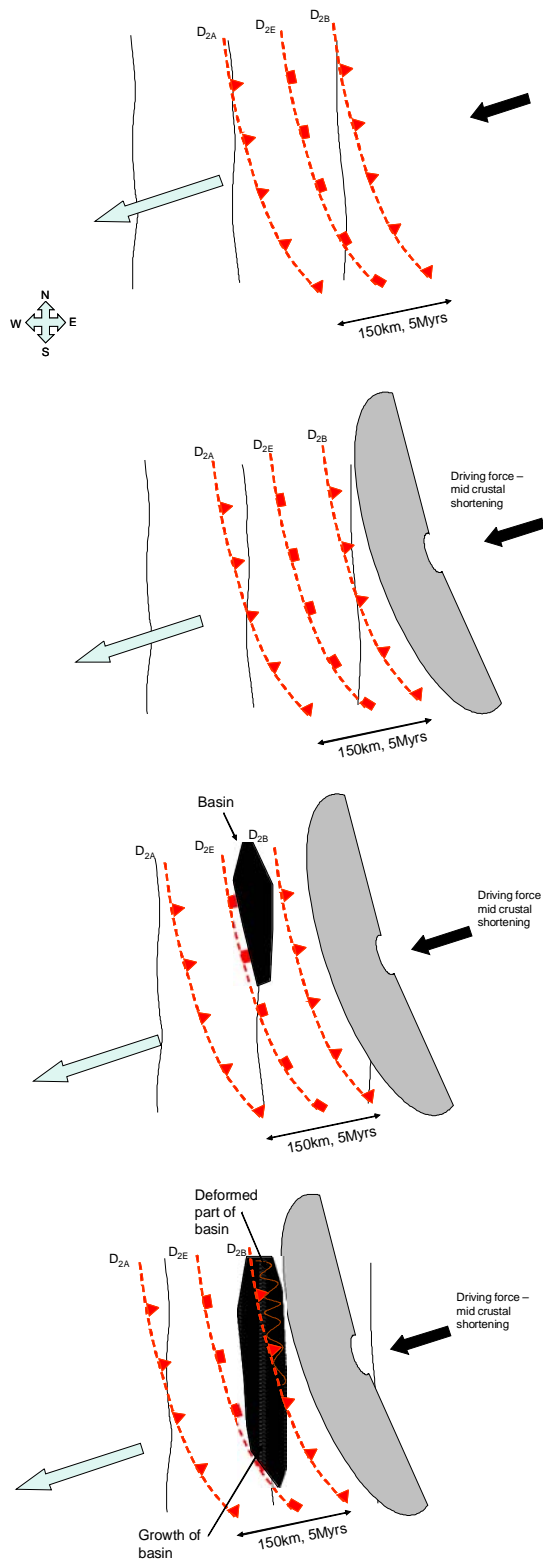
**Figure 8-6: Oblique D$_2$ collision imparted onto a N-S D$_E$ architecture, resulting in diachronous orogenesis (including basin formation), with the youngest events in the southwest of the EYC (around Kalgoorlie).**

The orogenic surge process has been animated to illustrate the schematic diagram with time (Kalinowski et al., 2004). A copy is available in Appendix 8-2.

## Implications for predictive mineral discovery

The orogenic surge model predicts and accounts for the diachroneity of the Late Basins, emplacement of the Mafic granites, and termination of the High-Ca granites. It also accounts for the fact that the Late Basins and granites cut earlier stages of $D_2$, are deposited/emplaced in an extensional regime, and yet are also overprinted by the main $D_2$ contraction. The diachroneity of deformation, and associated granites and basins, may explain some of the age differences found across the EYC. The driving force of the upper-crustal surge was the imbrication of the mid crust from behind and below. This mid-crustal deformation likely drove fluids via newly developing pathways into a pre-prepared architecture.

The orogenic surge model is an alternative hypotheses (to strike-slip amalgamation) for the development of the main '$D_2$' event. The model links the development of folds and thrusts at the crustal scale with the termination of High-Ca granites and the onset of mafic granite magmatism. The model places the Late Basins in a consistent temporal position with the diachronous from east to west (SW) development of the orogen.

The model predicts the switching of tectonic mode (extension-contraction) and thus provides alternating stress axes ($\sigma_1$ and $\sigma_3$) which are important for fluid flow or fluid mixing (magmatic-basinal fluids). Gold was been deposited at various stages of '$D_2$'. The direct dating of gold at a number of mining camps (Laverton, Chalice, Kambalda) places mineralisation during the waning stages of '$D_2$' (Figure 8-4). The orogenic surge model predicts that a favourable architecture was established in the upper crust in front of and above an imbricating mid crust. Deep crustal fluids were possibly driven subsequently into this pre-prepared ground in the foreland as the mid-crust imbricates "caught up" with the upper-crustal architecture.

The orogenic surge model predicts that metamorphic fluids and alteration would have reduced the strength of the active part of orogen, and maintained a high-strain focus at the toe of the foreland wedge (e.g., Willet, 1992). These fluids would have promoted the passage of the compression-extension couplet through the orogen by successively "lubricating" faults (preparing the ground), and facilitating a propagating wave of foreland surge and hinterland extension followed by inversion, uplift and annealing. In this way, the generation and driving processes of fluids are linked in one geodynamic model.

## Analogues of orogenic surge

Analogues are a partial validation of tectonic models. Examples of processes similar to the orogenic surge model outlined above are discussed below. These include the role of shear zones, granites, switching tectonic mode, and basin development.

In the Variscan Mondonedo nappe of NW Spain, large extensional shear zones were developed along with granite magmatism while the orogen was under contraction (Martinez-Catalan et al., 2003). Some of the extension occurs in the footwall of the thrusts, as foreland-directed extensional shear zones. The net result is a foreland-extruding wedge. This example illustrates that contraction, extension and granite magmatism can all occur in the same system. The foreland-dipping extensional shear

zones in the footwall may be equivalent to some of the west-dipping features visible in the mid crust in the seismic reflection profiles (see Chapter 3).

A similar mixed tectonic mode development of mechanically linked thrusts and extensional shear zones occurred in the High Himalayas (Searle, 1999). Foreland-directed extrusion of the Himalayas was accommodated by thrusting on the Khumbu Thrust and coeval hinterland collapse along down-to-the-north detachments in the Everest and Lhotse region (Searle, 1999). High Himalayan leucogranite sheets were emplaced during extension along the top of the High Himalayan slab. These granite sheets are up to ~1 km thick and were emplaced by hydraulic fracturing during simple shear. In this way, dilation occurs and facilitates the emplacement of granites in an overall contractional orogen. The mechanically linked contraction-extension is the geodynamic scenario Lister et al. (2001) used in their model of orogenic surge and has been applied by Blewett et al. (2004c).

Mixed mode (contraction-extension) basins occur in the Oligocene-Miocene basins of Calabria in southern Italy (Weltjie, 1992). These basins are sitting in a wedge-top or piggy-back position and are developed in the hinterland which is undergoing extension while the frontal thrust is under contraction (Figure 8-7). These Tertiary basins developed in a complex foreland system (DeCelles and Giles, 1996) perhaps partly analogous to the Late Basins of the EYC.
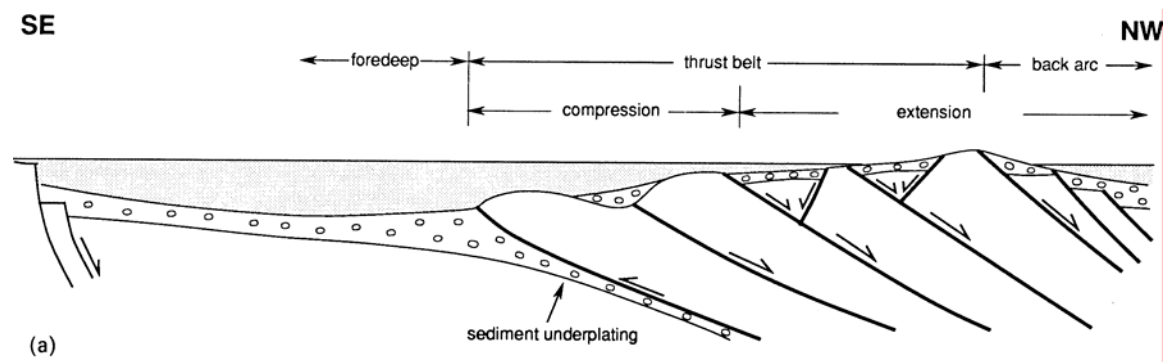


**Figure 8-7: Schematic cross section of the Oligocene-Miocene mixed-mode wedge-top basins in southern Calabria, Italy (from Weltjie, 1992). Note how the basins have a foreland-directed contraction accommodated on a frontal thrust and a coeval hinterland extension in the wedge-top or piggy-back position. Compare this section with the seismic interpretation of Smith (2004; Figure 6-12).**

## Numerical and analogue modelling of orogenic surge

Extension during contraction is not unique to the EYC. Others have attempted to model similar geodynamic scenarios. In the contractional Taiwan orogen, the central highlands are undergoing extension while they are still rising. Wang and Hung (2002) suggested that this was due to mid-crustal underplating and thickening. They attempted to model a thickening mid-crustal wedge (analogy with the EYC) with thrusts and coeval extension parallel to the orogen. Figure 8-8 shows their analogue modelling attempts, which resulted in the creation of localised extension just behind foreland-propagating thrusts. This contraction-extension linkage may be analogous to the development of the Late Basins in the EYC.
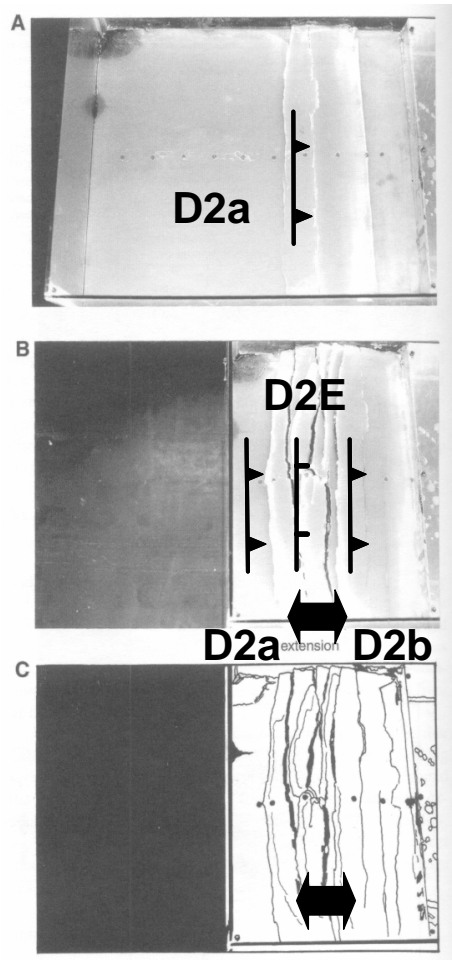
**Figure 8-8: Physical analogue modelling of Taiwan where the main mountain belt is undergoing extension in an overall contractional orogen (after Wang and Hung, 2002). Note that the thrusts propagate into the foreland (left) in A. Continued thrusting at the frontal thrust moves at a greater rate than the overall model leading to extension in the intermediate hinterland of the experiment in B. C is a line drawing of the final result B.**

Schreurs et al. (2002) made a number of experiments of thrust systems developing in sand (simulating the upper crust) with a variable-strength basal detachment layer. The rate of movement of different thrusts in a duplex system was shown to be different when the frontal thrust approached a strong domain in the basal layer. The result was a fast-propagating frontal thrust and a slow-propagating (or even extending) immediately hinterland thrust. This difference in thrusting rates resulted in a significant decrease in elevation behind the frontal thrust; a possible analogue for the space needed for Late Basin development? A copy of the Schreurs et al. (2002) animation is available in Appendix 8-3.

## Modelling extension during the orogenic convergence in the Yilgarn

*Y. Zhang, R.S. Blewett, B. Hobbs, A. Ord and P. Roberts*

178

## Introduction

The development of the architecture of the Yilgarn Craton involves a prolonged history of convergent orogenesis. Studies of structural signatures produced from this history (e.g., Swager 1997; Blewett et al., 2004; 2004d; Henson et al., 2004) reveal that under a broad convergent setting, several episodes of tectonic-mode switching occurred (between compression and extension). A question then arises concerning how compression switches to extension in an overall convergent orogenic belt, and what is the key geodynamic process behind this switch.

Lister et al. (2001) proposed three possibilities for tectonic-mode switching during orogenesis. Based on a general discussion of geological observations, but without any validation of fundamental geodynamics, these possibilities include:

1. lithosphere drop-off or slab tear (convective removal of a thermal boundary layer, reduced orogen strength and increase of potential energy, and the lateral spreading tendency of uplifted materials);
2. accelerated retreat of a subduction zone (essentially an extensional setting under slab retreat), and;
3. orogenic surges (a collapse event in the over-thickened continental crust due to ongoing convergence – Figure 8-9).
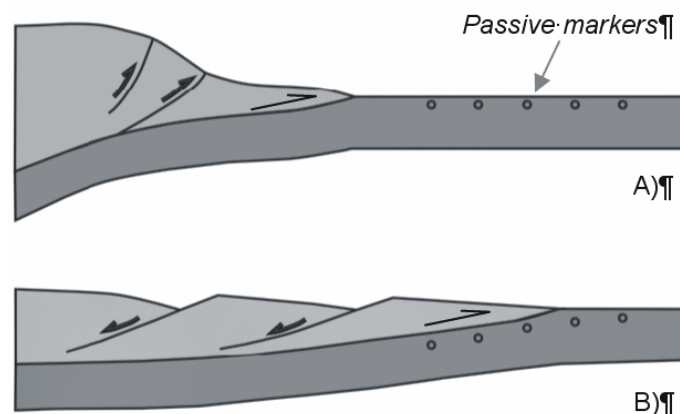


**Figure 8-9: The concept of the geometry of orogenic surge (adapted from Lister et al., 2001). A) Over-thickening of the orogenic wedge with the development of a new frontal thrust. B) The collapse of the orogen over the foreland and switch to extension in the immediate hinterland.**

The orogenic scenario has been proposed to explain the extensional events during the overall convergent process in the Yilgarn (Henson et al., 2004; Kalinowski et al., 2004). This mechanism suggests a local faulting/thrusting extrusion, which occurs when the crust is thickened to a certain level and topographical/gravitational loading reaches a certain magnitude.

The current numerical modelling seeks to approach this problem from several angles:

- development of reverse faults and associated deformation features;
- development of high topographic elevation along discrete thrusts and its thermal effects on deformation, and;
- extrusion of a frontal thrust wedge under topographic loading.

## Brief description of theoretical basis

The mechanical deformation of rocks in the current models follows two constitutive behaviours (rheology). These behaviours are Mohr-Coulomb elastic-plastic behaviour and linear-viscous behaviour.

The upper crust is simulated as a Mohr-Coulomb elastic-plastic material. Under this rheology, the material undergoing deformation behaves initially elastically until the stress reaches a critical value known as the yield stress, at which point it begins to deform plastically, and irreversibly, to high strain. A Mohr-Coulomb elastic-plastic model requires the specification of density, bulk and shear moduli, cohesion, tensile strength, friction angle and dilation angle. A strain-softening behaviour can be incorporated with the Mohr-Coulomb elastic-plastic deformation. This specifies that the material will become weaker (decrease of cohesion, tensile strength and friction angle) with accumulation of plastic strain, hence favouring the localisation of more strain.

The deformation of the lower crust is approximated by a linear viscous rheology. This formulation specifies that stress is related to strain rate by viscosity and, as such, the material can flow in a manner of viscous-creep under small stress and strain rates.

In the thrusting and topographic-elevation development models, mechanical deformation is coupled with thermal evolution. The thermal evolution follows the theories of conductive thermal transport (Fourier's Law). The model considers thermal conductivity, radioactive-heat production, and mantle thermal flux, and computes the distribution of geothermal gradients using structural geometries and densities. In these models, one slab is allowed to slide across other slabs along thrusts. The sliding is controlled by friction along thrusts (friction angle), which is also significantly affected by normal stresses on a thrust plane. Sliding occurs when the resolved shear stresses exceed frictional resistance along a thrust.

## Development of reverse faults and associated deformation features

The first sets of models explore what happens to a crust slab that is subjected to horizontal convergent deformation. The interest here is to see if extension can occur anywhere within the topographic elevation (the thickened part of the crust).

This model is 160 km long and 40 km thick, consisting of an upper-crust layer (20 km thick, Mohr-Coulomb elastic-plastic) and a lower-crust layer (also 20 km thick, linear viscous). Figure 8-10 illustrates the initial geometry.



**Figure 8-10: Initial geometry of a two-layer crust deformation model.**

For the upper crust, the following material properties have been used: density=2700 kg/m$^3$, bulk modulus=2.67e$^{10}$ Pa, shear modulus=1.6e$^{10}$ Pa, cohesion=1e$^7$ Pa, tensile strength=1e$^6$ Pa, friction angle=30° and dilation=2°. For the lower crust, a density of 2900 kg/m$^3$ and viscosity of 1e$^{21}$ Pa s have been used.

The model is first subjected to horizontal shortening. Figure 8-11 illustrates the patterns of shear strain distribution (whole model) and failure patterns (top level only). It is noted that diffuse shear zones are developed in the model as a result of the horizontal convergent deformation. These lead to the development of broad topographic elevation (the maximum of about 6 km). Tensile failure is predominantly located at the crest of the elevation (Figure 8-11, bottom). This reflects the effect of the lateral gravitational spreading tendency associated with high topographic elevation. It seems that such extensional features are confined to the shallow levels of the continental crust only, and particularly to the crest of high topographic elevations.
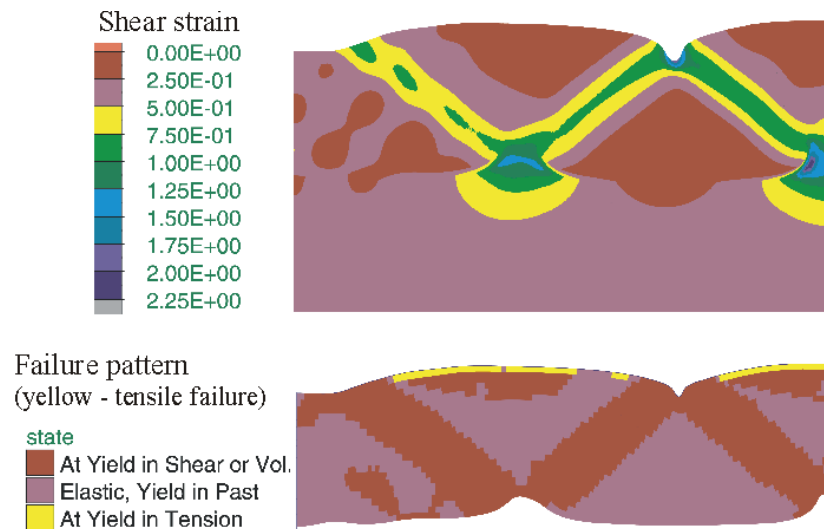


**Figure 8-11: The results of a two-layer model with horizontal convergent deformation (see Figure 8-10 for initial geometry). Top: shear strain contours. Bottom: failure pattern.**

In the next model, the behaviour of strain softening is incorporated in the model with identical geometry and properties to the model above. Strain softening behaviour promotes further strain localisation at sites where failure and plastic strain localisation occurred early in the shortening history (Figure 8-12). In this case, strain softening enables one shear zone or reverse fault zone to localize more strain and develop large displacement in the central part of the model, though other shear zones have also developed. High topographic elevation is developed as a result of thrusting. Consistent with the model above (Figure 8-11), the region of tensile failure is located at the crest of the maximum elevation. These are regions most likely to develop second-order gravitational sliding (extensional) faults.
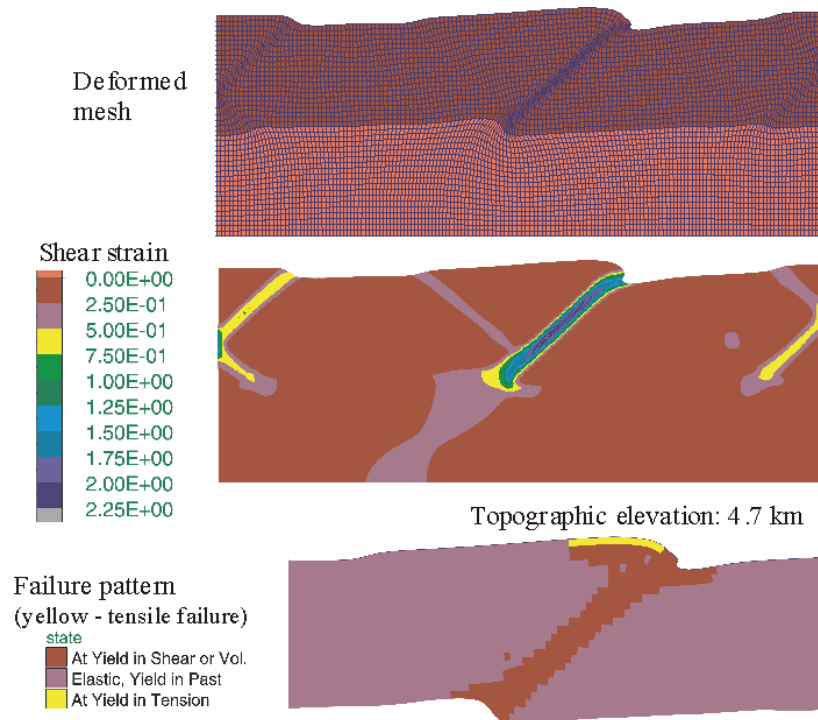
**Figure 8-12: Deformed mesh (top), shear strain contours (middle) and failure patterns (bottom) for a two layer model involving strain softening.**

To test the reverse faulting or thrust scenario further, a new model with three initial mechanical perturbations was constructed (Figure 8-13a). As illustrated in Figure 8-13b and 8-13c, these mechanical perturbations control and facilitate the locations and development of three shear zones or reverse fault zones (thrusts). Topographic elevations with amplitudes of 4.0-4.6 km are developed. Tensile failure only occurred at the crest of these elevations (Figure 8-13d), suggesting that only shallow crustal levels are favourable locations for gravitational extension. This feature is also related to buckling of the surface layer associated with reverse faulting or thrusting.
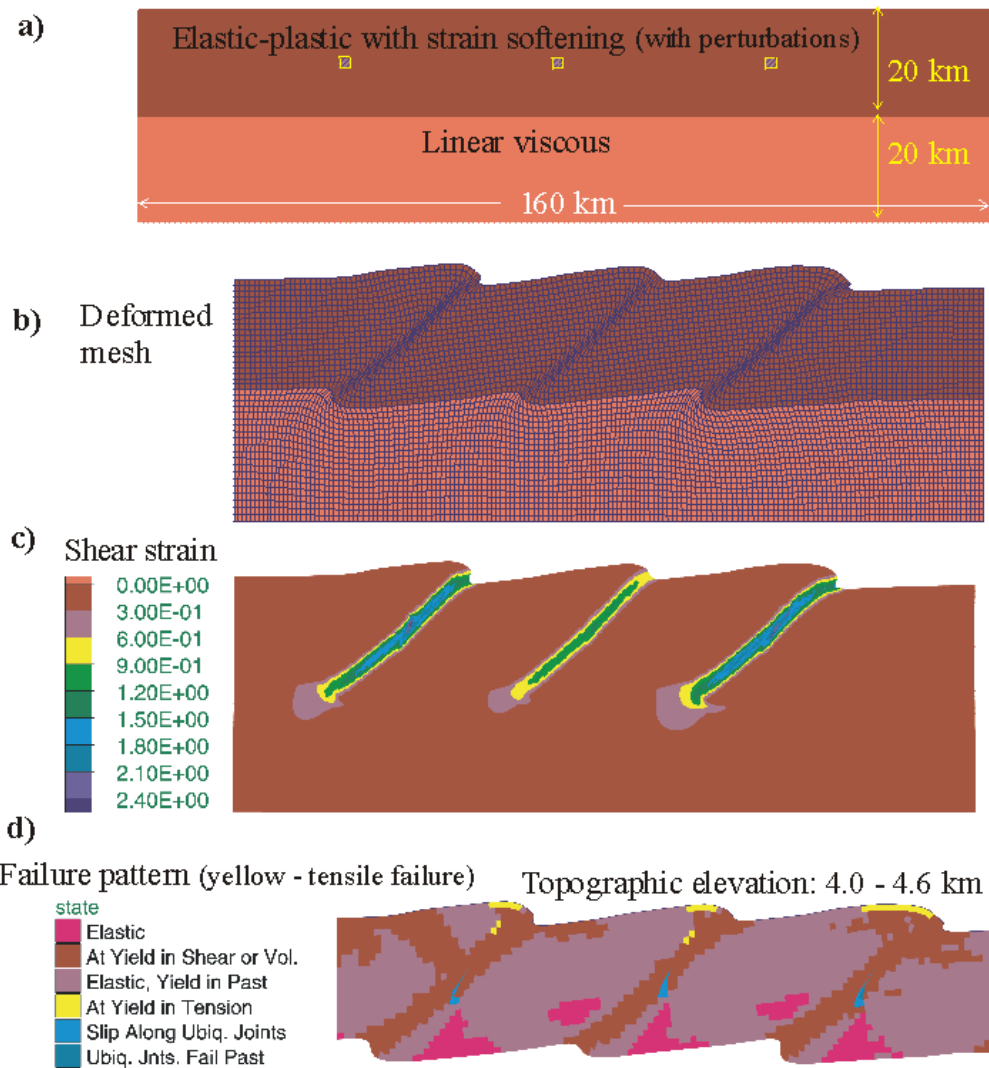
**Figure 8-13: The results of a model involving strain softening and three initial mechanical perturbations. a) Initial geometry and locations of mechanical perturbations. b) Deformed mesh. c) Shear strain contours. d) Failure patterns.**

# Development of high topographic elevation along discrete thrusts and its thermal effects on deformation

## Coupled mechanical-thermal thrust model

The set of models presented in this section simulate large displacements along thrust faults, the development of high topographic elevations, and raised geothermal anomalies associated with high topography and crustal thickening. Our interest here is to estimate the locations of tensile failure in a thrusting slab that experiences large displacement, and to find out if any part of thrust faults could possibly become extensional (normal displacement) during thrusting displacement and convergence.

Figure 8-14a shows the initial geometry of the model. The model consists of an upper crust and a lower crust, both being simulated as Mohr-Coulomb elastic-plastic slabs. The material properties of the upper crust are: density=2750 kg/m$^3$, bulk modulus=2.33e$^{10}$ Pa, shear modulus=1.4e$^{10}$ Pa, cohesion=5e$^6$ Pa, tensile

strength=5e6 Pa. For the lower crust, the material properties are: density=2850 kg/m$^3$, bulk modulus=4.67e$^{10}$ Pa, shear modulus=2.8e$^{10}$ Pa, cohesion=1e$^7$ Pa, tensile strength=1e$^7$ Pa. A friction angle of 30° and a dilation angle of 2° are used for both layers. The model contains pre-existing discrete thrusts (see Figure 8-14a). The activation of these thrusts is controlled in such a way that a foreland-propagating (piggy-back) sequence is achieved.
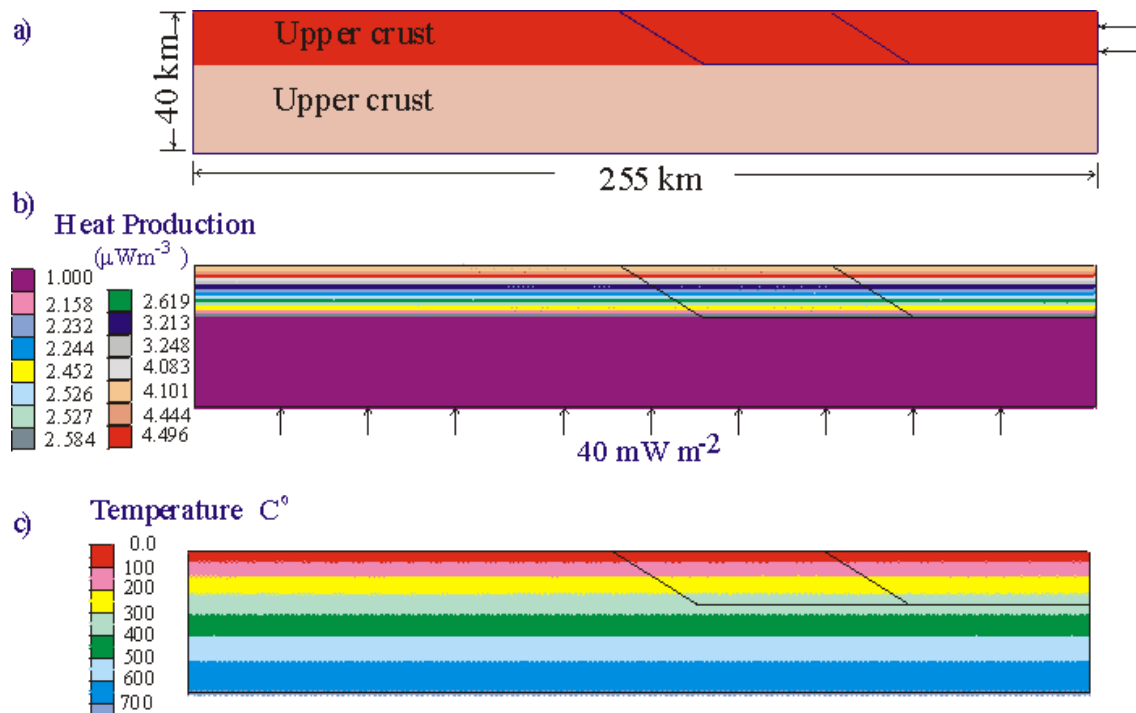


**Figure 8-14: Initial conditions of the coupled deformation-thermal model involving pre-existing discrete thrust faults. a) Initial geometry (arrows indicate the applied boundary displacement rate for thrusting). b) Initial heat production and mantle thermal flux distributions; these values are based on previous work. c) Initial equilibrium temperatures before the onset of thrusting.**

In the model, mechanical deformation is coupled with thermal transport. This allows the development of high-temperature fields along with topographic elevation and crustal thickening. The heat production and mantle thermal flux distributions are illustrated in Figure 8-14b and the equilibrium temperatures before the onset of thrusting are given in Figure 8-14c. The structural development and thermal evolution of the system (along with thrusting) are illustrated in Figure 8-15 and 8-16, respectively.
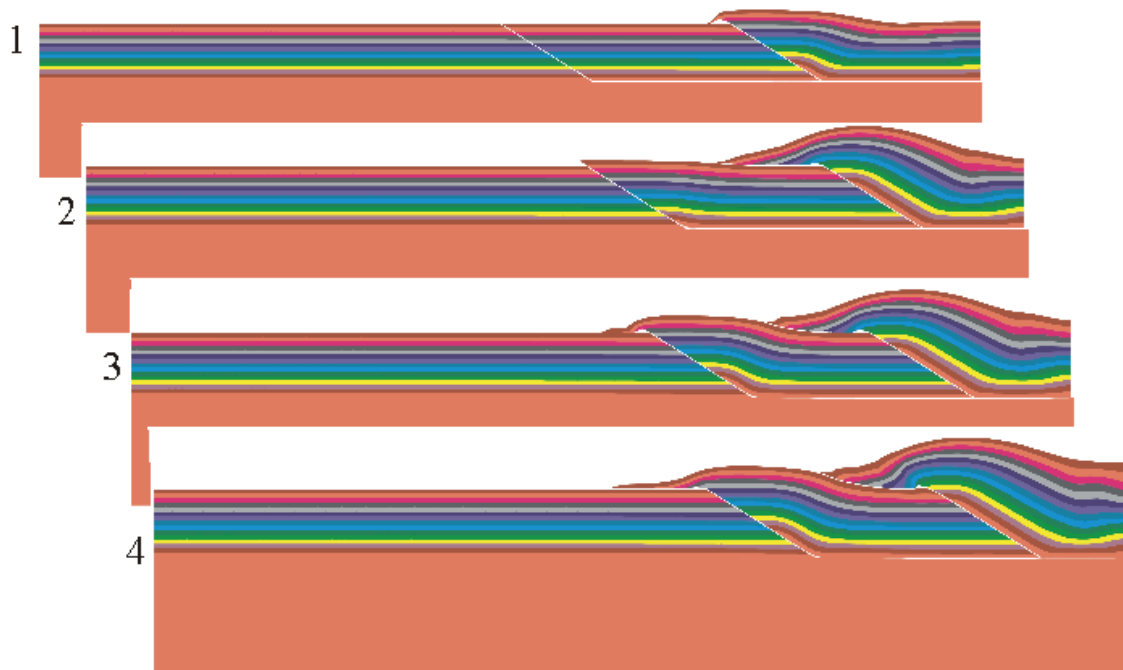
**Figure 8-15: Structural development of thrust slabs. Note the thickening of the crust and large displacement highlighted by the bedding markers.**

The model simulated the structural process of foreland-propagating or piggy-back thrusting (Figure 8-15). The thrust on the right side is first activated, leading to a large thrusting displacement of the hangingwall slab and crustal thickening above the ramp. Then the second thrust (further left) is activated, and thrusting and tectonic movement along this thrust become dominant in the later part of the thrusting process. Crustal thickening is also localised above the thrust ramp. The maximum crustal thickening (elevation) of the model is about 10 km, developing above the first thrust near the convergent edge.

As crust becomes thickened, its temperature gradient is increased (a function of new crustal thickness, heat production rate, flux rate and thermal conductivity). The maximum temperature rise is about 200°C beneath the portion of the maximum topographic elevation or crustal thickening (Figure 8-16).

Figure 8-17a illustrates the locations of tensile failure. Wedge-shaped tips of the two thrusting slabs show extensive tensile failure, coinciding with high shear strain localisation there (Figure 8-17b). The crest areas of thrusting-resultant topographic highs also show significant tensile failure. These are the locations which are mostly likely experiencing gravitational collapse or extension. The model also displays the tendency for the development of back thrusts, as reflected by two broad high shear strain zones (Figure 8-17b). Displacement vectors (Figure 8-17c) essentially reflect the feature of convergent deformation and thrusting movement. No extensional movement or normal faulting displacement can be observed along the main thrusts.
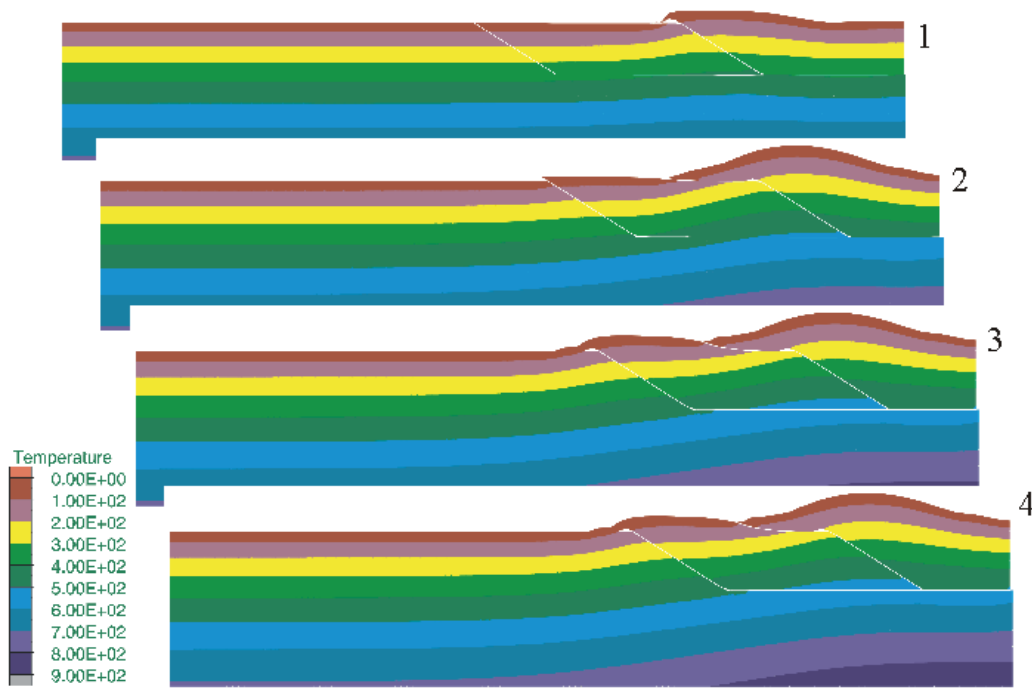
**Figure 8-16: Temperature distribution and evolution in thrust slabs during thrusting.**
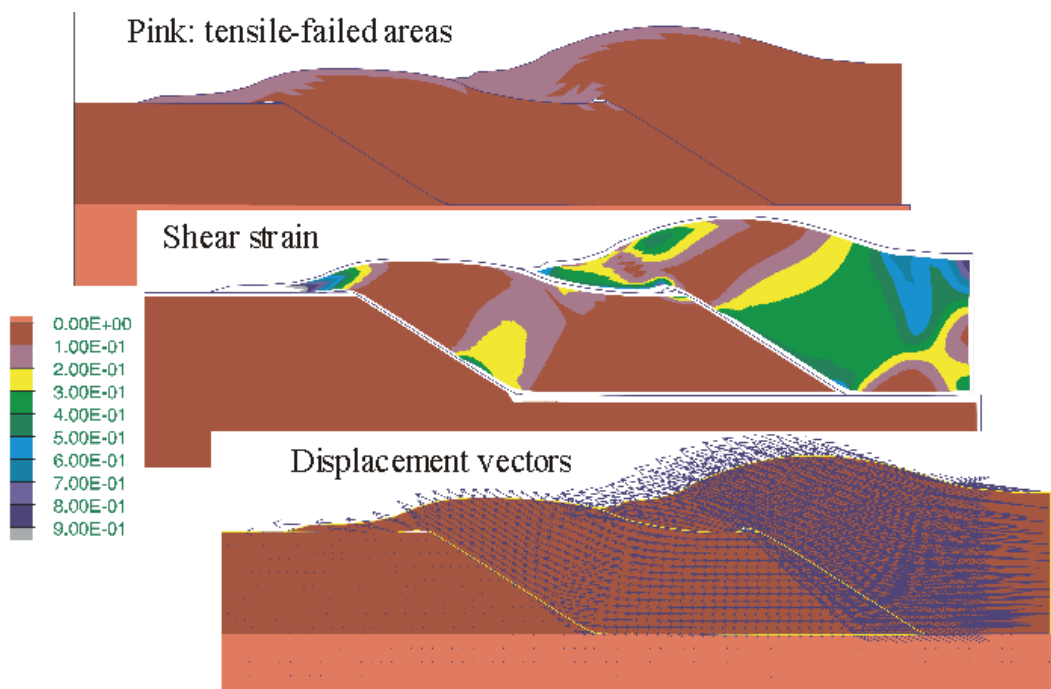


**Figure 8-17: Final deformation features of the thrusting slabs. a) Failure patterns. b) Shear strain contours. c) Displacement vectors.**

## Effect of change of rheology according to temperatures

It is noted that temperatures in much of the model are above 573 K or 300°C, particularly beneath the thrusting-induced topographic elevated areas. In these areas, rock deformation might conform to a power-law creep rheology, which means that

rocks are in effect weaker. Therefore, in the following model, the rheology of the model at an early stage of thrusting/convergent deformation is switched to power-law creep rheology if the temperature is above 573 K (Figure 8-18). This higher temperature specification creates a weaker root area beneath the thrust-induced topographic elevation. (Figure 8-18c). The continuation of the modelling simulation is conducted under two scenarios. The first is simply a continuation of convergent deformation and thrusting. In the second case, convergent shortening velocities at the left edge of the model are removed, so that the model sits with its potential gravitational loading following thickening.
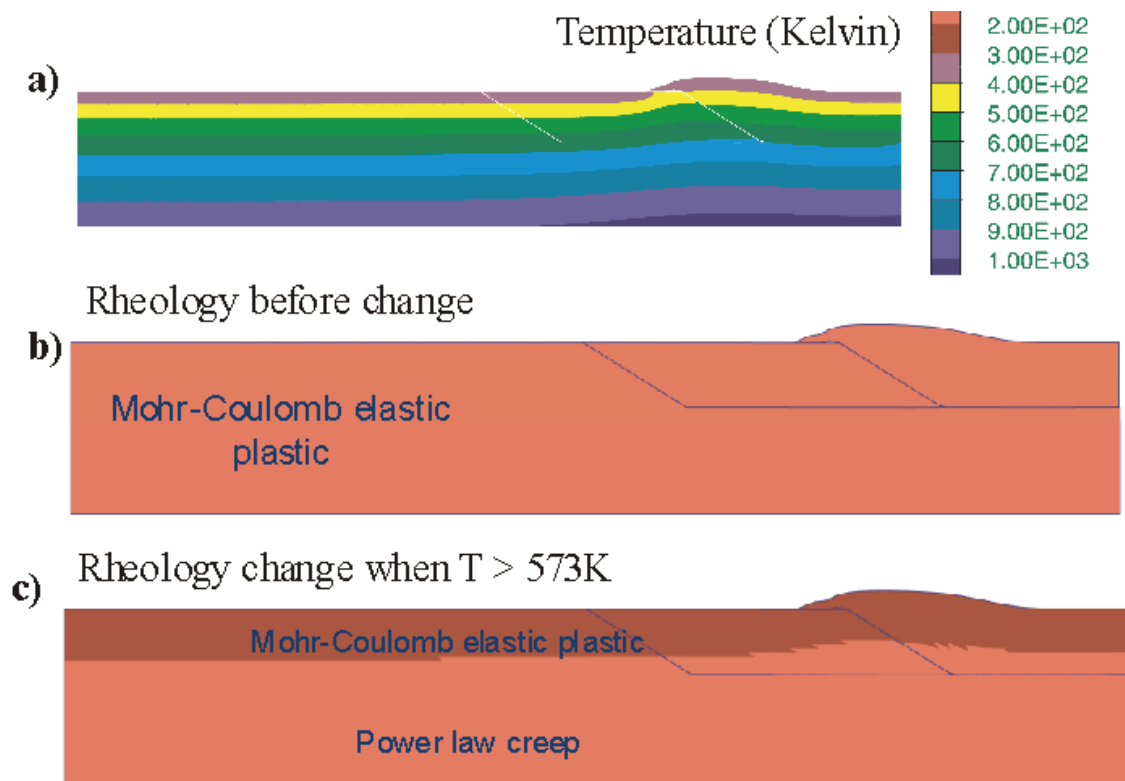


**Figure 8-18: Illustration of a model with rheology change according to temperatures. a) Temperature distribution. b) Rheology of the model before change. c) Rheology pattern of the model after change from elastic-plastic to power law when temperature is large than 573 K (300°C). Simulation is continued after a change of rheology.**

The displacement field for the first case (continuation of convergence) is illustrated in Figure 8-19a. Displacement vectors in the thrusting hangingwall slab still dominantly reflect thrusting and convergent movement; that is, no normal faulting movement can be detected along the main thrust fault. However, displacement vectors in the footwall slab and lower crust domains exhibit significant downward components. In particular, materials in deep levels of the lower crust display sideways movement patterns, indicating that material here tends to creep away. This is different to the patterns from the model without a rheology switch (cf. Figure 8-17).

In the second case where the convergent boundary velocities are removed (Figure 8-19b), we observe a further change in displacement patterns. Now displacement vectors in both the hangingwall and footwall slabs possess major downward components. In the deep levels of the lower crust, a sideways displacement pattern is also observed, again suggesting the creep-away movement of materials.
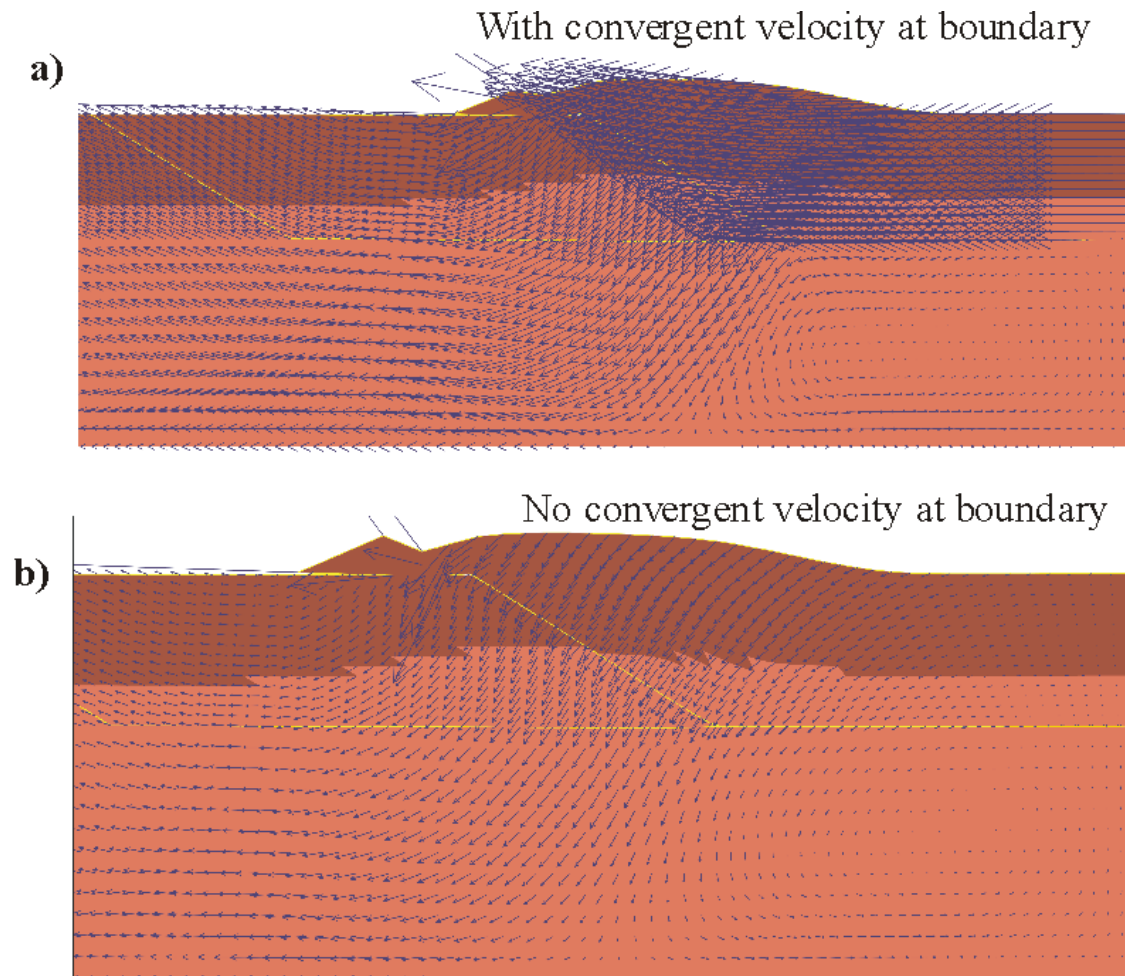
**Figure 8-19: Displacement patterns for the models with rheology change. a) The model with ongoing convergent deformation. b) The model with the removal of displacement rates at the right edge of the model for convergent deformation.**

## Effect of change of material strength property according to temperature

High temperatures (for example, >600°C) might lead to partial melting of some mineral compositions, and this should lead to the reduction of strength of the bulk rocks. Such property changes could result in a major change in the mechanical behaviour of the model. The following model is constructed to explore this scenario. The model adopts the geometry and temperature field developed in a previous model (Figure 8-20a; also see Figure 8-16), and is subject to property changes (reduction of cohesion, tensile strength and friction angle) if the temperature at a location is greater than 600°C. This leads to, for example, the new cohesion distribution pattern shown in Figure 8-20b. Note that the model now involves a weaker root beneath the maximum topographic elevation near the right edge. The simulation is continued again for two scenario cases. The first is the continuation of convergent deformation and thrusting. In the second case, convergent shortening velocities at the left edge of the model are removed (no further convergence).
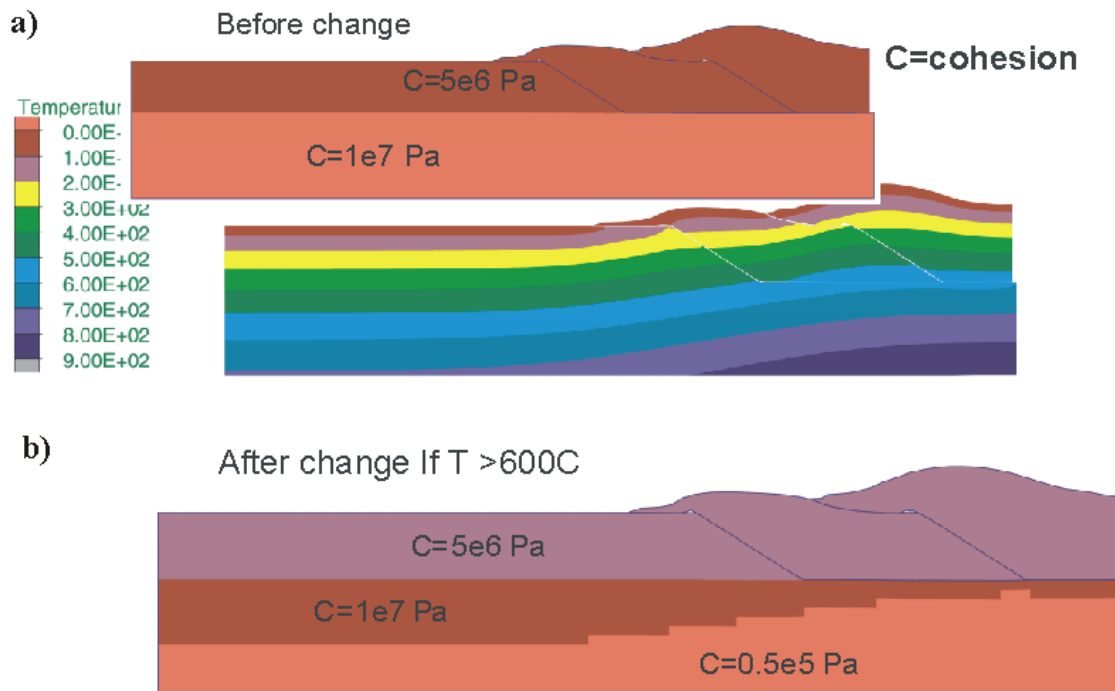
**Figure 8-20: Illustration of a model with the change of strength properties according to temperature. a) Temperature distribution and cohesion before change. b) Cohesion patterns after change (reduced if T > 600°C). Simulation is continued after change of strength parameters.**

The displacement vectors for the case of continuation of convergence are presented in Figure 8-21a. It is noted that displacement vectors in much of the thrusted slabs are predominantly left-directed, reflecting movements associated with thrusting and convergence. But further deep large downward displacement components are observed in the footwall wedge area beneath the maximum topographic high and in the lower crust region. This phenomenon is related the presence of a weak root beneath, and gravitational loading associated with, the topographic high ("mountain").

In the scenario where convergent shortening velocities at the left edge of the model are removed (Figure 8-21b), the displacement fields around the maximum topographic high (including the hangingwall area), and deeper areas, are all dominated by downward movement, showing that gravity-driven relaxation leads to the "sinking" of the "mountain". Note that the hangingwall thrust wedge at the right side of the model continues to show dominant left-directed thrusting driven by the gravitational load from the topographic high. The contrasting displacement pattern between the two thrust slabs seems to suggest that there might be some extension between the thrust slabs (that is, the more-elevated slab pushes the less-elevated slab forward). Tensile failure areas (Figure 8-21c) are also located in the wedge-shaped tip areas of the two thrusting slabs and the crest region of topographic highs, consistent with the patterns from the models above (cf. Figure 8-17).
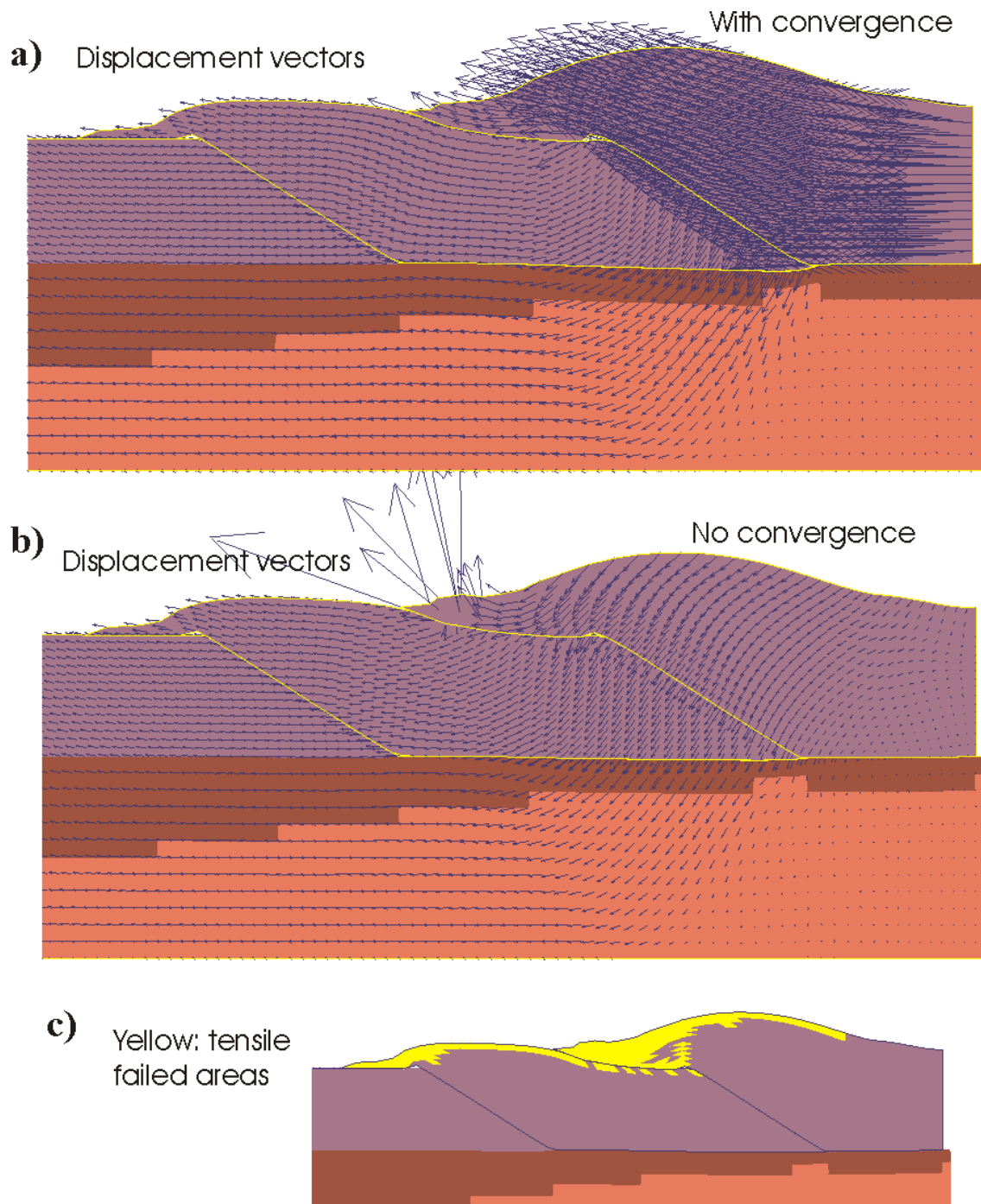
**Figure 8-21: Results of the models with rheology change. a) Displacement patterns for the model with ongoing convergent deformation. b) Displacement patterns for the model without convergent deformation (convergent rates at the right edge are removed).**

## Concluding remarks

The current models have successfully simulated large distance displacements and the geothermal response associated with crustal-scale thrusting. The results show that extensional regions (tensile failure) due to gravitational collapse of topographic highs ("mountains") are dominantly localised at the wedge-shaped tip areas of the thrust slabs, and at the crest regions of topographic highs. This seems to reflect the gravitational gliding situation reported for the Alps (Figure 8-22; France, 1987). But

the results of the models in this section are not sufficient to support the surge scenario as depicted in Figure 8-9.
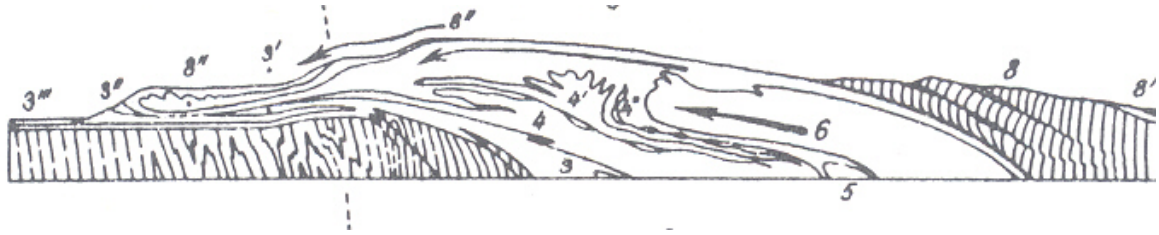


**Figure 8-22: A section showing a development stage of the Alps from the Tethys Geosyncline (after France, 1987).**

However, the current results show that crustal-scale thrusting could lead to significant temperature elevation in the root regions beneath the emerged topographic highs. These regions should become weakened due to rheology change or partial melting. If this happened, as demonstrated by the current results, gravitational relaxation and collapse might lead to downward material movement or the sinking of the topographic highs. This is particularly true when convergent motion in the nearby domain is temporarily suspended (e.g., slow-down of plate motion). Such motion may have the potential to generate extension (normal faulting) along the major thrusts beneath topographic highs.

## Extrusion of thrust wedge under topographic loading

### Introduction

In the preceding section, we achieved some understanding of the extensional structure associated with crustal-scale thrusting and high topographic elevations. The models did not provide numerical validation of the surge scenario model illustrated in Figure 8-9. In the models presented in this section, a simpler approach has been taken. The models do not concern the structural process of the development of thrusting and high topographic elevation, but simply assume the presence of a topographic high (Figure 8-23). The following models assume the existence of weak thrust faults bounding wedge-shaped crustal blocks. A straightforward question to explore is: given the presence of high orogenic topographic elevation and a thrust wedge similar to the structure defined in the original surge model (Lister, 2001), can the thrust wedge be extruded by the topographic load?

The material properties used in this set of models are identical to those used in previous models: for the upper crust, density=2700 kg/m$^3$, bulk modulus=2.67e$^{10}$ Pa, shear modulus=1.6e$^{10}$ Pa, cohesion=1e$^7$ Pa, tensile strength=1e$^6$ Pa, friction angle=30° and dilation=2°; for the lower crust, a density of 2900 kg/m$^3$ and viscosity of 1e$^{21}$ Pa s have been used. Thrust faults have been made weak by using a cohesion of 1e$^6$ Pa, tensile strength of 1e$^5$ Pa and friction angle of 5°.

### Models with the maximum topographic elevation of 10 km

The first set of models involves an extreme topographic elevation (about 10 km), as illustrated in Figure 8-23. Three scenarios are explored here:

1. the static case – no further convergent deformation (lateral edges are fixed at this stage);
2. continuation of convergent deformation with a smaller strain rate ($1e^{-14}$), and;
3. continuation of convergent deformation with a greater strain rate ($5e^{-14}$).
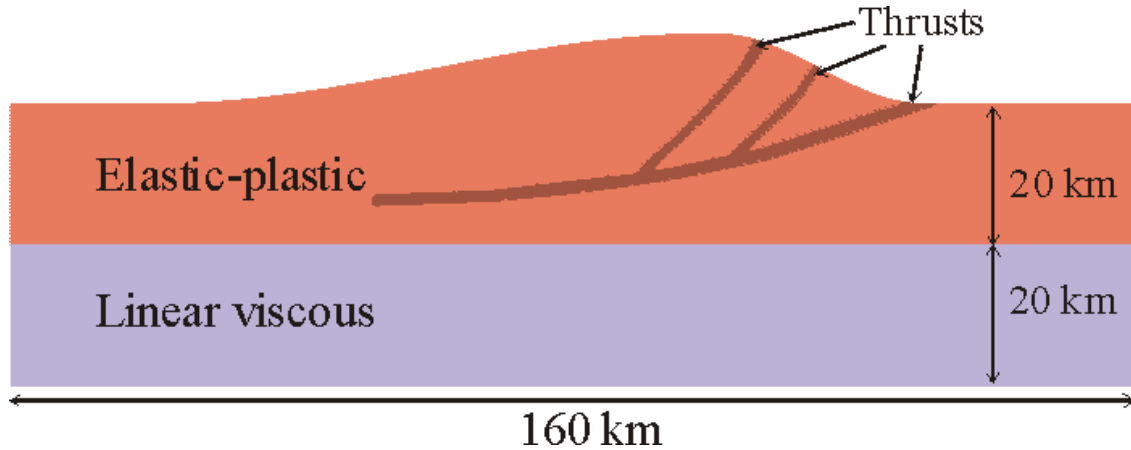


**Figure 8-23: Initial geometry of the thrust-wedge extrusion model with the maximum topographic elevation of about 10 km.**

### *Static case – no convergent deformation*

The displacement pattern of the model is shown in Figure 8-24. There is a strong downward material movement due to gravitational relaxation. This leads to lateral movement in the lower-crust domain and a corresponding rise of material at the edges of the model. In the highly elevated portion of the model, there is a pronounced bulk-material movement toward the foreland. Such gravitational relaxation in combination with the presence of favourably-oriented faults/thrusts results in some extrusion of the thrust wedge and slice (Figure 8-24b). This is reflected as normal faulting displacement along two shorter faults but reverse faulting displacement along the low-angle frontal detachment fault.
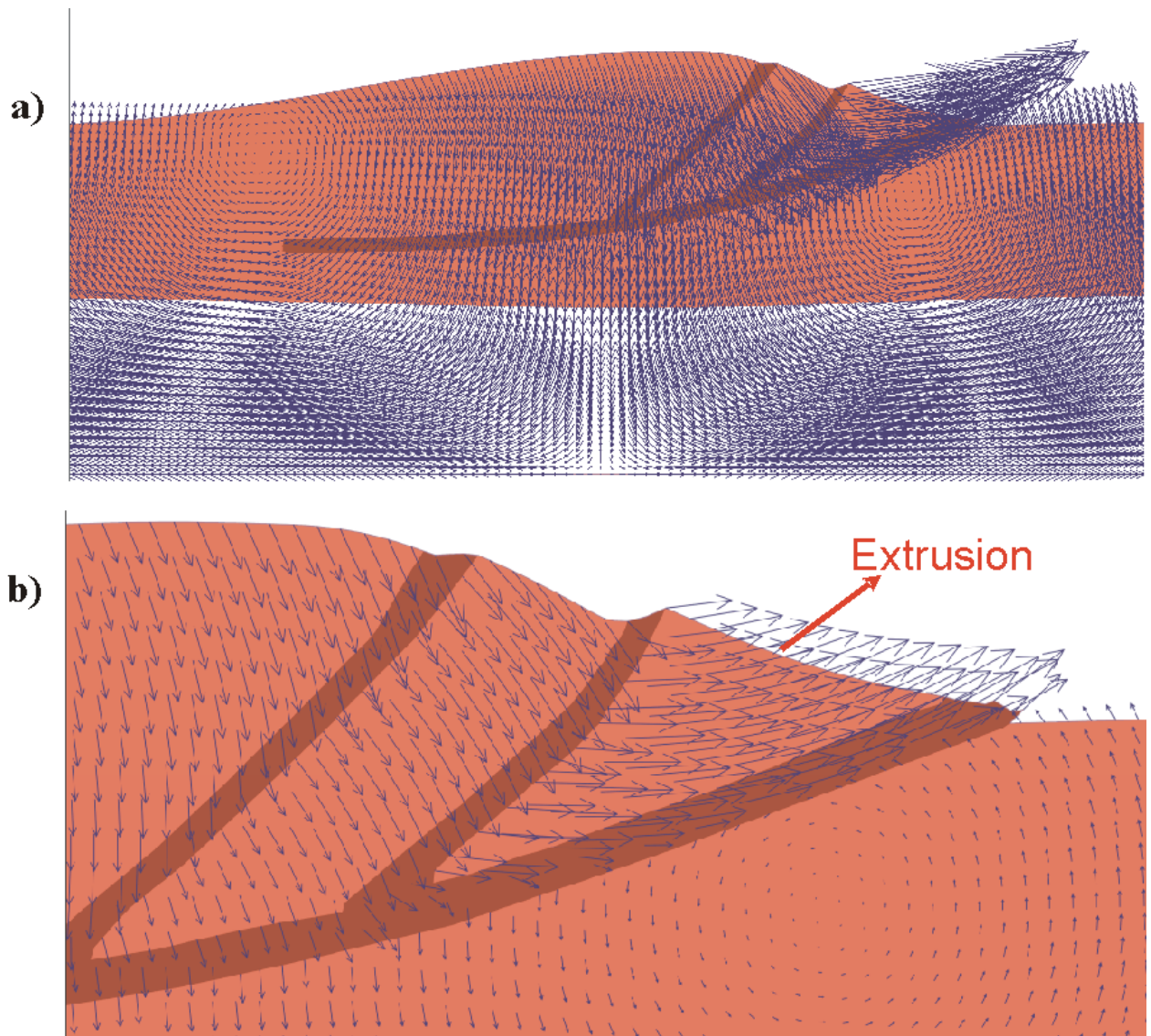
**Figure 8-24: Displacement vectors for a thrust-wedge extrusion model with a topographic elevation of about 10 km and without convergent deformation. a) Central part of the model; b) Detailed view of the foreland region of the model.**

*Convergent deformation: strain rate = $1e^{-14}$ / s*

The only change in this model from the model above is that an east-directed convergent deformation (corresponding to a strain rate of $1e^{-14}$) is incorporated. The displacement pattern of the model is shown in Figure 8-25. The pattern of downward material movement, which is observed in the model above, has entirely disappeared here. Now the displacement field is completely dominated by east-directed convergent movement. It is noted that the crustal wedge, which is confined by a short fault and the detachment fault, displays anomalous east-upward motion (Figure 8-25b), indicating the occurrence and tendency of structural extrusion of this block. This can also be seen in the final geometry of the model, featured by normal displacement along the short fault and reverse displacement along the detachment fault.
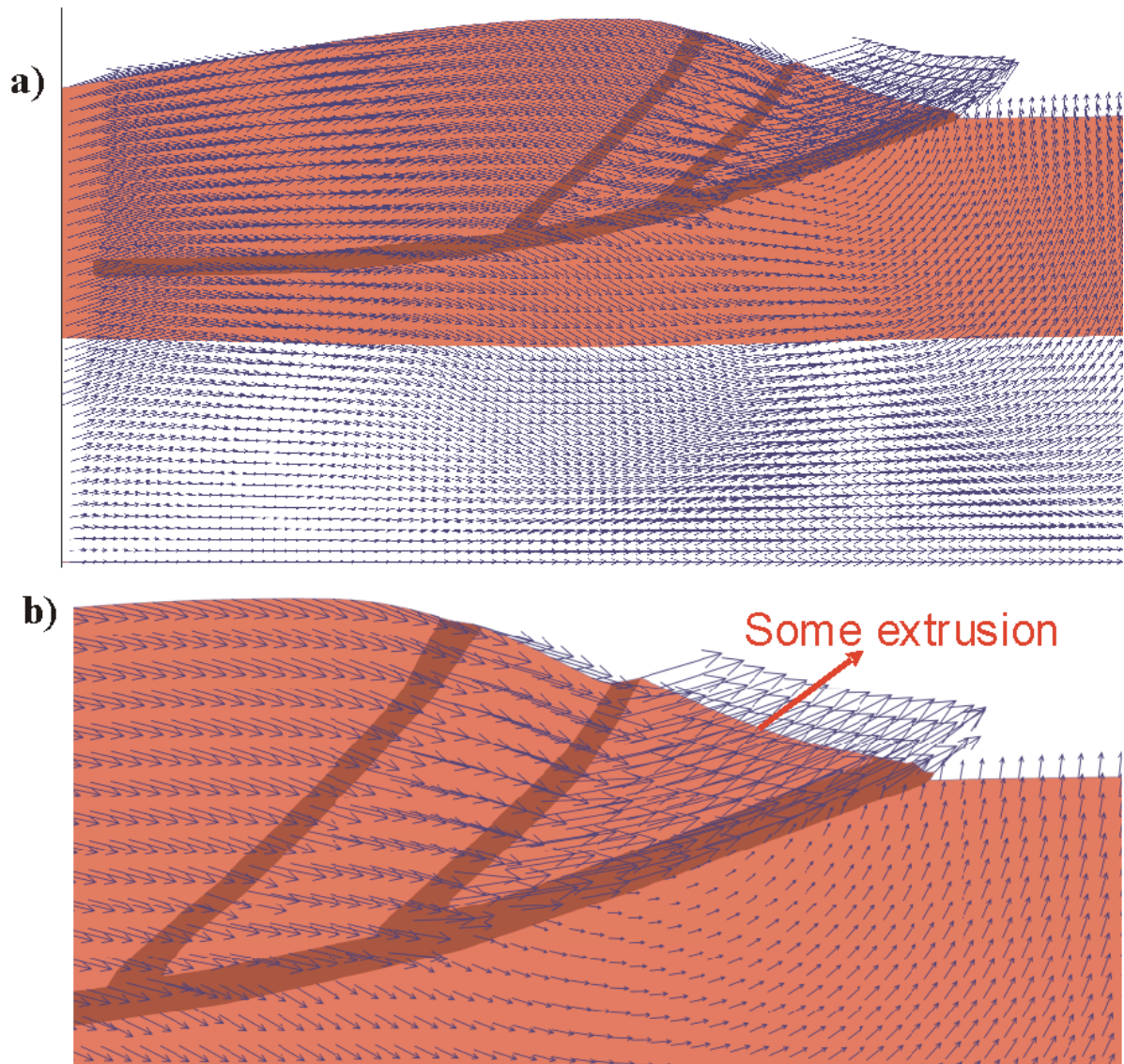
**Figure 8-25: Displacement vectors for a thrust-wedge extrusion model with a topographic elevation of about 10 km and with convergent deformation (strain rate=1e$^{-14}$). a) Central part of the model; b) Detailed view of the foreland region of the model.**

*Convergent deformation: strain rate = 5e$^{-14}$ / s*

In this model, the east-directed convergent deformation is also incorporated but at a greater rate. The corresponding strain rate is 5e$^{-14}$ / s, that is, five times higher than the previous model. The displacement pattern of this new model is shown in Figure 8-26. In this model, the whole rock package above the detachment fault has a consistent eastward motion. The crustal wedge sandwiched between the short fault and the detachment fault does not exhibit any extrusion (Figure 8-26b); note that the weak fault zones themselves are flattened more.
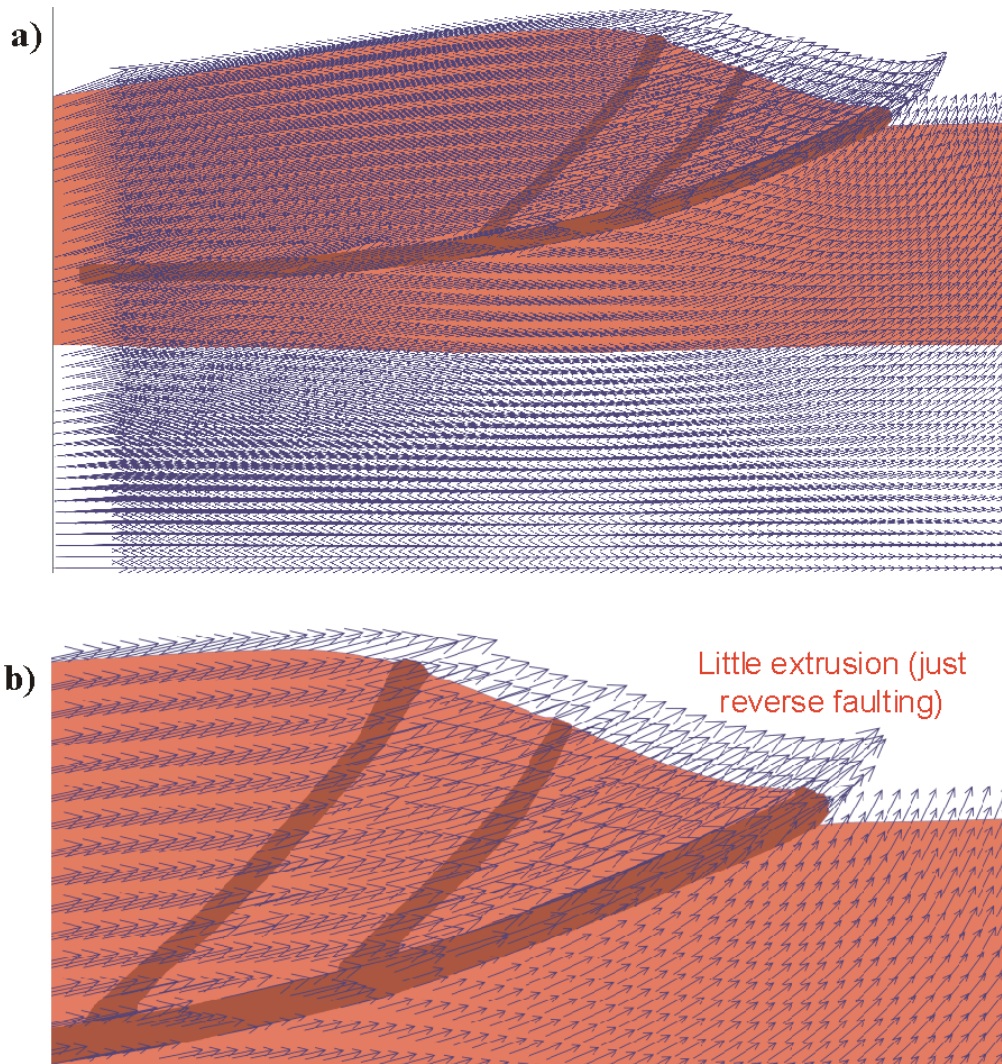
**Figure 8-26: Displacement vectors for a thrust-wedge extrusion model with a topographic elevation of about 10 km and with convergent deformation (strain rate=5e$^{-14}$). a) Central part of the model; b) Detailed view of the foreland region of the model.**

## Models with the maximum topographic elevation of 5 km

This set of models (Figure 8-27) involves a lower-amplitude topographic elevation (about 5 km). Three scenarios are also explored here:

1. static case – no further convergent deformation (lateral edges are fixed);
2. static case – no further convergent deformation but with weaker faults, and;
3. with convergent deformation at a slower strain rate of 1e$^{-14}$.
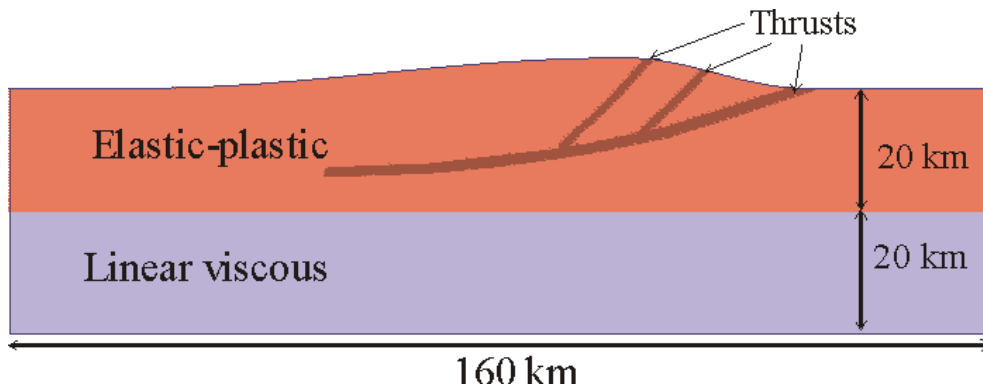
**Figure 8-27: Initial geometry of the thrust-wedge extrusion model with the maximum topographic elevation of about 5 km.**

### Static case – no convergent deformation

In comparison with the higher topographic elevation case (10 km, see Figure 8-24), the current model displays generally similar displacement patterns (Figure 8-28), that is, downward movement around the region of elevation, lateral motion in the lower crust, and a small upward motion near the lateral edges. However, the current model does not show any extrusion of the crustal wedge or slice sandwiched between the weak faults. This seems to suggest that a 5 km topographic elevation does not generate sufficiently-strong gravitational loading for wedge extrusion.
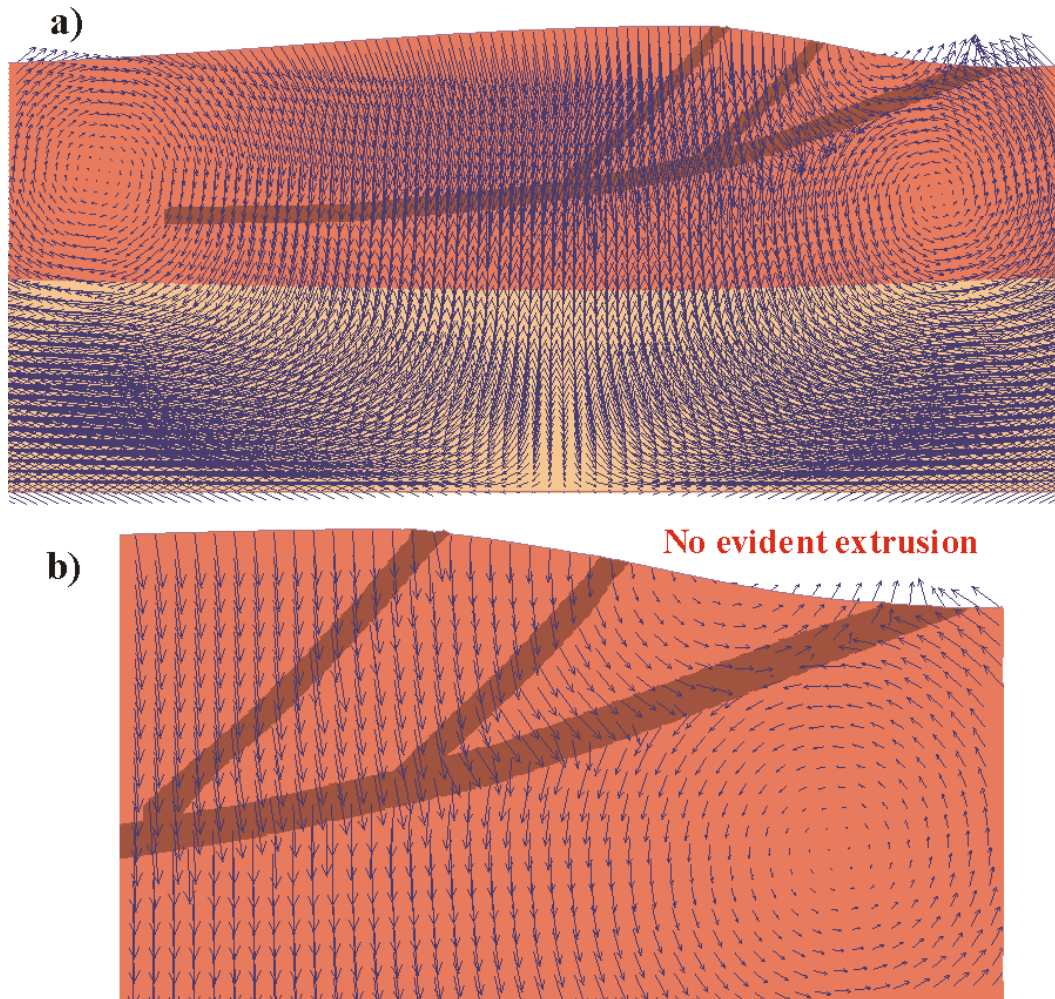
**Figure 8-28: Displacement vectors for a thrust-wedge extrusion model with an initial topographic elevation of about 5 km and without convergent deformation. a) Central part of the model; b) Detailed view of the foreland region of the model.**

### *Static case – no convergent deformation and weaker faults*

The purpose of this model is to see what happens to extrusion if faults are made even weaker. This is done by the adoption of cohesion=$2e^5$ Pa, tensile strength=$1e^5$ Pa and friction angle=1° for faults. The results show that when faults are weaker (easier to slide) a 5 km topographic elevation can generate sufficient gravitational loading to cause the clear extrusion of both the thrust wedge and slice (Figure 8-29b). This generates extension in the hangingwall side of the two short faults near surface.
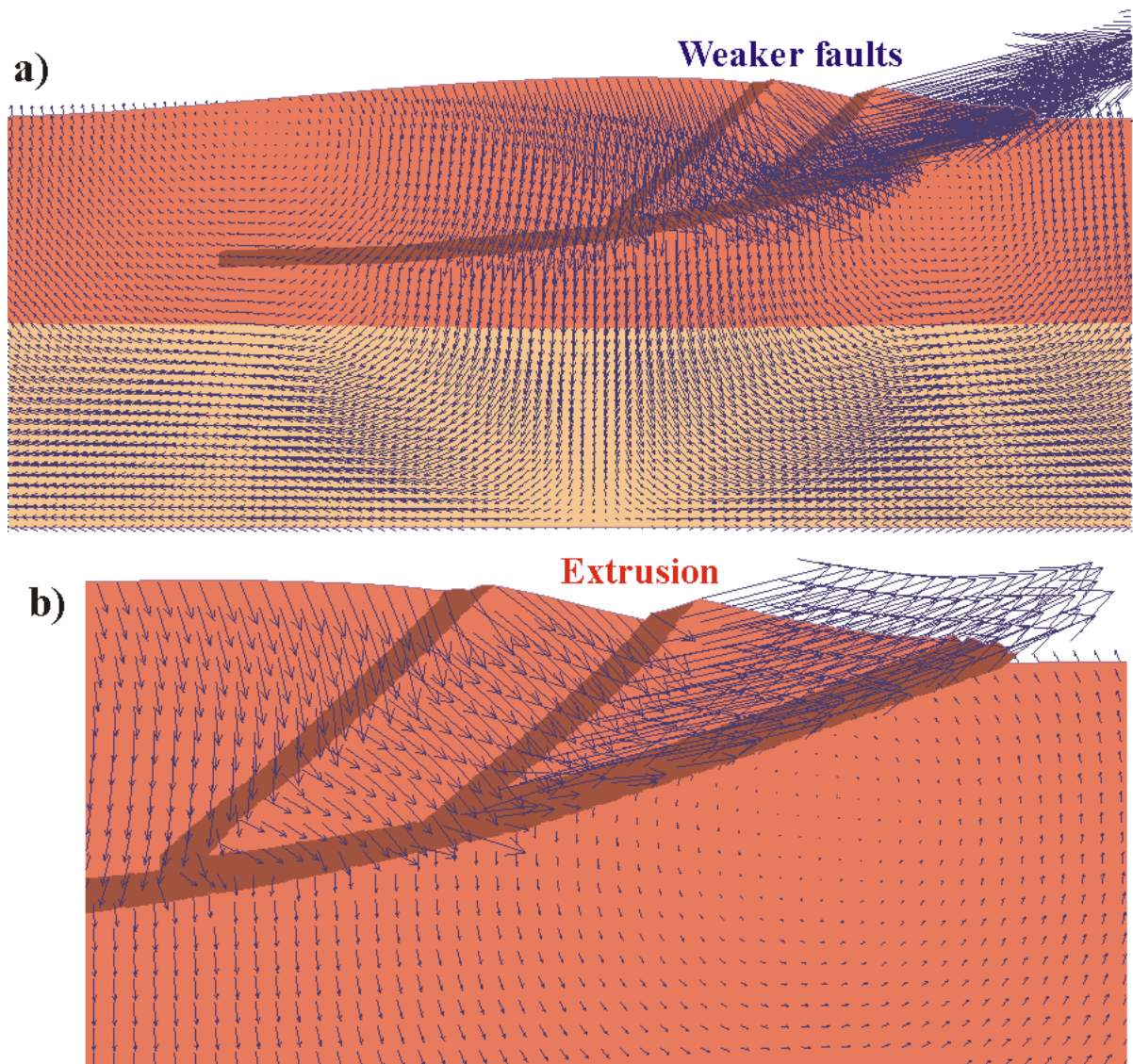
**Figure 8-29: Displacement vectors for a thrust-wedge extrusion model with an initial topographic elevation of about 5 km and without convergent deformation (weaker fault situation). a) Central area; b) Detailed view of the foreland region of the model.**

### *With convergent deformation*

In this model, an east-directed convergent deformation (strain rate=1e$^{-14}$) is applied. Displacement vectors are illustrated in Figure 8-30. It seems that the convergent deformation (even at a relatively slower rate) has entirely overpowered the gravitational effect associated with a 5 km topographic elevation. East-directed tectonic transport predominantly occurs along the low-angle detachment, the orientation of which is favourable for sliding. No wedge extrusion is observed in this case.
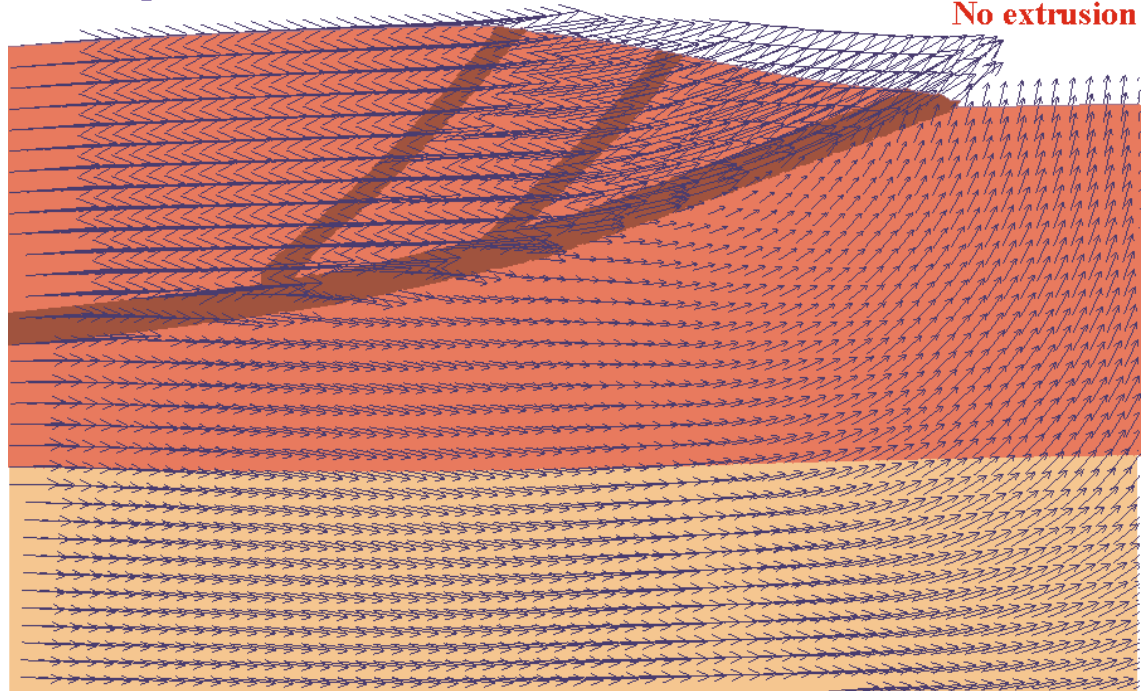
**Figure 8-30: Displacement vectors for a thrust-wedge extrusion model with an initial topographic elevation of about 5 km and with convergent deformation; detailed view of the foreland region of the model.**

## Implications for predictive mineral discovery

The results of the models in this section show that under conditions of high topographic elevation and the presence of certain fault/thrust geometries, which confines wedge structures (e.g., the geometry in Figure 8-9), structural extrusion of thrust wedges or thrust slices is possible, in particular near the foreland regions of the orogen. The extrusion could generate local extensional environments as a result of relative faulting movements. The occurrence of such extrusion and associated extension are promoted by following favourable factors:

- higher topographic elevation;
- pause of local convergent deformation or slower convergent rate, and;
- weaker faults/thrusts for easier structural sliding.

It needs to be pointed out that a limitation of the current continuum extrusion model is that is does not allow extrusion to take place at its full freedom. Simulation of faults in a continuum mesh limits fault movement and hence the extent of extrusion; it is difficult to create discrete, sliding faults with curved or complex geometries. Conceptually, a free-sliding fault situation should allow greater extrusion and extension (Figure 8-31). More specifically, the extrusion wedge may "leap" forward a large distance, and the overlying thrust slab could then collapse downward due to extrusion-generated space. This may lead to a broad area of extension. Such extension should probably be confined to the shallow levels of the crust.
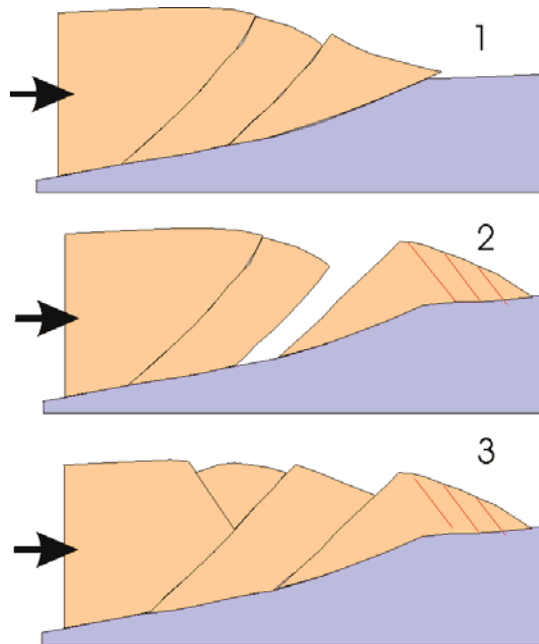
**Figure 8-31: Cartoon illustrating extrusion and extension process. 1 – Onset of structural extrusion of a thrust wedge; 2 – Large extrusion and potential space; 3 – Collapse of thrusting topographic high. Note that 2 and 3 are simultaneous. Red lines in the thrusting frontier indicate potential normal faults due to gravitational sliding.**

Further work is needed to model the involvement of the whole crust in the process of orogenic surge (e.g., Figure 8-5). This model is predicted not to require extreme topographic elevations, as the driving force is behind and below, not from above.

## Alternative arguments for Late Basin formation

*R.S. Blewett*

Some workers have suggested that the Late Basins were **not** developed in a modified foreland setting, as the orogenic surge model proposes. The following section outlines some of these views and responds to them with examples from well-known complex foreland systems.

Arguments that the Late Basins did not develop in a modified foreland setting include:

1. the Late Basin sequences fine upwards;
2. wedge-top basins do not get deformed (and these basins are deformed);
3. wedge-tops don't get preserved (and these basins are [partially] preserved);
4. Late Basins have axially derived source areas;
5. they are remnant ocean basins, or;
6. they are strike-slip basins.

### *The Late Basins fine up*

Some of the Late Basins appear to fine upwards (Glikson, 1971; Krapež et al., 2000; Hand et al., 2002). However, due to erosion, the full basin sequence is not preserved

and, consequently, the complete stacking pattern is equivocal. Fining up sequences are atypical of foreland basins, which coarsen up as the source approaches and thrusting continues.

However, not all of the basins fine up. Some coarsen upwards, others are neutral in their stacking patterns (e.g., Yilgangi, Wallaby). This suggests that simple end-member models are not applicable.


### *Wedge-top basins do not get deformed*

The Late Basins in the EYC have a strong cleavage ($S_{2b}$ and younger), and are folded and thrusted. There are many examples of foreland and wedge-top basins that are deformed, including the Siwaliks of Nepal, the basins of western Taiwan, and the Mula-Pliego Basin in southeast Spain.

The Siwaliks are wedge-top basins deposited in western Nepal. Mugnier et al. (1999) noted that early thrusts have become bevelled by unconformities and deposition of sediments in the wedge-top position. Subsequent overlap sediments have then been deformed by inner or hinterland break-back thrusts. These thrusts overprint and deform the basins.

The Pingtung wedge-top basin of western Taiwan has a thrust with up to 2 km of throw, bringing Miocene basement over the Pleistocene basin (Chiang et al., 2004). These basins are up to 5 km deep and were deposited rapidly in around 1 My. To the north, the Western Foothills are former wedge-top sediments that have been folded, thrusted and uplifted into low hills that were cannibalised to provide detritus for the evolving basins to the south (Chiang, et al., 2004).

The Mula-Pliego Basin in southeast Spain (Martin and Martin, 2002) is a Tertiary wedge-top basin that was controlled by a flexural tectonic event to create the basin. A series of blind-fault-propagation folds deformed the basin progressively from south to north. Finally, a tectonic event destroyed the basin.


### *Wedge-top basins do not get preserved*

Wedge-top basins are regions of rapid uplift and erosion and their preservation potential is relatively low. This suggests that the Late Basins would be unlikely to be visible today (preserved) if they were in this geodynamic setting. However, in the Andean orogenic wedge of southern Bolivia, Oligocene to late Miocene wedge-top basins have been preserved despite having developed above the toe of the orogenic wedge at low elevations, and are now being exposed >250 km west of the active thrust front and at >3 km elevation (Horton, 1998). The Late Basins are only small structural remnants of a larger system of basins, so only the bases of the basins are locally preserved.


### *The Late Basins have an axial source*

Sedimentalogical studies (including palaeocurrent analysis) suggest that much of the Late Basin detritus was derived from the north or northwest (Krapež et al., 2000).

This is considered atypical of foreland settings (when viewed in two dimensions) which would expect to be "seeing" the emergent highlands from the east.

However, many foreland basins do have an axial source. For example, in the southern Pyrenean wedge-top foreland basins, the deep water Ainsa basin passes along strike to the shallow water (subaerial) Tremp basin over a distance of 50 km. The sediment fill is from transverse alluvial fans with the main dispersal being axial (Figure 8-32). The development of two sub-basins is due to the nature of the underlying lateral ramps of the main south-directed thrust sheets. An analogous situation could be the fluvial Merougil and deep-marine Kurrawang Late Basins in the Kalgoorlie terrane. Their depocentre control may also be due to the underlying thrust sheets.
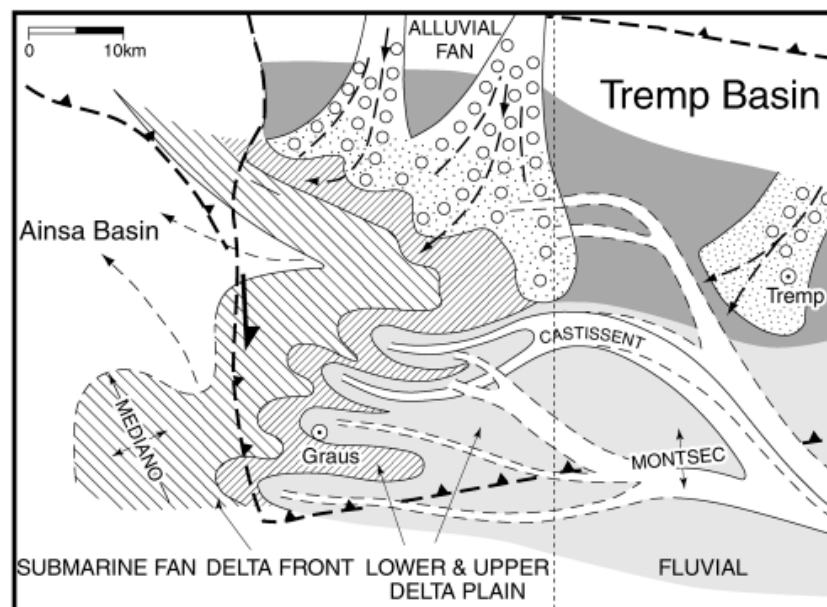


**Figure 8-32: Map of the Tremp and Ainsa basin system in the southern Pyrenees (Spain). The basin depocentres are controlled by lateral ramps that permit the passage of detritus axially from the east to the deep water in the west (after Clevis et al., 2004).**

A similar pattern occurs in the Taiwan orogen. Here, the main mountain belt is being unroofed and eroded, with the detritus being shed axially to the south into deep-water wedge-top basins above west-vergent thrusts (Figure 8-33). The architecture of these Taiwan basins may be partly analogous to the Late Basins of the EYC.
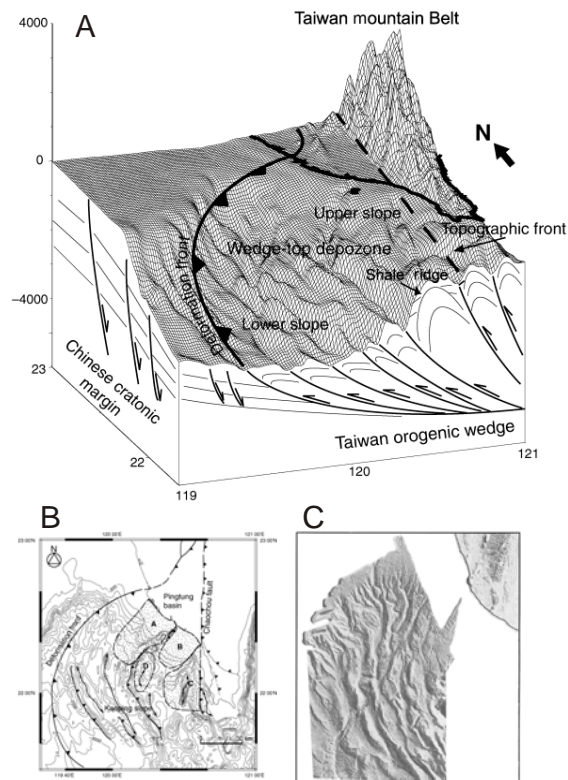
**Figure 8-33: The Taiwan orogen is a good modern example of oblique arc-continent collision. The obliquity in collision has resulted in a diachronous deformation front. In the north the orogen has arc collapse/subduction, while in the south intra-oceanic subduction occurs. Uplift in the north has resulted in the detritus being shed mostly to the south (axially) into wedge-top basins developed above west-directed foreland propagating thrusts systems (figures from Chiang et al., 2004). A – DTM with wedge-top basins in the south, along strike from the growing mountain belt. B – Position of sub-basins in the wedge-top positions above the west-directed thrusts. C – Sea floor topography showing the axial control of drainage superimposed on subparallel thrust architecture.**

### *The Late Basins are Remnant Ocean Basins (?)*

An alternative interpretation for the Late Basins is that they are Remnant Ocean Basins. Ingersoll et al. (2003) define Remnant Ocean Basins by:

- their huge sediment flux from collision into adjacent remnant basin (ocean crust) where collision has **yet to occur**;
- a flysch to mollase transition as the remnant ocean develops into a pro-foreland basin with ongoing collision, and;
- a sequence that **coarsens** upwards.

The Late Basins do not satisfy this definition. The Late Basins were not deposited on oceanic crust; some are even fluvial in origin. The Late Basins were also deposited when collision had already occurred. They lie with an unconformity on pre-folded sequences ($D_1$ and $D_{2a}$).

### The Late Basins are strike-slip basins (?)

Strike-slip basins are a special kind of narrow fault-controlled basin developed where space problems occur with wrenching curved structures. Strike-slip basins characteristically have:

- great stratigraphic thickness relative to basin size (*Late Basins are thin now – this is a real difficulty if there was a single Late Basin* [see Krapež, 1997]);
- thick asymmetric sedimentary sequences and facies patterns (*some Late Basins are symmetrical such as the Kurrawang Basin*);
- marginal fault-bounded coarse and central fine deposits (*not observed*);
- a dominant longitudinal mode of basin infill (*some Late Basins*);
- greater structural complexity than rift basins (*Late Basins are relatively simple*);
- rapid (lateral and vertical) thicknesses and facies changes in small areas (*not observed in Late Basins*);
- strike-slip evidence including displaced fan/source relationships; skewed fans; and tectonic straie (*not observed at sedimentation time in Late Basins*);
- successive overlap of basement by sediments (*possibly*), and;
- deposition in steep-faulted architectures such as negative flower structures (*this has not been observed*).

The characteristics of strike-slip basins outlined above are not matched by the evidence for the Late Basins in the EYC. On the balance of the available evidence, the Late Basins therefore developed in a geodynamic setting other than a Remnant Ocean Basin or a strike-slip setting.

## *Question 2—Architecture*

*R.S. Blewett*

### Introduction

The Y2 project was principally concerned with defining the architecture of the EYC through the building of a series of integrated 3D maps. Chapter 2 outlines the details of the process of building the maps, and Appendix 2 contains the Gocad objects of the 3D maps. This section of Chapter 8 highlights some of the new understanding of the EYC architecture. The section discusses the receiver function data and possible provinciality in the velocity structure of the crust, deep-penetrating faults, and upper crustal features of the 3D map.

### What is special about the Kalgoorlie Terrane: a receiver function perspective?

Chapter 4 details the receiver function technique. This section is an interpretation of the differences in crustal velocity between the Southern Cross and the terranes of the EYC (Kalgoorlie and Kurnalpi). Figure 8-34 shows the location of three recording stations in these terranes. The map also shows that the Low-Ca granite types are largely external to the greenstones and are likely underneath them.
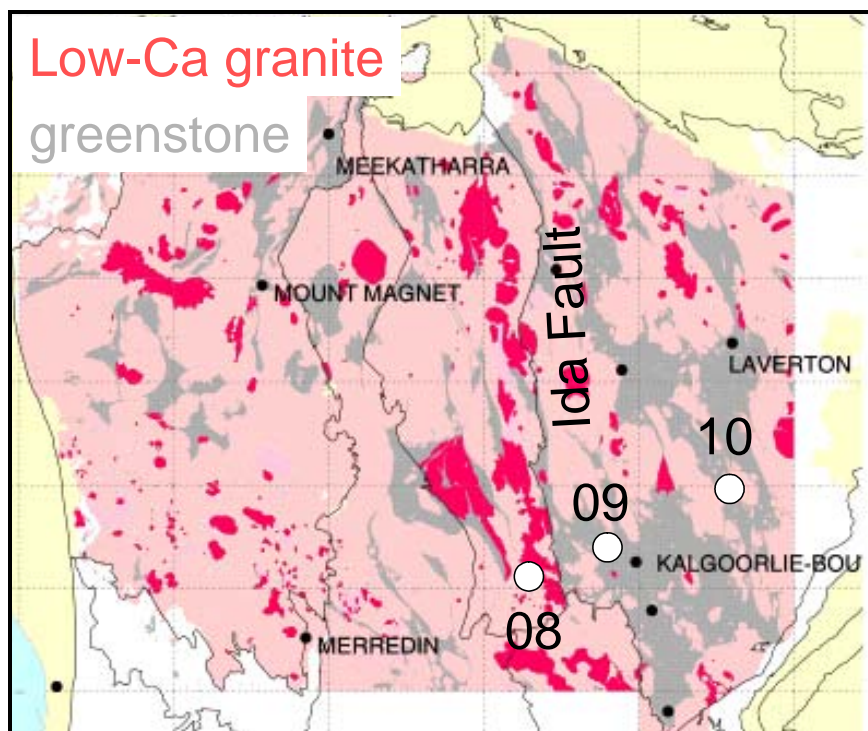


**Figure 8-34: Map of the Yilgarn Craton showing that the Low-Ca granites are largely external to (underneath) the greenstones. Sites 08, 09, 10 are from the WT survey of Reading et al. (2003). See Chapter 4 for more details on the technique.**

The velocity of seismic waves in rock is strongly governed by their density. The denser the lithology, the faster the passage of seismic energy. This means that dense greenstones (basalts and ultramafic rocks) have fast velocities, and granitic rocks which are on average less dense (see rock property determinations in Barlow, 2004b, and Chapter 2) have relatively slower velocities.

Receiver functions map the velocity profile for the column of crust upon which the recorder is located. Figure 8-35 (modified from Reading et al., 2003) shows three crustal velocity profiles through the Southern Cross (WT08), Kalgoorlie (WT09), and Kurnalpi (WT10) Terranes respectively.
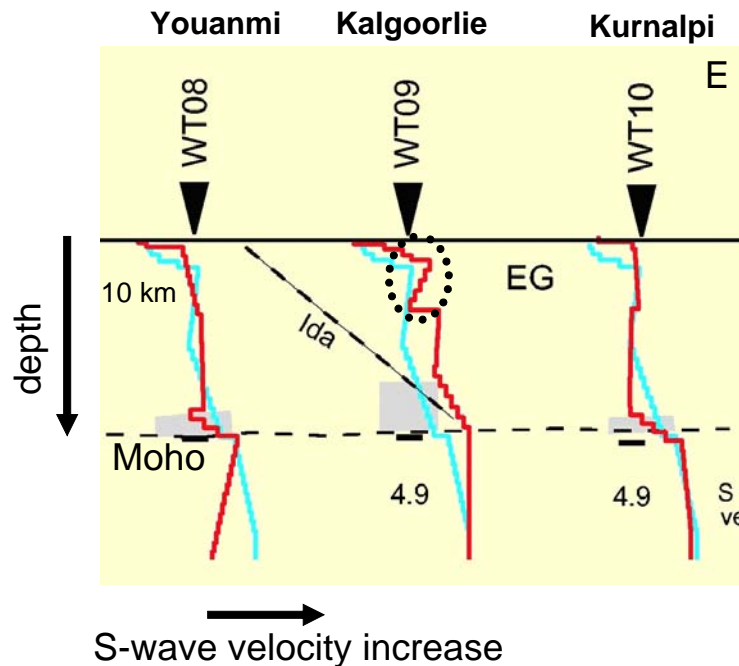


**Figure 8-35: Velocity profiles for Youanmi (Southern Cross), Kalgoorlie, and Kurnalpi Terranes. The blue line is the average profile for the Australian crust, the red line is the calculated profile for the terrane at the recording station (after Reading et al., 2003). Note the velocity anomaly (dotted ellipse) at around 10 km in the Kalgoorlie Terrane.**

The Kalgoorlie Terrane crustal profile is significantly different to the adjacent terranes' profiles (Figure 8-35). Despite an overall increase in velocity with depth to the base of the crust (Moho), there is a marked velocity drop from around the base of the greenstones (~5 km) to ~15 km depth. This velocity drop brings the velocity profile close to the Australian crustal average (blue line), in contast to the overall higher velocity (than Australian average) at depth.

As velocity is a largely a function of density, the interpretation is that a significant amount of light (therefore slow) granites occur at these levels, relative to the overall faster velocities at depth for this terrane. These granites may be the Low-Ca granite types which are inferred to lie beneath many of the greenstones (see Figure 8-34). This inference is based on the observation that Low-Ca granites are largely only exposed external to (that is beneath) now eroded greenstones. The corresponding relative velocity high deeper in the crust of the Kalgoorlie Terrane velocity profile is interpreted to reflect a more dense (hence fast) restite from Low-Ca granite anatexis.

The significance of these observations is that there are architectural differences in terms of the velocity structure (i.e. lithology) between the various terranes of the Yilgarn Craton. The Kalgoorlie Terrane is on average faster than the Australian average (the other terranes are similar to it). The Kalgoorlie Terrane is also the most endowed part of the Yilgarn for gold and nickel.

Does the velocity structure have a bearing on the endowment, and therefore prospectivity, of a terrane? Interestingly, the linkage between the velocity anomaly under the Kalgoorlie Terrane can be interpreted as a function of greater volumes of Low-Ca granites. The important relationship between domes, granites and gold is discussed elsewhere in this chapter. The receiver function data are consistent with the observations and interpretations of other data such as seismic reflection, gravity, geochemistry, and geological understanding.

## 3D interpretation of the eastern Yilgarn: New architectural insights from construction of the 3D map

*P. Henson and R.S. Blewett*

Following the initial interpretations of seismic lines in the EYC, construction of the 3D map has raised some questions about aspects of the initial interpretations. Although most of the original interpretations have held true, additional information derived from industry datasets and the integration of potential-field techniques have increased our understanding and therefore allowed a more-informed view of the 3D architecture.

The integration of multidisciplinary techniques has improved our understanding, and provided a framework to construct surfaces and develop an architecture that builds on the interpretations of previous workers (Drummond et al., 1997).

The highlights of this work are set out in the following paragraphs, which describe some of the techniques used and implications of the reinterpretation of the 3D architecture.

### Zuleika Fault and the Kurrawang ('late') Basin

The construction of the 3D map within the Kalgoorlie-Kambalda region required all geological relationships to be accounted for. While working on the Zuleika Fault and Kurrawang Basin it became evident that some inconsistencies occurred within the published data. The original seismic interpretation of the Zuleika Fault was an east-dipping structure (Drummond et al., 2000a) with the Kurrawang Basin located proximal to its east. A field trip to the region revealed that structurally it appeared to be a west-dipping structure with east-verging overturned limbs to the Kurrawang Basin in the footwall of the Zuleika Fault (Tripp, 2004). The dip of the structure was confirmed by deep drilling near the Kundana Mine by Placer Dome Asia Pacific.

The composite magnetic and gravity image of the Kurrawang Basin revealed a complexity within the basin interpreted to be an internal fault (Figure 8-36). In order

to verify the occurrence of this structure in the third dimension, the 99AGSY1 seismic line was used. It crosses the Kurrawang Basin and the Zuleika Fault in the northern region, and provided independent evidence for the occurrence of the internal fault and revealed the shape of the basin (Figure 8-37).
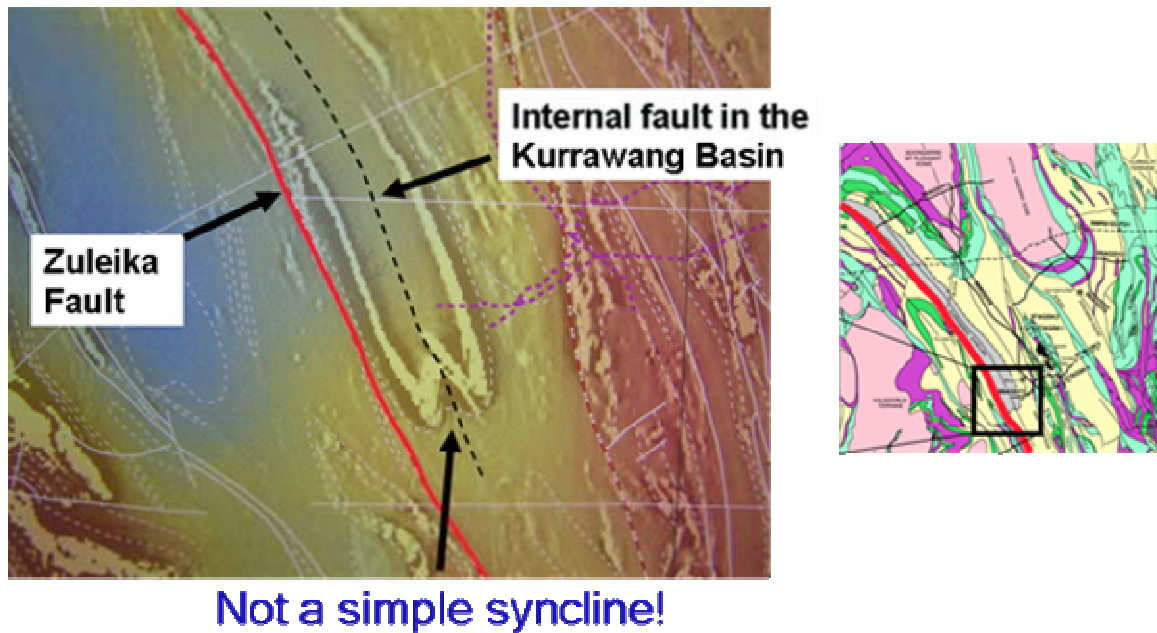


**Figure 8-36: Composite magnetic and gravity image of the southern extent of the Kurrawang Syncline, showing complexity interpreted as an internal fault.**
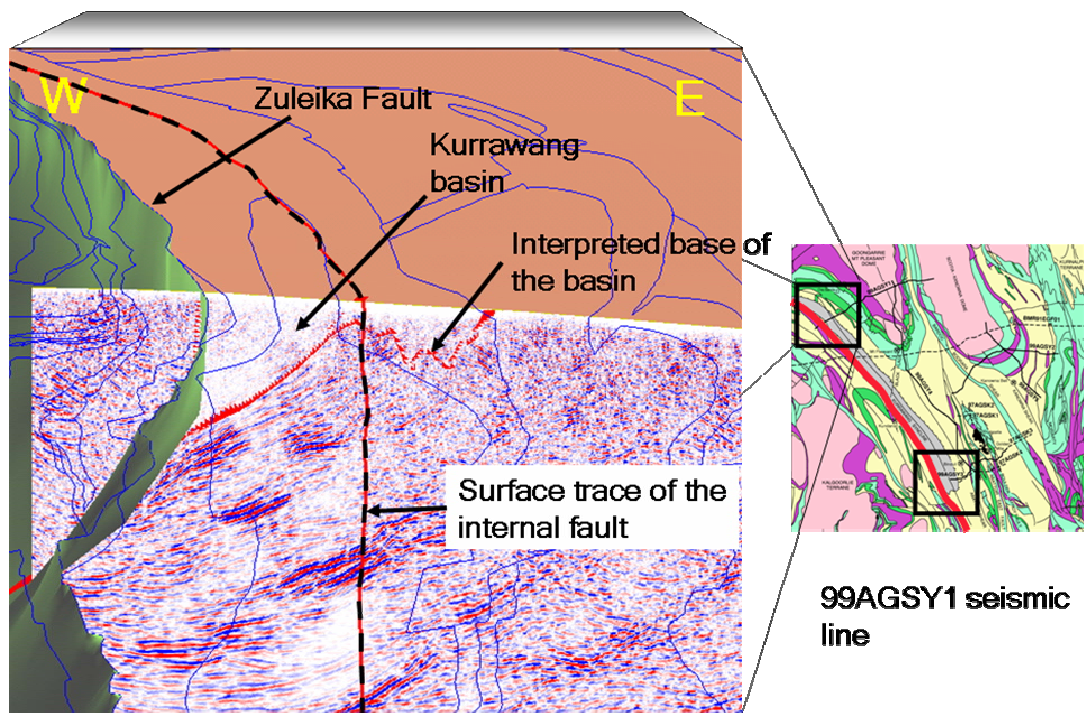


**Figure 8-37: 3D image from Gocad displaying the geometries of the interpreted Zuleika Fault, the Kurrawang Basin, and the surface trace of the internal fault within the basin.**
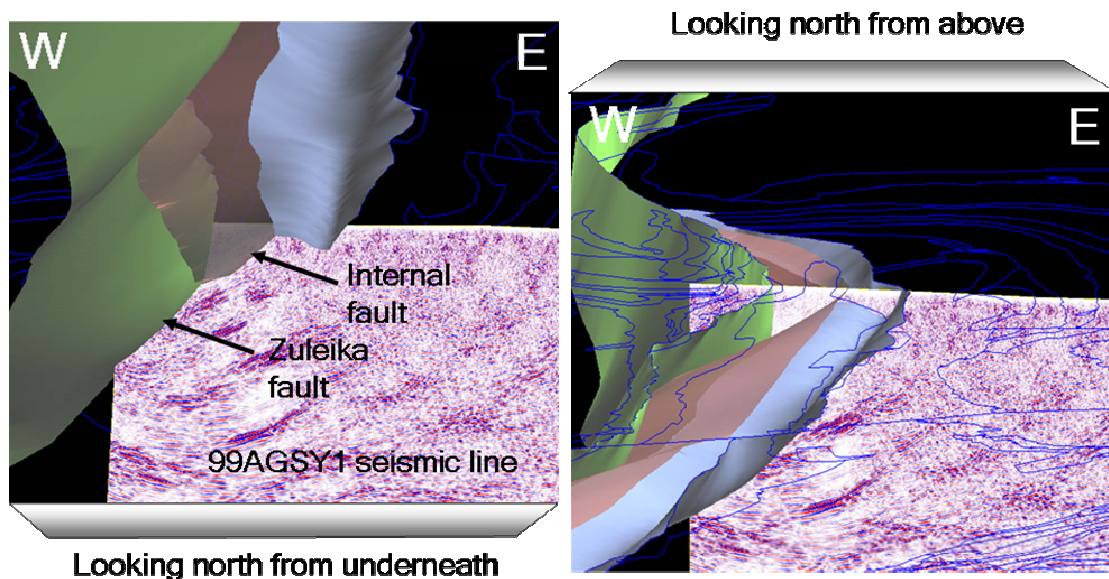
**Figure 8-38: Screen capture from Gocad showing the reinterpretation of the Zuleika Fault and the Kurrawang Basin, including a new interpreted internal fault through the basin.**

The reinterpreted seismic line combined with structural and drillhole data have significantly changed the original interpretation of the Zuleika Fault and the Kurrawang Basin sequence. Constructing surfaces in the 3D map from the reinterpretation provides a revealing insight into the 3D geometries and possible additional fluid pathways within the sequence (Figure 8-38).

## *Reinterpretation of the northern Ida Fault*

Previous workers have recognised the significant break (Ida Fault) that occurs across the NNW-trending fault zone that divides the Kalgoorlie Terrane in the east from the older Southern Cross Terrane in the west. The break has been mapped by a series of techniques, including geology, geochemistry, geophysics, and geochronology. This section describes a reinterpretation of the architecture of this important boundary between the EYC and terranes to the west.

The Sm-Nd model ages (Cassidy et al., 2002a) define a significant difference in the crustal residence ages between the two terranes (Figure 8-39). Cassidy et al. (2002a) also defined a zone of Low-Ca granites that appears to stop abruptly at the NNW-trending boundary of the Ida Fault in the south, although it is not so clearly defined in the northern zone (Figure 8-39).
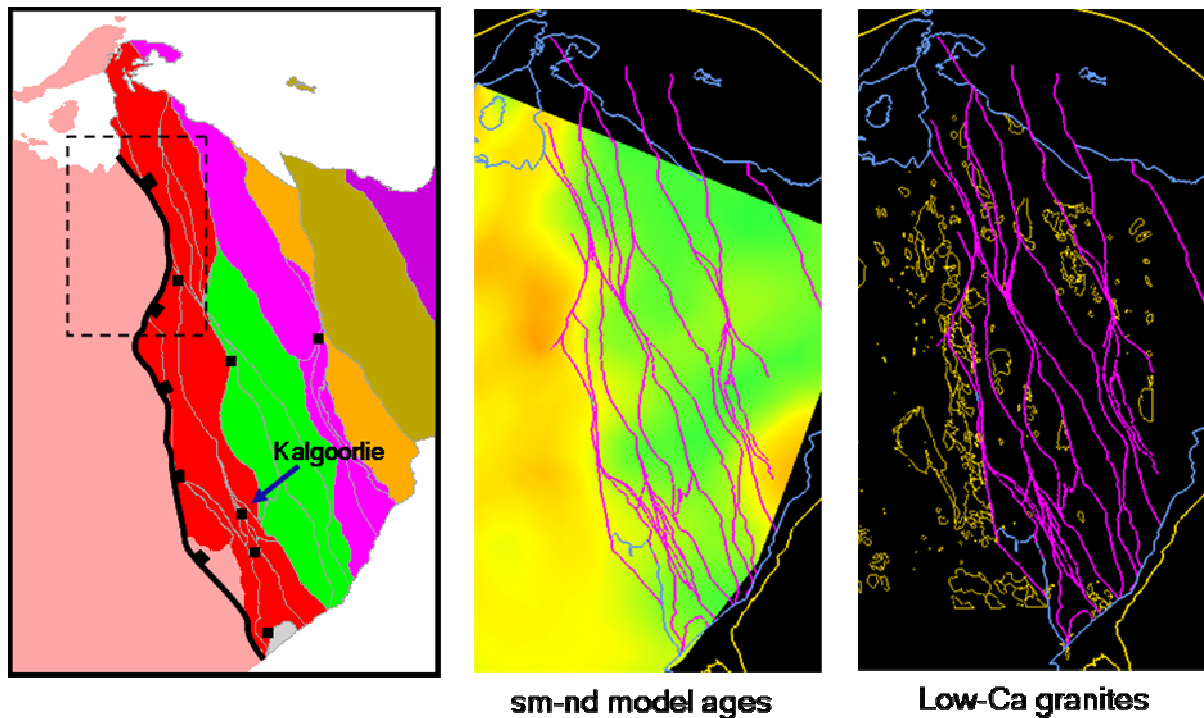
**Figure 8-39: Image showing the original interpretation of the Ida Fault and a dashed box delineating the area of reinterpretation in this study; an image of the Sm-Nd model ages, after Champion & Sheraton (1997) showing a significant crustal age difference on either side of the Ida Fault, and the spatial distribution of Low-Ca granites (yellow polygons) after Cassidy et al., (2002a).**

The Ida Fault was originally interpreted as a broadly east-dipping fault with a normal sense of displacement (Figure 8-39). The minor exception was the region where the younger west-dipping Waroonga Fault cuts the top off the Ida Fault (see Figure 8-40). The geometry of the southern part of the Ida Fault is typical of a normal sense of movement, although the northern segment does not match this interpretation. Close inspection of this structure using "worm" strings, proved that it was more plausible to reinterpret the northern Ida as a structure that had been truncated by west-dipping thrust faults (the Waroonga Fault System) (see Figure 8-41). This interpretation also explains some of the complexities in the spatial occurrence of the Sm-Nd model ages and the Low-Ca granites in the region around the northern Ida Fault.

In light of this new understanding, the northern Ida Fault is interpreted as a blind (east-dipping) structure that has been thrust out by the younger west-dipping Waroonga Fault System (Figure 8-41).
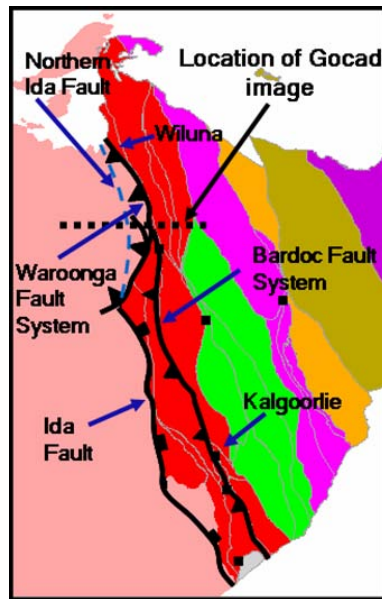
**Figure 8-40: The "blind" northern Ida Fault (blue dashed line) "concealed" by the west-dipping Waroonga Fault System.**
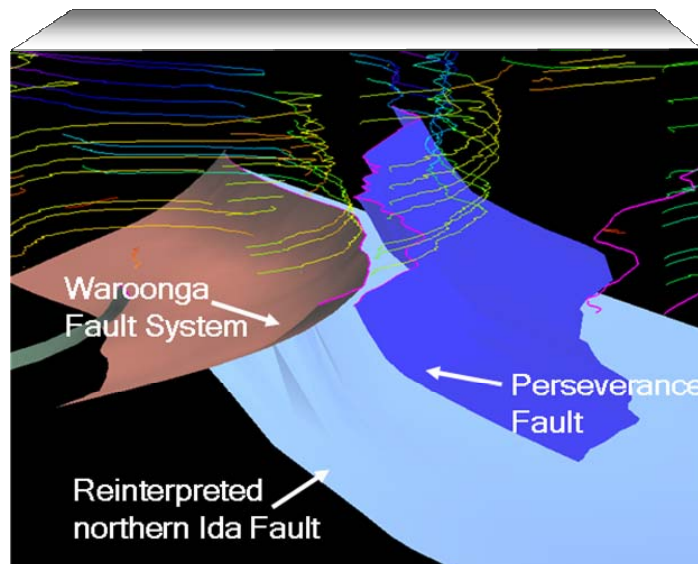


**Figure 8-41: Screen capture from Gocad looking north, displaying the reinterpretation of the northern Ida Fault and the Waroonga Fault System, using "worm" strings to constrain the dip direction of faults.**

## *The 'Golden Corridor', the region's hot property*

The Boorara and Kambalda Domains of the Kalgoorlie Terrane are the most-richly endowed regions of the Yilgarn Craton (Figure 8-42). They contain world-class gold deposits such as The Golden Mile; Kanowna Belle and Kambalda. A 'Golden Corridor' exists from Kambalda to Wiluna (and possibly as far north as Plutonic), along the axis of the Kalgoorlie Terrane. This section outlines the architecture of this Golden Corridor, from the south (where it is best defined, due to data density) to the north.

In the south, this mineralised zone lies on a NNW trend bounded on its western side by the Bardoc Fault System (Figure 8-42). Seismic reflection data across the EYC reveal that the majority of faults are east-dipping and west-verging, consistent with the geometries generally associated with a fold-and-thrust belt. Within the Kalgoorlie region, though, faults dip both east and west, with prominent faults such as the Bardoc Fault System occurring as a west-dipping structure.
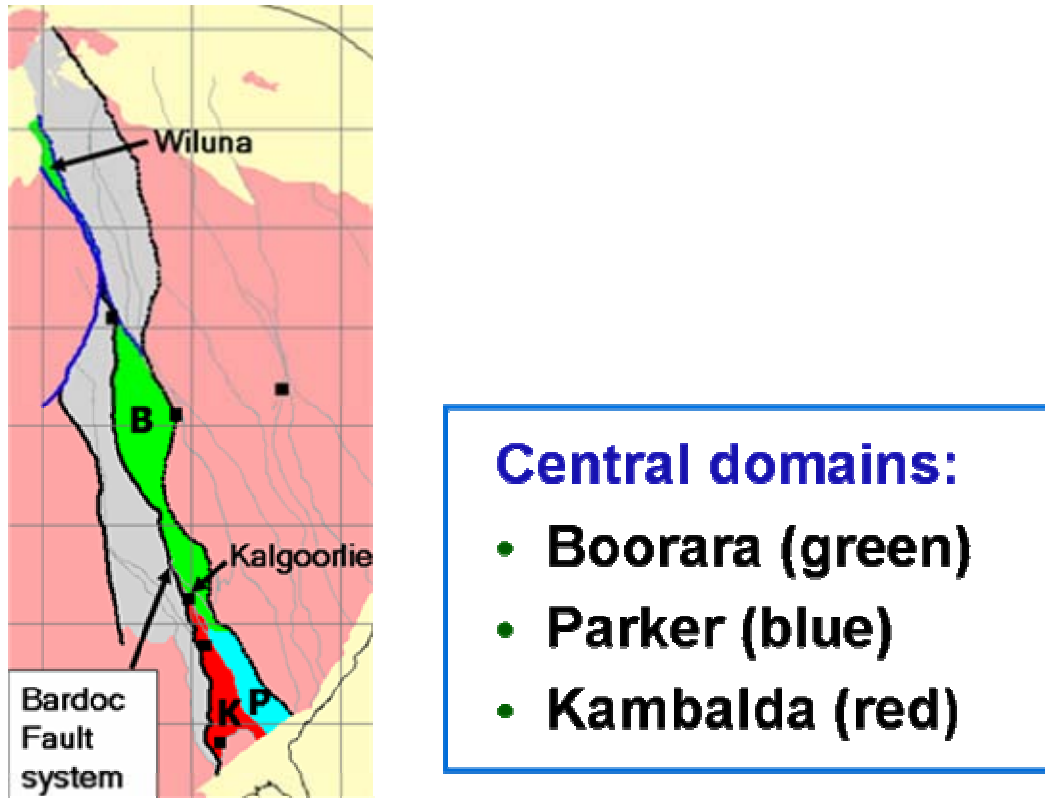


**Figure 8-42: Image showing the domains to the east of the Bardoc Fault System within the EYC.**

Interpretation of the subsurface geometries made during the construction of the 3D map of the Kalgoorlie-Kambalda region, revealed that a significant anticlinorium occurs in a corridor stretching from Kambalda to Kalgoorlie and northwards (Figure 8-43). This structure is a broadly north-south trending antiform with an undulation about an east-west axis. The interference of the north-south and east-west fold structures results in a series of elongate domical structures along a north-south corridor. To the east of this antiform is the reinterpreted Lefroy Fault, which has been reinterpreted from a west-dipping to an east-dipping structure using seismic reflection data recently acquired by Goldfields.

Overall the region is an antiform with major faults dipping in opposing directions away from its apex (Figure 8-44; see also Figure 8-70 and discussion later in the chapter). This places the major gold deposits in the footwall of these master faults and in two locations in sub-parallel subsidiary faults to the master faults. At The Golden Mile, mineralisation occurs within the steeply west-dipping Golden Mile Fault (sub-parallel to the Bardoc Fault System), which could be interpreted as a minor fault with genetic links to the Bardoc Fault System. At Kambalda the east-dipping Playa Shear appears to be related to the east-dipping Lefroy Fault.
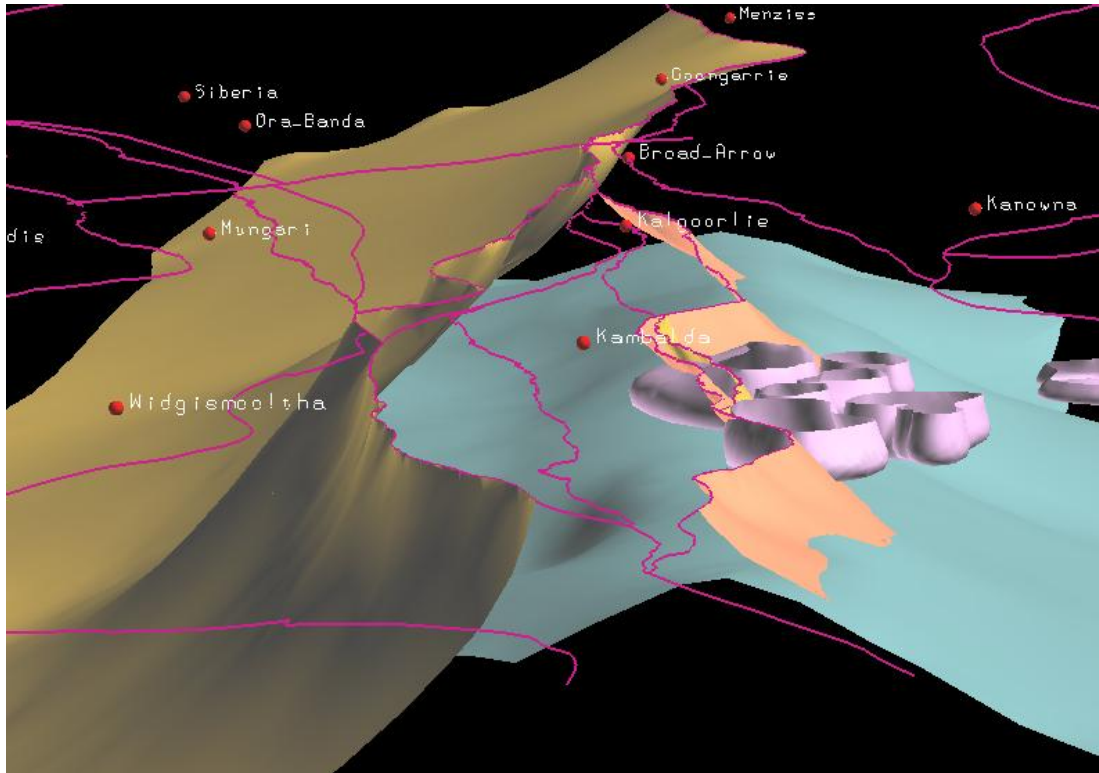
**Figure 8-43: Screen capture from Gocad of the southern section of the Golden Corridor looking north showing the anticlinorium beneath the Kalgoorlie-Kambalda region. Bardoc Fault (gold), Lefroy Fault (orange), LASH/antiform (blue), granites (pink).**
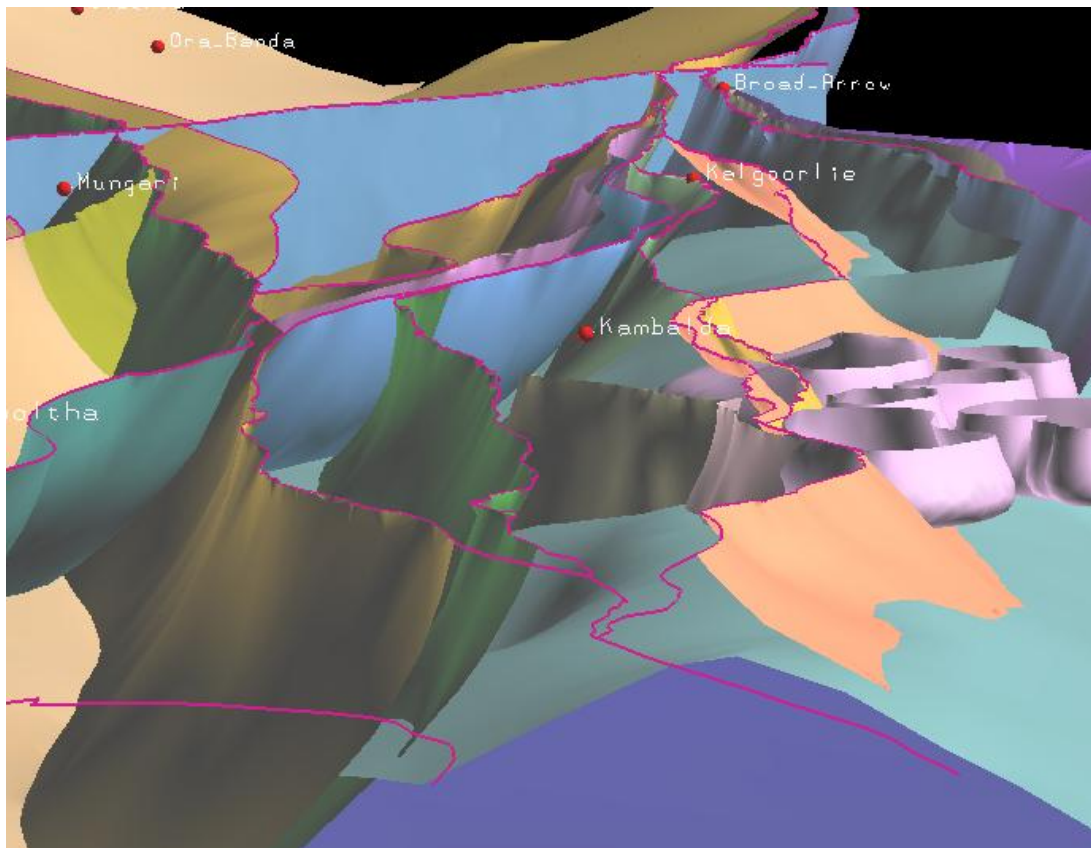


**Figure 8-44: Screen capture from Gocad looking north, showing the Kalgoorlie-Kambalda section of the Golden Corridor and additional minor faults.**

213

Regionally, the Bardoc Fault System continues north until it intersects the reinterpreted northern Ida Fault at depth and the Waroonga Fault System, as previously described (Figure 8-46). At this location it is difficult to separate the faults because they both dip west and appear to merge. If the Bardoc Fault System continued and merged with this structure it would place the gold deposits at Wiluna in the same structural position as The Golden Mile and Kambalda (with respect to the dip of master fault and the associated anticlinorial axis).

Close analysis of the deposit-scale structures reveal that there are striking structural similarities between the Wiluna gold deposits and their southern counterparts. Additionally, the deposits occur within anticlinoriums located in the footwall of the west-dipping Waroonga Fault System which is interpreted as an extension of the Bardoc Fault System (Figure 8-46).
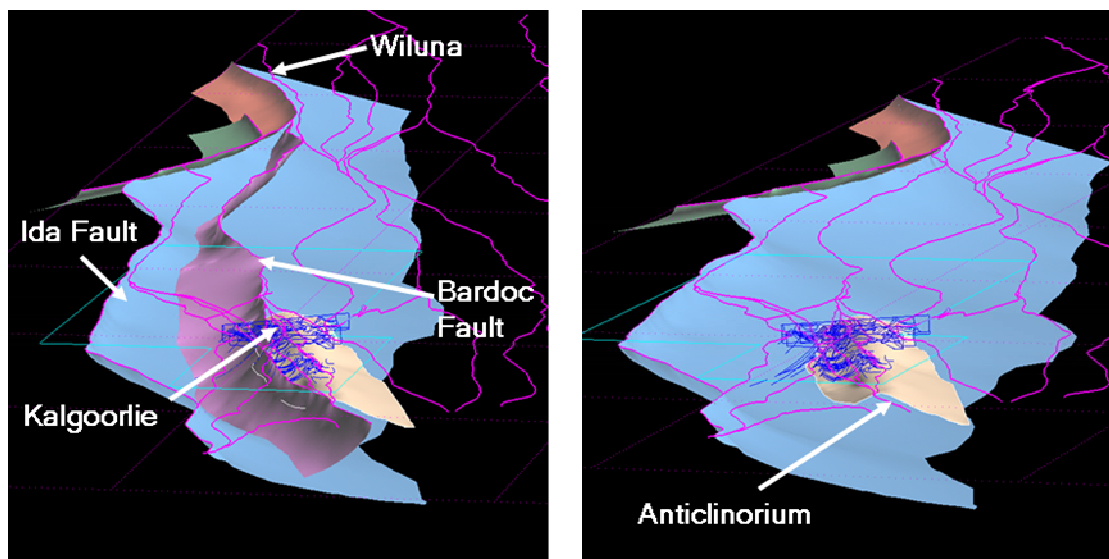


**Figure 8-46: Screen capture from Gocad looking north, showing the reinterpretation of the northern Ida Fault, the Bardoc Fault System and the anticlinorium beneath Kalgoorlie-Kambalda (the Golden Corridor).**

To the north of Wiluna, the Waroonga Fault System extends under relatively thin Proterozoic cover as far as Plutonic Bore (Figure 8-47), and appears to maintain a similar geometrical relationship with the greenstone belts to its immediate east. The Plutonic Bore gold deposit lies just to the east of the same general trend as the Bardoc Fault System and thus is likely the northernmost extension of the Golden Corridor. This northern extension of the Golden Corridor under cover may have **significant area selection potential**, as the region is dominated by significant gravity highs, indicative of a reasonable thickness of greenstone.
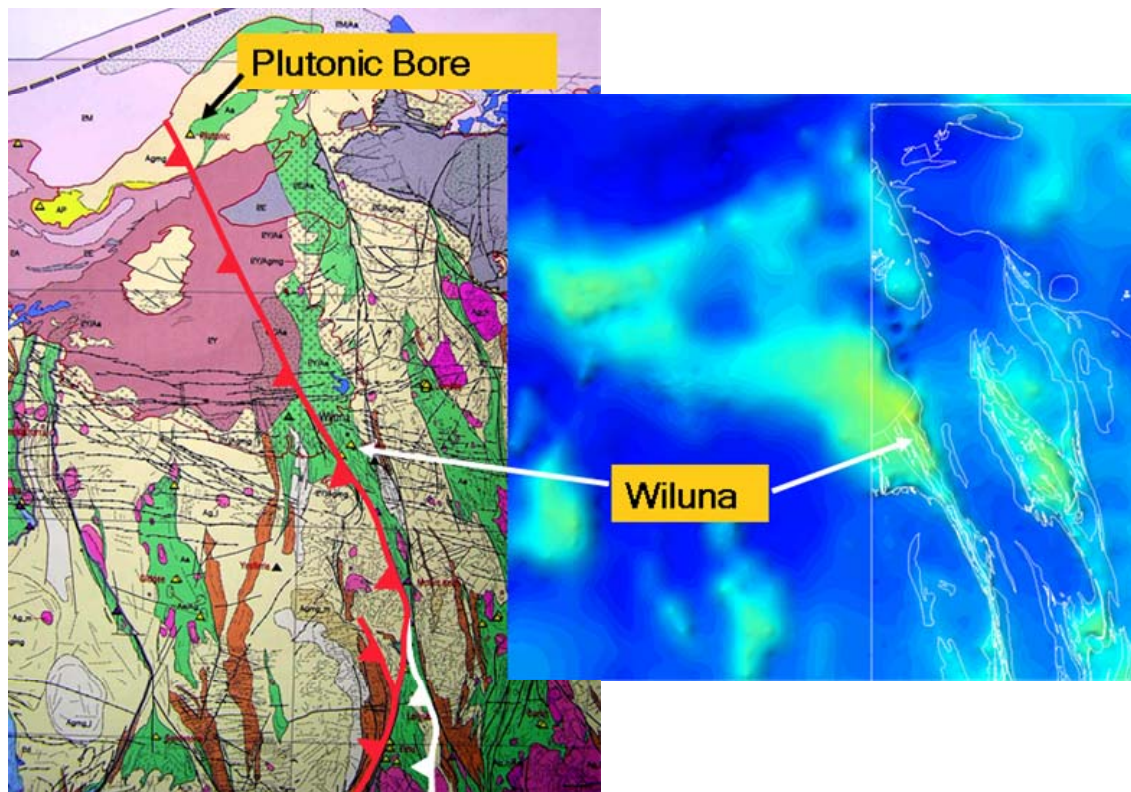
**Figure 8-47: Image displaying the magnetic interpretation of the Yilgarn Craton from Whitaker and Bastrokova (2002). Bardoc Fault System (white thrust); Waroonga Fault System and a possible northern extension to Plutonic Bore (red thrust). False colour gravity image of the Wiluna region shows significant mass and therefore greenstones to the east of the major west-dipping Bardoc and Waroonga Fault Systems.**

## *Implications for predictive mineral discovery*

The architecture of the system defines the fluid pathways of the orogenic gold mineral system. A number of changes to previous models have been outlined above. These include new changes to the Kurrawang Basin and Zuleika Fault, the nature of the Ida Fault, and the definition of a "Golden Corridor".

This Kurrawang Basin and Zuleika Fault region is known for significant gold deposits, including Kundana Mine, and there are additional small deposits located along the length of the Zuleika Fault. An understanding of the geometry of the basin and associated faults is required for any numerical modelling of fluid flow (see Potma, 2004). New findings suggest that the basin is not a simple syncline, rather it comprises two synclines separated by a largely faulted anticline. The fault that divides the basin is a moderately west-dipping splay from the steep listric west-dipping Zuleika Fault.

The Ida Fault, although largely unmineralised, is a fundamental boundary of the Yilgarn Craton. The tracing of this boundary beneath a younger thrust (Waroonga Fault System) infers significant late contraction following the extensional movement on the Ida Fault (see Swager, 1997). This observation has implications for geodynamics through the structural history and any late gold mineral systems.

The architecture of the Golden Corridor may partly explain why the Kalgoorlie Terrane is so well endowed. The unifying theme appears to be the relationship between major faults and regional anticlinoria, with periodic undulations or perturbations resulting in elongate domes. The Golden Corridor stretches from Kambalda possibly to Plutonic, with locations under thin cover providing new opportunities for exploration (i.e., north of Wiluna).

## Crustal penetrating faults, do they or don't they?

*R.S. Blewett*

Interpretations of the fault architecture below the greenstone base or in the granite areas are restricted to seismic reflection data. This is because of the inability of alternative potential-field methods to map structure effectively at depth (via rock-property contrasts) or in felsic crust (as discussed above).

Early interpretations of the seismic reflection data around Kalgoorlie (e.g., Goleby et al., 1993; Swager et al., 1997) noted a number of structures that penetrated the upper crustal detachment, and in some cases intersected the Moho. Similar interpretations were made of the northeastern Yilgarn seismic line (01AGSNY1), with three crustal-penetrating shear zones interpreted (Goleby et al., 2003). These shear zones include the Ockerberry (Mt George), Laverton, and Yamarna shear zones (see Chapter 3 and associated appendices).

There is little doubt that there are significant mid-crustal reflectors that dip consistently and are approximately aligned with known major faults at the surface. However, the unambiguous interpretation that links these mid-crustal reflectors with known surface faults is debatable. In this section, two examples are discussed. The Ockerberry Fault, which is a terrane boundary between the Kalgoorlie and Kurnalpi Terranes, and the Laverton Fault, which is internal to the Kurnalpi Terrane (see Chapter 1 for maps of the faults).

Figure 8-48 shows little evidence for a direct connection between mid-crustal reflectors (fault) and the interpreted upper-crustal fault plane. The Ockerberry is a major fault that separates distinct terranes. Figure 8-49 is a seismic section of the upper half of the crust showing well-developed mid-crustal reflectivity that possibly "connects" with an upper-crustal intra-terrane fault plane.

The implications of these observations is that the amalgamation of the terranes was relatively thin-skinned and its subsequent deformation (post-'$D_2$') involved a thick-skinned component. Breaking the entire crust with a single fault plane under contraction is mechanically difficult to achieve, but is easier under extension. It is likely that these through-going crustal penetrating faults developed late in the orogenic process (post-'$D_2$') and represent late-stage extensional collapse (see also Swager, 1997; Swager and Nelson, 1997; Blewett et al., 2002a; 2002b; Blewett, 2003; Davis and Maidens, 2003).
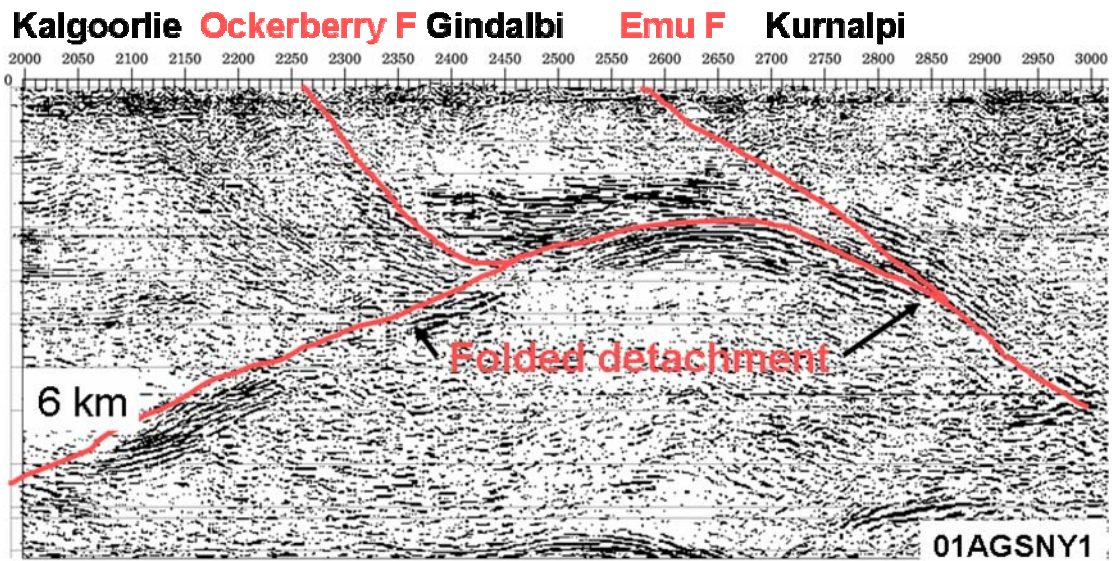
**Figure 8-48: Despite being a terrane boundary, the seismic reflection profile across the Ockerberry Fault suggests that it is thin-skinned and rolls onto a low-angle shear (LASH) or detachment.**
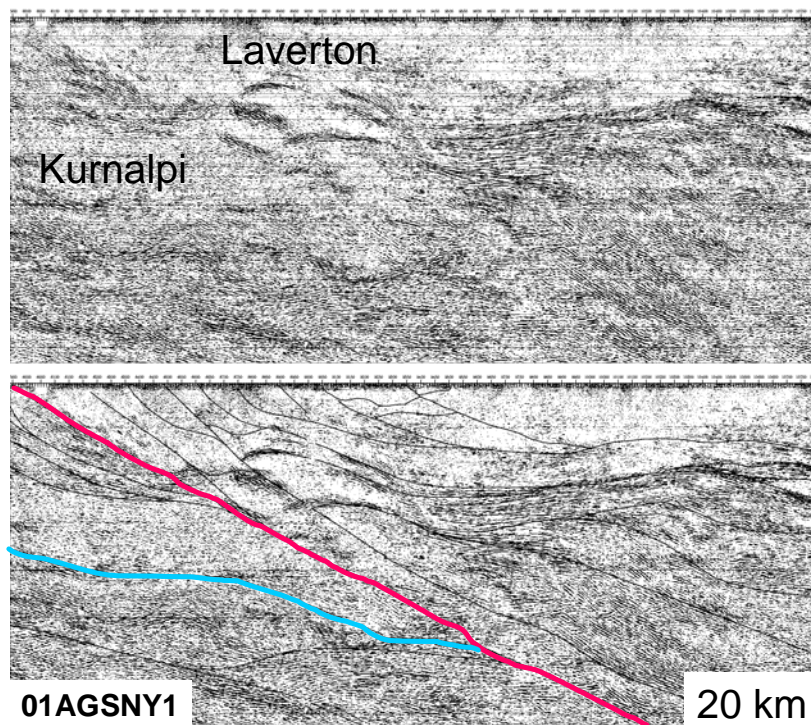


**Figure 8-49: Alignment of reflectivity in the mid crust appears to breach the upper crustal LASH and "crop out" at the Laverton Fault. This is an intra-terrane fault of the Kurnalpi Terrane (see Chapter 1 for maps and terrane nomenclature).**

217

# Failure of the lithosphere and development of crustal-penetrating faults

*K. Regenauer-Lieb*

Chapter 3 described the deep-penetrating faults visible in the seismic reflection profiles, and their importance for the architecture and possible fluid pathways. The Y2 project requested the Modelling team at CSIRO to examine what conditions were necessary to allow failure of the whole crust/lithosphere. The answer to this question has obvious geodynamic implications such as the initiation of subduction.

A prerequisite for plate tectonics is that the lithosphere becomes faulted, fractured and fragmented. A fundamental question is what critical geodynamic factor(s) controlled the yield of an originally intact lithosphere and initiated subduction. This geodynamic question is fundamental because it drove other subsequent tectonic processes (e.g., subduction-related accretion and orogenic convergence).

The yielding of a lithospheric slab is the fundamental mechanical prerequisite for the nucleation and propagation of discrete structures such as lithosphere-scale shear zones. This plays a key role in the initiation of subduction zones, which can lead to convergent deformation, orogenesis and mineralisation such as those observed in the Yilgarn.

Klaus Regenauer-Lieb and co-workers (Regenauer-Lieb et al., 2001; Regenauer-Lieb and Yuen, 2003) explored the issue of shear zone and subduction initiation in the lithosphere via a set of numerical models. The results of these models demonstrated the significance of the presence of water in the lithosphere. Water facilitated the rupture of the lithosphere, the initiation of lithospheric-scale shear zones, and subsequent subduction (Figure 8-50). In the dry rheology situation (Figure 8-50, left), the simulated lithosphere is only locally deformed. There is no major shear strain localisation, which might indicate the initiation of subduction. In contrast, by involving water in the wet rheology situation (Figure 8-50, right), shear strain is strongly localised in a zone that suggests the initiation of a major shear zone and subduction zone.
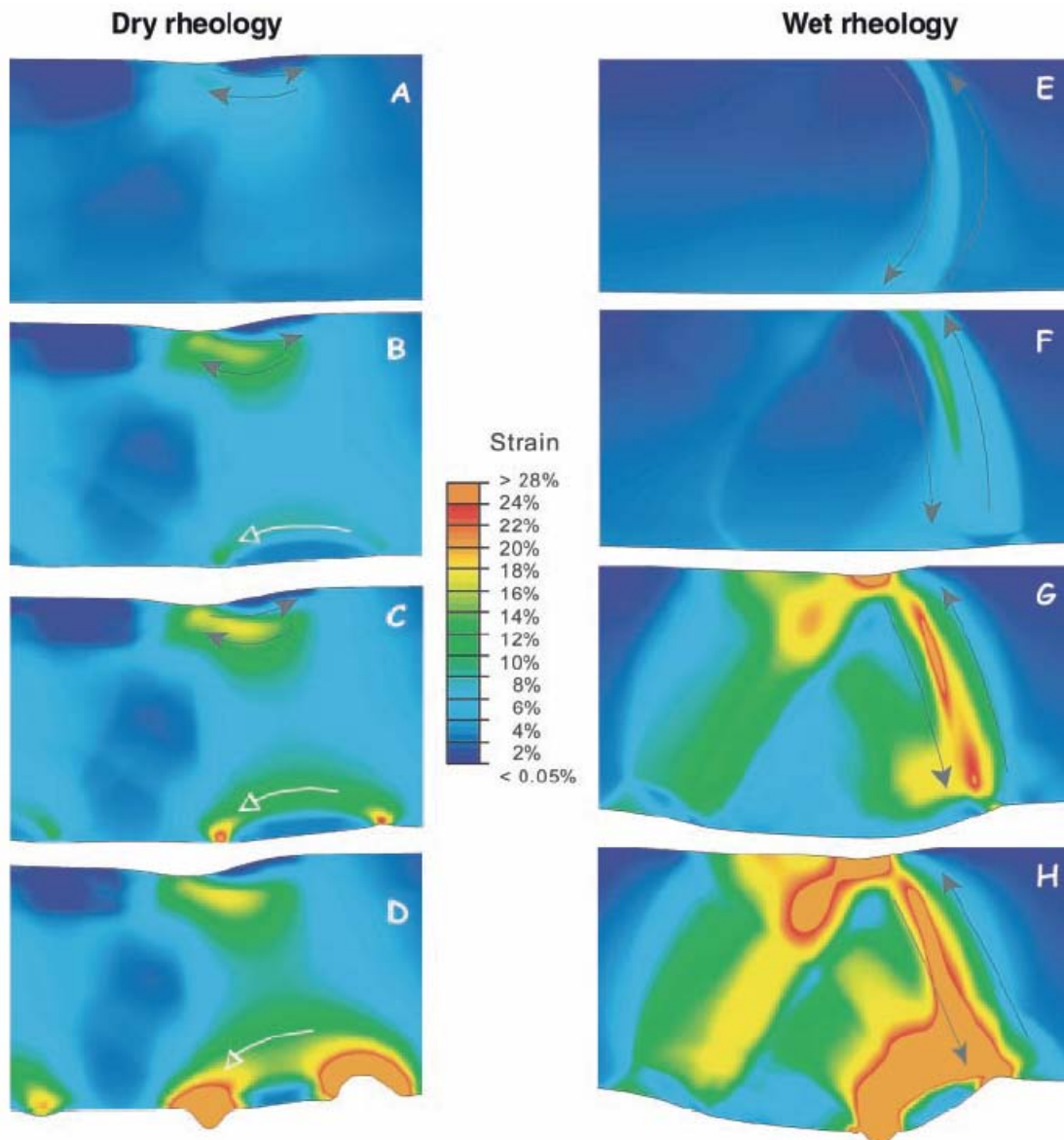
**Figure 8-50: Evolution of shear strain patterns in the dry (left column) and wet (right column) cases (Regenauer-Lieb et al., 2001). A to D give the results at the model times of 38, 64, 69, 72 My, respectively. Similarly, E to H show the results at the model times of 25, 30, 35, 35.5 My, respectively.**

## Importance for Yilgarn architecture and predictive mineral discovery

*R.S. Blewett*

The nature of the failure of the lithosphere was a question for the interpreters of the deep seismic reflection profiles (see Chapter 3). The question concerned whether (or not) the terrane bounding faults (e.g., Ockerberry, Celia, Laverton, Emu Faults) penetrated the crust. The question is not necessarily answered by this modelling, however, it does suggest that faults may transect the crust when fluid is available. Connectivity of the mantle and lower crust with the upper crust by deep-penetrating faults is considered an important pathway for components (fluids/metals?) of the

mineral system. Could the fluids available to break the crust (generate the through-going fractures previously linked to major gold camps) also be the same ones that enrich the upper crust?

## *Question 3—Fluid flow drivers and pathways*

*R.S. Blewett*

The question regarding fluid drivers was not specifically answered by the Y2 project. The common mechanisms include:

1. compaction of sedimentary basins;
2. topography;
3. thermal input from igneous complexes, and;
4. metamorphism and deformation.

The orogenic surge model discussed above touches on all four mechanisms:

1. The Late Basins are interpreted to have developed during the surging stage of the process, with inversion of faults and the development of elongate depocentres in the immediate hinterland. These localised extension areas where then inverted and the basins buried by over-riding thrusts. The result would be a compaction and metamorphism of the basinal sediments.
2. Some topography is required to drive the surge process (see numerical modelling section above), and it may have been important in driving the orogen and the development of the faults and the basins. Even if the model is incorrect, some topography is inferred on the basis of the exhumation of granitoids and their detritus being shed into Late Basins.
3. The localised extension facilitated Mafic granite-type intrusion into the system. These are temporally and spatially associated with many deposits and the remnants of Late Basins. Their thermal input may have contributed to fluid flow. The delamination of a restite layer late in the orogenic sequence is interpreted to be a cause for crustal anatexis and generation of Low-Ca granites.
4. The process of contraction and mid-crustal imbrication resulted in thickening of the crust, melting and metamorphism. These processes would all have likely played a role in driving fluids through favourable pathways. The switching in tectonic mode (extension-contraction) and rotation of stress axes may have also been significant as a fluid driver, or provided a driver for different fluids for mixing.

## Question 4—Fluids, their sources and reservoirs

*B. Hobbs, B. Drummond and A. Ord*

The involvement of mineralising fluids is critical to the development of the gold-rich mineralisation in the Yilgarn. Questions to be answered are:

- how mineralisation-relevant fluid reservoirs developed at mid-crust levels, and;
- how the upper crust (where deposits occur) is coupled with the lower crust.

## Introduction and statement of problem

Iio and Kobayashi (2002) proposed that seismogenic faults in the upper crust may be associated with localised extensions into the lower, viscous crust and that aseismic accumulation of strain within these aseismic zones ultimately nucleates seismic failure on the upper-crustal fault. Furthermore, they proposed that precursor, aseismic slip accelerates prior to the seismic event and that such accelerated motion may be expressed as accelerated tilt and/or distortion at the surface, thereby providing an observable precursor deformation in advance of a major seismic event.

The proposal is that there is an example of such a downward continuation of a seismogenic fault in the Sendai region of northeast Japan where the Nagamachi-Rifu Fault can be imaged by seismic methods down to the base of the seismogenic zone. This fault was the site of a magnitude 5 earthquake in 1998 at a depth of 12 km. In addition, seismic studies reveal the existence of a thin, shallow dipping S-wave reflector, below the base of the seismogenic zone, which is interpreted as a fluid-filled shear zone (see Umino et al., 2002; Drummond et al., 2004). It is proposed that localised, aseismic shear flow within this shallow dipping zone preceded and nucleated the main seismic event on the Nagamachi-Rifu Fault higher in the crust.

These observations prompt the following important questions regarding earthquake nucleation:

- What are the processes that lead to the accumulation of fluid rich regions in the mid crust?
- What is the geometry of such regions?
- Are these regions shear zones that could act as sites for aseismic slip?

Exploring these questions will facilitate our understanding of the accumulation of mineralising fluids at deep crustal levels and any feedback interaction between the deep and the shallower crustal levels.

For simplicity we consider a two-dimensional situation with Cartesian coordinate axes $x_i$ (i=1,2) and $x_2$ vertical, in which the total stresses are $\sigma_{ij}$, with $\sigma_1 \geq \sigma_2$ and compressive stresses positive. We define the deviatoric stresses to be $\sigma'_{ij}$ given by:

$$\sigma'_{ij} = \sigma_{ij} - \delta_{ij}\, \sigma^o \qquad (1)$$

where $\sigma^o$ is the mean normal stress in the rock mass, i.e., $\sigma^o = \sigma_{kk}/2$. $\delta_{ij}$ is the Kronecker delta. We also define the effective stresses by:

$$\sigma_{ij}{}^{eff} = \sigma_{ij} - \delta_{ij} P_f \qquad (2a)$$

$$\sigma_{ij}{}^{/\,eff} = \sigma_{ij}{}^{/} - \delta_{ij} P_f \qquad (2b)$$

where $P_f$ is the fluid pressure in the rock pore space. The concept of a deviatoric stress was introduced historically because the constitutive behaviour of viscous (pressure insensitive/temperature sensitive) materials is not (to first order) influenced by normal stresses but by only the shear stresses (see Nadai, 1950). On the other hand, the constitutive behaviour of plastic (pressure sensitive/temperature insensitive) materials is strongly influenced by normal stresses. Thus, the concept of effective stress was introduced (see Paterson, 1978, for a discussion) specifically for the plastic deformation of materials where the strain is influenced by the pore-fluid pressure that tends to force the grains apart. The notions surrounding the concepts of deviatoric stress and effective stress are commonly used interchangeably in a loose manner in the geoscience literature but the distinctions between them become fundamental in this discussion. Note that from (1) and (2),

$$(\sigma_1 - \sigma_2) = (\sigma'_1 - \sigma'_2) = (\sigma_1{}^{eff} - \sigma_2{}^{eff}) \qquad (3a)$$

$$(\sigma_1 + \sigma_2) = (\sigma'_1 + \sigma'_2) + 2\sigma^o = (\sigma_1{}^{eff} + \sigma_2{}^{eff}) + 2P_f \qquad (3b)$$

What defines the values and orientations of principal stresses in a deforming rock mass? In general the constitutive relations plus the boundary conditions define the values and orientations of principal stresses. However some general statements can be made without becoming specific about constitutive relations and boundary conditions. The condition for dynamic equilibrium is given by the generalisation of Newton's first law of motion:

$$\rho_r \frac{\partial u_i}{\partial t} = \frac{\partial \sigma_{ij}}{\partial x_j} + \rho_r g_i \qquad (4)$$

where $\rho_r$ is the rock density, $u_i$ are the components of the particle velocity and $g_i$ are the components of the acceleration due to gravity. If we neglect particle accelerations and shear stresses parallel to $x_1$ and $x_2$, and gradients in stress parallel to $x_1$, then (4) reduces to:

$$\frac{\partial \sigma_{22}}{\partial x_2} = -\rho_r g_2 \qquad (5)$$

so that for these conditions the vertical normal stress (which under these conditions is equal to $\sigma_2$) is given by $\rho_r gh$ where h is the vertical distance below the surface of the Earth and $g=g_2$ is the vertical component of the acceleration due to gravity. If particle accelerations are significant or shear stresses parallel to $x_1$ and $x_2$ are important, as is the case with regional buckling or the development of horizontal detachment zones then (5) is not necessarily approximately true. Some examples are given by Petrini and Podladchikov (2000).

For a power law viscous material, the value of $\sigma_1$ is then fixed by the constitutive relation and (3a):

$$\sigma_1 - \sigma_2 = \sigma'_1 - \sigma'_2 = A^{1/N} D^{-1/N} \exp \{Q/NRT\} \qquad (6)$$

where A is a material constant, D is the deformation rate, Q is an activation energy, R is the gas constant, T is the absolute temperature and N is an exponent normally in the range 1-5 (see Nicolas and Poirier, 1976). It is important to note that the constitutive relation for power-law viscous materials is written in terms of the second invariant of the deviatoric stresses, but can be reduced to (6) (see Jaeger, 1962).

For a plastic material, typically represented by a Mohr-Coulomb or a Drucker-Prager material, the stress state is governed by a flow rule which specifies the direction and magnitude of the incremental plastic strain as a vector normal to a plastic potential surface which, in turn, is defined in terms of q, a scalar function of the stresses and of the dilatancy of the material. For a Mohr-Coulomb material (see Vermeer and de Borst, 1984):

$$q = \sigma_1^{eff} - N_\varphi \, \sigma_2^{eff} - 2c\sqrt{N_\varphi} \qquad (7)$$

Here, $N_\varphi = (1+\sin \varphi)/(1- \sin \varphi)$, c is the cohesion and $\varphi$ is the dilation angle.

The stress rate can then be expressed in terms of the deformation rate and the total (elastic plus plastic) strain rate (see Vermeer and de Borst, 1984, p 24). In general the stress rate cannot be analytically integrated to obtain the stresses for a given strain history and numerical procedures are required. Thus the values and orientations of the principal stresses in a Mohr-Coulomb material are not defined solely by the constitutive relation, as is the case in an elastic or a power-law viscous material, but also by the history of incremental strains, which in turn is a function of the history of dilatancy.

## Fluid pressure distribution in deforming materials

It is widely observed that the uppermost crust is divided into more or less horizontal compartments in which the pore pressure gradient alternates between approximately hydrostatic to approximately lithostatic (see Hunt, 1990). In the absence of a non-hydrostatic stress field, over a specific column of rock, the mean pore pressure and the mean pore pressure gradient must be lithostatic. This follows from the fact that in a porous rock under a hydrostatic stress state the fluid pressure in the rock must be less than or sufficient to keep the pore space open, so that if the confining pressure is close to the strength of the rock, the pore pressure at a particular point must be similar in magnitude to the mean pressure given by $\rho_r gh$. This is the value of pore pressure classically adopted by metamorphic petrologists. The observed distribution of compartments seems to be the result of self-organisation resulting from two competing processes:

1. The tendency to move towards a global equilibrium state where the pore pressure gradient is everywhere hydrostatic even though the mean pore pressure is lithostatic. The time scale, $\tau$, for this to happen is given by the diffusion equation,

$$\tau = L^2/\kappa \qquad (8)$$

where L is a length scale for the system and $\kappa$ is the hydraulic diffusivity that in turn is given by (see Phillips, 1998)

$$\kappa = Kc^2/\mu\phi \qquad (9)$$

where c is the isothermal speed of sound in the rock (~$1.4 \times 10^3$ m/s), $\mu$ is the kinematic viscosity of the fluid (~$10^{-6}$ m$^2$/s for water at $0^o$C), and $\phi$ is the porosity. This means that for a rock with porosity 0.1, the magnitude of $\kappa$ is ~$1.96 \times 10^{13}$ K. Hence, layers 5 km thick, of different permeabilities, will evolve towards this global hydrostatic state at different rates depending upon their permeabilities. A layer with permeability of $10^{-17}$ m$^2$ will take ~3,950 years to reach an equilibrium hydrostatic gradient condition whereas the same thickness layer with permeability $10^{-18}$ m$^2$ will take ~39,500 years. These time scales are short geologically so that in the absence of devolatilisation or supply of fluids from the mantle, a lithospheric pore pressure gradient will rapidly relax to a hydrostatic gradient.

2.  The mechanical necessity that only columns of finite height of fluid with hydrostatic pore pressure gradients can be supported. This height is controlled by the generation of tensile effective stresses at the top of the column that hydrofracture the top of the column and the generation of compressive deviatoric stresses at the base of the column that tend to close the pore space by viscous flow.

The development of fluid pressure compartments by these processes has been elegantly discussed by Connolly and Podladchikov (2000). The above discussion is true for a rock mass under hydrostatic stress conditions. If the rock mass is deforming, other considerations need to be made and these are considered below.

## Fluid pressure distribution in a deforming power-law viscous material

We first explore the proposal that for a porous power-law viscous material under non-hydrostatic stress the pore pressure needed to keep the pores open is equal to the mean total stress, $(\sigma_1 + \sigma_2)/2$ (Figure 8-51a). This can be substantially greater than the lithostatic pressure since the mean deviatoric stress in such a material (see Stuwe and Sandiford, 1994) is:

$$(\sigma'_1 + \sigma'_2)/2 = \sigma'_2 + 0.5\, A^{1/N} D^{-1/N} \exp\{Q/NRT\} \qquad (10)$$

The mean total stress in a power law viscous material is given by:

$$(\sigma_1 + \sigma_2)/2 = \sigma_2 + 0.5\, A^{1/N} D^{-1/N} \exp\{Q/NRT\}, \qquad (11)$$

which approaches $\sigma_2$ as T increases and/or D decreases.

If $\sigma_2$ is solely due to the overburden pressure, then the mean stress approaches lithostatic for high T and/or low D but otherwise is substantially larger (see Stuwe and Sandiford, 1994 for a discussion).
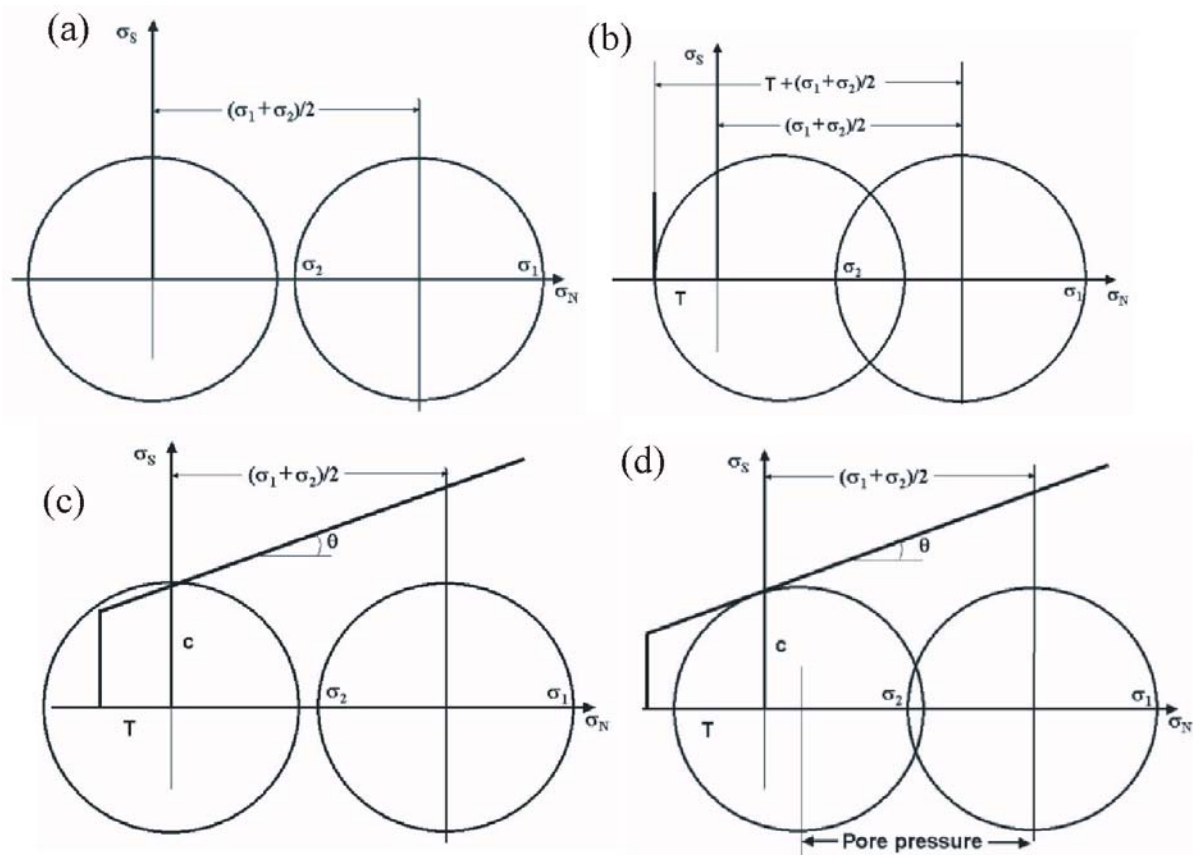


**Figure 8-51: (a) Transformation of a stress state defined by $\sigma_1$ and $\sigma_2$ in a viscous solid with no tensile yield due to a fluid pressure equal to the mean stress. (b) Transformation of a stress state defined by $\sigma_1$ and $\sigma_2$ in a viscous solid with a tensile yield stress, T, due to a fluid pressure less than the mean stress by an amount T. (c) Transformation of a stress state defined by $\sigma_1$ and $\sigma_2$ in a Mohr-Coulomb solid with a tensile yield stress, T, and failure envelope defined by the cohesion, c, and the friction angle, $\theta$, due to a fluid pressure equal to the mean stress. The effective stress state exceeds both the Mohr-Coulomb failure envelope and the tensile failure criterion and hence cannot be sustained. (d) Transformation of a stress state defined by $\sigma_1$ and $\sigma_2$ in a Mohr-Coulomb solid with a tensile yield stress, T, and failure envelope defined by the cohesion, c, and the friction angle, $\theta$, due to a fluid pressure that just enables yield to occur.**

The above discussion regarding the magnitude of the pore fluid pressure in a deforming porous power law material is true so long as the material can support relatively large tensile effective deviatoric stresses. If the viscous material exhibits a tensile failure mode then the situation is better represented by Figure 8-51b. It should be noted that experimental work in order to establish constitutive relations for power law viscous materials containing fluids is singularly lacking. Some of the best approaches are those of Tvergaard (1987), Needleman (1994) and Bercovici and Ricard (2002) discussed by Regenauer-Lieb (1999) and Regeneauer-Lieb and Yuen (2002). These constitutive relations show yield behaviour, a feature that is lacking in the classical constitutive relations for geological viscous materials and such yield behaviour would further restrict the possible states of fluid pressure as illustrated for plastic materials below.

## Fluid pressure distribution in a deforming plastic, Mohr-Coulomb material

In the upper part of the crust, the deformation style is dominated by plastic (that is, pressure dependent, temperature independent) constitutive behaviour. Various forms of behaviour may be assumed but the common one is characterised by the Mohr-Coulomb constitutive law where the constitutive behaviour is characterised by a yield surface defined (see Vermeer and de Borst, 1984) by:

$$f = \sigma_1^{eff} - N_\theta \sigma_2^{eff} - 2c\sqrt{N_\theta} \tag{12}$$

Here, f is the yield function, $N_\theta = (1+\sin\theta)/(1-\sin\theta)$, c is the cohesion and $\theta$ is the friction angle. Note the resemblance to the plastic potential function, q, defined in (7). If f=q the constitutive relation is associative; otherwise it is non-associative. For f=0 the material is at plastic yield in shear and for $\partial f/\partial t = 0$, remains at yield, where t is time; for f<0 the material is undergoing elastic deformation; the material cannot support stress states for which f>0. It follows from (12) and (3) that, at yield:

$$(\sigma_1 + \sigma_2)/2 = \sigma_2(N_\theta+1)/2 - P_f(N_\theta-1)/2 + c\sqrt{N_\theta} \tag{13}$$

For $\theta = 30^o$, $N_\theta = 3$ and so, $(\sigma_1 + \sigma_2)/2 = \rho_r gh + c\sqrt{3}$ for $\sigma_2 = \rho_r gh = P_f$. Notice also that the shear stress is given by:

$$(\sigma_1 - \sigma_2)/2 = \sigma_2(N_\theta-1)/2 - P_f(N_\theta-1)/2 + c\sqrt{N_\theta} \tag{14}$$

For $\theta = 30^o$ and $\sigma_2 = \rho_r gh = P_f$, $(\sigma_1 - \sigma_2) = 2c\sqrt{3}$ which is independent of fluid pressure. Here $P_f$ is the pore fluid pressure and in this instance corresponds to that pore fluid pressure required to induce yield.

Also, if $P_f = 0$ in expression (13), then one recovers the result of Petrini and Podladchikov (2000) that the mean stress in a dry, cohesionless Mohr-Coulomb material with $\theta = 30^o$ is $2\rho_r gh$. However, the outcome of assuming the pore fluid pressure is equal to the mean stress is illustrated in Figure 8-51c where it is clear that the effective stress state now exceeds the yield in shear and commonly also in tension.

Although expressions (13) and (14) give the mean stress and the shear stress at yield for a plastic material we still need the pore pressure needed to take the total stress to yield (see Figure 8-51d). This is given by:

$$P_f = (\sigma_1 + \sigma_2)/2 - (\sigma_1 - \sigma_2)/2 \sin\theta + 2c/\tan\theta \tag{15}$$

This is the pore pressure at failure that just keeps the pore space open without exceeding the yield stress. For $\theta = 30^o$ the largest $\sigma_1$ can be is $(3\sigma_2 + 2\ c\sqrt{3})$ which corresponds to the situation where the stress circle just touches the failure envelope with no fluid present. Otherwise, if one assumes that $\sigma_2 = \rho_r gh$, then $P_f$ is always less than $(\rho_r gh\ + 2\ c\sqrt{3})$ and, in particular, the fluid pressure is hydrostatic for $\sigma_1 = 2.26$ $(\rho_r gh + 2\ c\sqrt{3})$ assuming a crustal density of 2700 kg/m$^3$. Thus it is quite possible in a deforming Mohr-Coulomb material to have a hydrostatic pore fluid pressure that satisfies the mechanical constraints of keeping the pore volume open.

## Implications for fluid flow regimes in the crust

The governing equations for pore fluid flow are (see Bear, 1972; Scheidegger, 1974):

$$\frac{\partial v_1}{\partial x_1} + \frac{\partial v_2}{\partial x_2} = 0 \tag{16}$$

$$v_1 = \frac{K}{\mu}(-\frac{\partial P_f}{\partial x_1}) \tag{17}$$

$$v_2 = \frac{K}{\mu}(-\frac{\partial P_f}{\partial x_2} + \rho_f g) \tag{18}$$

where $v_i$ are the components of Darcy fluid flow velocity, K is the permeability, $\mu$ is the dynamic fluid viscosity, $\rho_f$ is the fluid density. Equation (16) is the continuity equation that describes the mass conservation of pore-fluid at each point in the crust for an incompressible fluid with no internal fluid sources; equations (17) and (18) are the Darcy equations for flow along horizontal and vertical pressure gradients in the crust. In the simple case we want to consider here we assume that there is no horizontal pore pressure gradient and so $v_1=0$.

Connolly and Podladchikov (2004) have discussed the significance of assuming the fluid pressure to be equal to the mean stress in the viscous regime and have shown, on the basis of such an assumption, that just beneath the plastic/viscous transition there exists a regime where the gradient of hydraulic head is negative so that fluid flow is downwards. Below this is a regime where the gradient in hydraulic head is zero; this corresponds to a regime of stagnant fluid flow. Connolly and Podladchikov then proceed to discuss the implications of the existence of these regimes for the interpretation of layering identified by seismic imaging in the lower crust.

## Coupling between the upper crust and lower crust

Application of expressions (16) and (18) indicates that at the boundary between plastic and viscous materials, the vertical component of fluid flow and the gradient of pore pressure must be continuous. If one adopts (15) and (11) as the expressions for the pore fluid pressure in the plastic and viscous regimes respectively, then these conditions of continuity are not fulfilled at the boundary in the general case, since the pore pressure in the viscous material at the boundary exceeds that in the plastic material by approximately [0.5 $A^{1/N}$ $D^{-1/N}$ exp {Q/NRT}]. The maximum pore

pressure at the boundary is fixed by the plastic material and since the matching pore pressure in the viscous material is significantly less than that given by (11), the pore space in the viscous material must collapse with a resultant decrease in permeability. This collapse in permeability presumably results in very low permeabilities however increases in permeability induced by deformation can result in the transient development of higher permeability. This has been incorporated into the numerical models presented in the following section in the form of hydrofracturing; this means that for plastic materials, if f=0, where f is the yield condition defined by (12), or the tensile yield strength is reached for plastic or viscous materials then the permeability is increased by a factor of ten. Thus the outcome of imposing conditions of continuity of fluid flow across the plastic-viscous boundary is the development of a low permeability boundary just below the interface with overpressured fluid below the layer. The thickness of this layer is governed by expressions (15) and (11) and hence is a function of the geothermal gradient and the constitutive parameters relevant to a particular lithology.

## Numerical simulation of an example

In order to be specific about the principles discussed above we present a numerical example of a section through the crust, 100 km wide and 30 km deep. The top 15 km is comprised of a plastic, elastic-Mohr-Coulomb material whilst the lower 15 km is comprised of an elastic-power law viscous material. The crust is lithologically homogeneous with constitutive properties similar to those of granite. A weaker, plastic fault dipping at 45º is included in the plastic part of the crust in order to simulate the Nagamachi-Rifu Fault in the Sendai situation (see Figure 8-52a). The temperature at the top of the crust is fixed at $0^o$C whilst that at the base is fixed at $600^o$C, corresponding to the Sendai situation. We also consider the result of increasing the thermal gradient so that the base of the crust is $1200^o$C. The crust is fully saturated with water. No advection of heat in the fluid as it moves is included. The fluid pressure in the plastic part of the model is given by expression (15). The permeability of the crust is set initially everywhere at $10^{-15}$ m$^2$. In the viscous part of the crust, if the mean stress given by expression (11) is greater than ($\sigma_2$+T), where T is the tensile strength of the viscous material, the pore pressure is set at ($\sigma_2$+T) and the permeability collapsed to $10^{-16}$ m$^2$; otherwise the pore pressure is set to $\sigma_2$. The model is shortened horizontally at $0.7$x$10^{-13}$/s. In order to simulate natural observations, a pressure seal consisting of a layer with permeability $10^{-16}$ m$^2$ is placed at a depth of 3 km with a hydrostatic fluid pressure gradient above the seal.

Figures 8-52 and 8-53 show the distribution of stress, pore pressure and deformation after 2% total horizontal shortening. Figure 8-52b is the vertical distribution of ($\sigma_1$-$\sigma_2$) and illustrates the influence of pore pressure particularly on the plastic part of the crust where the concept of effective stress is important. The stress difference in the plastic part of the crust is 2c√3 as indicated above whereas in the viscous part the stress difference is given by expression (6). Figure 8-52c shows the vertical distribution of the mean total stress; this again follows expressions (11) and (15); the mean stress is approximately ($\rho_r$gh + c√3) in the plastic regime but increases rapidly at the plastic/viscous boundary as discussed by Stuwe and Sandiford (1994) and indicated by expression (6). Figure 8-52d shows the vertical distribution of pore fluid pressure. Notice that this distribution is close to lithostatic, in the low geothermal

gradient example. In the high geothermal gradient example, the pore pressure rises above lithostatic in the region of porosity collapse just below the plastic/viscous transition but ultimately recovers to lithostatic towards the base of the crust. The vertical distribution of hydraulic head that follows from Figure 8-52d in the low geothermal gradient example indicates that there are no regions of downward flow or of stagnant flow whereas in the high geothermal gradient example two stagnant flow layers are developed (see Connolly and Podladchikov, 2004).
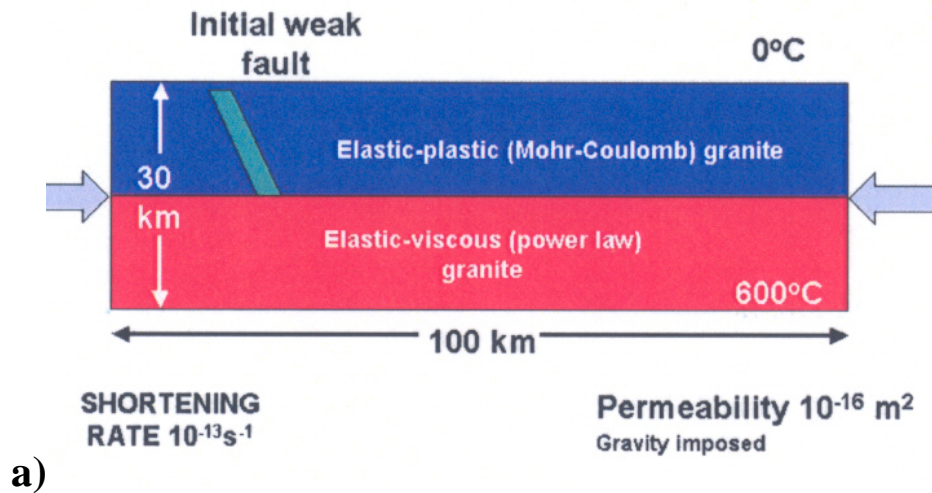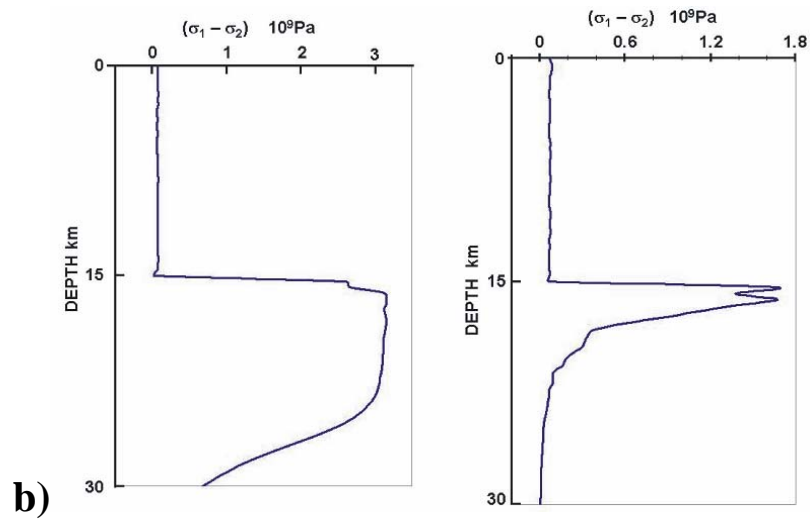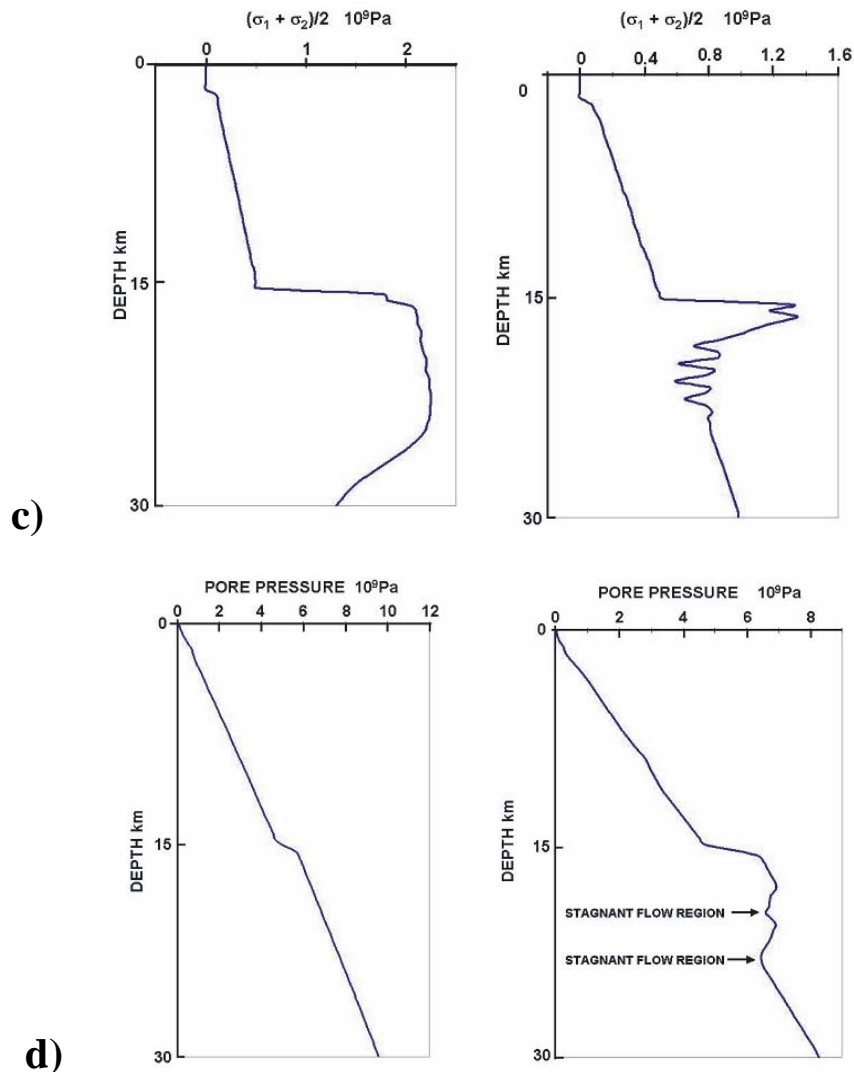
**Figure 8-52: (a) Initial geometry and boundary conditions for the numerical models. Some models were run with the lower temperature fixed at 1200°C; (b) Plot of ($\sigma_1$ - $\sigma_2$) against depth for low geothermal gradient (20°C/km) on the left and high geothermal gradient (40°C/km) on the right; (c). Plot of the mean stress, ($\sigma_1$ + $\sigma_2$)/2, against depth for low geothermal gradient (20°C/km) on the left and high geothermal gradient (40°C/km) on the right; (d). Plot of pore fluid pressure against depth for low geothermal gradient (20°C/km) on the left and high geothermal gradient (40°C/km) on the right.**

For the low geothermal gradient, the pore pressure jumps by an amount equal to the viscous tensile strength at the plastic/viscous transition but otherwise the gradient is close to lithostatic except in the top 3 km. For the high geothermal gradient, the pore pressure again jumps by an amount equal to the viscous tensile strength (somewhat exaggerated here to emphasise the effect) at the plastic/viscous transition but otherwise, again, the gradient is close to lithostatic except in the top 3 km. Following the arguments presented by Connolly and Podladchikov (2004) there are now two zones defined in the lower crust where fluid stagnation occurs. Above each of these zones the fluid flow is downwards whilst below each of these zones the fluid flow is upwards.

Figure 8-53a shows the spatial distribution of ($\sigma_1$-$\sigma_2$) and highlights the discontinuity of stress at the top of the viscous layer. This correlates with a concentration of the maximum shear strain rate in Figure 8-53b indicating a listric transition from the

230

initial fault dipping at 45$^o$ into a shear zone corresponding to the base of the plastic regime. Figure 8-53c shows the spatial distribution of pore pressure whilst Figure 8-53d shows the spatial distribution of permeability arising from hydrofracture evolution.

Both the plastic and viscous portions of the crust dilate during deformation and the patterns of dilatancy are shown in Figure 8-54 for various amounts of shortening and for the two geothermal gradients of 20$^o$C/km and 40$^o$C/km. These dilatant regions correspond to regions of higher porosity and hence higher fluid content. It is proposed that these correspond to the "bright-spots" identified in S-wave seismic images. The dilatant regions are commonly tabular in shape with shallow dips and correspond to dilatant zones on the immediate hanging-wall of the fault as shown in Figure 8-54b or to *en echelon* dilatant arrays as shown in Figure 8-54c. This *en echelon* array is particularly well developed in Figure 8-54c. In all cases these dilatant regions have failed in tension and correspond to regions of increased permeability. Fluid flow is instantaneously increased at yield with strong flow upwards across the isotherms as shown in Figure 8-56. These regions are not "ponding zones" but regions of active transport of fluid when yielding occurs.



231
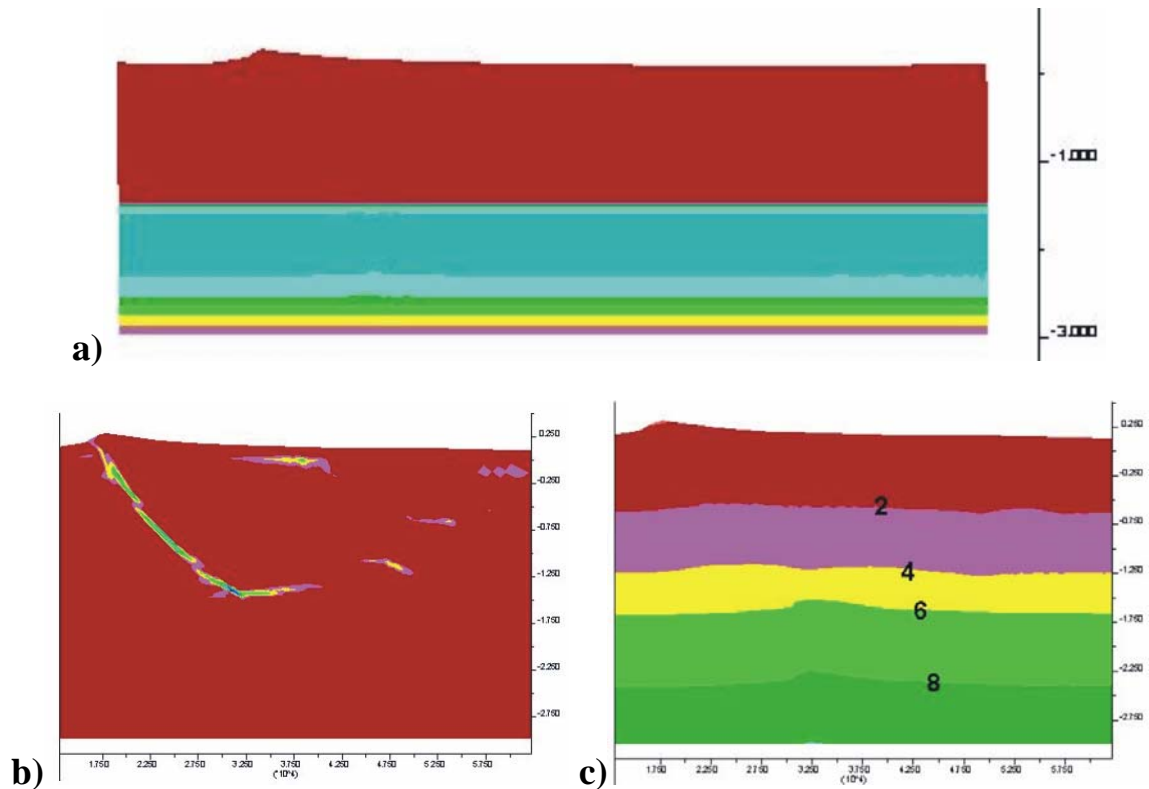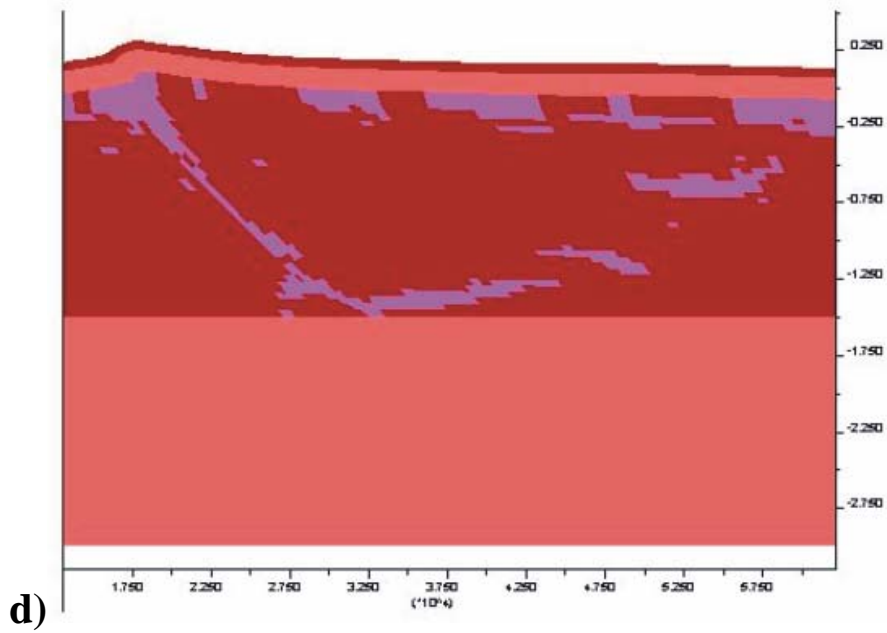
**Figure 8-53: (a) The spatial distribution of ($\sigma_1$-$\sigma_2$), highlighting the discontinuity of stress at the top of the viscous layer. This correlates with a concentration of the maximum shear strain rate in (b) indicating a listric transition from the initial fault dipping at 45° into a shear zone corresponding to the base of the plastic regime. (c) shows the spatial distribution of pore pressure whilst (d) shows the spatial distribution of permeability arising from hydrofracture evolution.**
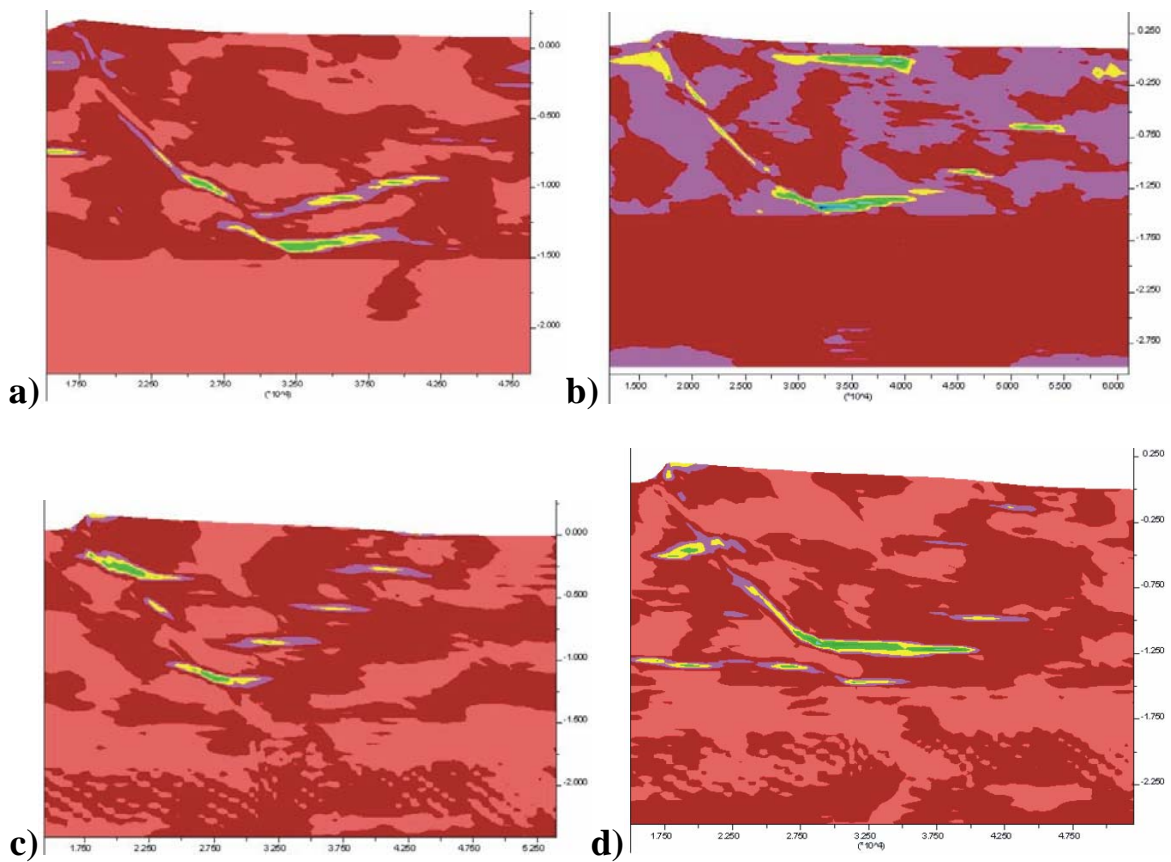
Figure 8-54: (a) Zoom into model with geothermal gradient 20°C/km. Plot of instantaneous volumetric strain rate. Red: $1.6 \times 10^{-11}$ /s, blue: $1.2 \times 10^{-11}$ /s, yellow: $0.8 \times 10^{-11}$ /s. Contour interval: $4 \times 10^{-12}$ /s. Total shortening 1.3%; (b) Zoom into model with geothermal gradient 20°C/km. Plot of instantaneous volumetric strain rate. Light green: $6 \times 10^{-11}$ /s, dark blue: $1.4 \times 10^{-11}$ /s, yellow: $4 \times 10^{-12}$ /s. Contour interval: $2 \times 10^{-12}$ /s. Total shortening 2%; (c) Zoom into model with geothermal gradient 40°C/km. Plot of instantaneous volumetric strain rate. Dark green: $3.2 \times 10^{-11}$ /s, yellow: $2.4 \times 10^{-11}$ /s: Purple: $1.6 \times 10^{-11}$ /s. Contour interval: $0.8 \times 10^{-11}$ /s. Total shortening 1.5%; (d) Zoom into model with geothermal gradient 40°C/km. Plot of instantaneous volumetric strain rate. Dark green: $2 \times 10^{-11}$ /s, yellow: $1.2 \times 10^{-11}$ /s, purple: $0.8 \times 10^{-11}$ /s. Contour interval: $4 \times 10^{-12}$ /s. Total shortening 2%.
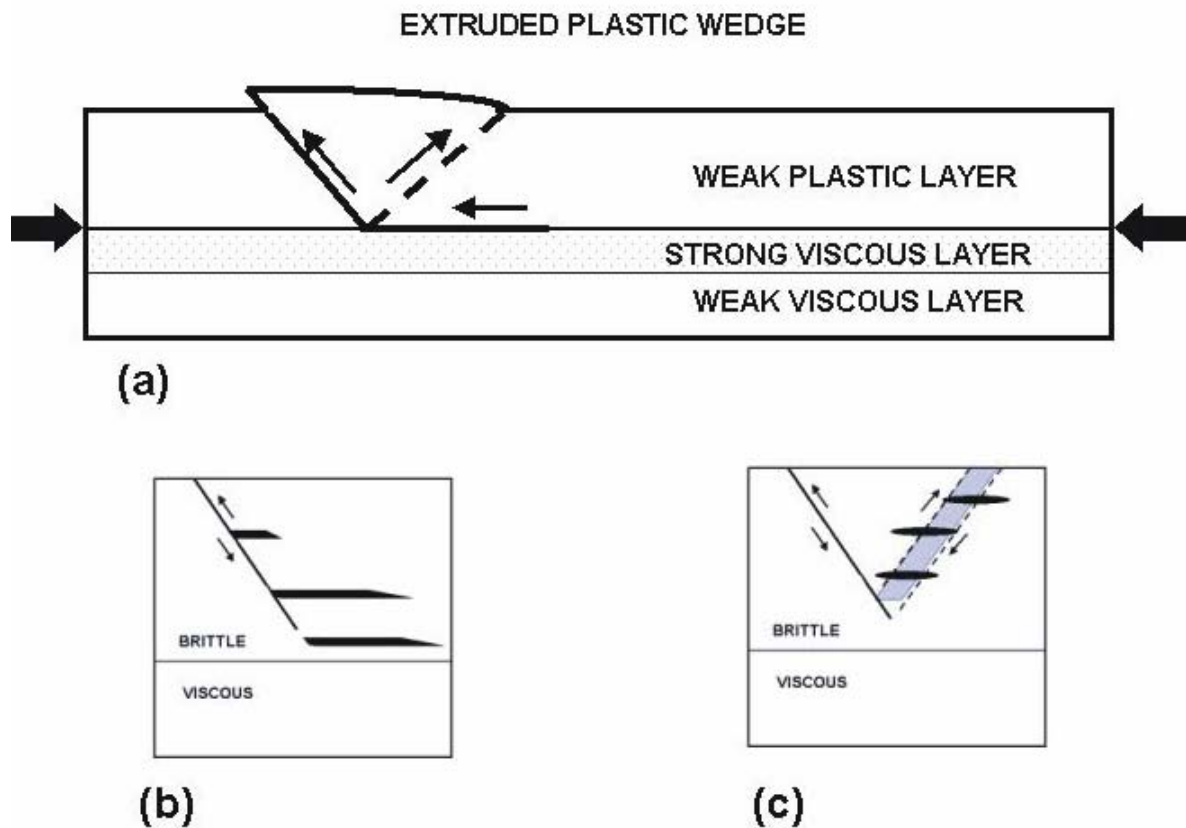


Figure 8-55: (a) Cartoon summarising the essence of the results. Almost all of the strain in the model is partitioned to form a plastic wedge, bounded on the right by the initial weak fault. The development of this wedge is accommodated by sliding on the boundary between the weak plastic upper crust and the strong portion of the viscous lower crust; (b) Cartoon showing the development of tensional dilatant zones on the footwall of a thrust fault; (c) Cartoon showing the development of tensional en echelon dilatant zones within a broad shear zone on the footwall of a thrust fault.

## Summary

At first sight, the proposal that the pore pressure in a deforming rock mass should be equal to the mean rock stress seems quite realistic. However, this situation is not possible in a plastic material characterised by a yield function because in general the material will yield either in shear or tension before this pore pressure is attained. In a Mohr-Coulomb material with a friction angle of 30° and with $\sigma_2 = \rho_r gh$ the pore pressure at yield is always less than $(\rho_r gh + 2\ c\sqrt{3})$. Moreover, in the viscous regime,

233

continuity of normal stress, pore pressure and pore pressure gradient across the plastic/viscous transition means that large pore pressures consistent with the mean stress distribution discussed by Stuwe and Sandiford (1994) cannot be achieved and the pore space within the upper part of the viscous regime must collapse since the pore pressure cannot match the mean rock stress. This situation is reinforced if the viscous material cannot support significant effective tensile stresses when the maximum fluid pressure possible is $(\sigma_2 + T)$, or approximately $(\rho_r gh + T)$ where T is the tensile strength of the viscous material.

The outcome is that the fluid pressure distribution through the crust must be close to lithostatic except at the base of the region of porosity collapse below the plastic/viscous transition where regions of down-flow or of fluid stagnation occur if the geothermal gradient is high. The result is a discontinuity in the pore pressure at the plastic/viscous transition but the jump is only as large as the tensile strength of the viscous material.
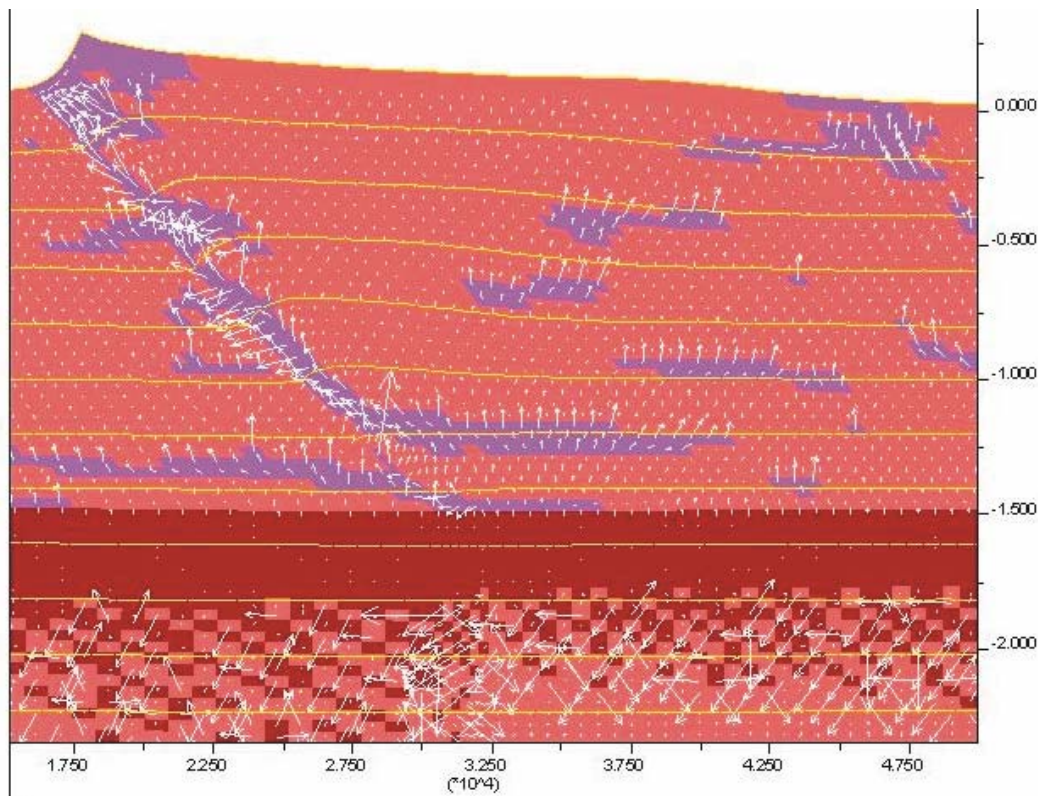


**Figure 8-56: Zoom into model with geothermal gradient 40$^{o}$C km$^{-1}$. Permeability 10$^{-16}$ m$^2$, red; 10$^{-15}$ m$^2$, pink; 10$^{-14}$ m$^2$, purple. Isotherms at 100$^{o}$C intervals with 0$^{o}$C at the surface. Darcy fluid flow vectors in white; maximum 6x10$^{-7}$ m s$^{-1}$.**

With the above basic principles in mind, it is then possible to model the geometry of the Nagamachi-Rifu Fault. Dilatant zones, representing zones of increased porosity and hence fluid content, develop as approximately horizontal tabular regions mainly on the hanging wall of the fault and as en echelon arrays along a diffuse shear zone conjugate to the main fault. This pattern of dilatancy is the direct result of the formation of a plastic wedge and the shear accommodation at the base of the plastic upper crust as shown in Figure 8-55a. As the deformation continues the main region

of dilatancy is concentrated in a horizontal tabular zone coincident with the listric continuation of the original fault. This mimics the observed seismic images of the Nagamachi-Rifu Fault system quite closely and suggests a general origin for seismic reflectors in other environments (see Drummond et al., 2004).

In particular, as indicated in Figure 8-56, the dilatant regions that develop are regions of strong instantaneous fluid flow upwards across isotherms. Hence, following the arguments of Phillips (1991, p. 107) that the rate of mineral alteration is proportional to the scalar product of Darcy flow and the temperature gradient, one would expect mineral alteration haloes such as precipitation of quartz and alteration of feldspar to micas in association with these regions. Although the increase in fluid content associated with increased porosity is presumably what is imaged by seismic studies in modern terrains, it is perhaps this alteration that is identified in modern seismic images of ancient "bright spots".

## Implications for predictive mineral discovery

Regions of stagnant fluid flow develop in the viscous lower crust. Here, reversals in the gradient of hydraulic head in the lower crust result in down flow and up flow regions with stagnant flow regions between.

Mineral alteration will still be associated with these zones but the style of alteration will be asymmetric in the sense that it will be different on the upper and lower surfaces of the layers. This arises since the top of one of these layers is associated with fluid flow *up* a thermal gradient whereas the base of the layer is associated with fluid flow *down* a thermal gradient.

Perhaps future seismic imaging can distinguish between the symmetric alteration patterns to be expected with bright spots in the upper crust as opposed to asymmetric alteration to be expected with bright spots in the lower crust?

## Metamorphism and the 3D distribution of isograds

*P. Henson and R.S. Blewett*

Within the *pmd*\*CRC Y2 project an attempt has been made to delineate metamorphic isograds in the third dimension based on the work by Mikucki and Roberts (2003) (Figure 8-57). These data are complex although there are several major observations that will be analysed in an attempt to understand better the patterns we see in the two-dimensional data and then extrapolate them into the third dimension.
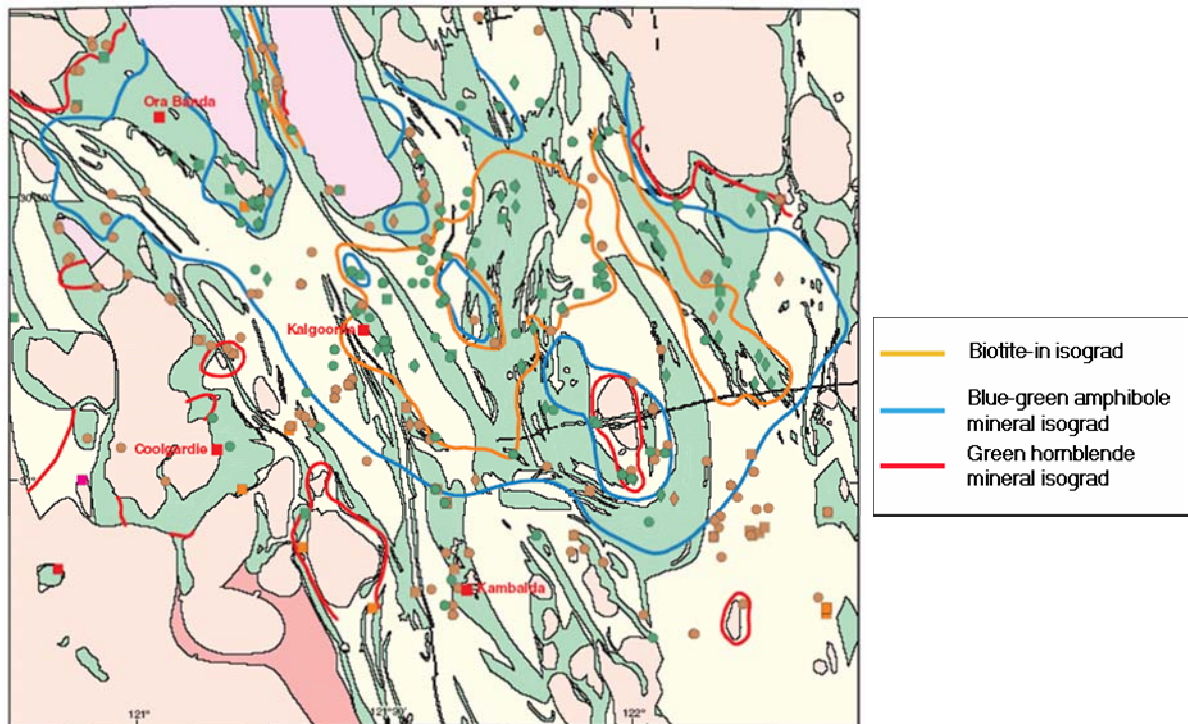
**Figure 8-57: 2D image of the metamorphic isograds in the Kalgoorlie/Kambalda region from Mikucki and Roberts (2003).**

This study was not intended to answer all of the questions posed from the original data set, instead it is an example of viewing and analysing the data using a 3D medium and some of the additional insights that can be learned from this technique. Some of the 2D and 3D questions that these data pose are:

- How many metamorphic events are there?
- What is the metamorphism related to? deformation? granites? both?
- What is the 3D distribution of isograds?
- Why do isograds cross-cut major structures?
- Why do concentric, high metamorphic grade zones correspond to gravity highs?

These questions are clearly linked to the geodynamic processes in the eastern Yilgarn and therefore need to be incorporated into the overall interpretation of the region and the construction of the 3D map. Their patterns also relate to fluids and their sources or reservoirs.

## Methods

There are four distinct metamorphic zones delineated by Mikucki and Roberts (2003):

- rocks absent of biotite (Biotite absent);
- rocks containing biotite (Biotite-in isograd);
- rocks containing blue amphibole (Blue amphibole mineral isograd), and;
- rocks containing green hornblende (Green hornblend isograd).

The process of incorporating metamorphic isograds into the third dimension requires a semi-continuous isograd (see Chapter 2 for discussion of the surface construction methodology). This required discontinuous segments of an isograd to be joined for continuity and once the isograd is delineated, a surface can be constructed from the 2D isograd. The constructed surface could then be constrained to absolute (drillhole data), or interpreted locations of the metamorphic isograd in the third dimension. Due to lack of metamorphic data from drillhole locations, this interpretation was based purely on an interpretation of the approximate metamorphic grade in the third dimension.

Two surfaces were built in the 3D map: 1) biotite-in isosurface, and 2) blue amphibole mineral isosurface. The green hornblende isosurface could not be constructed due to its discontinuous representation in the original 2D data. These two surfaces therefore delineate the three lowest metamorphic grade regions within the Kalgoorlie-Kambalda region in the third dimension.

## Interpretation of the 3D isosurfaces

Regions of biotite-absent rocks host both the Golden Mile and Kanowna Belle deposits (Figure 8-57), which lie close to the boundary with rocks containing biotite. Biotite occurs at depth beneath these deposits, and it is likely that the mineral system or alteration envelope mirrors the shape of the 3D biotite isograd at depth.

## Explanation for the low-grade zone at Kalgoorlie

The Kalgoorlie region lies within an anomalous depression of low metamorphic grade rocks (biotite absent). This depression in the isograds can not be explained easily by the architecture of the area, which is a north-plunging anticline. The metamorphic grade cross-cuts major '$D_2$' structures and, therefore, the metamorphism is probably related to post-'$D_2$' thermally induced sources. One possible explanation for this anomaly lies in the transfer of heat within country rocks through both conduction and/or convection.

Work by Spear (1995) indicates that the major perturbations in the isosurfaces will occur above a heat source, which is variable depending on the convection cells generated by it. Spear's modelling indicates that the isosurfaces will be asymmetrically distributed about the thermal source, with a broad region above and narrow region on the flanks of the source.

Little is known about the geometries of metamorphic isograds in the third dimension, although the introduction of 3D technologies facilitates a greater degree of understanding of the metamorphic process and its implications for mineral systems. At Kalgoorlie there is a perturbation in the biotite-in isograd corresponding to an anomalous low metamorphic grade zone at Kalgoorlie, which could be induced by localised convection. On the assumption that convection reduces metamorphic grade, could we view anomalous low (metamorphic grade) zones as areas where convection has operated during the process of metamorphism? Additionally, are these zones regions where significant fluid flow has occurred during the process of convection? Hagemann and Cassidy (2001) implied that meteoric fluid played a part in the formation of gold deposition in the EYC. Furthermore, Heath's (2003) studies on the

Golden Mile indicated that meteoric fluid played a large part in the formation of this deposit and that significant fluid was involved in the overall metamorphic assemblages and ore forming processes. There are however, numerous other processes that could explain the current day metamorphic isograds, and the timing of events has not been thoroughly researched.

Construction of 3D metamorphic isograds of the EYC has proven to be very thought provoking and could have real implications for mineral systems. A depression in the biotite-in isograds at Kalgoorlie could reflect a region where interaction between hot gold-rich metamorphic/distal and/or magmatic(?) fluids interacted with meteoric fluids. These scenarios have been postulated by Hagemann and Cassidy (2001) and Heath (2004) (Appendix 8-4). This interaction could have lowered heat within the region through increased convection and therefore the metamorphic isograds reflect a depression in the 3D isosurface. If this were correct, other major fault systems with anomalously low-grade zones could indicate that hydrothermal cells were operating. Can we therefore use anomalous depressions in the biotite-in isograd as a proxy to determine where hydrothermal cells operated and, if this is possible, can we use it as a targeting tool for exploration?

## Metamorphic highs: granites or other sources?

A comparison of the metamorphic isograds with potential-field data reveal that metamorphic highs are often independent of structures (overprint them) and may, or may not, correspond to gravity lows. Figure 8-58 shows the correlation between metamorphic highs and potential-field data at three locations on a NNW trend. One location is just north of Kanowna Belle and the remaining two locations are to the south of it.

The southern location corresponds to a Low-Ca granite and consequently has a gravity low spatially associated with it. A thermal anomaly associated with emplacement of this granite is suspected here. However, the other two locations have the same relatively high metamorphic grade but are coincident with relative gravity highs (high density). The gravity high is unlikely to be due to significant granite providing heat, another cause is likely. It is not conclusive that the relative high-density area is genetically related in any way to the relatively high-grade metamorphic area (they are simply spatially coincident).

An obvious question concerns the cause of the metamorphic grades, and are we viewing the representation of several metamorphic events or multiple sources (including dense mafic intrusions)?
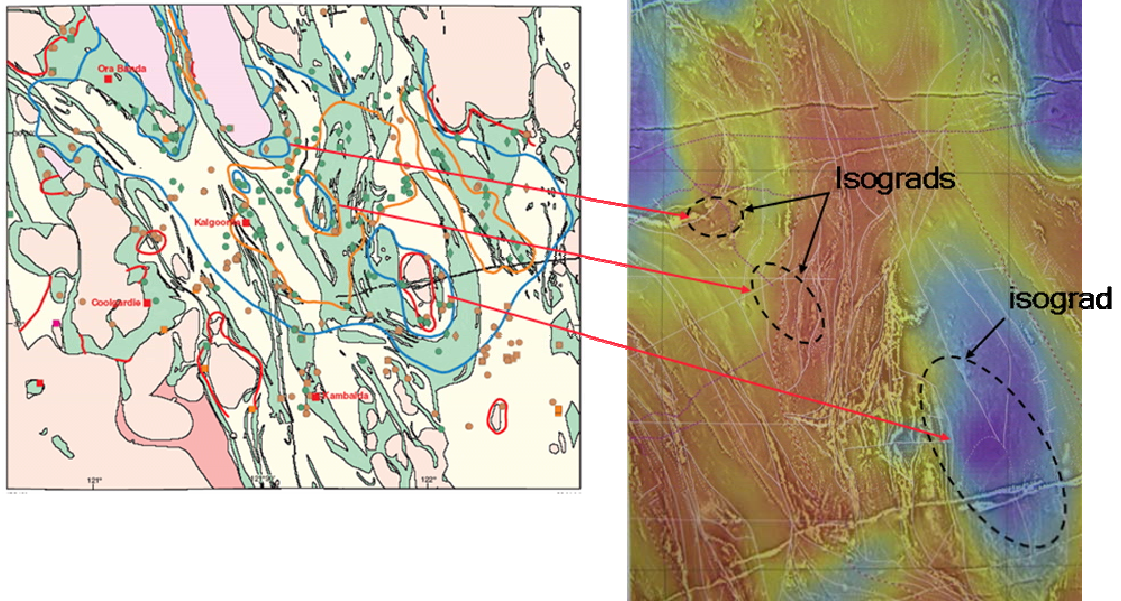
**Figure 8-58: Concentric zones of high metamorphic grade from Mikucki and Roberts (2003), compared spatially to potential-field data displayed as a composite magnetic and false colour gravity image. Note the southern anomaly is coincident with a mapped granite and associated gravity low (blue colour). The northern two anomalies are coincident with relatively high gravity (red colours), these are unlikely to be caused by significant volumes of granites.**
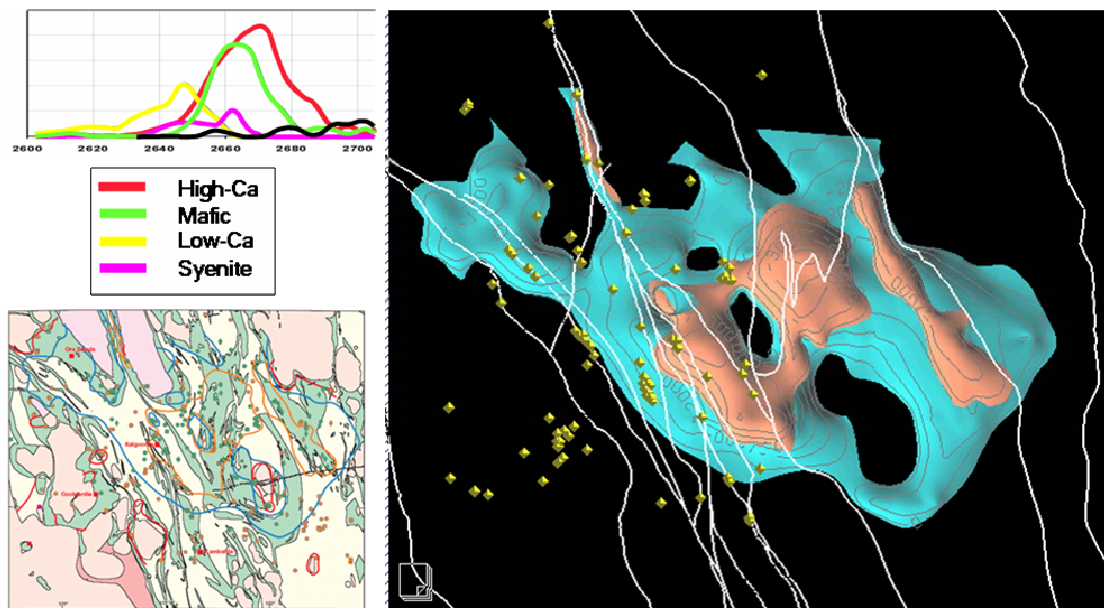


**Figure 8-59: 3D movie of the spatial and age relationships between High-Ca granites (red polygons); Low-Ca granites (yellow polygons); mafic granites (green polygons) and syenites (purple polygons); with gold deposits (gold diamonds) and metamorphic isosurfaces: biotite-in isosurface (orange); blue-green amphibole mineral isosurface (blue), in the Kalgoorlie-Kambalda region.**

Appendix 8-4 is an animation showing the metamorphic isograds and their relationship to other features of the 3D map. **(Appendix 8_4 Metamorphic movie.avi)**

## Implications for predictive mineral discovery

Constructing three-dimensional metamorphic isosurfaces from 2D isograds has introduced an additional way to view and interpret metamorphic assemblages. Further integration of drillhole data into this process could refine the location of isosurfaces in the third dimension, which would contribute to our understanding of mineral systems and their heat- and fluid-flow regimes.

Anomalous low metamorphic grade areas have been identified as regions of possible fluid down-flow zones, associated with the interaction between meteoric fluids and gold-rich fluid (possible gold indicators)? Anomalous areas of higher metamorphic grade may correspond to zones rich in mafic granites/porphyries and the indicators of favourable regions for gold.

## Low-angle shears (LASHs), fluids, and the brittle-ductile transition

The seismic reflection data reveal several strong reflections within homogeneous(?) felsic gneiss (beneath the base of greenstone) that have ambiguous origins. These features have been called Low-angle shears or LASHs (see Chapter 3 and associated appendices for further images). The hypothesis proposed here is that these strong reflectors represent faulting or shearing that was principally localised onto discrete planes (~10 km depth) that represent the seismogenic brittle-ductile transition.

In the modern-day San Andreas Fault, numerous monitoring locations of seismic activity indicate that the majority of movement occurs at approximately ~10 km depth. This level approximates the present day brittle-ductile transition (Figure 8-60).
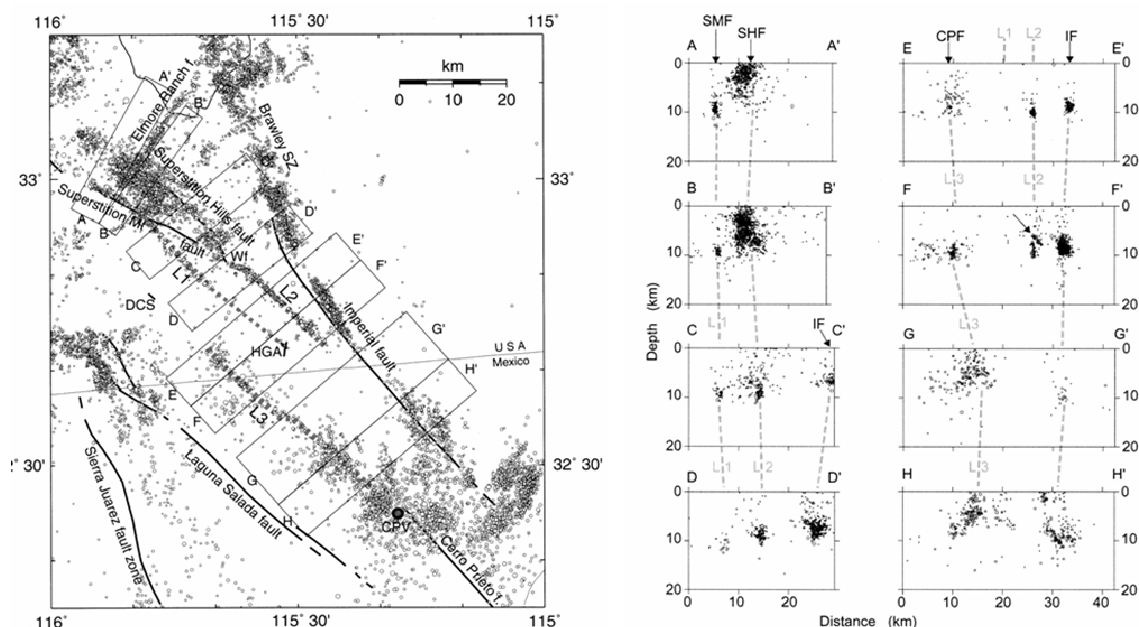


Figure 8-60: Image from Magistrale (2002) displaying the focus of seismicity with depth within the San Andreas Fault system. Note that the peak of the hypocentres (seismicity) is located at around 10 km depth. It is postulated that this is a region of enhanced fluids and weakening and/or represents the brittle-ductile transition.

Assuming that this brittle-ductile transition hypothesis is correct for the formation of the LASHs, we must then explain why there is a velocity contrast corresponding to a

240

shear zone (i.e., a seismic signature). Fluids and alteration have been postulated as likely causes. Klaus Regenauer-Lieb (*pers. comm.*, 2004 ) suggested that the LASHs represent a fluid interface. Barry Drummond (*pers. comm.*, 2004) and Drummond et al. (2004) suggested that the strong reflectors represented a fluid-ponding interface.

Either way, this region or crustal level would be a zone of weakness developed during stress driven deformation processes and could therefore develop a variation in seismic character detectable today.
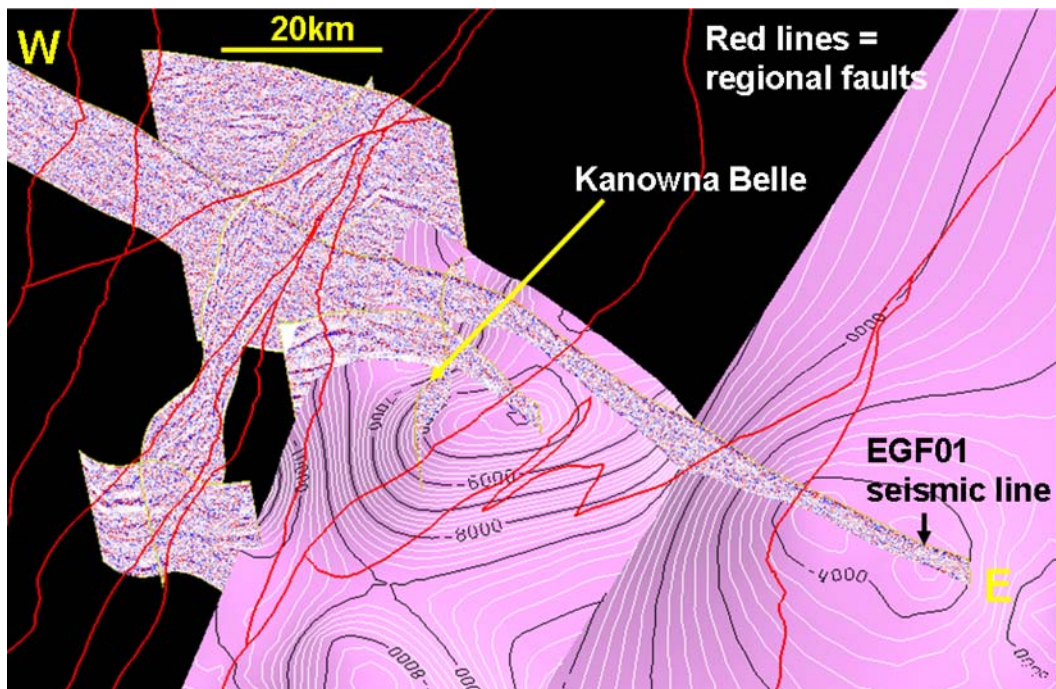


Figure 8-61: Screen capture from Gocad displaying a series of seismic reflection lines (purple and white surfaces) in the Kanowna Belle region. The pink surfaces are domical structures interpreted from seismic reflections.

The LASHs display a complex structural history and are now clearly at a much higher crustal level due to erosion as well as several orthogonal deformations. One example is the domical shear beneath Kanowna Belle. This dome is approximately 30 km across with depths ranging from 4 km in the centre to 9 km at its margin (Figure 8-61). Estimates of erosion from the preserved metamorphic grade at the present surface indicate that about 5-8 km of material has been eroded.

If the estimate of the eroded depth is added to the present day depth of the LASH under Kanowna Belle, a depth of 10-12 km can be inferred for the formation of this structure. This is similar to the present day depths of the brittle-ductile transition.

The presence of vertically stacked LASHs, if produced at the brittle-ductile transition as suggested, can then be used to provide relative histories of uplift and burial for the region during multiple (D1? D2?, D3?) deformation events (Figure 8-62). Figure 8-62 shows a seismic section from Leonora to the Kilkenny fault zone to a depth of about 15 km. Note the series of stacked LASHs in the section. Successive uplift and erosion events occur between each main deformation event ($D_1$, $D_2$, $D_3$). This results in the previous (palaeo)brittle-ductile transition "rising" in the crust and becoming

deformed. With time and depth, the successive LASHs becomes simpler and flatter. For an alternative interpretation of this geometry, see the later section in this chapter on diverging seismic reflections.
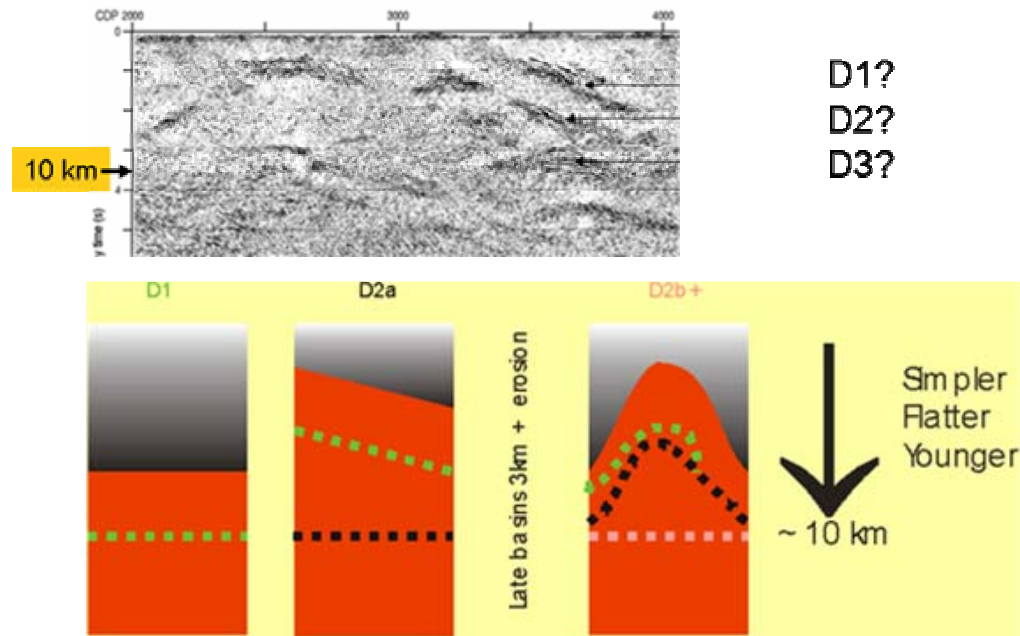


**Figure 8-62: The development of shearing at the brittle-ductile transition during multiple deformation events is revealed by multiple LASHs in the seismic section (example from far western end of 01AGSNY1 between Leonora and the Kilkenny shear zone). Uplift and erosion between successive events means that the previous (palaeo)brittle-ductile transition "rises" in the crust and itself becomes deformed. In the cartoon, D1 is the green line, D2 is the black dashed line and D3 is the pink dashed line. Note how that LASH becomes simpler, flatter and younger with depth.**

## Implications for predictive mineral discovery

The interpretation of the LASHs as reflecting (pun intended) the (palaeo)brittle-ductile transition has important implications for fluid flow and a source or reservoir for mineralising fluids.

The ability to track the history of the development of this surface in the crust through time has implications for the geodynamic evolution of the region. The cycles of deformation, uplift and erosion appear to broadly tracked in the seismic data.

## *Question 5—Metal transport and depositional processes*

*P. Henson and R.S. Blewett*

Ellis (1939) was ahead of his time in articulating a mineral systems approach to the understanding of lode gold in the Yilgarn. He suggested that structure (pathways) and

the presence or absence of cross-folding was of paramount importance in determining the localities of gold deposition.

The following section discusses one of the principal findings of the Y2 project – the role of a domical architecture at various scales and crustal levels and their possible role in focussing fluids for gold deposition.

## Domes and basins and their role in fluid focussing

The EYC contains the majority of known major gold deposits within the Yilgarn Craton, and as a result, has had intense scientific research directed at it for decades. The surface exposure of the Yilgarn Craton consists of a variety of lithological units although it is dominated by a suite of geochemically unique, variable aged granites and gneisses. These units are mantled by thin greenstone sequences that in some cases form **domical** structures around their margins.

The significance of these domical structures should not be underestimated and in fact several world-class gold deposits are situated above or on the margins of these structures (e.g., Kanowna Belle; Wallaby Mine; St Ives and Golden Mile). The question therefore is; what do the domical structures have to do with fluid focussing and can we use these geometries to find other world-class gold deposits?

## History of domes and gold deposits

This study has identified the significance of domical structures in the EYC through detailed analysis of geophysical and structural datasets, although the significance of domical structures and their relationship to gold deposition was first identified by Ellis (1939). He recognised that cross-folding, or orthogonal folding, in the Southern Cross Province produced a pronounced dome and basin geometries. Spatial correlation between these structures and gold deposition lead him to conclude that the domical parts of this geometry were zones of preferential gold deposition (Figure 8-63).
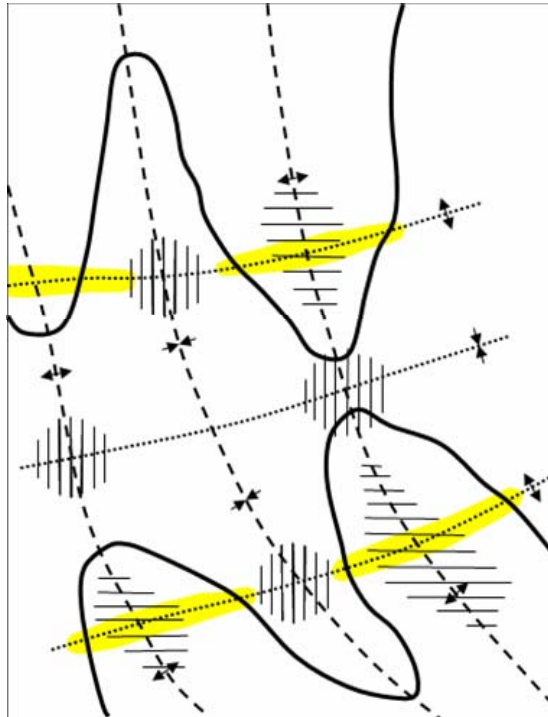
**Figure 8-63: Sketch of cross folding in the Southern Cross Province, Yilgarn Craton, from Ellis (1939) showing the areas of most favourable gold deposition (yellow) at the junction of two overprinting antiforms (see also Chapter 7).**

Close inspection of seismic data throughout this region reveal that there are several different layers within the crust that contain domical structures including:

1. middle crust imbricates;
2. domes/anticlines within the felsic gneiss below the base of the greenstones, and;
3. domes/anticlines within the upper crustal greenstone units.

The following section considers the development of the domes from the long-wavelength deeper domes in the mid crust up to short-wavelength domes in very upper crust. All these domes stack upon each other and form ever finer "funnels" for delivering focussed fluids to the deposition site.

## Domes in the mid crust

Structures within the mid crust resembling large crustal imbricates were first identified by Drummond et al. (1997) (Figure 8-64). The initial interpretation was mainly based on the east-west orientated 91BMREGF01 seismic line through the Kalgoorlie region, which imaged a series of large west verging imbricate structures. The process also attempted to identify the 3D geometry of these structures using seismic cross lines through the region, and although there were only limited data, it was concluded that the structures clearly have a domical geometry. In the north, the Leonora Laverton 01AGSNY1 seismic line also clearly imaged west-verging structures thought to be mid crust imbricates, further suggesting that the structures are regionally significant. These domical structures occur beneath what the early researchers (Drummond et al., 1997) termed the detachment surface, which was

interpreted as a semi-continuous zone at the base of the upper crust in the 91BMREGF01 seismic line.
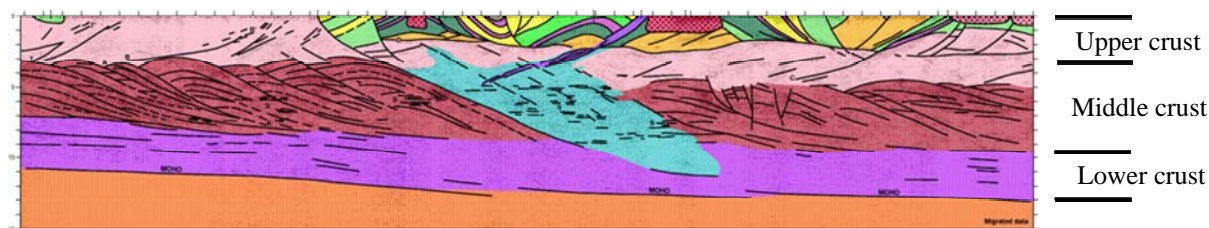


**Figure 8-64: 91BMREGF01 seismic line, from Drummond et al. (2000) showing mid crustal imbricates (dark red layer). In 3D these imbricates are domical.**

## Domes in the felsic upper crust (below the greenstone base)

A series of reflectors occur below the base of greenstone sequences and in at least one location at Kanowna Belle have been interpreted to represent a domical structure. The structure was identified using the mig99Y2 and mig99Y5 seismic lines that cross each other in the vicinity of the Scotia Kanowna Granite. This domical structure occurs above the original detachment surface although is well below the base of greenstone, determined using potential field modelling within the region. It therefore questions the interpretation of the "detachment" surface (from 91BMREGF01 seismic line) being a semi continuous layer.

Close inspection of the 01AGSNY1 seismic line through Leonora and Laverton also revealed that a series of discontinuous reflections and not a continuous structure occur below the base of greenstone. The 'detachment' is likely to be a series of discontinuous sub-horizontal thrusts developed at different times at around the crustal level of the brittle-ductile transition (see section on LASHs above).

## Domes in the upper crust (within the greenstones)

The solid geology map of the EYC clearly depicts domical structures on both a small and a large scale. Regionally the erosional remnants of domical structures are evident around numerous granitic bodies and the overall the architecture of the area displays an elongate NNW trending dome and basin geometry. These geometries are clearly complex and in many locations truncated by variably orientated late-stage faults. Many of the domes in the upper crust are attributed to thrust stacking although they may also be linked to granitic intrusions (laccoliths) coeval with deformation.

| Swager, 1997 | | | This study | | | |
|---|---|---|---|---|---|---|
| DE | N-S? extension | ⇕ | $D_E$ | N-S extension | ⇕ | |
| $D_1$ | N-S contraction | ↧ | $D_1$ | N-S? contraction | ↧ | |
| | | | $D_{2a}$ | E-W contraction | →←| Orogenic Surge |
| $D_{2e}$ | E-W extension | ←→ | $D_{2E}$ | E-W extension ('late basins') | ←→ | |
| $D_2$ | E-W contraction | →←| $D_{2b}$ | E-W contraction | →←| |
| | | | $D_3$ | ~N-S contraction | ↧ | Domes |
| $D_3$ | E(NE)-W(SW) contraction | ↗↙ | $D_4$ | E(NE)-W(SW) contraction | ↗↙ | |
| $D_4$ | E-W regional contraction | →←| $D_5$ | E-W regional contraction | →←| |
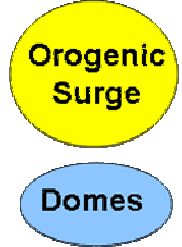
**Figure 8-65: Comparison between the Swager (1997) deformation history and the *pmd*\*CRC Y2 project study. Main differences are the more complex $D_2$ series of events (Wangkathaa orogeny) and the late ($D_3$) N-S contraction. The superposition of the east-west $D_2$ contraction and the north-south $D_3$ contraction is believed to be important further developing the domical geometry, at least in the upper crust.**

The development of the LASHs into domical structures is clearly linked to the deformation history and geodynamics. Construction of the 3D map identified additional deformations adding to the complexity of the Swager's (1997) definition (Figure 8-65) including a post $D_2$ N-S contractional event ($D_3$ this study).
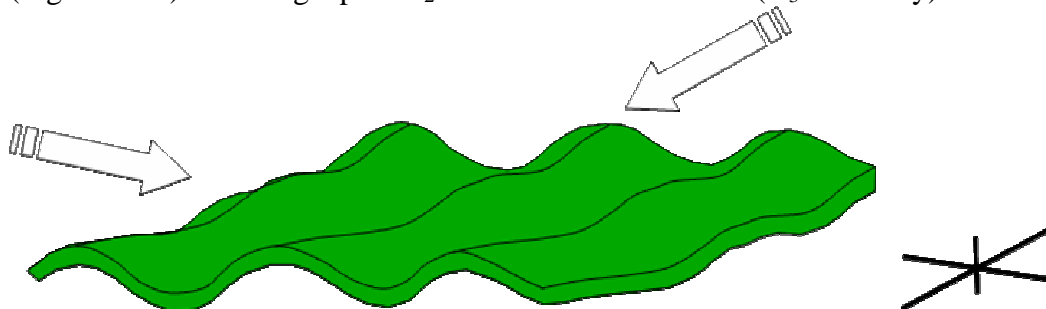


**Figure 8-66: Schematic diagram of the dome and basin development produced by two orthogonal deformation events (Type I fold interference pattern of Ramsay, 1987).**

The development of the domes may therefore be a result of regional north-south trending anticlines (developed during $D_2$) that were in turn folded orthogonally during the $D_3$ event (Figures 8-65; 8-66).

There is also a possibility that the domical architecture was partially developed during the east-west thrusting via differential movement along thrust planes (Figure 8-67). Thrusts do not continue along strike to infinity, despite the 2D cross-sectional view commonly envisaged. Thrusts typically develop antiformal stacks or culminations (Butler, 1983) which results in the development of domes, or the differential movement on the thrust planes also creates a dome.
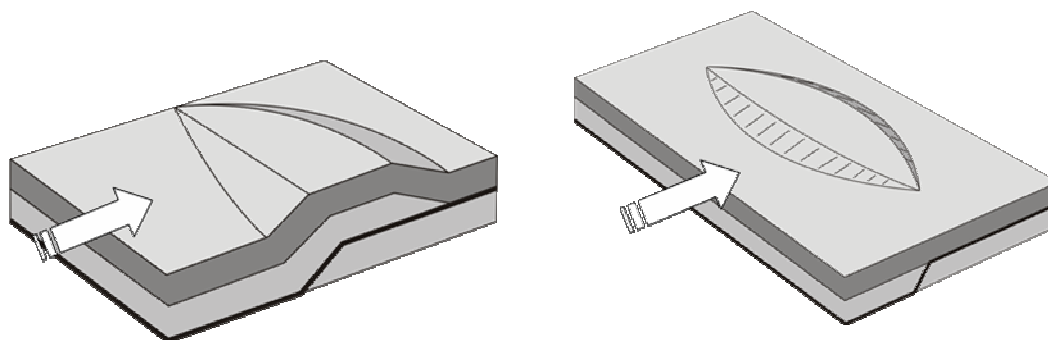
**Figure 8-67: Localised dome development from differential movement on thrust surfaces.**

The third process that could have played a role on developing domes in the upper crust is the intrusion of granitic sills/or laccoliths associated with the deformation process.

It is likely that all three processes outlined above had a role in developing the architecture of the domes. The importance for the mineral system is the timing of the fluids with respect to the development of the focussed pathways (domes) and the traps.

## Significance of domes for fluid focusing and gold deposition

Worldwide there appears to be a close association between anticlinoriums and in many cases domical structures with major gold deposits. The significance of this can not be understated, and if these structures are in fact a critical aspect in gold formation then we should endeavour to identify their locations within areas of outcrop and more significantly in areas undercover.

Along east-west oriented seismic lines these LASHs are clearly folded into broad antiforms and locally disrupted (interpreted to reflect continued $D_2$ contraction - $D_{2a}$, $D_{2b}$). A number of important deposits, e.g., Kanowna Belle, Golden Mile, are located in the region above these domes, suggesting a relationship between domes and gold mineralisation. Late structural breaches (late-$D_2$, $D_3$-$D_4$) of the domes associated with deformation may allow concentration of gold-rich fluids (formed at the brittle-ductile transition?) within the domical structures to migrate higher in the crust. The somewhat loose analogy is with the petroleum system, where oil and gas migrate up gradients using permeable pathways into antiformal or domical trap areas.

Mapping of the LASHs could therefore be a critical step in area selection for possible sites of gold mineralisation. The combination of large-scale faults intersecting domical traps may prove to be a viable fluid pathway during gold mineralisation (as per the petroleum analogy). The combination of a fluid pathway (fault system) and focusing mechanism (stacked series of domes) may explain the system. Empirically, this conjunction of pathway and focussing architecture has been demonstrated by the *pmd*\*CRC A1 project (see Chapter 7). Temporally however, it is only when the domes are breached (during late-$D_2$, $D_3$-$D_4$) that mineralisation occurs in the upper-crustal units, suggesting that mineralisation is largely late in the $D_2$ sequence of events (e.g., Groves, 1993).

## Area selection techniques and mapping domes

The processes involved in dome development are complex, although there occurrence clearly correlates with gold deposits in the Yilgarn Craton and worldwide (Chapter 7). Domical structures appear to develop at different levels in both the middle crust and upper crust and therefore could provide an architecture that can potentially focus Au-rich fluids via a similar mechanism to oil migration (less dense hot fluids). Identification of domes at different levels of the mid and upper crust could be interpreted as a multilevel focussing geometry, focussing fluids into locations of deposition (Figure 8-68).
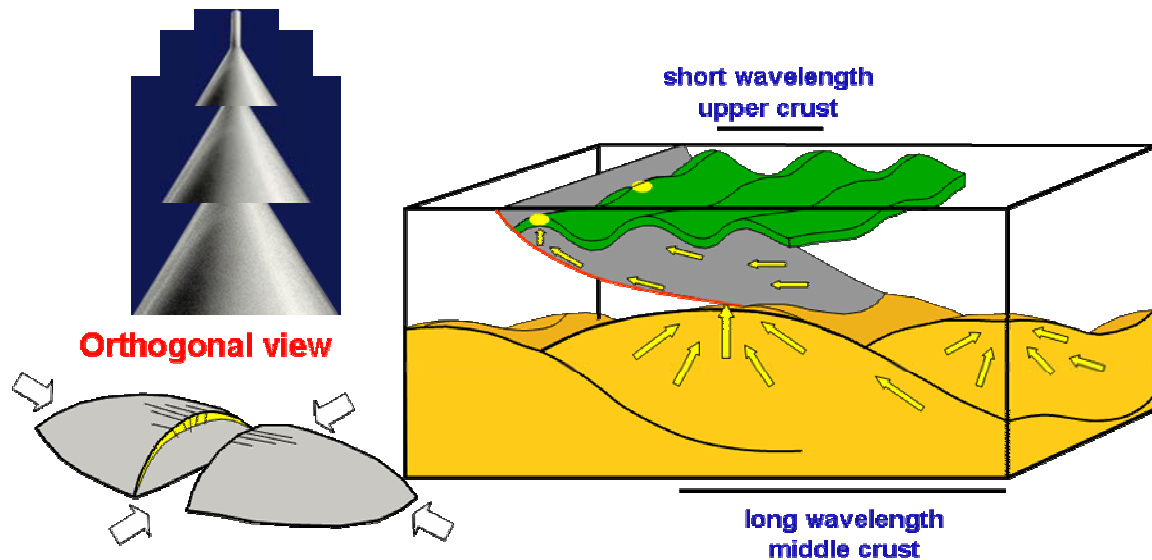


**Figure 8-68: Cartoon of the differing wavelengths of coincident or stacked domes at various levels in the crust. The wavelength of the domes increases with depth. The result of stacking ever-more focussed domes one on top of the other results in the delivery of very highly focussed mass and fluid flux into the upper crustal traps. The fault planes that are folded into the domes are the fluid pathways, which on breaching by later faults releases the fluid up the breaching the fault to net highest and more focussed level. A simple analogy is stacking of smaller and small funnels on top of one another.**

The identification of domical structures using seismic reflection data may prove to be effective for area selection. However, the coverage of regional seismic data will always be limited.

The process of comparing domes interpreted using seismic techniques with 3D isosurfaces developed using 3D inversion of potential field data may prove a viable and effective for mapping domes at a regional scale. Further work is needed to refine the process and constrain the detail needed to define domes in areas of complex geology (see Chapter 2).

The process of seismic interpretation within the *pmd*\*CRC Y2 project was initially conducted using the conventional method of interpreting individual paper copies of the seismic lines. During this process interpretations were made of individual seismic lines and some thought was given as to how they relate to other cross-lines and lines in close proximity although this is a difficult task due to the lack of spatial correlation. Using Gocad seismic lines can be positioned in true georeferenced space, enabling seismic cross-lines and lines in close proximity to be compared against one another.

There are major benefits in using this technique, including: spatial comparison between domes interpreted using seismic techniques with potential field data, including 3D inversions of gravity data.
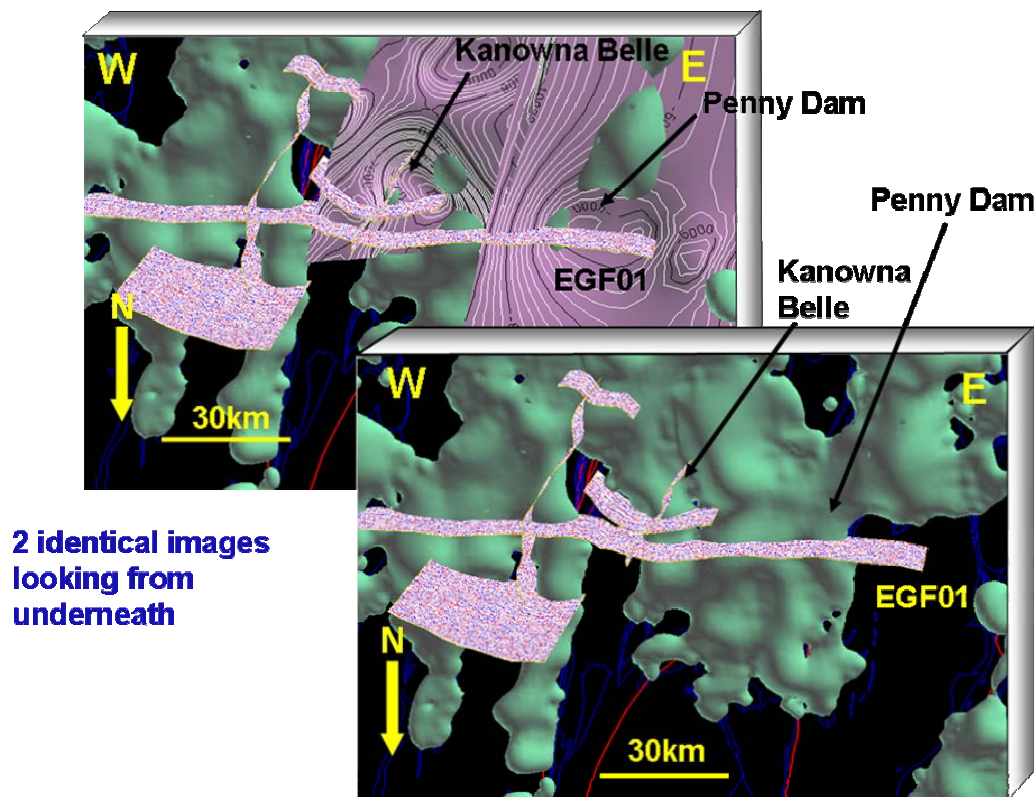


**Figure 8-69: Two identical screen captures from Gocad looking from underneath 1) Displaying the dome interpreted at Kanowna Belle (pink surface with contours) using seismic reflection lines superimposed on the 3D gravity inversion isosurface (green surface) and the seismic reflection lines. 2) Identical image without the surface interpreted from seismic. An additional dome was also interpreted at Penny Dam although it was only constrained using one seismic line.**

3D inversion data have proved to closely match the gross geometries seen in the seismic data at Kanowna Belle. At this location domical structures were also identified in the interpreted base of greenstone (Figure 8-69). Inversion techniques are still in development and further study would be needed to prove that the technique identifies similar features to seismic data in all locations. The advantage of this technique is that it is a regional coverage and therefore it has the potential to provide a tool to explore for domical targets both in areas of outcrop and undercover.

## Diverging seismic reflections: Implications for gold deposition

The role of granites in the minerals system need so be factored into any model for the EYC. The significance of granites is dependant on the part they play in both pre; syn and post gold deposition architecture and possible syn-gold fluids that they introduce to the processes.

As discussed above, several large gold deposits in the EYC are associated with domes or anticlinoriums. In two locations: 1) Wallaby Mine; 2) St Ives, these domes are well imaged by seismic reflection lines that run through the mine regions. A common

feature of both these areas is presence of a sub-horizontal reflector that diverges from the overlying anticlinal reflector (Figure 8-70). Interestingly, where the maximum divergence between these reflectors occurs, large gold deposits are found (Figures 8-70; 8-71; 8-72).
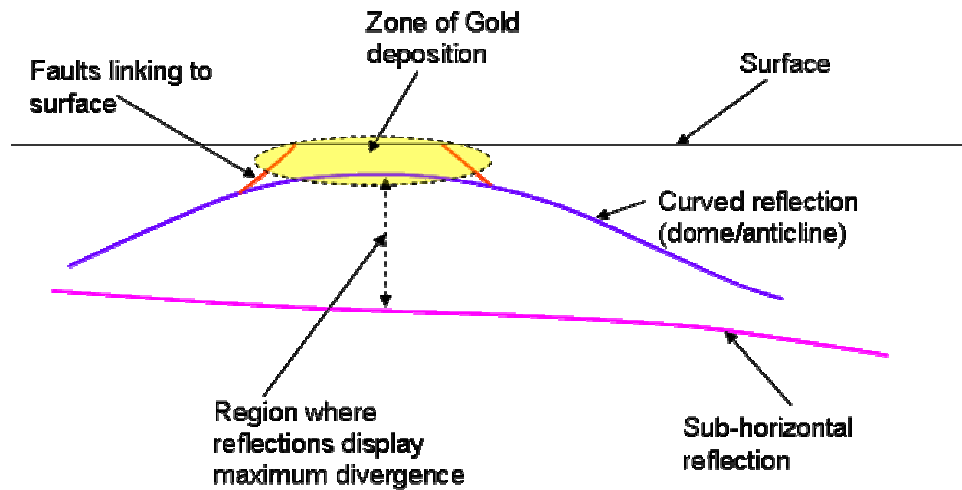


**Figure 8-70: Schematic diagram of diverging reflectors and structures associated with gold deposition (see seismic data in Figures 8-71 and 8-72). Gold deposits are located above the region of maximum divergence. Is the location of gold here related to crustal level and/or the geometry of the dome and underlying sub-horizontal reflector?**
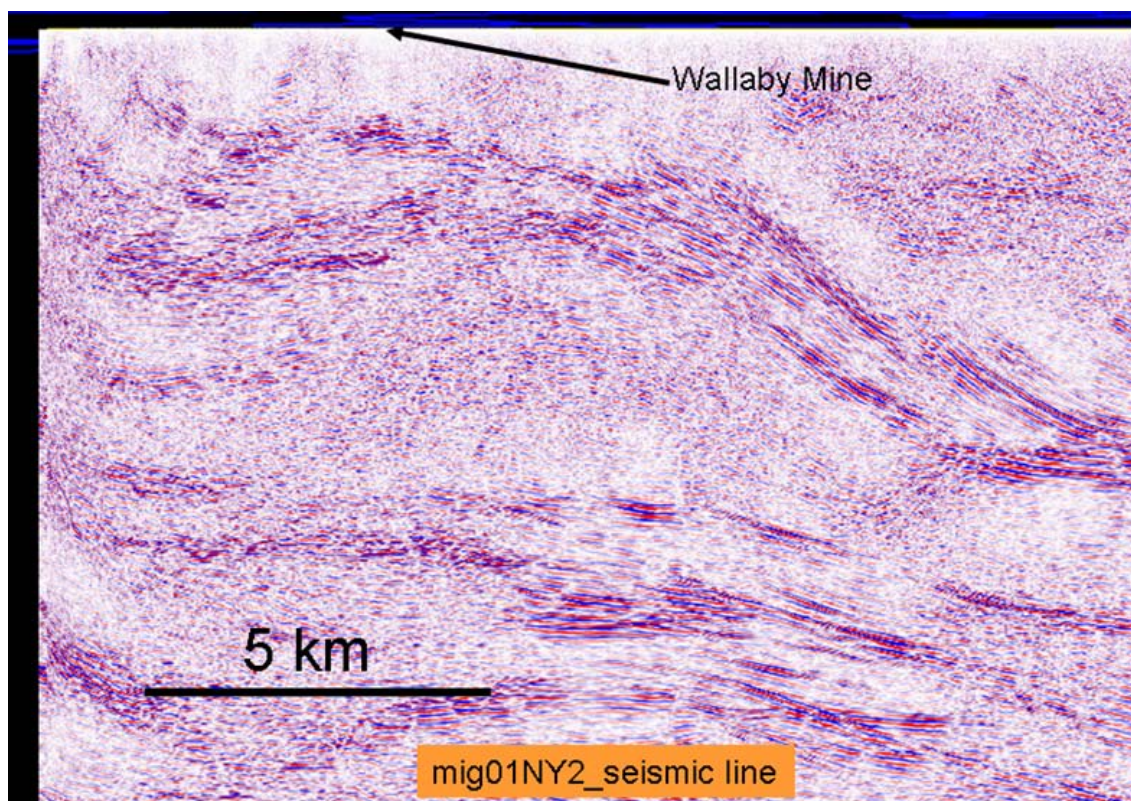


**Figure 8-71: Screen capture from Gocad of the mig01NY2 seismic line through the Wallaby gold mine. Note the pronounced antiform of reflectors (dome) with an underlying set of sub-horizontal reflectors. Note the relatively featureless seismic character which is suggestive of granite rather than thrust horses making up the dome.**
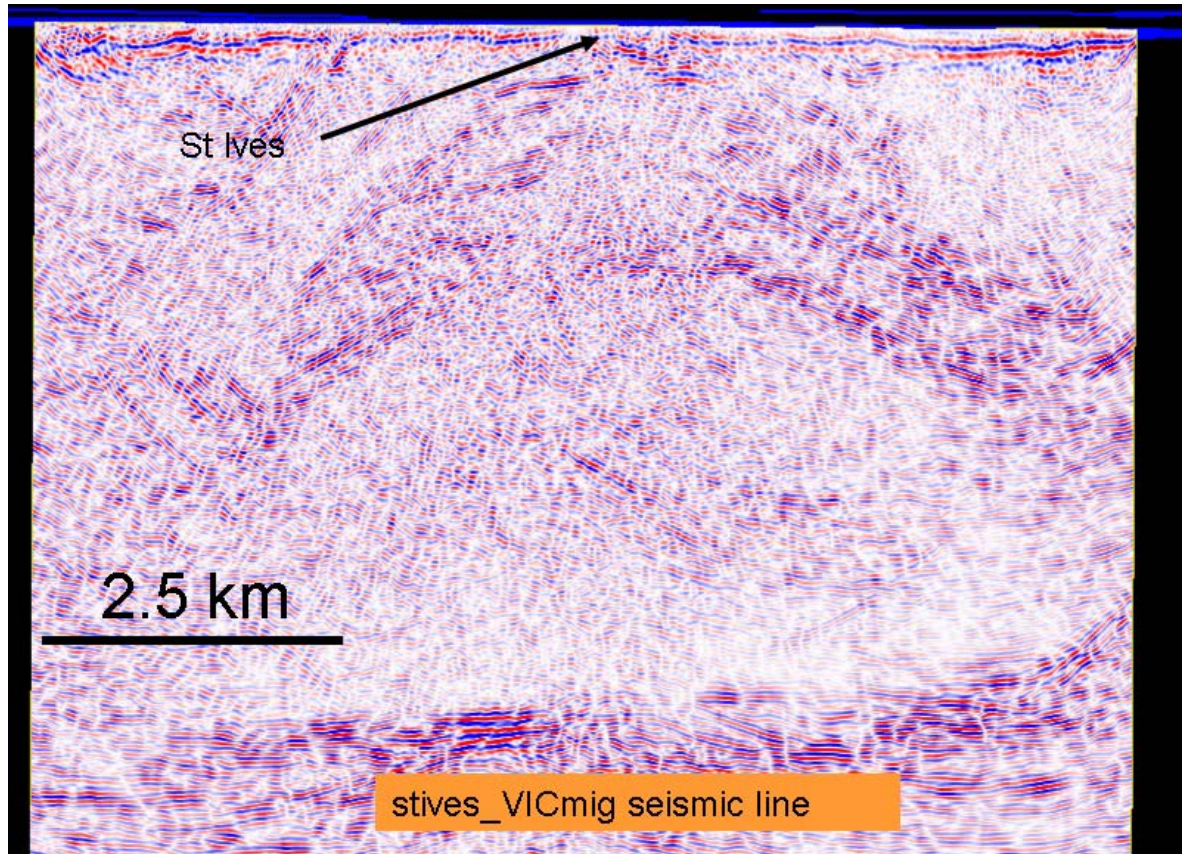
**Figure 8-72: Screen capture from Gocad of the VICmig seismic line through the St Ives region. Note the pronounced antiform of reflectors (dome) with an underlying set of sub-horizontal reflectors. Image courtesy of St Ives Goldfields of Australia. Note the relatively featureless seismic character which is suggestive of granite rather than thrust horses making up the dome.**

The question arises as to what these diverging reflectors represent and what processes operated during their formation, and when this occurred. Drummond and Goleby (1997) postulated by that the domes represent a series of thrust stacks (Figure 8-73). Alternatively they may represent regions of general thrusting into which granite laccoliths have intruded above the sole thrust (Figure 8-73). Emplacement of granite as a sill or laccolith would require $\sigma_1$ to be sub-horizontal and $\sigma_3$ to be sub-vertical, consistent with sub-horizontal dilation during thrusting (Sibson, 1990). Supporting the granite-dome hypothesis is the lack of any reflections within the diverging zone indicating a series of thrust stacks (Figures 8-71 and 8-72). The seismic reflection data show that this is a zone of random reflectors, more characteristic of a granite intrusion.

The potential field modelling does not distinguish from thrust stacked granite and gneiss as opposed to granite intrusions. The low density and relatively slow velocities (see Chapters 2 and 4) show that the region is underlain by felsic rocks. The seismic reflection data are the only available dataset able to distinguish and map these features.

251
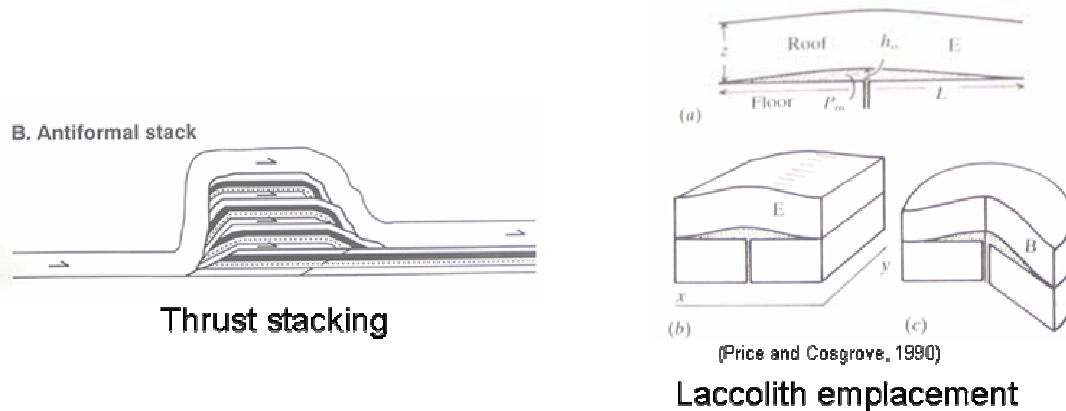
**Figure 8-73: Forming a dome via thrust stacking (Ramsay, 1987), or by laccolith emplacement (Price and Cosgrove, 1990).**

The buckle folding of a competent body results in differing stress across the fold. Typically the outer arc of a buckle fold undergoes extension while the inner arc undergoes contraction (Figure 8-74). Between the extensional and contractional domain lies the neutral surface. Folds typically occur in pairs (i.e., antiforms and complementary synforms), which results in a switch in the location of maximum extension about the fold profile (Figure 8-74).
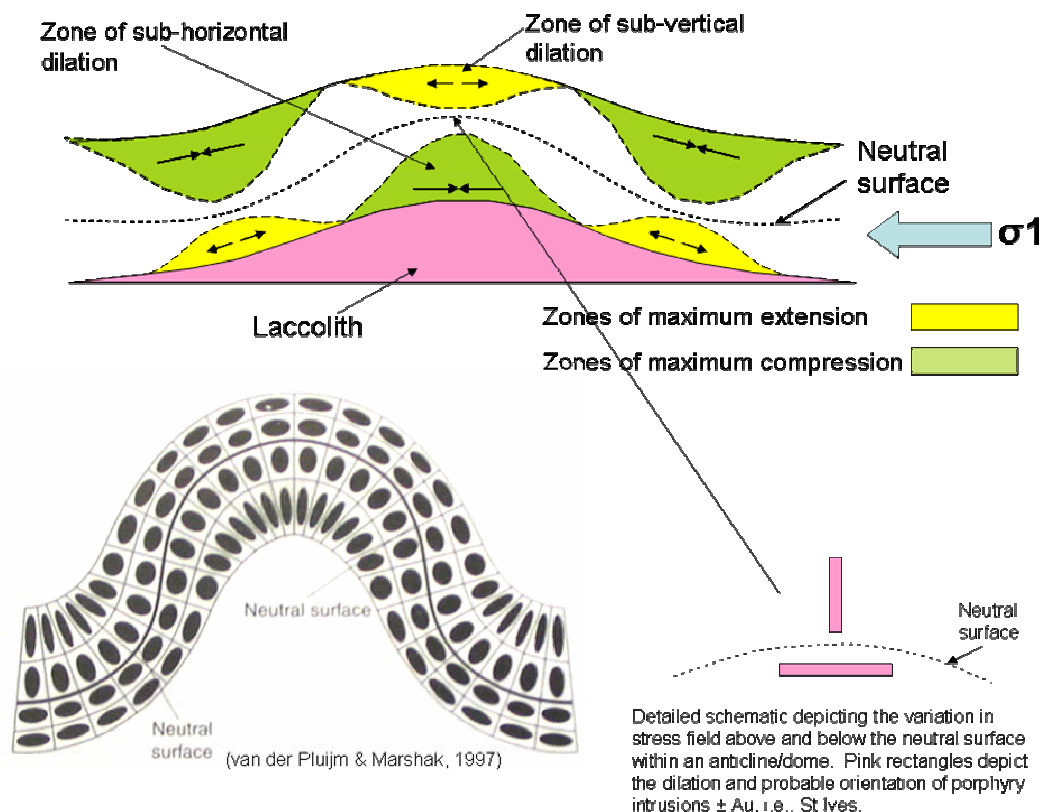


**Figure 8-74: Strain ellipses developed in a buckle fold (after van der Pluijm and Marshak, 1997). Developed during a laccolith intrusion within a regional contractional stress field.**

This change in local stress state about the fold profile gives rise to areas of dilation which would be favourable for developing permeability. At these sites (outer arc of

252

the fold), vertical dykes and extension veins are likely to occur despite regional $\sigma_1$ being horizontal (Figure 8-74). In contrast, the areas of contraction (inner arc of the fold) have both local and regional $\sigma_1$ as subhorizontal. At these sites, the dominant extension vein sets and intrusions will be flat lying (Figure 8-74). Deep drilling at St Ives has defined both sills and dykes of porphyry (Mafic-type granites), consistent with their position with respect to the neutral surface of the regional antiform (Dave Champion, *pers. comm.* 2004).

The development of the laccolith in the inner arc of the fold (Figure 8-74) is consistent with the diverging reflectors (Figure 8-70) and the seismic data at St Ives (Figure 8-72). The presence and role of the large-scale intrusions (laccoliths) during the main 'D$_2$' deformation would have had a significant impact on the architecture as well as the thermal and fluid evolution of the region.

## Implications for predictive mineral discovery

A number of components of the mineral system or five questions are integrated in the section on domes above. The key points for predictive mineral discovery include:

- that there is an empirical relationship globally and in the EYC between domes and mineralisation;
- domes occur at three levels in the crust and are stacked and linked by breaching faults so that an ever increasingly focussed fluid is channelled upward;
- domes are best mapped by seismic reflection data, however 3D gravity inversions have successfully mapped them regionally;
- the role of granites and their emplacement is determined by their position in space with respect to the regional fold structure, and;
- the underlying 'core' of the domes appears to be granite laccoliths (Mafic-type?), with a flat base along a sole thrust and convex or domal upper surface that is folded in harmony with the regional anticlinoria.

## *Tectonic synthesis and interpretation*

*R.S. Blewett and K.F. Cassidy*

The following section is a **speculative** assessment of the geodynamic evolution of the EYC from ~2.7 to ~2.6 Ga. There are many caveats to this interpretation, many of which are given in the body of this report. They are omitted here for brevity of this section.

The earliest events involve the rifting of the ancestral Yilgarn Craton with the development of much of the Kalgoorlie Terrane and establishment of the main N-S trending architecture of the region. The effect of this rifting is visible in the tomography showing a coincidence of the Kalgoorlie Terrane with a velocity anomaly at a depth of 220 km.

Remnants of the older material occur throughout the Kalgoorlie, Kurnalpi and Burtville Terranes. A large mantle plume has been hypothesised for much of this

extension, although no seismic record of this exists today. Separation (rifting) was enough for subduction to occur, and possibly development of a marginal sea such as that double subduction {subduction on both sides} resulted in its closure of marginal sea. There is no evidence for subduction in the seismic record. Differing sequences between the terranes also developed at this time.

A large-scale melting and extensional event (with N-S polarity?) occurred at around 2.675 Ga, and much of the High-Ca granite was likely generated and emplaced during extension (backarc?). However, as this magmatism occurred in both the Kalgoorlie and Kurnalpi Terranes, then by ~2.675 Ga both terranes must have been in close proximity (i.e., some form of closure had taken place). Some of this extension may have resulted in the development of domes (core-complex?).

The $D_1$ contractional event is enigmatic. Many of the features ascribed to $D_1$ appear to be late, overprinting the main $D_2$ structural elements. Other $D_1$ features may be developed during extension. However, the close proximity of the Kalgoorlie and Kurnalpi Terranes could be explained by a $D_1$ contraction event of some kind.

The main $D_2$ orogenic event involved both contraction and extension about a largely co-axial ~E-W direction. The main $D_2$ orogeny resulted in (thin-skinned) accretion of Kurnalpi and Kalgoorlie terranes onto ancestral Yilgarn post ~2.66 Ga. With the onset of contractional deformation, the main phase of High-Ca magmatism terminated. This deformation and termination of magmatism occurred diachronously from NE to SW over about 10 My. Delamination of a dense High-Ca granite residue was a direct consequence of the $D_2$ accretion/orogeny, resulting in termination of High-Ca magmatism (nothing left to melt). The driver of this accection and orogeny was located further east of the EYC. The Nd model ages for the Low-Ca granites have an older crustal signature fits, consistent with this interpretation.

The development of mid-crustal imbricates drove the upper crust forward (into the foreland in the west), with an extrusion of the frontal wedge onto the foreland at a rate greater than the overall shortening. This orogenic surge model explains why the Late Basins were diachronous and developed in the immediate extending hinterland (inverted earlier thrusts) to the surging frontal thrusts. Mafic- and Syenitic- (in the Kurnalpi Terrane) type granite magmatism was associated with this localised extension, which was also diachronous from east to west. The imbrication of the mid-crust drove deep metamorphic fluids upwards and into the foreland, which was pre-prepared by the earlier stages of the surge event. This time 'delay' from driving the deep fluid upwards and into the foreland accounts for diachronous late $D_2$ gold.

The deformation in the mid-crust developed large-scale duplexes with an antiformal or domal geometry in 3D. Similarly the upper crustal $D_2$ thrusts developed culminations and domes, which also controlled the location of Late Basin depocentres. The intrusion of Mafic- and syenitic-type granites were facilitated by the hinterland (surge) extension and further granite emplacement occurred as sills and laccoliths into the progressively evolving domes. Fluid pathways (dilatant zones) were developed at the brittle-ductile transition, a region of high seismicity and now imaged as 'bright spots' or strong reflectors from the now altered and sheared rock. The higher and deformed 'bright spots' would have formed during early deformation (e.g., $D_{2a}$ or earlier) and then acted as acquitards for ponded fluids below. The

ongoing deformation folded these pathways into fluid focussing domal structures. Breaching of the domal reservoirs by late faults delivered a focussed fluid higher into the crust.

Domes were further developed and amplified by a post-$D_2$ stage of N-S contraction. Warping and cross folding resulted in elongate Type I inference patterns, with a wavelength of ~ 30 km (which is the spacing of the main gold deposits). Some 20-30 My after the delamination of the dense High-Ca restite layer (visible in the tomography data) and the concomitant thermal pulse at the base of the crust, Low-Ca granites were emplaced at the base of the greenstone sequence and into the apex regions of earlier developed domes. These high-temperature crustal melts (Low-Ca granites) were emplaced across the entire Yilgarn Craton. The oldest Low-Ca granites were emplaced in the east (~2655 Ma), followed by a rapid event at around 2640 Ma, reflecting the thermal delay in the thermal spike and emplacement of the granites. Especially thick accumulations of Low-Ca granite are inferred to underlie the Kalgoorlie Terrane, providing heat and/or fluid to be feed into the domal pathways above, and develop the late orogenic gold. Alternatively, fluids that ponded below the domes were breached and driven upwards along new pathways developed during the emplacement of the Low-Ca granites.

Associated with this Low-Ca event was wide-spread extension and exhumation. Crustal-scale penetrating normal faults developed mainly within the annealed terranes, rather than at the boundaries of earlier $D_2$ amalgamation (except the Ida Fault System). Numerical modelling has suggested that fluids facilitate the breaking of the rigid crust, and these fluids may also be essential ingredients that used these new deep pathways to the upper crustal domes.


## *Appendix 8*

8-1: **Appendix 8_1 tomography.avi** animation of the Yilgarn Craton tomography to a depth of 350 km.

8-2: **Appendix 8_2 Kalinowski.avi** animation of the Orogenic Surge model presented at Barossa 2004 (Kalinowski et al., 2004). Process is discussed in Appendix 8-9.

8-3: **Appendix 8_3 Schruers.avi** animation of the development of thrusts with a variable strength detachment (from Schruers et al., 2002). Shows (relative) extensional movements on hinterland thrusts analogous to orogenic surge.

8-4: **Appendix 8_4 metamorphic movie.avi** animation from the 3D map showing the metamorphic isograds in 3D.

8-5: **Appendix 8_5 Blewett AGC2004 Talk.pdf** converted Powerpoint presentation by Blewett et al. (2004c) on orogenic surge at the 2004 AGC meeting in Hobart.

8-6: **Appendix 8_6 Orogenic surge paper submitted.pdf** paper submitted for Geology (requires resubmitting) by Blewett et al. in prep.

8-7: **Appendix 8_7 Henson Barossa poster.pdf** poster presented at Barossa 2004 outlining the structural history of the eastern Yilgarn Craton.

8-8: **Appendix 8_8 Henson et al Barossa Poster Abstract.pdf** abstract of the Henson poster for the Barossa CRC meeting in June 2004.

8-9: **Appendix 8_9 Kalinowski Barossa talk.pdf** talk presented at Barossa 2004 on how the 4D animation was constructed (Appendix 8-2).

8-10: **Appendix 8_10 Kalinowski Barossa 2004 Abstract.pdf** is the Abstract of the Kalinowski et al. (2004) talk at the Barossa CRC meeting in June 2004.

8-11: **Appendix 8_11 Henson Barrossa 2004 Abstract.pdf** is the Abstract of the Henson et al. (2004) talk at the Barossa CRC meeting in June 2004.

8-12: **Appendix 8_12 Henson Barossa 2004 talk.pdf** is the talk by Henson et al. (2004) talk at the Barossa CRC meeting in June 2004. The talk was a dynamic view of orogenesis and the development of the Eastern Yilgarn.

8-13: **Appendix 8_13 Blewett SEG 2004 Abstract.pdf** is the abstract for a talk presented (Blewett et al., 2004d) at the SEG meeting in September 2004 in Perth.

8-14: **Appendix 8_14 Blewett SEG 2004 talk.pdf** is the talk presented at the SEG meeting in September 2004 in Perth.

8-15: **Appendix 8_15 pdt 2004 Blewett D2orogeny.pdf** is a talk on orogenic surge presented at the December 2005 CRC Yilgarn PDT meeting in December 2004 in Perth.

8-16: **Appendix 8_16 pdt 2004 Blewett Y2 5Q summary.pdf** is the talk presented to the December 2004 PDT meeting in Perth regarding the main conclusions of the Y2 project.

8-17: **Appendix 8_17 2004 Henson Domes and basins.pdf** is the talk presented to the December 2004 PDT meeting in Perth regarding the development of the domes and basins and their role in fluid focussing and fluid flow.

8-18: **Appendix 8_18 pdt 2004 Henson&Champion new insights.pdf** is the talk presented to the December 2004 PDT meeting in Perth regarding many of the new insights of the geodynamics and architecture from building the 3D map.

# Chapter 9: Conclusions

*R.S. Blewett and K.F. Cassidy*

## Introduction

The principal outcomes of the Y2 project were:

- the successful building and interrogation of 3D maps of the eastern Yilgarn Craton (EYC) and the Kalgoorlie-Kambalda district;
- a new 1:500 000 scale solid geology and GIS that incorporates the granite attributes of AMIRA project P624;
- a new work flow process for building 3D maps;
- a new set of interpretations for the region's seismic reflection data;
- a new tomographic velocity model for the Yilgarn Craton;
- compilation of all publicly available geochronology into a time-space plot;
- a revised tectonic history;
- a novel geodynamic model for $D_2$ deformation (orogenic surge);
- mapping of the 'Golden Corridor' from Kambalda to Wiluna (and possibly Plutonic) and the corridor's relationship to the regional architecture, and;
- the importance of mutli-layered domes, which have a spacing in the upper crust of ~30 km domes and fluid flow models/drivers.

Project data and results have been transferred to sponsors in several forums, including the Perth 'PDT' meeting in December 2004 (see various appendices).

This chapter encompasses the principal conclusions of the project in chapter order. Chapter 8 is arranged as a synthesis of information relevant to each of the *five questions*. It also contains a summary of the proposed geodynamic evolution for the EYC. The implications for predictive mineral discovery are given at the end of each section through the report. Future research directions in the *pmd*\*CRC Y-New project are outlined in Chapter 10.

## Chapter 1

Chapter 1 sets the geological scene and defines the tectono-stratigraphic nomenclature used throughout. A synthesis of available geochronology shows terrane-specific spatial variations in the age of the various granite types. These temporal-spatial variations (specifically the cessation of High-Ca magmatism) are interpreted to reflect initiation of a specific geodynamic process (orogenic surge) leading to the delamination of a restite layer at the base of the crust (resulting in Low-Ca magmatism some >20 My afterwards). A time-space plot illustrates the temporal-spatial variations and is a useful supplement to the GIS developed as part of the 3D maps by providing the fourth dimension, time, to our understanding.

Information sharing between researchers and sponsors has helped the development of a standardised terrane and fault nomenclature for the eastern Yilgarn. This has been pivotal in the successful building of the 3D maps.

## Chapter 2

Chapter 2 highlights the work flow process and metadata for the building of the comprehensive 3D maps of Kalgoorlie-Kambalda and the Norseman to Wiluna region. These 3D maps constitute the main achievement and deliverable of the Y2 project and involved an iterative process developed over the life of the project. The maps were built on a foundation of 2D solid geology maps from government agencies, universities and industry. These data were integrated with various geophysical datasets (seismic reflection, refraction, broad band recording, receiver function, gravity and magnetic data plus various derivatives such as 'Worms', and forward and inverse models), geochemical datasets (e.g., from AMIRA P624), and geochronological datasets (from AMIRA P624 and earlier projects as well as published data).

All datasets were integrated so that the interpretations are fundamentally sound because they use blended/integrated datasets. The seismic reflection data are invaluable for building the 3D maps, especially below the base of the greenstones. Verification by intersecting seismic lines [?? Do you mean the interpreted lines or crossing seismic lines?], together with interpreting actively in 3D space (e.g., Geoscience Australia's 3D visualisation room) is essential for a full appreciation of the richness of the seismic data. Testing interpretations with the potential field data are also required.

The 3D GeoModeller (formerly 3DWEG) software was tested on part of the Kalgoorlie-Kambalda 3D map area. It proved to be a useful tool in rapidly testing many scenarios, but was not a substitute for the Gocad map in scope or detail. However, GeoModeller appears to offer exciting new opportunities for the modelling a region's geological structure. Following further development and testing, GeoModeller will be integrated into GA's work flow process where it is expected to facilitate new insights into the 3D character of the EYC and other Australian provinces.

## Chapter 3

The seismic reflection and wide-angle refraction data and interpretations gathered across the EYC are the subject of Chapter 3. There is now a transect of over 400 km of semi-continuous seismic reflection data from the western margin to nearly the eastern margin of the EYC. Around some of the mining districts (Kalgoorlie, St Ives and Laverton), shorter lines have been acquired (outside of the pmd*CRC, but access was provided following the appropriate confidentiality periods). These seismic reflection data are invaluable for understanding the third dimension. The 3D maps quality and reliability 'fall off' away from the seismic lines.

There has long been a debate regarding steep *vs.* shallow structures. Seismic reflection data can indirectly image steep structures (by terminations and cut offs). Interpretations are supported by potential field forward models, and these models have been tested for their sensitivity to dip changes between steep and shallow.
The relationship between the deep-penetrating fault systems (e.g., Ida, Laverton) and mineral deposits has been extensively reported. Some of the early interpretations have been refined, so that the terrane bounding faults are now viewed as being thin

skinned. The deep-penetrating faults are probably the result of late extension mostly within the terranes themselves.

The project experimented with wide-angle reflection acquisition synchronous with the deep seismic reflection acquisition. The results were encouraging and velocity structure of the upper crust has been better refined.

The way seismic data are processed can have a major impact on the geometry of the reflectors and, therefore, the interpretations. This is especially true for the upper 2 seconds of data (~6 km depth). The project tested pre-stack migration and this changed some of the earlier processed data. Pre-stack migration is very labour intensive and so careful decisions are needed whether this route should be taken.

It is possible to use seismic data consider more than simply <u>architecture. T</u>he data can be interpreted to show the passage of fluids and alteration, the development of a (palaeo) brittle-ductile transition and its exhumation and deformation. These interpretations have an impact on understanding fluid flow in the crust.

## *Chapter 4*

Chapter 4 incorporates the mapping the lithosphere (at the Yilgarn Craton scale) and its velocity structure by using broad band seismic recording (tomography) and receiver function data (velocity profiles). The tomography experiment was very successful with high-quality data returned. A new 3D map of the Yilgarn Craton's lithosphere (velocity structure) is a major advance on the early SKIPPY data. A number of interesting geodynamic inferences and speculations have been made regarding the nature and origin of some of the velocity anomalies. The tomography show a velocity stratification to the mantle lithosphere, with a fast S-wave velocity layer present at around 100-120 km depth. More work is needed to refine these velocity models.

The receiver function data showed significant differences between the various terranes of the Yilgarn Craton. The Kalgoorlie Terrane is especially anomalous with respect to its velocity profile. It is speculated that a thick Low-Ca granite sheet underlies the greenstone belts, at least across the profile where the receiver function data were collected. Both the receiver function and tomography data pick a seismic Moho at the same level as the seismic reflection data; substantiating the importance of integration of data sets to test and verify interpretations.

## *Chapter 5*

Chapter 5 outlined the limited study that was made of the distribution of the chalcophile elements across the EYC. This output was terminated on recommendation of the project sponsors. The main findings of this output were that gold is the best tracer of gold deposit-associated fluid pathways. Arsenic is associated with gold to some extent. Other elements thought to have some association with gold include Ag, Bi, Mo, and W.

## Chapter 6

The utility of the 3D maps is discussed in Chapter 6. The uptake and now routine process of building regional and camp-scale 3D maps by sponsors of this project is a clear indication of the impact of added utility gained through developing a 3D understanding (with time) versus traditional 2D approaches. The process of building a 3D map necessitates a far greater degree of rigour than that needed for traditional 2D maps, because it requires each adjacent relationship to be considered in 3D. From this approach a temporal understanding of all unit and event relationships is developed. Building 3D maps is a worthwhile despite being a very labour intensive exercise. Team work was enhanced through building the 3D maps and promotes development of a shared vision within the project team..

Development of a structural framework and its likely geodynamics were not an explicit task or deliverable for the Y2 project. However, the model building process has meant the development of a new structural paradigm for the EYC.

## Chapter 7

The prospectivity analysis output was terminated by sponsors at the December 2003 PDT meeting in Perth, on the basis that more-sophisticated prospectivity analysis tools were being developed external to the *pmd*\*CRC. Chapter 7 outlines the prospectivity analysis conducted by the A1 project using the Y2 project data. The A1 work showed that domes (or anticlinoria) with adjacent major faults were the most mineralised areas of the EYC. The empirical finding supports the major conceptual models presented in this report.

## Chapter 8

Chapter 8 is a synthesis of the project's findings arranged around the *five questions*. As Ellis (1939) first said, architecture is the key ingredient to finding mineral deposits. This project has provided 3D maps for the Norseman to Wiluna and the Kalgoorlie-Kambalda areas of the EYC. These maps provide the building blocks and regional province-wide framework for a 4D analysis and investigation for predictive mineral discovery.

Integrating the observations described throughout this report permit speculations regarding the overall geodynamics of the EYC's orogenic gold mineralisation. Early extension (mantle plume driven?) 'imprinted' an architecture into the EYC. Magmatism associated with extension and subduction was terminated with the onset of the main contraction which involved mid crustal imbricates driving the upper crust onto the foreland (orogenic surge). This process resulted in diachronous deformation and associated Late Basin sediments and Mafic magmatism. This contractional event terminated the High-Ca magmatism. Delamination of High-Ca granite restite at the base of the thickened crust allowed the influx of heat under the thinned lower crust. This influx melted the crust across the craton and generated the late-stage Low-Ca granites. These granites were contemporaneous with late-stage extension and the development of crustal-penetrating structures which provided new pathways for orogenic fluids. Late-stage orogenic gold and these granites were coeval.

## *Appendix 9:*

9-1:   **Appendix 9_1 November 2003 CRC Review.pdf** is a presentation made to sponsors and the review panel in November 2003.

9-2:   **Appendix 9_2 Nov 2003 panel session slides.pdf** are the summary session slides made to sponsors and the review panel in November 2003.

9-3:   **Appendix 9_3 December 2003 CRC PDT meeting.ppt** is a presentation made to sponsors at the December 2003 PDT meeting in Perth.

9-4:   **Appendix 9_4 April  2004 CRC PDT meeting.ppt** is a presentation made to sponsors at the April 2004 PDT meeting in Perth.

9-5:   **Appendix 9_5 ERC Reporting progress Y2 Sep 2004.ppt** is a progress report to the ERC Review committee fro September 2004.

# Chapter 10: Y-New project and future research directions

*R.S. Blewett*

## Summary objective

The Y-New project is entitled *"Predictive mineral discovery using a holistic study of the 4D evolution of the Eastern Yilgarn."* The project will run for 2.5 years (January 2005 until June 2007). The principal outcome for the Y-New project will be a multi-scaled 4D understanding of the world-class orogenic gold mineral system of the Eastern Yilgarn. A performance measure will be the successful application of this understanding to predictive targeting of undiscovered resources in near mine areas, as well as concepts/hypotheses that can be applied to targeting in data-poor areas.

Y-New will be the integrated successor project of the *pmd*\*CRC activities in the Eastern Yilgarn Craton (except Y1 AMIRA project P763). The project will build on the existing knowledge and expertise developed in the *pmd*\*CRC, AGCRC, and AMIRA/MERIWA projects not in confidentiality.

The project philosophy will be guided by the Five Questions to test hypotheses at a range of scales in an integrated and focussed manner. The project outcome will be achieved by collaborative research towards a robust understanding of the geodynamics, architecture, fluid sources and drivers, together with gold depositional mechanisms for the Eastern Yilgarn. The project will use the well-developed tools of the enabling technologies such as geochronology, numerical modelling, and chemical and fluid modelling to answer key questions and test hypotheses.

## Question One: Geodynamics
- New time-space event history database, charts, and maps
  - *Includes: greenstone and magmatic stratigraphy, metamorphism, deformation, mineralisation/alteration*
  - *To be developed on GA databases using map/chart-making tools*
  - *Build and update SRK and Y2 time-space plots*
- Reports and maps updating the structural history/stratigraphy (unravelling the D's)
  - *Focus on early extensional history through to Black Flag Group deposition*
  - *Test the veracity of $D_1$ N-S shortening*
  - *Linked to specific sites of mineralisation*
  - *PhD reports by Hodge, Tripp, & Morey*
- Maps of regional metamorphism, together with reports on the PT*t* evolution integrated with structural and alteration history
  - *Will contract aspects of the work if GSWA do not participate*
- Report including workshop(s) on likely geodynamic models of the Yilgarn, with appropriate tests and possible analogues
  - *Will be a key deliverable in the Synthesis*

## Question Two: Architecture

- 3D maps/GIS of specific districts to be built on Y2 regional 3D map
  - *Areas include Laverton, Agnew-Wiluna*
- Interpretation and characterisation of key faults, especially the deep-tapping 'cracks'
  - *Includes MT (acquire), seismic (incorporate industry lines), and ongoing tomography data reduction (Goleby and RSES)*
  - *Morey PhD*
  - *Revise deep seismic reflection profile interpretations*
- Report on an improved methodology for geologically intelligent geophysical inversions, supported by a rock property database
  - *Incorporate Y2 learnings*
  - *Williams PhD*

## Question Three: Fluid sources/reservoirs

- Reports and chemical models on the end-member fluids (magmatic, basinal, meteoric, metamorphic, mantle?)
- Reports, maps and databases on integrated mineral paragenesis and architecture and chemical modelling for selected camps and deposits

## Question Four: Pathways and drivers

- Reports on integrated numerical models of fluid flow for generic and site specific scenarios
  - *Focussed on areas where we will collect detailed structural and mineral paragenesis information*
- Regional footprint maps of alteration and fluid flow based on geochemistry, ASTER, HYMAP etc
  - *ASTER maps will be for coverage of 3D map and calibrated to the GSWA HYMAP study in Kalgoorlie*
  - *A range of minerals (eg white micas) will be mapped*
  - *A set of lithological discrimination presentations will be prepared*

## Question Five: Depositional mechanisms

- Maps and reports on the chemical and PT gradients for selected sites
  - *Initially will be focussed at Wallaby, Sunrise, St Ives, KB*
- Reports on the integrated structural controls of ore shoots with the regional framework, linked to alteration and mineralogy
  - *Initially will be focussed at Wallaby, Sunrise, St Ives, KB*
- Report on reactive transport models tested against specific sites where paragenesis and structure understood

## Integrated Synthesis

- Synthesis report (including DVDs with accompanying data) to accompany a workshop addressing the Five Questions across scales for the Eastern Yilgarn. The goal will be a holistic view of the 4D evolution and its relationship to the world-class mineral system, and how this understanding can be applied to predictive mineral discovery.

# Acknowledgements

# References

Anderson, E.M., 1951. The Dynamics of Faulting. Oliver and Boyd, Edinburgh, 206p.

Archibald, N.J., 1979. Tectonic-metamorphic evolution of an Archaean terrain. University of Western Australia, PhD thesis (unpublished).

Archibald, N.J., Bettenay, L.F., Binns, R.A., Groves, D.I., and Gunthorpe, R.J., 1978. The evolution of Archaean greenstone terrains, Eastern Goldfields Province, Western Australia. Precambrian Research, 6, 103-131.

Arenas, R., and Catalan, J.R.M., 2003. Low-P metamorphism following a Barrovian-type evolution. Complex tectonic controls for a common transition, as deduced in the Mondonedo thrust sheet (NW Iberian Massif). Tectonophysics, 365, 143-164.

Ayer J., Ketchum J.W.F., and Trowell N.F., 2002a. Project Unit 95-024, New Geochronological and Neodymium Isotope Results from the Abitibi Greenstone Belt, with Emphasis on the Timing and the Tectonic Implications of Neoarchean Sedimentation and Volcanism. In Summary of Field Work and other Activities 2002, Ontario Geological Survey, Open File Report 6100, 5-3.

Ayer J., Amelin Y., Corfu F., Kamo S., Ketchum J., Kwok K., and Trowell N., 2002b. Evolution of the southern Abitibi greenstone belt based on U-Pb geochronology: autochthonous volcanic construction followed by plutonism, regional deformation and sedimentation. Precambrian Research, 115, 87-101.

Barley, M.E., Krapež, B., Groves, D.I., and Kerrich, R., 1998. The Late Archaean bonanza: metallogenic and environmental consequences of the interaction between mantle plumes, lithospheric tectonics and global cyclicity. Precambrian Research, 91, 65-90.

Barley, M.E., Brown, S.J.A., Krapež, B., and Cas, R.A.F., 2002. Tectonostratigraphic Analysis of the Eastern Yilgarn Craton: an improved geological framework for exploration in Archaean Terranes. AMIRA Project P437A, Final Report.

Barley M.E., Brown, S.J.A., Cas, R.A.F., Cassidy, K.F., Champion, D.C., Gardoll, S.J., and Krapež, B., 2003. An integrated geological and metallogenic framework for the eastern Yilgarn Craton: Developing geodynamic models of highly mineralised Archaean granite-greenstone terranes. AMIRA Project P624, Final Report.

Barlow, M., 2004a. Yilgarn constrained gravity inversion. *pmd*CRC internal report (Appendix 2).

Barlow, M., 2004b. Density and susceptibility characterisation of the Minerie 100 000 geology sheet: implications for detailed gravity inversion. *pmd*CRC internal report (Appendix 2).

Bateman, R.J., Hagemann, S.G., McCuaig, T.C., and Swager, C.P., 2001. Protracted gold mineralisation throughout orogenesis in the Kalgoorlie camp, Yilgarn Craton, Western Australia: structural, mineralogical, and geochemical evolution. Geological Survey of Western Australia, Record 2001/17, 63-95.

Bateman, R., Swager, C.P., and McCuaig, C., 2002. Fimiston Lodes–deformation, structures, timings, and mineralisation. Australian Institute of Geoscientists Bulletin, 36, 6-8.

Bear, J., 1988. Dynamics of fluids in porous media. Elsevier, New York.

Bell, B., 2002. Application of potential field data to constrain three-dimensional geological modelling in the Leonora-Laverton transect area. In Cassidy, K.F. (Ed), Geology, geochronology and geophysics of the north eastern Yilgarn Craton, with an emphasis on the Leonora-Laverton transect area. Geoscience Australia, Record 2002/18, 75-82.

Bercovici, D., and Ricard, Y., 2003. Energetics of a two-phase model of lithospheric damage, shear localisation and plate-boundary formation. Geophysical Journal International, 152, 581-596.

Bijwaard, H., and Spakman, W., 1999. Tomographic evidence for a narrow whole mantle plume below Iceland. Earth and Planetary Science Letters, 166, 121-126.

Bijwaard, H., Spakman, W., and Engdahl, E.R., 2004. Closing the gap between regional and global travel time tomography, Journal of Geophysical Research.

Binns, R.A., Gunthorpe, R.J., and Groves, D.I., 1976. Metamorphic patterns and development of greenstone belts in eastern Yilgarn Block, Western Australia. John Wiley & Sons, New York, USA, 303-313.

Black, L.P., Champion, D.C., and Cassidy, K.F., 2005. Compilation of SHRIMP U-Pb geochronology data, Yilgarn Craton, Western Australia, 1996-2000. Geoscience Australia Record, 2005 (in press).

Blewett, R.S., Champion, D.C., Whitaker, A.J., Bell, B., Nicoll, M., Goleby, B.R., Cassidy, K.F., and Groenewald, P.B., 2002a. A new 3D model of the Leonora-Laverton transect: implications for the tectonic evolution of the eastern Yilgarn Craton. Australian Institute of Geoscientists Bulletin, 36, 18-21.

Blewett, R.S., Champion, D.C., Whitaker, A.J., Bell, B., Nicoll, M., Goleby, B.R., Cassidy, K.F., and Groenewald, P.B., 2002b. Three dimensional (3D) model of the Leonora-Laverton transect area: implications for Eastern Goldfields tectonics and mineralisation. In Cassidy, K.F., (Ed), Geology, geochronology and geophysics of the north eastern Yilgarn Craton, with an emphasis on the Leonora-Laverton transect area. Geoscience Australia Record, 2002/18, 83-100.

Blewett, R.S., Henson, P.A., Goleby, B.R., Champion, D.C., Cassidy, K.F., and Groenewald, P.B., 2003. On the deep crustal structure of the late Archaean Eastern Yilgarn Craton: a comparison to Palaeozoic and Modern analogues. Geological Society of Australia, Abstracts 72, p. 42.

Blewett, R.S., Cassidy, K.F., Champion, D.C., and Whitaker, A.J., 2004a. The characterisation of deformation events in time across the Eastern Goldfields Province, Western Australia. Geoscience Australia Record, 2004/10 [CDROM].

Blewett, R.S., Cassidy, K.F., Champion, D.C., Henson, P.A., Goleby B.R., and Kalinowski, A.A., 2004b. An orogenic surge model for the eastern Yilgarn Craton: implications for gold mineralising systems. In Muhling, J., et al., (Eds), SEG 2004, Predictive Mineral Discovery Under Cover. Centre for Global Metallogeny, The University of Western Australia, Publication 33, 321-324.

Blewett, R.S., Cassidy, K.F., Champion, D.C., Henson, P.A., Goleby, B.R., Jones, L., and Groenewald, P.B., 2004c. The Wangkathaa Orogeny: an example of episodic regional 'D2' in the late Archaean Eastern Goldfields Province, Western Australia. Precambrian Research, 130, 139-159.

Blewett, R.S., Cassidy, K.F., Champion, D.C., Henson, P.A., and Goleby, B.R., 2004d. Episodicity of Archaean tectonics: an orogenic surge model for the Eastern Yilgarn Craton. Geological Society of Australia, Abstracts 73, 146.

Boschetti, F., Hornby, P., and Horowitz, F., 2000. A new environment for analysis, processing and inversion of potential field data. International Geological Congress, Abstracts 31.

Bourne, B.T., Trench, A., Dentith, M.C., and Ridley, J., 1993. Physical property variations within Archean granite-greenstone terrane of the Yilgarn Craton, Western Australia: The influence of metamorphic grade. Exploration Geophysics, 24, 367-374.

Brooks, D.A., Carlson, R.L., Harry, D.L., Melia, P.J., Moore, R.P., Rayhorn, J.E., and Tubb, S.G., 1984. Characteristics of back-arc regions. Tectonophysics, 102, 1-16.

Brown, M.A.N., Jolly, R.J.H., Stone, W., and Coward, M.P., 1999. Nickel ore troughs in Archaean volcanic rocks, Kambalda, Western Australia: indicators of early extension. In McCaffrey, K.W.J., Lonergan, L., and Wilkinson, J., (eds), Fractures, fluid flow and mineralization. Geological Society Special Publications. 155, 197-211.

Brown, S.J.A., Krapež, B, Beresford, S.W., Cassidy, K.F., Champion, D.C., Barley, M.E., and Cas, R.A.F., 2001. Archaean volcanic and sedimentary environments of the Eastern Goldfields Province, Western Australia–a field guide. Western Australia Geological Survey Record, 2001/13, 66p.

Brown, S.J.A., Barley, M.E., Krapež, B., and Cas R.A.F., 2002. The Late Archaean Melita Complex, Eastern Goldfields, Western Australia: shallow submarine bimodal volcanism in a rifted arc environment. Journal of Volcanology and Geothermal Research, 115,303-327.

Brown, S.M., Fletcher, I.R., Stein, H.J., Snee, L.W., and Groves, D.I., 2002. Geochronological constraints on pre-, syn-, and post-mineralization events at the world-class Cleo gold deposit, Eastern Goldfields Province, Western Australia. Economic Geology, 97, 541-559.

Butler, R.W.H., 1983. Balanced cross-sections and their implications for the deep structure of the Northwest Alps. In Balanced cross-sections and their geological significance; a memorial to David Elliott. Journal of Structural Geology, 5, 125-137.

Cassidy, K.F., Champion, D.C., Fletcher, I.R., Dunphy, J.M., Black, L.P., and Claoue-Long, J.C., 2002a. Geochronological constraints on the Leonora-Laverton transect area, north-eastern Yilgarn Craton. In Cassidy, K.F., (Ed), Geology, geochronology and geophysics of the north eastern Yilgarn Craton, with an emphasis on the Leonora-Laverton transect area. Geoscience Australia Record, 2002/18, 37-58.

Cassidy, K.F., Champion, D.C., McNaughton, N.J., Fletcher, I.R., Whitaker, A.J., Bastrakova, I.V., and Budd, A.R., 2002b. Characterisation and metallogenic significance of Archaean granitoids of

the Yilgarn Craton, Western Australia. Minerals and Energy Research Institute of Western Australia (MERIWA), Report No. 222, 514p.

Cassidy K.F., and Champion D.C., 2004. Crustal evolution of the Yilgarn Craton from Nd isotopes and granite geochronology: implications for metallogeny. In Muhling, J., et al., (Eds), SEG 2004, Predictive Mineral Discovery Under Cover. Centre for Global Metallogeny, The University of Western Australia, Publication 33, 317-320.

Champion, D.C., 1997. Granitoids in the Eastern Goldfields. In Cassidy, K.F., Whitaker, A.J., and Lui, S.F., (Eds), Kalgoorlie '97. An International Conference on Crustal Evolution, Metallogeny and Exploration of the Yilgarn Craton – An Update. Australian Geological Survey Organisation, Record, 1997/41, 71-76.

Champion, D.C., and Sheraton, J.W., 1997. Geochemistry and Nd isotope systematics of Archaean granites of the Eastern Goldfields, Yilgarn Craton, Australia; implications for crustal growth processes. Precambrian Research, 83, 109-132.

Champion, D.C., and Cassidy, K.F., 2002. Granites in the Leonora-Laverton transect area, north eastern Yilgarn Craton: In Cassidy, K.F., (Ed), Geology, geochronology and geophysics of the north eastern Yilgarn Craton, with an emphasis on the Leonora-Laverton transect area. Geoscience Australia, Record 2002/18, 13-35.

Chen, S.F., Witt, W., and Liu, S.F., 2001. Transpressional and restraining jogs in the northeastern Yilgarn Craton, Western Australia. Precambrian Research, 106, 309–328.

Chen, S.F., Riganti, A., Wyche, S., Greenfield, J.E., and Nelson, D.R., 2003. Lithostratigraphy and tectonic evolution of contrasting greenstone successions in the central Yilgarn Craton, Western Australia. Precambrian Research, 127, 249-266.

Chen, S.F., Libby, J.W., Wyche, S., and Riganti, A., 2004. Kinematic nature and origin of regional-scale ductile shear zones in the central Yilgarn Craton, Western Australia, Tectonophysics, 394, 139-153.

Chiang, C.S., Yu, H.S., and Chou, Y.W., 2004. Characteristics of the wedge-top depozone of the southern Taiwan foreland basin system. Basin Research, 16, 65-78.

Claoué-Long, J.C., Compston, W., and Cowden, A., 1988. The age of the Kambalda greenstones resolved by ion microprobe - implications for Archaean dating methods. Earth and Planetary Science Letters, 89, 239-259.

Clark, M.E., Carmichael, D.M., Hodgson, C.J., and Fu, M., 1989. Wall-rock alteration, Victory gold mine, Kambalda, Western Australia; processes and P-T-X (sub CO2) conditions of metasomatism. In Keays, R.R., Ramsay, W.R.H., and Groves, D.I., (Eds), The geology of gold deposits; the perspective in 1988. Economic Geology Monograph, 6, 445-459.

Clevis, Q., de Jager, G., Nijman, W., and de Boer, P.L., 2004. Stratigraphic signatures of translation of thrust-sheet top basins over low-angle detachment faults. Basin Research, 16, 145-163.

Compston, W., Williams, I.S., Campbell, I.H., and Gresham, J.J., 1986. Zircon xenocrysts from the Kambalda volcanics: age constraints and direct evidence for older continental crust below the Kambalda-Norseman greenstones. Earth and Planetary Science Letters, 76, 299-311.

Connolly, J.A.D, and Podladchikov, Y., 2000. Temperature-dependent viscoelastic compaction and compartmentalisation in sedimentary basins. Tectonophysics, 324, 137-168.

Connolly, J.A.D, and Podladchikov, Y., 2004. Fluid flow in compressive settings: implications for mid-crustal reflectors and downward fluid migration. Journal of Geophysical Research, in press.

Cox, S.F., Etheridge, M.A., and Wall, V.J., 1990. Fluid pressure regimes and fluid dynamics during deformation of low-grade metamorphic terranes, implications for the genesis of mesothermal gold deposits. In Greenstone Gold and Crustal Evolution. Geological Association of Canada, 46-53.

Crowell, J.C., 1979. The San Andreas Fault system through time. Journal of the Geological Society of London, 136, 293-302.

Daigneault, R., Mueller, W.U., and Chown, E.H., 2002. Oblique Archaean subduction: accretion and exhumation of an oceanic arc during dextral transpression, Southern Volcanic Zone, Abitibi Subprovince Canada. Precambrian Research, 115, 261-290.

Davis, B.K., 2001. Complexity of tectonic history in the Eastern Goldfields Province, Yilgarn Craton: 4th International Archaean Symposium, Extended Abstracts. Geoscience Australia Record, 2001/37, 134-136.

Davis, B.K., 2002. The Scotia–Kanowna Dome, Kalgoorlie Terrane: Deformation history, structural architecture and controls on mineralisation. Australian Institute of Geoscientists Bulletin field guide, 61p.

Davis, B.K., and Maidens, E., 2003. Archaean orogen-parallel extension; evidence from the northern Eastern Goldfields Province, Yilgarn Craton, Precambrian Research, 127, 229-248.

DeCelles, P.G., and Giles, K.A., 1996. Foreland basin systems. Basin Research, 8, 105-123.

Dewey, J.F., 1980. Episodicity, sequence and style at convergent plate boundaries, In Stranway, D.W., (Ed), The continental crust and its mineral deposits. Geological Association of Canada Special Paper 20, 553-573.

Drummond, B.J., Goleby, B.R., Swager, C.P., and Williams, P.R., 1993., Constraints on Archaean crustal composition and structure provided by deep seismic sounding in the Yilgarn Block. Ore Geology Reviews, 8, 117-124.

Drummond, B.J, Goleby, B.R., and Hobbs, B.E., 2004. The role of crustal fluids in the tectonic evolution of the Eastern Goldfields Province of the Archaean Yilgarn Craton, Western Australia. Special volume of the Second International Symposium on slip and flow processes in and below the seismogenic region (10-14 March, 2004, The University of Tokyo).

Drummond, B.J., Goleby, B.R., and Swager, C.P., 2000a. Crustal signature of Late Archaean tectonic episodes in the Yilgarn craton, Western Australia: evidence from deep seismic sounding. Tectonophysics, 329, 193-221.

Drummond, B.J., Cox, S.F., and Goleby, B.R., 2000b. The role of fluids in the formation of regional-scale detachment surfaces. 9th International Symposium on deep seismic profiling of the continents and their margins, Ulvik, Norway, 18-23 June, 2000, abstracts, 51.

Dunphy, J.M., Fletcher, I.R., Cassidy, K.F., and Champion, D.C., 2003. Compilation of SHRIMP U-Pb geochronological data, Yilgarn Craton, Western Australia, 2001-2002. Geoscience Australia Record 2003/15, 139p.

Duuring, P., Hagemann, S.G., and Love, R.J., 2001. A thrust ramp model for gold mineralization at the Archaean trondhjemite-hosted Tarmoola Deposit; the importance of heterogeneous stress distributions around granitoid contacts. Economic Geology 96, 1379-1396.

Ellis, H.A., 1939. The Geology of the Yilgarn Goldfield south of the Great Eastern Railway. Geological Survey of Western Australia Bulletin, 97, 129-141.

Emerson, D.W., 1990. Notes on mass properties of rocks - density, porosity, permeability. Exploration Geophysics, 21, 209-216.

Fairclough, M.C., and Brown, J., 1998. Tarmoola gold deposit. In Berkman, D.A. and Mackenzie D.A., (Eds), Geology of Australian and Papua New Guinean mineral deposits: Australasian Institute of Mining and Metallurgy, Monograph 22, 173-178.

Fletcher, I.R., Mikucki, J.A., McNaughton, N.J., Mikucki, E.J., and Groves, D.I., 1998. The age of felsic magmatism and lode-gold mineralisation events in the Lawlers area, Yilgarn Craton, Western Australia. Geological Society of Australia, Abstracts no. 49, 146.

Fletcher, I.R., Dunphy, J.M., Cassidy, K.F., and Champion, D.C., 2001. Compilation of SHRIMP U-Pb geochronological data, Yilgarn Craton, Western Australia, 2000-2001. Geoscience Australia, Record 2001/47, 111p.

Fomin, T., Crawford, A. and Johnstone, D., 2003. A wide-angle reflection experiment with Vibroseis sources as part of a multidisciplinary seismic study of the Leonora-Laverton Tectonic Zone, Northeastern Yilgarn Craton. Exploration Geophysics, 34, 147–150.

Fomin, T., Goleby, B.R., and Nicoll, M., 2004. Some lessons from combined interpretations of wide-angle and conventional reflection data in the northern Yilgarn, Western Australia. Seismix 2004, the 11th International Symposium on Deep Seismic profiling of the Continents and their Margins, Programme and Abstracts, 26 September-1 October 2004, Centre des Congrès, Mount-Tremblant, Quebec, Canada.

France, D., 1987. Recumbent folds. In Seyfert, C.K., (Ed), The Encyclopaedia of Structural Geology and Plate Tectonics. Van Nostrand Beinhold Company, New York, 650-656.

Fukao, Y., Widiyantoro, S., and Obasyashi, M., 2001. Stagnant slabs in the upper and lower mantle transition region. Reviews of Geophysics, 39, 291-323.

Gee, R.D., 1979. Structure and tectonic style of the Western Australian Shield. Tectonophysics, 58, 327-369.

Gee, R.D., Baxter, J.L., Wilde, S.A., and Williams, I.R., 1981. Crustal development in the Archaean Yilgarn Block, Western Australia. Geological Society of Australia, Special Publication, 7, 43-56.

Glikson, A.Y., 1971. Archaean geosynclinal sedimentation near Kalgoorlie, Western Australia. Geological Society of Australia, Special Publication, 3, 443-460.

Goleby, B.R., Rattenbury, M.S., Swager, C.P., Drummond, B.J., Williams, P.R., Sheraton, J.E., and Heinrich, C.A., 1993. Archaean crustal structure from seismic reflection profiling, Eastern Goldfields, Western Australia. In Williams, P.R., and Haldane, J.A., (Eds), Kalgoorlie'93 – An international conference on crustal evolution, metallogeny, and exploration of the Eastern Goldfields. Australian Geological Survey Organisation, Record 1993/54.

Goleby, B.R., Bell, B., Korsch, R.J., Sorjonen-Ward, P., Groenewald, P.B., Wyche, S., Bateman, R., Fomin, T., Witt, W., Walshe, J., Drummond, B.J., and Owen, A.J., 2000. Crustal structure and fluid flow in the Eastern Goldfields, Western Australia. Australian Geological Survey Organisation, Record, 2000/34: 109p.

Goleby, B.R., Blewett, R.S., Champion, D.C., Korsch, R.J., Bell, B., Groenewald, P.B., Jones, L.E.A., Whitaker, A.J., Cassidy, K.F., and Carlsen, G.M., 2002a. Deep seismic profiling in the NE Yilgarn: insights into its crustal architecture. Australian Institute of Geoscientists Bulletin, 36, 63-66.

Goleby, B.R., Korsch, R.J., Fomin, T., Bell, B., Nicoll, M.G., Drummond, B.J., and Owen, A.J., 2002b. A preliminary 3D geological model of the Kalgoorlie region, Yilgarn Craton, Western Australia, based on deep seismic reflection and potential field data. Australian Journal of Earth Sciences, 49, 917-934.

Goleby, B.R., Blewett, R.S., Groenewald, P.B., Cassidy, K.F., Champion, D.C., Korsch, R.J., Whitaker, A., Jones, L.E.A., Bell, B., and Carlson, G., 2003. Seismic interpretation of the northeastern Yilgarn Craton seismic data. In Goleby, B.R., Blewett, R.S., Groenewald, P.B., Cassidy, K.F., Champion, D.C., Jones, L.E.A., Korsch, R.J., Shevchenko, S., and Apak, S.N., (Eds), The 2001 Northeastern Yilgarn Deep Seismic Reflection Survey. Geoscience Australia, Record 2003/28, 143p.

Goleby, B.R., Blewett, R.S., Kennett, B.L.N., Jones, L.E.A., Korsch, R.J., Drummond, B.J., Fomin, T., Reading, A.M., Cassidy, K.F., Champion, D.C., Henson, P., Groenewald, P.B., Nicoll, M., and Brennan, T., 2004. Seismic: a key tool in understanding crustal architecture and mineral systems. In Muhling, J., et al., (Eds), SEG 2004, Predictive Mineral Discovery Under Cover. Centre for Global Metallogeny, The University of Western Australia, Publication 33, 313-316.

Gower, C.F., 1976. Laverton, Western Australia, 1:250 000 Geological series–Explanatory Notes. Australian Government Publishing Service, Canberra, 30p.

Graham, S., Lambert, D., and Shee, S., 2004. The petrogenesis of carbonatite, melnoite and kimberlite from the Eastern Goldfields Province, Yilgarn Craton. Lithos, 76, 519-533.

Grant, F.S., and West, G.F., 1965. Interpretation Theory in Applied Geophysics, McGraw - Hill, Inc.

Griffin, T.J., 1990. Geology of the granite-greenstone terrane of the Lake Lefroy and Cowan 1:100 000 sheets, Western Australia. Geological Survey of Western Australia Report, 32, 53p.

Griffin, W.L., Belousova, E.A., Shee, S.R., Pearson, N.J., and O'Reilly, S.Y.O., 2004. Archean crustal evolution in the northern Yilgarn Craton: U-Pb and Hf-isotope evidence from detrital zircons, Precambrian Research, 131, 231-282.

Groenewald, P.B., 2002. Outcrop geology in the Leonora-Laverton region from the East Yilgarn Geoscience Database. Geoscience Australia Record, 2002/18, 7-10.

Groves, D.I., 1993. The crustal continuum model for late-Archaean lode-gold deposits of the Yilgarn Block, Western Australia. Mineralium Deposita, 28, 366-374.

Groves, D.I., and Batt, W.D., 1984. Spatial and temporal variations of Archaean metallogenic associations in terms of evolution of granitoid-greenstone terrains with particular emphasis on the Western Australian Shield. In Kroner, A., Hanson, G.N., and Goodwin, A.M., (Eds), Archaean Geochemistry: the Origin and Evolution of the Archaean Continental Crust, 73-98, Springer-Verlag.

Groves, D.I., Ho, S.E, and Houstoun, S.M., 1984. The nature of Archaean gold deposits in Western Australia with particular emphasis on parameters relevant to geophysical exploration. Geology Department and Extension Service, The University of Western Australia, Publication 10, 1-63.

Groves, D.I., Goldfarb, R.J., Knox-Robinson, C.M., Ojala, J., Gardoll, S., Yun, G.Y., and Holyland, P., 2000. Late kinematic timing of orogenic gold deposits and significance for computer-based exploration techniques with emphasis on the Yilgarn Block, Western Australia. Ore Geology Reviews, 17, 1-38.

Gustafson, J.K., and Miller, F.S., 1937. Kalgoorlie geology re-interpreted. Australian Institute of Mining and Metallurgy Proceedings, 106.

Hagemann, S.G., and Cassidy, K.F., 2000. Archaean orogenic lode gold deposits. In Hagemann, S.G., and Brown, P.E., (Eds), Gold in 2000. Reviews in Economic Geology, 13, 9-68.

Hallberg, J.A., 1985. Geology and mineral deposits of the Leonora–Laverton area, northeastern Yilgarn Block, Western Australia. Hesperian Press, Perth, Western Australia, 140p.

Hammond, R.L., and Nisbet, B.W., 1992. Towards a structural and tectonic framework for the Norseman-Wiluna Greenstone Belt, Western Australia. In Glover, J.E., and Ho, S.E., (Eds), The Archaean – Terrains, Processes and Metallogeny. Geology Department and University Extension, The University of Western Australia, Publication 22, 39-50.

Hammond, R.L., and Nisbet, B.W., 1993. Archaean crustal processes as indicated by the structural geology, Eastern Goldfields Province of Western Australia. In Williams, P.R., and Haldane, J.A., (Eds), Kalgoorlie '93–an international conference on crustal evolution, metallogeny, and exploration of the Eastern Goldfields. Australian Geological Survey Organisation Record, 1993/54, 105–114.

Hand, J.L., Cas, R.A.F., Ong, L., Brown, S.J.A., Krapež, B., and Barley, M.E., 2002. Syn- and post-eruptive volcaniclastic sedimentation in late Archaean subaqueous depositional systems of the Black Flag Group, Eight Mile Dam, Kalgoorlie, Western Australia. In Altermann, W., and Corcoran, P.L., (Eds), Precambrian sedimentary environments; a modern approach to ancient depositional systems. Special Publication of the International Association of Sedimentologists, 33, 235-258.

Harris, L.B., Koyi, H.A., and Fossen, H., 2002. Mechanisms for folding of high-grade rocks in extensional tectonic settings. Earth-Science Reviews, 59, 163-210.

Heath, C.J., 2003. Fluid Flow at the giant Golden Mile deposit, Kalgoorlie, Western Australia. Australian National University, PhD thesis (unpublished) 173p.

Henson, P.A., Blewett, R.S., Champion, D.C., Goleby, B.R. and Cassidy, K.F., 2004. A dynamic view of orogenesis and the development of the Eastern Yilgarn Craton. In Barnicoat, A.C., and Korsch, R.J., (Eds), Predictive Mineral Discovery Cooperative Research Centre: Extended Abstracts from the June 2004 Conference. Geoscience Australia, Record 2004/9, 91-94.

Hill, R.I., and Campbell, I.H., 1993. Age of granites in the Norseman area of Western Australia. Australian Journal of Earth Sciences, 40, 250-265.

Hill, R.I., Campbell, I.H., and Compston, W., 1989. Age and origin of granitic rocks in the Kalgoorlie-Norseman region of Western Australia: implications for the origin of Archean crust. Geochimica et Cosmochimica Acta, 53, 1259-1275.

Hill, R.I., Chappell, B.W., and Campbell, I.H., 1992. Late Archaean granites of the southeastern Yilgarn block, Western Australia: age, geochemistry and origin. Transactions of the Royal Society Edinburgh, Earth Science, 83, 211-226.

Hornby, P., Boschetti, F., and Horowitz, F.G., 1999. Analysis of potential field data in the wavelet domain. Geophysical Journal International, 137, 175-196.

Horton, B.K., 1998. Sediment accumulation on top of the Andean orogenic wedge: Oligocene to late Miocene basins of the Eastern Cordillera, southern Bolivia. Geological Society America, Bulletin 110, 1174-1192.

Horton, B.K., and DeCelles, P.G., 1997. The modern foreland basin system adjacent to the central Andes. Geology, 25, 895-898.

House, M., Dentith, M., Trench, A., Groves, D., and Miller, D., 1999. Structure of the highly mineralised late-Archean granitoid-greenstone terrain and the underlying crust in the Kambalda-Widgiemooltha area, Western Australia, from the integration of geophysical datasets. Exploration Geophysics, 30, 50-67.

Houseman, G.A., McKenzie, D.P., and Molnar, P., 1981. Convective instability of a thickened boundary layer and its relevance for the thermal evolution of continental convergent belts. Journal of Geophysical Research, 86, 6115-6132.

Hronsky, J.A., 1993. Gold ore-shoots at Lancefield gold deposit, WA. University of Western Australia, PhD thesis (unpublished).

Hronsky, J.M.A., 2004. The science of exploration targeting. In Muhling, J., et al., (Eds), SEG 2004, Predictive Mineral Discovery Under Cover. Centre for Global Metallogeny, The University of Western Australia, Publication 33, 129-133.

Hunt, J.M., 1990. Generation and migration of petroleum from abnormally pressured fluid compartments. AAPG Bulletin, 74, 1-12.

Iio, Y., and Kobayashi, Y., 2002. A physical understanding of the beginning of large intraplate earthquakes. Earth Planets Space, 54, 1001-1004.

Ingersoll, R.V., Dickinson, W.R., and Graham, S.A., 2003. Remnant-ocean submarine fans; largest sedimentary systems on Earth. In Chan , M.A. and Allen, W.A. (Eds), Extreme depositional environments; mega end members in geologic time. Geological Society America, Special Paper 370, 191-208.

Jaeger, J. C., 1962. Elasticity, Fracture and Flow. Methuen, London, 208p.

Jones, L.E.A., Goleby, B.R., Johnstone, D.W., and Barton, T.J., 2002. Seismic data acquisition and processing - 2001 Northern Yilgarn seismic reflection survey (L154). In Cassidy, K.F., (Ed), Geology, geochronology and geophysics of the north eastern Yilgarn Craton, with an emphasis on the Leonora-Laverton transect area. Geoscience Australia, Record 2002/18, 111-118.

Kalinowski, A.A., Henson, P.A., Blewett, R.S., Champion, D.C., Goleby, B.R., and Cassidy, K.F., 2004. 4D visualisation: bringing animation to geoscience. In Barnicoat, A.C., and Korsch, R.J., (Eds), Predictive Mineral Discovery Cooperative Research Centre: Extended Abstracts from the June 2004 Conference. Geoscience Australia, Record 2004/9, 101-104.

Karato, S., 1992. On the Lehmann discontinuity. Geophysical Research Letters, 19, 2255-2258.

Kennett, B.L.N., 1997. The mantle beneath Australia. AGSO Journal of Australian Geology and Geophysics, 17, 49-54.

Kennett, B.L.N., Engdahl, E.R., and Buland, R., 1995. Constraints on seismic velocities in the Earth from travel times. Geophysical Journal International, 122, 108–124.

Kent, A.J.R, 1994. Geochronological constraints on the timing of gold mineralisation in the Yilgarn Craton, Western Australia. Australian National University, PhD thesis (unpublished), 268p.

Kent, A.J.R., and McDougall, I., 1995. 40Ar -39Ar and U-Pb age constraints on the timing of gold mineralization in the Kalgoorlie gold field, Western Australia. Economic Geology, 90, 845-859.

Krapež, B., 1997. Sequence-stratigraphic concepts applied to the identification of depositional basins and global tectonic cycles. Australian Journal of Earth Sciences, 44, 1-36.

Krapež, B., Brown, S.J.A., Hand, J., Barley, M.E., and Cas, R.A.F., 2000. Age constraints on recycled crustal and supracrustal sources of Archaean metasedimentary sequences, Eastern Goldfields Province, Western Australia: Evidence from SHRIMP zircon dating. Tectonophysics, 322, 89-133.

Lacombe, O., Mouthereau, F., Angelier, J., and Deffontaines, B., 2001. Structural, geodetic and seismological evidence for tectonic escape in SW Taiwan, Tectonophysics, 333, 323-345.

Li, Y., and Oldenburg, D.W., 1996. 3-D inversion of magnetic data. Geophysics, 61, 494-408.

Li, Y., and Oldenburg, D.W., 1998. 3-D inversion of gravity data. Geophysics, 63, 109-119.

Lister, G.S., Forster, M.A., and Rawling, T.J., 2001. Episodicity During Orogenesis. In Miller, J.A., Holdsworth, R.E., Buick, I.S., and Hand, M., (Eds), Continental Reactivation and Reworking. Geological Society, London, Special Publications, 184, 89-113.

Liu, S., and Chen, S., 1998. Structural framework of the northeastern Yilgarn Craton and implications for hydrothermal gold mineralisation. Australian Geological Survey Organisation Research Newsletter, 29, 21-23.

Liu, S.F., Stewart, A.J., Farrell, T., Whitaker, A.J., and Chen, S.F., 2000. Solid Geology of the north Eastern Goldfields, Western Australia. Geoscience Australia 1:500 000 scale print on demand map (Catalogue No 53233).

Magistrale, H., 2002. Relative contributions of crustal temperature and composition to controlling the depth of earthquakes in Southern California. Geophysical Research Letters, 29, 1447.

Marsalia, K.M., 1995. Interarc and backarc basins. In Busby, C.J., and Ingersoll, R.V., (Eds), Tectonics of Sedimentary Basins. Blackwell Science, 299-330.

Martin, M.M., and Martin, A.A., 2002. Thrust sequence and syntectonic sedimentation in a piggy-back basin; the Oligo-Aquitanian Mula-Pliego Basin (internal Betic Zone, SE Spain). Comptes Rendus - Academie des sciences. Geoscience, 334, 363-370, Elsevier. Paris, France.

Martinez-Catalan, J.R., Arenas, R., and Diez, B.M.A., 2003. Large extensional structures developed during emplacement of a crystalline thrust sheet; the Mondonedo Nappe; NW Spain. Journal of Structural Geology, 25, 1815-1839.

Martyn, J.E., 1987. Evidence for structural repetition in the greenstones of the Kalgoorlie district, Western Australia. Precambrian Research, 37, 1-18.

Matheson, R.S., 1940. Reports on some Mining Groups in the Yilgarn Goldfield. Geological Survey of Western Australia Report for 1939, 18-43.

McMath, J.C., 1953. The geology of the country about Coolgardie, Coolgardie Goldfields, W.A. GSWA Bulletin 107.

McNaughton, N.J., Cassidy, K.F., Groves, D.I., and Perring, C.S., 1990. Timing of mineralization. In Ho, S.E., Groves, D.I., and Bennett, J.M., (Eds), Gold Deposits of the Archaean Yilgarn Block, Western Australia: Nature, Genesis and Exploration Guides. Geology Department and Extension Service, University of Western Australia, Publication 20, 221-225.

Mikucki, E.J., 1998. Hydrothermal transport and depositional processes in Archaean lode-gold systems: a review. Ore Geology Reviews, 13, 307–321.

Mikucki, E.J., and Roberts, F.I., 2003. Metamorphic petrography of the Kalgoorlie region, Eastern Goldfields Granite-Greenstone Terrane: METPET database. Western Australia Geological Survey Record, 2003/12.

Mueller, A.G., Harris, L.B., and Lungan, A., 1988. Structural control of greenstone-hosted gold mineralisation by transcurrent shearing; a new interpretation of the Kalgoorlie mining district,

Western Australia. In Ho, S.E., and Groves, D.I., (Eds), Advances in understanding Precambrian gold deposits – Volume II. Geology Department and Extension Service, University of Western Australia, Publication 12, 355p.

Mugnier, J.L., Leturmy, P., Huyghe, P., and Chalaron, E., 1999. The Siwaliks of western Nepal II. Mechanics of the thrust wedge. Journal of Asian Earth Sciences, 17, 643-657.

Myers, J.S., 1995. The generation and assembly of an Archaean supercontinent – evidence from the Yilgarn Craton, Western Australia, In Coward, M.P., and Ries, A.C., (Eds), Early Precambrian Processes, Geological Society London, Special Publication 95, 143-154.

Myers, J.S., 1997. Preface; Archaean geology of the Eastern Goldfields of Western Australia; regional overview. Precambrian Research, 83, 1-10.

Nadai, A., 1950. Theory of Flow and Fracture of Solids. McGraw-Hill, New York, 572p.

Needleman, A., 1994. Computational modelling of material failure. Applied Mechanics Reviews, 47, 34-42.

Nelson, D.R., 1995. Compilation of SHRIMP U-Pb zircon geochronology data, 1994. Western Australia Geological Survey, Record 1995/3, 244p.

Nelson, D.R., 1996. Compilation of SHRIMP U-Pb zircon geochronology data, 1995. Western Australia Geological Survey, Record 1996/5, 168p.

Nelson, D.R., 1997a. Evolution of the Archaean granite-greenstone terranes of the Eastern Goldfields, Western Australia: SHRIMP U-Pb zircon constraints. Precambrian Research, 83, 57-81.

Nelson, D.R., 1997b. Compilation of SHRIMP U-Pb zircon geochronology data, 1996. Western Australia Geological Survey, Record 1997/2, 189p.

Nelson, D.R., 1998. Compilation of SHRIMP U-Pb zircon geochronology data, 1997. Western Australia Geological Survey, Record 1998/2, 242p.

Nelson, D.R., 1999. Compilation of geochronology data, 1998. Western Australia Geological Survey, Record 1999/2, 222p.

Neumayr, P., 2004. Camp- to deposit-scale architecture, hydrothermal alteration and location of gold deposits. Predictive Mineral Discovery CRC project development team meeting Perth December 2004. [https://pmd-twiki.arrc.csiro.au/twiki/bin/view/Pmdcrc/YilgarnPdt]

Newton, P.G.N., Brown, S.M., and Ridley, J.R., 2002. The Sunrise-Cleo Au deposit, Laverton, Western Australia. In WA Gold Giants, Extended Abstracts Volume. School of Earth and Geographical Sciences, University of Western Australia, 35-43.

Nicolas, A., and Poirier, J.P., 1976. Crystalline plasticity and solid state flow in metamorphic rocks. Wiley, London.

Norrish, K., and Chappell, B.W., 1977. X-ray fluorescence spectrometry. In Zussman, J., (Ed), Physical Methods in Determinative Mineralogy (2nd ed.). Academic Press, New York, 201–272.

Nutman, A.P., Bennett, V.C., Kinny, P.D., and Price, R., 1993. Large-scale crustal structure of the northwestern Yilgarn Craton, Western Australia: evidence from Nd isotope data and zircon geochronology, Tectonics, 12, 971-981.

Ojala, V.J., McNaughton, N.J., Ridley, J.R., Groves, D.I., and Fanning, C.M., 1997. The Archaean Granny Smith gold deposit, Western Australia: Age and Pb-isotope tracer studies. Chronique de la Recherche Miniere, 529, 75-89.

O'Leary, R., 2003. Distortion Effects of Faults on Gravity 'Worm' Strings. Internal report to Predictive Mineral Discovery CRC Y2 project (Appendix 2).

Oversby, B., 1994. A proposed extensional transfer structure in the Archaean of the Eastern Goldfields, AGSO Research Newsletter, 21, 11-12.

Passchier, C.W., 1994. Structural geology across a proposed Archaean terrane boundary in the eastern Yilgarn craton, Western Australia. Precambrian Research, 68, 43-64.

Paterson, M.S., 1978. Experimental Rock Deformation. The Brittle Field. Springer-Verlag, 254p.

Petrini, K., and Podladchikov, Y., 2000. Lithospheric pressure-depth relationship in compressive regions of thickened crust. Journal of Metamorphic Geology, 18, 76-77.

Phillips, O.M., 1991. Flow and Reactions in Permeable Rocks. Cambridge University Press, 285p.

Pidgeon, R.T., and Wilde, S.A., 1990. The distribution of 3.0 Ga and 2.7 Ga volcanic episodes in the Yilgarn Craton of Western Australia. Precambrain Research, 48, 309-325.

Pidgeon, R.T., and Hallberg, J.A., 2000. Age relationships in supracrustal sequences of the northern part of the Murchison Terrane, Archaean Yilgarn Craton, Western Australia: a combined field and zircon U-Pb study, Australian Journal of Earth Sciences, 47, 153-165.

Platt, J.P., 1986. Dynamics of orogenic wedges and the uplift of high-pressure metamorphic rocks. Geological Society of America Bulletin, 97, 1037-1053.

Platt, J.P., Whitehouse, M.J., Kelley, S.P., Carter, A., and Hollick L., 2003. Simultaneous extensional exhumation across the Alboran BasIn Implications for the causes of late orogenic extension. Geology, 31, 251-254.

Potma, W., 2004. Modelling of controls on ore deposition in the Eastern Yilgarn. Predictive Mineral Discovery CRC project development team meeting Perth December 2004. [https://pmd-twiki.arrc.csiro.au/twiki/bin/view/Pmdcrc/YilgarnPdt]

Price, N.J., and Cosgrove, J.W., 1990. Analysis of geological structures. Cambridge University Press, Great Britain, 80p.

Qiu, Y., and Groves, D.I., 1999. Late Archaean collision and delamination in the southwest Yilgarn Craton: the driving force for Archaean orogenic lode gold mineralisation? Economic Geology, 94, 115-122.

Qiu, Y.M., McNaughton, N.J., Groves, D.I., and Dalstra, H.J., 1999. Ages of internal granitoids in the Southern Cross region, Yilgarn craton, Western Australia, and their crustal evolution and tectonic implications. Australian Journal of Earth Sciences, 46, 971–981.

Ramsay, J.G., 1987. The Techniques of Modern Structural Geology, Volume 2: Folds and Fractures. Academic Press Inc, London.

Ramsay, J.G., and Huber, M.I., 1983. The Techniques of Modern Structural Geology, Volume 1: Strain Analysis. Academic Press Inc, London, 307p.

Rattenbury, M.S., 1993. Tectonostratigraphic terranes in the northern Eastern Goldfields. In Williams, P.R., and Haldane, J.A., (Eds), Kalgoorlie'93 – An International Conference on Crustal Evolution, Metallogeny, and Exploration of the Eastern Goldfields. Australian Geological Survey Organisation, Record 1993/54, 73-75.

Reading, A.M., Kennett, B.L.N., and Goleby, B.R., in prep. The deep seismic structure of Precambrian terranes within the West Australian Craton and implications for crustal formation and evolution. To be submitted to Precambrian Research.

Reading, A.M., Kennett, B.L.N., and Dentith, M.C., 2003. Lithospheric structure of the Pilbara Craton, Capricorn Orogen and northern Yilgarn Craton, Western Australia, from teleseismic receiver functions. Australian Journal of Earth Sciences, 50, 439–445.

Reading, A.M., Kennett, B.L.N., and Dentith, M.C., 2003. Seismic structure of the Yilgarn Craton, Western Australia. Australian Journal of Earth Sciences, 50, 427–438.

Regenauer-Lieb, K., 1999. Dilatant plasticity applied to Alpine collision: ductile void growth in the intraplate area beneath the Eifel volcanic field. Journal of Geodynamics, 27, 1-21.

Regenauer-Lieb, K., Yuen, D., and Branlund, J., 2001. The initiation of subduction: Criticality by addition of water? Science, 294, 578-580.

Regenauer-Lieb, K., and Yuen, D.A., 2003. Modelling shear zones in geological and planetary sciences: Solid-fluid and fluid-thermal-mechanical approaches. Earth Science Reviews, 63, 295-349.

Revenaugh, J., and Jordan, T.H., 1991. Mantle layering from ScS reverberations: 2. the transition zone. Journal of Geophysical Research, 96, 19763-19780.

Rodgers, J., 1995. Lines of basement uplifts with external parts of orogenic belts. American Journal of Science, 295, 455-487.

Ross, A.A., Barley, M.E., Ridley, J.R., and McNaughton, N.J., 2001. Two generations of gold mineralisation at the Kanowna Belle gold mine, Yilgarn Craton, In Cassidy, K.F., Dunphy, J.M., and Van Kranendonk, M., (Eds), 4th International Archaean Symposium 2001, Extended Abstracts. AGSO – Geoscience Australia, Record 2001/37, 398-399.

Ross, A.A., Barley, M.E., Brown, S.J.A., McNaughton, N.J., Ridley, J.R., and Fletcher, I.R., 2004. Young porphyries, old zircons: new constraints on the timing of deformation and gold mineralisation in the Eastern Goldfields provided by SHRIMP U-Pb zircon ages from the Kanowna Belle Gold Mine, Western Australia. Precambrian Research, 128, 105-142.

Rudnick, R.L., 1995. Making continental crust. Nature (London), 378 571-578.

Salier, B.P., Groves, D.I., McNaughton, N.J., and Maidens, E., 2001. Isotopic constraints on the genesis of alteration at Wallaby gold deposit, WA. In Cassidy, K.F., Dunphy, J.M., and Van Kranendonk, M., (Eds), 4th International Archaean Symposium 2001, Extended Abstracts. Australian Geological Survey Organisation, Record 2001/37, 400-402.

Scheidegger, A.E., 1974. The physics of flow through porous media, University of Toronto Press, Toronto.

Schreurs, G., Hann, R., and Vock, P., 2002. Analogue modelling of transfer zones in fold and thrust belts: a 4-D analysis. Journal of the Virtual Explorer, 6, 43-49.

Searle, M.P., 1999. Extension, compression and exhumation along the high Himalaya; evidence from the Everest-Lhotse Massif. Journal of Geological Society of London, 156, 227-240.

Sibson, R.H., 1990. Faulting and fluid flow. In Fluids in Tectonically Active Regimes of the Continental Crust. MAC Short Course on crustal fluids, 18, Vancouver, May 1990.

Smithies, R.H., and Champion, D.C., 1999. Geochemistry of felsic igneous alkaline rocks in the Eastern Goldfields, Yilgarn Craton, Western Australia: a result of lower crustal delamination? - implications for Late Archaean tectonic evolution. Journal of the Geological Society of London, 156, 561-576.

Spear, F.S., 1995. Metamorphic Phase Equilbra and Pressure-Temperature-Time Paths. Mineralogical Society of America, USA, 50-51.

SRK Consulting, 2000. Global Archaean Synthesis – Yilgarn module. Unpublished consultants report, 88 p.

Stewart, A.J., 1998. Recognition, structural significance, and prospectivity of early F1 folds in the Minerie 1:100,000 sheet area, Eastern Goldfields, Western Australia. Australian Geological Survey Organisation Research Newsletter, 29, 4-6.

Stewart, A.J., 2001. Laverton–Western Australia 1:250 000 Explanatory Notes (2nd edition). Western Australia Geological Survey, 34p.

Stuwe, K., and Sandiford, M., 1994. Contribution of deviatoric stresses to metamorphic P-T paths: an example appropriate to low-P high-T metamorphism. Journal of Metamorphic Geology, 12, 445-454.

Swager, C.P., 1989. Structure of the Kalgoorlie greenstones regional deformation history and implications for the structural setting of gold deposits within the Golden Mile. Western Australia Geological Survey Report 25, 59-84.

Swager C.P., 1997. Tectono-stratigraphy of late Archaean greenstone terranes in the southern Eastern Goldfields, Western Australia, Precambrian Research, 83, 11-42.

Swager, C.P., and Griffin, T.J., 1990. An early thrust duplex in the Kalgoorlie-Kambalda greenstone belt, Eastern Goldfields Province, Western Australia. Precambrian Research, 48, 63-73.

Swager, C.P., and Nelson, D.R., 1997. Extensional emplacement of a high-grade granite gneiss complex into low-grade granite greenstones, Eastern Goldfields, Western Australia. Precambrian Research, 83, 203-209.

Swager, C.P., Witt, W.K., Griffin, T.J., Ahmat, A.L., Hunter, W.M., McGoldrick, P.J., and Wyche, S., 1992. Late Archaean granite-greenstones of the Kalgoorlie Terrane, Yilgarn Craton, Western Australia, In Glover, J.E., and Ho, S.E., (Eds), The Archaean – Terrains, Processes and Metallogeny. Geology Department and Extension Service, University of Western Australia Publication 22, 107-122.

Swager, C.P., Goleby, B.R., Drummond, B.J., Rattenbury, M.S., and Williams, P.R., 1997. Crustal structure of granite-greenstone terranes in the Eastern Goldfields, Yilgarn Craton, as revealed by seismic reflection profiling. Precambrian Research, 83, 43-56.

Tornatora, P.M.A., 2002. Structure and mineralisation of the Western Shear Zone, Cleo-Sunrise gold deposit, Western Australia. University of Tasmania MSc thesis (unpublished).

Trench, A., House, M., Miller, D.R., Withers, J.A., Goleby, B.R., and Drummond, B.J., 1993. On the gravity signature of Archean greenstones in the Widgiemooltha-Tramways area, Eastern Goldfields, Western Australia. Exploration Geophysics, 24, 811-818.

Tripp, G., 2004. Kalgoorlie Archaean Symposium: Regional geological traverse. Placer Dome Asia Pacific field guide (unpublished).

Trofimovs, J., Davis, B.K., and Cas, R.A.F., 2004. Contemporaneous ultramafic and felsic intrusive and extrusive magmatism in the Archaean Boorara Domain, Eastern Goldfields Superterrane, Western Australia, and its implications. Precambrian Research, 131, 283-304.

Tvergaard, V., 1987. Effect of yield surface curvature and void nucleation on plastic flow localisation. Journal of Mechanics and Physics of Solids, 35, 43-60.

Umino, N., Ujikawa, H., Hori, S., and Hasegawa, A., 2002. Distinct S-wave reflectors (bright spots) detected beneath Nagamachi-Rifu fault, NE Japan. Earth Planets Space, 54, 1021-1026.

van der Hilst, R., Kennett, B.L.N., Christie, D., and Grant, J., 1994. Project Skippy explores the mantle and lithosphere beneath Australia, EOS, 75, 177,180,181.

Van der Pluijm, B.A., and Marshak, S., 1997. Earth Structure: An Introduction To Structural Geology and Tectonics. WCB/McGraw-Hill, USA.

Vearncombe, J.R., 1998. Shear zones, fault networks, and Archaean gold. Geology, 26, 855-858.

Vearncombe, J.R., Barley, M.E., Eisenlohr, B.N., Groves, D.I., Houstoun, S.M., Skwarnecki, M.S., Grigson, M.W., and Partington, G.A., 1989. Structural controls on mesothermal gold mineralization; examples from the Archean terranes of Southern Africa and Western Australia. Economic Geology, Monograph 6, 124-134.

Vermeer, P.A, and de Borst, R., 1984. Non-associated plasticity for soils, concrete and rock. HERON, 29, 1-64.

Vielreicher, N.M. Groves, D.I., Fletcher, I.R., McNaughton, N.J., and Rasmussen, B., 2003. Hydrothermal monazite and xenotime geochronology: a new direction for precise dating of orogenic gold mineralisation. Society of Economic Geologists, Newsletter, 53, 9-16.

Wang, W.H., and Hung, W.J., 2002. Synorogenic extension, Taiwan; implications of physical and numerical modelling. In Byrne, T.B., and Liu, C.S., (Eds), Geology and geophysics of an arc-continent collision, Taiwan, Special Paper - Geological Society of America, 358, 137-146.

Weinberg, R.F., Moresi, L., and van der Borgh, P., 2003. Timing of deformation in the Norseman-Wiluna Belt, Yilgarn Craton, Western Australia. Precambrian Research, 120, 219-239.

Whitaker, A.J., and Bastrokova, I.V., 2002. Yilgarn Craton aeromagnetic interpretation (1:1 000 000 scale data). Geoscience Australia, Canberra, Australia.

Whitaker, A.J., Blewett, R.S., and Fokker, M., 2002. Leonora-Laverton transect area solid geology. In Cassidy, K.F., (Ed), Geology, geochronology and geophysics of the north eastern Yilgarn Craton, with an emphasis on the Leonora-Laverton transect area. Geoscience Australia, Record 2002/18, 59-74.

Wilde, S.A., Valley, J.W., Peck, W.H., and Graham, C.M., 2001. Evidence from detrital zircons for the existence of continental crust and oceans on Earth 4.4 Gyr ago: Nature, v.409, p.175-178.

Willett, S. D., 1992. Kinematic and dynamic growth and change of a Coulomb wedge. In McClay, K.R., (Ed), Thrust Tectonics, Chapman & Hall. London, UK, 19-31.

Williams, I.R., 1974. Structural subdivision of the Eastern Goldfields Province, Yilgarn Block, Annual Report–Western Australia Geological Survey 1973, 53-59.

Williams, P.R., 1993. A new hypothesis for the evolution of the Eastern Goldfields Province. In Williams, P.R., and Haldane, J.A., (Eds), Kalgoorlie '93 – An International Conference on Crustal Evolution, Metallogeny, and Exploration of the Eastern Goldfields. Australian Geological Survey Organisation, Record 1993/54, 73-83.

Williams, P.R., and Whitaker, A.J., 1993. Gneiss domes and extensional deformation in the highly mineralised Archaean Eastern Goldfields Province, Western Australia, Ore Geology Reviews, 8, 141-162.

Williams, P.R., Etheridge, M.A., Witt, W., and Swager, C.P., 1989. Gold potential of early shear zones near Leonora, WA. Bureau of Mineral Resources Research Newsletter, 10, 6-7.

Witt, W.K., 1994. Geology of the Bardoc 1:100 000 sheet. Geological Survey of Western Australia, 1:100 000 Geological Series Explanatory Notes.

Wyche, S., Nelson, D.R., and Riganti, A., 2004. 4350-3130 Ma detrital zircons in the Southern Cross Granite-Greenstone Terrane, Western Australia: implications for the early evolution of the Yilgarn Craton: Australian Journal of Earth Sciences, v.51, p.31-45.

Yeats, C.J., McNaughton, N.J., Ruettger, D., Bateman, R., Groves, D.I., Harris, J.L., and Kohler, E., 1999. Evidence for diachronous Archaean lode-gold mineralization in the Yilgarn Craton, Western Australia: A SHRIMP U-Pb study of intrusive rocks: Economic Geology, 94, 1259-1276.

Yeats, C.J., Kohler, E.A., McNaughton, N.J., and Tkatchyk, L.J., 2001. Geological setting and SHRIMP U-Pb geochronological evidence for ca. 2680-2660 Ma lode-Au mineralisation at Jundee-Nimary in the Yilgarn Craton, Western Australia, Mineralium Deposita, 36, 125-136.